The multi-disciplinary science of Rheology

Towards a healthy and sustainable development

ISBN 978-84-697-5123-7

Edited by:
M. J. Hernández,
T. Sanz, A. Salvador,
F.J. Rubio-Hernández, R. Steinbrüggen

Design by imedes

Preface

It is a pleasure to introduce this collection of reviewed papers related to some of the posters and oral communications presented in Ibereo 2017, held in Valencia (Spain) in September 2017 and hosted by the Universitat de Valencia and IATA-CSIC.

The Ibereo 2017 is the sixth of a series of conferences on Fundamental and Applied Rheology, organized jointly by the Portuguese Society of Rheology (SPR) and the Spanish Group of Rheology (GER). The conference is a forum that aims to connect and strength relationships among professionals of a wide variety of disciplines, revealing the fact that Rheology is a multidisciplinary science.

In 2017 edition important consideration has been given to the connection between rheology and industry, with emphasis in the relationships between research, development and innovation. Health and sustainable development have also been main drivers of the conference, in accordance to what society requires. We are grateful to both SPR and GER, together with the sponsors (EPL, IFI, TA Instruments, Massó, IESMAT, Kern Pharma, RNB, Korott, MICOS and Applied Rheology), since they have helped to make Ibereo 2017 possible.

The applications of Rheology to Food and Pharmaceutical Sciences have taken centre stage in the book, due to the unavoidable influence of Ibereo 2017organizing chairs. Both subjects are undoubtedly related to Formulation and Product Design, so the latter is also an outstanding topic. Moreover, other topics as Polymers &Biopolymers, Colloids& Suspensions are also covered with very interesting contributions, following the main tradition of the Conference and the relevance of rheology in the study of those systems. The book ends with some new developments in Rheometry & Experimental methods.

Special acknowledgements are given to all authors who have prepared the manuscripts of this book and the Ibereo 2017 Scientific Committee for improving them with their suggestions and corrections. Finally, all credit for the content of every contribution should be given to the authors themselves.

The Editors

REVIEWERS (Ibereo 2017 Scientific Committee)

María Dolores Álvarez
(ICTAN-CSIC, Madrid, Spain)

María Teresa Cidade
(Universidade Nova de Lisboa, SPR President, Portugal)

José María Franco
(Universidad de Huelva, Spain)

Carlos Gracia
(TA Instruments, Spain)

Antonio Guerrero
(Universidad de Sevilla, GER President, Spain)

Catarina Rosa Leal
(Instituto Politécnico de Lisboa-ISEL, Portugal)

José Muñoz
(Universidad de Sevilla, Spain)

Miguel Nóbrega
(Universidade do Minho, Portugal)

Pedro Partal
(Universidad de Huelva, Spain)

María GraçaRasteiro
(Universidade do Coimbra, CIEPQPF-UC, Portugal)

Helena Ribeiro
(Universidade de Lisboa, Portugal)

Antxon Santamaría
(Universidad del País Vasco, Spain)

Isabel de Sousa
(Universidade de Lisboa, Portugal)

Clara Asunción Tovar
(Universidad de Vigo, Spain)

Contents

Invited Contributions

Rheological Aspects of Dysphagia Diagnosis and Management

C. Gallegos, G. Assegehegn, M. Turcanu, E. Brito

I&D Centre Complex Formulations & Processing Technologies, Fresenius Kabi Deutschland GmbH (Germany)

Introduction

Swallowing is defined as "the function of clearing food through the oral cavity, pharynx and esophagus into the stomach at an appropriate rate and speed".

Dysphagia is a dysfunction of the transfer of the bolus from the mouth to the stomach, which may involve any of the stages of the above-mentioned normal swallowing sequences and may result in misdirection of transferred bolus. Thus, patients with structural or physiologic deficits in the mouth, pharynx, or esophagus may demonstrate signs and symptoms of dysphagia. From a pathological perspective, dysphagia may result from a variety of diseases or medical conditions or from treatment of diseases or medical conditions.

The rheological characterization of food boluses is highly relevant, as it is linked to the performance of the deglutition or swallowing process. The rheological properties of foods entering into the mouth are fundamentally a function of the food composition. However, once in the mouth, the rheological behaviour is modified during the formation of the bolus, which is largely influenced by subjective sensorial perceptions. Thus, rheological properties play an important role in perceptions of food textures or consistencies.

Food bolus flow is a dynamic process that depends on the characteristics of the applied force. Thus, the bolus during the swallowing process is submitted to shear and extensional flows. However, the focus is usually centred on the measurement of shear viscosity. Likewise, structured food systems may exhibit solid-like behaviour. In this case, more sophisticated rheological studies should be used to describe the rheological behaviour of food boluses.

Even though the elongational properties of dysphagia products have not been extensively studied up to now, they might provide important insights on the dynamics of food bolus during the swallowing process. Thus, it is assumed that higher extensional properties of food bolus could be correlated to higher cohesiveness during the oral processing. This is particularly important since a cohesive bolus will fracture/breakup less during the pharyngeal phase of the swallowing, which could decrease the risk of aspiration for patients with dysphagia.

Management of dysphagia is commonly done by the prescription of texture-modified diets. The rationale behind modifying the texture or viscosity of foods and drinks is to change the rate at which the bolus is transported through the pharynx and, thus, to reduce the risk of aspiration and pneumonia [1]. Texture (or viscosity) modification of liquids or solids is commonly done by using powder thickeners (based on starch or, more recently, on alpha-amylase resistant gums). An alternative to this practice is the use of prescribed ready-to-use oral nutritional supplements (ONS), specially designed for the nutritional support at different stages of dysphagia. This practice has some advantages, as they are designed for complete nutrition of the patient.

On the other hand, the most appropriate modification of food consistencies should follow from a clear assessment of the swallowing problem [2]. The goal of the diagnostic strategy for dysphagia is to evaluate two deglutition-defining characteristics: (a) efficacy; and (b) safety [3]. Among the several diagnostic assessment methods, instrumental assessment provides more accurate and objective diagnosis. Instrumental assessment uses fiberoptic endoscopic evaluation of swallowing (FEES) or videofluoroscopy (VFS) to evaluate the safety and efficacy of deglutition, to characterize the alterations of deglutition, and to help select and assess specific therapeutic strategies. During the FEES or VFS assessment, the swallowing process can be visualised either by using a ready-to-use commercial contrast medium (i.e. Varibar® or Gastrografin®) or by mixing food with, for instance, barium sulphate. Nevertheless, the lack of standardisation is apparent [4]. In addition, it is worth mentioning that the rheological properties of the radiopaque bolus prepared by mixing with normal food are quite different from those of the normal food used as

a "vehicle" for the videofluoroscopic tests. A more detailed clinical diagnosis and nutritional management of dysphagia have discussed by some of the authors elsewhere [5].

Care professionals are increasingly relying on national guidelines for the dietary management of dysphagia patients. There are several guidelines from different dysphagia professional associations around the world concerning a "rheological" classification of fluids for dysphagia management. All of them are referring to viscosity as the only rheological property involved in diet modification for dietary management of dysphagia. In addition, only one of these guidelines proposes objective viscosity borders and ranges for thickened liquids or food boluses (nectar, honey and spoon-thick). In this case, the classification and ranges are based on shear viscosities measured at a single shear rate (50 s^{-1}) and a temperature of 25°C [6], without any scientific evidence or rationale given on the temperature and shear rate chosen for this scale. In fact, a wide range of shear rates, ranging from 5 to 1000 s^{-1} are feasible [7, 8].

It is quite clear that more research needs to be conducted to determine normative rheological values for the complex swallowing process and, consequently, for its application to dysphagia diagnosis and management.

In this sense, this paper gathers up-to-date information on the rheology of swallowing and dysphagia (including shear and elongational flows) and its influence on the characteristics of the enteral nutrition for dysphagia management (ready-to-use oral nutritional supplements and thickening powders), with special focus on the real characteristics of the bolus after mixing with human saliva.

Experimental Methods

Materials

Starch-based, gum-based, mixtures of starch and gum-based powder thickeners, and ready-to-use dysphagia products (ONS) were used in this study. These commercial dysphagia products were obtained from their corresponding manufacturers and were used according to the usage instruction of the manufactures without further modification. In the case of powder thickeners, the desired amount of powder was weighed and dissolved in tap water to obtain thickened fluids.

Contrast medium (Gastrografin®), with iodine concentration of 370 mg/mL, was obtained from Bayer Hispania, S.L., Barcelona, Spain.

Lyophilized human saliva was obtained from LEE BioSolutions (LEE^{SM}, BioSolutions, USA).

Methods

Some commercially available dysphagia products were characterised in terms of their shear and elongational behaviour. For the thickened fluids, the powder thickener was dissolved, either in tap water or in a mixture of tap water and Gastrografin® (1:1). In addition, the effect of salivary α-amylase on these products was also studied.

Viscous flow behaviour in steady shear

A controlled-stress rheometer (Haake MARS III, Thermo Haake GmbH, Karlsruhe, Germany) was used to perform shear characterization of selected dysphagia products. All the measurements were carried out at 25 °C and in a shear rate range of 1-300 s^{-1}.

Elongational behaviour

In order to highlight the elongational properties of some commercially available dysphagia fluids, uniaxial elongational measurements were performed by using a capillary break-up extensional rheometer (CaBER-1, Thermo Haake GmbH, Karlsruhe, Germany) with an attached high-speed camera (Photron Fastcam Mini UX100, Photron, USA). The filament thinning of the samples was induced by separating the 6 mm diameter parallel plates of the extensional rheometer from an initial gap of 3 mm to a final gap of 11 mm, within 50 ms. Mid-filament diameter was monitored with the standard laser micrometer of the device until the filament breakup. Both filament evolution and breakup time were qualitatively and quantitatively compared.

Effect of saliva on viscous flow and elongational behaviours

The first step during swallowing is mixing of food bolus and saliva. During this mixing process, the viscosity of the food bolus may decrease because of a hydrolysis reaction with salivary α-amylase and, to some extent, because of dilution with saliva. This viscosity reduction can be significant and may severely affect the safety and efficiency of dysphagia management. Some selected thickened fluids and ready-to-use products were characterized in terms of their resistance to hydrolysis reaction with saliva. For this study, a mixing rheometer [9] was used, as it has many advantages over conventional geometries. These advantages include providing an effective mixing of the bolus and saliva as it happens in the mouth, providing continuous visual observation of the hydrolysis reaction, providing

real-time information of the reaction, avoiding errors during sample preparation, and allowing the calculation of reaction kinetics. With this aim, a helical ribbon mixer, as mixing element, was coupled to a Haake, MARS III rheometer. In order to obtain the effective shear rate imposed by the mixer on the food bolus, the helical ribbon geometry was calibrated and tested before use [9]. During the saliva test experiment, a sample was added to the rheometer and, after the torque reached a constant value, simulated saliva was added, in a concentration of 10% v/w [10], and the hydrolysis reaction was followed. In addition to the shear measurements, elongational properties of food boluses, before and after the addition of simulated saliva were performed using CaBER. All measurements were performed at 25 °C.

Results and Discussion

Current practice of dysphagia diagnosis and management relies in many occasions on subjective evaluation of viscosity using verbal descriptors. However, this practice shows poor repeatability for safe and efficient dysphagia treatment. This is due to the fact that many variables may affect the consistency of, for instance, a thickened fluid prepared from powder thickeners, such as thickener nature, beverage type, fluid temperature, human saliva, shear rate, and time. Thus, for instance, several brands of powder thickeners are available in the market with differences in constituent ingredients (mainly starch, gums, or their blends) and instructions for use, which may complicate attempts for subjective judgment. From the diagnosis point of view, care must be taken not to directly implement the manufacturers' dosage information to prepare thickened fluids containing contrast medium. As shown in Figure 1, the same amount of thickener powder dissolved in water and in a mixture of water and Gastrografin® yields significantly different viscosity values at 50 s^{-1}, with the latter yielding a 5-fold higher viscosity value (shown as a single shear rate value). This clearly shows that additional rheological characterization should be performed in order to achieve rheological similarities between thickened fluids dissolved in only water and in a fluid containing contrast medium.

The flow curves in Figure 1 represent rheological similarities of a powder dissolved in only water and in a 1:1 ratio of water and Gastrografin®. In order to achieve such similarities, the amount of powder dissolved in the latter was decreased down to 4 g/100 mL of solvent. Other authors have developed a ready-to-use product with similar rheological characteristics (see Table 1) to Varibar® pudding, aiming to avoid differences between diagnosis and management of dysphagia [2].

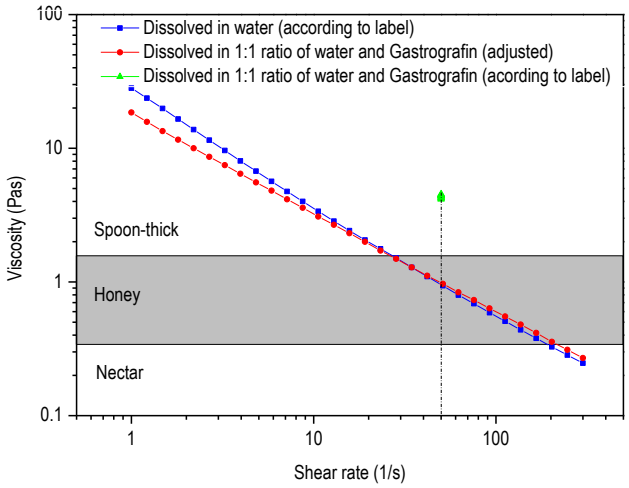

Figure 1. Viscous flow behaviour of a thickened fluid with and without contrast medium

As mentioned before, texture modification of foods and beverages is one of the most common methods of dysphagia management. Consistency classes, which vary from country to country, are prescribed for dysphagia patients based on their swallowing impairment, dysphagia phenotype, age and gender, which are assessed during diagnosis.

However, for a safe and efficient dysphagia management, it is therefore indispensable to have a clear definition of the fluid consistency. In other words, it is necessary to characterise the viscous flow behaviour of the thickened fluids and ONS in a wide range of shear rates. Figure 2 shows viscous flow curves of fluids thickened with some of commercially available powders and ready-to-use (ONS) dysphagia products. Figure 2a shows a representative graph of the shear-thinning behaviour of fluids thickened with starch-based powder, gum-based powder, and mixture of both thickeners thereof. The thickened fluids were prepared according to the manufacturers' guidelines for spoon-thick/pudding consistency. As shown in that Figure, it has been proven that the values of the flow index, n, and the consistency index, K, significantly differ depending on the thickener composition and manufacturer for all the products studied. Similar differences were also observed for nectar and honey consistencies (data not shown). The degree of shear-thinning behaviour is closely related to the safety of thickened products swallowing. A thickened product with low flow index reduces its viscosity to rather low values as shear rate increases (e.g. in pharynx), and this may increase the risk of aspiration in dysphagia patients. On the other hand, a thickened product with a high flow index remains relatively viscous at high shear rates (e.g. in the

pharynx), and thus may facilitate the safe swallowing process. It is, therefore, highly recommended that standardized objective definitions, in terms of viscosity level, shear-thinning behaviour, and elasticity of each dysphagia stages, taking into account dysphagia phenotype, swallowing impairment, gender, and age of the patients, are set. Figure 2b shows the viscous flow behaviour of different thickened fluids and ONS with remarkable similarities in their viscous flow behaviour.

Table 1: Rheological similarities of a ready-to-use product and a Varibar® pudding contrast medium [2].

	Sisko's model parameters		
	η_∞[Pa.s]	K [Pa.s^n]	n [-]
RTU pudding-like product	0.9	155	0.16
Varibar® pudding	0.7	143	0.14

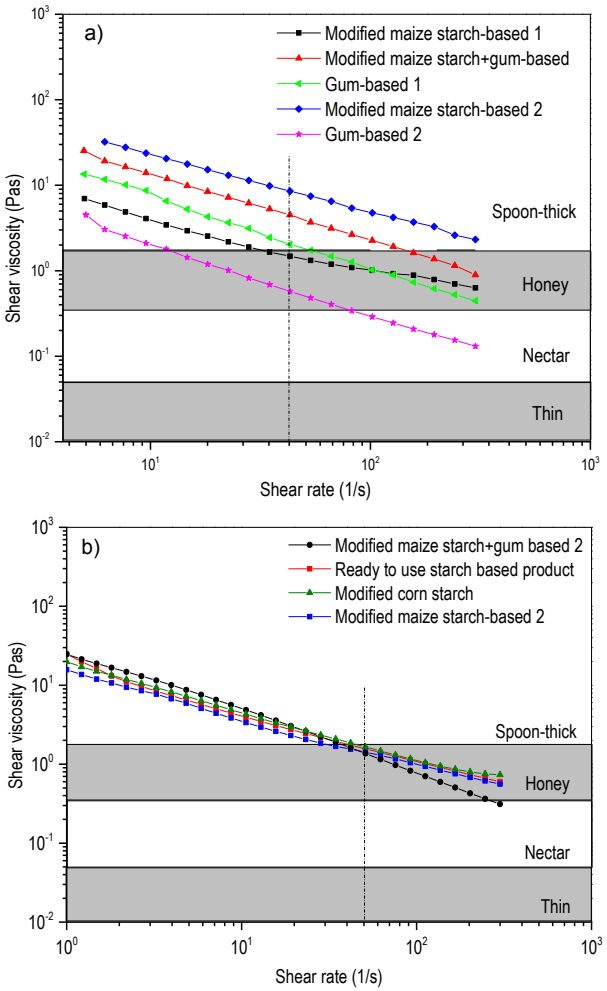

Figure 2. Viscous flow behaviour of thickened fluids with commercial available powders and ONS: a. different shear viscosity at 50 s^{-1}; and b. similar shear viscosity at 50 s^{-1}.

Concerning the elongational behaviour of fluids for dysphagia management, the filament shapes of the four dysphagia products shown in Figure 2b are illustrated in Figure 3.

In contrast to their very similar shear viscosities (1.7 Pa.s) at 50 s^{-1}, these fluids show different elongational responses for the same imposed uniaxial deformation profile. It was observed that, in general, ready-to-use products tend to form more homogenous filaments and have longer breakup times than thickened fluids for the same range of shear viscosities. Ready-to-use products are subjected to thermal treatment during sterilization which ensures high product homogeneity. On the other hand, thickened fluids might not be totally hydrated in the limited time suggested by the manufacturer, which could explain the complex filament profiles observed in Figure 3.

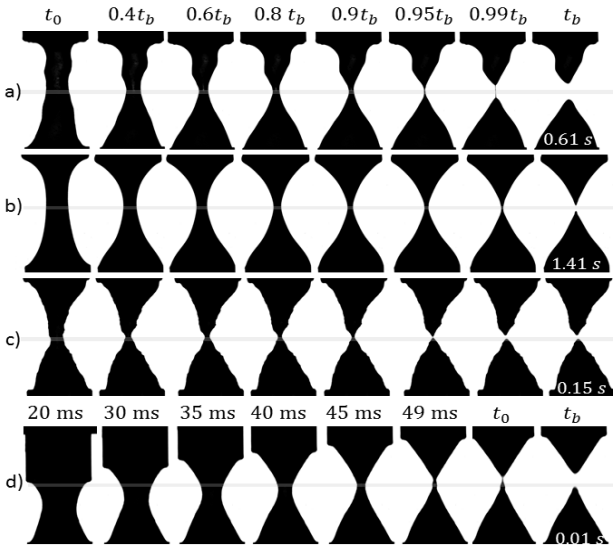

Figure 3. Filament shapes (in CaBER) of a ready-to-use dysphagia oriented product (b) and of different thickened fluids (a, c, d), classified by their main thickening ingredient as gum-based (GB:a) and starch-based (SB:b,c,d). t_0: starting time, and t_b: break-up time

The first product is a thickened fluid containing, in addition to modified maize starch, xanthan gum (Figure 3a). The elasticity resulting from the presence of gums is illustrated through the formation of an ideal cylindrical thread shortly before filament breakup (0.95 t_b). The second fluid (Figure 3b) is a ready-to-use product based on starch as thickener. This product forms a homogenous filament, highly curved in the centre, that necks and breaks up right in the middle, after more than 1 s. This type of evolution is generally observed for the majority of starch-based ready-to-use dysphagia designed fluids. The third filament (Figure 3c) is a starch-based thickened fluid. This filament shows high

non-homogeneity and breaks within the first 15 ms after the end of the imposed deformation. The fast filament breakup is due to the lack of elasticity of starches, in contrast to gums that form structural networks that disentangle during stretching and eventually break. The last filament (Figure 3d) is a starch-based thickened fluid as well, but less concentrated. In this case, the filament breaks right after the end of the imposed elongation profile (0.01 ms).

From the previous results, it is clear that, even though shear viscosities and shear-thinning behaviour are very similar for the four fluids shown in Figure 2b, their elongational behaviour and capillary breakup times are significantly different (Figure 3).

Furthermore, until now, the discussion was restricted to neat dysphagia designed fluids. In reality, these fluids are always in contact with human saliva during swallowing. Therefore, both shear and elongational behaviours of these products may be altered during oral processing.

It is well known that the enzyme α-amylase, which is found in human saliva, is responsible for the early break down of starch components. This phenomenon has a direct implication in dysphagia management as many dysphagia products contain starch as thickener. It has been found that, in less than 10 s after mixing with saliva (or α-amylase), honey consistency shows almost a 10-fold decrease of its original viscosity [11]. When foods made with unmodified starch are mixed with α-amylase, their viscosity can be reduced by more than half within 1-10 s [12]. In this paper, the effect of α-amylase on fluids thickened with starch-based or gum-based powders, as well as with mixtures of both thickeners, is analysed. This is shown in Figure 4, where the starch-based thickened fluid reduces its viscosity level significantly within very short period of time. Comparing the three curves, it is easy to conclude that having starch as a major component leads to a significant viscosity reduction, being this reduction almost instantaneous. This might lead to an increased risk of aspiration for the patient.

The superiority of gum-based thickened fluids over starch-based thickened fluids in terms of α-amylase resistance can be observed not only in relation to the shear viscosity, but also in the elongational behaviour, through the evolution of breakup time.

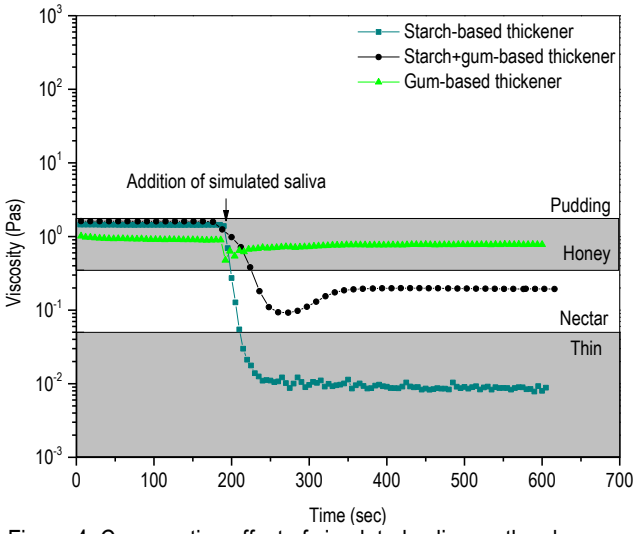

Figure 4. Comparative effect of simulated saliva on the shear viscosity at 50 s^{-1} of fluids thickened with starch, gums, or mixtures of starch+gums (1 mL saliva/10 mL sample, 25°C).

Figure 5 gathers both shear viscosities, at 50 s^{-1}, and elongational breakup times for two thickened fluids, one based on starch and the other one based on gums, before and after the addition of simulated saliva (or water, as a control). With such representation, it is easy to screen the enzymatic effect of α-amylase on a pure starch based thickened fluid, when compared to a gum based thickened fluid. In the presence of simulated saliva, the decrease in both shear viscosity and elongational breakup time of a starch-based thickened fluid are significant, while, for a gum-based thickened fluid, these functions are affected in the same manner as after its dilution with water.

Even though the in-vitro studies performed in this work clearly highlight the effect of alpha-amylase, it is worth mentioning that the elongational properties of the bolus may be quite different when mixed with real human saliva. Thus, some of the authors have shown that an unexpected increase in filament lifetime of a starch-based food product in the presence of whole human saliva occurs (coming from a healthy person), which is triggered by the presence of highly elastic mucins, naturally secreted during food oral processing [13].

However, human saliva is a personal pattern. In addition, the rheological characteristics of this fluid will also depend on the level of dysphagia of the patient. Consequently, it is not reliable to generalise these findings taking into account the current level of research. Therefore, more research is currently in process, in order to better understand the role of elongational flow in the swallowing process of dysphagia designed fluids.

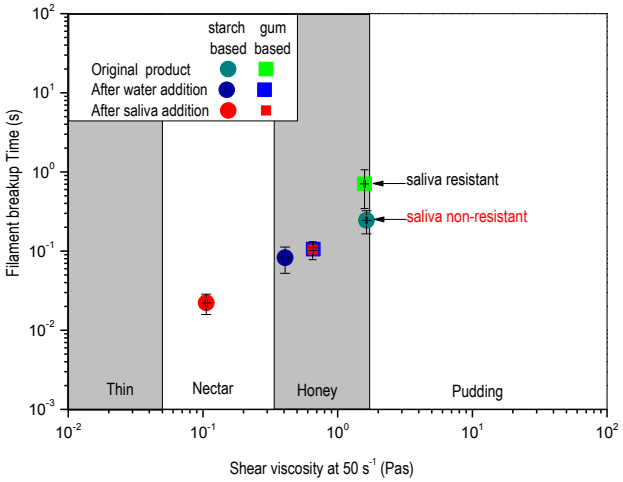

Figure 5 Comparative effect of simulated saliva on the shear viscosity at 50 s^{-1} and elongational breakup time of a starch based thickened fluid and a gum based thickened fluid (1 mL saliva (or water)/10 mL sample, 25°C).

Concluding remarks

Dysphagia is a dysfunction of the transfer of a bolus from the mouth to the stomach, which may involve any of the stages of the normal swallowing sequence and may result in misdirection of transferred bolus. Individuals with inadequately managed dysphagia can be expected to experience bolus aspiration, leading potentially to aspiration pneumonia or other aspiratory problems. Dysphagia can also result in dehydration and malnutrition rendering the individual susceptible to further serious health problems.

Diagnosis of dysphagia is an important first step, which helps evaluate the efficacy and safety of dysphagia patients. During the instrumental assessment, such as using VEF or FEES, thickened powders are dissolved in fluids containing contrast medium and, as shown in this paper, significant rheological differences are observed in thickened fluids prepared with or without contrast medium. Therefore, it is highly recommended that a thorough rheological characterization of thickened fluids used during diagnosis and management is performed and that a good rheological similarity is achieved in a wide range of shear rates.

Management of dysphagia is commonly done by the prescription of texture-modified diets in an aim to decrease the rate at which the food/drink transported through the pharynx or esophagus, so that the muscles and nerves, involved in the swallowing process, get enough time to direct the food bolus through the correct swallowing path. Until recently, healthcare professionals mainly rely on subjective national guidelines to assess the different consistencies during management of dysphagia patients. These national guidelines, however, do not consider the effect of different conditions, such as shear rate, temperature, time, and human saliva on the rheological properties of thickened products and hence lead to a greater risk for dysphagia patients. In an agreement with this, results from this paper have shown that manufacturers' dosage information for the same consistency level yielded significantly different shear and elongational rheological properties. In addition, the effect of salivary α-amylase on starch-based thickened fluids was significant, reducing the initial viscosity by up to 90% within 60 seconds.

Therefore, for a safer and more efficient management of dysphagia, additional research is needed to better understand the rheology of food bolus and how its properties affect the complex swallowing process. Furthermore, there is an urgent need for standardization of food bolus consistency descriptors, terminology, and viscosity measurements.

References

1. Quinchia, L. A., Valencia, C., Partal, P., Franco, J. M., Brito-de la Fuente, E., & Gallegos, C. (2011). Linear and non-linear viscoelasticity of puddings for nutritional management of dysphagia. Food Hydrocolloids, 25, 586–593.
2. Brito-de la Fuente, E., Staudinger-Prevost, N., Quinchia, L. A., Valencia, C., Partal, P., Franco, J. M., et al. (2012). Design of a new spoon-thick consistency oral nutrition supplement using rheological similarity with a swallow barium test feed. Applied Rheology, 22, 53365.
3. Clavé, P., de Kraa, M., Arreola, V., Girvent, M., Farré, R., Palomera, E., et al. (2006). The effect of bolus viscosity on swallowing function in neurogenic dysphagia. Alimentary Pharmacology & Therapeutics, 24, 1385–1394
4. Brito-de la Fuente, E., Ekberg, O., & Gallegos, C. (2012). Rheological aspects of swallowing and dysphagia. In O. Ekberg (Ed.), Dysphagia: Diagnosis and treatment (pp. 493–506). Berlin: Springer.
5. Gallegos C., Brito-de la Fuente E., Clavé P., Costa A., and Assegehegn G. (2017). Nutritional Aspects of Dysphagia Management. In: Fidel Toldrá (Ed.), Advances in Food and Nutrition Research, Vol. 81, pp. 271-318. Burlington: Academic Press.
6. National Dysphagia Diet Task Force. (2002). National dysphagia diet: Standardization for optimal care. USA: American Dietetic Association.
7. Salinas-Vázquez, M., Vicente, W., Brito-de la Fuente, E., Gallegos, C., Márquez, J., & Ascanio, G. (2014). Early numerical studies on the peristaltic

flow through the pharynx. Journal of Texture Studies, 45, 155–163.

8. Gallegos, C., Quinchia, L. A., Ascanio, G., Salinas-Vázquez, M., & Brito-de la Fuente, E. (2012). Rheology and dysphagia: An overview. Transactions of the Nordic Rheology Society, 20, 3–10.
9. Assegehegn, G. (2012). Viscous flow behaviour of thickeners for management of dysphagia. European Masters in Engineering Rheology. Spain: Master Thesis Universidad de Huelva.
10. Hanson, B., O'Leary, M.T., Smith, C.H. (2012). The effect of saliva on the viscosity of thickened drinks. Dysphagia 27:10–19.
11. Chen J. (2009) Food oral processing-A review. Food Hydrocoll 23:1–25
12. Ferry, A. L., Hort, J., & Mitchell, J. R. (2004). Effect of amylase activity on starch paste viscosity and its implications for flavor perception. Journal of Texture Studies, 35, 511–524.
13. Turcanu, M., Siegert, N., Tascon, L., Omocea, I.L., Balan, C., Gallegos, C., Brito-de-la-Fuente,E. (2015). The role of human saliva on the elongational properties of a starch-based food product, Proceedings of E-Health and Bioengineering Conference (EHB), ISBN 978-1-4673-7544-3, pp. 1-4.

The role of rheology in the development of green emulsions

J. Muñoz, M.C. García, L. A. Trujillo-Cayado, J. A. Carmona, J. Santos

Universidad de Sevilla, Grupo de Reología Aplicada. Tecnología de Coloides. Facultad de Química. C/ Profesor García González, 1, 41012, Sevilla (Spain)

Introduction

The objective of green chemistry is to achieve sustainability through science and technology. The 3rd, 7th and the 10th principles of Green Chemistry are related to the use of safer and eco-friendly formulations. The use of traditional organic solvents in agrochemical formulations has been restricted since they posed health hazards for farmers and because of its harmful effects on the environment [1]. Therefore, the chemical industry is paying more and more attention to eco-friendly or better, green solvents. These solvents not only must derive from renewal resources and exhibit enhanced biodegradability but also must possess the expected functional properties. Water-based formulations are by far preferred to oil-based ones for ecological reasons. The non-polar character of most organic solvents prevents their incorporation into aqueous homogeneous solutions due to thermodynamic incompatibility [2]. Thus, they first have to be converted into a colloidal dispersion consisting for instance of an oil phase dispersed as small droplets within an aqueous phase [3].

This work highlights that rheology is a powerful tool for emulsion engineering if used cooperatively with different techniques, such as optical microscopy (bright field, polarising microscopy, phase contrast), confocal scanning laser microscopy (CSLM) and scanning electron microscopy (SEM, cryo-SEM), laser diffraction, and multiple light scattering. Therefore, the role of rheology to detect and control destabilization by creaming as well as to understand oil flocculation, coalescence and Ostwald ripening will be assessed.

Materials

The scope of this work involves formulations based on different green solvents, eco-label surfactants, copolymers, hydrocolloids and clays. The composition of the oil phase has a major influence on the formation and stability of emulsions. N,N-dimethyldecanamide (Agnique® AMD-10, BASF) is considered as an eco-friendly solvent which may find applications in matrices for agrochemical products [4]. D-Limonene, a natural hydrocarbon, is a biosolvent derived from the rinds of citrus fruits such as grapefruit, lemon, lime, and, in particular, oranges. Another monoterpene susceptible to be an interesting alternative solvent is α-pinene. It represents the major constituent of turpentine oils from most conifers and a component of the wood and leaf oils obtained from plants such as rosemary or parsley. Thyme oil has antiseptic and antibacterial properties so that it may be used in cleansing and cosmetic formulations. Sweet fennel oil can be used in food systems.

Ecological surfactants have attracted much attention recently. We report here results of emulsions formulated with surfactants that exhibit the European eco-label; namely, a) an alkyl (C14-C18) poly-pentoside (Appyclean™ 6548, Wheatoleo) derived from wheat biomass and b) a polyoxyethylene glycerol ester (Levenol™ C-201, KAO) derived from coconut oil. In addition, results of emulsions formulated with amphiphilic copolymers (Atlas™ G-5000 and Atlox™ 4913, Croda) are also reported.

Organic (gum polysaccharides) and inorganic (clays) stabilizers have been used to extend the shelf-life of emulsions studied. Their ability to increase the viscosity of a solution depends principally on their molecular characteristics (molecular weight, conformation, etc.).
We have used several microbial polysaccharides, Welan, Rhamsan, Xanthan, Gellan and Diutan gums, kindly provided by CP-Kelco. In addition, a fumed silica (Aerosil™ 200, Evonik) and a clay based on sepiolite (Pangel™ S9, Tolsa) were used as inorganic stabilizers.

Results and Discussion

The rheology of emulsions from both a fundamental and an applied point of view is an important tool to characterize green emulsions. A huge amount of emulsions must be formulated and processed such that they are classified as “flowable materials” showing submicron mean droplet sizes. For this reason, the scope of this work involves the use of formulations

based on different green solvents, eco-label surfactants, copolymers, hydrocolloids and clays.

Rheology is directly related to the structure of dispersed systems. For instance, an analysis of flow curves in emulsions formulated with Agnique® AMD-10 and d-limonene or α-pinene with very similar droplet size distributions allowed different flocculation grades to be detected [4, 5, 6]. In addition, this fact could be checked by analysing the corresponding mechanical spectra [7, 8]. The "flowable" properties of these emulsions, formulated with mixtures of green solvents, were supported by their apparent viscosity values. The study of zero shear viscosity is a great tool to differentiate between destabilization mechanisms in emulsions. The drop of zero shear viscosity with aging time is a clear indication of droplet size increase for emulsions [5, 7, 10, 11]. In addition, an analysis of the evolution of the plateau modulus can detect coalescence in dispersed systems. In fact, a decrease in this parameter with aging time was shown by concentrated green emulsions undergoing coalescence, as indicated by laser diffraction [9, 11]. By contrast, the creaming process involves an increase in zero shear viscosity and a decrease in the flow index with aging time, provided sampling is made from the middle or upper part of the container [11]. Creaming occurs when gravitational separation outweighs the free movement of droplets. Rheology was an important tool to study the influence on emulsion properties and physical stability of several formulation variables like ratio of solvents [10], surfactant concentration [7, 8, 12] or dispersed phase concentration [10, 11]. Furthermore, rheology was able to distinguish between different processing variables [5,6] and emulsification methods [6]. On top of that, the analysis of the viscoelastic properties can suggest the occurrence of different structures in emulsions formulated with different eco-friendly surfactants and detect destabilization mechanisms like depletion flocculation. An excess of free micelles in the continuous phase is expected to trigger depletion flocculation, influencing the rheological properties of the emulsion. This rheological change may be due either to an increase in viscosity of the continuous phase and/or the formation of a stronger oil network due [7,8,12]. In addition, longer relaxation times may be associated to stronger droplet−droplet interactions, which can be correlated with longer macroscopic stability against creaming in emulsions.

Given that the rheology of many "flowable" emulsions is controlled by the rheology of the continuous phase, different case studies will be discussed. In this way, relevant examples of the rheology of polysaccharide solutions, weak gels, fluid (sheared) gels and suspensions of clays will be analysed. Fluid gels prepared with low-acyl gellan gum and either Na^+ or Ca^{2+} can be used as dispersion stabilizers due to the fact they show a high zero-shear viscosity and a dominant elastic response when linear viscoelastic behavior is guaranteed. As a consequence, in the quiescent state, fluid gels exhibited a structural network. Fluid gel microstructure tends to break progressively down as shear stress increases. Thus, these materials exhibited time-dependent flow properties before reaching steady state response. For this reason, their thixotropic properties must be assessed in order to evaluate their role as dispersion stabilizer. Rheological properties of low-acyl gellan gum samples with promising applications as emulsions stabilizers have been reported in several fairly recent articles [13, 14, 15, 16].

Biopolymers are frequently used to stabilize aqueous suspensions or O/W emulsions. These polymers can stabilize emulsions through different mechanisms. Thus, the formation of an extended hydrated polymer network results in high viscosity of the continuous phase at low shear, thus slowing down the droplet motion. In addition, polymeric material may surround the oil droplets, ensuring effective steric hindrance of droplet coalescence. A combination of Gellan and Xanthan gums was utilized to achieve O/W emulsions containing α-pinene and two amphiphilic copolymers (Atlas™ G-5000 and Atlox™ 4913) [17]. Small amplitude oscillatory shear results supported the likely occurrence of three different relaxation mechanisms and microstructures, which were dependent on hydrocolloid system used. The relaxation spectrum of the emulsion containing both polysaccharides indicated the existence of thermodynamic incompatibility between both polysaccharides. Flow curves fitted the Carreau-Yasuda model and highlighted the occurrence of negative synergism between Gellan and Xanthan gums. Furthermore, the influence of different ratios of amphiphilic copolymers (Atlas™ G-5000 and Atlox™ 4913) in emulsions formulated with Gellan gum and d-limonene [18] or α-pinene [19] as dispersed phase was studied. Results of these investigations indicated that the ratio of emulsifiers had significant effects on the physical stability, droplet size, viscoelasticity, and viscosity of these emulsions. An increase in Atlas™ G-5000 enhanced both the G´ and G´´ values and also the viscosity, providing higher stability to emulsions. Adding Gellan gum yielded viscoelastic spectra with a weak frequency dependence of G' and G'', according to the formation of a faint gel-like matrix.

The rheological properties of concentrated welan gum aqueous solutions with different polymer concentration

have been studied at 20ºC. Flow curves and mechanical spectra were determined at several gum concentrations by step-wise and SAOS tests. The results showed shear thinning behavior and weak gel-like viscoelastic behavior in the range of concentrations studied (0.1-0.6 wt %). Another interesting technique used was the parallel superposition rheology, which consists of applying steady shear in parallel with oscillatory shear. Thus, a change from weak gel-like viscoelastic behavior to fluid like viscoelastic behavior was observed when the steady shear increased. The frequency locating the G' and G'' crossover shifted to higher frequencies values as the steady-state shear stress applied was increased. In other words, increasing shear stress values resulted in decreasing terminal relaxation times, congruently with a weaker and weaker microstructure. This technique allowed obtaining linear viscoelastic snapshots while the sample microstructure was progressively disrupted.

A detailed study of the rheological properties of mixtures of Rhamsan gum and Welan gum solutions containing an eco-friendly surfactant has been reported elsewhere [20]. By using a response surface methodology, the effects of surfactant concentration, Rhamsan/Welan mass ratio and total concentration of polysaccharides were investigated. A second order polynomial equation fitted the influence of surfactant concentration, Rhamsan/Welan mass ratio and total concentration of polysaccharides, the latter being the most significant variable. Systems containing blends of Rhamsan and Welan did not show synergism but made it possible to adjust the linear viscoelastic and low shear rate flow properties in order to achieve values in between those of systems containing either Rhamsan or Welan as the only polysaccharide. All the systems studied exhibited weak gel rheological properties as the mechanical spectra displayed the plateau or rubber-like relaxation zone, the linear viscoelastic range was rather narrow and flow curves presented shear thinning behavior, which fitted the power-law equation. Furthermore, the influence of total gum concentration and Rhamsan/Welan gum ratio on rheological properties, droplet size distribution and physical stability of eco-friendly O/W emulsions formulated with α-pinene and stabilized by an ecological surfactant were studied. Rheological properties of emulsions showed an important dependence on the two studied variables. Flow curves were fitted to the power-law model and no synergistic effect between Rhamsan and Welan gums was demonstrated. Multiple light scattering illustrated that creaming was practically eliminated by the incorporation of polysaccharides. The use of Rhamsan and Welan gums as stabilizers improved the emulsion rheology and physical stability in comparison with the formulation without gum.

Small amplitude oscillatory shear (SAOS) is a useful tool to study the viscoelasticity of a wide range of materials. This technique requires that tests are conducted within the linear viscoelastic range (LVR), which guarantees the material microstructure is not destroyed by shear. In the LVR the properties of materials can be defined by two properties storage modulus in phase with the strain G' and viscous modulus out phase 90º with strain G". Although this conditions of low deformation are not near real flow conditions, such as those typical of processing and transport. When the strain increases above a critical value the classic linear viscoelastic approach is not longer valid. This is due to the fact that the response is not a simple sinusoidal function and it is necessary to use another method like that proposed by Ewoldt et al [22] to provide a unified physical interpretation of large amplitude oscillatory shear (LAOS) results. We have reported the applications of LAOS for xanthan gum aqueous dispersions at different NaCl concentrations [23] and different polymer concentration [24]. LAOS was demonstrated to be much more sensitive than small amplitude oscillatory shear (SAOS) when studying the influence of NaCl concentration. This technique allows gaining a deeper insight into the viscoelastic properties of materials under non-linear conditions, which is closer to real flow conditions. The rheological LAOS characterization was carried out by means of both full-cycle (average elastic modulus and dynamic viscosity) and local methods (strain-hardening and shear-thickening ratios) [23, 24]. The plot of the maximum value of the local shear-thickening parameter (T) obtained by LAOS against concentration showed a change of the viscoelastic behavior associated to the modification of the gum structure.

As far as the development of "flowable" concentrated thyme oil in water emulsions formulated with a (C14-C18) alkyl poly-pentoside is concerned, Welan gum turned out to be quite efficient to get emulsions showing weak-gel viscoelastic behavior and shear thinning flow properties with adjustable plateau modulus and zero-shear viscosity values.

Pangel ™ S9 sepiolite and Aerosil ™ 200 fumed silica are good examples of inorganic stabilizers. The former is able to form a viscous suspension at 3 % (m/m) exhibiting gel-like viscoelasticity and very shear thinning behavior, such that the values of the dynamic viscoelastic functions, the zero-shear viscosity and the apparent yield stress can be tuned by adding either a cationic or an anionic surfactant. Aerosil™ 200 /water dispersions show gel properties at pH 7 from 8 wt% fumed silica. These dispersions can be used as

stabilizers even in emulsions with large droplets (>5 microns). 7 wt% fennel oil/W emulsions containing just 4 wt% of Aerosil™ 200 showed an apparent yield point and gel behavior in SAOS. These rheological properties conferred these green emulsions very long stability.

Acknowledgements

The financial support received (Projects CTQ2011-27371 & CTQ2015-70700) from the Spanish Ministerio de Economía y Competitividad (MINECO) and from the European Commission (FEDER Programme) is kindly acknowledged.

References

1. Anastas, P. T., & Warner, J. C. (1998). Principles of green chemistry. *Green chemistry: Theory and practice*, 29-56.
2. Israelachvili, J.N. (1992). *Intermolecular and Surface Forces*, Academic Press, London, UK
3. McClements, D. J., & Rao, J. (2011). *Critical Reviews in Food Science and Nutrition*, 51(4), 285-330.
4. Bigorra, J. (2010). Innovative solvents based on renewable raw materials. Proceedings of 40th Annual Meeting of CED. Barcelona, Spain.
5. Santos, J., Trujillo-Cayado, L. A., Calero, N., Alfaro, M. C., & Muñoz, J. (2016). Journal of Industrial and Engineering Chemistry, 36, 90-95.
6. Trujillo-Cayado, L. A., Santos, J., Alfaro, M. C., Calero, N., & Muñoz, J. (2016). Industrial & Engineering Chemistry Research,*55*(27), 7259-7266.
7. Santos, J., Calero, N., & Muñoz, J. (2015). Chemical Engineering Research and Design, 100, 261-267.
8. Trujillo-Cayado, L. A., Alfaro, M. C., García, M. C., & Muñoz, J. (2017). Colloids and Surfaces B: Biointerfaces, *149*, 154-161
9. Santos, J., Calero, N., & Muñoz, J. (2016). RSC Advances, 6(62), 57563-57568.
10. Santos, J., Trujillo-Cayado, L. A., Calero, N., & Muñoz, J. (2014). AIChE Journal, 60(7), 2644-2653.
11. Trujillo-Cayado, L. A., Garcia, M. C., Santos, J., Carmona, J. A., & Alfaro, M. C. (2017). ACS Sustainable Chemistry & Engineering, *5*(5), 4127-4132.
12. Pérez-Mosqueda, L.M.,Ramírez, P., Trujillo-Cayado, L. A., Santos, J., & Muñoz, J. (2014). Colloids and Surfaces B: Biointerfaces, 123, 797-802.
13. García, M.C., Alfaro, M.C., Calero, N., &Muñoz, J. (2011). Biochemical Engineering J., 55(2), 73-81.
14. García, M. C., Alfaro, M. C., & Muñoz, J. (2015). Journal of Food Engineering, 159, 42-47.
15. García, M. C., Alfaro, M. C., & Muñoz, J. (2016). Biochemical Engineering Journal, 114, 257-261.
16. García, M. C., Alfaro, M. C., & Muñoz, J. (2016). Food Science and Technology International, 22(4), 325-332.
17. García, M. C., Alfaro, M. C., Calero, N., & Muñoz, J. (2014). *Carbohydrate polymers*, *105*, 177-183.
18. Trujillo-Cayado, L. A., García, M. C., Muñoz, J., & Alfaro, M. C. (2016). *Journal of Applied Polymer Science*, *133*(34), 43838 (1- 7).
19. García, M.C., Alfaro, M.C., & Muñoz, J. (2015). *Colloids and Surfaces B: Biointerfaces*, *135*, 465-471.
20. Trujillo-Cayado, L. A., Alfaro, M. C., Raymundo, A., Sousa, I., & Muñoz, J. (2016). Colloids and Surfaces B: Biointerfaces, *145*, 430-437.
21. Trujillo-Cayado, L. A., Alfaro, M. C., Muñoz, J., Raymundo, A., & Sousa, I. (2016). Colloids and Surfaces B: Biointerfaces, *141*, 53-58.
22. Ewoldt, R. H., Hosoi, A. E., & McKinley, G. H. (2008). Journal of Rheology, 52(6), 1427-1458.
23. Carmona, J.A., Ramirez, P., Calero, N., & Muñoz, J. (2014). Journal of Food Engineering, 126, 165-172.
24. Carmona, J. A., Lucas, A., Ramírez, P., Calero, N., & Muñoz, J. (2015). Rheologica Acta, 54(11-12), 993-1001.

Contact Address:

José Muñoz (jmunoz@us.es)
Department of Chemical Engineering
Faculty of Chemistry
University of Seville
C/ Profesor García González, 1, 41012, Sevilla (Spain)
Telf.: +34 954 556447

IBEREO valencia 2017

The multidisciplinary science of rheology
Towards a healthy and sustainable development

VNIVERSITAT DE VALÈNCIA

iata Instituto de Agroquímica y Tecnología de Alimentos

CSIC

Food Rheology

Rheological characterization of *Spirulina* gluten-free cookie doughs

A.P. Batista, I. Bursic, A. Miranda, S. Fragoso, P. Fradinho, A. Raymundo, I. Sousa

LEAF-Linking Landscape, Environment, Agriculture and Food. Instituto Superior de Agronomia. Universidade de Lisboa (Portugal)

Introduction

Spirulina (*Arthrospira platensis*) is a cyanobacteria widely used in human nutrition due to its nutritional properties - rich in proteins, gamma-linolenic acid (GLA), vitamins (e.g. B_{12}) and phycobilliproteins. Besides this, the addition of *Spirulina* has been associated to both positive [1] and negative [2] structural effects in different food matrixes (pastas and gelled desserts, respectively). Therefore a thorough investigation is needed to assess the rheological and microstructural implications of *Spirulina* addition in food systems, namely its potential in the challenging design of gluten-free products.

Experimental

Sweet cookie doughs were prepared with wheat and rice (gluten-free) flours, according to a previously optimised formulation [3]. *Spirulina* biomass (lyophilised) was added at 2, 4 and 6%, replacing the corresponding amount of flour. Furthermore, *Spirulina* concentration was kept constant (2% for rice and 6% for wheat) while the flour concentration was reduced and replaced by water. Formulations are presented in Tables 1 and 2. All percentages in the paper are based in mass ratio, expressed as weight/weight (w/w).

The ingredients were kneaded in a food processor for 60 s and moulded in 4 mm height sheets. Fresh cookie doughs were immediately analysed in a controlled-stress rheometer (Haake, RS-75), using serrated parallel plates (20 mm Ø) geometry with 1 mm gap, using the small amplitude oscillatory system, i.e. within the linear viscoelastic behaviour. Stress sweeps were carried out at 1 Hz to determine the linear viscoelastic region (LVR). Frequency sweep tests were then performed at a constant stress within the LVR (60-130 Pa), from 0.01 to 100 Hz.

Wheat flour, rice flour and *Spirulina* water and oil absorption capacities were also determined as described in [4].

All experiments were carried out at 20ºC, in triplicate. ANOVA Post-Hoc comparison at 95% probability level was performed by Scheffé Test.

Table 1. Wheat flour cookie dough formulations (%, w/w)

	C	F2	F4	F6	F6A	F6B
Spirulina	0	2	4	6	6	6
Wheat Flour	49	47	45	43	40	37
Water	10	10	10	10	13	16
Baking powder	1	1	1	1	1	1
Margarine	20	20	20	20	20	20
Sugar	20	20	20	20	20	20

Table 2. Rice flour cookie dough formulations (%, w/w)

	C	F2	F4	F6	F2A	F2B	F2C	F2D
Spirulina	0	2	4	6	2	2	2	2
Wheat Flour	49	47	45	43	44	42	40	38
Water	10	10	10	10	13	15	17	19
Baking powder	1	1	1	1	1	1	1	1
Margarine	20	20	20	20	20	20	20	20
Sugar	20	20	20	20	20	20	20	20

Results and Discussion

From the rheological mechanical spectra, presented in Fig. 1, a predominantly elastic behavior is observed for wheat flour-*Spirulina* sweet cookie doughs, with *G'* always higher than *G''*. For all samples, a dependence of the viscoelastic moduli with frequency is evident, with a tendency for moduli crossover both at lower and higher frequency values.

A linear increase in the wheat cookie dough's viscoelastic moduli, with *Spirulina* concentration was observed, as presented for *G'* values at 1 Hz frequency in Fig. 2 (R^2=0.97). This indicates that *Spirulina* incorporation can play a significantly role on the cookie dough structure development. These results are in agreement with higher texture parameters found for 6% *Spirulina* cookies in a previous study [3], which may be related to its high protein content and high water absorption capacity.

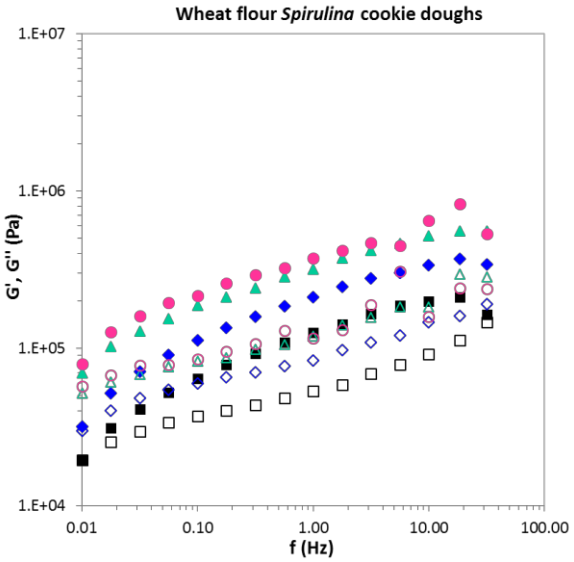

Figure 1. Mechanical Spectra of wheat flour (WF) cookie doughs with different *Spirulina (Sp) contents (w/w):* ■ *0 %Sp (control, 49% WF),* ♦ *2% Sp (47% WF),* ▲ *4% Sp (45% WF) and* ● *6% Sp (43% WF). G', closed symbol, G'' open symbol.*

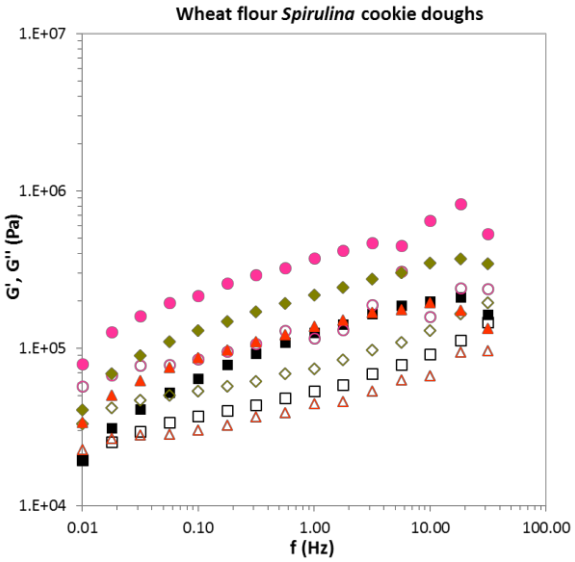

Figure 3. Mechanical Spectra of cookie doughs with 6% *Spirulina (Sp) and different wheat flour (WF) contents (w/w):* ■ *49% WF (control, 0% Sp),* ● *43% WF (6% Sp),* ♦ *40% WF (6% Sp),* ▲ *37% WF (6% Sp). G', closed symbol, G'' open symbol.*

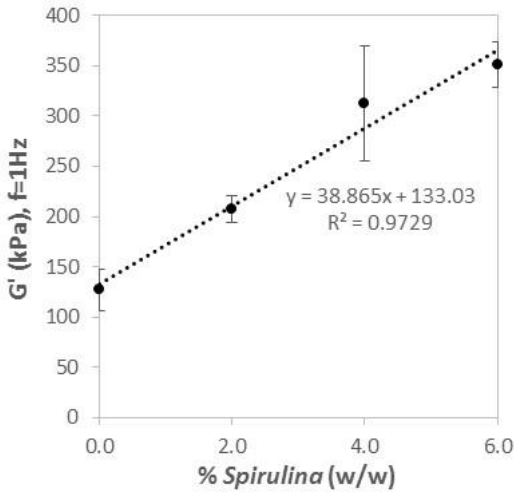

Figure 2. Evolution of viscoelastic moduli, at 1 Hz frequency (from frequency sweep tests), of wheat flour cookie doughs with increasing *Spirulina contents.*

Therefore, the possibility to reduce wheat flour content in the cookie dough formulation (replacing flour by water), while adding 6% *Spirulina*, was also evaluated.

From the resulting mechanical spectra (Fig. 3) it is evident that, with 6% *Spirulina*, reducing wheat flour from 43% to 40% results in a dough with significantly lower (p<0.05) *G'* values (351 vs. 222 kPa, at f=1Hz) but still significantly higher than the control (49% flour, 0% *Spirulina*) (222 vs. 127 kPa, at f=1Hz).

Further decreasing the wheat flour content down to 37%, with 6% *Spirulina*, resulted in a cookie dough with viscoelastic parameters similar (p>0.05) to the 49% wheat flour control. Nevertheless, due to the high water content (16%), this sample was quite sticky and difficult to manipulate.

These results are interesting and demonstrate the potential application of *Spirulina* biomass as techno-functional ingredient in bakery products. This *Spirulina* structuring effect can be particularly useful in the challenging formulation of gluten-free product, where the absence of a viscoelastic gliadin-glutelin network usually results in products with poor texture and sensory properties.

From mechanical spectra (Fig. 4) it can be seen that rice flour doughs present viscoelastic moduli significantly higher (p<0.05) than wheat flour (Fig. 3) doughs (G'_{1Hz}: 646 vs. 127 kPa for the rice and wheat control samples, respectively).

The addition of *Spirulina* to rice flour cookie doughs clearly contributed to a more elastic dough, with positive impact in the cookies sensory properties (results not shown). Even at the lowest alga concentration (2%) there is a pronounced structuring effect in relation to the control (52% increase in G'_{1Hz}), but when further increasing *Spirulina* content the differences are not statistically significant (p<0.05) (Fig. 5).

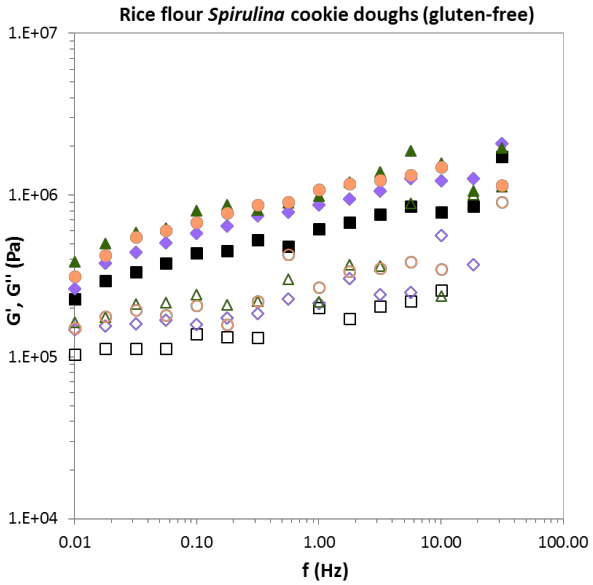

Figure 4. Mechanical Spectra of rice flour (RF) cookie doughs with different *Spirulina (Sp) contents (w/w):* ■ *0 %Sp (control, 49% RF),* ♦ *2% Sp (47% RF),* ▲ *4% Sp (45% RF) and* ● *6% Sp (43% RF). G', closed symbol, G" open symbol.*

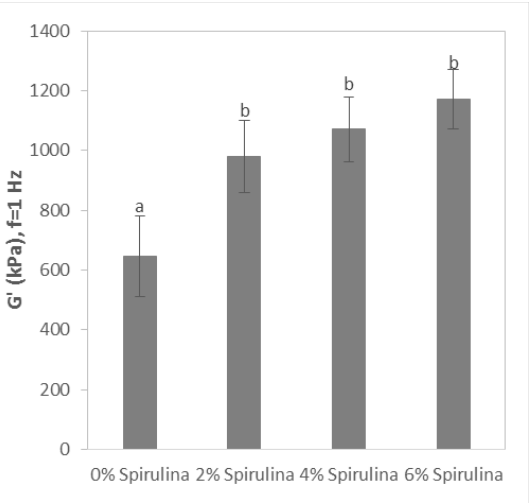

Figure 5. Values of G', at 1 Hz frequency (from frequency sweep tests), of rice flour cookie doughs with different Spirulina contents. Different letters correspond to significant differences (p<0.05).

A study on the potential of *Spirulina* to replace rice flour in cookie dough was carried out, similar to what was previously done with wheat flour (Fig. 3). In this case *Spirulina* was kept at only 2%, since there were no significant differences in the rice dough rheology for higher alga concentrations. By lowering rice flour content (and increasing water), in the presence of *Spirulina*, it was intended to attain formulations of doughs with viscoelastic properties similar to wheat flour doughs (target product).

Figure 6 presents the mechanical spectra of cookie doughs with 2% *Spirulina*, with observable viscoelastic functions decrease with decreasing rice flour contents.

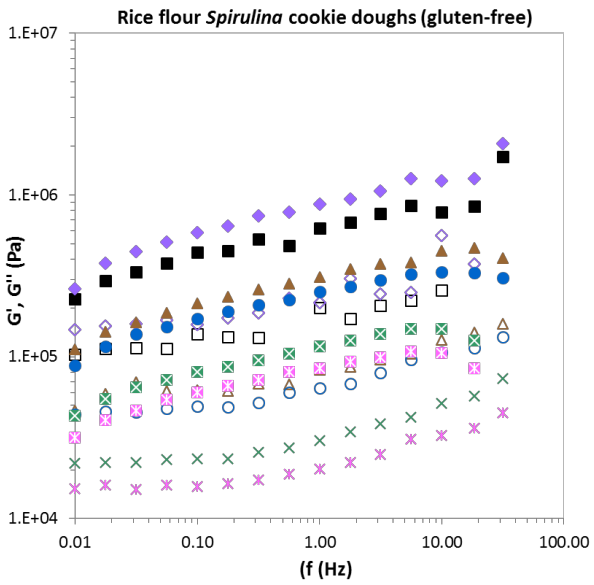

Figure 6. Mechanical Spectra of cookie doughs with 2% Spirulina (Sp) and different rice flour (RF) contents (w/w): ■ *49% RF (control, 0% Sp),* ♦*47% WF (2% Sp),* ▲ *44% RF (2% Sp),* ● *42% RF (2% Sp), x 40% RF (2% Sp),* ✶ *38% RF (2% Sp). G', closed symbol, G" open symbol.*

As expected, significant differences (p<0.05) were found on G' values upon rice flour decrease from 47% (G'_{1Hz}=980 kPa) to 38% (G'_{1Hz}=81 kPa). The evolution of G'_{1Hz} with rice flour follows an exponential behaviour (R^2=0.96) (Fig. 7). It should be noted that wheat flour samples showed G'_{1Hz} values around 100 to 300 kPa, so with some of these formulation changes we achieved values close to the target products. However, the high water content of these samples (13-19%) makes them quite adhesive and therefore difficult to manipulate, so further studies should be focused on overcoming this aspect.

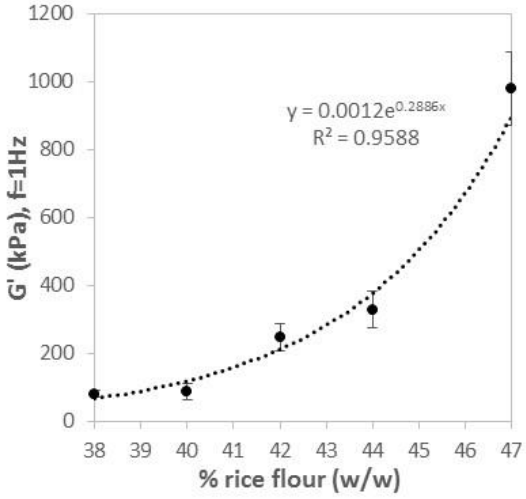

Figure 7. Evolution of viscoelastic moduli, at 1 Hz frequency (from frequency sweep tests), of Spirulina cookie doughs with increasing rice flour contents.

The observed techno-functional properties of *Spirulina* should be related to its high water and oil absorption properties (5.2 and 2.2, respectively) in relation to the flours (2.1-2.4 and 1.7, respectively), as can be observed in Fig. 8.

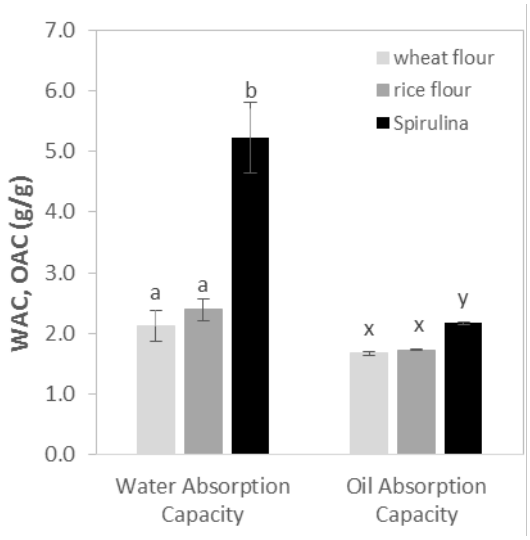

Figure 8. Water and oil absorption capacities of wheat flour, rice flour and Spirulina. Different letters correspond to significant differences ($p<0.05$).

Conclusions

The use of *Spirulina* biomass as functional ingredient in bakery gluten-free products is thus promising. Besides potential bioactive and nutritional benefits, *Spirulina* presents very interesting structuring properties that can be applied for gluten-replacement or "mimicking" effects highly required in the design of coeliac-directed bakery products.

Acknowledgements

The authors thank Prof. Mario Tredici Research Group from DISPAA–University of Florence (Italy) for providing *A. platensis* biomass and for all collaboration in this research project. This work was supported by national funds from Fundação para a Ciência e a Tecnologia (Portugal) through the research unit UID/AGR/04129/2013 (LEAF). Patrícia Fradinho acknowledges her PhD grant from Instituto Superior de Agronomia, Universidade de Lisboa and Ivana Bursic acknowledges Erasmus grant.

References

1. Fradique, M., Batista, A.P., Nunes, M.C., Gouveia, L., Bandarra, N.M., Raymundo, A. (2010). J. Sci. Food Agric. 90, 1656-1664.
2. Batista, A.P., Nunes, M.C., Fradinho, P., Gouveia, L., Sousa, I., Raymundo, A., Franco, J.M. (2012). J. Food Eng. 110, 182-189.
3. Batista, A.P., Niccolai, A., Fradinho, P., Fragoso, S., Bursic, I., Rodolfi, L., Biondi, N., Tredici, M.R., Sousa, I., Raymundo, A. (2017). Algal Research, Accepted
4. Raymundo, A., Fradinho, P., Nunes, M.C. (2014). Bioact. Carbohydr. Diet. Fibre 3, 96–105.

Contact Address:

paulabatista@isa.ulisboa.pt
LEAF – Linking Landscape, Environment, Agriculture and Food
Instituto Superior de Agronomia
Universidade de Lisboa
Tapada da Ajuda. 1349-017 Lisboa. Portugal.
Telf.: +351 213653100 Ext.: 2124

Rice Industry By-Products in Food Emulsions

P. Fradinho, I. Sousa, A. Raymundo

LEAF-Linking Landscape, Environment, Agriculture and Food, Instituto Superior de Agronomia, Universidade de Lisboa. (Portugal)

Introduction

Cereal industries generate high volumes of by-products with environmental impact. In Portugal, about 160 000 tons of paddy rice (*Oryza sativa* ssp.) are annually produced, which leads to high amounts of by-products, namely broken rice (10%) and rice bran (10%). These residues could be recovered and used in the production of added-value foods. Rice bran is a good source of fibre, vitamins, minerals, proteins, and especially lipids, which makes it an excellent functional ingredient that helps preventing several chronic diseases, such as high cholesterol, cancer and diabetes [1]. There has been increasing interest in rice bran's oil fraction, rich in vitamin E and antioxidants, namely γ-oryzanol, especially for cosmetic and pharmaceutic applications [2]. However, rice bran' high lipid content makes it favourable to lipase action, promoting oxidation and rancidity, which limits rice bran's applications [3]. Defatting rice bran is an industrial practice to overcome this limitation since rice bran' oil has a high market value. Therefore, several studies focus on using the defatted rice bran [e.g. 4]. The approach in this study, since bran oil is very interesting from the nutritional point of view, is based on the enzymatic inactivation of rice bran, prior to food incorporation, in order to prevent lipid oxidation. In a previous work [5], rice bran stabilization by thermal enzyme inactivation was optimized by response surface methodology: 138.3ºC/51.5 min with more than 90% inactivation.

Rice bran potential to act as texturing and stabilizing agent is investigated due to its ability to swell when absorbing water, which occurs due to the presence of fibres. Food emulsions are multiphasic systems, thermodynamically unstable, usually consisting of dispersions of oil in water [6]. As a source of fibre, rice bran could also contribute to lower the fat content of the emulsion, acting as fat mimetic [7].

Emulsifying agents are generally used to stabilize the emulsion and prevent droplet aggregation, which could lead to phase separation, they consist of amphiphilic molecules (comprising both polar and nonpolar groups) that are usually adsorbed in the interfacial region, such as proteins and polysaccharides. The potential of rice bran and rice flour to play this role will be investigated. The aim of this study was to prepare emulsions using rice bran and rice flour (obtained from broken rice milling) as stabilisers, adding value to by-products of the rice industry.

Experimental

Materials

Rice bran (RB) and rice flour (RF) from Ariete (*Japonica ssp.*), Guiana (*Indica ssp.*) and parboiled rice from Guiana variety were provided from a Portuguese milling company. Commercial vegetal oil made from a mixture of food grade vegetable oils was used for the preparation of the emulsions.

Methods

Raw materials characterisation

The chemical composition of rice flours and brans was determined according to AACC method 44-15.02:1999 (moisture), ISO20483:2006 (protein, with conversion factor of 5.95), NP518:1986 (ash) and NP4168:1991 (lipids) [8-11]. Oil absorption capacity (OAC) of all samples was determined following a modification of the method developed by Chandi and Sogi [12], and the water absorption index (WAI) at 20ºC was assessed by the method described by Anderson [13]. Each determination was performed at least in triplicate.

Emulsions preparation

Emulsions were prepared using rice bran (2 - 10%), rice flour (3 - 5%), oil (55 - 65%) and distilled water (30 - 40%) at different proportion combinations by dispersing rice bran (RB) and rice flour (RF) in water, under magnetic stirring for 30 min, followed by oil addition under mechanical stirring (T25 basic, IKA Labortechnik, Germany) at 13 000 rpm, 3 min. Emulsions were poured into glass containers (35 mm height, 32 mm diameter)

and stored at 4ºC for 24h to allow full maturation, before performing colour, texture and rheology measurements.

Colour measurements

The emulsions colour parameters were determined using a CR-400 colorimeter (Konica Minolta, Japan). Colour parameters (L*, a* and b*) were assessed by CIELAB system, where L* is the lightness and a* and b* are chromaticity parameters. Each emulsion preparation was measured eight times.

Texture measurements

Texture profile analysis of all emulsions was performed in a texturometer TA-XTplus (Stable Micro Systems, UK) in penetration mode, using a 10 mm cylindrical probe which penetrated the sample 15 mm, at 1 $mm.s^{-1}$. Firmness (N), cohesiveness and adhesiveness (-N.s) parameters were determined before performing any measurements, gels were allowed to equilibrate at 20 ºC for around 1 h in a temperature-controlled room. Each formulation was tested at least six times.

Rheology measurements

All rheology tests were performed in a MARS III controlled-stress rheometer (Haake) coupled to a UTC-Peltier system for temperature control. All assays were performed at 20°C.

The evaluation of the internal structure of the emulsions was assessed by small amplitude oscillatory shear (SAOS) measurements, using a cone and plate sensor system with 35 mm diameter and 2° angle. For each emulsion, the mechanical spectrum was obtained at 1Hz, within the viscoelastic linear range. The Plateau modulus (G^0_N) was estimated as the value of G' for the minimum value of the loss tangent (tan δ = G"/G') [14].

For steady-state flow measurements, a serrated parallel plate sensor system was used (35 mm diameter), in order to overcome slip effects [15].

Flow equations, which are an important contribution to predict the emulsions behaviour in the final product, were established according to the Carreau Model (1).

$$\eta = \frac{\eta_0}{\left[1+\left(\frac{\dot{\gamma}}{\dot{\gamma}_c}\right)^2\right]^s} \qquad (1)$$

The limiting viscosity values were calculated on the first Newtonian plateau (η_0), critical shear rate ($\dot{\gamma}_c$) and parameter s (related to slope of the viscosity decay with shear rate) of the emulsions were studied.

Statistical analysis

Experimental data was analysed by means of one-way ANOVA. When the former analysis indicated differences among means, a Scheffé test was performed to differentiate means with 95% confidence ($p < 0.05$). All statistical treatments were done using SPSS Statistics Version 20 (IBM SPSS Statistics, New York, NY, USA).

Results and Discussion

Selection of raw materials

The proximate physicochemical properties of rice flours and brans are presented in Table 1.

Table 1. Proximate physicochemical properties of rice flours (RF), stabilized rice brans (RBS) from Indica (Ind) and Japonica (Jap) varieties and Parboiled (Par) rice

Sample	(g/100 g dry basis)			
	Moisture	Lipids	Protein	Ash
RF Ind	13.9 ± 0.1	2.7 ± 0.3	4.9 ± 0.3	0.6 ± 0.0
RF Jap	11.5 ± 0.1	1.6 ± 0.1	5.7 ± 0.3	0.6 ± 0.0
RF Par	12.3 ± 0.1	4.5 ± 0.4	5.9 ± 0.3	1.1 ± 0.0
RBS Ind	3.2 ± 0.0	17.2 ± 0.6	14.2 ± 0.4	8.3 ± 0.1
RBS Jap	0.2 ± 0.0	19.2 ± 1.2	13.0 ± 0.3	10.0 ± 0.0
RB Par	8.9 ± 0.0	25.7 ± 1.5	12.2 ± 0.9	6.6 ± 0.1

All rice brans presented higher protein, lipid and ash contents than the flours from the same rice variety, which makes rice bran an excellent raw material for emulsion stabilisation. As expected, *RBS Ind* and *RBS Jap* presented lower moisture content than parboiled rice bran (*RB Par*), due to moisture loss during the enzyme inactivation procedure.

The selection of the most suited bran and flour varieties was based on physicochemical properties, especially protein and lipid contents, but also on water and oil absorption capacities (Fig.1).

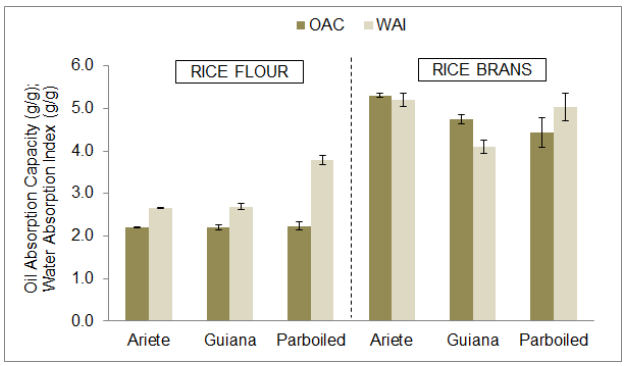

Figure 1. Oil absorption capacity (OAC) and water absorption index (WAI) of rice flours and brans

High oil absorption is essential for the formulation of food systems like sausages, mayonnaise and salad dressings [12], and water absorption between 1.5-4.7 g/g has revealed to be critical in viscous foods such as soups and gravies [16].

Considering oil and water absorption capacities (OAC: 5.30 ± 0.05 g/g d.b.; WAI: 5.20 ± 0.16 g/g d.b.) Ariete rice bran was chosen. For stabilizing the emulsion parboiled rice flour was chosen due mainly to its higher protein content (5.9 ± 0.03 g/100 g d.b.).

After selection of the raw materials, emulsions were prepared according to the described procedure. Formulations with 2, 3 and 10% RB did not allow emulsion preparation since phase separation was observed immediately or after 24h. Only the formulations that emulsify (Fig. 2) - A: 5% RB + 55% Oil; B: 5% RB + 60% Oil; C: 5% RB + 65% Oil; D: 5% RB + 62% Oil + 3% RF - were characterized in terms of colour, texture and rheology parameters.

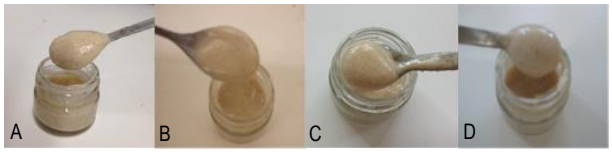

Figure 2. Emulsions prepared with Ariete rice bran, 55-65% oil (A, B, C) and 3% parboiled flour (D)

Texture measurements

In Figure 3 the main texture parameters used to characterize the emulsions are depicted.

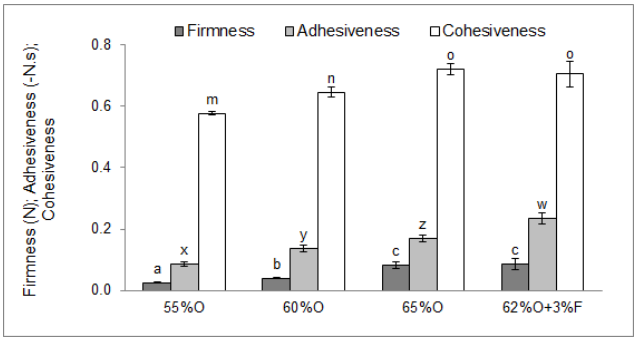

Figure 3. Texture parameters of 5% rice bran O/W emulsions with 55% -65% oil and 3% rice flour. Different superscript letters indicate significantly different values at p < 0.05 level.

The amount of oil in the emulsions influences positively its texture properties, namely firmness, cohesiveness and adhesiveness, as observed in previous works [17]. Rice flour incorporation (3%) affects positively the cohesiveness of the emulsion with the advantage of reducing the oil content (in 3%), for similar texture characteristics, acting as fat mimetic.

Rheology measurements

The effect of oil content and flour addition on viscoelastic parameters is depicted in Figure 4.

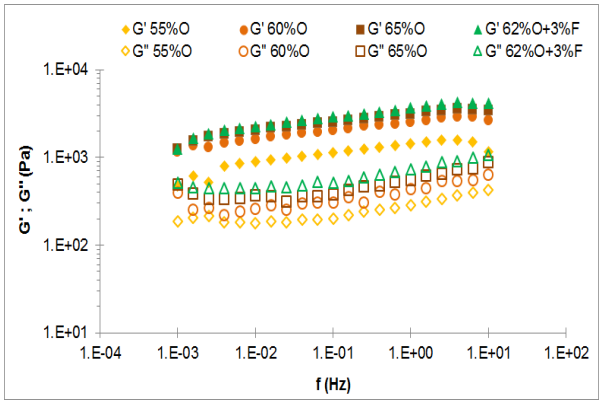

Figure 4. Mechanical spectra of 5% rice bran O/W emulsions with 55% -65% oil and 3% rice flour.

From the mechanical spectra of rice bran emulsions it is observed that G' is always higher than G" within the experimental frequency range, which translates a predominance of the elastic component. Both moduli present a slight frequency dependence of G' (Fig. 4), typical of this kind of food systems, showing a plateau region (plateau modulus-G^0_N) associated with a minimum in G". This is a viscoelastic parameter that is related with the density of the entangled network developed between polymeric molecules [18]. A similar pattern was observed for the three oil concentrations, with a clear increase in the linear viscoelastic functions with oil content. This reflects an increase in the level of structure, confirmed by the increase in G^0_N (Table 2).

Table 2. Plateau modulus (G^0_N) of the rice bran emulsions.

Sample	G^0_N (Pa)
55%O	1417
60%O	1995
65%O	2173
62%O+3% F	2888

It is evident that all the emulsions present a considerable degree of structuring, which will be compatible with high physical stability and thus a long shelf life, and is in agreement with the texture results (Fig. 3). Flour addition allows the reinforcement of the structure and at the same time allows the reduction of the oil needed for structuring the system.

A similar behaviour was observed in terms of steady-state flow curves (Fig. 5), with an increase of η_0 with the increase of the oil content. The addition of rice flour (62%O+3%F) induces similar flow behaviour to the emulsion with 65% oil, showing a fat mimetic behaviour of the rice flour-bran system, as it was previously reported for other type of systems [7]. All the emulsions show a shear-thinning behaviour: a Newtonian plateau followed by a region where the viscosity decreases with increasing shear rate.

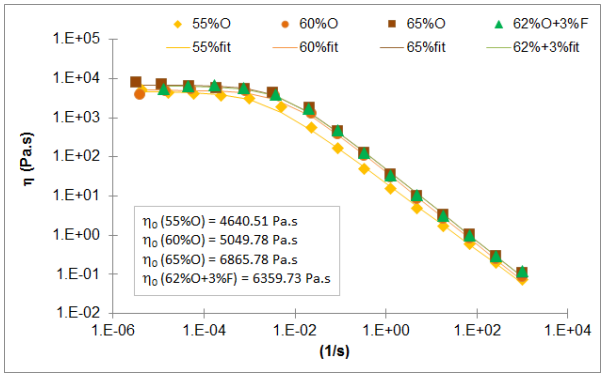

Figure 5. Viscosity curves of the 5% rice bran O/W emulsions. The lines indicate the adjustment of the Carreau model to the data.

Colour measurements

The effect of the oil concentration and flour incorporation on the colour parameters of the emulsion (L*, a*, b*) are presented in Figure 6.

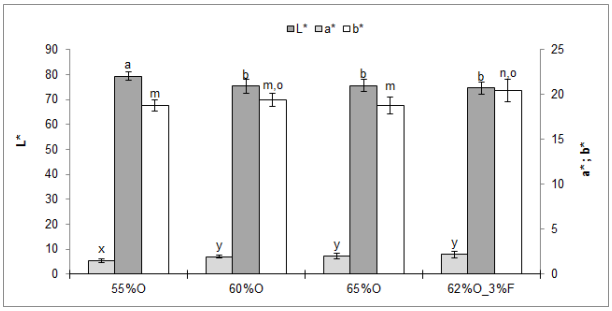

Figure 6. Colour parameters of the 5% rice bran O/W emulsions. Different superscript letters indicate significantly different values at p < 0.05 level.

The colour parameters of the 55% oil emulsion were significantly ($p<0.05$) higher in lightness (L*) and lower in redness (a*) from the ones obtained for the other emulsions prepared. There were no differences in the colour parameters of the rice bran emulsions as a function of the incorporation of rice flour.

Concluding remarks

It is possible to prepare food emulsions with rice bran and rice flour with suitable texture and rheology properties, adding value to these rice milling industry's by-products.

Acknowledgements

This work was supported by: i) COMPETE program: QREN – "Arroz +" project 38749/13, in co-promotion with two rice milling companies and ii) Portuguese Foundation for Science and Technology (FCT) through the research unit UID/AGR/04129/2013 (LEAF).

References

1. OECD Environment, Health and Safety Publications, Series on the Safety of Novel Foods and Feeds, 2004, nº10, pp38.
2. Juliano, C., Cossu, M., Alamanni, M.C. and Piu, L. (2005). Int. J. Pharm. 299: 146-154.
3. Sharma S., Kaur S., Dar B.N. and Singh, B. (2014). J. Food Sci & Tech. 51(3), 583-588.
4. Zhang, H.J., Zhang, H., Wang, L., Guo, X-N. (2012). Food Res. Int. 47, 359-363.
5. Fradinho P, Raymundo A, Sousa I. (2014). Pp 26-29. Livro de atas do 12º Encontro de Química dos Alimentos-SPQ. Lisboa. ISBN 978-989-98541-6-1.
6. Dickinson, E. and Stainsby, G. (1987). Food Technol. 41: 75-81.
7. Raymundo, A., Gouveia, L., Batista, A.P., Empis, J. and Sousa, I. (2005). Food Res. Int. 38: 961-965.
8. AACC International (1999). Approved Methods of Analysis, 11th Ed. Method 44-15.02, AACC International, St. Paul, USA.
9. ISO 20483 (2006). International Organization for Standardization.
10. Norma Portuguesa NP518 (1986). Instituto Português da Qualidade. Lisboa.
11. Norma Portuguesa NP4168 (1991). Instituto Português da Qualidade, Lisboa.
12. Chandi,G.K. and Sogi,D.S.(2007).J.Food Eng.79:592–597
13. Anderson, R.A. (1982). Cer. Chem. 59(4): 265-269.
14. Wu, S. (1989). J. Pol. Sci. 27: 723–741.
15. Franco, J.M., Gallegos, C. and Barnes, H.A. (1998). J. Food Eng. 36: 89–102.
16. Aletor, O., Oshodi, A.A., and Ipinmoroti, K. (2002). Food Chem. 78(1): 63–68.
17. Raymundo, A., Franco, J., Gallegos, C., Empis, J. and Sousa, I. (1998). Nahrung, 42 (3/4), S. 220–224.
18. Franco, J.M., Berjano, M. and Gallegos, C. (1997). J. Agric. Food Chem. 45: 713-719.

Contact Address:
Patrícia Fradinho
pfradinho@isa.ulisboa.pt
LEAF-Linking Landscape, Environment, Agriculture and Food, Instituto Superior de Agronomia, Universidade de Lisboa.
Tapada da Ajuda, 1349-017 Lisboa (Portugal).
Telf.: +351 3653100 (Ext. 2121)

Rheological evaluation of gelled structures of rice flour for the production of different food products

A. Raymundo, A. Morais, P. Fradinho, I. Sousa

LEAF-Linking Landscape, Environment, Agriculture and Food, Instituto Superior de Agronomia, Universidade de Lisboa. Tapada da Ajuda, 1349-017 Lisboa (Portugal).

Introduction

Portugal, the top country on rice consumption in Europe – 16 kg *per capita*, produces a specific type of Japonica variety – "carolino" rice - that is a traditional variety with differentiated starch properties to the development of gluten-free foods, namely gels. Rice milling creates about 40% of by-products (~ 20% hull; 10% bran; 10% broken rice), mainly forwarded to feed, which can still be of value to the human food chain, making the product life cycle more efficient aligning with the circular economy concept.

Rice flour is the most common cereal grain flour for the production of gluten-free products due to its bland taste, white colour, digestibility, lightness and hypoallergenic properties. The gelling ability of "carolino" rice flour was previously investigated [1,2,3] and its valorisation to obtain high added value gelled products should be an important contribution to improve the global efficiency of the rice industry.

A gel can be considered as a colloidal system in which a solid matrix is the continuous phase and a liquid is the discontinuous phase [4]. This implies an internal structure formed by all sorts of intermolecular linkages, including hydrogen-bonding and hydrophobic interactions.

Food gels are viscoelastic substances and several gelled products can be designed based on this structure, with different applications, such as toppings for pastry, puddings and baby foods.

The gelling agents, used in food, are usually polysaccharides and proteins. In the present work, the use of rice flour as a gelling agent was studied, in order to obtain products with different market positions, particularly for the gluten-free food sector.

The main objective of this work is to stablish the minimum critical rice flour concentration to design gels with commercial application. The effect of sugar and sweeteners (xylitol and stevia) on rice gel behaviour was also evaluated as well as the impact of hydrocolloids addition on gel properties, in order to obtain different food-gel products.

Experimental

Materials

The "carolino" flour was provided by Novarroz - Produtos Alimentares. Hydrocolloids (xanthan gum, k-carrageenan and gelatine) and sweeteners (xylitol and steviol glycosides) were purchased to Sosa. Sucrose and commercial references of food gels were acquired in the local market.

Gels preparation

Suspensions of rice flour with different concentrations (5, 7, 10 and 15% w/w) were prepared, at room temperature, in distilled water, under stirring (600 rpm) for 30 min. Different sugar or sweetener concentrations were added, as well as the hydrocolloid (xanthan, gelatine or k-carrageenan), depending on the specific propose.

For the rheological assays, gelation was performed *in situ*, placing these suspensions on the rheometer and performing a heating cycle from 20 to 90 °C for 30 min, followed by cooling to 5 °C, during the same period of time (f=1hz). The gels for texture evaluation were prepared in a similar manner, but they were cooled down first to room temperature and then in the fridge down to 5ºC with no control of the cooling rate.

Rheology measurements

Small amplitude oscillatory measurements (SAOS) - temperature cycles (heating/cooling), time and frequency sweep tests, were set up inside the linear viscoelastic region of each formulation. The linear viscoelastic range was ensured by determining the critical stresses at each stage of the heating/cooling cycle. A controlled stress rheometer – Mars III (Haake), coupled with a Peltier system was used. A PP35 probe (serrated parallel plate system, 35mm diameter) to overcome the slip effect [5] was used, with a gap of 1 mm and f=1Hz. The exposed edges of the sample were

covered with liquid paraffin so as to avoid evaporation of water during measurements.
Texture properties of the gels (texture profile analysis - TPA) were performed using a Texturometer TA-XTplus (Stable Microsystems), using a cylindrical probe (10 mm diameter) and a penetration of 5 mm with a probe velocity of 1 mm/s, at 20ºC. Firmness (N), considered as the maximum resistance to the penetration of the probe, was calculated as the height of the force peak during the first penetration cycle. This texture parameter was the one that allowed to discriminate more effectively the studied samples, as verified in other works with gels [6].
Gel syneresis was determined by weighing the liquid released using filter paper [7].

Results and Discussion

Texture (Figure 1) and SAOS measurements (Figure 2) characterisation of commercial toppings, puddings and baby foods was performed and the respective results were used as a target for each category.

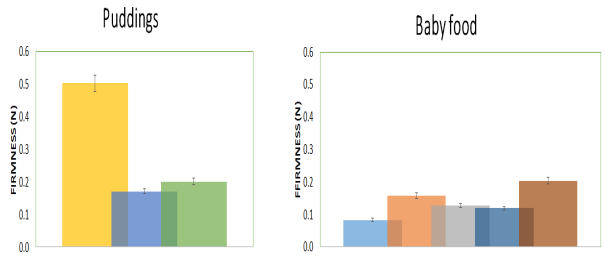

Figure 1.Texture of commercial gels performed at 20ºC.

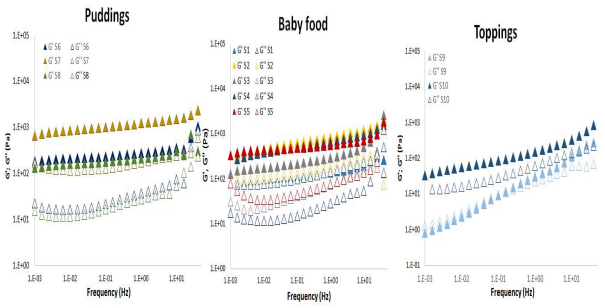

Figure 2. Mechanical spectra of commercial gels samples, performed at 5ºC. "s" is the sample code.

From these results it turns out that baby foods are softer gels, comparing with puddings, that are the most structured gels – elastic moduli (G') and loss moduli (G'') higher. It is also evident that the commercial toppings are the less structured gels, with G' values close to G'', even presenting crossing over zones.
The rice flour gelling capacity and the critical rice concentration to obtain gels with commercial interest was investigated performing frequency sweep tests, at 5ºC (after de heat/cooling cycle) – Figure 3. The respective appearance of the model gels can be seen on Figure 4.

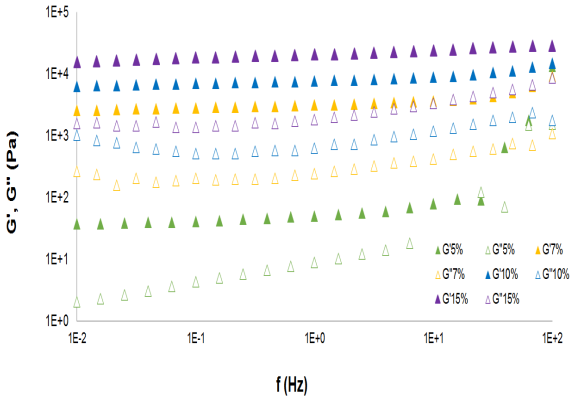

Figure 3. Mechanical spectra of rice gels prepared with different concentrations (5, 7, 10 e 15% w/w), at 5ºC, after a heating/cooling cycle.

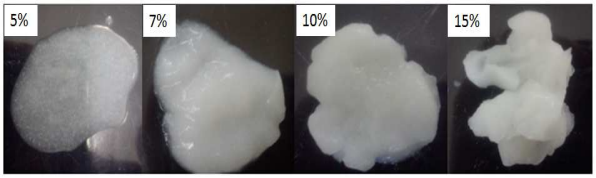

Figure 4. Appearance of rice gels prepared with different concentrations, at room temperature.

From the above results it can be considered that a critical value of rice flour (japonica Portuguese variety – *carolino*) concentration of 5% (w/w) was obtained to the development of food gels with commercial purposes. Nevertheless, for this concentration G' and G'' is highly dependent on the frequency, and a pronounced gel syneresis is also observed. In addition, the gel with more than 8% of rice flour showed a negative impact on the sensory perception of these gels (results not shown). Therefore, the gel with 7% (w/w) of rice flour was considered the most appropriate concentration, which allows to maximize the incorporation of flour and to guarantee promising sensory characteristics. These results are in agreement with other gel studies, revealing a reinforcement of the gel structure with the increase of the macromolecules concentration, with a contribution to the development of the entangled network [8].
The impact of sucrose and sweeteners, from 1 to 6% (w/w), on the development of the gel structure was also evaluated and a slight effect on gel rheological behaviour was observed (Figure 5).

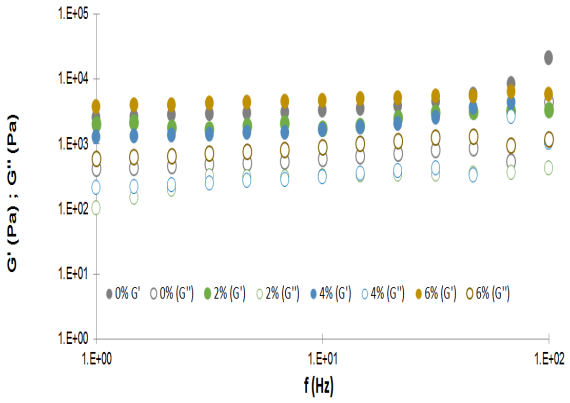

Figure 5. Impact of sugar sucrose concentration on mechanical spectra of rice gels obtained with 7% (w/w) of rice flour, at 5ºC.

In other work of our group [1], a decrease of gel firmness with sucrose and sweeteners concentration was observed, however higher concentrations were involved (from 5 to 25%). In this case, the decrease of firmness was attributed to the formation of large and complex interactions between rice starch and sugar, disrupting the starch-starch (amylose network) bridging, leading to gels with lower firmness values.

In this work, a markedly impact of sucrose addition on syneresis was found (Figure 6). There was a substantial increase of the excluded water, after 8 days of storage, which is more pronounced for the higher sugar concentration. This may be related to the contraction of the gel structure at higher sugar concentrations, which results in lower water retention in the gel matrix. 3% (w/w) of sucrose is the concentration that leads to lower syneresis.

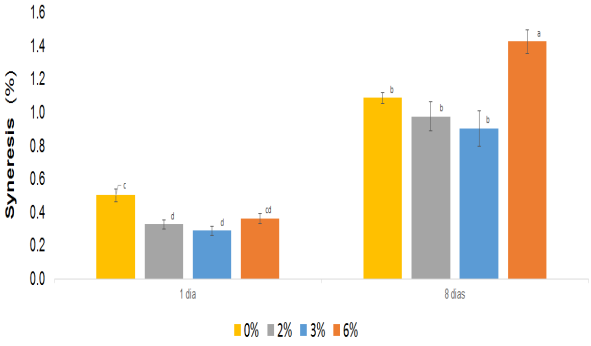

Figure 6. Syneresis of rice gels prepared with different concentrations of sucrose after preparation and after 8 days of storage, at room temperature.

In order to obtain rice gels with physical properties close to those of similar products in the market, the use of hydrocolloids was studied. The use of these macromolecules to produce complex binary systems with rice flour was the key to design gel structures for the three different fields of applications proposed. A wide range of concentrations of each hydrocolloid was tested and the impact of its addition on texture, rheology and syneresis was evaluated.

Considering all the physical characteristics, it was found that, for a gel prepared with 7% (w/w) of rice flour and 0.25% (w/w) of xanthan gum it is possible to obtain a typical topping gel structure. When adding 1% of gelatine, a pudding like structure was found. With 0.25% of k-carrageenan, a baby food like structure can be produced. The mechanical spectra of these selected gels are represented on Figure 7.

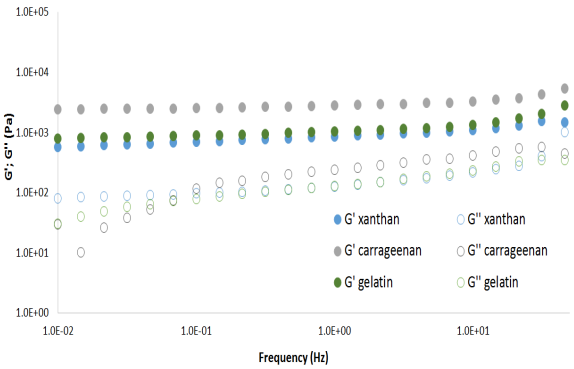

Figure 7. Mechanical spectra of rice gels prepared with 0.25% of xanthan, 1% of gelatine and 0.25% of k-carrageenan, for a rice flour concentration of 7% (w/w, at 5ºC.

The gel texture analysis of the different types of gels produced, provide important and complementary information to correlate the results with the sensory evaluation. On Figure 8 the firmness values, of the rice flour gels for each market category considered, are represented.

The gels produced with 0.25% of k-carrageen exhibit higher values of elastic modulus and a certain dependence of G'' with frequency, more evident at low frequencies, which is generally associated with a shear-induced gelation process.
These systems showed higher values of firmness and general sensory characteristics close to the Baby Food structures. The role of k-carrageenan to act as a filler in protein/starch structures, reinforcing the texture perception, was previously reported by Nunes et al (2016) [8].

The mechanical spectra obtained with 0.25% (w/w) and 1% (w/w) of gelatine are quite similar. Nevertheless, the gelatine system evidenced higher firmness and sensory behaviour as a pudding, with a pronounced retention of the structure, when removed from the storage container. This different behaviour is related with the different role

of xanthan gum and gelatine on the development of a gel structure. The action of xanthan gum results essentially from its thickener effect, whereas the role of gelatine is well recognised as a gelling agent [9].

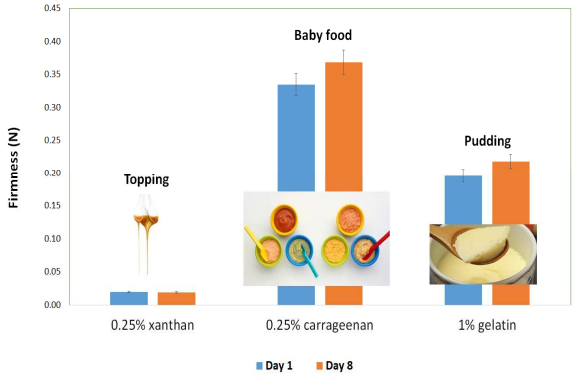

Figure 8. Firmness of 7% (w/w) rice four gels with addition of 0.25% of xanthan gum, 0.25% of k-carrageenan and 1% of gelatine and its relation with target materials, at 20ºC.

Concluding remarks

The use of rice flour for the design of gels with different market positions was investigated. The optimum concentration of rice flour for gelation was 7% (w/w). Addition of 3% (w/w) of sucrose is associated with lower syneresis, which is a key factor form the commercial point of view. Sucrose had more impact on syneresis reduction, than the sweeteners studied, since these are added at much lower concentrations.

The addition of hydrocolloids turned possible to design promising rice gels with rheology behaviour close to different types of products available in the market: 0.25% of xanthan gum to obtain a typical topping gel structure; 1% of gelatine for a pudding like structure and with 0.25% of k-carrageenan a baby food like structure can be produced.

Acknowledgements

This work was supported by: i) COMPETE program: QREN Arroz + project: 38749/13; ii) *Portuguese Foundation for Science and Technology (FCT) through the research unit UID/AGR/04129/2013 (LEAF).*

References

1. Torres, M.D., Raymundo A. and Sousa, I. (2013). Carb. Pol. 98: 249– 256.
2. Torres, M.D., Raymundo A., Fradinho, P., Sousa, I. (2014). *Food and Bioprocess Technology: An International Journal*. 7. (4): 1171-1182.
3. Torres, M.D., Raymundo A. and Sousa, I. (2014). *Carb. Pol*. 102: 30-37.
4. Sahin and Sumnu (2006). Physical Properties of Foods, Food Science Text Series. Pp 39-105.
5. Barnes, H. A., Hutton, J. F., & Walters, K. (1989). Elsevier Science Publishers BV.
6. Aguilar, J.M., Batista, A.P., Nunes, M.C., Cordobés F., Raymundo, A., Guerrero, A. (2011). *Food Hydrocolloids*. 25, 654-658.
7. Ako K. (2015). *Carb. Pol.* 115, 408-414 p.
8. Nunes, M. C., Raymundo, A., & Sousa, I. (2006). *Food Hydrocolloids*. 20, 106–113.
9. Saha, D. and Bhattacharya, S. (2010). *J Food Sci Technol.* 47(6): 587–597.

Contact Address:

Anabela Raymundo
Author's email: anabraymundo@isa.ulisboa.pt
LEAF-Linking Landscape, Environment, Agriculture and Food,
Instituto Superior de Agronomia, Universidade de Lisboa.
Tapada da Ajuda, 1349-017 Lisboa (Portugal).

Effect of inulin with different polymerization degree on wheat flour dough rheological properties of 1250 type

G. G. Codină[1], D. Zaharia[2], E. Todosi Sănduleac[1], A. Dabija[1]

[1] Ştefan cel Mare University of Suceava, Faculty of Food Engineering, 13 Universităţii Street, 720229, Suceava (Romania)
[2] S. C. Dizing S. R. L. Brusturi, Neam (Romania)

Introduction

From a structural point of view, inulin is a fructan formed of a mixture of fructo-oligosaccharides and of fructo-polysaccharides [1]. It is a soluble fiber which is not degraded until it reaches the colon, where the action of different bacteria finally deteriorates it to hydrogen, methane, carbon dioxide and short-chained fat acids: acetic, propionic, butyric as shown in the drawing below. It is well known that there are two types of fibers namely insoluble and soluble one. Insoluble edible fibers are represented by the vegetal material that is not digested by the enzymes present in the human digestive tract and are not soluble in hot water like cellulose, different types of hemicellulose, lignin, e.g. The soluble edible fibers are represented by the vegetal material that is not hydrolyzed by the enzymes present in the human digestive tract and is soluble in hot or warm water, precipitating whenever the water is mixed with four doses of ethylic alcohol: pectin, different types of hemicellulose, inulin, β-glucans, gums, e.g.

Even though it is only digested in the colon, inulin's transition from foods through different organs of the digestive apparatus has certain positive effects on the human body, effects that will be mention below. In the stomach, it increases satiety and ensures a better digestion of foods; in the small intestine, it provides a better digestion and decreases sugar absorption in the human body, which has a highly positive effect for diabetics; in the large intestine, it reduces constipation, thus leading to a better intestinal health. Research has shown that each short-chained fat acid produced from the degradation of inulin in the colon has a certain positive effect on the human body. Therefore, the propionic has an important role in lowering cholesterol, the butiric acid helps preventing colon cancer, while the acetic acid stimulates glycogenesis (known to be a forerunner of the cholesterol). Another important role that inulin has in the human body is that of functioning as a prebiotic – an indigestible food ingredient which influences the body in a positive way through the selective stimulation of the growth and/or the activity of some species or of a limited number of bacteria in the colon [2].

The intestinal micro flora is made of a complex of microorganisms which have a very important role for the human body. They interact with each other and with the host organism within the intestinal tract in which they coexist. In essence, they metabolize different endogenous substances in the human diet, forming products that can have positive effects on man's health both at a global and at the local level. The average intestinal micro flora can be modified through diet, medication, stress and/or environmental factors. Thus, it is possible for the natural balance between different groups of microorganisms to be disordered during the life of a human being, this having negative consequences for one's health. By inulin consummation is stimulated the increase of the number of *bifidobacteria* and *lactobacteria*, leading also to an increase in the availability of calcium and magnesium. The absorption of Ca and Mg in the body is completed according to a process that has not yet been clarified [3].

Inulin is a functional ingredient because it provides a series of benefits for human health: an increase of fiber content; the stimulation of good bacteria in the digestive system (the bifidogenic effect); the improvement of calcium absorption, thus contributing to an increase in the mineral density of the bones; a lower risk of cardiovascular diseases and colon cancer; the inhibition of diarrhea and the elimination of constipation [1].

The inclusion of prebiotic elements in food processing is a way of developing new commodity markets and new products. From a technical point of view, both inulin and oligofructose are easy to use and contribute to the taste and aspect of the products they are used for. The

inclusion of inulin in wheat flour in order to obtain bread has been previously studied [1]. But it is well known that to obtain a bread of good quality the dough rheological properties must confer some good characteristics, especially a good elasticity and extensibility. The effect of inulin on dough rheological properties has been published before, and it was reported that its addition up to a certain level decreases water absorption of wheat flour dough, dough stability and extensibility [4]. Also an important influence on dough rheological behavior presents the inulin chain length that varies from 2 to 60 from the degree of polymerization (DP) point of view, a DP less than 10 corresponding to an oligofructose [1].

The aim of this study was to investigate the effect of inulin addition (from 2.5% to 10% on dry matter - wheat flour plus inulin) on wheat flour dough rheological properties of a low extraction rate due to the fact that it presents a high content of fibers (in especially insoluble ones) and also important amounts of vitamins and minerals.

Experimental

Materials

The research has been carried on 1250 flour type (harvest 2016) obtained from S.C. Dizing SRL (Brusturi, Neamț, Romania). According to Romanian or international standard methods the flour used in the experiments presents the following characteristics: moisture content 14.5% (ICC methods 110/1), ash content 1.25% (ICC 104/1), protein content 15.6% (ICC 105/2), wet gluten content 36.7% (ICC 106/1), gluten deformation index 3 mm (SR 90:2007), falling number 363 s (ICC 107/1).

As inulin products, an instant inulin with a degree of polymerization (DP = 10) and an oligofructose (DP =5.5) derived from chicory root were used

Dough empirical rheological properties during fermentation

Dough empirical rheological properties during fermentation were made by using the Chopin Rheofermentometer (Chopin Rheo, type F3, Villeneuve-La-Garenne Cedex, France). Total CO_2 volume production (VT, mL), maximum height of gaseous production (H'm, mm), and volume of the gas retained in the dough at the end of the test (CO_2 retention, VR, mL) were recorded.

Dynamic rheology

Dough fundamental rheological properties were investigated by using a Haake dynamic rheometer. The plate and plate system was used with a diameter of 40 mm and a gap between plates of 2 mm. The dough sample was placed between the rheometer plates and the excess dough was carefully removed. A thin layer of vaseline was applied to the exposed dough surface to prevent drying during testing. In a first stage stress sweep tests (1 Hz at 25 ℃) were made in order to determine the linear viscoelastic region of the dough samples. Next, frequency sweep tests from 1 to 20 Hz in the linear viscoelastic region were performed for dough samples. The storage modulus (*G'*), loss modulus (*G''*) and loss tangent (tan *δ*) were assessed. The moduli and tan *δ* were also determined for dough samples during heating (25-90 ℃) at the rate of 4 ℃ per minute. All experiments were made to optimal fibre-enriched dough water abortion established to Farinograph. More replications were made for each dynamic test.

Results and Discussion

The wheat flour type 1250 was of a strong one for bread making with a low deformation index. Also it presented a low alpha amylase activity due to its Falling Number value (363 s).

Before making the rheological tests fibre-enriched dough water absorption were determined in order to obtain a dough consistency of 500 BU. The water absorption ranged between 65.0-47.3% for native inulin addition and between 65.0-44.1% for oligofructose addition. The water absorption value is a very important aspect for the bread making technology with inulin addition because a water addition similar to those for the control sample make the dough very difficult to process. The decrease of the water absorption value proportional with the increase level of inulin addition may be attributed to the increase of the osmotic pressure outside to the protein micelle which will reduce the water osmotic absorption. This is a consequence of the presence of the fructose molecule in the dough system by inulin addition which is in a higher amount in oligofructose than in native inulin. Similar results were also found by [3].

In Table 1 are shown the empirical rheological properties during fermentation time for wheat flour dough enriched with inulin and oligofructose at different levels. Total CO_2 volume production decreased with increasing levels of inulin and oligofructose more for oligofructose than for inulin addition. Also at 10% soluble fibre addition a lower value were obtained for

maximum height of gaseous production (H'm, mm) for oligofructose than for inulin addition.

Table 1. Effect of inulin and oligifructose addition on Rheofermentograf rheological properties

Fiber addition (%)	H'm (mm)		VT (mL)		VR (mL)	
	OF	In	OF	In	OF	In
0.0	66.7		1443		1137	
2.5	69.1	67.7	1212	1392	1017	1130
5	66.7	66.9	1179	1291	991	1011
7.5	60.2	65.8	1105	1282	963	972
10	56.5	64.8	1078	1268	940	959

In, inulin; OF, oligofructose; VT, total CO2 volume production; H'm maximum height of gaseous production; VR, volume of the gas retained in the dough at the end of the test.

The dynamic rheological properties evaluated for wheat flour dough enriched with inulin and oligofructose at Farinograph water absorption are shown in Figures 1-4. Figures 1 and 2 show frequency sweep results for doughs containing wheat flour 1250 type-inulin blends and Figures 3 and 4 present the results for doughs containing wheat flour 1250 type-oligofructose blends.

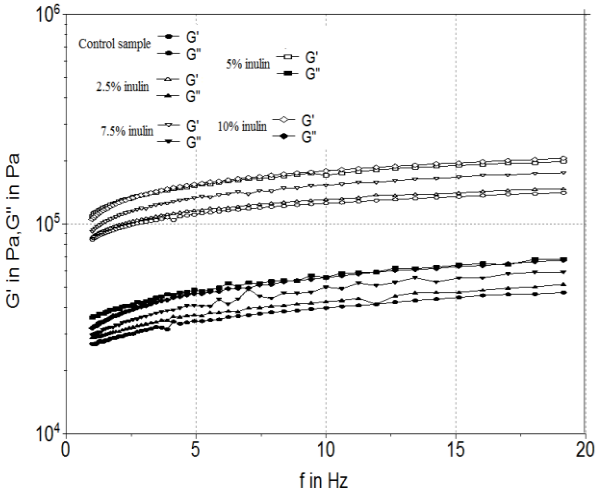

Figure 1. Storage and loss modulus vs. frequency for wheat flour dough enriched with inulin at Farinograph water absorption

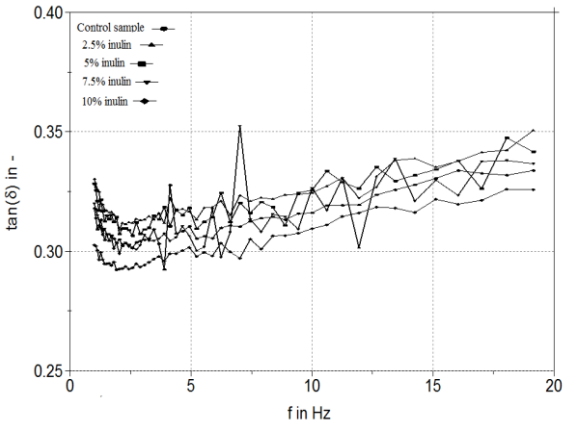

Figure 2. Loss tangent vs. frequency for wheat flour dough enriched with inulin at Farinograph water absorption

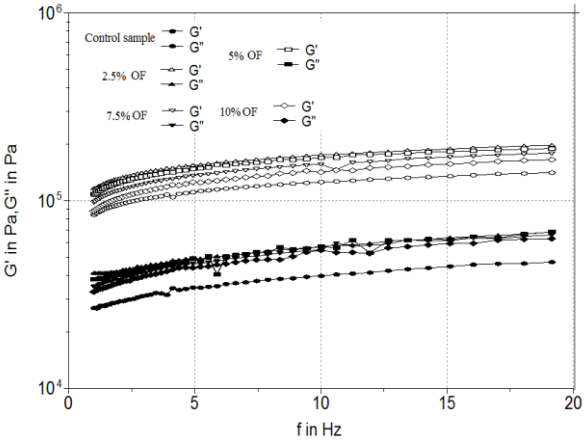

Figure 3. Storage and loss modulus vs. frequency for wheat flour dough enriched with oligofructose at Farinograph water absorption

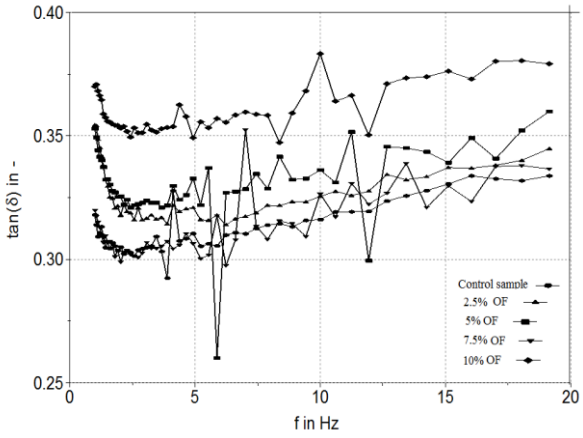

Figure 4. Loss tangent vs. frequency for wheat flour dough enriched with oligofructose at Farinograph water absorption

The addition of inulin with different DPn conducted to significant changes in linear viscoelastic properties of dough. The storage and loss moduli increased and tan δ decreased with increasing level of inulin addition. Inulin addition at 5% resulted in moduli values about 3 times higher than those of the control flour. Higher storage and loss values and lower tan δ indicate a more solid-

like material. More elastic and stable doughs were obtained by oligofructose addition than by inulin incorporation. For all the samples inulin with different DP addition presents higher elasticity and solid-like behaviour than the control sample. Similar results were also obtained by Peressini and Sensidoni [4].

The changes of storage and loss moduli and of tan δ during heating of dough samples enriched with inulin and oligofructose are shown in Figures 5-8.

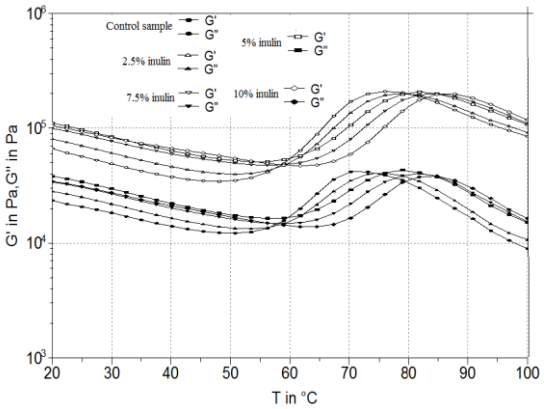

Figure 5. Storage and loss modulus during heating for wheat flour dough enriched with inulin at Farinograph water absorption

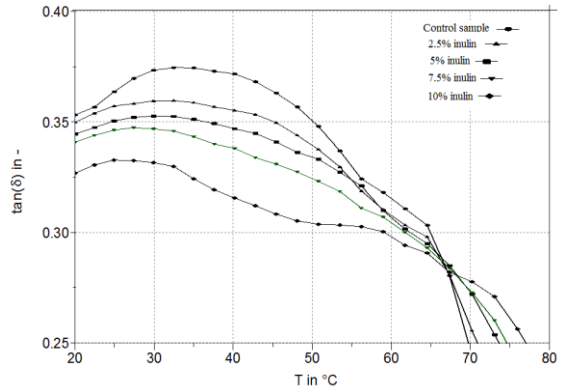

Figure 6. Loss tangent during heating for wheat flour dough enriched with inulin at Farinograph water absorption

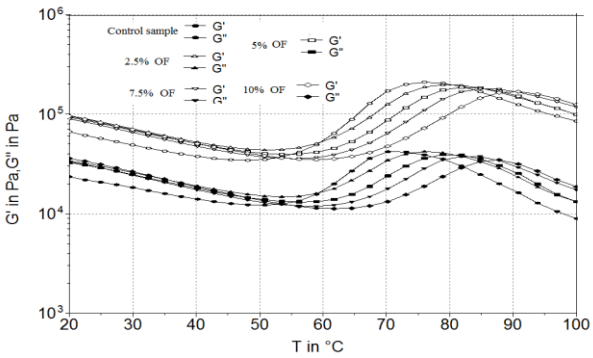

Figure 7. Storage and loss modulus during heating for wheat flour dough enriched with oligofructose at Farinograph water absorption

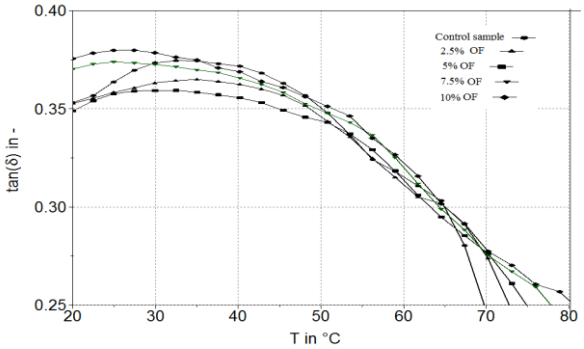

Figure 8. Loss tangent during heating for wheat flour dough enriched with oligofructose at Farinograph water absorption

It can be observed that both G' and G" values showed the same tendency as the temperature increased. On the other hand, in the presence of inulin the inflection point temperatures for both moduli were also higher.

Concluding Remarks

The partial replacement of flour by two inulin types (with different DP) at increasing levels (2.5 to 10%) significantly changes the dough rheological properties. Both types of inulin caused a strengthening effect, although the reinforcement was more pronounced with oligofructose addition than with inulin incorporation. Nevertheless, inulin addition increases the solid-like properties of doughs but reduces dough expansion during fermentation. Samples with inulin addition also presented a delay in the starch gelatinization temperature compared with the control sample.

Acknowledgements

This work was supported by a grant of the Romanian National Authority for Scientific Research and Innovation, CNCS/CCCDI – UEFISCDI, project number PN-III-P2-2.1-BG-2016-0079, within PNCDI III.

References

1. Morris, C. and Morris, G.A. (2012). Food Chemistry, 133, 237–248.
2. Peressini, D., Foschia, M., Tubaro, F. and Sensidoni, A. (2015). Food Hydrocolloids, 43, 73-81.
3. Meyer, D. and Peters, B. (2009). Agro Food Industry Hi-Tech, 20 (3), 48-50.
4. Peressini, D., and Sensidoni, A. (2009). Journal of Cereal Science, 49(2), 190–201.

Contact Address:
G.G. Codină (codina@fia.usv.ro);
Phone: +40 745 460 727

Effect of tomato skins powder addition on rheological and physicochemical characteristics of milk yoghurt

A. Dabija, G. G. Codină, M. A. Oroian, S. Mironeasa

Stefan cel Mare University of Suceava, Faculty of Food Engineering, 13 Universităţii Street, 720229, Suceava (Romania)

Introduction

In the last decades increased demand for food products that contributes directly to consumers' health. Development of food which to provide not only necessary nutrients for humans but also to prevent nutrition-related diseases and improve physical and mental well-being of the consumers has gained special attention from food scientists and industries [1].

Yoghurt is a fermented dairy product usually manufactured by fermenting milk with a starter culture consisting of *Lactobacillus delbruckii subsp.* and *Bulgaricus Streptococcus thennophilus* used individually or in combination [2], which produces lactic acid. The gel structure of yoghurt appears as result of coagulation of the milk proteins by the lactic acid produced. Due to its nutrient profile that comprise of more than ten essential nutrients in particular, certain minerals and vitamins [3], yoghurt has numerous health benefits, such as improve lactose digestion, decrease risk of cancer, reduce blood cholesterol, improve vitamin nutritive value, and help the body to assimilate protein, calcium and iron.

Fermented dairy products and yoghurt in particular are increasingly sought after and appreciated by consumers around the world. Therefore, the varieties and types of yoghurts available in the market are increasing and must fulfil the consumer's expectancy for products that are simultaneously relish and healthy. The acceptability of novel yoghurt products by the consumer is still based on satisfactory textural and sensory properties. Also, rheological property of yoghurt (viscosity) is one of the important factors regarding the quality, low viscosity of the product being a desirable feature [4].

In this context, many researchers have tried yoghurt fortification to improve the quality of yoghurt by supplementing with various ingredients that increase these nutritional properties. Some fortification may contribute to a better uniformity of curd or even modify the gel structure of yoghurt [5].

Many researchers studied texture characteristics of yoghurts due to the addition of some stabilizers such as gelatine, pectin, k-carrageenan that can influence the sweetness and flavour sensory characteristics and can prevent syneresis of the yoghurt.

Incorporating tomato skins flour in yoghurt formulation can improve its quality especially from the point of view of its nutritional value and antioxidant (carotenoids) intake in the human diet. The antioxidant and nutrient composition of the final products can be improved, changing their technological quality.

Numerous studies have focused on beneficial components of tomato skins [6] which is recognized as rich source in nutrients and bioactive compounds due to its content in organic acids, pigments, fibre, proteins, oils, sugars, antioxidants and vitamins. Studies on antioxidant compounds in some tomato genotypes were reported that had higher levels of total phenolics, total flavonoids, lycopene and ascorbic acid was found in skins.

Experimental

Materials

Cow milk was purchased from a milk dispenser (Suceava, Romania). A freeze-dried lactic culture which contained a mixture of *Streptococcus thermophilus* and *Lactobacillus bulgaricus* was kindly supplied by S.C. Enzymes@Derivates S.A. Romania (Costisa,Neamț). Tomato skins powder was prepared from tomato skins separated from pomace. After drying, tomato skins were ground with a grinder to a tomato skins powder for yoghurt formulation. The following yoghurt samples was prepared with various concentrations of tomato skins

powder: C (control sample) without any addition, S1 (0.2%), S2 (0.4%), S3 (0.6%) and S4 (0.8%).

Tomato skins powder and milk analysis

The chemical composition of tomato skins powder was determined according to the Romanian or international standards: moisture (SR EN ISO 712:2010), fat content (SR EN ISO 11085:2010), protein content (SR EN ISO 20483: 2014) and ash as a percentage of the dried substance (SR ISO 2171:2009). The carbohydrate content was determined as a difference of the average: 100 – (the quantity in percentage of the moisture content, ash, protein and oil). The physical–chemical parameters of the milk (fat, protein, lactose, solid non fat, mineral content) were determined by using a precalibrated milk analyzer (Lacto Star, Funke Gerber, Germany).

The characteristics of the tomato skins powder, as a percentage from dried substance, are the following: moisture 5.60%, lipids 5.90%, protein 8.78%, ash 3.42% and carbohydrates 76.30 %.

Determination of pH and acidity

The pH of the yoghurt samples was determined using a digital pH-meter (Hanna Instruments, HI 98180, Woonsocket, RI, USA) by immersing the sensor in the yoghurt. The fermentation was considered completed when a pH of 4.5 was reached. Before making the tests, the yoghurt samples were cooled and stored at 4-5 °C for 24.

Acidity, expressed as Thorner degree, was determined by titration with 0.1N NaOH using phenolphthalein as indicator.

Syneresis

After 24 h of storage at 4 ± 1°C, the syneresis of the yoghurt samples was determined through the centrifugation procedure. Approximately 5 g of yoghurt was transferred into a 10 mL glass tube and was centrifuged (Hermle Labortechnick, Z 306 model, Wehingen, Germany) at 3500 rpm for 15 min at 20 °C.

Rheological measurements

The rheological measurements were carried out with a Brookfield rotational viscometer (Model RVDV-I Prime,

Brookfield Engineering Laboratories Inc., Lorch, Germany) equipped with a RV3 spindle selected according to the samples' viscosity. The measurements were carried out at 4±1°C and five rpm levels of 5, 10, 20, 50 and 100. For each sample, three readings were taken. The power law (Ostwald-de-Wael) model was developed from the data obtained in viscometer to characterize the rheological behaviour of the yoghurt samples. The parameters of this model, consistency index (k) and flow behavior index (n) were calculated according to the Eq. (1)

$$\sigma = K \dot{\gamma}^{n} \quad (1)$$

where, σ is the shear stress (Pa), k is the consistency coefficient (Pa s^n), γ is the shear rate (1/s) and exponent n is the flow behaviour index (dimensionless).

The empirical data measured with the viscometer for yoghurt samples were converted to shear stress and shear rate using the method described by Mitschka (1982) [7] and Briggs and Steffe (1997) [8]. The apparent viscosity, η (Pa s) was calculated using the Eq. (2).

$$\eta = \frac{\sigma}{\gamma} \quad (2)$$

The experimental data obtained for yoghurt samples at different shear rates were calculated.

Results and Discussion

Effect of tomato skins powder addition on pH and acidity during fermentation

A 43°C fermentation temperature was chosen as an optimum one for the thermophilic lactic acid bacteria, i.e., *Streptococcus subsp. thermophilus* and *Lactobacillus delbrueckii subsp. Bulgaricus [2]*.

The influence of tomato skins powder on the lactic acid bacteria metabolism was monitored during the fermentation process. The lactic fermentation process was stopped when the control sample reached a pH value of 4.6. The variations of pH and acidity for all the samples analyzed are shown in Fig. 1 and Fig. 2.

As can be seen, the yoghurt samples supplemented with tomato skins powder had a much higher decrease in the pH compared to the control sample prepared without tomato skins powder addition (Figure 1).

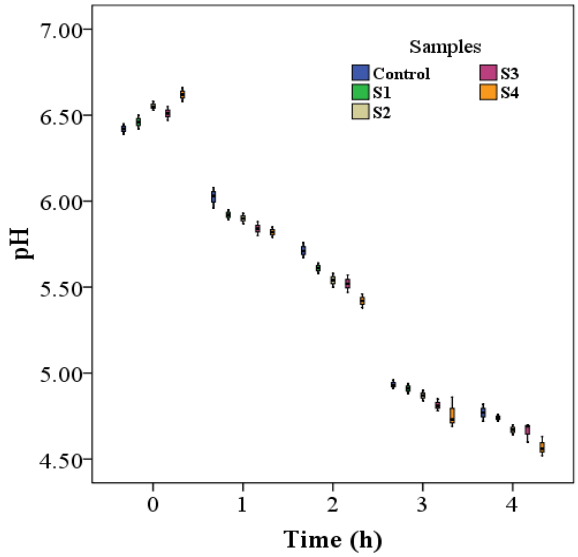

Figure 1. Variation of pH value during thermostatic time in yoghurt samples with different levels of tomato skins powder: 0% (Control), 0.2% (S1), 0.4% (S2), 0.6% (S3), 0.8% (S4)

Also, a much higher increase in the total acidity during the fermentation process was obtained in all samples with tomato skins powder addition comparatively with the control sample (Figure 2). Therefore, the tomato skins powder influenced the growth of yoghurt starter culture and the production of lactic acid probably due to the composition in nutrients of tomato skins [6].

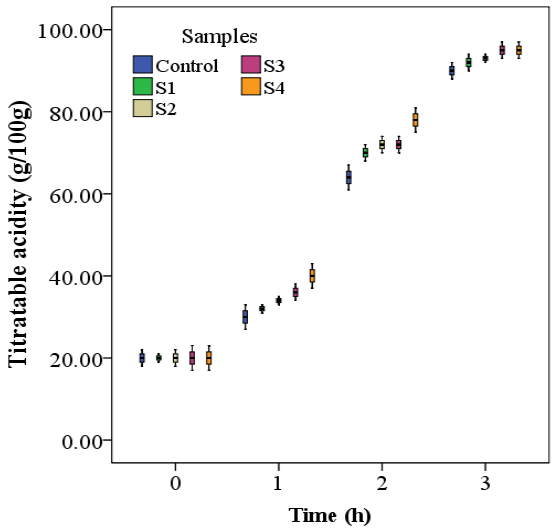

Figure 2.. Titratable acidity value of yoghurt samples with Different levels of tomato skins powder: 0% (Control), 0.2% (S1), 0.4% (S2),0.6% (S3), 0.8% (S4)

Determination of syneresis showed a higher level of whey in sample with 0.8% tomato skins powder probably due to the tomato skins particles that damage the continuity of protein gel network.

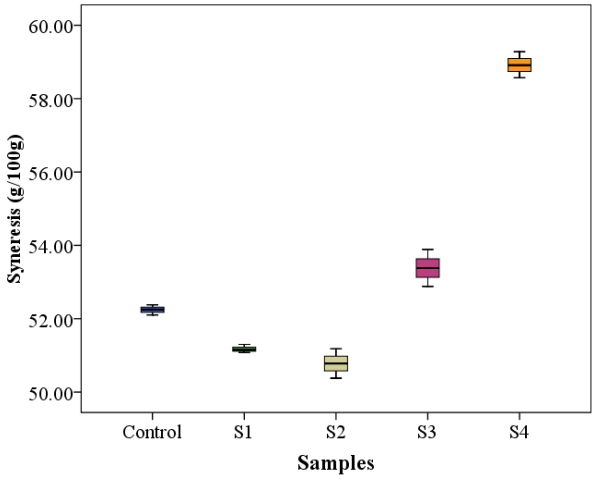

Figure 3. Variations in syneresis in yoghurt samples with different levels of tomato skins powder: 0% (Control), 0.2% (S1), 0.4% (S2), 0.6% (S3), 0.8% (S4)

Regarding the rheological properties, shear stress value decreased by increasing tomato skins powder level from 0.2 to 0.8% as compared with control sample addition. A decrease in apparent viscosity with increase in shear rate from 2.57 to 70.2 (1/s) was obtained in all yoghurt samples indicating a non-Newtonian fluid and shear-thinning behaviour. The sample with 0.8% tomato skins powder has a lower apparent viscosity than the control one. This fact indicates that a high amount of tomato skins powder addition can destroy the yoghurt curd, increasing the proportion of whey.

The Ostwald-de-Wael model appears to be suitable ($R^2 > 0.99$) for describing the flow behaviour of yoghurt with different tomato skins powder concentrations.

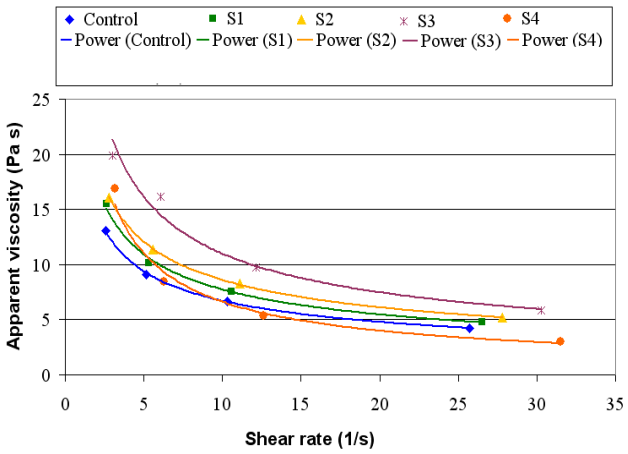

Figure 4. Apparent viscosity related to the shear rate for yoghurt samples with different levels of tomato skins powder: 0% (Control), 0.2% (S1), 0.4% (S2), 0.6% (S3), 0.8% (S4)

The consistency index increased with the increase of tomato skins powder level, while the flow index

decreased with the increase of tomato skins powder addition at this level (Table 1).

Table 1. Rheological parameters of Ostwald-de-Waele model

Samples	Cod sample	k ($Pa \cdot s^n$)	n (dimensionles)	R^2
Tomato skins powder (%)				
0.0	Control	21753	0.41	0.997
0.2	S1	28200	0.38	0.999
0.4	S2	32391	0.36	0.999
0.6	S3	40980	0.33	0.984
0.8	S4	15123	0.45	0.997

k, consistency coefficient; n, flow behaviour index; R^2, coefficient of determination.

Results show that samples containing tomato skins powder up to 0.6% have a higher viscosity, because tomato skins powder can bond water in samples and consequently increase the viscosity.

Concluding Remarks

Tomato skins powder addition had an influence on the pH value, whey loss and rheological properties of milk yoghurt. A shear thinning profile was registered in all samples analyzed. The samples with tomato skins powder up to 0.6% addition have higher apparent viscosity and lower whey loss.

Acknowledgements

This work was supported by a grant of the Romania National Authority for Scientific Research and Innovation, CNCS/CCCDI – UEFISCDI, project number PN-III-P2-2.1-BG-2016-0089, within PNCDI III

References

1. Menrad, K. (2003). Journal of Food Engineering, 56(2), 181-188.
2. Lee, W.J. and Lucey, J.A. (2010). Asian-Aust. J. Anim. Sci. 23, 1127 – 1136.
3. Weerathilake, W.A.D.V., Rasika, D.M.D., Ruwanmali, J.K.U. and Munasinghe, M.A.D.D. (2014). International Journal of Scientific & Research Publications 4, 1-10.
4. Nilsson L.-E., Lyck S. and Tamime A.Y. (2006) In: A. Tamime (Ed.) Fermented Milks, Society of Dairy Tehnology-Blackwell Science Ltd, UK, 2006, pp. 95-128.
5. Loveday S.M., Sarkar A. and Singh H. (2013). Trends Food Sci. Technol. 33, 5 – 20.
6. Peng Y.Y., Zhang, Y.W. and Ye J. N. (2008). Journal of Agricultural and Food Chemistry, 56(6),1838–1844.
7. Mitschka L.P. (1982). Rheol. Acta 21, 207–209.
8. Briggs J.L. and Steffe J.F. (1997). J Journal of Texture Studies 28, 517–522.

Contact Address:
S. Mironeasa (silviam@fia.usv.ro)
Ştefan cel Mare University of Suceava, Faculty of Food Engineering, 13 Universităţii Street, 720229, Suceava, Romania
Telf. +40 741 985 648

Rheological characterization of yogurt with different types of fibres

A. Dabija, M. A. Oroian, A. M. Sidor, G. G. Codină

Faculty of Food Engineering, Stefan cel Mare University of Suceava, Universitatii Street, 13, Suceava (Romania)

Introduction

Yogurt has been recognized as an important dairy-fermented product known to bring many positive effects for individuals. Research and development in yogurt has focused on reducing whey syneresis, improving product firmness and texture, as well as reducing gelation time. Consequently, there is a growing demand to discover new manufacturing technology which enables the production of high-quality clean label yogurt: less fat and no stabilisers [1, 2].

In the past decades, the food industry has started to use fibres in more and more innovative ways due to their health benefits and in an attempt to develop a variety of products which fit consumer needs. Among the main source of fibres utilized by the food industry we find cereal polysaccharide, while residues of fruits and vegetables are more a non-conventional source. Although edible, the dietary fibre found in plants and cereals are resistant to digestion in the small intestine, but attains complete (partial) fermentation in the large intestine. Dietary fibre includes oligosaccharide, polysaccharides, lignin and secondary plant substances provided by the cell wall of fruits, vegetables or cereals. By adding fibre in cookies, cakes, breakfast cereals, bread, yogurt, beverages and even meat products, the obtained end-products have been reported with favourable results [3, 4].

Research so far has recorded various types of fibers being added to yogurt formulation in order to enhance the texture, structure and quality of the finished product. Adding fibers has been proven to reduce yogurt syneresis and lipid retention, improve texture and structure (increased gel firmness) and reduce finished product's caloric content by acting as a bulking agent. Intake of high fibre yogurt may prevent or decrease hypertension, obesity, diabetes, hypercholesterolemia, gastrointestinal disorders, coronary heart disease, and colon cancer.

The effects of apple, wheat, bamboo, or inulin fibres on organoleptic and rheological properties of yogurt were studied by Dello Staffolo *et al.* (2004). Their findings demonstrated that even though some rheological features were modified, the obtained high fibre yogurts were acceptable to end consumers [5]. Yogurt's microstructure, texture, organoleptic and rheological characteristics depend on a sundry of factors: formula of the milk base, particularity of bacterial culture used, variety of ingredients added during production process, as well as packaging and storage [6, 7].

Inulin is a good example of added ingredient which is recognized to reduce caloric value while providing dietary fibres. The prebiotic effects of inulin have been subjected to countless research due to its beneficial effects on the gastrointestinal and immune systems. Furthermore, inulin has been proven to augment the absorption of calcium and magnesium in the body, as well as influencing the formation of blood glucose, and reducing cholesterol and serum lipids levels [8].

The aim of this study was to determine the effects of addition of different fibres, such as: pea fibres, wheat fibres, oat fibres and inulin fibres on the rheological properties of yogurt samples.

Experimental

Materials

The raw and auxiliary materials used in order to obtain the yogurt samples under laboratory conditions were: cow's milk (composition: 3.5% fats, 4.5% carbohydrates and 3% protein); lactic bacteria culture (*Lactobacillus bulgaricus* and *Streptococcus thermophillus*, provided by Danisco Romania S.R.L); different types of fibres (inulin, oat, pea and wheat fibres, supplied by Enzymes & Derivates Costișa, Neamț). Pea fibres are extracted from the endosperm of the yellow pea and they contain 20.0% total dietary fibre, of which 5.5 % soluble fibre and 12.5% insoluble fibre. Wheat fibres contain 12.6% total dietary fibre, of which 10.2 % soluble fibre and 2.3 % insoluble fibre. Oat fibres contain 10.3 % total dietary fibre, din care 6.5% soluble fibre and 3.8% insoluble

fibre. Inulin is produced by extraction from chicory roots, with a degree of polymerization of ~10 and a dietary fibre content in dry matter of more than 90%.

Yogurt preparation

The yogurt preparation phase of the study followed the ensuing steps: pasteurization of cow's milk (90°C for 15 minutes); cooling the milk to 45°C; direct inoculation of milk with starter culture of *Lactobacillus bulgaricus* and *Streptococcus thermophillus* (0.02% w/v); milk active stir for a homogenous culture distribution; direct dosing of fibres in the yogurt jars (varying proportions from 1 to 2.5%); transfer of the inoculated milk over dosed inulin, oat, pea and wheat fibres. After that, the fermentation process was monitored at 40°C, until a pH of 4.6 was reached and the yogurt samples could be stored at 4÷6°C for the next 24 h. Afterwards, the yogurt samples (see coding in table 1) were rheologically analysed.

Methods

In order to study the structural modification of yogurt by fibres addition, a rotational rheometer Thermo Haake Mars was used. The rheological properties (viscosity and shear stress) depending on shear rate (rinsing curve from 0.02 to 100 s^{-1} and descending curve from 100 to 0.02 s^{-1}, at 8°C) were determined. Hysteresis was determined as the area between the curves and the models of Ostwald-de-Waele, Casson, Bingham and Herschel-Bulkley were adjusted for the upward curves. Also, viscosity was measured at a constant shear rate of 100 s^{-1} as a function of time during 10 minutes. Haake RheoWin Data Manager software was employed.

Results and Discussion

Table 1 shows the values of the hysteresis areas (in Pa/s) for the studied yogurt samples. Given the rheological behaviour described by the η (viscosity) and τ (shear stress) curves depending on $\dot{\gamma}$ (shear rate), all samples presented non-Newtonian time-dependent behaviour. The rheograms of yogurts with different amounts of fibres were distinct, indicating the importance of the fibres' type and concentration in the rheological properties of a sample. All analysed samples showed a distinctive hysteresis area, this characteristic being related to the degree of structure breakage of yogurt samples during shearing. The $YP_{2\%}$ sample showed the lowest hysteresis area, 567Pa/s.

Figures 1, 2, 3 and 4 are the graphical representation of the curves of shear stress and viscosity depending on the applied shear rate for yogurt samples with same proportion of different type of fibres (1%, 1,5%, 2% and, respectively, 2,5% inulin, oat, pea and wheat fibres). The areas between the curves represent the samples' hysteresis.

Table 1. Samples' coding and hysteresis values of yogurt samples

Sample coding	Type of addition in sample	Hysteresis (Pa/s)
$WY_{control}$	White yogurt (control sample)	831
$YI_{1\%}$	Yogurt with 1% inulin fibres	879
$YO_{1\%}$	Yogurt with 1% oat fibres	1399
$YP_{1\%}$	Yogurt with 1% pea fibres	755.5
$YW_{1\%}$	Yogurt with 1% wheat fibres	1863
$YI_{1.5\%}$	Yogurt with 1.5% inulin fibres	799.3
$YO_{1.5\%}$	Yogurt with 1.5% oat fibres	1474
$YP_{1.5\%}$	Yogurt with 1.5% pea fibres	580.1
$YW_{1.5\%}$	Yogurt with 1.5% wheat fibres	1749
$YI_{2\%}$	Yogurt with 2% inulin fibres	827.1
$YO_{2\%}$	Yogurt with 2% oat fibres	1350
$YP_{2\%}$	Yogurt with 2% pea fibres	*567*
$YW_{2\%}$	Yogurt with 2% wheat fibres	1496
$YI_{2.5\%}$	Yogurt with 2.5% inulin fibres	1214
$YO_{2.5\%}$	Yogurt with 2.5% oat fibres	2388
$YP_{2.5\%}$	Yogurt with 2.5% pea fibres	691.9
$YW_{2.5\%}$	Yogurt with 2.5% wheat fibres	1589

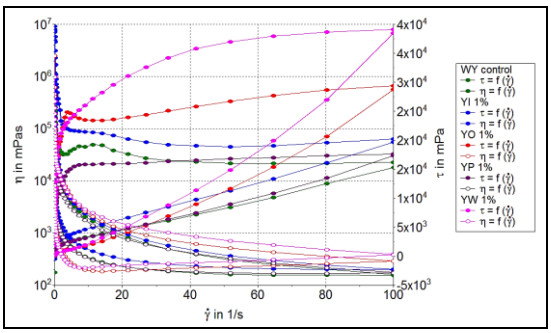

Figure 1. Flow and viscosity curves of yogurt samples with 1% fibres

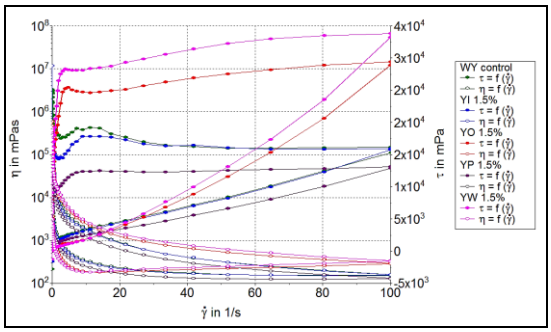

Figure 2. Flow and viscosity curves of yogurt samples with 1.5% fibres

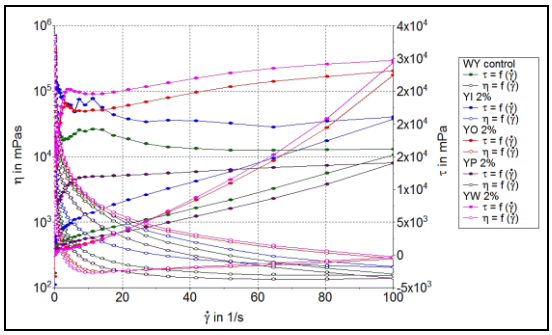

Figure 3. Flow and viscosity curves of yogurt samples with 2% fibres

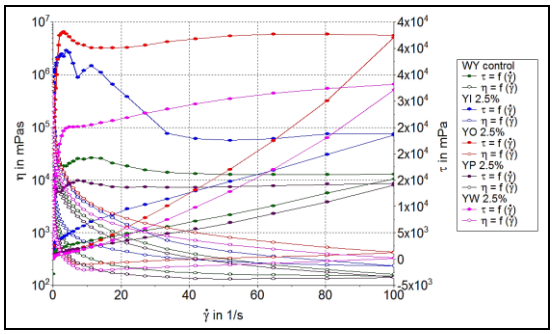

Figure 4. Flow and viscosity curves of yogurt samples with 2.5% fibres

Tables 2 and 3 show the values of the regression coefficient *r* for models adjusted for the upward flow and, respectively, viscosity curves of yogurt samples. The study of formed casein gels microstructure is important for evaluating the yogurt quality and also for obtaining products with well-defined properties. Gel formation can be traced without affecting its structure by dynamic rheology methods at low variations of shear rate. To model the viscosity profile and determine *r* values, consistency index (*k*) and flow index, mathematical models are used: the Power-Law rheological model (Ostwald de Waele), the Herschel-Bulkley model, as well as Bingham and Casson, for modelling visco-plastic components. Decreasing viscosity with increasing shear rate is typical of acidic dairy products. This rheological behaviour is called "shear-thinning". Since the viscosity value depends on the shear rate, there is no absolute viscosity. According to the Ostwald de Waele model, the samples $YW_{1\%}$, $YW_{2.5\%}$, $YO_{1.5\%}$, $YO_{2.5\%}$ had high *r* index, between 0.9989 and 0.9674, explained by the proportional variation of the viscosity depending on the shear rate, on the linearity zone. The $YI_{2.5\%}$ sample showed a small correlation index, $r < 0.2$. The determination of the Bingham model parameters and of the limit viscosity have highlighted that $YO_{2.5\%}$ and $YP_{2.5\%}$ samples had high *r* index, 0.9987 and, respectively, 0.9998. The yogurts are creamier due to the growth of the plastic component. The Herschel-Bulkley model describes the plastic and viscous behaviour (non-newtonian, power law type). According to this model, $YP_{2.5\%}$ sample showed the highest *r* index, $r = 1$. The Casson model highlighted the 0.9835 *r* index for $YW_{1\%}$ sample. The $r > 0.99$ values confirm the appropriate model to characterize the rheological behaviour of yogurts.

Table 2. The regression coefficient (r) for the models adjusted to the flow curves of the samples

Sample	Models adjusted to the flow curves			
	Bingham	Ostwald Weale	Casson	Herschel-Bulkley
$WY_{control}$	0.9424	0.9893	0.9704	0.9942
$YI_{1\%}$	0.4239	0.9120	0.7514	0.9123
$YO_{1\%}$	0.6730	0.9300	0.9212	0.9347
$YP_{1\%}$	0.7093	0.8602	0.8313	0.8811
$YW_{1\%}$	0.7857	0.9894	0.9835	0.9939
$YI_{1.5\%}$	0.2078	0.4108	0.3971	0.4111
$YO_{1.5\%}$	0.6778	0.9338	0.8114	0.9364
$YP_{1.5\%}$	0.6407	0.6246	0.7204	0.7268
$YW_{1.5\%}$	0.6665	0.9523	0.8036	0.9684
$YI_{2\%}$	0.5037	0.5253	0.5810	0.5386
$YO_{2\%}$	0.7236	0.9155	0.8335	0.9156
$YP_{2\%}$	0.7814	0.8548	0.8788	0.9022
$YW_{2\%}$	0.7070	0.9220	0.8310	0.9223
$YI_{2.5\%}$	0.7416	0.2866	0.6861	0.3010
$YO_{2.5\%}$	0.4973	0.8766	0.6695	0.9121
$YP_{2.5\%}$	0.5013	0.7766	0.6526	0.7767
$YW_{2.5\%}$	0.7309	0.9674	0.8523	0.9731

Table 3. The regression coefficient (r) for the models adjusted to the viscosity curves of the yogurt samples

Sample	Models adjusted to the viscosity curves			
	Bingham	Ostwald Weale	Casson	Herschel-Bulkley
$WY_{control}$	0.9879	0.9471	0.8690	0.9930
$YI_{1\%}$	0.3373	0.9888	0.9806	0.9900
$YO_{1\%}$	0.9715	0.9936	0.9643	0.9967
$YP_{1\%}$	0.3800	0.9484	0.9483	0.9957
$YW_{1\%}$	0.9404	0.9902	0.9656	0.9967
$YI_{1.5\%}$	0.9756	0.9464	0.8980	0.9892
$YO_{1.5\%}$	0.9970	0.9989	0.8460	0.9988
$YP_{1.5\%}$	0.9925	0.9265	0.9600	0.9937
$YW_{1.5\%}$	0.9805	0.9880	0.9120	0.9891
$YI_{2\%}$	0.9507	0.9588	0.9342	0.9897
$YO_{2\%}$	0.9553	0.9724	0.9036	0.9776
$YP_{2\%}$	0.9951	0.9953	0.9218	0.9953
$YW_{2\%}$	0.9903	0.9907	0.9264	0.9907
$YI_{2.5\%}$	0.9922	0.9388	0.9587	0.9985
$YO_{2.5\%}$	0.9987	0.9985	0.9737	0.9990
$YP_{2.5\%}$	0.9998	0.9190	0.9715	1.000
$YW_{2.5\%}$	0.9916	0.9922	0.9127	0.9923

The variation of viscosity versus time at a constant shear rate for yogurt samples with same concentration of inulin, oat, pea and wheat fibres is graphically represented in figures 5, 6, 7 and 8 (1%, 1.5%, 2% and, respectively, 2.5% fibres addition).

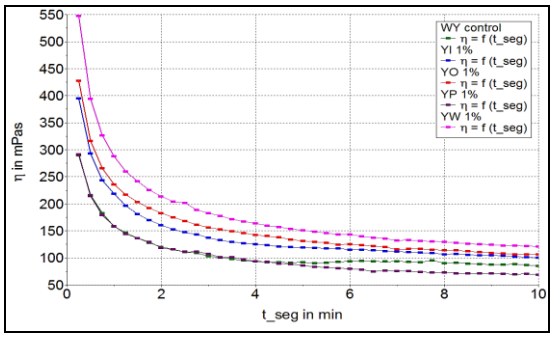

Figure 5. Curve of viscosity versus time of testing thixotropy of yogurt samples with 1% fibres

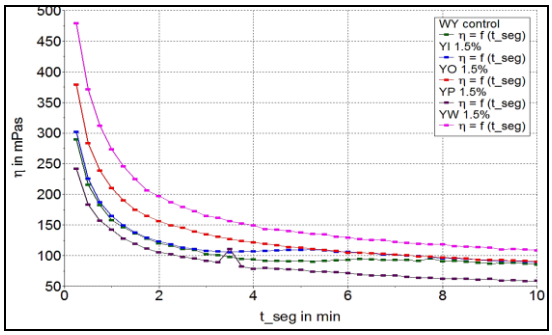

Figure 6. Curve of viscosity versus time of testing thixotropy of yogurt samples with 1.5% fibres

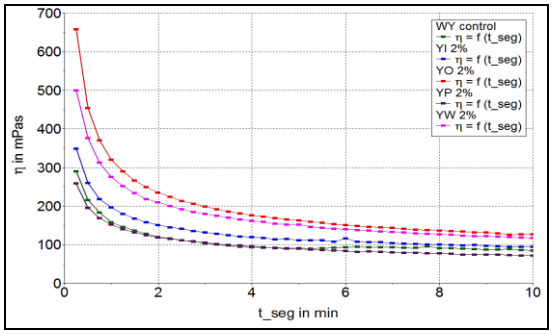

Figure 7. Curve of viscosity versus time of testing thixotropy of yogurt samples with 2% fibres

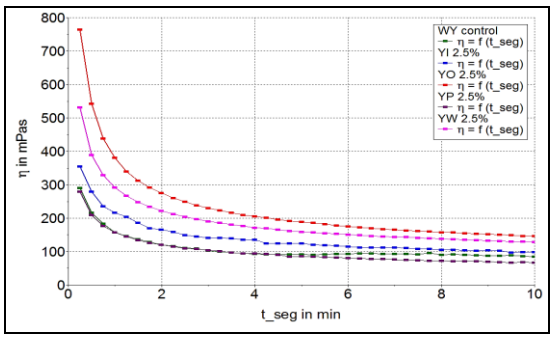

Figure 8. Curve of viscosity versus time of testing thixotropy of yogurt samples with 2.5% fibres

There was observed a decrease in viscosity over time, at constant shear rate for all yogurt types. The smallest changes in time viscosity were recorded by yogurts with added oat and wheat fibres, for all amounts of fibres added in yogurt (YW and YO).

Concluding remarks

All samples showed behaviour of non-Newtonian and pseudo- plastic fluid. The smallest changes in time of viscosity were recorded by yogurts with added oat and wheat fibres, for all amounts of fibres added in yogurt (YW and YO). All the fibres obtained as a by-product of industrial food processing were compatible with the yogurt manufacturing process, so the enriched yogurt would be considered an alternative to incorporate fibres in the human diet.

Acknowledgement

This work was supported by a grant of the Romania National Authority for Scientific Research and Innovation, CNCS/CCCDI – UEFISCDI, project number PN-III-P2-2.1-BG-2016-0089, within PNCDI III.

References

1. Gahruie, H.H., et al. (2015). In Food Science and Human Wellness, vol. 4, pp. 1–8.
2. Dhingra, D., Michael, M., Rajput, H., Patil, R.T (2012). In Journal of Food Science and Technology, vol. 49, issue 3, pp. 255–266.
3. Tejada - Ortigoza, V., Garcia - Amezquita, L.E., Serna - Saldivari, S., Welti - Chanes, J. (2016). In Food Engineering Reviews, vol. 8, pp. 251–271.
4. Hashim, I.B., Khalil, A.H., Afifi, H.S. (2009). In Journal of Dairy Science, vol. 92, pp. 5403–5407.
5. Dello Staffolo, M., Bertola, N., Martino, M., Bevilacqua, A. (2004). In International Dairy Journal, vol. 14, pp. 263-268.
6. Crispín-Isidro., G., *et al.* (2015). In LWT - Food Science and Technology, vol. 62, pp. 438-444
7. Espírito-Santo, A.P., *et al.* (2013). In Food Research International, vol. 50, pp. 224-231.

Contact Address:

Adriana Dabija
adriana.dabija@fia.usv.ro
Faculty of Food Engineering, Stefan cel Mare University of Suceava
Address: Universitatii Street, 13, Suceava, Romania
Telf. :- ; Fax: 0040230216 / 0040230520080

Influence of fortification with vegetable and fruit powder on the rheological and physicochemical properties of yoghurt

S. Ropciuc, A. Dabija, A. M. Sidor, M. A. Oroian

Stefan cel Mare University of Suceava, Faculty of Food Engineering, Suceava (Romania)

Introduction

Rheology is the study of deformation and flow of food materials [1]. Yogurt is an acid dairy product with complex rheology that depends on the temperature of the product at the time of determination, the concentration of solids and the physical state of fats and proteins. Out of all fermented dairy products, yogurt is the most known and consumed product. It is easy to digest, has high nutritional value and is a rich source of carbohydrates, proteins, lipids, vitamins, calcium and phosphorus [2]. Natural yoghurt is obtained by adding certain cultures of lactic bacteria that cause irreversible changes: they increase the acidity of the milk, form the specific flavor, and give yogurt specific texture. The fundamental procedure in the conversion of milk to yoghurt is accumulation of casein micelles into athree-dimensional network structure. Casein represents about 80% of the total content of bovine milk protein and includes four main fractions: αs1, αs2, β and k [3].

You should arrange your contribution in the following order: Yoghurt may have two initial defects: the difference in viscosity and/or the serum expulsion (syneresis). The viscosity and syneresis characteristics of dairy products are controlled by adding vegetal materials in the form of powders that act as lipids replacers. These vegetal powders interact with the casein network and contribute to the formation of gels in two phases (liquid-solid). Fortification of yoghurt with vegetal materials powders (fruits or vegetables) has seen a significant increase in the last few years. The purpose of this study was to add vegetable and fruit powder in yogurt (seabuckthorn and carrot, peas and brier) to improve the viscosity, syneresis and chemical composition of yogurt. The search for a healthier diet becomes more and more widespread all over the world. Consumers are concerned about their health and wellbeing. An increasing demand for healthy products in the dairy products market leads to the production of functional foods by intake of protein, folic acid, vitamins A, B and minerals. The sea buckthorn (*Hippophae rhamnoides* L.) is rich in vitamin C, vitamins E, K, F, P, complex B (B2, B6, B9), carotenoids (beta carotene, xanthophylla), minerals and trace elements, polyunsaturated fatty acids, complex oils, pectins, tannins, amino acids, enzymes, phytosterols. It has antioxidant properties, it is depurative, anti-inflammatory and healing.

Carrot powder (*Daucus carota*) is an insoluble fiber rich in carotene, β-carotene, potassium, magnesium and vitamin C. Carrot is low in calories and lipids. The addition of pea powder (Pisum sativum L.) strengthens yogurt due to the high content of soluble sugars, proteins, vitamin K, vitamin B6, mineral salts, carbohydrates. It reduces the risk of cardiovascular disease, controles cholesterol levels in the blood and blood pressure and prevents heart rhythm disturbances. It gives yogurt sweet and fresh taste. Brier (*Rosa canina L.*) powder improves the chemical composition of yogurt via the vitamin complex (C, A, B1, B2), improves peripheral circulation. These powders added to the yoghurt modify the consistency and viscosity, the chemical composition and the caloric value together with the increased consumer acceptability.

The purpose of rheological analysis of yogurt samples with the addition of vegetal powders is to check the stability of the gel under the action of shear forces and to determine the optimal percentage of powder in the recipe. The viscosity of gels, like yoghurt, is non-Newtonian. Decreasing viscosity with increasing shear rate is typical for gels of acidic dairy products. Potential changes in the physicochemical and rheological characteristics were determined 24 hours after the yogurt was obtained and refrigerated samples were stored.

Materials

Obtaining yogurt samples with addition of vegetal powder

Yoghurt was developed and produced in the Microbiology Laboratory at the University of Food Engineering in Suceava.

Yoghurt samples were obtained from UHT milk with a fat content of 3.5%, the Rich® (Chr Hansen) original cultures (1 g L-1) containing a superconcentrated culture of the two strains of lactic acid bacteria Lactobacillus Bulgaricus and Streptococcus thermophilus.

Vegetable matter powders (seabuckthorn, carrot, peas and brier) were obtained by drying at a temperature of 55-60 ° C to a constant mass. They were then milled and sieved through a vibrating screening system. Granules of vegetal material powder were used ≤ 300 µm. Yoghurt was obtained using the following percentages of vegetal materials, according to Table 1.

Table 1. Percentage of addition of vegetal powder in yogurt

Sample	seabuckthorn : carrot (%)	peas : rosehip (%)
Ycontrol	0	0
Y_1	0.8 : 0.1	2 : 0.2
Y_2	0.8 : 0.2	2 : 0.4
Y_3	0.8 : 0.3	2 : 0.6
Y_4	0.8 : 0.4	2 : 0.8
Y_5	0.8 : 0.5	2 : 1
Y_6	0.8 : 0.6	2 : 1.2

The milk sample was heated to 38-40 °C where the lactic culture and the percentages of powder were mixed. The fermentation was done in a thermostat at 40 ° C. During the fermentation, at intervals of 30 minutes, the pH was monitored by direct measurement of the pH value using the Mettler Toledo. When the pH value reached 4.6, the process was stopped and the yogurt was cooled to 4 ° C and stored at this temperature. The yogurt obtained falls within the group of dense acidic products [5].

Physico-chemical and rheological determinations were done after 24 hours of storage at 4 ° C.

Experimental methods

pH determination was done after 24 hours of refrigerated sample storage by direct reading of the pH value using the pH meter.

Determination of the acidity of the yoghurt with added vegetal powder was carried out by titration with sodium hydroxide in 10 g of yoghurt sample mixed with 10 ml of distilled water.

Calculation:

$$A = \frac{V \times 0.9}{m} \times 100, g\ acid \frac{lactic}{100g}$$

Where: V is the volume (in ml) of 0.1 M sodium hydroxide, m is the mass (in g) of the sample and 0.9 is the conversion factor of the lactic acid. The result was expressed in g of lactic acid / 100 g of product.

Syneresis was determined by measuring the water-holding capacity by the procedure reported by Guzmán-González, Morais [4]. A sample of about 20g of yoghurt (Y) was centrifuged at 1250 x g for 10 min at 4 °C. The whey expelled (W) was removed and weighed. The waterholding capacity (WHC, gxkg−1) was calculated as: WHC = (Y – W) /Y x 1000.

Color determination of yogurt samples was carried out with a Konica Minolta CM-3500d spectrocolorimetry (Konica Minolta Business Technologies, Inc., Tokyo, Japan) and the results were expressed in accordance with the CIELAB system. The parameters determined were L* [L* = 0 (black) and L* = 100 (white)], a* (-a* = greenness and +a* = redness), b* (-b* = blueness and +b* = yellowness).

Rheometry analysis was performed in triplicate with a Thermo Haake MARS rotational rheometer, equipped with geometry plate/plate of 40mm diameter and a gap of 1mm. Shear rate was increased from 0.02 s^{-1} to 100.0 s^{-1} and then decreased from 100.0 to 0.02 s^{-1}. Temperature control was carried out with a Haake Mars Peltier. Temperature was fixed at 8 ºC for all analyses.
Before performing the assay, samples were mixed twice and then a sample for rheological determination was collected.

Results and Discussion

1. pH and acidity

In foods, the acidity indicates the content of free acids and other chemical compounds, due to this, in an acidic food as the yogurt; a decrement of pH indicates the release of lactic acid (hydroniumions H_3O^+) in the medium by lactic acid bacteria (LAB). Results for determinations of pH and acidity (Table 2) showed no significant differences between fresh formulations with powder addition and no differences were observed respect to the control. In the overall analysis for pH and acidity of all samples, no significant differences were found because the fortified. yogurts have the same characteristics as the control yogurt.

Table 2. Physicochemical properties of fortified yoghurt

Samples	pH	Acidity, Lactic acid /%	Syneresis (g/100 mL)	Color values			Samples	pH	Acidity, Lactic acid /%	Syneresis (g/100 mL)	Color values		
				*L**	*a**	*b**					*L**	*a**	*b**
Yogurt control S+ C	4.19	0.9612	42.49	85.77	-7.00	11.59	Yogurt control P+R	4.04	1.094	34.43	86.42	-7.21	12.42
Y_0.8 S+0.1 C	4.17	1.081	43.70	79.72	-3.63	13.72	Y_ P+0.2 R	4.06	1.114	38.83	80.75	-4.24	14.97
Y_ 0.8 S+0.2 C	4.14	1.089	48.20	78.17	-3.25	13.47	Y_ 2 P+0.4 R	4.02	1.133	23.78	79.96	-3.18	16.92
Y_ 0.8 S+0.3 C	4.10	1.130	45.01	78.74	-2.11	14.59	Y_ 2 P+0.6 R	3.97	1.171	36.26	78.35	-2.49	18.28
Y_ 0.8 S+0.4 C	4.07	1.171	43.68	78.95	-2.24	13.67	Y_ 2 P+0.8 R	3.99	1.230	38.48	77.52	-2.08	18.57
Y_ 0.8 S+0.5 C	4.09	1.211	43.60	78.73	-1.86	14.47	Y_ 2 P+1 R	3.91	1.218	31.23	76.32	-1.47	19.81
Y_ 0.8 S+0.6 C	4.12	1.219	43.26	76.98	-0.70	15.45	Y_ 2 P+1.2 R	3.96	1.253	26.77	75.34	-1.02	20.42

S- (seabuckthorn); C- (carrot); P- (peas); R- (rosehip)

The decrease in pH during the storage was due to the production of lactic acid by the bacteria present in the yogurt. The acidity of the yogurt in the samples with added peas and rosehip increases slightly compared to buckthorn and carrot samples. Drago and Valencia (2002), they reported values of acidity higher than 1.0 for a yogurt enriched with asparagus fibre.

2. Syneresis it is an important attribute in determining the quality of yogurt and other dairy products Yogurts fortified with vegetable powder. The samples fortified with powder were more stable; this can be attributed to the size of the protein and the presence of fibres, which promotes water retention due to its gel-like structure.

Syneresis showed significant differences (Table 2), increasing significantly in all samples. This effect may be related to a decreasing of pH below 4.6, that contributes to caseins rearrangement and water release.

3. The comparative statistical analysis of the three color parameters based on the Hunter scale, for all samples are included in Table 2. For the L, a* and b* parameters, found in the fresh samples fortified with seabuckthorn and carrot the control, added to the formulation is brown, it produced a decrease in luminosity (L), a significant decrease in the parameter a* which indicates a tendency to brown, and a increase in the parameter b*. The addition of pea and rose powder colours the yogurt in red, lowers the brightness, lowers the white color of a* and increases parameter b*.

4. Flow properties

The viscosity values as a function of the shear rate for the white yogurt and the yogurts enriched with various types of seabuckthorn and carrot fibre showed that within the range of shear rates studied the flow curves occur in the pseudoplastic zone; in other words, viscosity decreases with increased shear rate.

In the present work. hysteresis loop areas were larger for the fortified yogurt in comparison with the control sample yogurt.

Hysteresis loop areas increases with the increase in the amount of plant powder added per unit volume (Figure 1 and Figure 2).

This can be revealed from the increase in the area of hysteresis loops based on the increase in the plant powder content. Addition of vegetable powder also resulted in an overall increased in compactness of the yoghurt microstructure. The values of hysteresis loop area ranged from 580.3 to 1402 for seabuckthorn addition and carrot and from 566.6 to 1238 for peas and rosehip addition.

Table 3. Effect of sample in rheological parameters

Sample	Hysteresis (Pa/s)	μ_final /μ_initial, %	Sample	Hysteresis (Pa/s)	μ_final/ μ_initial, %
Y_Control	580.3	8.047	Y_Control	566.6	9.084
Y_ 0.8 S+0.1 C	864.2	9.410	Y_ 2 P+0.2 R	547.4	8.386
Y_ 0.8 S+0.2 C	1125	9.354	Y_ 2 P+0.4 R	819.5	10.451
Y_ 0.8 S+0.3 C	1019	13..10	Y_ 2 P+0.6 R	1223	13.647
Y_ 0.8 S+0.4 C	848	12.199	Y_ 2 P+0.8 R	829.1	13.063
Y_ 0.8 S+0.5 C	844.7	25.130	Y_ 2 P+1 R	1238	16.380
Y_ 0.8 S+0.6 C	1402	31.979	Y_ 2 P+1.2 R	937.8	19.046

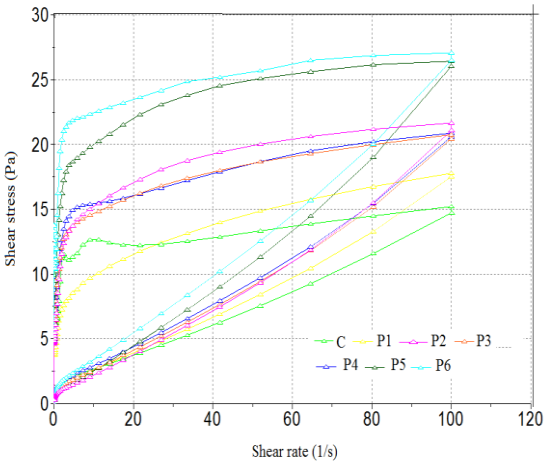

C- yogurt control; P1-0.8 S+0.1 C; P2-0.8 S+0.2 C; P3-0.8 S+0.3 C; P4-0.8 S+0.4 C; P5- 0.8 S+0.5 C; P6- 0.8 S+0.6 C

Figure 1. Hysteresis loop of the yogurt sample with different levels of seabuckthorn and carrot vegetable powders.

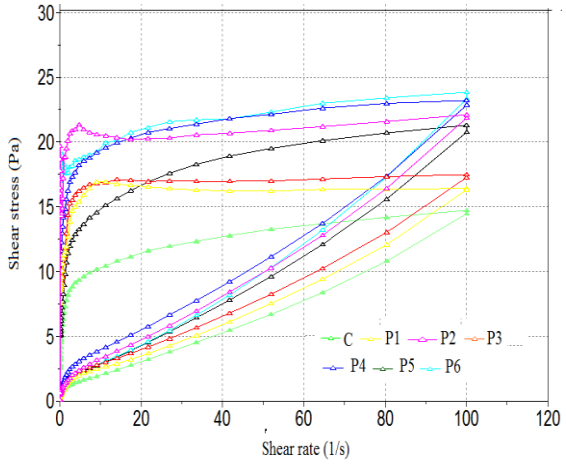

C- yogurt control; P1- 2 P+0.2 R; P2- 2 P+0.4 R; P3- 2 P+0.6 R; P4-2 P+0.8 R; P5- 2 P+1 R; P6- 2 P+1.2 R

Figure 2. Hysteresis loop of the yogurt sample with different level of vegetable powder from peas and rosehip.

Conclusions

Yogurts fortified with different vegetable and fruit fibers with a functional food role were evaluated. Analysis of physico-chemical and rheological properties was carried out on samples kept in the refrigerator for 24 hours. pH and acidity did not change significantly when the plant powders were added. Significantly different values were reported in color parameters. Syneresis decreased significantly in some samples with the addition of peas and rosehip. The viscosity of the yoghurt samples is optimal with an addition of 1.2% horseradish powder and 2% pea's powder. For the addition of seabuckthorn powder. the optimum is recorded with the addition of 0.8% seabuckthorn powder and 0.2% carrot powder.

Acknowledgements

This work was supported by a grant of the Romanian National Authority for Scientific Research and Innovation. CNCS/CCCDI – UEFISCDI. project number: PN-III-P2-2.1-BG-2016- 0089 within PNCDI III.

References

1. W. J. Lee and J. A. Lucey. (2010). Formation and Physical Properties of Yogurt. Asian-Aust. J. Anim. Sci. 23(9). 1127-1132.
2. S.. Drago & M. E. Valencia (2002). Effect of fermentation on iron zinc and calcium availability from iron-fortified dairy products. Journal of Food Science 67. 3130- 3134.
3. Y.Morvarid. L.. Nateghi. A.. Elham (2013). Effect of different concentration of fruit additives on some physicochemical properties of yoghurt during storage. Annals of Biological Research. 4(4). 244-249.
4. Z. Tarakci (2010). Influence of Kiwi Marmalade on the Rheology Characteristics. Color Values and Sensorial Acceptability of Fruit Yogurt. Kafkas Üniversitesi Veteriner Fakültesi Dergisi. Kafkas Univ Vetriner Fakul Dergisi16 (2) 173-178

Contact address
sorina.ropciuc@fia.usv.ro
Food Engineering
Stefan cel Mare University of Suceava
Telf.: +40 230 216147
Fax: +40 230 523267

The effect of cooking procedures on the rheological properties of olive oils

A. Bettencourt, C. Marques, L. Pinheiro

Research Institute for Medicines (iMed.ULisboa), Faculty of Pharmacy, Universidade de Lisboa (Portugal)

Introduction

Extra virgin olive oil (EVOO), obtained from the fruit of the olive tree by mechanical or physical processes under thermal settings that do not lead to modifications, is a key bioactive food for its health beneficial effects, being part of the mediterranian diet [1-6]. EVOO is a complex mixture composed mainly by triglycerides and a minor unsaponificable fraction, the latter constituted by squalene, sterols, terpenic and aliphatic alcohols, polyphenols, tocopherols, pigments and volatile compounds. EVOO overall therapeutic characteristics can be ascribed to the fatty acid profile (high in monounsaturated fatty acids such as oleic acid) and its content in antioxidant tocopherols and polyphenols [1,2,4,5].

The use of raw EVOO added to foods after cooking (or as a salad dressing) is the best way to express the original flavour and to maximize the intake of the compounds accountable for its bioactivity. However, other cooking methods involving EVOO include also microwave heating and frying. With regard to the latter, the exposure to water (from foods) and to atmospheric oxygen, the high temperatures (about 180 ºC) and the repeated heating cycles associated with frying can lead to physical, chemical and biological changes. Under these circumstances, EVOO experience oxidation, polymerization, hydrolysis, cyclization, and isomerization [7-10], which may impair the nutritional and sensory properties.

While frying is the most studied cooking method, studies dealing with the EVOO subject to other conditions (e.g. soup preparation and stewing, using temperatures around 100ºC) are less common.

One of the consequences of the abovementioned thermal degradation of EVOO is an increase in viscosity, which depends on the chain lengths of triglyceride fatty acids and saturation/unsaturation [11]. Viscosity is an essential rheological descriptor in olive oil quality control, being highly correlated with its sensory properties and structural evaluation. Thus among the different quality properties, viscosity of EVOO can be indicative of microstructural changes and allow understanding in more detail the mechanisms of olive oil degradation after thermal treatment in distinct cooking processes [11,12]. It has been well recognized that viscosity depends strongly on temperature [11,12], and also on shear rate, both being sensitive parameters for the appropriateness of EVOO in the frying process.

In this study, the effect of temperature on the rheological behaviour of four Portuguese EVOO samples was evaluated, before and after different simulated cooking conditions.

Experimental

Four commercial Portuguese extra virgin Protected Designation of Origin olive oils were purchased from a local supermarket: one monovarietal (Norte Alentejo, hereinafter represented as A) and three resulting from a mixture of several cultivars (Trás-os-Montes, Moura and Ribatejo, hereinafter represented as T, M and R, respectively).

Viscosity measurements of EVOO samples were assessed with a programmable Brookfield LVDV II+Pro digital viscometer using spindle S61.

Experiments were carried out in two categories to explore viscosity changes based on cooking processes and temperature. In the first (Test A), within the rotating speed range of 6-90 rpm, the samples were subjected to different heating temperatures (20, 60, 100 and 180 ºC) during a period of thirty minutes to simulate different cooking conditions and, after cooling, the viscosity was measured at 20 ºC; for the 180 ºC, three heating cycles were performed. In the second experimental setting (Test B), viscosity data was collected for six temperatures (from 20 ºC to 70 ºC), at varying rotating speed in the range 15-80 rpm.

The effect of temperature on the EVOO samples viscosities followed an Arrhenius-type model, enabling the calculation of the activation energy (Eq. (1)):

$$\eta = \eta_0 \exp(E_a/RT) \quad (1)$$

where η is the viscosity (Pa.s), η_0 the pre-exponential constant (Pa.s), E_a the flow activation energy (J/mol), R the universal gas constant (8.314 J/mol K), and T the absolute temperature (K).

Results and Discussion

Regarding the results obtained from Test A (heating and cooling process), all samples exhibited a newtonian behaviour (illustrated in Figure 1) as already observed by other type of EVOOs [9,13].

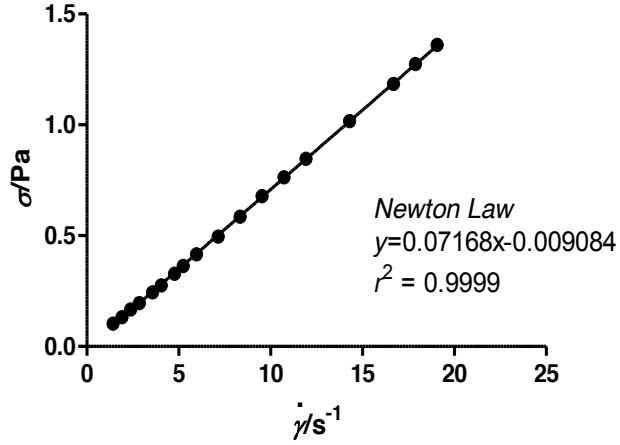

Figure 1. Olive Oil "Norte Alentejo" behavior after being subjected to 100 ºC (rotating speed range of 6-90 rpm); n=3.

The observed behaviour was obtained by plotting shear stress (σ) against shear rate ($\dot{\gamma}$) of each sample data, considering the slope as the dynamic viscosity (η) of olive oil at experimental temperature, according to Newton´s law of flow (Eq.(2)) [13]:

$$\sigma = \eta \dot{\gamma} \quad (2)$$

Furthermore, Figure 2 shows that among the tested EVOOs, olive oil A shows the higher value of viscosity at room temperatute (20ºC), suggesting a stronger attraction force between its molecules. Considering that in the production process of EVOOs, the higher viscosity is related to the difficulty in pumping, higher energy costs will be involved in the production process of olive oil A. On the other hand, considering EVOO transference through pumps, pipes and valves, the higher the viscosity, the more careful actions must be taken in order to avoid turbulence and shaking, which may cause large energy dissipation, air absorption and emulsion formation, compromising its sensory properties [15].

EVOO's average viscosity after heating/cooling process was similar for T and M olive oils, for all the tested temperatures (Figure 2). Both EVOO´s showed a decrease in viscosity at 60ºC. On the contrary, olive oils A and T showed a viscosity increase at 60ºC. Interestingly, viscosity values at 100 and 180ºC did not differ significantly between the different tested EVOO´s. The interpretation of these results is not straightworth as many physico-chemical parameters may change with temperature (as density, pH, phenol content, etc) and will affect the viscosity of each olive oil [13,16]. Nevertheless, differences among EVOOs suggests that different cooking procedures may have distinct effects on their properties that deserve further evaluation.

Results regarding the changes in viscosity after being subjected to 3 heating cycles (180 ºC) show that for olive oils A and T the viscosity does not significantly change after the 1st and 2nd frying cycles, but shows an increase after the 3rd cycle, (Table 1). On the other hand, the viscosity increase after each cycle is greater for olive oil R. Olive oil M presents the smaller viscosity changes with different frying cycles. As changes in viscosity can be related to degradation mechanisms in the EVOO compounds namely fatty acid levels [11], it may be indicative of microstructural changes and the suitable of the oils for frying purposes. Thus, the present study suggests that in particularly, the olive oils from "Norte Alentejo" "Tras-os-Montes" and "Ribatejo" are not suitable to be used in different frying cycles.

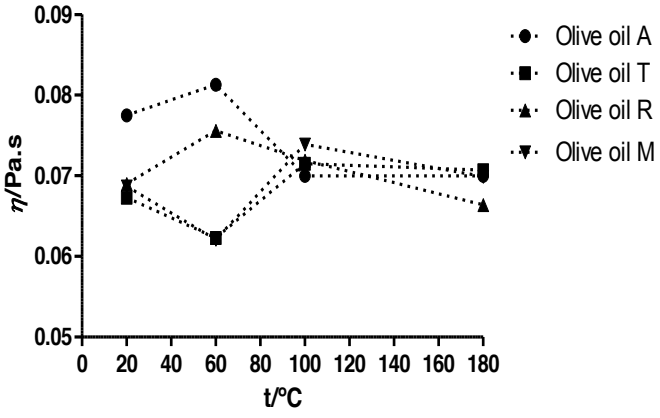

Figure 2. EVOO's average viscosity after heating/cooling process (rotating speed range of 6-90 rpm) for each studied heating temperature. A=Norte Alentejo; B = Trás-os-Montes; R = Ribatejo; M = Moura; n=3.

Table 1. EVOO's average viscosity after 3 cycles at 180 ºC (rotating speed range of 6-90 rpm). A=Norte Alentejo; B = Trás-os-Montes; R = Ribatejo; M = Moura; n=3.

	η (Pa.s)		
Type of Olive Oil	***1st***	***2nd***	***3rd***
A	0.0721	0.0733	0.0776
T	0.0723	0.0717	0.0749
R	0.0681	0.0738	0.0777
M	0.0750	0.0760	0.0777

The second experimental setting (Test B) evaluated the effect of temperature on viscosity. An exponential decreased in dynamic viscosity as a function of temperature was observed and experimental data was fitted to an Arrhenius-type model viscosity (Eq. 1). This is a significant relationship in terms of the production process of olive oil, resulting from the energy obtained to overcome the resistance to flow, which may be due to the atractive forces among the olive oil molecules. The activation energy gives a direct estimation of the sensitivity of olive oil to quality degradation factors. Results showed that flow activation energy values presented slightly differences among samples in terms of temperature sensibility (Table 2).

Table 2. Fitting of the Arrhenius-type model to experimental data (20, 30, 40, 50, 60, 70 ºC, in the linearized form of Eq (1)); rotating speed range of 15-80 rpm. A=Norte Alentejo; B = Trás-os-Montes; R = Ribatejo; M = Moura; *n*=3

Type of Olive Oil	η_0 (Pa.s)	E_a (kJ/mol)	r^2
A	1.6072E-06	25.9629	0.9986
T	2.7802E-06	24.4723	0.9949
R	2.4097E-06	24.8713	0.9924
M	2.7913E-06	24.5088	0.9968

The effect of temperature on viscosity may be explained by an increase in the thermal movement of the molecules decreasing the intermolecular forces of attraction and consequently the viscosity of the EVOOs [17].

The increase in flow energy shows the sensibility of viscosity to changes in temperature [11,16] meaning that small fluctuations will have a high effect. Table 2 shows that among the tested EVOOs, the highest value of flow energy is of olive oil A, suggesting a higher content in monounsaturated fatty acids [16]. This fact means that it will be the one more influenced by temperature changes and consequently it should be used with care in cooking procedures that involves high temperatures.

Conclusion

It´s important to note that viscosity variations for each EVOOs changed among them, meaning that different cooking techniques (even the more aggressive ones, at 100 or 180 ºC) will not have the same effect on olive oils nutritional properties. As for the determination of activation energies, results suggest that the combined effects of temperature and shear stress lead to unsaturation of EVOO samples, expressed by a decrease of the viscosity values. The present study shows that rheological evaluation can be an important tool in the context of the EVOOs quality control and safety assessment.

Acknowledgments

This work was supported by FCT - *Fundação para a Ciência e Tecnologia, Portugal* (PEst-OE/SAU/UI4013/2014).

References

1. Owen, R.W., Giacosa, A., Hull, W.E., Haubner, R., Spiegelhalder, B. and Bartsch, H. (2000). Eur. J. Cancer. 36, 1235-124.
2. Capannesi, C., Palchetti, I., Mascini M. and Parenti, A. (2000). Food Chem. 71, 553–562.
3. Silva, L., Pinto, J., Carrola, J. and Paiva-Martins, F. (2010). Food Chem. 121, 1177–1187.
4. Garcia, B., Magalhães, J., Fregapane, G., Salvador, M.D. and Paiva-Martins, F. (2012). Eur. J. Lipid Sci. Technol. 114, 1070–1082.
5. Sousa, C., Gouvinhas, I., Barreira, D., Carvalho, M.T., Vilela, A., Lopes, J., Martins-Lopes, P. and Barros, A.I. (2014). J. Am. Oil Chem. Soc. 91, 599–611.
6. Abedinzadeh, S., Torbali, M., and Azadmard-Damirchi, S. (2016). Adv. Pharm. Bull. 6, 597–606.
7. Bester, E., Butinar, B., Bucar-Miklavcic, M. and Golob, T. (2008). Food Chem. 108, 446–454.
8. Casal, S., Malheiro, R., Sendas, A., Oliveira, B.P.P. and Pereira, J.A. (2010). Food Chem. Toxicol. 48, 2972–2979.
9. Bonnet, J-P., Devesvre, L., Artaud, J. and Moulin, P. (2011). Eur. J. Lipid Sci. Technol. 113, 1019–1025.
10. Martinez-Pineda, M., Ferrer-Mairal, A., Vercet, A. and Yagüe, C. (2011) . CyTA – J. Food. 9(4), 301–306.
11. Ashrafi, N. (2012). Appl. Rheol. 22, 34203.1-34203.7.

12. Kalogianni, E.P., Karapantsios, T.D. and Miller, R. (2011). J. Food Eng. 105, 169–179.

13. Gila, A., Jiménez, A., Beltrán, G. and Romero, A. (2015). Eur. J. Lipid Sci. Technol. 117, 366–376.

14. Faustino, C., Bettencourt, A.F., Alfaia, A., and Pinheiro, L. (2015). J. Chem. Educ. 92, 936–939.

15. Abramovic, H., and Klofutar, C. (1998). Acta Chim. Slov. 45(1), 69-77.

16. Escudero, A., Ramos, N., La Rubia, M.D. and Pacheco, R. (2016). J. Anal. Methods Chem. 1-10.

17. Kim, J., Kim, D.N., Lee, S.H., Yoo, SH. and Lee, S. (2010). Food Chem. 118, 398–402.

Contact Address:

asimao@ff.ulisboa.pt (Ana Bettencourt) and
lpinheiro@ff.ulisboa.pt (Lidia Pinheiro)
Department of Toxicological and Bromatological Sciences
Faculty of Pharmacy, University of Lisbon
Av. Prof. Gama Pinto, 1649-003 Lisbon, Portugal
Telf.: +351 217946400; Fax: +351 217946470

Viscosity Profile of Selected Monofloral Portuguese Honeys

L. Pinheiro, J. Gonçalves, C. Faustino

Research Institute for Medicines (iMed.ULisboa), Faculty of Pharmacy, Universidade de Lisboa (Portugal)

Introduction

Honey has been used for nutrition and medicinal purposes throughout the centuries, mainly due to its antioxidant, anti-inflammatory and antimicrobial properties [1,2]. Honey is a highly viscous supersaturated solution of sugars (mainly fructose and glucose) with low water content (usually below 20% w/w) and minor concentrations of bioactive compounds, including phytochemicals, organic acids, amino acids, proteins, vitamins and minerals [1].

The viscosity of honey is an important rheological parameter that influences the sensory properties of the product, such as appearance, texture, consistency and flavor release [3]. The flow properties and the rheological behavior of honey are key parameters for quality control, manufacturing processes, stability and storage [4]. Viscosity and rheological properties of honey are mainly influenced by temperature and physicochemical properties, such as moisture, sugar content and degree of crystallization, presence of colloidal material and pollen grains, which in turn are strongly dependent on honey floral origin, geographical location, climate, harvesting process, storage conditions and aging [1,5].

Most honeys described in the literature have been characterized as Newtonian fluids at a wide range of temperatures [6–8], however non-Newtonian behavior has also been observed, mainly for manuka, heather, buckwheat and eucalyptus honeys [9–12]. Colloidal substances, such as high protein content, have been held responsible for the shear-thinning and thixotropic behavior of heather and buckwheat honeys [10] while the shear-thickening behavior of some *Eucalyptus* sp. honeys has been attributed to the presence of polymeric dextran [9,11]. Although physicochemical characterization of some Portuguese raw honeys and commercial honeys has been achieved [13–15], limited and scarce information is available regarding their rheological properties.

Experimental

Commercial Portuguese orange blossom, eucalyptus, lavender and heather monofloral honeys were purchased from a local supermarket in Lisbon. Viscosity measurements of honey samples were performed at varying shear rates in the range 0.5–60 rpm with a programmable Brookfield LVDV-II+Pro digital viscometer using spindle S64. The viscosity measurements were performed at 20 °C in the original containers of each sample and shear rate was determined according to Eq. (1):

$$\dot{\gamma} = 2\omega R_c^2 R_s^2 / [r^2 (R_c^2 - R_s^2)] \qquad (1)$$

where $\dot{\gamma}$ is shear rate (s^{-1}), R_c and R_s are the container and the spindle radius (cm), respectively, ω is angular velocity (which depends on the number of revolutions of the spindle per minute) and r (cm) is radius at which shear rate is being determined [16].

Results and Discussion

The Portuguese commercial honey samples studied were monofloral honeys from different botanical and geographical origins (Table 1).

Table 1. Characterization of the Portuguese monofloral honeys at 20ºC

Honey	Orange blossom	Lavender	Eucalyptus	Heather
Floral origin	*Citrus* spp.	*Lavandula* spp.	*Eucalyptus* spp.	*Erica* spp.
Region	Algarve	Serra Malcata	Beira Litoral	Serra Estrela
Color	Light amber	Light amber	Amber	Dark amber
Water (% w/w)	15.7	15.9	16.5	16.0
Total soluble solids (ºBx)	82.5	82.2	81.6	81.8
pH	3.50	3.43	3.56	4.18
Electrical conductivity (mS/cm)	0.256	0.215	0.385	0.609

The rheological behavior of the Portuguese monofloral honeys was characterized from viscosity measurements at different shear rates using a digital Brookfield viscometer. The influence of time on the rheological behavior of the analyzed samples was also addressed. In these studies, viscosity measurements at increasing shear rates were performed and the procedure was then repeated at decreasing shear rates. Care was taken to ensure constant time intervals between measurements at different shear rates. Viscosity was the same for increasing and decreasing shear rates for honey samples with the exception of heather honey (Figure 1A).

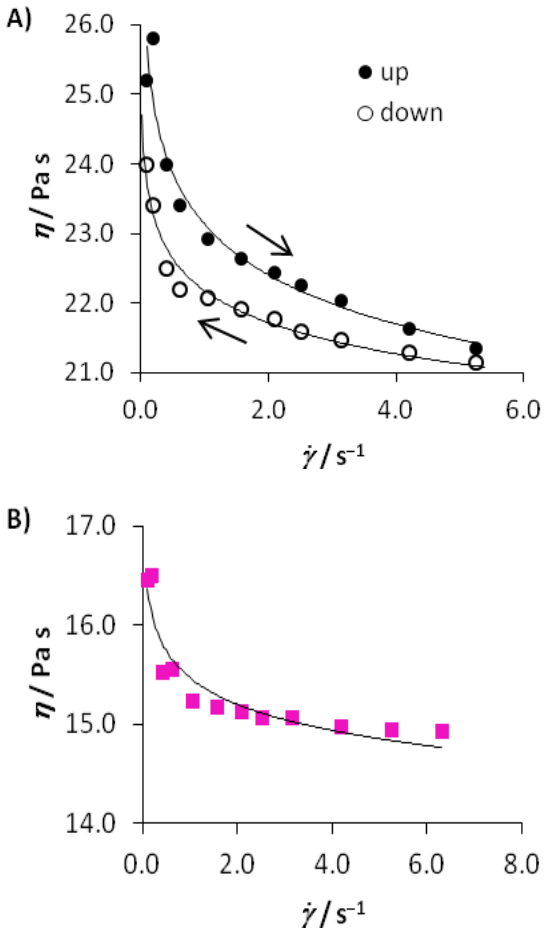

Figure 1. Viscosity flow curves for A) heather honey and B) eucalyptus honey. The lines are fits to the Power Law model.

Heather honey showed lower viscosity at decreasing shear rate compared to viscosity values obtained at increasing shear rates, a phenomenon known as thixotropy. Thus, the viscosity flow curve of this sample was characterized by a hysteresis loop (Figure 1A), since the curves for increasing and decreasing shear rates do not coincide. Thixotropy has been described in the literature for New Zealand manuka honey and also for heather honey from different geographical locations, which has been reported to possess consistency and rheological behavior similar to that of manuka [10,11]. For the other monofloral honey samples, viscosity values were the same at increasing and decreasing shear rates and these samples did not exhibit time-dependent flow behavior.

Regarding the influence of shear rate on the viscosity of the analyzed honey samples, different behaviors were observed. The viscosity of orange blossom and lavender honeys was constant and independent of the applied shear rate at the temperature of the experiment, corresponding to Newtonian behavior (Figure 2A). Therefore, a straight line with zero intercept was obtained by plotting shear stress against shear rate for these samples (Figure 2B) where the slope corresponds to the dynamic viscosity of the fluid at the temperature of the experiment, according to Newton's law of flow (Eq. (2)):

$$\sigma = \eta \cdot \dot{\gamma} \qquad (2)$$

where σ is shear stress (Pa), $\dot{\gamma}$ is shear rate (s^{-1}) and η is viscosity (Pa s) [17].

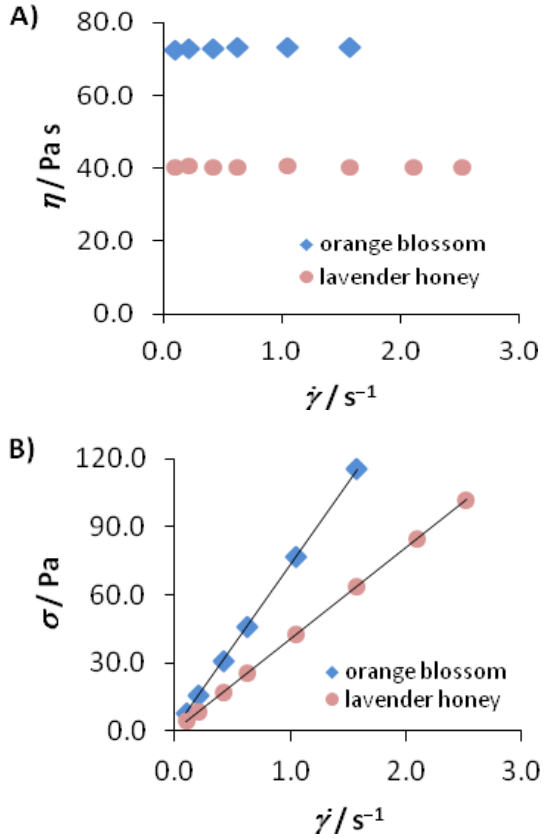

Figure 2. Influence of shear rate on A) viscosity and B) shear stress for orange blossom and lavender honeys. Lines are fits to the Newtonian model.

The influence of shear rate on rheological properties is usually more pronounced at low shear rates [17]. For the studied heather and eucalyptus honey samples, viscosity decreases with increasing shear rate and the effects are more pronounced at low shear rate values (Figures 1A and 1B). Thus, these honeys show non-Newtonian behavior and can be classified as shear-thinning fluids, whose viscosity decreases with increasing shear rate.

The Ostwald-De Waele or Power Law model (Eq. (3)) was employed to fit the experimental rheological data for the non-Newtonian honey samples:

$$\eta_{app} = K \cdot \dot{\gamma}^{n-1} \qquad (3)$$

where η_{app} is the apparent viscosity (Pa s), $\dot{\gamma}$ is the shear rate (s^{-1}), K is the consistency coefficient (Pa s^n) and n is the flow behavior index [17]. This simple model reduces to Newton's law of flow when $n = 1$ whereas $n < 1$ for shear-thinning fluids and $n > 1$ for shear-thickening fluids.

The Ostwald-De Waele parameters, K and n, obtained by applying Eq. (3) to heather and eucalyptus honeys (Figure 1) are presented in Table 2. According to this model, eucalyptus and heather honeys have $n < 1$ and thus behave as shear-thinning fluids. Regarding the thixotropic heather honey, the Ostwald-De Waele model was applied to both increasing and decreasing shear rate ramps (Figure 1A), and the parameters presented in Table 2 are mean values.

Table 2. Rheological parameters at 20 ºC for monofloral Portuguese honeys

Honey	Newtonian model	Ostwald-De Waele (Power Law) model	
	η (Pa s)	n	K (Pa s^n)
Orange blossom	73.21±1.83	–	–
Lavender	40.35±1.24	–	–
Eucalyptus	–	0.975±0.006	15.47±0.53
Heather	–	0.963±0.004	23.23±0.78

The non-Newtonian behavior of eucalyptus and heather honeys was very similar to the one described for honeys from Galicia (Spain) [18] and Germany [10]. Galician honeys showed shear-thinning behavior with flow behavior index between 0.933–0.982 and consistency coefficients in the range 7.887–14.279 Pa s^n according to the Power law model [18] while for German honeys flow behavior indexes of 0.901–0.997 and consistency coefficients of 13.39–30.34 Pa s^n have been obtained [10]. Moreover, thixotropic behavior has also been found for the German heather honey, being more pronounced at lower temperatures (≤ 20°C) for which a yield stress value (σ_0 = 0.15 Pa at 20 °C) could also be detected [10]. The characteristic rheological behavior of the German heather honey was attributed to its high protein content. Similarly, a high protein amount up to 0.6% (w/w) can be found in the studied heather honey according to the manufacturer label, while typical protein content for the other honey samples are around 0.2–0.3% (w/w).

Shear-thinning behavior (flow behavior indexes of 0.92–0.99 and 0.966–0.996) has also been described for some monofloral Indian [19] and Iranian [20] honeys, which showed consistency coefficients between 0.47–15.98 Pa s^n and 54.40–101.52 Pa s^n, respectively. Stelmakiene *et al*. [12] studying eucalyptus honeys from Lithuania found a pronounced shear-thinning behavior, characterized by flow behavior index of (0.5219 ± 0.04) and consistency coefficient of (119.59 ± 28.83) Pa s^n at 20 °C, and also thixotropy, which was attributed to the crystalline structure of the honey sample. The same authors also reported a decrease in consistency coefficients and a corresponding increase in flow behavior indexes with increasing water content, which was also observed in the Portuguese shear-thinning honeys.

For the Newtonian samples studied, orange blossom honey showed higher viscosity than lavender honey (Table 2) due to lower moisture content and higher sugar content (ºBx). The viscosities of orange blossom and lavender honeys are consistent with values obtained at 20 °C for light-colored Jordanian honeys (28.28–78.45 Pa s) [21] and Greek honeys (9.9–200.0 Pa s) [7], being slightly higher than the ones obtained for Polish honeys (18.0–43.8 Pa s) [8]. Lower viscosities were reported for Spanish (5.558–13.970 Pa s at 25 °C) [22], Tunisian (6.83–10.23 Pa s) [23] and Turkish (12.46–26.73 Pa s) [24] honeys. Newtonian behavior was also found for Indian [3, 25] and Chinese [26] honeys, the latter exhibiting small viscosity values, in the range 0.33–6.30 Pa s, associated with their high water content [26].

Acknowledgments

This work was supported by FCT - *Fundação para a Ciência e Tecnologia* (PEst-OE/SAU/UI4013/2014).

References

1. Faustino, C., and Pinheiro, L. (2015). In The Battle Against Microbial Pathogens: Basic Science, Technological Advances and Educational Programs (Méndez-Vilas, ed.), Vol. 2, pp. 98–108, Formatex, Badajoz.
2. Bogdanov, S., Jurendic, T., and Sieber, R. (2008). Am. J. Coll. Nutr. 27, 677–689.
3. Anupama, D., Bhat, K.K., and Sapna, V.K. (2003). Food Res. Intl. 36, 183–191.
4. Yanniotis, S., Skaltsi, S., and Karaburnioti, S. (2006). J. Food Eng. 72, 372–377.
5. Dobre, I., Georgescu, L.A., Alexe, P., Escuredo, O., and Seijo, M.C. (2012). Food Res. Int. 49, 126–132.
6. Bhandari, B., D'Arcy, B., and Chow, S. (1999). J. Food Eng. 41, 65–68.
7. Lazaridou, A., Biliaderis, C.G., Bacandritsos, N., and Sabatini, A.G. (2004). J. Food Eng. 64, 9–21.
8. Juszczak, L., and Fortuna, T. (2006). J. Food Eng. 75, 43–49.
9. Steffe, J.F. (1996). Rheological Methods in Food Process Engineering, 2nd edn., Freeman Press, East Lansing.
10. Smanalieva, J., and Senge, B. (2009). Eur. Food Res. Technol. 229, 107–113.
11. Witczak, M., Juszczak, L., and Galkowska, D. (2011). J. Food Eng. 104, 532–537.
12. Stelmakienė, A., Ramanauskienė, K., Briedis, V., and Leskauskaitė, D. (2012). Afr. J. Biotechnol. 11, 12406–12414.
13. Aazza, S., Lyoussi, B., Antunes, D., and Miguel, M.G. (2013). J. Food Sci. 78, C1159–C1165.
14. Iglesias, A., Feás, X., Rodrigues, S., Seijas, J.A., Vázquez-Tato, M.P., Dias, L.G., and Estevinho, L.M. (2012). Molecules 17, 8561–8577.
15. Gomes, S., Dias, L.G., Moreira, L.L., Rodrigues, P., and Estevinho, L. (2010). Food Chem. Toxicol. 48, 544–548.
16. Brookfield Engineering Laboratories (2014). More Solutions to Sticky Problems, Brookfield Engineering Laboratories, Middleboro.
17. Faustino, C., Bettencourt, A.F., Alfaia, A., and Pinheiro, L. (2015). J. Chem. Educ. 92, 936–939.
18. Gómez-Díaz, D., Navaza, J.M., and Quintans Riveiro, L.C. (2006). Eur. Food Res. Technol. 222, 439–442.
19. Ahmed, J., Prabhu, S.T., Raghavan, G.S.V., and Ngadi, M. (2007). J. Food Eng. 79, 1207–1213.
20. Mehryar, L., Esmaiili, M., and Hassanzadeh, A. (2013). American-Eurasian J. Agric. Environ. Sci. 13, 807–819.
21. Zaitoun, S., Ghzawi, A.-M., Al-Malah, K.I.M., and Abu-Jdayil, B. (2001). Int. J. Food Prop. 4, 139–148.
22. Oroian, M., Amariel, S., Escriche, I., Leahu, A., Damian, C., and Gutt, G. (2014). Int. J. Food Prop. 17, 2228–2240.
23. Boussaid, A., Chouaibi, M., Rezig, L., Hellal, R., Donsì, F., Ferrari, G., and Hamdi, S. (2014). Arabian J. Chem., in press. Doi: 10.1016/j.arabjc.2014.08.011.
24. Kayacier, A., and Karaman, S. (2008). J. Texture Stud. 39, 17–27.
25. Nayik, G.A., Dar, B.N., and Nanda, V. (2016). Arabian J. Chem., in press. Doi: 10.1016/j.arabjc.2015.08.017.
26. Junzheng, P., and Changying, J. (1998). J. Food Eng. 36, 165–168.

Contact Address:

lpinheiro@ff.ulisboa.pt (Lídia Pinheiro)
Department of Toxicological and Bromatological Sciences
Faculty of Pharmacy
University of Lisbon
Av. Prof. Gama Pinto, 1649-003 Lisbon, Portugal
Telf.: +351 217946400; Fax: +351 217946470

Rheological and biochemical study of Afuega'l Pitu cheese (PDO)

L. Piñeiro[2], I. Franco[1], C.A. Tovar[2]

[1] *Área de Tecnología de los Alimentos, Facultad de Ciencias de Ourense, Universidad de Vigo (Spain)*
[2] *Departamento de Física Aplicada,* Facultad de Ciencias de Ourense, *Universidad de Vigo (Spain)*

Introduction

Afuega'l Pitu cheese is made in the northern of Spain (Asturias) from pasteurized cow's milk by predominantly acid coagulation. It is protected with a Denomination of Origin (PDO) since 2004 (Commission Regulation (EC) No. 723/2008). There are four varieties according to its form, troncoconic (*atroncau*) or pear shape (*trapu*), and its colour, with (*roxu*) or without (*blancu*) paprika added. The elaboration is a slow and unhurried process resulting in a soft paste which becomes gradually harder during ripening.

This type of cheese is an acid milk gel made at pH near to the isoelectric point of caseins, resulting in a particulate gel (coarse-structured) formed by aggregation of casein micelles of heterogeneous size distribution [1, 2]. The structure of the gel may be affected by different cheesemaking conditions during manufacturing (rennet dose, coagulation temperature, consistency of the curd, kneading time, etc.). These factors have influenced mostly in the curd moisture content and pH [3]. The rheological properties of cheese are quality attributes that are important to the manufacturer and consumer [1]. Previous studies have analyzed microbiological and biochemical changes during ripening [4]. However, to date no research has been reported regarding rheological parameters of Afuega'l Pitu cheese (PDO). The aim of this work was to analyze the viscoelastic and biochemical parameters of *Atroncau blancu* variety of Afuega'l Pitu cheese (PDO) made by different manufactures at fixed ripening time.

Experimental

Two batches of cheese were produced by eight different farms of Asturias following traditional methods [4] and ripened for 30 days. Each sample was split into two halves; one was ground and held in an air-tight container at -40 ºC until biochemical analysis, while the other was directly subjected to the rheological test on the same day.

The following determinations were carried out: moisture by IDF 4 (2004), fat content by IDF 5 (2004), protein by IDF 20-1 (2001) and pH by AOAC 920.124 (1990). All measurements were carried out at least in duplicate.

The viscoelastic tests were performed with a Haake RS600 controlled stress rheometer (Thermo Electron, Corp. Germany) using parallel-plate geometry (20 mm diameter and 1 mm gap). Samples were tempered at ambient temperature and allowed to rest. Temperature was controlled to within 0.1 °C using a Peltier element on the lower plate. Viscoelastic parameters in the linear viscoelastic (LVE) range were obtained from stress sweeps at 1Hz and 20 °C from the initial shear stress (σ_i= 75 Pa) to final stress (σ_f= 4,700 Pa). Frequency sweeps were performed between 10 and 0.1 Hz at fixed strain γ= 0.1% in the LVE range at 20, 50 and 75 °C. All dynamic measurements were performed at least in quadruplicate.

Biochemical data were subjected to an analysis of variance (ANOVA) using the General Linear Model procedure of the computer programme Statistica© 8.0 for Windows (Statsoft Inc., Tulsa, OK, USA). A Tukey HSD test (significance level of P<0.05) was performed to compare the mean values by the different cheeses. Statistical correlations between the biochemical, and viscoelastic parameters were determined by multiple regression with confidence intervals of 95% (P<0.05), 99% (P<0.01) and 99.9% (P<0.001), by the use of the same statistical program. Rheological results are presented as mean values with expanded uncertainty limit (EUL) data as the maximum and minimum deviation from the respective mean value. Trends were considered significant when means of compared sets differed at P<0.05 (Student's test).

Results and Discussion

Biochemical parameters

The values of physicochemical parameters for the eight samples (P1–P8) analyzed (Table 1) are within the specification for the Afuega'l Pitu PDO. However, the moisture content was different among samples. Specifically, sample P5 showed a significant (P<0.05) lower amount and P8 had the highest moisture content

(Table 1). These changes could be caused by different conditions of drainage time between cheesemakers. The fat and protein contents were similar in the eight samples (Table 1) and they were also similar than those reported for other cow's milk acid coagulated cheeses [5]. All samples showed pHs lower than that the isoelectric point (pI~ 4.6) within the range stablished by PDO regulation (pH= 4.1–5) (Table 1). Despite lactic acid is primarily responsible for the decrease in pH, the actual pH attained is strongly affected by the buffering capacity of the milk and curd [1].

Table 1. Biochemical parameters of Afuega'l Pitu cheese

Sample	Moisture[1]	Fat[2]	Protein[2]	pH	MPR
P1	44.80^{a}	53.87^{a}	37.22^{a}	4.32^{a}	1.20^{ac}
P2	41.51^{ab}	50.37^{a}	38.74^{a}	4.27^{bc}	1.07^{ab}
P3	37.74^{b}	50.54^{a}	35.70^{a}	4.38^{a}	1.06^{ab}
P4	38.18^{b}	52.65^{a}	35.82^{a}	4.34^{ac}	1.07 ^{ab}
P5	33.84^{c}	52.44^{a}	37.96^{a}	4.22^{bd}	0.89^{b}
P6	40.61^{ab}	52.16^{a}	35.77^{a}	4.09^{e}	1.13^{ab}
P7	49.07^{d}	52.89^{a}	34.64^{a}	4.14^{de}	1.42^{c}
P8	51.39^{d}	54.47^{a}	36.06^{a}	4.52^{f}	1.43^{c}
SEM	1.030	0.285	0.271	0.023	0.032
Sig.	***	*	*	***	***

*[1] g/100 g cheese; [2] g/100 g TS; MPR: moisture:protein ratio; SEM: Standard error of mean values; Sig.: Statistical significance *** P<0.001, ** P<0.01, * P<0.05; [a-f] Different letters in the same column indicate significant differences (P<0.05).*

Linear viscoelastic range

Stress sweeps were carried out to determine the LVE range in terms of stress (σ_{max}) and strain (γ_{max}) amplitudes. It was observed that P5 had the highest σ_{max} and low γ_{max} (Table 2) indicating a more stable but less deformable micellar network, as consequence of the lowest moisture:protein ratio (MPR). So, a low moisture content promotes a higher number of cross-links among caseins resulting in a more packed casein matrix. Conversely, P8 had the greatest moisture content and consequently the highest MPR, thus, the gel network is a more hydrated structure that exhibits the lowest σ_{max} and the highest γ_{max} (Table 2). These trends were assessed applying the Pearson correlation coefficient, that showed a positive correlation of γ_{max} (0.68**) and a negative high correlation of σ_{max} (-0.91***) with MPR. As consequence of acid-induced gels calcium phosphate is solubilised. In all samples, the loss of Ca^{2+} ions produced a less cohesive micellar network [6] which explains the low values of γ_{max}< 0.34% comparing with those obtained by rennet-induced coagulation (γ_{max}> 0.60%) at similar ripening time [7]. Linkage of the rennet-altered micelles is a diffusion-controlled aggregation of hydrophobic colloids and probably occurs at definite surface sites [1] which could explain the enhanced deformability of casein network. Moreover, the presence of Ca^{2+} ions facilitates the formation of ionic bonds that stabilize the casein network. Thus, the resulting rennet gels exhibited a greater conformational flexibility (high γ_{max}).

Table 2. Viscoelastic parameters in the linear viscoelastic (LVE) range for different commercial producers (P1−P8) at 1Hz and 20 °C

Sample	σ_{max} (Pa)	γ_{max} (%)
P1	526±53^{a}	0.257±0.030^{ab}
P2	551±55^{a}	0.273±0.030^{ab}
P3	609±61^{a}	0.292±0.023^{ab}
P4	848±85^{b}	0.329±0.039^{ac}
P5	1003±100^{b}	0.257±0.023^{b}
P6	555±56^{a}	0.296±0.026^{abc}
P7	323±32^{c}	0.309±0.035^{abc}
P8	166±17^{d}	0.339±0.019^{c}

[a-d] Different letters in the same column indicate significant differences P<0.05 among samples.

Mechanical spectra

Mechanical spectra were analyzed using the power-law fit (Eq. 1), being G_0' the storage modulus at 1 rad/s and n' the power law exponent:

$$G' = G_0' \cdot \omega^{n'} \qquad (1)$$

Table 3. G_0' and n' parameters (Eq. 1) of mechanical spectra at 20 °C

Sample	G_0' (kPa)	n'	r^2 Eq. (1)
P1	174±32^{ab}	0.1366±0.0003^{a}	1.000
P2	170±12^{a}	0.1454±0.0006^{b}	1.000
P3	175±8.8^{a}	0.1454±0.0006^{b}	1.000
P4	251±53^{b}	0.1532±0.0004^{c}	1.000
P5	327±18^{c}	0.1452±0.0006^{b}	1.000
P6	159±13^{a}	0.1482±0.0003^{d}	1.000
P7	100±7.9^{d}	0.1422±0.0003^{e}	1.000
P8	41±1.9^{e}	0.1400±0.0006^{f}	1.000

Values are given as mean ± expanded uncertainty limit (EUL); [a-f] Different letters in the same column indicate significant differences (P<0.05).

Specifically at 20 ºC, all samples behaved as solid-like materials since the elastic character (*G'*) predominates over the viscous (*G''* not shown). Nevertheless, P5 exhibited the highest G_0' value (Table 3) indicating that the network is formed by a stiffer casein matrix as consequence of a greater fusion of casein micelles resulting in a higher contact area between them [8]. This result is in agreement with its brittle structure reported by stress sweeps (low γ_{max}). By contrast, P8 showed the lowest G_0' value (Table 3), which indicates a softer structure produced by a less concentrated casein matrix. The greater percentage of stiffness for P5 relative to P8

was maintained at high temperatures (50 and 75 ºC; Table 4 and 5 respectively), showing the principal role of the protein phase in the gel network. Exponent *n'* provides network time-stability [9], reflecting the level of intermolecular association among strands [10]. At 20 ºC all samples showed *n'* values between 0.14 and 0.15 (Table 3); similar values have been reported by [11] and [12] for other types of acid casein gels.

Table 4. G_0' and n' parameters (Eq. 1) of mechanical spectra at 50°C

Sample	G_0' (kPa)	n'	r^2 Eq. (1)
P1	9.039±0.003[a]	0.1859±0.0003[a]	1.000
P2	14.65±0.023[b]	0.1983±0.0014[b]	0.999
P3	11.60±0.011[c]	0.2080±0.0008[c]	1.000
P4	16.20±0.008[d]	0.2068±0.0004[c]	1.000
P5	30.90±0.044[e]	0.2079±0.0013[c]	0.999
P6	15.87±0.020[f]	0.1965±0.0011[b]	0.999
P7	6.399±0.003[g]	0.1860±0.0004[a]	1.000
P8	3.026±0.001[h]	0.1966±0.0004[b]	1.000

Values are given as mean ± expanded uncertainty limit (EUL); [a-h] Different letters in the same column indicate significant differences (P<0.05).

Table 5. G_0' and n' parameters (Eq. 1) of mechanical spectra at 75°C

Sample	G_0' (kPa)	n'	r^2 Eq. (1)
P1	2.12±0.008[a]	0.144±0.003[a]	0.989
P2	3.40±0.012[b]	0.158±0.003[b]	0.993
P3	3.36±0.023[c]	0.143±0.006[a]	0.965
P4	3.74±0.022[d]	0.163±0.005[bc]	0.98
P5	7.13±0.042[e]	0.169±0.005[c]	0.982
P6	3.31±0.014[f]	0.173±0.004[c]	0.99
P7	0.809±0.004[g]	0.155±0.005[b]	0.983
P8	0.628±0.003[h]	0.140±0.004[a]	0.982

Values are given as mean ± expanded uncertainty limit (EUL); [a-h] Different letters in the same column indicate significant differences (P<0.05).

The thermal behavior of mechanical spectra was evidenced in the decrease of G_0' parameter with temperature up to 75 ºC (Tables 3–5), more noticeable between 20 and 50 ºC. Part of this softening is related to the liquefaction and coalescence of fat (~ 40 ºC), which could contribute to the decrease of the contact area between caseins, but the major overall effects relate to the weakening of casein-casein interactions (kinetic variations) [13, 14]. These facts may also be observed in the increase of *n'* exponent for all samples at 50 ºC (Table 4) based on the reduction in the number and strength of bonds and the subsequent lower degree of connectivity among strands in the casein matrix, resulting in a less stable and more weak gel [15].

The thermal responses are also reflected in the increase in the loss factor (*tanδ*) at 50 and 75 ºC comparing with the corresponding data at 20 ºC (Figure 1 and 2; X-axis in logarithmic scale), remarkably at the high frequency range, from 10 to 63 rad/s. These results could be explained because at high temperatures the rates of spontaneous rearrangements are higher [16] thus, the relaxation times are lower comparing with the process time at short-term behavior. The proportion between both times involves a low Deborah number (N_{De} <1), indicating a greater liquid-like property [17].

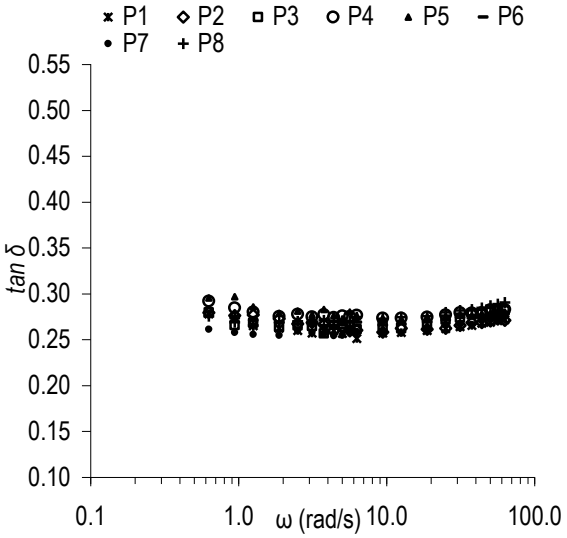

Figure 1. Effect of frequency on loss factor (tanδ) at 20 ºC

However, at 75 ºC thermal response of *tanδ* was different at low frequency range comparing with that at high frequencies. Specifically, from 10 to 0.1 rad/s *tanδ* values were significantly lower (Figure 2b). This result indicates that at 75 ºC a shear-induced gel formation occurred with decreasing the angular frequency [16]. This effect was particularly noticeable in P8, whose net decrease of *tanδ* was more intense. However, P5 exhibited a minor decrease of *tanδ* down to 0.6 rad/s (Figure 2b). These trends are consistent with the *n'* values of both samples at 75 ºC, so, for P8 it was found a more stable network reflected in a less frequency dependent of G_0' (Table 5), showing the stabilizing role of water molecules in the casein matrix (P8). The increase in the solid-like character and the decrease in rigidity (elastic) modulus are mutually compatible. This fact may be explained by Eq. (2), which relates the elastic shear modulus (*G'*), with diverse structural parameters [10]:

$$G' = C \cdot N \cdot \frac{d^2V}{dx^2} \qquad (2)$$

where *V* is the Gibbs energy of interaction between two structural elements when moved with respect to each other over a distance, dx; *C* is a constant of dimension length whose value depends on the geometry of the network; *N* is the number of connections between structural elements per unit cross-section perpendicular

to x. So, heating could reduce the connectivity in the network (low N) decreasing the contact area among caseins (Eq. 2). On the other hand, shearing at high temperature increased the energy content (*V* parameter) of bonds in casein matrix resulting in a more ordered structure, which is reflected in the notable decrease of the loss factor at 75 °C at the low frequency range. Thus, combining two opposite (geometrical and energy) contributions, it is reasonable the net diminish of G' at high temperature (Table 5).

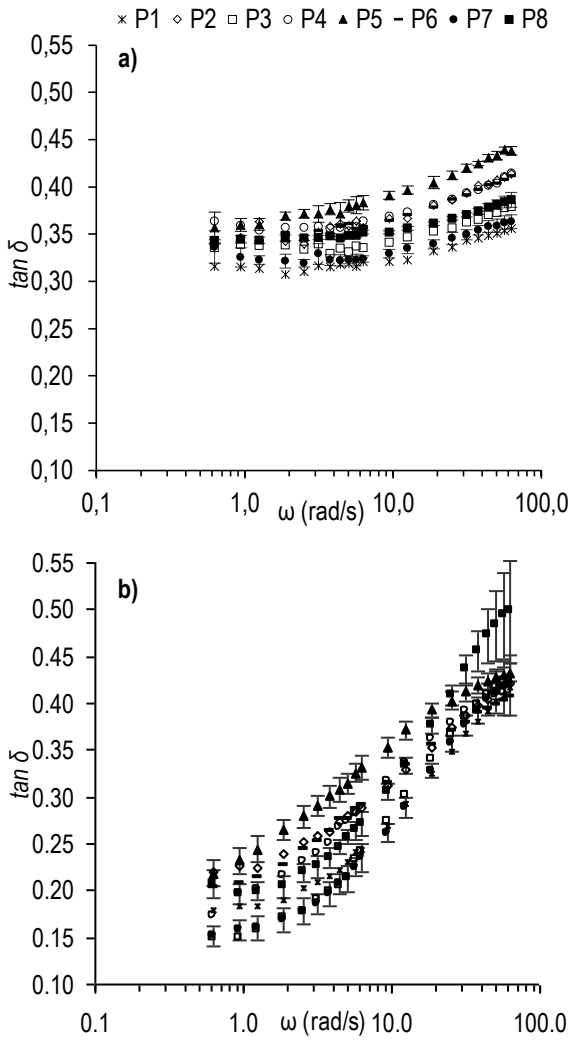

Figure 2. Effect of frequency on loss factor (tanδ) at: a) 50 ºC and b) 75 ºC

Concluding Remarks

The moisture content was determinant to distinguish the rheological differences between samples P5 and P8. The lower moisture content of P5 explained the more rigid and brittle structure, while the high moisture content in P8 justified its softer and more deformable network. At 75 °C it was observed some increase of the solid-like character in the low frequency range, indicating a more energy stable casein matrix.

References

1. Fox, P.F., Guinee, T.P., Cogan, T.M., and McSweeney, P.L.H. (2000). Fundamentals of Cheese Science, Aspen Publishers Inc., Gaithersburg.
2. Rao, M.A. (2007). Rheology of Fluid and Semisolid Foods. Principles and Applications, 2nd edn., Springer, New York.
3. Lucey, J.A., Mishra, R., Hassan, A., and Johnson, M.E. (2005). Int. Dairy J. 15, 645–653.
4. Cuesta, P., Fernández-García, E., González de Llano, D., Montilla, A., and Rodríguez, A. (1996). J. Dairy Sci. 79, 1693–1698.
5. Arenas, R., González, L., Sacristán, N., Tornadijo, M.E., and Fresno, J.M. (2014). J. Sci. Food Agric. 95, 851–859.
6. Hui, Y. H., Cross, N., Kristinsson, H. G., Lin, M. H., Nip, W. K., Siow, L. F., and Stanfield, P.S. (2006). In Food biochemistry & food processing (Hui, Y.H., ed.), pp. 351–378, Blackwell Publishing, New Jersey.
7. Bargiela, V., Franco, I., and Tovar, C.A. (2012). Queso San Simón da Costa (DOP). Editorial Académica Española, Saarbrücken.
8. Lucey, J.A. (2002). J. Dairy Sci. 85, 281–294.
9. Lapasin, R. and Pricl, S. (1999). Rheology of industrial polysaccharides: Theory and applications. Aspen Publishers Inc., Gaithersburg.
10. Walstra, P. (2003). Physical Chemistry of Foods, Marcel Dekker Inc., New York.
11. Roefs, S.P.F.M., de Groot-Mostert, A.E.A., and van Vliet, T. (1990). Formation and model of gel network, Colloids Surf. 50, 141–159.
12. Arshad, M., Paulsson,M., and Dejmek, P. (1993). J. Dairy Sci. 76, 3310–3316.
13. Lucey, J.A., and Singh, H. (2003). In Advanced Dairy Chemistry, 3rd Edition. Part B, (Fox, P.F., and McSweeney, P.L.H., eds.), Vol. 1 Proteins, pp.1001–1025, Kluwer Academic/Plenum Publishers, New York.
14. Tunick, M.H. (2010). Int. Dair. J. 20, 680–685.
15. Clark, A.H. and Ross-Murphy, S.B. (1987). Adv. Polym. Sci., 83, 57–192.
16. Larson, R.G. (1999). The structure and rheology of complex fluids, Oxford University Press, Inc., New York.
17. Steffe, J.F. (1996). Rheological Methods in Food Process Engineering, 2nd edn., Freeman Press, Lansing.

Contact Address:

Clara Asunción Tovar Rodríguez (tovar@uvigo.es)
Dpto. Física Aplicada, Facultad de Ciencias de Ourense. Universidad de Vigo, As Lagoas s/n, 32004, Ourense (Spain)
Telf.: +34 988387241; Fax: +34 988387001.

Effect of high pressure processing on the rheological properties of 5% glucomannan gels at several pHs

C. A. Tovar[1] , J. Borderias[2], B. Herranz[3]

[1] Department of Applied Physics, Faculty of Science of Ourense, University of Vigo (Spain)
[2] Department of Products, Institute of Food Science, Technology and Nutrition (ICTAN-CSIC) (Spain)
[3] Department of Characterization, Quality and Safety, Institute of Food Science, Technology and Nutrition (ICTAN-CSIC) (Spain)

Introduction

Konjac glucomannan (KGM), a neutral hydrocolloid extracted from *Amorphophallus konjac* C. Koch [1], is a gelling agent proposed in previous work for making restructured fish products [2]. Physical gelation of glucomannan (GM) occurs through the formation of a three-dimensional network by associating domains (junction zones) which involve hydrogen bonds and other physical interactions [3]. It is crucial to make appropriate gels that junctions between molecules do not grow too large. Thus, there must be some means of control the growth of these molecular domains [4]. Moreover, the effect of the alkalinisation on the deacetylation ratio of samples is also important for designing gels with adequate textural characteristics for a specific technological purpose. So, when pH increased the increase of inter-chain associations promoted the formation of larger junctions and more elastic gel networks [5]. In previous research it has been analysed the influence of high hydrostatic pressure (HHP) on GM gels at pH=11 (completely deacetylated), to produce gels which could be used to make restructured seafood analogues. So, at 600 MPa the crystalline regions in GM matrix became reinforced, while 200 MPa produced softer and more flexible physical networks [6]. The present paper is focused on combine both pH and constant HHP (400 MPa), in order to optimize the degree of alkalinisation to obtain suitable rheological properties of 5 g/100 mL GM gels for making the appropiate texture to make restructured seafood analogues.

Experimental

Sample preparation

Three lots of GM gels at 5 g/100 mL were made: "Lot C" (control-native GM gels), "Lot A" (weakly deacetylated GM gels), and "Lot B" (completely deacetylated GM gels) from KGM (average molecular mass $11 \cdot 10^5$ Da, Guinama, Valencia, Spain) were prepared according to the methodology described in [7]. One third of the 5 g/100 mL GM gels was the lot control without coagulant agent (lot C, pH= 5.2). The second third of the 5 g/100 mL GM gels was weakly deacetylated by adding 1.5 mL/100 mL of 0.6 mol/L KOH (Panreac Química, S. A., Barcelona, Spain), raising pH to about 9.1 (Lot A). The other third of the 5 g/100 mL GM gels was completely deacetylated by adding 4 mL/100 mL of 0.6 mol/L KOH (Lot B, pH=11). Petri dishes were then filled with the three lots (C, A and B) and set by heating, first at 30 °C for 1 h and then at 5 °C for 4 h as setting conditions. Lots A and B gels were then placed in a citrate-phosphate buffer at pH 5 (1:10 gel:buffer proportion) for 20 h at 5 ºC to lower pH to neutral values. Then A, B, and C gels were immediately vacuum packed in double plastic bags to prevent contact with pressurization fluid and subjected to HHP processing= 400 MPa for 10 min at 10 ºC (Stansted Fluid Power CTD, FPG 7100:-2C. Harlow, Essex, UK.). Samples were named C0, C400 for lot C subjected to: 0, and 400 MPa, A0, A400 for lot A and B0, B400 for lot B. All gels were warmed to 25 ºC before analysis. Analyses were conducted after one day of chilled storage at 5 ºC.

Viscoelastic measurements

Small amplitude oscillatory shear (SAOS) data were gathered using a RS600 Haake rheometer (Thermo Electron Corporation Karlsruhe, Germany). The measurement system was the parallel plate (20 mm in diameter and 1 mm gap). Temperature in the lower plate was kept at 25.0±0.1 ºC. Stress sweeps were obtained from 1 to 1,500 Pa at angular frequency 6.28 rad/s. Frequency sweeps were performed over the range 0.063–63 rad/s, keeping constant strain (γ=1%) within the linear viscoelastic (LVE) region. Temperature sweep tests were performed using dynamic thermo-mechanical analysis (DTMA) from 25 to 90 ºC at a linear

heating rate (1 °C/min). Frequency (0.63 rad/s) and strain γ=1% within the LVE range were fixed.

Results and Discussion

Linear viscoelastic (LVE) range

Figure 1 shows the influence of HHP at 400 MPa on the limit parameters which characterize the LVE range: stress (σ_{max}) and strain (γ_{max}) amplitudes for 5 g/100mL GM gels with increasing pH. For control native GM gels (pH=5.2), 400 MPa strongly and significantly ($p<0.05$) increased σ_{max} (Figure 1a) and γ_{max}, (Figure 1b), showing a specific structural benefit for the control pressurized gel evidenced in the higher structural stability and conformational flexibility of the network.

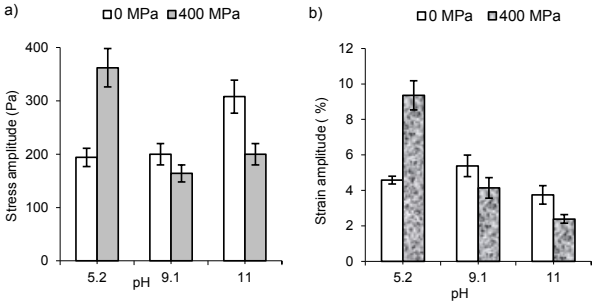

Figure 1. Influence of high pressure(400 MPa) on stress (a) and strain (b) amplitudes of 5% GM gels made at pH=5.2; 9.1 and 11. T=25°C.

So, pressure reduces the excluded-volume force and the free volume in native GM matrix [8], increasing GM-GM associations, by hydrogen bonds, van der Waals, and hydrophobic interactions, which are weak and reversible [8]. These rearrangements are random in nature, due to the practical absence of electric charge at pH=5.2, thus, the conformational flexibility in pressurized GM matrix is enhanced (Figure 1b).

At pH=9.1, HHP processing at 400 MPa did not practically altered neither σ_{max} nor γ_{max} values (Figure 1a,b). However, when GM was completely deacetylated (pH=11), HHP significantly decreased σ_{max} (Figure 1a) and γ_{max} (Figure 1b) making a more brittle matrix in B400 *vs* B0. In this case, deacetylation of GM naturally produces repulsive electrostatic forces due to the greater density of $CH_3\text{-}COO^-$ anions, meanwhile new inter-chain associations by hydrogen bonding were formed after applying 400 MPa, thus, total level of orientational order in pressurized GM matrix was notably enhanced [8]. Therefore, this new reticular order reinforces the existent crystalline microstructures promoting a less deformable (low γ_{max}) polymeric matrix of B400 *vs* B0 (Figure 1b).

Frequency sweeps

From elastic (*G'*) and viscous (*G''*) modulus of mechanical spectra can be calculated the fraction of ideal network (*fin*) (Eq. 1) which gives a measurement of the level of order in a gel network [9].

$$f_{in} = \left(\frac{G'}{G'+G''} \right) \cdot 100 \qquad (1)$$

In case of native GM gels (C0), 400 MPa did not produce relevant changes in all frequency range, so, for both C0 and C400, *fin* exhibited low values which notably decreased with decreasing the angular frequency (ω) down to 0.1 rad/s (Figure 2).

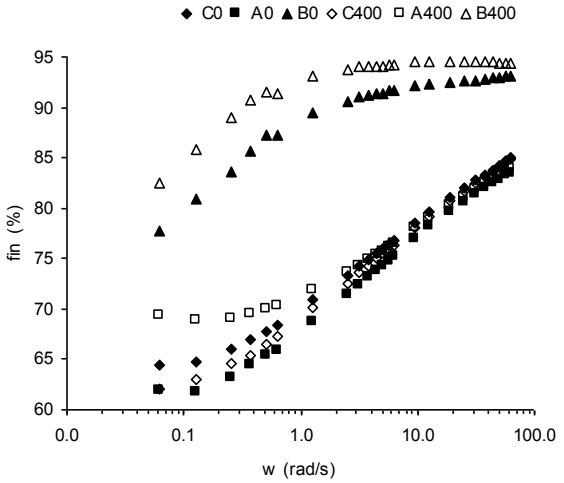

Figure 2. Influence of high pressure (400 MPa) on mechanical spectra in terms of the fraction of ideal network for 5% GM gels made at pH=5.2; 9.1 and 11.T=25°C.

This result is a natural consequence of shear stress in a weak network, which became less energy stable and consequently more time-dependent at higher shearing times (low frequencies). So, shear stress disrupts more effective junctions reducing consequently the ability of C0 and C400 networks to store mechanical energy at low frequencies. When GM was weakly deacetylated in both A0 and A400 the *fin* parameters, at higher frequencies, were similar than those of C0 and C400. However at lower frequencies specifically at 0.63-0.063 rad/s range, HHP notably increased the *fin* values in A400 *vs* A0 (Figure 2). This result suggests that when GM was weakly deacetylated the repulsive (excluded-volume) force something decreased, compared with C0, increasing some orientational order in the polymeric matrix. So, in this way, 400 MPa reinforced the time stability and the level of intermolecular order increasing the energy capability in A400 network at low frequencies.

At pH=11, as deacetylation of the GM chains was practically total, the degree of electrostatic and orientational order in network is maximum, thus, the *fin* values for B0 were notably higher than in the other gels (A0, A400, C0, C400) in all frequency range.

However, the frequency-dependence of *fin* in B0 was different of C0-C400 and A0-A400 gels. At the high-frequency range (from 63 to 6 rad/s), *fin* values flattened, while, in the low-frequency range (6 to 0.06 rad/s) *fin* continuously decreased to the lowest frequency (Figure 2). Thus, the viscoelastic response at the high frequency range shows some mechanical resistance due to strength of junctions. Conversely, in the low frequency range there is a progressive disruption of physical bonds produced by internal rearrangements (molecular relaxations), when shear time increased. The *fin* parameter for the pressurized sample (B400), exhibited a similar pattern in all frequency range than in B0; however the *fin* values of B400 were higher than those of B0 (Figure 2). This result shows that processing at 400 MPa reinforced the orientational order enhancing the level of connectivity in B400 matrix, thus the degree of permanency of the interconnections, principally by hydrogen bonding, is also enhanced in B400 vs B0. This trend could explain the lower rate of *fin* drop at the low frequency range in B400 comparing with B0 matrix (Figure 2).

Dynamic thermo-mechanical analysis

As regards to thermal profile of control (C0) sample from 25 to 55 °C, *G'* values exhibited a plateau zone up to ~55 °C (Figure 3). From 55 °C to 90 °C, *G'* exhibited a weak minimum at ~70 °C reaching *G'* similar values than at ~25 °C at higher temperatures (~90 °C) (Figure 3).

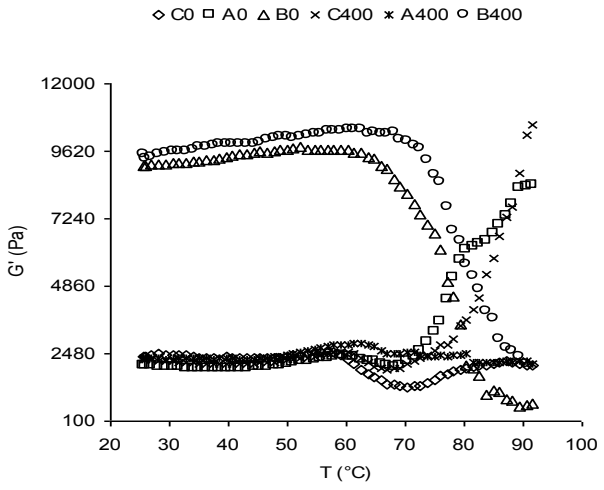

Figure 3. Influence of high pressure (400 MPa) on thermal profiles in terms of storage modulus of 5% GM gels made at pH=5.2; 9.1 and 11. f=0.1 Hz.

However, *G''* moduli progressively decreased up to 75 °C (Figure 4), producing a second gelation process after T>40 °C for C0 gel.

HHP= 400 MPa changed the pattern of thermal profile of C0 producing a rubber elastic (entropy elastic) response at T>70 °C in C400 (Figure 3). It is possible that HHP could induce the formation of some randomly cross-linked chain segments that could adopt multiple conformations capable of free rotation about their backbone [4]. Comparing Figure 3 and Figure 4 can be observed that for C400, the rate of thermal increase in *G'* was higher than that of *G''*, hence, a second gelation process was produced, specifically from 50 to 90 °C. At pH=9.1, A0 exhibited a similar thermal pattern than C400, however at pH=9.1, 400 MPa cancelled the rubber-like elasticity founded in A0 gel so, at T>70 °C, *G'* moduli progressively decreased up to 90 °C reaching *G'* values similar that those at 25 °C (Figure 3). *G''* moduli progressively decreased from 25 °C to 90 °C (Figure 4), inducing a second gelation process with increasing temperature (A400).

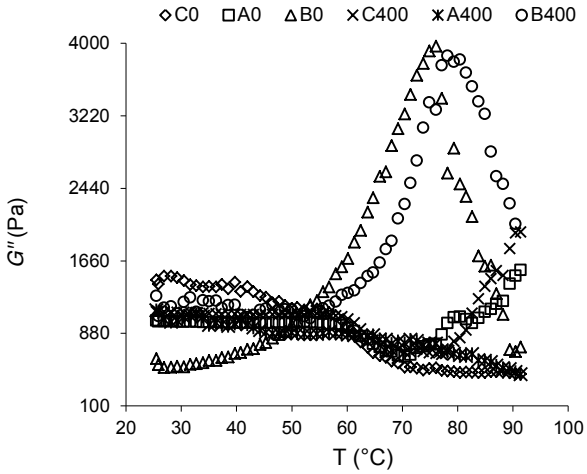

Figure 4. Influence of high pressure (400 MPa) on thermal profiles in terms of loss modulus of 5% GM gels made at pH=5.2; 9.1 and 11. f=0.1 Hz.

Conversely, at pH=11 when GM was completely deacetylated, the greater size and extent of junction zones by hydrogen bonding reinforced the molecular packing forming a hard physical gel with higher *G'* moduli in the plateau zone in B0 comparing with C0 and A0 (Figure 3). The strong gel (B0) is similar in some sense to a glass [6] and the observed increase of *G''* up to 75 °C and the maximum-peak in *G''* at 75 °C (Figure 4) is sometimes used as the definition the glass transition (Tg) [4]. The effect of 400 MPa on the thermal profile maintained similar pattern than in B0, however Tg exhibited a slight shift at higher values for B400 (Tg

~80 °C). This trend could be explained because as pressure reduced the free volume, the degree of orientational order in GM matrix has been enhanced, increasing more the structural stabilisation of the gel network (B400) which involves a greater density of cross-links, evidenced in the greater *G'* moduli up to 70 °C in B400 *vs* B0 (Figure 3), thus, Tg is shifted to at higher values.

Concluding Remarks

The effect of high pressure processing on the viscoelastic properties of 5 g/100 mL glucomannan gels varied depending on pH. When glucomannan gel was in native state (pH=5.2), HHP processing improved the structural stability and deformability in the gel network, inducing some random conformations in GM chains, which promote the rubber-like elasticity at high temperature, as a characteristic thermo-rheological response. However, when glucomannan gel was completely deacetylated (pH=11), processing at 400 MPa increased the level of orientational order that existed in the initial gel (pH=11, 0 MPa), resulting in a reinforced intermolecular-packing, forming a more brittle polymeric network, due to a new vitrification process in the pressurized matrix. The strong rigidity of gels produced characteristic thermal profiles which permit analyse the evolution of the glass transition interval.

Acknowledgements

Thanks to the Xunta de Galicia for its financial support under the Consolidation and restructuring program of competitive research units: Strategic Research Partnerships (2009/060) and project AGL2011-24693.

References

1. Nishinari, K., Williams, P. A., & Phillips, G. O. (1992). Food Hydrocolloids 6, 199–222.
2. .Herranz, B., C. A. Tovar, Solo-de-Zaldivar, B., & Borderias, A. J. (2012). Food Hydrocolloids 27(1), 145–153.
3. Lapasin, R., & Pricl S. (1999). Rheology of Industrial Polysaccharides: Theory and Applications, Aspen Publishers, Gaithersburg.
4. Sperling, L.H. (2001). Physical Polymer Science. John Wiley & Sons, Canada.
5. Solo-de-Zaldívar, B., Tovar, C. A., Borderías, A. J. and Herranz, B. (2014). Food Hydrocolloids 35, 59–68.
6. Moreno, H. M., Herranz, B., Borderías, A. J. & Tovar, C. A. (2016). Food Hydrocolloids 60, 437–444.
7. Herranz B., Tovar, C. A., Solo-de-Zaldívar, B. &. Borderias, A. J. (2013). LWT-Food Sci. Technol. 51, 500–506.
8. Larson, R. G. (1999). The Structure and Rheology of Complex Fluids, Oxford University Press, New York.
9. Bargiela, V. Moreno, H. M., Herranz, B., Borderías A.J. and Tovar, C.A. (2015). In Challenges in Rheology and Product Development, pp. 95–98, E-rheo-iba, Coimbra.

Contact Address:

tovar@uvigo.es
Department of Applied Physics,
Faculty of Science of Ourense.
University of Vigo
As Lagoas s/n, 32004 Ourense (Spain)
Tel.: +34 988 38 72 75; Fax: +34 988 38 72 14

Rheology of aqueous methylcellulose/tragacanth gum dispersions

R. Moreira, F. Chenlo, C. Silva, M.D. Torres

Department of Chemical Engineering, Universidade de Santiago de Compostela, rúa Lope Gómez de Marzoa, Santiago de Compostela, E-15782 (Spain).

Introduction

The use of hydrocolloids is common in many industrial fields, but, particularly, in the food sector it has considerably grown in the last years due to the demand of ready-to-eat meals, low-fat food or long-life food, among others [1,2]. Among hydrocolloids, the methylcellulose (MC) and tragacanth (T) gums has been widely used in the food for batter formulas, gluten-free products or edible coats, among others. The rheological properties of MC and T systems depend on several factors, among which are: the polymer concentration, pH, ionic strength, the molecular weight, the presence of additives, or the temperature [3,4]. Concerning temperature, one of the most widely explored features of MC solutions is the thermo-reversible gelation, strongly influenced by pH or salt concentration [1,2]. Therefore, the rheological characterisation of systems with semi-synthetic and non-ionic gums as MC or their interactions with natural plant exudates and ionic gums as T, in a wide range of operating conditions (temperature, concentration, pH, etc.), is clearly an interesting subject to the industry.

In the last decade, some MC/hydrocolloid mixtures have been also explored [4-6]. Particularly, the excellent pH stability of MC/alginate solutions in the presence of NaCl has been determined, especially relevant to be used as vehicle in the selective release of bioactive proteins in the intestine. Later on, the study of the rheological behaviour of MC/xanthan gum mixtures in the presence of NaCl (0.1 M) at different polymer ratios revealed no synergic effect or specific interactions between components. Recently, MC and k-carrageenan mixtures have received particular attention for their particular behaviour, showing very interesting double thermal-reversible transition gel-sol-gel upon heating. This specific thermal behaviour provides a liquid state of the system between gel-states at low and high temperatures controlling the polymer content. This fact suggests that this system should be further tested as potential carrier for various functional colloidal systems.

In the food industry, T gum has been used as thickener to enhance the viscosity of ready meal or sauces, where MC was added as gelling agent. MC:T gums were also jointly employed as stabilisers in fruit juices [5]. The use of other cellulose derivatives and T has been proposed for personal care applications, as both thickeners and emulsifiers [6]. Despite their potential industrial applications, among various combinations of bi-component polysaccharide systems, the rheological behaviour of binary systems MC and T has not been yet reported. The interactions understanding between biopolymers in food and non-food formulations is critically relevant in order to control the rheological, mechanical, structural or storage stability characteristics of the derived products, especially important for those biopolymers with complex characteristics, as T [4].

Besides many papers were published on the rheology of water-soluble cellulose derivatives elsewhere [5], one of the drawbacks of the previous scientific research was lack of in-depth studies on steady and dynamic shear rheology of MC solutions and their mixtures at temperatures below the gel formation temperatures, which is critically relevant in industrial application processes. In this context, the main aim of this work is to explore the rheology of aqueous methylcellulose/ tragacanth (MC:T) dispersions at different gum ratios and temperatures below the gel formation temperatures.

Experimental

Raw materials

Methylcellulose gum, MC (CAS 9004-67-5, Sigma-Aldrich, Inc., St. Louis, MO) and tragacanth gum, T (CAS 9000-65-1, Merck KGaA., Darmstadt, Germany), from commercial food grade polymers, were employed without further purification. Both gums were equilibrated at a constant moisture content using a chamber with constant relative humidity generated by saturated aqueous NaCl solutions at room temperature (a_w 0.75) to avoid concentration variations during its handling, due

to its hygroscopic nature. Moisture content was determined following standard methods [3].

Samples preparation

Two independent stock aqueous MC solution (20 g L^{-1}) and T dispersion (10 g L^{-1}) were prepared in order to obtain systems with comparable apparent viscosities. MC:T dispersions were prepared at different polymer ratios 0:100, 0.25:0.75, 0.5:0.5, 0.75:0.25 and 100:0 and were kept at 4ºC at least 12 h before rheological tests.

Rheological measurements

Steady-shear and dynamic rheological tests were conducted on a controlled stress rheometer (MCR 301, Paar Physica, Austria) with either parallel plates (diameter 50 mm, 1 mm gap) and Couette (bob diameter 24 mm, cup diameter 26 mm, bob height 25 mm) geometries. The tests were made at different temperatures (5 to 35 ±0.01ºC, in steps of 10 ºC), controlled by a Peltier system. In all experiments, samples were covered with light paraffin oil in order to prevent water evaporation. Samples were rested between plates or cup during 10 min at the studied temperature before conducting the measurements. All experimental measurements were carried out, at least, in triplicate.

Steady-shear measurements

Steady-shear flow curves (apparent viscosity, η (Pa s), vs. shear rate, $\dot{\gamma}$ (s^{-1})) of MC:T dispersions were obtained by, firstly, decreasing (downwards) and, then, increasing (upwards) shear rate following a logarithmic ramp, at different shear rates (0.1 - 300 s^{-1}), and no hysteresis was observed.

Oscillatory measurements

Mechanical spectra (elastic, G', and viscous, G", moduli (Pa), *vs.* angular frequency, ω (rad s^{-1})) of MC:T dispersions were measured at linear viscoelasticity conditions. Strain sweep tests at 1 Hz at the studied concentrations and temperatures were previously conducted in order to define the linear viscoelasticity range of strain (γ: 0-10%). Subsequently, frequency sweeps (upwards and downwards) were programmed at a strain value of 5% over an angular frequency range of 0.1 - 62.8 rad s^{-1}. No differences were observed between up and down curves. Experimental mechanical spectra were correlated using the Maxwell equations,

$$G';G''(\omega) = \frac{a\omega^b}{1+c\omega^d} \quad (1)$$

being a, b, c and d the fitting parameters.

Statistical analysis

Fitting parameters were analysed using one-factor analysis of variance (ANOVA) by PASW Statistics. A Scheffé test was made to differentiate means with 95% confidence ($p < 0.05$) when the analysis of variance indicated differences among means.

Results and Discussion

Steady-shear tests of MC:T gum dispersions

Figure 1 shows the steady shear flow curves of MC:T dispersions at representative polymer ratios and different temperatures.

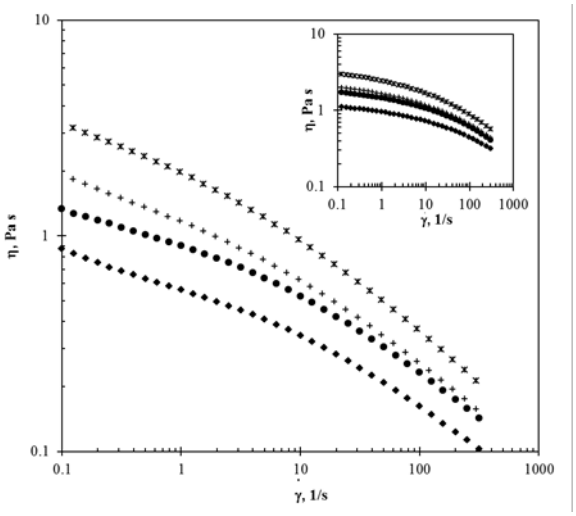

Figure 1. Steady-shear experimental data for MC-T dispersions at different polymer ratios (1:3, (inset) 3:1) and temperatures: (*) 5, (+) 15, (•) 25, (•) 35ºC

MC:T dispersions exhibited shear thinning behaviour at each temperature and decrease on apparent viscosity with increasing temperature, as expected from the single components features. At higher MC content a trend to a Newtonian plateau at low shear rate and at higher T content a high shear thinning behaviour, reducing the Newtonian plateau and consequently decreasing the critical shear rate.

Additionally, the dependence of the apparent viscosity with temperature at selected shear rates for MC:T dispersions using the Arrhenius function, $\eta = A_A \exp(-E_a / RT)$, has been evaluated and the fitting parameters values at different polymer ratios are presented in Table 1. In all cases, the activation

energy, E_a, decreased with increasing shear rate, which indicate that changes in viscosity with temperature occur more rapidly at low shear rates. In the shear thinning region, density of entanglements is constantly decreasing and a lower E_a value is required to start the flow. A similar trend has been described in some studies with other polymers [5].

Table 1. Fitting parameters of Arrhenius function of apparent viscosity with temperature for MC-T dispersions at different polymer ratios and shear rates

MC:T *ratio*	$\dot{\gamma}$ *, 1/s*	$A_A \cdot 10^5$*, Pa s*	E_a*, kJ/mol*	R^2*, -*
0.25:0.75	0.1	0.42±0.01^{i}	31.3±0.2^{a}	0.997
	1	0.78±0.02^{h}	28.7±0.1^{c}	0.987
	10	4.2±0.3^{f}	23.2±0.3^{f}	0.977
	100	12.6±0.2^{e}	18.4±0.2^{i}	0.968
0.50:0.50	0.1	0.44±0.03^{i}	31.0±0.1^{a}	0.995
	1	0.36±0.05^{i}	30.7±0.1^{b}	0.996
	10	0.80±0.01^{h}	27.6±0.3^{d}	0.995
	100	1.6±0.3^{g}	24.2±0.2^{e}	0.994
0.75:0.25	0.1	16.5±0.3^{d}	22.7±0.3^{f}	0.990
	1	21.9±0.5^{c}	21.5±0.1^{g}	0.988
	10	39.8±0.4^{b}	19.3±0.3^{h}	0.985
	100	100±0.9^{a}	15.7±0.2^{j}	0.988

Data are presented as means ± standard deviation. Data value with different superscript letters in columns are significantly different, $p \leq 0.05$.

Mechanical spectra of MC:T gum dispersions

Figure 2 shows the influence of temperature on the viscoelastic properties for representative MC:T dispersions. G´ and G´´ values increased with angular frequencies and decreased with temperature. The dependence of both moduli with the angular frequency was more pronounced at 0.75:0.25 ratio, which is in well harmony with the results obtained for single components, as the range of values of G´ and G´´ for MC encompasses about four magnitude orders (from 0.01 to 100 Pa) whereas for T only three (from 0.01 to 10 Pa) (data not shown). Although all samples exhibited predominantly viscous behaviour (G´´ > G´) at the studied angular frequency and temperature ranges, the dependence of G´ modulus with the angular frequency was higher than that showed by the corresponding G´´ modulus. Experimental data from mechanical spectra of MC:T dispersions at different polymer ratios were also satisfactorily (R^2 > 0.99 and s < 0.005 Pa) correlated with angular frequency at each temperature trough Maxwell model, Eq. (1). The thermal influence on rheological moduli can be estimated by means of the Eq. (1) exponents. Note here those exponents (b and d) exhibited values in the range of those corresponding to the single systems, and could be successfully estimated using a mixing rule based on the polymer ratios and exponents for single systems.

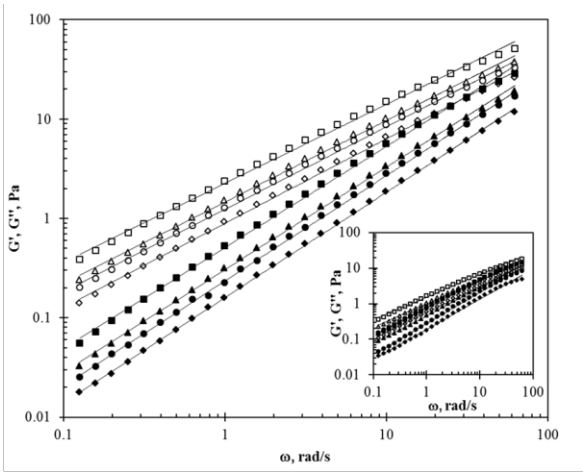

Figure 2. Oscillatory shear experimental data for MC:T dispersions at different polymer ratios (1:3, (inset) 3:1) and temperatures: (■) 5, (▲) 15, (•) 25, (•) 35 ºC (G´, full symbols; G´´, empty symbols)

It should be indicated that the MC and T systems showed the highest and the lowest tan δ (G''/G') values, respectively, at angular frequencies below 10 rad s^{-1}. The values of tan δ for MC:T mixtures were intermediate to those obtained for the single systems with lower values when MC:T ratio decreased (data not shown). In all cases, the values of tan δ decreased with increasing frequency, indicating a more liquid-like behaviour, mainly at the lowest angular frequencies. Specifically, at 35ºC, MC:T dispersions prepared at MC:T ratio > 50:50 tended to a relative maximum in tan δ at low angular frequencies, which is more evident for MC:T dispersions at the highest MC:T ratio (75:25).

The presence of a relative maximum in tan δ at low angular frequencies has been previously noticed for biopolymer suspensions with spheroidal and cylindrical particles, being promoted at the highest temperatures [1]. Later on, Balaghi et al. [4] also observed differences in the maximum of tan δ for six T samples with different insoluble fraction content. Latter authors attributed this behaviour to differences in the insoluble fraction, which with its swelling power and its greater Sauter diameter, contributed to the modification of the viscoelastic character of the samples.

The dependence of the elastic and viscous moduli with temperature at selected angular frequencies (0.13, 1, 10, 62.7 s^{-1}) for MC:T dispersions using the Arrhenius

function has been also evaluated and the corresponding fitting parameters (R^2 > 0.95 and s < 0.018 Pa) at different polymer ratios, Table 2.

Table 2. Representative data of the fitting parameters of Arrhenius function of storage modulus (G') with temperature for MC:T dispersions. Energy of activation.

		G´		
MC:T	***w*, rad/s**	***A_A*, Pa s**	***E_a*, kJ/mo1**	***R^2*, -**
0.25:0.75	0.13	$2.6 \cdot 10^{-8} \pm 1.0\ 10^{-9}$ g	35.9±0.2 c	0.980
	1	$2.3 \cdot 10^{-7} \pm 1.4\ 10^{-8}$ f	34.7±0.1 d	0.999
	10	$3.5 \cdot 10^{-5} \pm 1.3\ 10^{-6}$ d	27.3±0.1 h	0.991
	62.8	$4.4 \cdot 10^{-4} \pm 1.8\ 10^{-5}$ c	24.1±0.2 j	0.950
0.50:0.50	0.13	$4.0 \cdot 10^{-7} \pm 2.3\ 10^{-8}$ f	28.1±0.3 g	0.999
	1	$4.7 \cdot 10^{-7} \pm 1.9\ 10^{-8}$ f	32.6±0.2 e	0.999
	10	$1.4 \cdot 10^{-5} \pm 1.5\ 10^{-6}$ d	29.4±0.3 f	0.999
	62.8	$8.5 \cdot 10^{-5} \pm 2.1\ 10^{-6}$ d	27.3±0.1 h	0.989
0.75:0.25	0.13	$6.5 \cdot 10^{-7} \pm 1.8\ 10^{-8}$ f	26.1±0.5 i	0.990
	1	$2.9 \cdot 10^{-6} \pm 2.3\ 10^{-7}$ e	27.9±0.2 g	0.995
	10	$1.2 \cdot 10^{-4} \pm 1.9\ 10^{-5}$ c	24.8±0.4 j	0.984
	62.8	$5.4 \cdot 10^{-3} \pm 2.0\ 10^{-4}$ b	19.8±0.4 k	0.974

Data are presented as means ± standard deviation. Data value with different superscript letters in columns are significantly different, p ≤ 0.05.

Overall, the trend of E_a of both moduli decreased with increasing angular frequency, although some statistical differences can be observed in a restricted range, which indicate that the changes on the viscous or elastic component with temperature are promoted at lower frequencies [5]. Besides, it was also noticed that the values of energy of activation determined for G´ were higher than those corresponding to G´´.

Cox-Merz analysis

Evaluation of the Cox-Merz rule for representative MC:T gum dispersions are shown in Figure 3. The most of the MC:T dispersions obeyed the Cox-Merz rule, although slight differences at the highest shear rates for samples with the highest MC content (75:25) and at the lowest shear rates for samples with the highest T (25:75) content were observed. This behaviour was independent of the tested temperature and consistent with the previous results for MC and T [3]. At low shear rate/frequencies, deviations from the Cox-Merz rule were also previously reported for particulates systems [5] or algae suspensions [6]. Latter authors indicated that this empirical relationship is only obeyed for homogeneous systems, which is in well harmony with the results found for tested gums, taking into account the insoluble fraction present in the tragacanth gum [3].

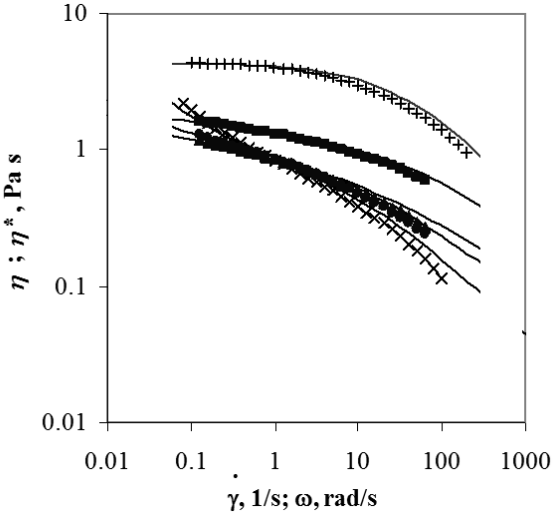

Figure 3 Cox-Merz relationships for complex (lines) and apparent viscosity (symbols) for: (|) T 10 g L-1, (+) MC 20 g L-1, and (•) MC:T (1:3), (▲) MC:T (1:1), (■) MC:T (3:1), at 25 ºC

This behaviour is confirmed here, since samples with the highest tragacanth ratio (25:75) exhibited the largest deviations. These departures in other hydrocolloids mixed systems were attributed to the presence of high density entanglements resultant from very specific polymer/polymer interactions ('hyper-entanglements') [6].

References

1. Farzia, M., Yarmanda, M.S., Safaria, M., Emam-Djomeha, Z., and Mohammadifar, M.A. (2015). Int. J. Biol. Macromol. 79, 433-439.
2. Chenlo, F., Moreira, R., Pereira, G., and Silva, C. (2009). LWT - Food Sci. Technol. 42, 519-524.
3. AOAC (2000). *Official Methods of Analysis*.
4. Balaghi, S., Mohammadifar, M.A., Zargaraan, A., Gavlighi, H.A., and Mohammadi, M. (2011). Food Hydrocol. *25*, 1775-1784.
5. Teimouri, S., Abbasi, S., and Sheikh, N. (2016). Food Hydrocol. 59, 9-16.
6. Razavi, S. M. A., Alghooneh, A., Behrouzian, F., and Cui, F. S. W. (2016). Food Hydrocoll. 60, 67-76.

Contact Address:

M.D. Torres (mariadolores.torres.perez@usc.es)
Department of Chemical Engineering, Universidade de Santiago de Compostela, rúa Lope Gómez de Marzoa, Santiago de Compostela, E-15782, Spain.
Tel: +34 881816752; fax: +34 981528050

Seaweed-Enriched Gluten-Free Chestnut Doughs: Effect of *Bifurcaria bifurcata* Addition on Rheological Behaviour

R. Moreira, J. Sineiro, F. Chenlo, S. Arufe, M.D. Torres

Department of Chemical Engineering, Escola Técnica Superior de Enxeñaría, Universidade de Santiago de Compostela (Spain)

Introduction

Given the increasing demand of gluten-free products adequate for people suffering some of the three pathologies associated with the gluten intake (*i.e.* gluten allergy, coeliac disease, and gluten sensitivity), the development of new formulations is necessary. In this sense, brown seaweed *Bifurcaria bifurcata*, commonly found in Europe on the Atlantic coast, is suitable for human consumption [1]. It can be employed in gluten-free formulations based on flour made from dried and milled chestnut fruits (*Castanea sativa*), a autochthonous Mediterranean raw material, to improve nutritional and antioxidants properties.

Recent studies on chestnut flour indicated that the presence of this flour may be a promising frontier to improve overall appearance, quality, sensory properties and shelf life of gluten-free baked products [2]. Overall, chestnut flour and *Bifurcaria bifurcata* seaweed powder offer a range of excellent choices, both as a base or additive, for gluten-free baked products. A challenge for the coming years would be to introduce these and other novel additives with attractive antioxidant properties in gluten-free products, optimising processing conditions and doses of the compounds [3].

Common gluten-free flours present certain technological limitations, mainly high viscosity values or lack of suitable viscoelastic properties owing to the absence of gluten [4]. The thermo-rheological characterization of novel gluten-free doughs is critically relevant in order to accomplish the optimisation of formulations and the characterisation of the final products in terms of technological aptitude and textural acceptance.

The enhancement of the functional properties of gluten-free products remains an important task for research and development, which is a concomitant challenge towards the improvement of technological and sensory characteristics. In this context, the main objective of this work is to study the effect of *Bifurcaria bifurcata* seaweed powder addition on the thermo-rheological characteristics of the chestnut flour doughs.

Experimental methods

A gluten-free formulation (control, BB0) based on chestnut (*Castanea sativa*) flour, 2% of guar gum (flour basis, f.b.) and 1.8% f.b. of sodium chloride was supplemented with different amounts of *Bifurcaria bifurcata* seaweed (BB) dried powder (3, 6 and 9% f.b.), labelled as BB3, BB6 and BB9, respectively, and mixed in a laboratory kneader (Mixolab®) to obtain seaweed-enriched chestnut flour doughs with similar torque (1.10 ± 0.07 Nm).

The rheological characterization was carried out using a controlled stress rheometer (MCR 301, Anton Paar Physica, Austria) equipped with a chamber (CTD 450, Anton Paar Physica, Austria) with parallel plates (50 mm diameter, 2 mm gap) at 30ºC (± 0.1ºC). Doughs obtained with Mixolab® at the target consistency were placed between the plates. The dough that came out of the plate was trimmed. The sample edge was coated with paraffin (Panreac Química S.A., Spain) to prevent water evaporation during the measurements. A rest time of 5 min was applied to all samples before measuring. All tests were carried out at least in triplicate.

The linear viscoelastic region (LVER) of every sample was determined by means of a strain sweep (γ: 0.01 - 10%) at standard frequency of 6.28 rad s^{-1} (1 Hz).

In order to determine the mechanical spectra of doughs, frequency sweep tests were carried out from 1 to 100 rad s^{-1} of angular frequency (ω) at 0.1% strain value, inside the LVER of the sample, to determine the storage, G´, and loss, G´´, moduli (Pa) and the loss tangent ($\tan\delta$ = G´´/G´). Experimental data of G´ and G´´ *vs* ω were fitted using Eqs. (1) and (2):

$$\log G' = \log a' + b' \log \omega \quad (1)$$

$$\log G'' = \log a'' + b'' \log \omega \quad (2)$$

where a', a'', b' and b'' are the corresponding fitting parameters.

Creep and recovery tests were performed by application of a constant stress (σ) of 50 Pa during 60 s (t_{max}) out of the LVER (creep step) and allowing strain recovery during 180 s after stress removal, $\sigma = 0$ (recovery step). Experimental data of creep and recovery were analysed by means of creep compliance rheological parameters J(t) (Pa^{-1}) = γ/σ [5] and correlated by Burgers model [6] using the following Eqs. (3) and (4) for creep and recovery steps, respectively:

$$J(t) = J_0 + J_m\left(1 - \exp\left(\frac{-t}{\lambda_c}\right)\right) + \frac{t}{\eta_0} \quad (3)$$

$$J(t) = J_{max} + J_0 + J_m\left(1 - \exp\left(\frac{-(t-t_{max})}{\lambda_r}\right)\right) \quad (4)$$

where J_0, J_m and J_{max} (Pa^{-1}) are the instantaneous, viscoelastic and maximum creep compliance, respectively, t (s) is the phase time, λ_c and λ_r are the mean retardation times of creep and recovery steps respectively and η_0 (Pa·s) is the zero-shear viscosity. The recovery compliance, J_r (Pa^{-1}), is calculated by the sum of J_0 and J_m corresponding to the recovery phase, Eq. (4). The J_r/J_{max} ratio gives information on relative elastic component of the maximum creep compliance.

Thermomechanical characteristics of doughs were measured inside the LVER of the doughs (0.1 % of strain, 1 Hz of frequency). Temperature was increased from 30 to 100ºC with a constant heating rate of 4ºC/min. Values of G´, G´´, and tanδ were determined to analyse the temperatures associated with thermal transitions using Rheoplus/32 software (version 3.21, Anton Paar, Ostfildern, Germany).

Statistical analysis

Experimental data of different properties of the tested flour doughs were statistically analysed. Differences among means were identified by one-factor analysis of variance (ANOVA), followed by the Scheffe test and considering significant P-values ≤ 0.05 (IBM SPSS Statistics 22).

Results and Discussion

BB addition increased water absorption (WA) of doughs to obtain similar consistencies. Control doughs had the lowest WA 57.7 ± 2.3 % d.b. BB powder addition had a strong influence on WA. In fact, just a 3% of seaweed powder addition already produced a significantly increase on WA (62. 5± 0.9%) whereas the maximum WA was obtained for dough with 9% of BB (70.8 ± 0.8%). The increase of WA of doughs with seaweed powder addition could be explained by the higher water retention capacity of seaweed powders 10.40 g water·(g d. solid)$^{-1}$ compared to those of chestnut flour, 3.80 g water·(g d. solid)$^{-1}$.

Frequency sweep tests showed that G´ and G´´ values increased with angular frequency (ω) (Figure 1). ANOVA test indicated that no significant differences existed on moduli dependence with ω (b´ and b´´ values corresponding to tested doughs samples) (Table 1). G´ values were larger than G´´ showing that elastic proportion was dominant over the viscous one, a typical trend observed in gluten-free doughs [4]. Finally, addition of BB > 6% significantly increased G´ values whilst G´´ values did not exhibit statistical differences for all assayed doughs.

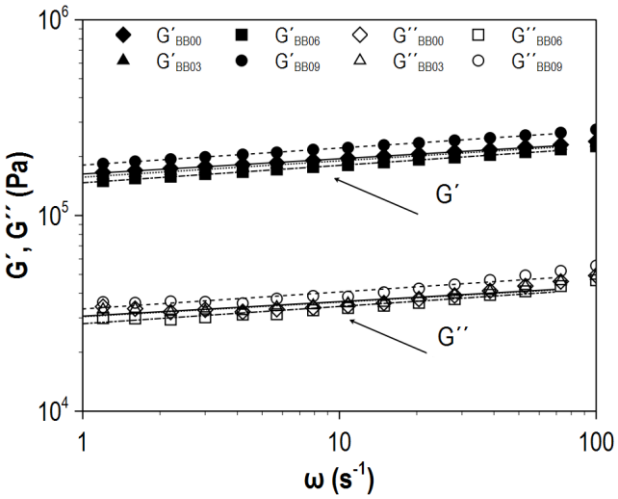

Figure 1. Experimental data of G´ (filled markers), G´´ (empty markers) chestnut and seaweed-enriched chestnut doughs. Lines correspond to Eqs. (1) and (2).

*Table 1. Rheological parameters of chestnut and seaweed-enriched chestnut doughs for oscillatory shear modelling: Eqs. (1) and (2).**

Dough	a´ ·10^{-3} (Pa s$^{-b´}$)	b´ ·10^3	R^2	a´´ ·10^{-3} (Pa s$^{-b´´}$)	b´´ ·10^3	R^2
BB00	163±4^{a,b}	78±1^a	0.99	31±2^a	74±13^a	0.80
BB03	157±12^{a,b}	83±9^a	0.99	30±2^a	79±20^a	0.85
BB06	147±2^a	89±2^a	0.99	28±1^a	88±1^a	0.92
BB09	181±1^c	87±2^a	0.99	33±1^a	87±1^a	0.87

**Data are presented as means ± standard deviation. Data value with different superscript letters in columns are significantly different, P ≤ 0.05.*

Creep and recovery results revealed similar viscoelastic behaviours of doughs (Figure 2). During creep phase compliance increased and then, during recovery phase, a sensible decrease on compliance was observed until almost achieved the steady state. Similar curves were also reported by other authors for gluten-free doughs [7].

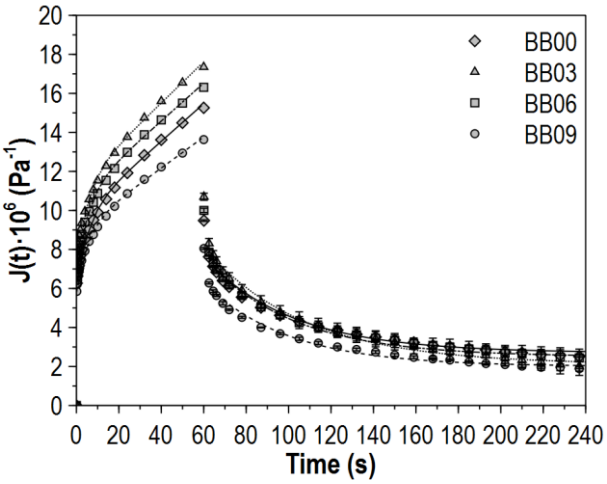

Figure 2. Experimental data creep and recovery data of chestnut and seaweed-enriched chestnut doughs. Lines correspond to Eqs. (3) and (4).

Parameters values obtained after fitting of experimental data employing Eqs. (3) and (4) for creep and recovery, respectively, are shown in Table 2. No significant differences were observed on λ_c for all assayed doughs. However it was observed a significant difference on instantaneous and viscoelastic compliance (J_0 and J_m) and zero shear viscosity (η_0) when amounts of *Bifurcaria bifuracata* seaweed powders > 6% were added. Indeed, BB addition seems to increase (η_0) that could lead to lower values of J_0 and J_m. Other authors [8] also reported a positive increment on viscosity when fibre was added to wheat flour doughs and suggested to be due to a filler like effect of particles added as it could be happening in our case.

*Table 2. Rheological parameters of chestnut and seaweed-enriched chestnut doughs: creep, Eq. (3), and recovery, Eq. (4), models.**

Parameter	BB00	BB03	BB06	BB09
		Creep		
$J_0\ 10^6$ (Pa^{-1})	$5.9\pm0.2^{a,b}$	6.7 ± 0.1^{c}	$6.3\pm0.1^{b,c}$	5.5 ± 0.1^{a}
$J_m\ 10^6$ (Pa^{-1})	3.7 ± 0.1^{b}	4.4 ± 0.1^{c}	4.2 ± 0.1^{c}	3.4 ± 0.1^{a}
λ_c (s)	4.8 ± 0.1^{a}	4.3 ± 0.0^{a}	4.4 ± 0.1^{a}	4.5 ± 0.2^{a}
$\eta_0\ 10^{-6}$ (Pa·s)	10.1 ± 0.2^{b}	9.2 ± 0.2^{a}	9.9 ± 0.1^{b}	12.1 ± 0.1^{c}
R^2	0.98	0.98	0.98	0.98
		Recovery		
$J_{máx}\ 10^6$ (Pa^{-1})	13.4 ± 0.1^{b}	14.9 ± 0.1^{d}	14.2 ± 0.2^{c}	11.8 ± 0.1^{a}
$J_0\ 10^6$ (Pa^{-1})	$5.9\pm0.1^{a,b}$	6.7 ± 0.2^{c}	6.3 ± 0.1^{b}	5.5 ± 0.1^{a}
$J_m\ 10^6$(Pa^{-1})	4.9 ± 0.3^{a}	6.0 ± 0.2^{b}	$5.2\pm0.3^{a,b}$	4.3 ± 0.1^{a}
λ_r (s)	41.9 ± 3.7^{a}	47.5 ± 0.4^{a}	39.8 ± 2.4^{a}	39.7 ± 1.0^{a}
J_r (%)	80.6 ± 1.7^{a}	85.6 ± 2.9^{a}	81.6 ± 2.6^{a}	82.6 ± 0.6^{a}
R^2	0.96	0.96	0.96	0.95

**Data are presented as means ± standard deviation. Data value with different superscript letters in rows are significantly different, P ≤ 0.05.*

Concerning recovery parameters, J_0 and J_m showed similar behaviour of those corresponding for creep step whilst J_{max} showed its maximum value for doughs enriched with 3% of BB and then decreased to lower values compared to control dough with BB addition of 9%. This seems to indicate that BB addition < 6% did not significantly worsen the recovery behaviour of doughs.

As it can be observed in Figure 3, all assayed doughs showed similar thermomechanical behaviour. Firstly, at low temperatures both moduli diminished due to proteins weakening of dough until achieve a minimum (T_0'). T_0' determines the beginning of gelatinization process as it has been reported to be related to swelling of starch granules. Then both moduli increases due to the growing turgor of starch granules defining an inflection point of the curve (T_0) until achieve a maximum (T_p). Finally, both moduli decrease as consequence of thermal degradation of doughs components once gelatinization transition has finished (T_f). Temperatures associated to gelatinization transition of doughs were studied by DMTA employing the protocol established in literature [9] which defines how to determine the different points associated to this transition (T_0', T_0, T_p and T_f) following G´ values.

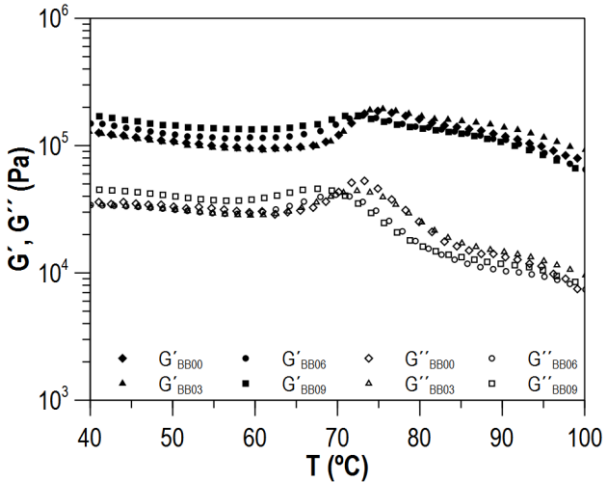

Figure 3. G´ and G´´ moduli vs temperature (T) for chestnut and seaweed-enriched chestnut doughs.

As it can be observed in Table 3, no significant differences were observed on T_0' which seem to indicate that the different water absorption of doughs as consequence of BB addition did not modify the beginning of swelling process of starch granules. However, T_0 and T_p significantly increased for dough with BB addition ≥ 3%, this fact indicates that BB addition modifies the process of disintegration of granules and starchy polymers melting. The interactions between starch and seaweed particles at these temperatures are not studied, up to our knowledge.

However, this modification can be explained by the higher water absorption of dough with BB addition > 6% that, even if it did not modify the beginning of swelling process of the starch, aids the water acquisition by the starch granules and hence the need of lower temperatures to start the disintegration of granules and melting polymers of starch.

*Table 3. Temperatures associated to gelatinization transition of chestnut and seaweed-enriched chestnuts doughs determined by DMTA.**

Peak	BB00	BB03	BB06	BB09
T_0'	60.2±1.0^a	60.2±1.2^a	57.1±1.8^a	58.6±1.5^a
T_0	70.0±0.5^b	70.7±0.1^b	68.5±0.2^a	68.2±0.1^a
T_p	75.3±0.3^b	75.1±0.1^b	72.3±1.1^a	72.5±0.1^a
T_f	83.5±0.7^a	82.9±2.3^a	81.8±0.4^a	80.3±1.6^a

**Data are presented as means ± standard deviation. Data value with different superscript letters in rows are significantly different, P ≤ 0.05.*

Concluding Remarks

The rheological study of seaweed-enriched chestnut flour doughs allowed the determination of a threshold value of BB addition that do not modify seaweed-enriched chestnut flour doughs properties compared to a control formulation. A maximum value of 6% of BB addition seems to be adequate due to it allows the maintaining of oscillatory, creep and recovery and thermomechanical properties in the same range of those obtained for control formulation.

Acknowledgements

The authors acknowledge the partial financial support of the Ministerio de Economía y Competitividad of Spain and FEDER (CTQ 2013-43616/P).

References

1. Gómez-Ordóñez, E., Jiménez-Escrig, A. and Rupérez, P. (2010). Food Res. Int. 43, 2289-2294.
2. Paciulli, M., Rinaldi, M., Cirlini, M., Scazzina, F. and Chiavaro, E (2016). LWT – Food Sci. Technol. 70, 88–95.
3. Torres, M.D., Arufe, S., Chenlo, F. and Moreira, R. (2017). Int. J. Food Sci. Technol. 52, 81-90.
4. Moreira, R., Chenlo, F., Arufe, S., and Rubinos, S.N. (2015). J. Food Sci. Technol. 52, 7954-7963.
5. Steffe, J.F. (1996) Rheological methods in food process engineering, 2nd ed., Freeman Press, East Lansing.
6. Burgers, J.M. (1935) First report on viscosity and plasticity. Nordemann Pub, New York.
7. Lazaridou, A., Duta, D., Papageorgiou, M., Belc, N. and Biliaderis, C.G. (2007). J. Food Eng. 79, 1033-1047.
8. Bonnand-Ducasse, M., Della Valle, G., Lefebvre, J., and Saulnier, L. (2010). J. Cereal Sci. 52, 200-206.
9. Moreira, R., Chenlo, F., and Arufe, S. (2015). Carbohydr. Polym. 127: 160-167.

Contact Address:

ramon.moreira@usc.es
Chemical Engineering Department
Escola Técnica Superior de Enxeñaría (ETSE)
Universidade de Santiago de Compostela
Rúa Lope Gómez de Marzoa s/n, Campus Vida, 15782 Santiago de Compostela, Spain.
Telf.: +34 881 816 797
Fax: +34 881 528 060

Rheological Properties of Wheat Flour Dough Enriched with *Fucus vesiculosus* Brown Seaweed Powder

R. Moreira[1], J. Sineiro[1], F. Chenlo[1], S. Arufe[1], H. Chiron[2], G. Della Valle[2]

[1] Chemical Engineering Department, Escola Técnica Superior de Enxeñaría, Universidade de Santiago de Compostela (Spain)
[2] UR 1268 Bliopolymères Interactions Assemblages (BIA), Institut National de la Recherche Agronomique (INRA) (Nantes, France).

Introduction

The European Commission of European Union recently classified the brown edible seaweed *Fucus vesiculosus* like a "novel food" for human consumption and consequently an increase in its demand as food is expected. *Fucus vesiculosus* is a dominant specie of macroalgae on the coast bathed by the Atlantic Ocean in Europe. It is mainly constituted by (% dry mass): 47.8 carbohydrates, 17.5 minerals, 10.5 polyphenols, 10 proteins, 4.8 lipids and 9.4 other components [1] and some of these components are reported to have relevant antioxidant capacity [1,2]. These characteristics suggest that the study of this seaweed to improve nutritional properties of foods could be interesting.

Wheat is one of the most employed sources of nutrients by world population, typically in the form of bread [3]. However, nutritional properties of wheat bread can still be improved by the use of new ingredients as well as food additives like hydrocolloids, which has become a common practice in the baking industry in order to improve also dough handling properties, bread quality and to extend the shelf life of stored bread [4]. In this sense, the use of *Fucus vesiculosus* seaweed powder in order to improve wheat bread properties and also to develop alternative uses of this seaweed seems to be an interesting starting point. However, the addition of this seaweed to wheat can alter final bread texture, dough rheological properties and processing behaviour.

The main aim of this work is to determine the effect of *Fucus vesiculosus* addition to wheat flour on rheological properties of the corresponding doughs in order to determine the feasibility this seaweed addition as ingredient in breadmaking from a technological point of view.

Experimental

Dough Formulation and Mixing

Different formulations of wheat dough were studied: one of wheat flour used as reference (control), and other with *Fucus vesiculosus* (FV) seaweed powder added to wheat flour at different levels to modify the standard procedure. Control formulation consisted of 300 g wheat flour, 192 g tap water, 5.4 g salt and 0.006 g ascorbic acid. Several seaweed powder amounts were added to obtain different bread compositions, labelled as FV0X, with X as 2, 4, 6 and 8 % of seaweed powder (flour basis, f.b.). Tap water addition, Table 1, was adjusted by an expert baker for each formulation in view of dough behaviour in order to obtain a comparable dough consistency at the end of mixing [5].

Mixing was carried out in a spiral mixer in three different steps. Initially, wheat flour and seaweed powder were mixed at 60 rpm for 1 min in order to homogenize the solid mixture. Then, ascorbic acid and water were added and a pre-mixing step was carried out at 60 rpm during 2 min. Finally, a mixing step was developed for 7 min at 120 rpm. Salt was added 4 min before the end of the mixing. Experiments were carried out at least in triplicate.

Table 1. Composition of wheat dough and enriched wheat dough with Fucus vesiculosus seaweed powder (FV).

Dough	Flour (g)	FV (g)	Water (g)
FV00	300	0	192
FV02	300	6	196
FV04	300	12	200
FV06	300	18	204
FV08	300	24	208

Dough Characterization

Elongational characterisation of dough was carried out at large bi-extensional deformations by Lubrificated Squeezing Flow test (LSF) using a traction/compression machine (Instron Corporation, Type 1122, USA) with a plate-plate geometry (20 mm diameter) equipped with a force sensor (100 N). Cylindrical samples (14 mm height, 20 mm diameter) of mixed dough samples (≈ 5 g) were moulded in Teflon cylinders lubricated with paraffin oil and kept at room temperature for 30 min [6].

Then the homogeneous samples were removed from the cylinders and placed between the plates also lubricated with paraffin oil. The cylindrical samples were compressed by the upper plate, attached with a movable crosshead, until a final height of 1 mm, at several constant speeds (5, 10 or 100 mm/min). The force applied was recorded as function of sample displacement. Data were processed according to a previous procedure [7]. The biaxial (Hencky) strain ε_b was calculated and related to the time in order to calculate the strain rate, $\dot{\varepsilon}_b$ (s^{-1}). Then $\dot{\varepsilon}_b$ was related to the stress, calculated as the ratio between the force applied and the surface of the plate, in order to obtain the bi-extensional viscosity, η_e (Pa·s). The variations of η_e with $\dot{\varepsilon}_b$ at constant ε_b, were fitted by the power law equation, Eq. (1):

$$\eta_e = K \cdot (\dot{\varepsilon}_b)^{n-1} \quad (1)$$

where K ($Pa \cdot s^n$) is the consistency index and n (-) the flow behaviour index.

Viscoelastic properties of doughs were studied by dynamic mechanical thermal analysis (DMTA) using a controlled stress rheometer (MCR 301, Anton Paar, Austria) equipped with a chamber (CTD 450, Anton Paar, Austria) with parallel plates (50 mm diameter, 2 mm gap). After mixing, dough rested 20 min at ambient temperature (≈ 25°C). Then a dough sample was placed between the plates, excess volume of dough sample, in relation to the volume given by gap between plates, was trimmed and the edge was coated with paraffin to prevent water evaporation during the measure. A rest time (5 min) was applied to all samples before measuring. Experiments were carried out at 1 Hz, 0.1% of strain (inside the linear viscoelastic region). Temperature was increased from 25 to 115°C with a constant heating rate of 3°C/min. Values of viscoelastic moduli (G´, G´´ and tan δ = G´´/G´) were determined. Minimum and maximum values of G´ were obtained and their ratio calculated to provide an interpretation of starch gelatinization and gluten reticulation [8]. All measurements were carried out at least in duplicate.

Statistical Analysis

The goodness of fitting of experimental data to the different model applied was evaluated from the corresponding coefficients of determination (R^2) and root mean square error (E_{RMS}). Differences among means were identified by one-factor analysis of variance (ANOVA), followed by the Scheffe test and considering significant P-values ≤ 0.05 (IBM SPSS Statistics 22).

Results and Discussion

The biaxial extension measurements of all studied doughs were satisfactorily fitted ($R^2 > 0.94$) using power law equation, Eq. (1). For ε_b value of 1, the values of consistency index (K) varied between 6.6 and $22.1 \cdot 10^3$ $Pa \cdot s^n$ (Table 2) in the same interval as those reported for wheat flour doughs containing different bran amounts [9]. The flow index (n) values varied in a narrow interval (0.24-0.29), were lower than those encountered by other authors [9] and reflected a clear shear-thinning behaviour for all assayed doughs. Large values of n were attributed to modifications of gluten network structure [10]. In our case, the increase of K, and consequently of elongational viscosity, due to seaweed powder addition, can be explained by the physical action of seaweed powder particles. Indeed, this is in agreement with previous results [11,12] that showed, for elongational and shear viscosities, respectively, that solid particles could increase dough viscosity through a filler-like effect in the dough matrix. In this case, the FV particles could perform this role. A similar increase in the elongational viscosity of wheat flour dough, by adding bran, was reported [9] and related to the high water absorption capacity and insolubility of the added particles. Given this, it could be suggested that, in this case, *Fucus vesiculosus* seaweed powder could play the same role as bran particles due to its high water retention capacity and insolubility (> 90%).

*Table 2. LSF parameters of wheat dough and enriched wheat dough with Fucus vesiculosus seaweed powder (FV).**

Dough	$k \cdot 10^{-3}$ ($Pa \cdot s^n$)	n (-)	R^2 (-)	$E_{RMS} \cdot 10^{-3}$ (Pa·s)
FV00	6.6 ± 0.01^d	0.24 ± 0.01^b	0.991	4.87
FV02	10.7 ± 0.01^c	0.29 ± 0.01^a	0.999	1.87
FV04	15.3 ± 0.02^b	$0.26 \pm 0.01^{a,b}$	0.983	16.09
FV06	21.7 ± 0.03^a	0.28 ± 0.01^a	0.998	4.41
FV08	22.1 ± 0.01^a	0.28 ± 0.01^a	0.998	7.20

**Data are presented as means±standard deviation. Data value of each parameter with different superscript letters in columns are significantly different, P ≤ 0.05.*

To have a better insight on the possible structural mechanisms governing the changes of dough extensional properties, employing DMTA, its properties in the viscoelastic domain (small strains). In this purpose, G'_{max}/G'_{min} ratio was measured and it has been considered as a potential indicator of gluten network structuration or cross-linking. Indeed, a lower value of the ratio is related to a less efficient heat effect promoting thermal aggregation of proteins, showing that the gluten network was already cross-linked before heating [8,10]. In our case, the modulus ratio strongly

decreased with FV content (Figure 1) from 28 (FV00) to 8 (FV08).

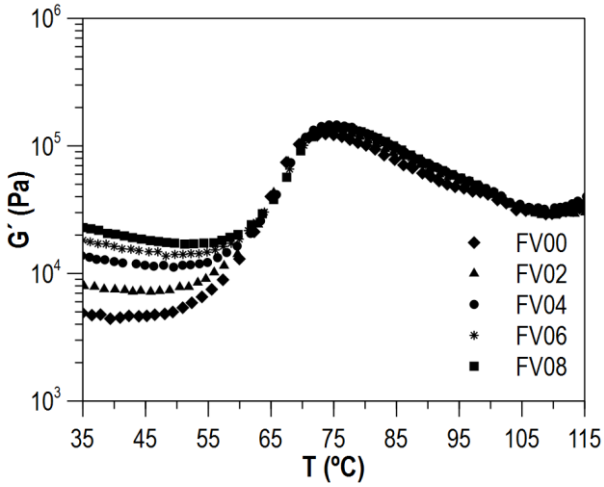

Figure 1. G´ vs temperature (T) for wheat dough and enriched wheat dough with Fucus vesiculosus seaweed powder (FV).

The correlation between the G'_{max}/G'_{min} ratio, measured at low strains, and K obtained at large strains (LSF) was similar of that obtained for wheat dough obtained under different mixing conditions [10]. Acceptable correlation ($R^2 > 0.90$) was found between the G'_{max}/G'_{min} ratio and K by an Arrhenius type equation, Eq. (2):

$$K = 4.79e^{\frac{13.65}{\left(\frac{G'_{max}}{G'_{min}}\right)}} \quad (2)$$

Large values of elongational viscosity are coincident with low G'_{max}/G'_{min} values that indicate a high structuration of dough gluten network [10], since in this case gluten network formation was likely influenced by the mixing conditions. In our case, such mechanism is still questionable because solid particles, like FV powder, are better known to preclude the formation of gluten network either by competing for available water or because of steric hindrance [9,13]. The obtained result could be related to the physical effect of seaweed particles which impairs gluten aggregation during heating by DMTA.

Concluding Remarks

Fucus vesiculosus seaweed powder addition significantly modified wheat dough properties. It incremented elongational viscosity due to a filler-like effect in the dough matrix of seaweed powders and decreased G'_{max}/G'_{min} ratio.

From a technological point of view the use of *Fucus vesiculus* as ingredient in breadmaking seems to be feasible taking into account the rheological changes of the enriched dough compared to a typical wheat flour dough.

Acknowledgements

The authors acknowledge the financial support of the Ministerio de Economía y Competitividad of Spain and FEDER (CTQ 2013-43616/P).

References

1. Hahn, T., Lang, S., Ulber, R., and Muffler, K. (2012). Process Biochem. 47, 1691-1698.
2. Moreira, R., Chenlo, F., Sineiro, J., Arufe, S., and Sexto, S. (2016). J. Appl. Phycol. 28, 2485–2494.
3. Peña, R.J. (2002). In Bread Wheat Improvement and Production. (Curtis, B.C., Rajaram, S. and Macpherson, H.G. eds.), Food and Agriculture Organization of the United Nations, Rome.
4. Mamat, H., Matanjun, P., Ibrahim, S., Amin, S.F.M., Hamid, M.A. and Rameli, A.S. (2014). J. Appl. Phycol. 26, 1057-1062.
5. AFNOR, (2002). BIPEA, standard method for French breadmaking, V03 716, Association Française de Normalisation, Paris.
6. Launay, G., and Michon, C. (2008). J. Texture Stud. 39, 496-529.
7. van Vliet, T. (2008). J. Cereal Sci. 48, 1-9.
8. Angioloni, A., and Dalla Rosa, M. (2005). J. Cereal Sci. 41, 327-331.
9. Le Bleis, F., Chaunier, L., Chiron, H., Della Valle, G. and Saulnier, L. (2015). J. Cereal Sci. 65, 167-174.
10. Turbin-Orger, A., Shehzad, A., Chaunier, L., Chiron, H. and Della Valle, G. (2016). J. Food Eng. 168, 129-136.
11. Cavella, S., Romano, A., Giancone, T. and Masi, P. (2008). In Bubbles in Food 2-Novelty, Health and Luxury (Campbell, G.M., Scanlon, M.G. and Pyle, D.L. eds.), pp. 311-322, Eagan Press, St Paul.
12. Bonnand-Ducasse, M., Della Valle, G., Lefebvre, J., and Saulnier, L. (2010). J. Cereal Sci. 52, 200-206.
13. Noort, M.W.J., van Haaster, D., Hemery, Y., Schols, H.A. and Hamer, R.J. (2010). J. Cereal Sci. 52, 59-64.

Contact Address:

ramon.moreira@usc.es
Chemical Engineering Department
Escola Técnica Superior de Enxeñaría (ETSE)
Universidade de Santiago de Compostela
Rúa Lope Gómez de Marzoa s/n, Campus Vida, 15782 Santiago de Compostela, Spain.
Telf.: +34 881 816 797 Fax: +34 881 528 060

Influence of sugars on the apparent viscosity enhancement of aqueous tragacanth gum dispersions

R. Moreira, F. Chenlo, C. Silva, M.D. Torres

Department of Chemical Engineering, Universidade de Santiago de Compostela, rúa Lope Gómez de Marzoa, Santiago de Compostela, E-15782 (Spain).

Introduction

The understanding of interactions between biopolymers and other main components commonly used in food formulations is critically relevant in order to control the rheological, mechanical, structural or storage stability characteristics of the derived products. This is particularly important for those biopolymers with complex characteristics, as the natural plant exudate tragacanth gum (T) obtained from stems and branches of different *Astragalus* species [1,2].

T gum is a complex heterogeneous anionic branched polysaccharide with high molecular weight (~ 8.4 105Da) [3], that has been used in a wide range of food, cosmetic, pharmaceutical and other diverse industrial applications. It consists of two main portions – one tragacanthin is water soluble and other bassorin is water swellable - with different physicochemical and rheological properties [4]. Earlier works have also demonstrated that the soluble and insoluble ratios strongly vary between species. The effect of biopolymer concentration (from 0.6 to 7.6 g/L) on the steady shear flow properties (at shear rates from 3 to 1000 s^{-1}) of aqueous T dispersions at fixed temperature of 25ºC has been already reported [3], indicating pseudoplastic behaviour with an approximation to Newtonian behaviour as gum concentration decreases. Even though, further insight is necessary concerning the effect of temperature on steady shear flow properties of this biopolymer dispersions, which have not been extensively studied. These differences can result in an extended pallet of rheological functionalities highly dependent of interactions with other components which is necessary to analyse.

The use of this biopolymer is the result of its unique properties of high viscosity, ease of emulsification, acid stability, smooth and creamy mouthfeel [5]. In the last decade, the T gum (E413) has been used in numerous food formulations, where sugars (s), essentially sucrose (S) and glucose (G), are present in noteworthy amounts. Namely, this biopolymer has been used as thickening agent in gluten-free flour doughs, as fillings or sauces; as emulsifier in baked goods, relishes or dairy products or as stabiliser in processed fruits and fruit juices, acid dressings or fermented dairy products. In these applications, the common range of T gum concentration is from 0.1% up to 2.0% [4,5,6].

Sucrose is one of the most studied sweeteners, as it plays a key role as a preserving agent or ingredient in many formulations and technological processes. Commonly the presence of sucrose improves the product flavour, structures and texture, prolongs freshness or contributes to moisture retention. Currently, glucose is used with more frequency as ingredient, mainly in syrups.

Considering that apparent viscosity and physical stability of a food formulation could be modified by the presence of sugars, at larger content than the used for gums, the research of these mixtures is justified. Previous works have hypothesised that the changes could arise from the hydrogen bonds rupture, solvent structural change, polymer hydration modifications or alteration of the polymer-water interactions [5]. Moreover, the presence of sugar solutions changes the carbohydrate – water interactions, suggesting an organisation increase of the water molecules with sodium salts in aqueous sugar solutions. In view of these results, the study of such more complex mixtures (hydrocolloid – sugar – salt) turns interesting for many applications in food formulations [3]. Many food products have optimal ranges of rheology and texture, and it is important to stay within these limits even when the sugar/salt conditions are changed.

Therefore, this work is aimed to study the impact of sugars (sucrose and glucose), over a wide range of concentrations and temperatures, on the rheological properties of aqueous tragacanth gum dispersions and to determine the corresponding model equations.

Experimental

Raw materials

The tragacanth gum, (T) (Merck KGaA., Darmstadt, Germany) from commercial food grade polymers was used without further purification. Due to its hygroscopic character, it was equilibrated at a constant moisture content using a chamber containing saturated NaCl solution at room temperature (a_w 0.75). Sucrose (commercial table sugar), anhydrous D(+)-glucose (PA-ACS, Panreac Química, Spain) and sodium chloride (PRS-Codex, Panreac Química, Spain) were also used previous hygroscopic equilibration.

Samples preparation

A stock T (2.5 g L^{-1}) aqueous dispersion was prepared following the protocol established in the literature [2]. The sugar/water ratio (*i.e.* S or G) ranged from 0 to 0.40 (w/v). G and S, previously dissolved in distilled water were added to the stock T with stirring at 1400 rpm for 30 min at room temperature, Table 1.

Table 1. Composition, wi (g/100 mL), and mass component ratios of aqueous tragacanth gum dispersion (T-s0), tragacanth-sugar (T-si). T, tragacanth gum; s, sugar; W, water.

	T-s0	T-s1	T-s2	T-s3
w_T	0.25	0.23	0.21	0.18
w_s	-	9.07	16.63	28.52
w_w	99.75	90.70	83.16	71.30
T/s	-	0.025	0.013	0.0062
T/W	0.0025	0.0025	0.0025	0.0025
s/W	-	0.10	0.20	0.40

Rheology

Steady-shear flow tests were conducted, at different shear rates, $\dot{\gamma}$, (1 – 1000 s^{-1}), on a controlled stress rheometer (MCR 301, Paar Physica, Graz, Austria), with either parallel plates (geometry 50 mm, 1 mm gap) or Couette geometry (2 mm gap, bob diameter and height of 24 and 25 mm). All measurements were controlled by a Peltier system (± 0.01). Temperature effect on some selected dispersions (tragacanth gum T–s0 and tragacanth–sugar at s/W 0.40) was studied from 5 to 65ºC. In order to prevent water loss, all samples were covered with paraffin oil. Before conducting the measurements, all samples were rested in the device during 10 min.

Experimental data of apparent viscosity *vs.* shear rate for T dispersions in the presence of sugars were correlated following the Cross-Williamson model, Eq. (1),

$$\eta = \frac{\eta_0}{1 + k(\dot{\gamma})^{(1-n)}} \approx \frac{A}{1 + k(\dot{\gamma})^{(1-n)}} \quad (1)$$

being η_0 (Pa s) the zero shear rate viscosity renamed to A corresponding to the apparent viscosity value at shear rate of 1 s^{-1}, because of the lack of Newtonian plateau in T systems below this shear rate; n (-) the flow index and k (s^{1-n}) the model parameter related to the consistency index.

Statistical analysis

One-factor analysis of variance (ANOVA) was used to statistically analyse the fitting parameters. When the ANOVA indicated differences among means, a Scheffé test was performed to differentiate means with 95% confidence ($p \leq 0.05$). The statistical treatments were made using IBM SPSS Statistics.

Results and Discussion

Rheology: effect of sugars on tragacanth dispersions

Flow curves of aqueous T gum-sugar dispersions (T-S and T-G) at polymer concentration of 0.25% and different sugar contents (0, 10, 20 and 40%) indicated that the sugar presence increased apparent viscosity in the whole shear rate range (Figure 1). This behaviour has been previously reported for other hydrocolloid-sucrose systems, where the increasing in apparent viscosity was associated to synergistic effects [2,3]. The increase in apparent viscosity is non-linear with sugar content and it is enhanced from values higher than 20% s/W. The trend to increase viscosity at low shear rate values (< 5 s^{-1}), specific of T gum, is softened with increase on sugar content.

Figure 1 gives more insight on the impact of each sugar on the flow behaviour of T gum dispersions. The apparent viscosity of T gum dispersions increased depending on the sugar type/content and the shear rate by the addition of both sugars. Particularly, the enhanced viscosity was larger at each shear rate for T samples added with glucose. The enhanced viscosity progressively increased in the presence of sucrose, more sharply at low shear rates and tending to a plateau at higher shear rates, which was shifted from 2 to 10 s^{-1}, with increasing sucrose content from 10 to 40%. Interestingly, the enhanced viscosity exhibited a maximum around the same values of shear rate in the presence of glucose. Analysing the data sets in terms of moles of sugar by gram of tragacanth in order to

compare T-S2 (~ 0.23 mol/g) to T-G1 (~ 0.22 mol/g) and T-S3 (~ 0.46 mol/g) to T-G2 (~ 0.44 mol/g), the outcomes suggest that the interactions between the polymer and sugars are favoured at low shear rates (< 10 s^{-1}) in the presence of sugars with low molecular size, which is consistent with those results for other hydrocolloids as dextran [4] or sage seed gum affected by various sugars [6]. Latter authors indicated that the highest viscosity increase at low shear rates in the presence of low molecular size sugars is related to increasing the number of junction zones.

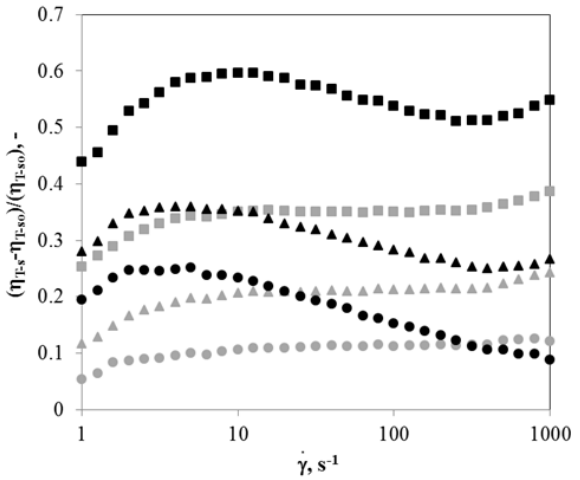

Figure 1. Enhanced viscosity [$(\eta_{T-s}-\eta_{T-s0})/(\eta_{T-s0})$] due to sugars presence for tragacanth gum- sucrose (T-S) (grey) and tragacanth gum-glucose (T-G) (black) solutions at 5 ºC. Symbols: (•) T-s1, (▲) T-s2, (■) T-s3.

In contrast, at high shear rates, these junction zones can be easier broken than those formed in the presence of sugars with high molecular weight, in this case the sucrose, which allow easily stabilizing their structure and apparent viscosity shows a plateau in this region of shear rates. The obtained outcomes support the hypothesis that interactions through hydrogen bonds between the biopolymer and sugar-OH groups, more and more stable junction zones between the biopolymer chains and the influence of the spatial structure and the interplay between water and sugar on interactions with the polymer are favoured at low shear rates in the presence of low molecular size polymers as glucose.

Concerning steady-shear data modelling, an adequate balance between low number of parameters and fitting quality was attained using Cross-Williamson model (Eq. 1). Table 2 collects the corresponding parameters for T-S and T-G systems at 5 ºC, as well as the reference (T-s0) at the same temperature. It should be noted that larger parameter values were found for tragacanth-glucose systems when compared with those obtained for tragacanth-sucrose systems. In all cases, as sugar content increased, A parameter significantly increased whereas k statistically decreased. Note here that the flow index, n, was invariant 0.64±0.02 for sucrose and glucose systems.

Table 2. Parameters of Cross-Williamson model, Eq. (1) $\eta = f(\dot{\gamma})s/W$, for aqueous tragacanth gum (T-s0) and tragacanth gum-sugar (T-S and T-G) dispersions at 5ºC. Average value n=0.64±0.02.

System	A 10^2(Pa s)	k (s^{1-n})	R^2
T-s0	6.31 ± 0.03	0.37 ± 0.01	0.985
T-S1	6.47 ± 0.09^c	0.34 ± 0.01^a	0.996
T -S2	6.72 ± 0.01^b	0.30 ± 0.01^b	0.994
T -S3	7.92 ± 0.01^a	0.24 ± 0.01^c	1.000
T -G1	7.59 ± 0.07^c	0.36 ± 0.01^a	0.995
T -G2	8.19 ± 0.01^b	0.33 ± 0.01^b	0.994
T -G3	8.54 ± 0.01^a	0.26 ± 0.01^c	0.999

Data are presented as means ± standard deviation. Data value with different superscript letters in columns per each sugar system are significantly different, $p \leq 0.05$.

Rheology: Effect of temperature on tragacanth-sugar dispersions

Flow curves of tragacanth-sucrose and tragacanth-glucose at the highest tested sugar content (T-S3 and T-G3) at different temperatures are presented in Figure 2. The dependency of apparent viscosity with temperature followed a similar trend to that noticed for the reference system T-s0. Flow curves at different temperatures did not converge at the lowest or highest shear rates, indicating that the temperature effect is independent on shear rate.

For both sugar added systems, apparent viscosity decreased non-linearly with increasing the temperature. Namely, the magnitude of the enhanced viscosity at each shear rate decreased with increasing temperature, exhibiting similar patterns at each temperature to those previously reported for sugar content (Figure 1). The enhanced viscosity exhibited a maximum in T-G3 samples, which was less marked at the highest assayed temperatures. In contrast, the enhanced viscosity of T-S3 samples gradually increased with increasing shear rate up to plateau behaviour. Both, the plateau and the maximum were shifted to lower shear rates (from 10 to 1 s^{-1}) with increasing temperature. The enhanced viscosity behaviour with temperature suggests that as temperature increased, the molecules of the insoluble fraction are probably more able to glide along each

other promoted by the viscosity drop with temperature; therefore the sample flow is favoured [4].

(a)

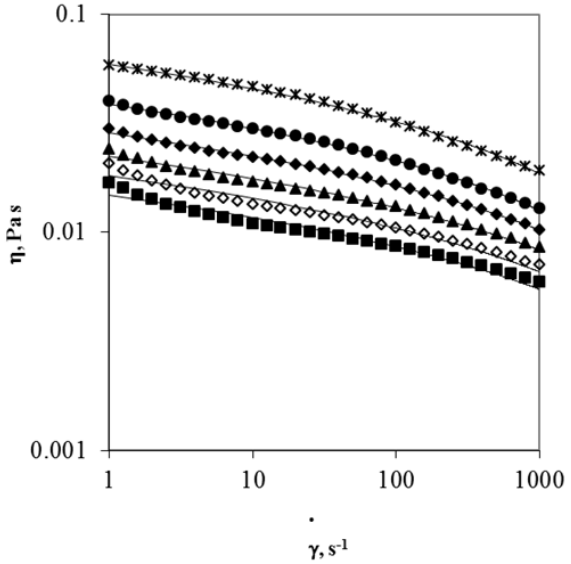

(b)

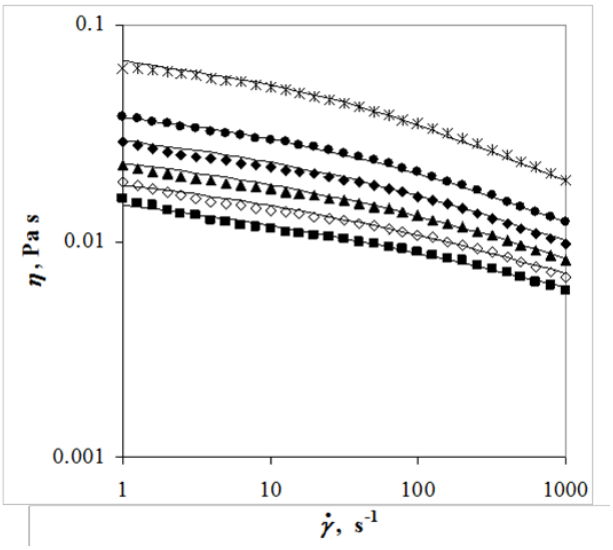

Figure 2. Flow curves for (a) tragacanth gum- sucrose (T-S3) and (b) tragacanth gum-glucose (T-G3) dispersions at different temperatures (ºC). Symbols: (*) 5, (•) 25, (♦) 35, (▲) 45, (◊) 55, (■) 65. Lines correspond to the correlation $\eta = f(\dot{\gamma}, T)$.

In all cases, the effect of the sugar (sucrose or glucose) decreased the apparent viscosity in the low shear rates region, a feature which allowed obtaining a satisfactory fitting by means of the Cross-Williamson model at each temperature. The corresponding parameters are summarised in Table 3, which were adequately correlated by means of the Arrhenius function for A and k parameters whereas a linear fitting was obtained for the flow index. It should be highlighted that the proposed function is able to reproduce the experimental steady-shear flow data with a maximum deviation of 7.4 and 8.0% for T-S3 and T-G3, respectively.

Table 3. Fitting parameters of Cross-Williamson model, Eq. (1) $\eta = f(\dot{\gamma})T$, for representative aqueous tragacanth gum-sugar dispersions at different temperatures (S, sucrose; G, glucose).

System	T (ºC)	A 10^2(Pa s)	k (s^{1-n})	n (-)	R^2
T-S3	5	7.18±0.09^{a}	0.24±0.01^{f}	0.57±0.01^{f}	1.000
	25	4.48±0.01^{b}	0.35±0.01^{e}	0.65±0.01^{e}	1.000
	35	3.29±0.01^{b}	0.45±0.01^{d}	0.6 ±0.01^{d}	0.998
	45	3.00±0.07^{c}	0.56±0.01^{c}	0.72±0.01^{c}	0.995
	55	2.78±0.01^{d}	0.70±0.01^{b}	0.78±0.01^{b}	0.992
	65	2.38±0.01^{e}	1.07±0.01^{a}	0.81±0.01^{a}	0.992
T-G3	5	8.54±0.06^{a}	0.18±0.01^{f}	0.62±0.01^{a}	0.999
	25	4.47±0.04^{b}	0.26±0.01^{e}	0.64±0.01^{a,b}	0.998
	35	3.39±0.01^{c}	0.31±0.01^{d}	0.66±0.01^{b,c}	0.995
	45	2.69±0.01^{d}	0.37±0.01^{c}	0.68±0.01^{c}	0.995
	55	2.62±0.01^{e}	0.47±0.01^{b}	0.75±0.01^{b}	0.990
	65	2.12±0.01^{f}	0.80±0.02^{a}	0.79±0.01^{a}	0.988

Data are presented as means ± standard deviation. Data value with different superscript letters in columns per each sugar system are significantly different, $p \leq 0.05$.

References

1. Yousefi, A.R., Eivazlou, R., and Razavi, S.M.A. (2016). Int. J. Biol. Macromol. 91, 1018–1024.
2. Chenlo, F., Moreira, R., Silva, C. (2011). J. Food Eng. 107, 234-240.
3. Pereira, P. A. P., Souza, V. R., Teixeira, T. R., Queiroz, F., Borges, S. V., and Carneiro, J. D. S. (2013). Food Hydrocoll. 42, 404–412.
4. Mohammadifar, M. A., Musavi, S. M., Kiumarsi, A., and Williams, P. A. (2006). Int. J. Biol. Macromol. 38, 31-39.
5. Kulkarni, V.S., and Shaw, C. (2016). Use of polymers and thickeners in semisolid and liquid formulations. In: Mclauglhin, M., East, K., Halterman, K. (Ed.) Essential chemistry for formulators of semisolid and liquid dosages. Academic Press, San Diego, USA.
6. Kurt, A., Cengiz, A., and Kahyaoglu, T. (2016). Carbohyd. Polym. 143, 116–123.

Contact Address:

M.D. Torres (mariadolores.torres.perez@usc.es)
Department of Chemical Engineering, Universidade de Santiago de Compostela, rúa Lope Gómez de Marzoa, Santiago de Compostela, E-15782, Spain
Tel: +34 881816752; fax: +34 981 528 050

Flow behaviour and viscoelasticity of nanoemulsions with different thickening agents

C. Arancibia[1], S. Fiszman[2], A. Tárrega[2]

[1] Food Science and Technology, Technological Faculty, University of Santiago of Chile (Chile)
[2] Instituto de Agroquímica y Tecnología de los Alimentos (IATA-CSIC) (Spain)

Introduction

Nanotechnology is a relevant science for food industry due to the increasing consumers' demand for healthier products and the need for edible systems able to encapsulate, protect, and release functional compounds [1]. Nanoemulsions consist on small oil droplets (diameter < 100 nm) dispersed within a continuous phase that can often be designed to have novel texture and to increase the bioavailability of bioactive lipid compounds encapsulated within them [2].

The incorporation of biopolymers represents one of the most common strategies used to stabilize emulsions, since one of the greatest problems of food emulsions is that they are unstable and tend to break during certain processing operations or upon storage [3]. The main role of most hydrocolloids in emulsions is that they act as structuring, thickening or gelling agents in the aqueous phase. The ability of hydrocolloids to thicken aqueous solutions is useful for inhibiting fat droplet creaming, and for providing some of the textural attributes on reduced-fat product [3, 4].

Starch is one of the most widely used thickeners in the food industry; it is present in many emulsion-based foods as sauces, dressings, soups, and dessert, since it gives smoothness, good texture, and improves physical stability of emulsions [4]. On the other hand, carboxymethyl cellulose (CMC), xanthan gum (XAN) and carrageenan (CAR) are also being used as an alternative to starch in thickened food and as fat replacer in semi-solid matrices due to several technological, sensory and nutritional advantages. Nevertheless, some authors have reported that the structural differences between cellulose- and starch-based matrices may result in different rheological and sensory properties [5, 6].

In this context, the objective of this study was to evaluate the effect of different type of hydrocolloids on the rheological properties of nanoemulsions based on avocado oil.

Experimental

Samples composition and preparation

Oil in water (O/W) nanoemulsions were prepared with avocado oil (10g/ 100 g) (Casta de Peteroa, Terramater S.A., Chile), Tween 80 (emulsifier) (7.5 g/ 100 g)(Sigma-Aldrich S.A., France) and purified water. Different hydrocolloids were used as thickeners: medium cross-linked modified tapioca starch (ST, C* Creamtex 75720, Cargill Ibérica SL, Spain), CMC (Akucell AF3265, AzkoNobel, The Netherlands), λ-carrageenan (CAR, Satiagum ® ADC 25, Degussa, Spain) and xanthan gum (XAN, Santiaxane CX910, Cargill Ibérica, Spain).

Four samples were prepared by adding different hydrocolloids to the emulsion: one sample with only starch (ST) (5 g/ 100 g) and three samples containing starch and a second hydrocolloid: CMC-0.1 g/ 100 g, CAR-0.2 g/ 100 g, and XAN-0.2 g/ 100 g.

The nanoemulsion-base was prepared according to the following procedure: first, Tween 80 was dispersed in water using a magnetic stirrer (Arex, Velp Scientifica, Italy) at 300 rpm-20 min. Then, oil was added slowly to the aqueous phase and the mixture was stirred using a high-performance dispersing homogenizer (Wiggen Hauser D130, Germany) at 16800 rpm for 10 min in a water bath at 5±1 ºC. In order to obtain nanoemulsions, the coarse emulsions were homogenized using a sonicator (VCX500, SONICS & Materials, USA) at 80% amplitude and 20 KHz of frequency during 20 min. Nanoemulsion-base had a particle size between 100 and 120 nm, which was determined in a Zetasizer (NanoS90, Malvern Instruments, UK).

After the nanoemulsion-base was prepared, a 100 g batch of each thickened sample was prepared. Hydrocolloids were weighed and added into nanoemulsions and mixed using a Thermomix (Vorverix, Germany) at 300 rpm-70 ºC for 10 min. After this time, samples were cooled at room temperature in a closed flask and stored under refrigeration (4±1 ºC for 24 h) prior to rheological measurements.

Rheological measurements

Rheological measurements were carried out in a controlled stress rheometer RS1 (Thermo Haake, Germany), using a parallel plates geometry (60 mm diameter; 1-mm gap) and a sample temperature of 10±1ºC.

Flow Behaviour. Flow curves of samples were obtained by recording shear stress values when shearing the samples at linearly increasing shear rates from 1 to 200 s^{-1} through 60 s and down in reverse sequence for the same time. Experimental data from ascending flow curve were described by a Ostwald de-Waele model as follow (Eq. 1):

$$\sigma = K\dot{\gamma}^{n} \quad (1)$$

where σ is the shear stress (Pa), $\dot{\gamma}$ is the shear rate (s^{-1}), K is the consistency index (Pa s^n) and n is the flow behaviour index. Apparent viscosity values at 10 s^{-1} (η_{10}) were calculated using Eq. 2.

$$\eta_{10} = K\dot{\gamma}^{(n-1)} \quad (2)$$

Viscoelastic Properties. Strain sweeps at a frequency of 1 Hz were performed in all samples to determine the linear viscoelasticity zone. Frequency sweeps tests were then performed from 0.01 to 10 Hz. The oscillatory rheological parameters used to compare the viscoelastic properties of the samples were: storage modulus (G'), loss modulus (G''), complex dynamic viscosity (η^*), and loss angle tangent (tan δ) at 1 Hz.

Statistical analysis

ANOVA was applied to rheological parameter values. Minimum significant differences were determined by the Tukey's test (α=0.05) (XLSTAT-Pro software v.2015, Adinsoft, Paris, France).

Results and Discussion

Flow behaviour

Flow curves obtained for nanoemulsion-based systems are shown in the Figure 1. All the samples exhibited a typical shear-thinning behaviour and observable hysteresis loops when they were sheared during a complete cycle. This behaviour is typical of semi-solid emulsion-based matrices, which corresponds to the resistance of deformation of the structure, given by the characteristics of the disperse phase (oil droplets), and the thickened continuous phase. The incorporation of a second hydrocolloid increased the resistance to flow of samples due probably to the formation of transient network structure in the aqueous phase [4].

In order to characterise the flow behaviour of each sample, data of the ascending curve were fitted to the Ostwald–de Waele model (R^2>0.99); the values of consistency index (K), the flow index (n) and apparent viscosity at 10 s^{-1} (η_{10}) obtained are shown in Table 1.

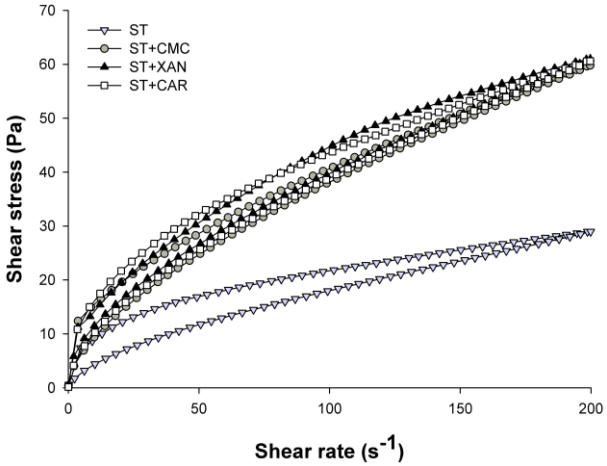

Figure 1. Flow curves of nanoemulsions with different thickening agents: ST (starch), ST+CMC (starch+carboxymethyl cellulose), ST+XAN (starch+xanthan gum) and ST+CAR (starch+carrageenan)

In general, it was observed that the incorporation of a second hydrocolloid increased significantly ($p<0.05$) apparent viscosity of starch-based nanoemulsions; however, no significant differences were found among different thickening agents. In addition, the second hydrocolloid did not have a significant ($p>0.05$) impact on K and n values.

Table 1. Rheological parameters of nanoemulsions with different thickening agents

Rheological Parameters[1]	Samples[2]			
	ST	ST+CMC	ST+XAN	ST+CAR
K (Pa s^n)	3.11[a]	4.00[a]	4.56[a]	5.22[a]
n	0.42[a]	0.50[a]	0.49[a]	0.46[a]
η_{10} (Pa s^{-1})	0.71[a]	1.26[b]	1.41[b]	1.50[b]
G' (Pa)	16.76[a]	22.84[a]	30.18[a]	19.72[a]
G" (Pa)	5.14[a]	12.58[b]	16.35[c]	16.73[c]
tan δ	0.31[a]	0.56[b]	0.56[b]	0.83[c]
η^* (Pa s)	2.79[a]	4.15[ab]	5.50[b]	4.15[ab]

[1] K: consistency index, n: flow index, η_{10}: apparent viscosity at 10 s^{-1}, G': storage modulus at 1 Hz, G": loss modulus at 1 Hz, tan δ: loss angle tangent at 1 Hz, η^*: complex dynamic viscosity at 1 Hz.
[2] ST: starch, CMC: carboxymethyl cellulose, XAN: xanthan gum, CAR: carrageenan
[a-c] Means within a row with common superscripts did not differ significantly (p>0.05)

Viscoelastic properties

All thickened nanoemulsions exhibited weak-gel behaviour, with the elastic response predominating over the viscous one (G' >G") (Figure 2). The incorporation of a second hydrocolloid reinforced the structure, but

storage (G') and loss modulus (G") values were more dependent on the frequency. For comparative purposes G', G", η^*, tan δ values at a frequency of 1 Hz were considered. Results from ANOVA showed that the addition of a second hydrocolloid affected significantly ($p<0.05$) G", η^* and tan δ values (Table 1). G" and η^* increased with second hydrocolloid, but this increase was different depending on type of thickener. In general, the samples with starch+xanthan-gum showed the highest G', G" and η^* values, which could indicate the formation of a three-dimensional network in the aqueous phase that leaded to more structured systems. It was also observed that the incorporation of a second hydrocolloid decreased significantly ($p<0.05$) tan δ values.

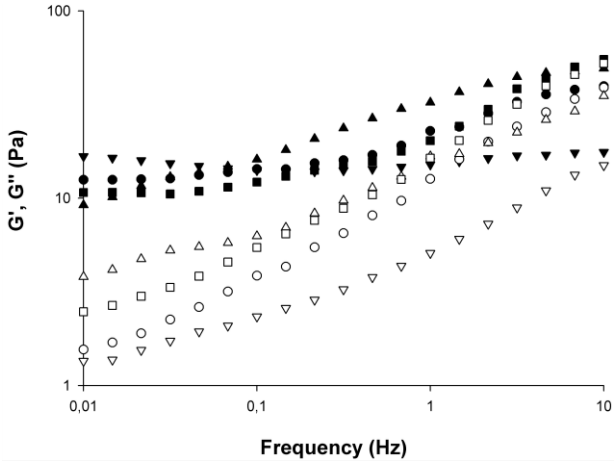

Figure 2. Mechanical spectra of nanoemulsions with different thickening agents: ▽ starch, ○ starch+carboxymethyl cellulose, △ starch+ xanthan gum, □ starch+carrageenan. G' (filled symbols) and G" (empty symbols).

Conclusions

It can be concluded that the incorporation of a second hydrocolloid into starch-based nanoemulsions modified their rheological properties, which depended on interactions of the different types of particles and polymers present in the system. The apparent viscosity and viscoelasticity of nanoemulsions increased by adding non-starch thickeners to the aqueous phase, obtaining food emulsions with comparable rheological behaviour. However, it is necessary to analyse thickener effects on other emulsion properties (droplet size, physical stability, etc.) in order to obtain food emulsions with full stability and adequate characteristics.

Acknowledgments

To CONICYT of Chile for financial support (FONDECYT POSTDOCTORADO Nº3150537 and PAI 79160091). To the Spanish Ministry of the Economy and Competitiveness for financial support (AGL-2016-75403-R) and for the Ramon y Cajal contract for author Tárrega, and gratefully acknowledge the financial support of EU FEDER funds.

References

1. Silva, H.D., Cerqueira, M.A., and Vicente, A.A. (2012). Food Bioprocess Tech 5(3), 854-867
2. Li, Y., and McClements, D.J. (2010). J Agri Food Chem 58(13), 8085-8092
3. McClements, D.J. (2015). Food Emulsions, 3th edn., CRC Press, Boca Raton.
4. Chung, C., Degner, B., and McClements, D.J. (2012). Food Res Inter 48, 641-649.
5. Ferry, A.L., Hort J., Mitchell J.R., Lagarrigue, S., and Pamies, B.V. (2004). J Texture Stud, 11–24
6. Arancibia, C., Jublot, L., Costell, E., and Bayarri, S. (2011). Food Res Inter 46 (6), 1632-1641.

Contact Address:

Carla Arancibia
carla.arancibia@usach.cl
Food Science and Technology Department,
Technological Faculty
University of Santiago of Chile
Obispo Umaña 050, Santiago, Chile
Telf.: +56227184518

Effect of pH and temperature on hydrocolloid solutions and hydrocolloid-based emulsions

M. Espert[1], T. Sanz [1], M.J. Hernández[2], A. Salvador[1]

[1] Department of Physical and sensory properties of food and consumer science. Institute of Agrochemistry and Food Technology (IATA-CSIC), Valencia (Spain).

[2] Department of Earth Physics and Thermodynamics, Faculty of Pharmacy, University of Valencia (Spain).

Introduction

Food hydrocolloids have been used for a long time in food systems as thickeners, emulsifiers, gelling agents, stabiliser, bulking agents, included in a wide variety of food products as bakery, beverages, confectionery and dairy based products.

A recent application of hydrocolloids in the food industry is the reduction of fat digestion in emulsions. It has been observed that fat digestion is related to the changes in the hydrocolloid structure.

The ether of cellulose methylcellulose (MC) is a non-ionic cellulose derivative with methyl groups added to the anhydroglucose backbone. Despite the fact that methyl moieties are hydrophobic groups, the polymer retains enough hydrophilicity to be highly water soluble. The introduction of these hydrophobic groups provides the polymer with surface activity and unique hydration-dehydration characteristics [1]. The ability to form thermal gels depends on the type and substitution degree of the hydrocolloid. The highest methoxyl substitution, the lowest gelling temperature.

Xanthan gum is an anionic polysaccharide, obtained by bacterial fermentation, with the ability to form high viscosity solutions stable over a wide range of temperature and pH. Xanthan gum does not show surface active properties, but it is very effective in emulsions as stabilizer of the continuous phase.

The decrease in fat digestion in emulsions has been related with the physical barrier exerted by the undigested continuous phase (hydrated hydrocolloid), which impedes fat release and the appropriate contact between fat and the digestive fluids, reducing the effectivity of the fat digestion process [2].

For the rational design of non digestible emulsions and to develop new applications of hydrocolloids, it is important to study the physical characteristics of the hydrocolloids and how they are affected during digestion conditions.

The objective of this work was to evaluate the influence of pH and temperature on the physicochemical properties of hydrated hydrocolloid systems and hydrocolloid based emulsions to better understand the structural changes that can be produced during the gastric digestion of these matrices.

Experimental

The hydrocolloids studied were: two types of methyl cellulose (MC) (A4M and MX) (The Dow Chemical Co) and xanthan gum (XG) (Cargill, France), always at a concentration of 2%.

Hydrated hydrocolloid solutions:

Two hundred grams of a solution of the different cellulose ethers (2% w/w) was prepared according to the hot/cold technique (The Dow Chemical Company). The powder was previously dispersed by gentle mixing with 1/3 of the total water at 80ºC for approximately 3 min (Heidolph stirrer at 800 rpm). Subsequently, the beaker with the dispersed cellulose ether was quickly transferred to a refrigerated water bath at 10ºC and the rest of the water was added at 1ºC and stirred continuously for 10 min, allowing a correct cellulose ether hydration.

In Xanthan gum water solution (2% w/w) the powder was hydrated by gentle mixing with water at room temperature for approximately 15 min (Heidolph stirrer at 800 rpm) increasing the stirring speed continuously up to 1800 rpm to allow a correct XG hydration.

Emulsions:

The emulsions were composed of sunflower oil (47%), water (51%) and the hydrocolloid (2%). To prepare cellulose o/w emulsions the cellulose ether was first dispersed in the oil using a Heidolph stirrer at the lowest speed for five minutes. The mixture was then hydrated by gradually adding the water at 1ºC while continuing to stir for 30 s. Stirring continued using a homogenizer (Ultraturrax T18, IKA, Germany) at 6500 (1 min−1) for 15 s and subsequently at 17500 (1 min−1) for 60 s until the emulsion was obtained.

In xanthan gum o/w emulsions the hydrocolloid was first dispersed in the water at room temperature using a Heidolph stirrer at 300-500 rpm for 10-12 minutes. Then the oil was gradually added while continuing to stir increasing the speed up to 1800 rpm. Stirring was maintained for additional 15 minutes. The mixture was finally homogenized using an IKA T18 basic (Ultra-Turrax) at 6500 (1 min−1) for 60 s, 13500 (1 min−1) for 60 s and subsequently at 17500 (1 min−1) for 60 s.

Viscoelastic properties

Rheological properties of the hydrocolloid hydrated solution and the O/W emulsions were analyzed by a controlled stress rheometer (AR-G2, TA Instruments (Crawley, England)) using a 40mm diameter plate-plate sensor geometry with serrated surface and 1mm gap between plates. Vaseline oil was used to prevent sample from drying during testing. In order to determine the linear viscoelastic range of each sample, deformation sweep tests were performed at a constant frequency (1 Hz). Temperature sweeps were carried out at a frequency of 1 Hz, 1°C/min, in the linear viscoelastic region, from 20°C to 70°C. Temperature sweeps were also carried out from 20°C to 37°C, followed by an oscillatory time sweep at 37°C during the time required to stabilize the sample. Once the sample structure is stable at 37°C, frequency tests (from 10 to 0.01Hz) were carried out. The samples were measured at the initial neutral pH and at pH 2.0 after adjusting with HCl (6N).

Results and Discussion

Hydrated hydrocolloid solutions

The changes in tan δ values during heating from 20 to 70°C for the different hydrocolloids, at neutral and at acidic pH are shown in Figure 1. At room temperature, the highest viscoelasticity was observed in Xanthan gum (XG), followed by Cellulose MX and Cellulose A4M. Thermal behavior was completely different for XG and cellulose ethers. In XG viscoelasticity was not affected by temperature, whereas thermal gelation is clearly observed in both A4M and MX, the gelation temperature being lower for MX type. In MX the increase in viscoelasticity (decrease in tan δ) occurs at a lower temperature in comparison to A4M, which is associated to its higher methoxyl content, as greater hydrophobicity reduces the gelling temperature. The pH does not affect the heating profile for any of the hydrocolloid solutions studied.

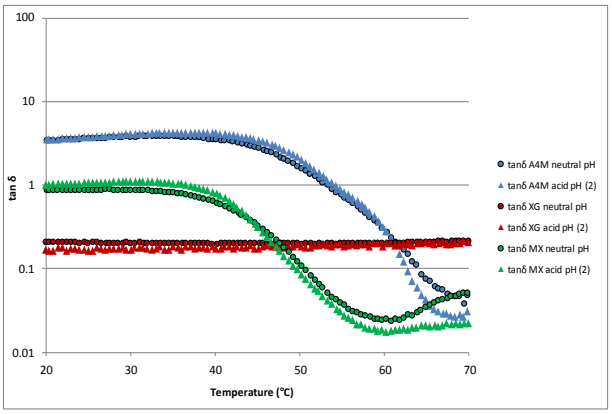

Figure 1. Tan δ values during heating for the hydrated hydrocolloid solutions.

The mechanical spectra at 37°C was investigated. In Figure 2 values of G' versus frequency are shown. A4M hydrated solution showed lower values of G' and higher frequency dependence than the others hydrated hydrocolloids. The highest G' values of cellulose MX in comparison to A4M are explained by two main reasons: 1) its higher molecular weight and 2) thermal gelation is already taking place at 37ºC in MX. No effect of pH was observed.

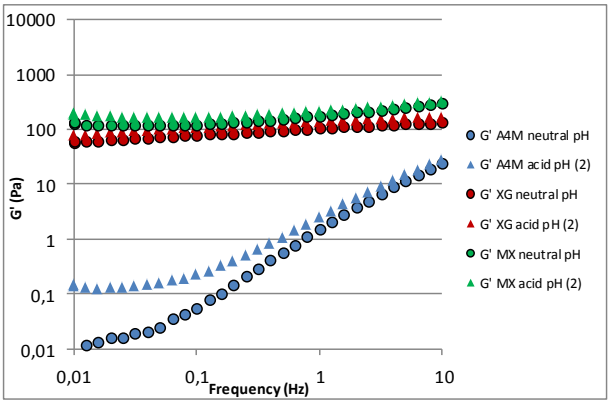

Figure 2. G' as a function of frequency for the different hydrated hydrocolloid solutions at 37°C.

Emulsions

The emulsion thermal behaviour is shown in Figure 3. Similarly to the behaviour found in the hydrated hydrocolloids, the XG emulsion viscoelastic behaviour was stable with temperature, while in A4M and MX emulsions a thermal dependence was observed. At 20ºC the highest viscoelasticity (lower tanδ) was found in the XG, followed by MX emulsion and A4M emulsion, which showed the lowest viscoelasticity. The increase in viscoelasticity with increasing temperature occurred at around 35ºC in MX emulsion and around 50ºC in the A4M emulsion. No effect of pH was observed in any of the samples. The fact that thermalgelation in the MX emulsion occurs at around body temperature in acidic pH conditions may have interesting implications, which should be considered for the rational design of food systems with novel properties, such as lower fat digestion in emulsions or development of satiating food.

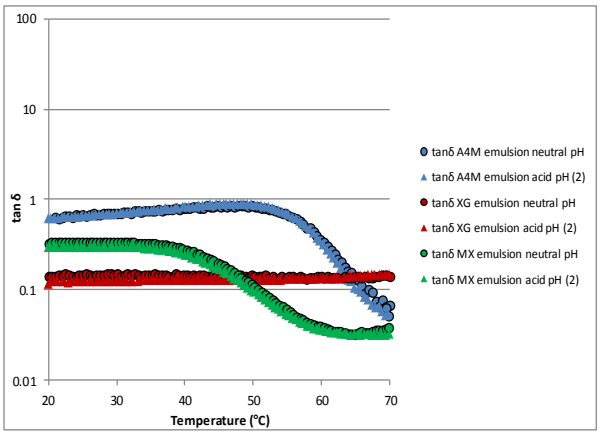

Figure 3. Tan δ values during heating for the hydrocolloid-based emulsions.

The evolution of G' with frequency at 37ºC is shown in Figure 4. The highest G' values were found in MX emulsion, while the A4M show significantly lower G' values with a big dependence with frequency. In emulsion A4M gelation has not already started at 37ºC. No effect of pH was observed in both cellulose emulsions. On the contrary, in the XG emulsion an increase in G' at pH 2 was observed. This higher effect of pH in the XG emulsions is expected to be associated to the anionic character of this gum.

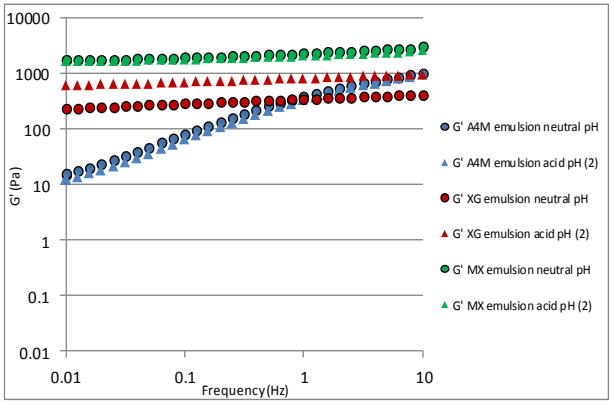

Figure 4. G' as a function of frequency for the different emulsions at 37°C.

Conclusions

This study contributes to better understanding the effect of pH and temperature in the structural properties of single hydrocolloids and hydrocolloid-based emulsions and will be helpful in the rational design of oil/water emulsions with reduced fat digestibility, and of other novel food applications, such as for example food with enhanced satiety. Future work is focused on the relationship among the rheological changes after simulated human digestion conditions and microstructure, emulsion droplet size and fat digestion. The increase in viscoelasticity will be also further investigated in terms of its relationship with fullness sensation.

Acknowledgements

Authors wish to thank Ministerio de Economía y Competitividad (Spain) for financial support (Project AGL2015-68923-C2-1-R).

References

1. Sarkar, N. (1975). J. Appl. Polym. Sc. 24, 1073-1087.
2. Espert, M., Borreani, J., Hernando, I., Quiles, A., Salvador, A., and Sanz, (2017). T. Food Hydrocolloid. 69, 76-85.

Contact Address:

mespert@iata.csic.es
Department of Physical and sensory properties of food and consumer science.
Institute of Agrochemistry and Food Technology (IATA-CSIC).
Avda. Agustín Escardino 7, 46980, Paterna, Valencia (Spain).
Telf.: +34 963 900 022

Release of flavonols in simulated *in vitro* gastrointestinal digestion and its relationship with viscosity in onion and apple products and commercial quercetin supplement

M.D. Alvarez, B. Herranz, I. Fernández-Jalao, C. Sánchez-Moreno, B. De Ancos

Department of Characterization, Quality and Safety, Institute of Food Science, Technology and Nutrition (ICTAN-CSIC), Madrid (Spain)

Introduction

Quercetin and quercetin derivatives are the major flavonoids found in onion and apple. The benefits on human health attributed to their consumption depend on their bioavailability that represents the end result of absorption, distribution, metabolic conversion of nutrients or bioactive compounds in the body and elimination via urine and faces. Bioavailability first requirement is the bioaccessibility of nutrients and bioactive compounds that is defined as the release of them from the food matrix during gastrointestinal digestion (GID) to be available for intestinal absorption [1]. *In vitro* digestion models represent a good system to understand the interaction food matrix-bioactive compounds during human GID and to determine their bioaccessibility obtaining results that are well correlated to those obtained *in vivo* digestion systems [2]. The GID phases are complex aqueous suspensions of particulate matter and solubilized nutrients, together with other components such as secreted enzymes, bile and mucin. Viscosity and other rheological properties of the digests change during their transit throughout the GID process so that digest rheology will be influenced by a combination of effects from continuous liquid and suspended particulate solid phases influencing the bioaccessibility of bioactive compounds (BC) [3]. The aim of this work was to study the release and bioaccessibility of flavonols in onion and apple products and in a commercial quercetin supplement and their possible relationships with the viscosity changes of the different gastrointestinal phases throughout *in vitro* GID process using a dynamic gastrointestinal digester. For that, flavonols release and viscosity changes at a physiological shear rate (10 s^{-1}) were studied. The changes in backscattered light monitored in time with a Turbiscan® were also measured to study the physical stability of the digests.

Experimental

Simulated GID procedure

A DGD, a multi-compartmental, dynamic and computer-controlled system developed at AINIA Technologic Center (Valencia, Spain) [4] was used to digest onion (*Allium cepa* L. var cepa, 'Recas', Carabaña, Madrid, Spain) and apple (*Malus Domestica*, 'Golden Delicious', Aragón, Spain) powder samples and quercetin supplements (500 mg; Solaray, Nutraceutical Corp. USA). The digestion process used is similar to that described in Villamejane et al. [5]. *In vitro* GID process was performed on 27 and 37.5 g of freeze-dried powder onion and apple, respectively, and on 70.5 mg of commercial quercetin powder from a pool of 5 capsules, in order to have similar total flavonol content at the beginning of GID.

Experimental analyses

For all the following analyses, digests of the different phases (ND, OP, GD and ID) for the three samples (onion, apple and commercial quercetin supplement) were performed in triplicate. The physical stability of the different digests was evaluated using a Turbiscan Lab instrument (Iesmat S.A., Alcobendas, Spain). The emulsion sample (7 mL) was transferred to a flat-bottom cylindrical glass vial and analyzed by a light beam emitted in near infrared (880 nm) wavelength which scanned the sample cell from the bottom to the top each minute for a period of 60 min.

The analysis of total flavonol was determined according to the methodology described by Bonoli et al. [6] using a UV-vis-Spectrophotometer (GE Amersham Biosciences Pharmacia, Sweden). Quantification was achieved using quercetin as external standard calibration curve in the range from 1 to 50 µg/mL. Total flavonol content was expressed as mg quercetin equivalents (QE) per 100 g dried weight (dw) of sample. Bioaccessibility was determined using equation: Bioaccessibility (%) =

($BC_{digested}/BC_{non\text{-}digested}$) x 100 with: $BC_{digested}$ = Concentration of BC in the soluble fraction of digested sample and $BC_{non\text{-}digested}$ = Concentration of BC in the non-digested sample.

Steady shear tests were carried out with a Kinexus Pro Rotational Rheometer (Malvern Instruments Ltd., Worcestershire, UK) equipped with a cone and plate geometry (4° cone angle, 40 mm diameter) at shear rates (100 to 0.1 s^{-1}) at 37 °C. A pre-shear was done at shear rate of 100 s^{-1} during 5 min. For gastric peristalsis, a maximum shear rate of 10 s^{-1} was reported by Kozu et al. [7] in liquid and liquid–solid gastric contents. For that reason, $\eta_{a,10}$ (apparent viscosity at shear rate of 10 s^{-1}) values were derived from apparent viscosity vs. shear rate curves and compared to *K* (consistency) values from power law fits.

Results and Discussion

The backscattering (BS) profiles of the digests in the different GID phases (ND, OP, GD and ID) for the three samples studied are shown in Figs. 1-4. All three samples presented a stable BS pattern in ND phase (Figs.1a-c). In OP and GD phases (Figs. 2,3), the BS profiles of onion (Figs. 2a,3a) and apple (Figs. 2b,3b) show an aggregation process by an increase of the BS in the middle of the sample, which is characteristic of the particle size increase, and at the same time, a notable creaming phenomenon (migration of particles) by the presence of cream layer (increase of BS) at the top part of the sample (right part of the graph). The cream layer increases with the time and it was more marked in onion (thicker layer; Figs. 2a,3a) than in apple (Figs. 2b,3b), However, in commercial quercetin supplement OP and GD phases (Figs. 2c,3c, respectively) were very stable. Note that in ID phase (Fig. 4) it was produced a remarkable change in the BS profiles for the three samples losing completely their previous patterns. This result could be related with the release of BC in the intestine. Therefore, the mild alkaline conditions of the intestinal phase seem to produce a change in the physical stability of the digests facilitating the release of the bioactive compounds.

These findings are in accordance with the results obtained for total flavonol contents in each product. A progressive decrease in total flavonols (Table 1) was observed in onion and quercetin supplement from ND to ID phases, meanwhile a significant increase in total flavonols release was observed in GD and ID phases of apple. Therefore, onion flavonols and quercetin in the commercial supplement appear to have been more resistant in the acidic conditions of the stomach than in the alkaline ones of the small intestine. However, the ID phase of apple product showed also a remarkable change in the BS profile in addition to presenting similar total flavonol content in GD and ID phases being significantly higher than in ND and OP ones. This different behavior detected in apple product may be due to a different physico-chemical composition of the food matrix since the apple presented higher pectin content, total fiber, soluble solids and acidity than onion which can makes apple powder more resistant to the intestinal phase than onion powder and quercetin supplement. Therefore, apple product presented the higher bioaccessibility (59.72%) followed by onion (16.55%) and quercetin supplement (4.12%). These results reflected the importance of the food matrix effect in the release and bioaccessibility of the flavonols.

Table 1. Effects of different in vitro GID phases on total flavonols

GID phases	Onion product
Non-digested (ND)	$382\pm19^{A}{}_{b}$
Oral-phase (OP)	$335\pm5.8^{B}{}_{b}$
Gastric digest (GD)	$338\pm12^{B}{}_{a}$
Intestinal digest (ID)	$292\pm3.5^{C}{}_{a}$
Bioaccessibility (%)	16.6 ± 2.3^{b}
GID phases	**Apple product**
Non-digested (ND)	$27.1\pm0.71^{B,C}{}_{c}$
Oral-phase (OP)	$26.2\pm2.7^{C}{}_{c}$
Gastric digest (GD)	$32.3\pm2.1^{A,B}{}_{c}$
Intestinal digest (ID)	$37.3\pm3.9^{A}{}_{c}$
Bioaccessibility (%)	59.7 ± 7.4^{a}
GID phases	**Quercetin supplement**
Non-digested (ND)	$840\pm19^{A}{}_{a}$
Oral-phase (OP)	$543\pm2.8^{B}{}_{a}$
Gastric digest (GD)	$168\pm4.5^{C}{}_{b}$
Intestinal digest (ID)	$88.0\pm7.0^{D}{}_{b}$
Bioaccessibility (%)	4.12 ± 0.27^{c}

Values are expressed as mg QE/100 g dw.
$^{A–D}$ for the same food matrix mean values with different letter Between different phases are significantly different ($P < 0.05$).
$^{a-c}$ for the same digestion phase among different products mean values with different letter are significantly different ($P < 0.05$).

Regarding rheological measurements, the flow curves of each GID phase for the three samples showed non-Newtonian shear-thinning behavior due to rearrangement in the conformation of the molecules in the dispersion as a result of shearing. As can be seen in Table 2, a decrease in *K* and $\eta_{a,10}$ values was observed for onion and apple products from ND to ID. However, in commercial quercetin, *K* and $\eta_{a,10}$ values were similar between different GID phases and much lower than those in onion and apple.

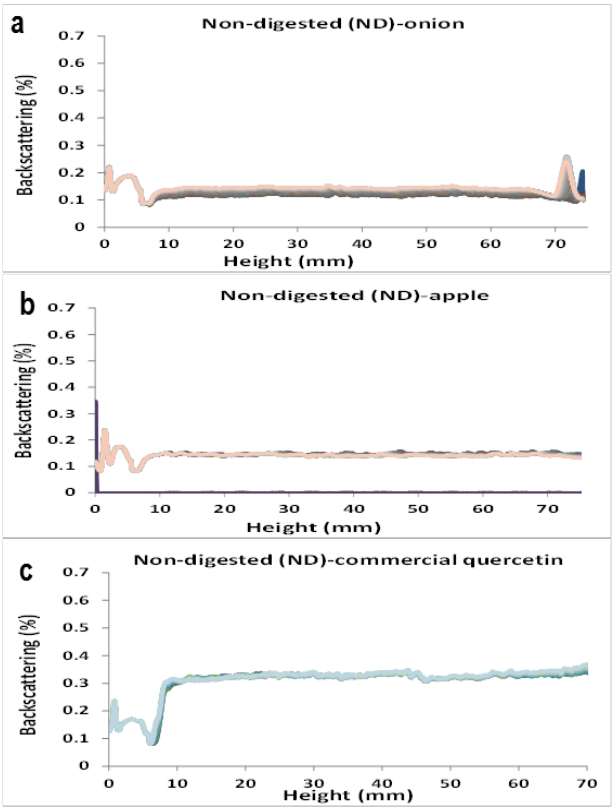

Figure 1. Backscattering (BS) profiles of the non-digested (ND) products

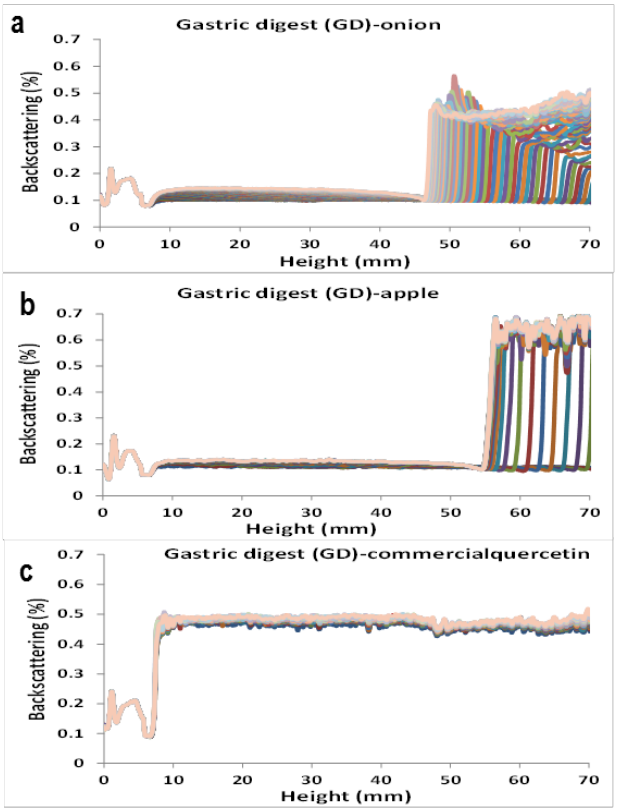

Figure 3. Backscattering (BS) profiles of the digests in gastric phase (GD)

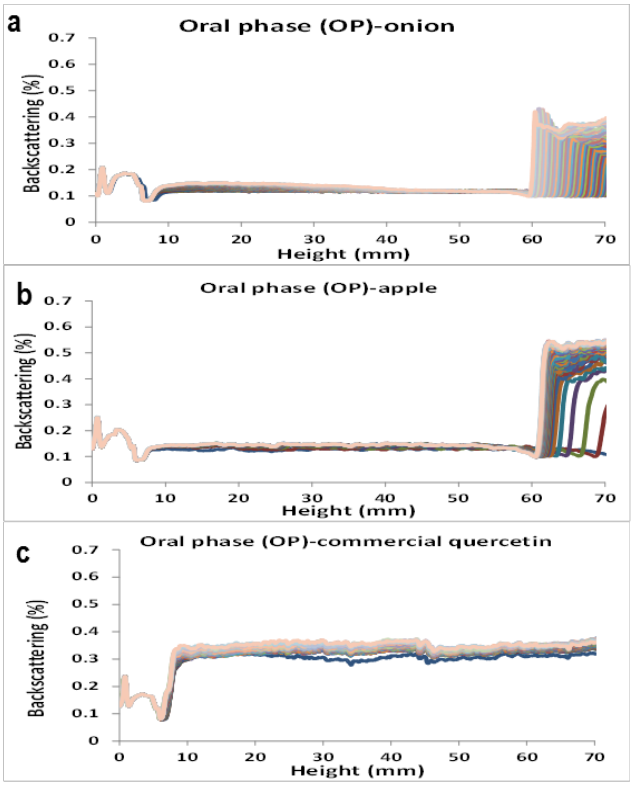

Figure 2. Backscattering (BS) profiles of the digests in oral phase (OP)

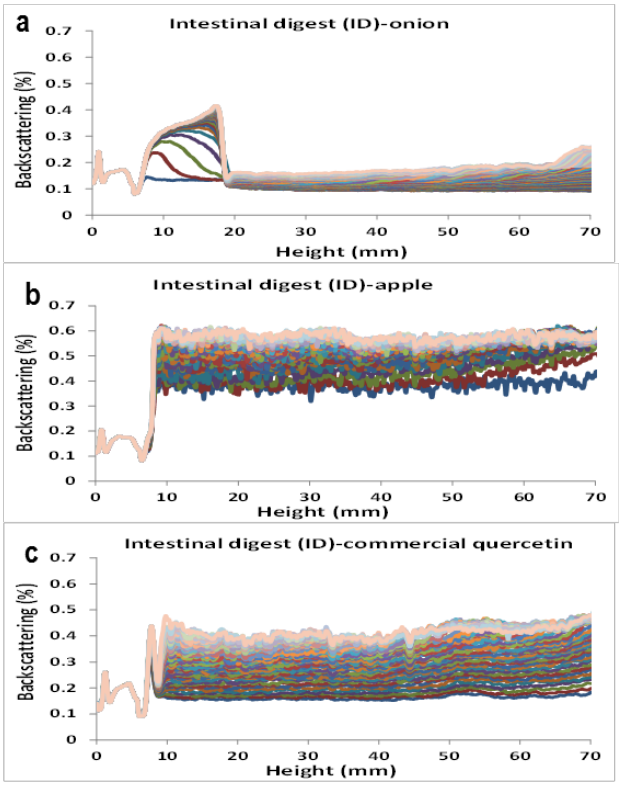

Figure 4. Backscattering (BS) profiles of the digests in intestinal phase (ID)

Table 2. Effects of different in vitro GID phases (ND, OP, GD and ID) and food matrix on steady shear rheological properties for different food products

Onion	***K* (mPa s^n)**	**$\eta_{a,10}$ (mPa s)**
ND	$237\pm18^{A}{}_{b}$	$48.0\pm11^{A}{}_{b}$
OP	$111\pm18^{B}{}_{b}$	$32.8\pm7.3^{B}{}_{b}$
GD	$22.3\pm2.5^{C}{}_{b}$	$4.77\pm1.1^{C}{}_{b}$
ID	$14.2\pm0.50^{C}{}_{b}$	$2.00\pm0.047^{C}{}_{b}$
Apple	***K* (mPa s^n)**	**$\eta_{a,10}$ (mPa s)**
ND	$376\pm13^{A}{}_{a}$	$72.2\pm17.6^{A}{}_{a}$
OP	$207\pm15^{B}{}_{a}$	$45.6\pm14.5^{B}{}_{a}$
GD	$178\pm21^{B}{}_{a}$	$23.7\pm8.60^{B,C}{}_{a}$
ID	$23.8\pm1.8^{C}{}_{a}$	$3.41\pm0.22^{C}{}_{a}$
Quercetin	***K* (mPa s^n)**	**$\eta_{a,10}$ (mPa s)**
ND	$12.2\pm0.18^{A,B}{}_{c}$	$1.60\pm0.038^{B}{}_{c}$
OP	$10.5\pm0.47^{C}{}_{c}$	$1.27\pm0.087^{C}{}_{c}$
GD	$12.8\pm0.37^{A}{}_{c}$	$1.78\pm0.076^{A}{}_{c}$
ID	$11.7\pm0.30^{B}{}_{c}$	$1.52\pm0.065^{B}{}_{c}$

$^{A-C}$ for each rheological property and the same matrix mean values with different letter between different phases are significantly different ($P < 0.05$).
$_{a-c}$ for each rheological property and the same GID phase mean values with different letter between different products are significantly different ($P < 0.05$).

Therefore, it seems that a diluting effect is produced in onion and apple products as the samples passed throughout GID. These results are in accordance with the previous BS profiles that were very stable for the all digestion phases in commercial quercetin while in onion and apple products showed a change in BS (destabilization phenomena) until it was achieved the ID phase. On the other hand, *K* and $\eta_{a,10}$ values correlated well with the bioaccesibility; apple had the highest *K* and $\eta_{a,10}$ values in ID, followed by onion and by last quercetin supplement.

Concluding Remarks

The release of bioactive compounds in the intestine corresponded with a change in the physical stability of the digest. There is a diluting effect throughout gastrointestinal digestion as it was shown by the *K* and $\eta_{a,10}$ values of the different GID phases of apple, onion and quercetin supplement. This diluting effect is related to the release of flavonols. Food matrices (apple and onion products) showed higher bioaccessibility than commercial quercetin supplement. Therefore, the evolution of the apparent viscosity and BS profiles throughout *in vitro* simulated GID can be related with the release of flavonols and their bioaccessibility.

Acknowledgements

This study has been funded by the Spanish project AGL2013-46326-R (Ministry of Economy and Competitiveness).

References

1. Carbonell-Capella, J. M., Buniowska, M., Barba, F. J., Esteve, M. J., Frígola, A. (2014). Compreh. Rev. Food Sci. Food Safety 13, 155-171.
2. Bouayed, J., Hoffmann, L., Bohn, T. (2011). Food Chem. 128(1), 14-21.
3. Marcano, J., Hernando, I., Fiszman, S. (2015). Food Hydrocolloids, 51, 16-22.
4. Viadel Crespo, B., Rivera Patiño, J. D., Navarro Fayos, M. T., Tenllado Llavador, I., Carreres Malonda, J. E., García Reverter, J., Blasco Piquer, M., Subirats Huerta, S. (2012). Equipo modular de digestión in vitro, Patent: ES 2 361 983 B1.
5. Villemejane, C., Denis, S., Marsset-Baglieri, A., Alric, M., Aymard, P., Michon, C., (2016). Food Chem. 190, 164-172.
6. Bonoli, M., Verardo, V., Marconi, E., & Caboni, M. F. (2004). J. Agric. Food Chem. 52, 5195-5200.
7. Kozu, H., Kobayashi, I., Neves, M. A., Nakajima, M., Uemura, K., Sato, S., & Ichikawa, S. (2014). Food Funct. 5, 1839–1847.

Contact Address:

María Dolores Alvarez (mayoyes@ictan.csic.es)
Characterization, Quality and Safety (DCCS), Institute of Food Science, Technology and Nutrition (ICTAN-CSIC), José Antonio Nováis 10, 28040 Madrid, (Spain)
Tel.: +34 91 5492300.Fax: +34 91 549 3627

A comparative study of flaxseed/chia-quinoa dough: thixotropic and viscoelastic behaviour

J. Rubio-Merino[1], E. Amate-Ruiz[2], A.I. Gómez-Merino[2], F.J. Rubio-Hernández[2], J.L. Arjona-Escudero[3], I.M. Santos-Ráez[3]

[1] *Unidad Docente Multiprofesional de Atención Familiar y Comunitaria Distrito Málaga-Guadalhorce, Málaga,(Spain)*
[2] *Dep. Física Aplicada II, Universidad de Málaga, Dr Ortiz Ramos s/n, Málaga (Spain)*
[3] *Dep. Ingeniería Mecánica Térmica y de Fluidos, Universidad de Málaga, Dr Ortiz Ramos s/n, Málaga (Spain)*

Introduction

Gluten is a source of vegetal protein. In terms of its nutritional value, gluten is considered to be poorer than proteins from animal sources and can cause allergic reactions and intolerances [1]. Quinoa, as other cereals, has attracted much interest because of its high nutritional value and for the absence of gluten. In spite of this, the absence of gluten in these flours, results in major problems for many pasta and bakery products. Attempts to use proteins from alternative flours as a partial substitute in wheat products have generally been unsuccessful, because of the contrasting differences between proteins: water-solubility, differences in primary structure and their size distributions, accounted for viscoelastic properties that are unique to wheat gluten proteins. The major protein fraction of quinoa seeds is formed by globulin, which does not possess the requisites to confer elasticity to the dough [2].

Hydrocolloids are a diverse group of long-chain polymers that are readily dispersive, fully or partially soluble, and prone to swell in water. They change the physical properties of the solution to form gels, or enable thickening, emulsification, coating, and stabilization [3]. Flaxseed (Linum usitatissimum) and Chia (Salvia hispanica L.) seeds are used as a potential source for functional food due to its unique nutrient profile. Chia and flaxseed are composed of proteins, lipids, carbohydrates and have high fiber content. These seeds contain a large amount of antioxidants, minerals and vitamins. Both chia and flaxseeds are rich in polyunsaturated omega-3 and omega-6 fatty acids, which constitute the central nervous system, total fatty acids, α-linolenic acid (ALA) [4]. They are also rich in hydrocolloids that could improve the elastic properties of the quinoa-chia or quinoa-flaxseed doughs. In this work, the effect of chia and flaxseed (10 % weight) addition to quinoa dough was studied. Special attention to thixotropic and viscoelastic properties of the dough was paid. A comparative study of the two hydrocolloids was carried out.

Experimental Methods

Commercially ecological chia and flaxseed were used in this study. The content of chia was: fat 31.0 % (omega-3-18.6%) ; protein 20.0, carbohydrates 39.9 %; salt content 0.04 %; and flaxseed was: fat 42.2 %; carbohydrates 28.8%; protein 18.3 %; salt content 0.0075; milled chia and flaxseed particles presented two peaks in the range of 100-400 nm and 1-3 μm. Quinoa flour showed a peak in the range 50-300 nm. All of them were obtained by DLS measurements.

Samples were prepared mixing 1.5 g of chia/flaxseed flour in 10 ml of deionised water. The mixture was stirred for two hours at 500 rpm until the mucilage was released. Then, 15 g of quinoa flour was added and stirred for 2 more hours. The resulting dough was left overnight and stored at 4 ºC. The wheat dough was prepared in the same concentration (1.5 wheat flour: 1 water).

Rheological experiments were carried out with a Peltier system for the control of the temperature, on a MARS III (Thermo-Haake, Germany) using parallel plate sensor system with a diameter of 20 mm and a gap of 1mm. Flow curves were conducted under steady shear. Shear was applied until the steady response was obtained in the range of 10^{-2} to 10^{3} s^{-1} of shear rate and 60 to 1300 Pa of stress. The hysteresis loop was carried out from 0.0005 to 1000 s^{-1} during 240 s de complete loop.

Strain sweep was performed to determine the linear viscoelastic region at 1 Hz. The frequency sweep was carried out in the linear region with γ=0.01, at a range of 0.01-10 Hz. Three measurement replicates were recorded for each sample. All measurements were performed at 25.0±0.1 ºC.

Results and Discussion

The rheological behaviour of gluten dough depends on its composition and microstructure i.e. spatial arrangement of its constituents. Dough development involves the hydration of gluten protein, the predominant fraction controlling the viscoelastic properties of dough. A very simplified model of gluten at the molecular level consists of two classes of protein: linear proteins, glutenins, and globular proteins, gliadins, which can be represented as spheres. The linear proteins interact with each other via the loop and train mechanism and by disulphide bonding [2]. As a first approximation, the chains are imagined to interact with the globular proteins by non-covalent forces such as Van de Waals interactions. During mixing, glutenins tend to align and form cross-links between gliadins molecules, leading to an increase in dough strength. The amount of glutenin in flour was found to be positively correlated with dough strength while gliadin promotes elongational resistance and dough extensibility. The hydrated gluten protein network provides a framework for holding starch granules and trapping air cells. Wheat flour dough is regarded as a composite material of starch granules embedded in a continuous gluten protein network, which confers viscoelastic properties [5]. However, quinoa proteins are mainly globulin or spheroproteins (70 % of total proteins) which do not provide dough elasticity. Chia seeds contain a significant quantity of oil as a linolenic acid (omega 3) and also dietary fiber, a polysaccharide with a high molecular weight. A tentative structure of the basic unit of the polysaccharide was proposed by as a tetrasaccharide with 4-O-metil-α-D-glucoronopyranosyl residues occurring as branches of β-D-xylopyranosyl on the main chain. Immediately the milled seeds are in contact with water, small filaments appear on the surface that began to stretch slowly until they become fully extended. When the seeds are totally hydrated, these filaments (mucilage fibers) are completely developed in a filiform structure which is uniformly distributed forming a framework where other molecules, i.e. globulins, starch, etc. can be trapped [6, 7]. The presence of elongated branched aggregates results in an increasing of the system viscosity.

Steady Flow

Fig. 1 shows the viscosity curves of the three doughs: wheat, quinoa-chia and quinoa-flaxseed. Considering the microstructure above explained, the viscosity of the wheat mass can be easily explained due to the solid-like behaviour of the gluten protein network. Chia mucilage has a similar rheological behaviour to gluten although is not so rigid. This characteristic improves the texture quality of the dough. The percentage of hydrocolloid affects considerably the viscosity of the dough. This can be easily solved by adding more water to the dough.

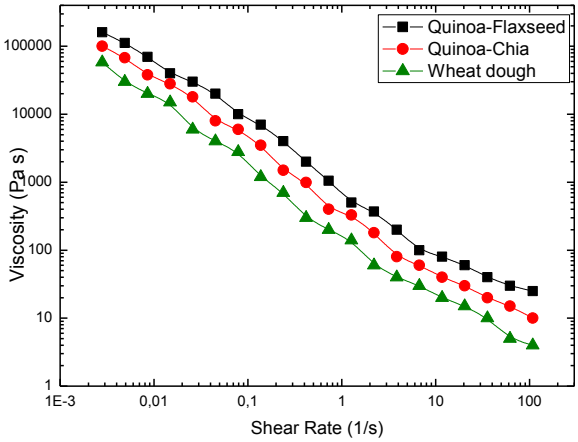

Figure 1. Viscosity curves of wheat (green), quinoa-chia (10%) (red) and quinoa-flaxseed (10%) at 25 ºC (black).

Table 1. Predicted values of K and n according to Power Law model (1) and yield stress according to Herschel-Bulkley model (2).

Material	*K* [Pa s]	*n*	τ_y [Pa]
Wheat	590.3±0.6	0.69±0.07	110±1
Quinoa-Chia	1420±1	0.68±0.05	2920±1
Quinoa-Lino	2510±1	0.64±0.03	5600±1

As a reference of the consistency of the mass, the two parameter of the Power Law are very useful:

$$\eta = K \cdot (\dot{\gamma})^{n-1} \qquad (1)$$

K, the consistency, is a constant related to the slope of the viscosity curve, it is named consistency while n, the flow index, refers to the sign of the slope (n<1, negative, shear thinning). Other interesting parameter is the yield stress, which can be evaluated by means of the Herschel-Bulkley model:

$$\tau = \tau y + K \cdot (\dot{\gamma})^{n} \qquad (2)$$

As we can see in Fig. 1, wheat dough is less viscous than chia-quinoa and flaxseed-quinoa, for the same solid concentration. Actually, the viscosity of the mixtures quinoa-chia and quinoa-flaxseed is in the suitable values taking into account that chia needs water to release the mucilage. Therefore, for commercial purposes, in the

mixtures quinoa-chia, for the same solid quantity, more water should be added to prepare the dough.

Hysteresis Loops

The thixotropy is a time-dependent property exhibited by certain materials that become less viscous when they are subjected to an applied stress. The area of the thixotropic loop (ascendant and descendant ramp) is useful in quality control or in comparative studies of behavior. In this work, the hysteresis area of the wheat dough can be a reference for preparing other masses with similar texture. Figure captions show the corresponding hysteresis area for each material. Figs. 2, 3 and 4 suggest that the wheat mass is the more thixotropic (8.6±1.8×10^5 Pa/s), although quinoa-flaxseed dough also presents a similar thixotropic area value (7.4±1.7×.10^5 Pa/s). This area could be a good reference for the estimation of the percentage of chia or flaxseed to obtain dough with similar characteristic.

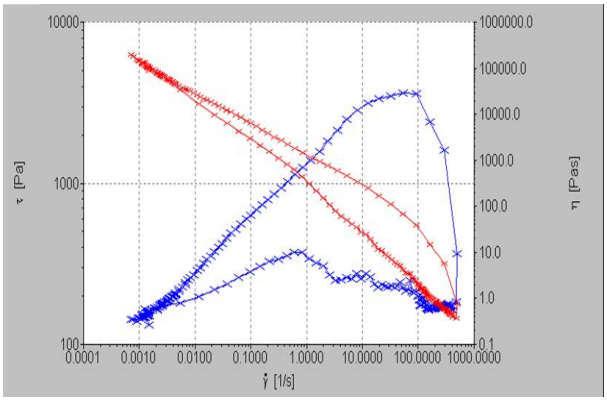

Figure 2. Thixotropic loop of wheat mass: stress loop (blue) and viscosity loop (red). The thixotropic area is 8.6±1.8.10^5 Pa/s.

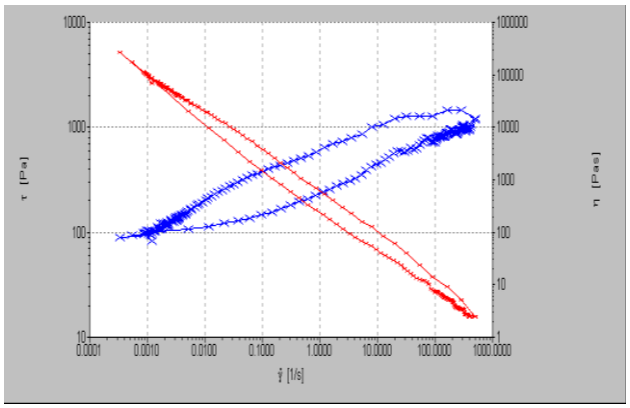

Figure 3. Thixotropic loop of quinoa-chia (10%) mass: stress loop (blue) and viscosity loop (red). The thixotropic area is 3.3. ±1.5×10^5 Pa/s.

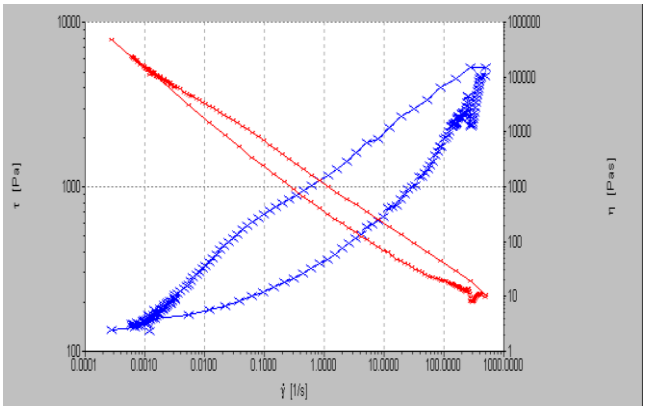

Figure 4. Thixotropic loop of quinoa-flaxseed (10%) mass: stress loop (blue) and viscosity loop (red). The thixotropic area is 7.4±1.7.10^5 Pa/s.

Viscoelasticity

Quinoa flour possesses the major content of spheroproteins in its microstructure which do not provide elastic properties to the dough [7,8]. However, the addition of chia and flaxseed improves the viscoelastic properties of the quinoa flour.

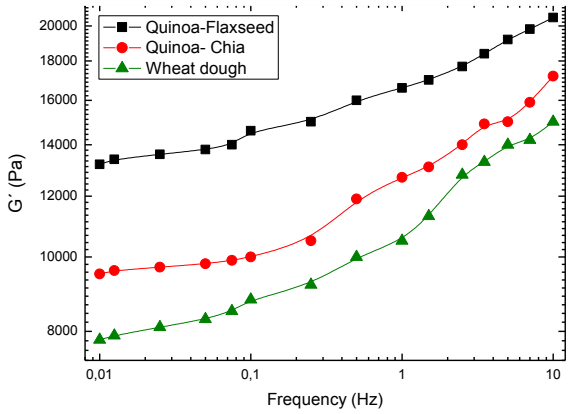

Figure 5. Elastic modulus (G´)of quinoa-flaxseed (10%) (black), quinoa-chia (10%) (red) and wheat (green) doughs.

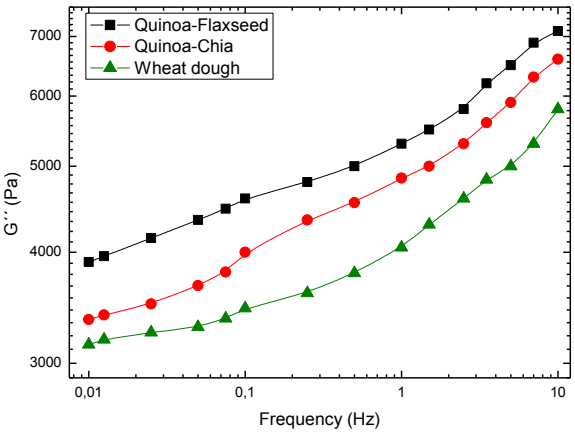

Figure 6. Viscous modulus (G´´) of quinoa-flaxseed (10%) (black), quinoa-chia (10%) (red) and wheat (green) doughs.

The mixtures quinoa-chia and quinoa-flaxseed display values of G´ and G´´ higher than those exhibited by the wheat dough. The explanation of this fact can be found in the interaction of the hydrocolloid filiform framework with the spheroproteins and starch present in quinoa flour giving place to a more consistent cross-linked structure.

In summary, the addition of hydrocolloids as chia and flaxseed flours to a quinoa improve the elastic properties of this substance at high frequencies. Flaxseed has better thixotropic and viscoelastic properties than chia seeds at high frequencies but at low values exhibited greater loss moduli. The explanation of this fact could be found in the different nature of the hydrocolloids versus the gluten structure, which is stronger due glutenin proteins. However, both of them are potential additives for gluten-free cereals.

Concluding Remarks

A comparative study of the flow properties of quinoa-chia and quinoa-flaxseed doughs was performed. In all the tested samples, the elastic properties of the resulting dough were improved.

After baking, the addition of chia and flaxseed increased the volume of the loaf and exhibited good sensory acceptance.

Both hydrocolloids are potential additives as flour improver in gluten-free cereals. However, flaxseed flour exhibited better elastic properties at high frequencies and it could be considered as a flavour enhancer.

References

1. Gallagher, E., Gormley, T. R., & Arendt, E. K. (2004). Trends in Food Science & Technology, 15(3), 143-152.
2. Tatham, A. S., Hayes, L., Shewry, P. R., & Urry, D. W. (2001). Biochimica et Biophysica Acta (BBA)-Protein Structure and Molecular Enzymology, 1548(2), 187-193.
3. Lilian E. Abugoch J., Advances in Food and Nutrition Research, 2009, 58 1-31.
4. Ayerza, R.; Coates, W. (2004). Tropical Science, 44, 131–135.
5. Shewry, P-S.; Popineau, Y.; Lafiandrax, D.; Belton, P. (2001) Trends in Food Science & Technology 11, 433–441.
6. Muñoz, L.A.; Cobos A.; Diaz, O.; Aguilera. J.M. (2012) Journal of Food Engineering. 108, 216–224.
7. Qian, K.; Cui, S.; Wu, Y.; Goff, H. (2012). Food hydrocolloids, 28, 275-283.
8. Lamacchia, C.; Chillo, S.; Lamparelli, S.; Suriano, N., La Notte, E.; Del Nobile, M. A. (2010). Journal of Food Engineering, 96, 97-106.

Contact Address:

aimerino@uma.es
Department of Fisica Aplicada II,
Escuela de Ingenierías Industriales
University of Málaga (Spain)
C/ Dr. Ortiz Ramos, s/n, Málaga (Spain)
Telf.: 951 952 294 ; Fax:

Effects of acidification and exogenous proteins on rheological properties of gluten-free starch-based doughs

M. Villanueva, S. Pérez-Quirce, F.Ronda

Department of Agriculture and Forestry Engineering, Food Technology. College of Agricultural and Forestry Engineering, University of Valladolid (Spain)

Introduction

Gluten has a very important role in products for their singular viscoelastic properties where gas is occluded and contained in the liquid phase during dough development from the flour, water and other ingredients [1]. Thus, the removal of gluten from gluten free (GF) products has a significant impact on their structure, texture and sensory attributes [2]. Nowadays in the market, there are several GF baked products with poor physicochemical and sensory quality, lack fibre, vitamins and nutrients, which results in a worsening effect on the already nutritionally unbalanced diet of celiac sufferers [3]. Utilization of proteins from different sources is commonly considered a good supplement to increase both nutritional and functional values in GF products. In addition, acetic and lactic acids produced by the exogenous microflora or added to breadmaking matrices confer suitable properties to final breads. Although dough acidification and protein addition are known to change the rheological properties of rice-based doughs and, therefore affect the quality of the final baked product [4, 5], the effect of acidification of protein-enriched GF doughs depending on the starch sources has not been reported so far. The impact of acid incorporation (acetic+lactic, 0.5%) into doughs formulated with two different starches (corn and potato) enriched with soy protein isolated (SPI) added at 5% dose, has been investigated on dough viscoelastic properties.

Experimental Methods

Dough preparation

A straight dough process was performed using the following formula on a 100 g corn or potato starch (or starch + protein) basis: 6 g oil, 5 g sucrose, 1.5 g salt, 2 g HPMC and 75 g water. The protein was added at 0 or 5 g/100g. Doughs were supplemented with (0.1 + 0.4) g/100 g of acetic and lactic acid, respectively, when acid-treatment was applied. GF dough-making was achieved by blending first solid ingredients and oil in a kitchen-aid professional mixer (KPM5). Then water was added and hand mixed. Finally the dough was mixed with dough hook at a speed 4 for 8 min. Acid blend, when added, was diluted in a small part of water (7% of total) and adjusted to the dough before the mixer was powered on.

Oscillatory and creep-recovery test

Oscillatory and creep–recovery tests were carried out with a RheoStress 1 rheometer (Thermo Haake, Karlsruhe, Germany) with parallel plate geometry (60 mm diameter) of serrated surface and with 3-mm gap. The excess of dough was removed, and vaseline oil was applied to cover the exposed sample surfaces. All measurements were done at 25 °C. Before each assay, the dough was allowed to rest for 10 min for relaxation. Frequency sweeps were carried out from 10 to 1 Hz in the linear viscoelastic region (LVR). A constant stress value of 1 Pa was chosen for the frequency sweeps of all doughs after establishing this value fell in the LVR of all doughs by means of stress sweeps from 0.1 to 100 Pa at 1 Hz. From the curves, the maximum stress beyond which the dough structure was broken, τ_{max}, was established. Frequency sweep data were fitted to the power law model:

$$G'(\omega) = G'_1 \cdot \omega^a \qquad (1)$$

$$G''(\omega) = G''_1 \cdot \omega^b \qquad (2)$$

$$\tan\ \delta(\omega) = \frac{G''(\omega)}{G'(\omega)} = \left(\frac{G''}{G'}\right)_1 \cdot \omega^{(b-a)} = (\tan\ \delta)_1 \cdot \omega^c \qquad (3)$$

Creep tests were performed by imposing a sudden step shear stress in the LVR for 150 s. In the recovery phase the stress was suddenly removed and the sample was allowed for 300 s to recover the elastic (instantaneous and retarded) part of the deformation. Each test was

performed in triplicate. The data from creep tests were modelled to the 4-parameter Burgers model:

$$J_c(t) = J_{0c} + J_{1c}\left(1 - \exp\left(\frac{-t}{\lambda_{1c}}\right)\right) + \frac{t}{\mu_0} \qquad (4)$$

$$J_r(t) = J_{max} - J_{0r} - J_{1r}\left(1 - \exp\left(\frac{-t}{\lambda_{1r}}\right)\right) \qquad (5)$$

Results and Discussion

The results obtained indicate that starch source, protein incorporation and dough acidification markedly affected to dough viscoelasticity. Corn starch led to the less consistent doughs, the lowest elastic, viscous moduli and steady viscosity and the highest compliances. Thus, potato starch dough had the highest elastic modulus. Supplementation of doughs with SPI led to a threefold more consistent matrices (higher viscoelastic moduli and steady viscosities, and lower instantaneous and retarded elastic compliances). SPI increased in higher extent the elastic (G') than the viscous (G'') modulus, decreasing the loss tangent significantly (-32% and -17% with respect to the non-enriched doughs, for corn and potato starch respectively) and denoting a higher solid like behaviour and a more structured dough.

The acidification of protein-enriched GF doughs decreased markedly these effects, lowering the viscoelastic moduli and steady viscosity and increasing all compliances and tan δ, regardless the starch used. However, the acidification effect was hardly observed in non-protein added doughs.

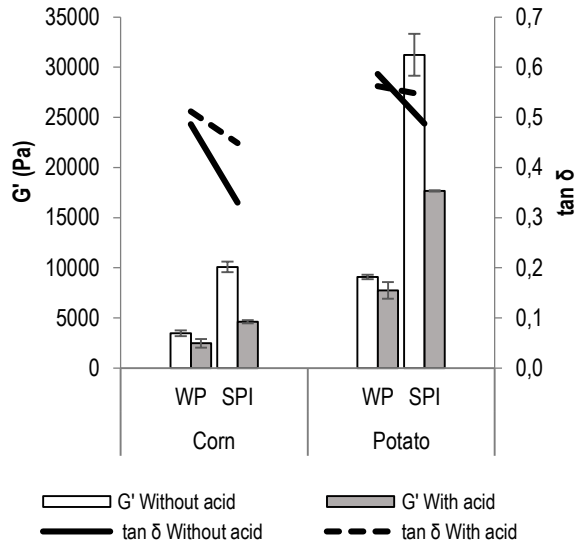

Figure 1. Rheological parameters of the samples without protein (WP) and with 5% of SPI.

Conclusions

Acidification of protein-enriched starch doughs allowed manipulation of its rheological properties which is of relevant importance in gluten-free bread development. Different interaction between protein and starches in the dough can justify the different viscoelastic behaviour. The molecular electrostatic association between protein and starch, affected by dough pH, also affects these interactions as can be concluded by the modulating effect of acidification on dough viscoelasticity.

Acknowledgement

Authors gratefully acknowledge the financial support of the Spanish Institutions Ministerio de Economía y Competitividad and the European Regional Development Fund (FEDER) (AGL2015-63849-C2-2-R) and Junta de Castilla y León for Marina Villanueva doctoral grant.

References

1. Ashraf, S., Saeed, S. M. G., SaYeed, S. A., and Ali, R. (2012). International Journal of Agriculture and Biology, 14, 365-370.
2. Witczak, M., Ziobro, R., Juszczak, L., Korus, J. (2016). Journal of Cereal Science, 67, 46-57.
3. Ronda, F., Pérez-Quirce, S., Angioloni, A., and Collar, C. (2013). Food Hydrocolloids, 32, 252-262.
4. Ronda, F., Villanueva, M., and Collar, C. (2014). LWT - Food Science and Technology, 59, 12-20.
5. Villanueva, M., Mauro, R.R., Collar, C. and Ronda, F. (2015) Eur Food Res Technol, 240, 783-794.

Contact Address:

fronda@iaf.uva.es
Department of Agriculture and Forestry Engineering
College of Agricultural and Forestry Engineering
University of Valladolid
Av. Madrid, s/n, 34004 Palencia, Spain
979 108339 / 983 184095

Formulation and Product Design

Impact of heat moisture treatment on the physical profiles of blended matrices made of barley and wheat flours

E, Armero, G, Sanmartín, C. Collar

Department of Food Science, IATA-CSIC, Avda. Catedrático Agustín Escardino, 7. 46980 Paterna (SPAIN).

Introduction

Heat moisture treatment (HMT) constitutes an environmentally friendly technique and a clean label alternative to chemical modification for altering the gelatinization and retrogradation properties of starches from different sources. Depending on the intensity of the process parameters, a reduction of microorganisms, the inactivation of enzymes or the modification of structural, physicochemical and nutritional properties of starches [1], and the enhancement of nutritional properties [2] and shelf-life extension [3] of starch-rich flours are achieved. In contrast to the extensive knowledge on the significance of hydrothermal treatment of starches, only limited information is available about the impact of HMT of cereal and grain flours, despite the application of the treatment is known to improve their food end uses [4]. HMT may positively impact on the structure restoration of diluted wheat matrices such as blends with non-gluten forming cereals like barley. Mixed breads obtained by 40 % replacement of wheat flour (WT) by barley flour (BL) exhibit superior nutritional quality than regular WT breads [5], but explicit impaired techno-functional performance compared to WT matrices, mainly ascribed to the lower viscoelasticity of diluted doughs.

The significance of HMT (15% moisture content, 1 h heating time at 120ºC) on the viscoelastic profiles of binary matrices (WTBL, 60/40, w/w) was evaluated in hydrated flours and doughs at different hydration levels based on their pasting/gelling and mechanical properties, extrusion and stress relaxation behaviours, by applying imitative instrumental techniques (viscometric and texture profile analysis and forward extrusion, penetration and stress relaxation tests).

Experimental

Materials

Commercial flours from refined common wheat *Triticum aestivum* (WT), and whole barley *Hordeum vulgare* L. (CB), were purchased from the Spanish market. Refined WT (70% extraction rate) of 200 x 10^{-4} J energy of deformation W, 0.6 curve configuration ratio P/L, and 57% water absorption in Brabender Farinograph, was used.

HMT

Single BL and WT flour samples were weighed and placed into screw-capped glass containers. Small amount of distilled water was added slowly with frequent stirring until moisture levels (w/w) of the total mixture reached 15%, and equilibrated for 24 h at room temperature. Hydrated samples were kept for 1h at 120 ºC in a convection oven. After cooling to room temperature, the samples were dried at 40 ºC overnight to a constant weight, and then passed through 100-mesh sieve for further analysis. Untreated native flours were used as controls. Untreated (-) and HMT (+) flours were used singly (WT, CB) and in binary blends (WT/CB, 60/40, w/w) for analysis. Blends were hydrated with 63% and 70% of water to make doughs of 163 and 170 of dough yield (DY), respectively. Four different blended doughs were obtained per DY: WT-CB-, WT-CB+, WT+CB-, WT+CB+.

Rheological assessment of hydrated flours and doughs

Viscometric profiles (gelatinization, pasting, and setback properties) of 14% (w/v) hydrated single (WT, CB) and blended (WT/CB, 60/40, w/w) untreated (-) and HMT (+) flours were obtained with a Rapid Visco Analyser (RVA-4) using ICC Standard 162. Pasting parameters were calculated from the pasting curve [6].

After RVA testing, canisters containing flour pastes were covered with paraffin film and kept at 4 ◦C for 24 h. Texture of gels in canisters (with a dimension of 20 mm in height and 38 mm in diameter) were determined in a TA- XT2 Texture Analyzer by compression to a distance of 15 mm at a speed of 2.0 mm/s using a cylindrical Perspex probe of 25 mm in diameter. The peak force measured in duplicate was reported as gel hardness.

Forward extrusion assays of untreated and HMT binary WTCB doughs made at DY of 163 and 170 were

performed in a TA-XT2 texture analyser equipped with a 30 kg-load cell and operating at 10 mm/s head speed. Compression force-time curve allowed evaluating maximum force, determined as the force at which the slope changed. The change of slope was visually detected, and the force at this point calculated using the Texture Analyser software. The curve plateau representing the force necessary to continue with the extrusion process and the area under the curve were both used to define the sample consistency. All measurements were performed in triplicate.

Texture Profile Analysis (TPA) of untreated and HMT binary WTCB doughs were performed by applying a double compression cycle in a TA-XT2 texture analyser using a 1 cm diameter probe, 75 s waiting period, and 60% compression, as described previously [7].

The stress relaxation data were collected by applying an instantaneous strain to the sample and the force required to maintain the formed deformation was observed as a function of time. Stress relaxation tests were applied on the gels obtained from RVA experiments after storage at 4 °C for 24 h. The stress–relaxation tests were conducted using the texture analyzer mentioned above fitted with a load cell of 30 kg and a P/25 cylindrical probe and the relaxation data were obtained under this configuration. The gel samples in the canisters were directly placed under a cylindrical plate and compressed to 30% a crosshead speed of 0.5 mm/s for 300 s at room temperature (25 °C). Stress relaxation tests were replicated twice. Doughs were submitted to uniaxial compression using an acrylic probe (37-mm diameter) to a 10% strain and the change in force with time was measured for 300 s. A pretest speed of 5 mm/s and test speed of 0.5 mm/s were used.

The obtained stress relaxation curves were normalized and linearized according to the Peleg and Pollak model as $F_0t/(F_0-F(t))=k_1 + k_2t$, where F_0 is the initial force, $F(t)$ is the momentary force at time (t) and k_1(s), k_2 are constants related to stress decay rate and to residual stress at the end of the experiment, respectively. In addition, percent stress relaxation *(% SR*= (F_0-F_{300}).100/F_0), 1/k_1 (initial rate of relaxation), 1/k_2 (extent of relaxation) and relaxation time (*RT* as the time required for F_0 to drop to 36.8% (gels) and 50% (doughs) of its values, respectively), representing viscoelastic behavior, were compared for the different samples.

Multivariate analysis of variance of data were performed by using Statgraphics V.7.1 program (Bitstream, Cambridge, MN). Multiple range test (Fisher's least significant differences, LSD) for analytical variables was applied to know the difference between each pair of means.

Results and Discussion

Impact of HMT on the pasting and gelling of single and blended flours

Pasting properties provide information on intermolecular bonding between densely packed starch granules and the rigidity of swollen starch granules during the heating process, derived parameters being strongly affected by HMT.The mean results pertaining to pasting properties of single (WT, CB) and blended (WT:CB, 60:40, w:w) flours as affected by HMT (15% moisture, 1 h, 120ºC) are plotted and displayed comparatively in Figure 1. HMT flours reached much higher viscosity values during earlier pasting and subsequent gelling than the corresponding native counterparts. Values for peak viscosity and total setback (mPa.s) respectively account for 2683 and 3257 vs 224 and 200 (BL), and 2908 and 1500 vs 2240 and 1156 (WT), confirming trends previously found (unpublished results, 2017). Similar patterns were reported earlier [8] for wheat flour submitted to mild hydrothermal treatment. Authors related the decrease in onset pasting time and increase in peak viscosity to the increased hydrophobicity of gluten proteins and to the occurrence of lipophilization of starch granules due to the change of the properties of the starch granule surface proteins from hydrophilic to hydrophobic. In addition, changes in the gluten protein structure encompassed a minor swelling of the starch granules that occurred in the presence of the moisture content in the flour, and observed increased retrogradation values compared to the untreated flours indicated a tendency of higher re-association ability of amylose [8]. Analogous increased hydrophobicity of prolamins and glutelins in CB+ could explain the prominent enhanced viscosity profile observed. Both additive and non-additive pasting behaviour has been already found for additive-wheat flour [6], and flour blends [9]. In this work, viscosity patterns during both pasting and gelling cycles of blended untreated and HMT flours were much lower than it could be expected from its compositional flours. Decrease was particularly relevant for blends with untreated CB (WT-CB-, WT+CB-) with viscosity values as low as 27% (peak viscosity), 7% (holding strength), 13% (final viscosity) and 19% (total setback) the expected values for an additive viscometric behaviour of single flours in blends, vs 55%, 30%, 39%, and 46% respectively in blends

with treated CB (WT-CB+, WT+CB+). In blended flours, HMT provided enhanced viscometric profiles during both pasting and gelling (Figure 1). Particular higher values of viscosity features were observed for the sample WT+CB+, followed by the sample WT-CB+, while on the contrary, lower profiles were reached by WT-CB- followed by WT+CB- (Figure 1) in good agreement with the significant single effect of HMT on the enhancement of CB flour viscometer parameters compared to those of WT counterparts. This is particularly true for peak viscosity (+194% vs +31%), holding strength (710% vs 38%), and viscosity at end of 95ºC (+612% vs 37%) during pasting, and total setback (+483% vs +24%), viscosity at 50ºC (+489% vs +28%) and final viscosity (+546% vs 29%) during gelling, respectively.

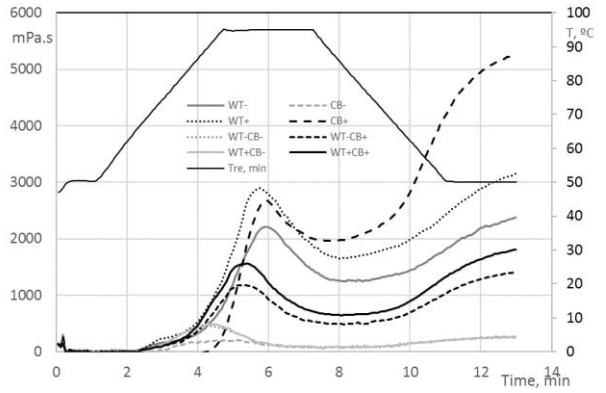

Figure 1.- Rapid Visco-Analyzer profiles of untreated (-) and Heat Moisture treated (+) single wheat (WT), commercial barley (CB) and blended (WTCB, 60:40, wt:wt) flours.

Impact of HMT on viscoelastic and textural behaviour of gels and doughs from single and blended flours

Physical parameters from stress relaxation, penetration, forward extrusion and texture profile analysis tests of untreated and HMT blended gel and dough matrices at different DY are compiled in Tables 1-2. Viscoelastic materials exhibit stress relaxation phenomena, which are some of the most important factors in characterizing agricultural materials. In stress relaxation tests, a constant strain is applied and the stress required to maintain the deformation is measured as a function of time. The measured relaxation time shows how fast the material dissipates stress after receiving a sudden deformation. It was reported that relaxation time is the time when the viscoelastic material dissipates its force to about 36.8% of the originally applied force. The relaxation constants are related to viscoelastic characteristics of samples.

The constant $1/k_2$ is related to the asymptotic level of stress not relaxed at long times, since the constant $1/k_1$ is related to the initial stress decay rate. At gel level, small variations were observed with HMT in therelaxation parameters, except for the initial force F_0 that followed the same trend as the gel strength during puncture test. The lowest k_1 values were noticed in both untreated WT-CB- and treated WT+CB+ gels (Table 1).

Table 1 .- Physical parameters[a] from stress relaxation tests of untreated (-) and heat moisture-treated (+) blended gel and dough matrices from wheat (WT) and commercial barley (CB) at 60:40, w:w.

sample	F_0, g	k_1 (s)	k_2	RT, s	%SR
gels, 14%					
WT-/CB-	134±2^{a}	6.17976±0.2051^{a}	1.4059±0.0424^{a}	35±4^{a}	70±2^{a}
WT-/CB+	503±1^{c}	6.23446±1.0324^{ab}	1.4131±0.0141^{a}	37±9^{a}	70±2^{a}
WT+/CB-	195±8^{b}	6.63628±0.2546^{b}	1.4072±0.0071^{a}	38±3^{a}	70±2^{a}
WT+/CB+	488±59^{c}	5.67061±0.6081^{a}	1.3898±0.0424^{a}	29±10^{a}	71±2^{a}
doughs, DY 170					
WT-/CB-	155±19^{a}	8.3797±0.5020^{a}	1.3935±0.0354^{a}	14±0^{a}	70±2^{bc}
WT-/CB+	158±51^{ab}	8.2669±1.5203^{ab}	1.3615±0.0424^{a}	13±2^{a}	72±2^{c}
WT+/CB-	190±14^{b}	9.3777±0.5869^{ab}	1.5129±0.0495^{b}	19±1^{c}	65±2^{b}
WT+/CB+	214±6^{b}	9.2087±1.0041^{ab}	1.4394±0.0566^{ab}	16±0^{b}	68±3^{bc}
doughs, DY 163					
WT-/CB-	304±30^{c}	12.1931±2.2345^{b}	1.4038±0.0495^{a}	20±2^{cd}	69±2^{c}
WT-/CB+	357±25^{cd}	12.4380±1.7961^{b}	1.4366±0.0566^{ab}	22±1^{d}	68±3^{bc}
WT+/CB-	374±24^{d}	11.8359±1.2657^{b}	1.5323±0.0707^{b}	25±1^{e}	64±3^{b}
WT+/CB+	530±4^{e}	14.0082±0.2546^{c}	1.8210±0.1061^{c}	78±3^{f}	54±3^{a}

[a]Mean values ± standard deviation. Within columns for blended gels and doughs respectively, values (mean of three replicates) with the same following letter do not differ significantly from each other ($p > 0.05$).
DY: dough yield, F_0 is the initial force, k_1(s), k_2 are constants related to stress decay rate and to residual stress at the end of the experiment, respectively, RT as the time required for F_0 to drop to 36.8% (gel) and to 50.0% (dough) to its values, F_{RT}, as the force corresponding to RT, % SR= $((F_0-F_{300})/F_0)100$.

No differences with HMT were obtained regarding either the relaxation time or the percent of stress relaxation (Table 1).

In excess of water (14% flour concentration), gelatinised and gelled mixed flours in RVA canisters exhibited increased strength to penetration with HMT, effect being larger for CB+ (190%) than for WT+ (21%), but lower than the increase provided by the simultaneous presence of WT+/CB+ (230%) in the binary mixture (Table 2). During HMT, increase in gel hardness has been attributed to the increased cross-linking between starch chains in the particular amylose portion. These allowed the formation of more junction zone in the continuous phase of the gel, resulting in the increased gel hardness. Under restricted water availability, samples such doughs showed differentiated viscoelastic and textural parameters with HMT of flours, often depending on DY (Table 2). Regardless DY, HMT of WT decreased dough consistency, % SR, cohesiveness and resilience, and increased k_2, while HMT of CB increased dough consistency (Table 2). At DY 170, HMT decreased the relaxation time by 12% for CB and increase by 35% for WT, while at DY 163, sharp increases by 93% (WT) and 73% (CB) were denoted. HMT changed dough hardness, adhesiveness, cohesiveness in variable extent only for WT (32%,-72%, -26%, respectively) when flour is incorporated to softer

doughs (DY 170), and specifically for CB (62%, -30%, -17%, respectively) when flour is mixed in harder doughs (DY 163). HMT of flours decreased dough resilience only for WT, being extent of depletion greater in softer than in harder doughs (-43% vs -31%). In general doughs made at DY170 compared to their counterparts made at DY163 explicited lower relaxation curves with small values for both k_1 (8.3-9.4 vs 11.8-14.0) and k_2 (1.4-1.5 vs 1.4-1.8), shorter relaxation times (13-19s vs 20-78s) and higher percent of stress relaxation (65-72% vs 54-69%), giving softer (70-117N vs 161-232N), more cohesive (0.51-0.73 vs 0.38-0.63), and adhesive (141-558 vs 72-122g.s) doughs (Tables1-2).

Table 2.- Physical parametersa from penetration, forward extrusion and texture profile analysis tests of untreated (-) and heat moisture-treated (+) blended gel and dough matrices from wheat (WT) and commercial barley (CB) at 60:40, w:w.

sample	Firmness/hardness, g		Cohesiveness	Adhesiveness, g.s	Resilience
gels, 14%	*Penetration*				
WT-/CB-	177±13[a]				
WT-/CB+	515±15[c]		-	-	-
WT+/CB-	215±10[b]				
WT+/CB+	585±9[d]				
doughs, DY 170	*Forward extrusion*		*TPA*		
WT-/CB-	8645±221[b]	107±5[a]	0.7210±0.0057[f]	543±54[d]	0.0725±0.0035[de]
WT-/CB+	11715±956[c]	98±6[a]	0.7335±0.0276[g]	558±46[d]	0.0670±0.0014[d]
WT+/CB-	6965±106[a]	127±3[b]	0.5840±0.0396[e]	163±45[c]	0.0400±0.0014[a]
WT+/CB+	8282±373[b]	142±9[c]	0.5055±0.0813[d]	141±43[bc]	0.0400±0.0028[a]
doughs, DY 163					
WT-/CB-	20881±2892[ef]	182±9[d]	0,6335±0.0290[e]	122±25[bc]	0.0775±0.0021[e]
WT-/CB+	23232±2855[f]	206±26[e]	0.4900±0.0127[c]	79±8[a]	0.0715±0.0092[de]
WT+/CB-	16076±2687[d]	101±7[a]	0.4270±0.0000[b]	96±9[b]	0.0465±0.0035[bc]
WT+/CB+	19322±496[e]	252±0[f]	0.3800±0.0156[a]	72±8[a]	0.0500±0.0042[c]

[a]*Mean values ± standard deviation. Within columns for blended gels and doughs respectively, values (mean of three replicates) with the same following letter do not differ significantly from each other (p > 0.05). DY: dough yield.*

It was reported in banana and plantain that the softer the gel samples become, the less viscous the cell wall contents become, the less polysaccharide entanglement and the faster the ability to dissipate the force [10]. This is in line with obtained results for untreated WT-CB- and WT-CB+ doughs at DY 170 with lower values for k_1 and k_2. This indicates a steeper descent in the relaxation curves toward a lower residual value, which is related to a more viscous-like character of the doughs in agreement with concomitant lower values for F_0, *RT* TPA hardness and higher values for cohesiveness and adhesiveness (Table 2). On the contrary, WT+CB+ at DY 163 provided the most elastic dough with the smallest depletion in initial rate of stress ($1/k_1$), as well as in the value asymptotically approached by normalized stress ($1/k_2$). It reflects the change in structure of dough, which under water restrictions becomes more elastic.

Conclusions

HMT of flours modified dough viscoelasticity and doughmaking functionality of diluted breadmaking wheat matrices made with 40% of wheat flour replacement by barley flour. The trend and extent of the changes closely depend on water availability. In excess of water, HMT provided enhanced viscometric profiles during both pasting and gelling in blended flours, particularly for samples with HMT treated barley, while on the contrary, lower profiles were reached by sample blends with native barley flour. The gelling ability of HMT treated barley provided harder gels, and may confer a suitable thickening effect to blended doughs that may improve gas retention in presence of a diluted gluten network. Under water restrictions, flour hydration governs viscoelasticity and mechanical properties of blended doughs, while HMT only modulates dough performance.

Acknowledgements

The authors acknowledge the institutions Ministerio de Economía y Competitividad (MINECO) and Federación Europea de Desarrollo Regional (FEDER) for funding the Project AGL2015-63849-C2-1-R.

References

1. Chung, H.J., Liu, Q., and Hoover, R. (2009). Carbohydr. Polym. 75, 436–447.
2. Satmalee, P., and Matsuki, J. (2011). Int. J. Food Sci. Technol. 12, 2628–2633.
3. Yadav, D.N., Kaur, J., Anand, T., and Singh, A. K. (2012). Int. J. Food Sci. Technol. 47, 2532–2537.
4. Ye, X., Lu, F.,Yao,T., Gan, R., and Sui, Z. (2016). Int. J. Biol. Macromolec. 93, 34–40.
5. Collar, C. and Angolan, A. (2014). Eur. Food Res. Technol. 238, 459–469.
6. Collar, C. (2003). Eur. Food Res. Technol. 216, 505-513.
7. Armero, E., and Collar, C. (1997). Z. Lebensm.-Unters. Forsch. A, 204, 136–145.
8. Bucsella, B., Takács, A., Vizer, V., Schwendener, U., and Tömösközi, S. (2016). Food Chem. 190, 990–996.
9. Collar, C. (2016). J. Cereal Sci. 69, 32-39.
10. Kajuna, S.T.A.R., Bilanski, W.K.. and Mitta, G.S. (1998). Appl. Eng. Agric. 14, 55-61.

Concha Collar
ccollar@iata.csic.es
Department of Food Science
IATA-CSIC
Avda. Catedrático Agustín Escardino, 7. 46980 Paterna (SPAIN).
Telf.: +34 963 90 00 22; Fax: +34 963 63 63 01

Orange juice obtained from powdered freeze-dried puree. Powder particle size and juice viscosity relationship

M.A., Silva, E., Algarra, M., Uscanga Ramos, M.M., Camacho, N., Martínez-Navarrete

Universitat Politècnica de València. Food Technology Department, Food Investigation and Innovation Group. Camino de Vera s/n, 46022, Valencia, (Spain)

Introduction

Fruits are essential components of a healthy diet, as they appear to contribute to the prevention of cardiovascular diseases and some cancers. This protection is attributed to its high bioactive compounds content that contributes to its antioxidant capacity [1]. Nevertheless, fruits have a short shelf life related to its high water content. Freeze-drying (FD) is a dehydration method that eliminates water of the fruit by sublimation and provides high quality products. Currently, a variety of fruit juices can be found in the market, but any of them obtained from a freeze-dried puree of the fruit. Some will be the advantages of applying FD process to obtain a fruit juice. On the one hand, the whole edible part of the fruit can be profited so that a more nutritive and functional product is obtained in a more sustainable way, with far fewer by-products generated, compared with other processes with which to obtain a juice. On the other hand, the product is not submitted to high temperatures with the corresponding benefits in product's quality. Additionally, the commercialization of the dehydrated fruit in a powdered vitreous state would have the advantages of its manipulation and storage, in relation to the smaller volume occupied and its physical, chemical and microbiological stability.

Nevertheless, dehydrated fruit could present problems related to the glass transition of its amorphous matrix, associated to the increase in the rate of deteriorative reactions and to the development of collapse phenomena leading to the loss of the structure, that becomes extremely sticky. The change from the highly stable glassy state to the more unstable rubbery one occurs when the glass transition temperature (Tg) of the sample is exceeded, which may occur in dehydrated products by small increases in humidity or temperature. To prevent this undesirable situation, it has been noted the use of high molecular weight solutes such as arabic gum or bamboo fiber, capable of increasing the glass transition temperature [2] [3]. After FD the mix fruit puree:solutes, a cake is obtained which must be rehydrated to obtain the juice. An important quality aspect of the obtained juice is its viscosity. In this paper, the relationship between the particle size of the freeze-dried and crushed orange puree and the rheological behavior of the juice obtained after its rehydration was studied.

Experimental Methods

Raw materials

Oranges (*Citrus x sinensis* var. Navel) used in this study were purchased in a local supermarket (Valencia, Spain). Fruit pieces were selected based on the size homogeneity, colour and good physical integrity.

Carriers used to obtain the dehydrated oranges samples were arabic gum (AG, Scharlab, Sentmenat, Spain) and bamboo fiber (BF, VITACEL®, Rosenberg, Germany).

Four commercial orange juices were purchased in a local supermarket in the city of Valencia, which will be called A, B, C and D. The compositional information according to its label is: A: orange juice and vitamin C; B: orange juice, pulp and vitamin C; C: orange juice; and D: orange juice from concentrated and vitamin C.

Orange juice samples obtained by rehydration of the powdered freeze-dried puree

The peeled oranges were cut and ground in a bench top electrical food processor (Thermomix TM 21, Vorwerk, Spain). Triturated fruit was mixed with 5 g AG/100 g orange puree and 1g BF/100 g orange puree [4] and was named mix. This mix was placed in aluminium plates, 0.5 cm thickness and immediately frozen at -45 ºC (Liebherr LGT 2325, Germany) until freeze-drying at least 48 h after. A Telstar Lioalfa-6 Lyophyliser, at 0.05 mbar, -45 ºC in the condenser and 40ºC in the shelve for

20h. The freeze-dried cakes were crushed, in the same bench top electrical food processor above mentioned, to obtain a powder. Batches of 40 g powder were passed through a set of sieves of 0.5, 0.4, 0.3, 0.2 and 0.15 mm coupled to the corresponding top and bottom (200/50 CISA, Barcelona, Spain), using a vibratory sieve shaker at 50 Hz for 5 min (AMP0.40 CISA, Barcelona, Spain). The sample with a particle size greater than 0.5 mm was discarded and that retained on each of the other sieves and on the bottom was collected in zip bags and stored at 4º C until its rehydration.

Rehydration was carried out in order to obtain the same mix before freeze-drying process. A mass balance, taking into account both the water content of the mix and that of each sieved powder, was applied to calculate the water content to be added to the powder to get the mix water content. Rehydration was carried out in jacketed beakers connected to water bath thermostated at 10 ºC with constant magnetic agitation (800 rpm) during 5 min (Multi-Channer Stirrer MS-51M, JEIO TECH Lab Companion, Daejeon, Korea). Analysis of the samples was carried out in triplicate as described below.

Water content

The mass fraction of water was obtained by drying the samples in a vacuum oven (Vaciotem, J.P. Selecta) at 60ºC ± 1ºC under p < 100 mm Hg until constant weight [5].

Rheological characterization

The flow behaviour of the mix, the rehydrated products and the commercial ones was obtained at 8 °C by means of a controlled shear stress rheometer (Haake RheoStress 1, Thermo Scientific, Karlsruhe, Germany) with a coaxial cylinder sensor system (Z34 DIN), coupled to a thermostatic bath (Viscotherm VT 10, Physica). A relax time of 300 s was selected for the sample before running the test. Shear rate ($\dot{\gamma}$) was increased from 0 to 120 s^{-1}, with the lowest shear rate measured being 1,1 s^{-1}, and shear stress (σ, Pa) was recorded. Results were fitted to Ostwald de Waele model (Eq. 1), to get the flow behaviour index (n) and the consistency index (K). Instead to select a concrete $\dot{\gamma}$ to indicate the corresponding apparent viscosity (η_{ap}, Pa·s), η_{ap} was calculated applying the mean value theorem (Eq. 2) to give a representative value of this variable in all the shear rate range considered in the study. Taking into account that for our samples η_{ap} follows Eq. (3), Eq. (2) can be expressed as Eq. (4) to give the referred representative value.

$$\sigma = K(\dot{\gamma})^n \quad (1)$$

$$\eta_{ap} = \frac{1}{\dot{\gamma}max} \int_0^{\dot{\gamma}max} \eta\,(\dot{\gamma})\, d(\dot{\gamma}) \quad \dot{\gamma}\epsilon\,[0, \dot{\gamma}\mathrm{max}] \quad (2)$$

$$\eta_{ap} = K(\dot{\gamma})^{(n-1)} \quad (3)$$

$$\eta_{ap} = \frac{K}{n}\,\dot{\gamma}\mathrm{max}^{(n-1)} \quad (4)$$

Where σ: shear stress (Pa), $\dot{\gamma}$: shear rate (s^{-1}), n: flow behaviour index, K: consistency index ($Pa.s^n$), $\dot{\gamma}_{max}$: maximum rate (s^{-1}) = 120 s^{-1}, η_{ap}: apparent viscosity (Pa.s).

Statistical analysis

An analysis of variance (ANOVA) was performed to establish the significant differences among the analysed samples (α = 0.05). Statistical analysis was conducted using Statgraphics Centurion XVI.II.

Results and Discussion

The water content of the mix and the different particle size powders (Table 1) allowed to calculate the water to be added in each case to obtain the different rehydrated products, all of them with the same water content of the mix.

Table 1. Water content of the mix and the different particle size powders.

Sample	g water/100g sample
Mix	83.88
P(0.5-0.4mm)	0.32
P(0.4-0.3mm)	0.38
P(0.3-0.2mm)	0.67
P(0.2-0.15mm)	0.86
P(<0.15mm)	0.54

The rheological behaviour of the mix, the rehydrated products and the commercial ones was analysed. The mix and the rehydrated products flow curves (Figure 1) showed a typical pseudoplastic behaviour. The mix prepared showed greater shear stress values, this indicating the impact of crushing the FD cake in the viscosity of the obtained juice.

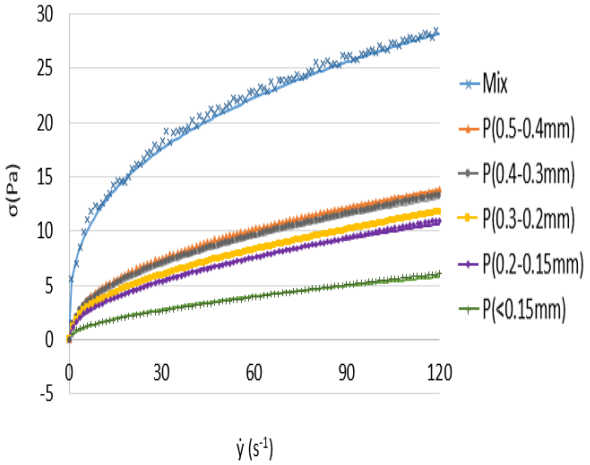

Figure 1. Flow curves of the mix and the rehydrated products obtained from the different particle size powders. Experimental data and Oswald-de Waele fitted model.

Figure 2 shows the flow curves of the commercial orange products. In this case, all the shear stress values were lower than those showed in Fig. 1 so that any of the commercial juices showed lower viscosity than those prepared from FD samples. B and C juices, both with visible pulp, presented a pseudoplastic behaviour while A and D ones, without pulp, showed a Newtonian behaviour.

Table 2 shows n and K parameters obtained when fitting the Ostwald-de Waele model to rheological data. From this values, a representative η_{ap} value in the whole shear rate studied range was obtained (Figure 3).

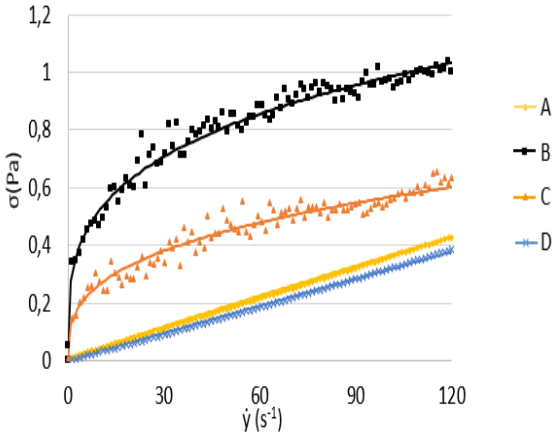

Figure 2. Flow curves of the commercial orange products. Experimental data and Oswald-de Waele fitted model.

Table 2. Consistency index (K), flow behaviour index (n) and R^2 of the different samples. The same lowercase letter within columns indicates homogeneous groups established by ANOVA ($p<0.05$) carried out without taking into account the mix sample.

Sample	n	K(Pa.s^n)	R^2
Mix	0.343(0.011)	5.5(0.4)	0.996
P(0.5-0.4mm)	0.462(0.009)^b	1.51(0.03)^f	0.995
P(0.4-0.3mm)	0.464(0.003)^b	1.411(0.007)^f	0.998
P(0.3-0.2mm)	0.480(0.002)^b	1.181(0.016)^e	0.999
P(0.2-0.15mm)	0.490(0.005)^b	0.97(0.08)^d	0.998
P(<0.15mm)	0.533(0.002)^b	0.45(0.02)^c	0.994
A	0.93(0.05)^c	0.005(0.002)^a	0.995
B	0.23(0.04)^a	0.37(0.09)^c	0.941
C	0.25(0.12)^a	0.22(0.13)^b	0.931
D	0.99(0.02)^c	0.0033(0.0005)^a	0.999

Values of n very close to 1, like those of A and D samples, confirm their Newtonian behaviour. B and C samples have the lower values of n and the rehydrated products have intermediate values, much lower than 1, which confirms their pseudoplastic behaviour.

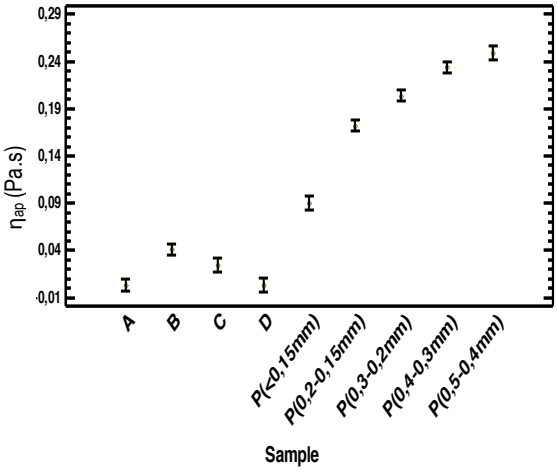

Figure 3. Mean and LSD intervals of apparent viscosity of the samples.

The representative viscosity of the mix was 0.69±0.03 Pa.s, value that stands out for being much greater than those of the others samples. The greater viscosity of the mix is related to the kind of sample, this being the orange puree added with the solutes. In this sense, the direct rehydration of the FD cake will lead to a similar viscosity value [6]. For this reason, it seems necessary to crush the cake before rehydration in order to get a value close to that of the commercial products. As it can

be seen in Fig. 3, the viscosity of the rehydrated powders with different particle size was between that of the mix and the commercial products, closer to the last ones. The viscosity decreased as the powder particle size decreased, so that it seems possible to obtain the desired juice viscosity by adequately fitting the powder particle size. In this case, the viscosity of the products obtained from the rehydration of the powder with a particle size lower than 0.15 mm was also greater than that of any commercial juice. To obtain a rehydrated product with a lower viscosity, sieves lower than 0.15 mm mesh should be used.

Conclusion

It is possible to apply freeze-drying to obtain a fruit juice. Nevertheless, it is necessary to crush the cake to a determined powder particle size before rehydration in order to obtain a juice with the desired viscosity. In this case a powder particle size lower than 0,15 mm will be needed to provide a viscosity after rehydration similar to that of the commercial orange juices.

Acknowledgements

The authors thank the Ministry of Economy and Competitiveness for the financing of this work through the AGL 2012-39103 project and the Ministry of Education, Culture and Sport for the FPU grant (FPU14 / 02633) granted to Ms. Andrea Silva.

References

1. De Ancos. B.; Gónzalex. E. M.; Cano. M. P. (2000). Ellagic acid. vitamin C. and total phenolic contents and radical scavenging capacity affected by freezing and frozen storage in raspberry fruit. Journal of Agriculture and Food Chemistry. 48, 4565–4570.
2. Barbosa-Canovas, G.; Ortega-Rivas, E.; Juliano, P.; Yan, H. (2005). Food powders: physical properties, processing and functionality. Kluwer Academic/Plenum Publisher, New York. 372.
3. Telis, V.R.N.; Martínez-Navarrete, N. (2009). Collapse and color changes in grapefruit juice powder as affected by water activity, glass transition and addition of carbohydrate polymers. Food Biophysics. 43, 44–751.
4. Agudelo. C. (2017). Selección del mejor proceso para la obtención de pomelo en polvo (*Citrus paradisi*) de alta calidad nutritiva. funcional y sensorial. Doctoral Thesis. Universidad Politècnica de València.
5. AOAC. (2000). Official Methods of Analysis of AOAC International. 17th ed., MD, Gaithersburg.
6. Silva. A. (2015) . Estudio del comportamiento reológico de zumo de fruta obtenido a partir de pomelo liofilizado. Master thesis. Universitat Politècnica de València. Escuela Técnica Superior de Ingeniería Agronómica y del Medio Natural.

Contact Address:

Marilú Andrea Silva Espinoza
masiles@doctor.upv.es
Food Technology Department
Polytechnical University of Valencia
Address: Camino de Vera s/n. 46022. Valencia. Spain.
Telf.: 0034693100059

Optimization of seabuckthorn fruit powder yogurt formulation using rheological analysis

A. M. Gâtlan, C. Mironeasa, M. A. Oroian, E.T. Sănduleac, S. Mironeasa

Faculty of Food Engineering, Stefan cel Mare University of Suceava, Universitatii Street, 13, Suceava, Romania

Introduction

Yogurt is the most consumed healthy and nutritious food around the world. Yogurt is now widely consumed mainly due to its availability in a large variety of flavors, and also for preventing or treating most of diseases, especially in young children. Therefore, it can be said that yogurt has a significant impact on improving the community health. The fruit enriched yogurt adds variety in a healthy diet, so the consumer can select the yogurt type which fits best his preferences. Also, a higher coagulum firming rates, compact structures, which not show syneresis are important quality indicators of yogurt, determining the acceptability and feasibility of the new product. The rheological characteristics of the yogurt are changed by adding various ingredients, at different doses.

Seabuckthorn is a unique plant, currently being domesticated in several countries like Romania, France, Germany, Finland, China, Russia, France, Nepal, Pakistan and India. This future food source has been gaining attention because of its nutritional benefits, as it has been reported to contain more than 190 nutritional compounds in the seeds, pulp, fruit and juice. These compounds include fat soluble vitamins (A, K, and E), fatty acids, lipids, organic acids, amino acids, carbohydrates, vitamins C, B1, B2, folic acid, tocopherols and flavonoids, phenols, terpenes and tannins. Many of the substances which are found in sea buckthorn are known to have beneficial effects on health. It has been well established in the literature that berries and seeds contain high amounts of natural antioxidants, the seabuckthorn berries being considered the most nutritious and vitamin rich fruits found in the plant kingdom [1, 2, 3].

Numerous studies indicate seabuckthorn berry and leaf extracts as well as isolated compounds to have pharmacological and therapeutic activities such as antioxidant, antibacterial, anti-radiation, antiviral, anti-stress, antiatherogenic, anticancer, immunomodulatory, hepatoprotective, adaptogenic, cardioprotective, and acute and chronic wound healing effects. Recent studies have shown that compounds obtained from seabuckthorn are considered to be valuable drugs in the treatment of cancer, gastric ulcers, skin diseases, inflammatory diseases, thrombosis, diabetes, injuries of tendons and the ligaments, which also possesses antibacterial and antiviral properties [4, 5].

Therefore, the supplementation of yogurt with seabuckthorn fruit powder will enhance its nutritional quality and will also bring therapeutic value for the final product. Due to this additional feature the consumer will be more inclinable to purchase seabuckthorn flavored yogurt.

The aim of this study was to determine the optimum proportion of seabuckthorn powder which, added in yogurt, will improve its rheological characteristics.

Experimental

Materials

The yogurt was developed and produced under laboratory conditions, using the following raw materials: integral cow's milk with 3.5% fats, 4.5% carbohydrates and 3% proteins, purchased from a local store; lactic bacteria culture (*Lactobacillus bulgaricus* and *Streptococcus thermophillus*), supplied by Danisco Romania SRL; seabuckthorn powder, obtained from well ripped sea buckthorn fruits (Hippophaë rhamnoides L.), by controlled drying at 40°C, grinding and sieving up to a particle size < 300 µm.

Yogurt preparation

The yogurt manufacture was performated by indicated classical technology under laboratory conditions. The milk was first pasteurized at 90°C for 15 minutes and cooled to about 45°C for the addition of ingredients. Then, it was inoculated with the starter culture. In all preparations, milk was directly inoculated with 0.02% (w/v) *Lactobacillus bulgaricus* and *Streptococcus thermophillus* starter cultures. The mixture was

homogenized for the evenly distribution of the culture. Then, the inoculated samples were transferred over seabuckthorn powder, which has been previously dosed directly into the yogurt jars in varying proportions from 0.2 to 1.2%. The fermentation process was carried out at 40°C. When the pH value reached 4.6, the process was interrupted, and afterwards the yogurt samples were cooled to 4°C and stored at this temerature.

Methods

The rheological properties of yogurt samples were determined using the Thermo Haake Mars Rheometer, equipped with a 40 mm titanium geometry plate. Each yogurt sample was stirred gently 10 times with a spoon and a small amount of sample was placed onto the bottom plate of the rheometer. Excess sample at the edge of the geometry was wiped away without excessively disturbing the sample. The measurement temperature was 8°C. To obtain the viscosity values, it was analysed the variation of viscosity as a function of ascending and descending shear rate from 0.02 to 100 s^{-1}. For the determination of elastic and viscous modules, there were conducted frequency dependency experiments from 0.05 to 10.0 Hz. In order to guarantee the existence of linear viscoelastic response according to previous stress sweeps carried out under the same conditions, the applied stress was always selected. Three determinations of each oscillatory dynamic test were conducted for each sample replicate [7].

Experimental design

Seven levels (0, 0.2, 0.4, 0.6, 0.8, 1.0 and 1.2% (w/v)) of seabuckthorn powder as independent variable were chosen (Table 1). Response surface methodology (RSM) was used to study the effect of independent variable on response variables: yogurt viscosity (η), elastic modulus (G') and viscous modulus (G''). The optimal doses of seabuckthorn powder were obtained using RSM by employing of seven-levels of one factor design.

Statistical analysis of responses

The responses (viscosity, elastic modulus and viscous modulus) for different experimental conditions were related to coded variable (A) by a second degree polynomial. Data were modelled by multiple regression analysis and statistical significance of the terms was examined by analysis of variance (ANOVA) for each response. The coefficients of each model were reported as coded values of the independent variable. The adequacy of the regression model was checked by coefficients of determination (R2), adjusted coefficients of determination (Adj-R^2), adequate precision and Fisher's *F* - test [8]. Design Expert 9.0 software (trial version) was used to design the experimental matrix, modeling data and to generate three dimensional plots for each regression model.

Results and Discussion

Table 1 shows the experimental design in coded values [8] and real values of independent variable used in this investigation.

Table 1. Experimental design matrix with coded and real values used in one factor RSM design

	Coded value	% Real value (w/ v)
Doses of seabuckthorn powder added in milk yogurt	-1.00	0.00
	-0.66	0.20
	-0.33	0.40
	0.00	0.60
	0.33	0.80
	0.66	1.00
	1.00	1.20

Viscosity

The quadratic regression model was fitted for viscosity. The coefficients of the model and other statistics are given in Table 2. The F-value of 20.02 implies that model is significant ($p < 0.05$). The R^2 and adjusted R^2 of the model are 0.85 and 0.80, respectively. The adequate precision value of 9.767 indicates that the model can be used to navigate the design space as it is greater than 4.0 [8]. Therefore, the quadratic model was selected for representing the variation of viscosity. The linear term of seabuckthorn powder variable (A) had highly significant positive effect, while the quadratic term (A^2) had a negative effect on viscosity.

Table 2. Regression coefficients of quadratic model and their significance for viscosity

Factor	Viscosity η (mPa·s)		
	Value	*F*	*p*
Constant	68.18		
A: Seabuckthorn powder	10.39	30.47	0.0009
A^2	-9.79	9.58	0.0175
R^2	0.85		
Adjusted R^2	0.80		
Adequate precision	9.767		
Model	-	20.02	0.0013

The effect of seabuckthorn powder doses added in milk yogurt formulation can be seen in Figure 1, indicating

that viscosity increases up to a concentration of 0.8% (w/v).

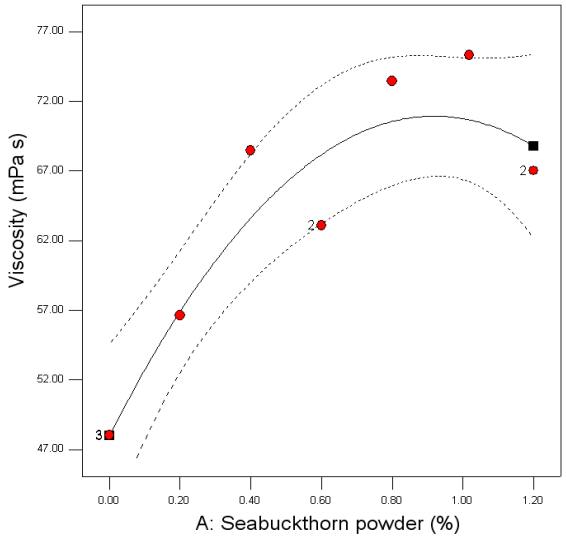

Figure 1. Response surface of yogurt viscosity versus dose of seabuckthorn powder

Elastic modulus

The effect of doses of seabuckthorn powder incorporated in milk yogurt on the elastic modulus G' expressed as their corresponding regression coefficients in the quadratic regression model is shown in Table 3. The quadratic term indicated a significant negative influence on the G'. The coefficient of determination (R^2 = 0.70) for quadratic regression model confirmed the adequacy of the model.

Table 3. Regression coefficients of quadratic model and their significance for elastic modulus

Factor	Elastic modulus G' (Pa)		
	Value	***F***	***p***
Constant	168.52		
A: Seabuckthorn powder	62.98	11.47	0.0128
A^2	-114.24	12.81	0.0090
R^2	0.77		
Adjusted R^2	0.70		
Adequate precision	7.892		
Model	-	11.91	0.0056

The response surface plot obtained for G' (Figure 2) showed that the increasing of seabuckthorn powder level up to at 0.8% added in milk yogurt increases G'.

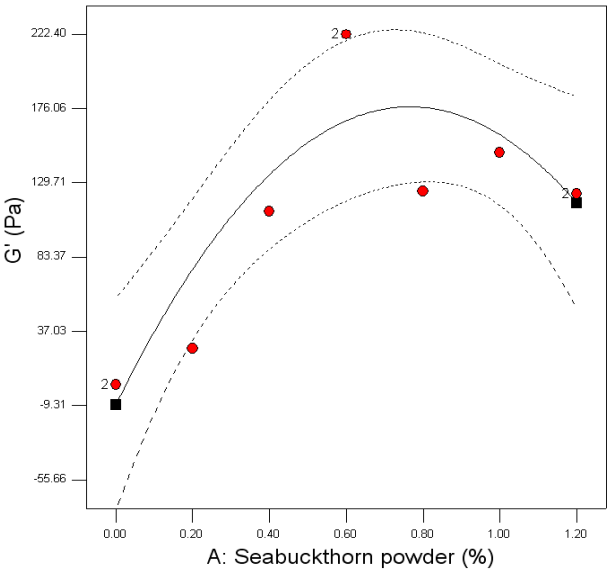

Figure 2. Response surface of elastic modulus versus dose of seabuckthorn powder

Viscous modulus

The quadratic regression model was used to determine the viscous modulus (G'') of milk yogurt. G'' was significantly associated ($p < 0.01$) with doses of seabuckthorn powder added in milk yogurt. Analysis of variance (Table 4) shows that *F*-values for linear and quadratic terms of seabuckthorn powder dose and *p* value are significant terms. The linear term had a positive effect on G'', while the quadratic term of seabuckthorn powder had negative effect on the viscous modulus (Figure 3).

Table 4. Regression coefficients of quadratic model and their significance for viscous modulus

Factor	Viscous modulus G'' (Pa)		
	Value	***F***	***p***
Constant	48.74		
A: Seabuckthorn powder	18.36	12.13	0.0102
A^2	-31.42	12.56	0.0094
R^2	0.77		
Adjusted R^2	0.71		
Adequate precision	8.029		
Model	-	12.35	0.0051

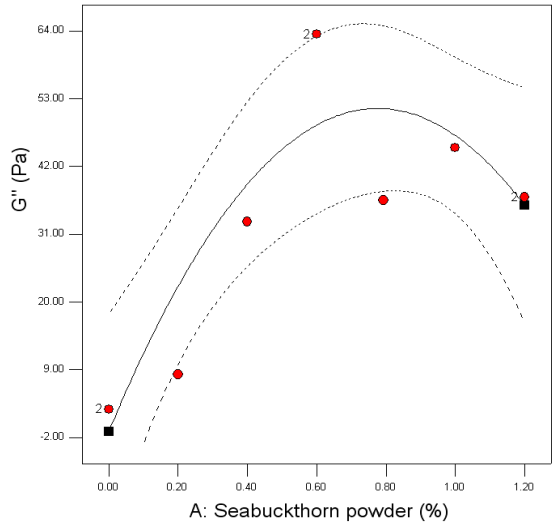

Figure 3. Response surface of viscous modulus versus dose of seabuckthorn powder

Optimization

The numerical optimization showed the optimum level of independent variable to achieve the desired response goals. Viscosity, elastic modulus and viscous modulus were desired maximal. Maximal value for these parameters at shear rate in 0.02 - 100 s^{-1} range and between 0.05 to 10.0 Hz frequencies lead to obtaining a yogurt with improved form firmer gels, with no syneresis, preferred by consumers. Rheological properties are important quality parameters playing a crucial role in consumers' acceptance.

The optimal value for dose of seabuckthorn powder (Figure 4) leading to the global desirability value (0.792) are 0.81% (w/v), with predicted response of 70.60 mPa·s for viscosity, 176.64 Pa for G' and 51.34 Pa for G''. G' is higher than G'', indicating elastic properties.

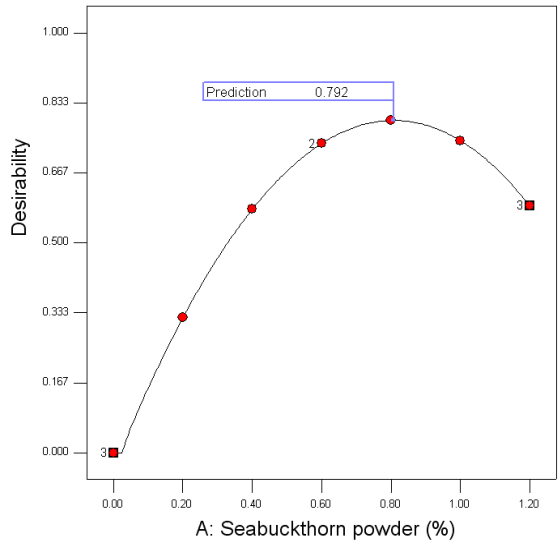

Figure 4. The contour plot of optimum values for seabuckthorn powder added in milk yogurt.

Conclusions

The seabuckthorn fruit powder yogurt formulation was optimized at the seabuckthorn powder content of 0.81% (w/v). The optimum parameters obtained by numerical optimization for rheological parameters of yogurt with seabuckthorn powder were found as viscosity, 70.60 mPa·s, G', 176.64 Pa and G'', 51.34 Pa. An improve in the coagulum firming rates can be obtained in yogurt with 0.81% (w/v) seabuckthorn powder, within the studied range of shear rates and frequency.

Acknowledgement

This work was supported by a grant of the Romania National Authority for Scientific Research and Innovation, CNCS/CCCDI – UEFISCDI, project number PN-III-P2-2.1-BG-2016-0089, within PNCDI III.

References

1. Bal, L., Meda, V., Naik, S.N., and Satya, S. (2011) Food Research International, 44, 1718-1727.
2. Selvamuthukumaran, M., and Khanum, F. (2015) Journal of Food Science and Technology, 52(2), 831–839.
3. Gunenc, A., Khoury, C., Legault, C., Mirrashed, H., Rijke, J., and Hosseinian, F. (2016) LWT - Food Science and Technology, 66, 490-495.
4. Fatima, T., Kesari, V., Watt, I., Wishart, D., Todd, J.F., Schroeder, W.R., Paliyath, G., and Krishna, P. (2015) Phytochemistry, 118, 181-191.
5. Olas, B. (2016) Food and Chemical Toxicology, 97, 199-204.
6. Mathias, T., Carvalho Junior, I., Carvalho, C., and Sérvulo, E. (2011) Alimentos e Nutrição Araraquara, 22:4, 521-529.
7. Miocinovic, J., Miloradovic, Z., Josipovic, M., Nedeljkovic, A., Radovanovic, M., and Pudja, P. (2016) International Dairy Journal, 58, 43-45.
8. Montgomery, D.C. (2001) Design and Analysis of Experiments, New York Wiley.

Contact Address:

Anca-Mihaela Gâtlan
anca.gatlan@fia.usv.com
Faculty of Food Engineering
Stefan cel Mare University of Suceava
Address: Universitatii Street, 13, Suceava, Romania
Telf. / Fax: 0040230216 / 0040230520080

Study of collagen and chitosan-based 3D matrices as potential scaffolds for Regenerative Medicine

V. Perez-Puyana, I. Carreño-Carmona, L. Cabrera-Correa, A. Romero

Department of Chemical Engineering, Faculty of Chemistry, University of Seville (Spain)

Introduction

Tissue Engineering is an emerging scientific field which is relevant in the Regenerative Medicine area. It is based on three main elements: cells, growth factors and scaffolds. A scaffold is a three-dimensional porous structure which should give a certain mechanical support for an optimal cell growth. Furthermore, this mechanical support must be maintained until the tissue formed has enough mechanical integrity and, even, the cells that make up the formed tissue must express the suitable genes in order to maintain the specific function of the tissues [1]. For that reason, the knowledge provided by Biomaterials Engineering gives the base for the development of porous 3D matrices which could act as scaffolds for Tissue Engineering [2].

There are several techniques to develop scaffolds. Among them, one of the most commonly used techniques consists of a freeze-drying process driven to hydrogels previously elaborated. The mechanical resistance of the scaffolds produced could be enhanced by a later dehydrothermal treatment at 105ºC or by the addition of a crosslinking agent (i.e. glutaraldehyde). In addition, an exhaustive characterization is subjected to the scaffolds by analyzing their mechanical and structural properties. Synthetic polymers are the most commonly used nowadays because it is possible to select and control easily the final properties of the scaffolds, however, present, among others, the disadvantages of being toxic or rather non biocompatible [3].Therefore, in the last years, there has been an increased use of biopolymers as collagen or chitosan as raw material because they provide biocompatibility, which is essential for scaffolds.

Indeed, the main objective of this work is the development of collagen and chitosan scaffolds studying the influence of the pH and the addition of a crosslinking agent on the structure and properties of the scaffolds fabricated, revealing that the conditions absolutely influence the properties of the scaffolds.

Experimental

Materials

Pork collagen (C) protein (named as Pork HI95) with a protein content of ca. 94 wt.% was supplied by Essentia Protein Solutions (Grasten, Denmark) and Chitosan (CH) of low molecular weight was supplied by Sigma Aldrich (Germany). Acetic acid and glutaraldehyde (GA) were purchased from Panreac Química, S.A. (Barcelona, Spain).

Preparation of Scaffolds

The scaffolds were fabricated s with a 50/50 collagen/chitosan ratio (named as C50-CH50), using a previously prepared solution, following a freeze-drying method described by O'Brien et al. (2004) [4]. The collagen was mixed with acetic acid 0.05 M in a centrifuge at 12,000 rpm (Medifriger BL-S, JP Selecta, Spain). The temperature of the solution was maintained at 4ºC. Scaffolds were then obtained by freeze-drying, with a two-stage method: a freezing stage at -40ºC for 1 h, followed by treatment under vacuum (<15 Pa) for 24 h, to cause the solvent to sublime from the sample using a freeze dryer (LyoQuest, TELSTAR, Japan). Furthermore, a dehydrothermal treatment at 105ºC was carried out to enhance the properties of the scaffolds.

Characterization of Scaffolds

Mechanical Characterization: Frequency sweep tests between 0.02 and 20 Hz and a constant strain (within the linear viscoelastic range) were carried out. The linear viscoelastic range and, consequently, the critical strain values were determined by performing strain sweep tests in compression mode at 1 Hz from $1 \cdot 10^3$ to 2%. The geometry used was two cylindrical plates (dia:15mm). The normal force of static force is an important parameter to be taken into account and, consequently, the static force is proportional to the dynamic force, but always without altering the structure.

Porosity measurements: The porosity (ε) of the scaffolds was obtained using a method that has been previously described [5]. The individual porosities were calculated using Eq. (1):

$$\varepsilon(\%) = (1 - \frac{\rho_s}{\rho_m}) \cdot 100 \qquad (1)$$

Where ρ_s is the density of the scaffold (calculated using weight and volume of each scaffold) and ρ_m is the density of the mixed system gelatin/chitosan, which is different for each case.

Results and Discussion

Influence of the pH

Mechanical characterization:

Figure 1 shows the evolution of the elastic and viscous moduli (E' and E'', respectively) with frequency for the scaffolds obtained from the system C50-CH50 at different pH values (2.0, 3.2, 5.0 and 7.0).

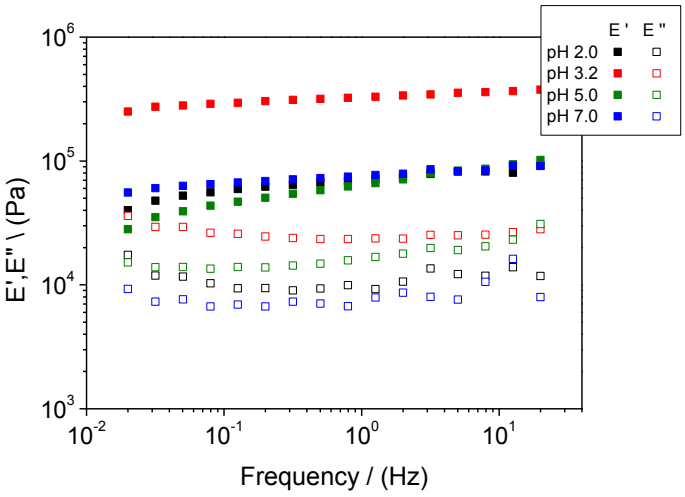

Figure 1. Evolution of E' and E'' with frequency in C50-CH50 scaffolds produced at different pH values (2.0, 3.2, 5.0 and 7.0)

It is observed the elastic solid behavior is maintained regardless the pH used. It is interesting to point out that the variation of the processing parameters affects the properties of the scaffolds produced. In the case of the pH, the optimal pH is 3.2-3.4 (in order to produce suitable scaffolds). For that reason, the variation towards higher or lower pH produces a significant decrease of the mechanical properties.

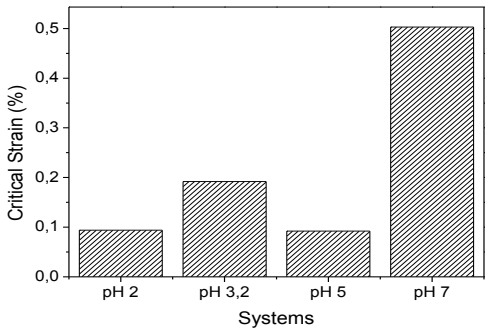

Figure 2. Critical strain of C50-CH50 scaffolds produced with a different pH values (2.0, 3.2, 5.0 and 7.0).

On the other hand, Figure 2 shows the critical strain of the scaffolds at different pH values (2.0, 3.2, 5.0 and 7.0). It is interesting to point out that the highest critical strain value corresponds to the system produced at pH 7.0, which means that the scaffolds produced present a higher elastomeric character.

Structural characterization:

Table 1 shows the porosity of the scaffolds produced at different pH values. As it can be seen, the porosity values show higher values (ca. 99%) and tend to decrease when the pH values increase above 3.2.

Table 1. Porosity values of the C50-CH50 scaffolds produced at different pH values (2.0, 3.2, 5.0 and 7.0).

Systems	Porosity (%)
C50-CH50 pH 2.0	99.0 ± 0.1
C50-CH50 pH 3.2	99.1 ± 0.1
C50-CH50 pH 5.0	98.4 ± 0.1
C50-CH50 pH 7.0	98.7 ± 0.1

Furthermore, an image of the each scaffold fabricated in can be observed in Figure 3. Interestingly, some physical changes take place because the scaffolds produced using a pH different from 3.2 shows characteristics (texture and physical appearance) different as the considered as distinctive for scaffolds.

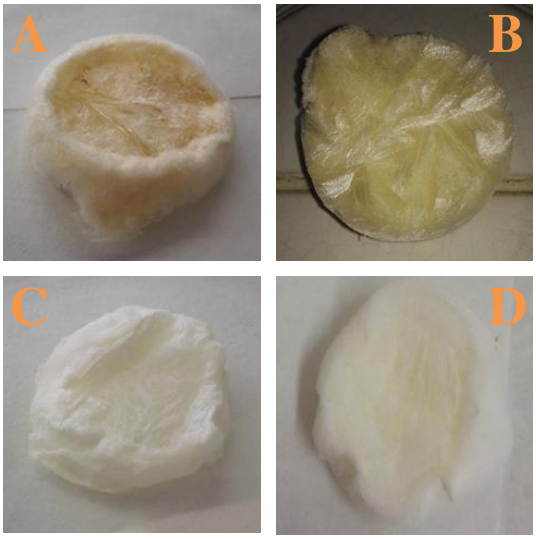

Figure 3. Images of the C50-CH50 scaffolds produced with a different pH values: 2.0 (A), 3.2 (B), 5.0 (C) and 7.0 (D).

Influence of the addition of glutaraldehyde

Mechanical characterization:

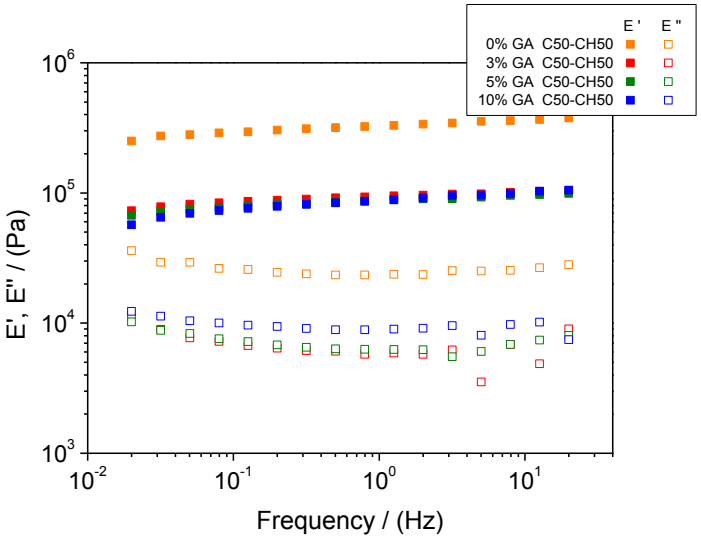

Figure 4. Evolution of E' and E'' with frequency in C50-CH50 scaffolds produced with a different concentration of glutaraldehyde (0, 3, 5 and 10%)

The results of the frequency sweep tests performed to C50-CH50 scaffolds with a different concentration of crosslinking agent (0%, 3%, 5% and 10%) are shown in Figure 4.

As it happened with the study of the pH, for all the systems E' is above E'', highlighting the elastic behaviour of the scaffolds. Furthermore, both moduli remain constant in all the frequency range (from 0.02 to 20 Hz), showing a gel-like behaviour. These measurements highlight the stability of the scaffolds produced. Moreover, it is clearly observed that the addition of glutaraldehyde does not produce an enhancement of the mechanical properties of the C50-CH50 scaffolds.

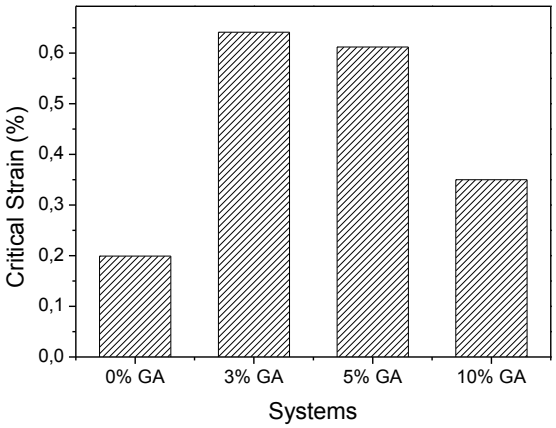

Figure 5. Critical strain of C50-CH50 scaffolds produced with a different concentration of glutaraldehyde (0, 3, 5 and 10%)

Otherwise, the influence of glutaraldehyde on the critical strain was also evaluated (Figure 5). Interestingly, the addition of GA produces an increase of the critical strain of the scaffolds, however, when it reaches a concentration of 10%, this effect is less marked.

Structural characterization:

The effect of the crosslinking agent in the porosity of the scaffolds is shown in Table 2.

Table 2. Porosity values of C50-CH50 scaffolds produced with a different concentration of glutaraldehyde (0, 3, 5, and 10%).

Systems	Porosity (%)
C50-CH50 GA 0%	99.11 ± 0.10
C50-CH50 GA 3%	95.24 ± 0.10
C50-CH50 GA 5%	95.30 ± 0.10
C50-CH50 GA 10%	98.89 ± 0.33

The addition of glutaraldehyde produces a decrease in the porosity of the systems compared with the system

without glutaraldehyde. However, the more the content of crosslinking agent, the more the porosity is.

In addition, the images showed in Figure 6 reveal that the crosslinking agent does not induce significant changes in the scaffolds formed.

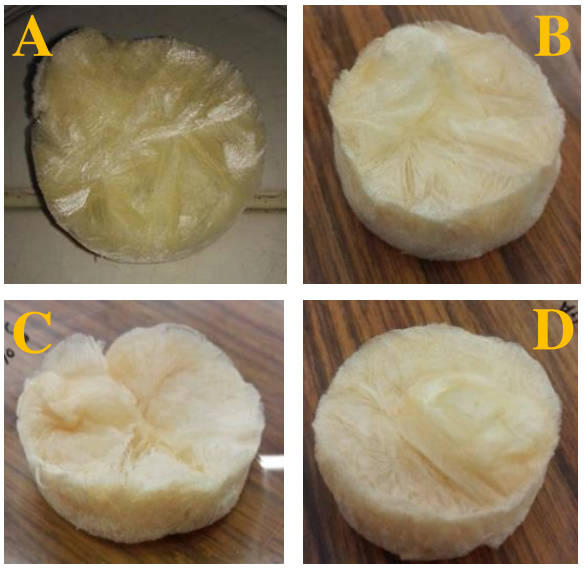

Figure 6. Images of the C50-CH50 scaffolds produced with a different concentration of glutaraldehyde: 0% (A), 3% (B), 5% (C) and 10% (D).

Concluding Remarks

A freeze-drying process has been followed for the development of collagen and chitosan scaffolds.

The study of the pH during the process reveal that working at a pH different than 3.2, the scaffolds do not present neither better optimal appearance nor the best mechanical properties.

On the other hand, the addition of glutaraldehyde to the initial formulation produces scaffolds with a more elastomeric character and a lower porosity.

Acknowledgements

This work is part of a research project sponsored "Ministerio de Economía y Competitividad" from the Spanish Government (Ref. CTQ2015-71164-P, MINECO/FEDER, UE). The authors gratefully acknowledge the University of Seville for the pre-doctoral scholarship of the VPPI-US of Victor M. Pérez Puyana, as well as "Ministerio de Educación y Cultura" for the Collaboration Grant of Isabel Carreño Carmona (csv: 23562025770558860482779 51). The authors gratefully acknowledge their financial support.

References

1. Jana, S., Tefft, B.J., Spoon, D.B., and Simari, R.D. (2014). Acta Biomater. 10, 2877–2893.
2. Van Vlierberghe, S., Dubruel, P., and Schacht, E. (2011). Biomacromolecules, 12, 1387–1408.
3. Geutjes, P.J., Daamen, W.F., Buma, P., Feitz, W.F., Faraj, K.A., and van Kuppevelt, T.H. (2006). Adv.Exp. Med. Biol. 585, 279-295.
4. O'Brien, F.J., Harley, B.A., Yannas, I.V., and Gibson, L. (2004). Biomaterials, 25, 1077–1086.
5. Al-Munajjed, A.A., Hien, M., Kujat, R., Gleeson, J.P., and Hammer, J. (2008). J. Mater. Med. 19, 2859–2864.

Contact Address:

alromero@us.es
Department of Chemical Engineering
Faculty of Chemistry
University of Seville
C/ Profesor García González
Telf.: +34 954557179

Development of collagen and chitosan-based membranes by electrospinning as potential scaffolds in Regenerative Medicine

V. Perez-Puyana, L. Cabrera-Correa, I. Carreño-Carmona, A. Romero

Department of Chemical Engineering, Faculty of Chemistry, University of Seville (Spain)

Introduction

Membranes formed by nanometric-size fibers present interesting characteristics such as a high specific surface, a high surface functionality and a greater mechanical behaviour. These properties make nanofiber materials excellent candidates in many applications: chemical, electronic, or biomedical [1]. Considering the possible biomedical applications, these materials could be used as potential scaffolds for Regenerative Medicine.

These membranes are processed by electrospinning. This is an innovative process which allows the continuous production of fibers with diameters in a range between 3 nm and 1 μm with great flexibility [2]. This technique is based on the elongation of a viscoelastic solution to form a filament. A polymer solution is projected from a syringe into a collector due to a voltage applied. The membrane constituted by fibers is formed on the surface of the collector [3].

The stability of the three-dimensional structure of biopolymers (proteins and polysaccharides) does not allow the optimal formation of the continuous filament. For that reason, synthetic polymers are commonly incorporated such as polyethylene oxide (POE) or polyvinyl alcohol (PVA). In this sense, the aim of this work is to optimize the electrospinning process of fish collagen (CG) and chitosan (CH) systems, by evaluating the incorporation of a water-soluble polymer, POE.

The electrospinning process was not achieved for the systems with CG and/or CH, so a synthetic polymer (POE) was included in the initial formulation. Systems with different CG/POE and CG/POE concentrations were elaborated and evaluated. The conductivity, surface tension, density and viscosity of the binary solutions were measured as well as the structure including the fiber diameter of the membranes obtained from electrospinning.

Experimental

Materials

Fish Collagen (CG) with a protein content of ca. 98 wt.% was supplied by Henan Boom Gelatin Co. Ltd (China). Chitosan (CH) of low molecular weight and Polyethylene oxide (POE) (Mw of 600,000) were purchased from Sigma Aldrich (Germany).

Preparation of solutions

First, solutions of POE, CH and CG are made varying the concentration. Concentrations of 0.85 wt.% and 5 wt.% were selected as the optimal concentration for CH and CG, respectively (the weight percentage, wt.%, is named as % in the rest of the text).

In addition, different binary solutions are prepared taking into account the CH-POE (0.85%/3.0%, 0.85%/3.5% and 0.85%/4.0%) and CG-POE (5.0%/3.0%, 5.0%/3.5% and 5.0%/4.0%) ratio. Acetic acid (10%) is used as solvent to improve biopolymer solubility. In addition, in order to achieve optimum solubility, magnetic stirring was carried out for 4-5 h.

Characterization of solutions

Electrical conductivity: The electrical conductivity was measured with a EC-Meter Basic 30+ equipment (Crison instruments, Spain). All the measurements were determined at 25ºC.

Surface Tension: Surface tension of the different solutions was measured using a Sigma 701 tensiometer (KSV, Finland) based on the Wilhelmy method. The temperature was maintained at 25ºC with a thermostat.

Density: The density was obtained at 25 ºC by means of a Densito 30PX Portable Density Meter (Mettler Toledo, USA).

Viscosity: Viscosity measurements were carried out by means of an AR2000 (TA Instruments, New Castle, DE, USA) rheometer. All the flow curves from 1 to 200 Pa were carried out at 25ºC (controlled by a Peltier connected to a thermostatic bath) using 40 mm

diameter aluminium serrated plates (both upper and lower plates).

Besides, for a Newtonian fluid, the shear rate is calculated by the following relation (Eq. 1):

$$\gamma = 8D/u \quad (1)$$

Where D is the diameter of the needle and u is obtained as follows (Eq. 2):

$$u = Q/A \quad (2)$$

Where Q is the flow rate and A is the circular area.

For that reason, considering the needle (G22) and the flow rate (0.4 mL/h) used, the theoretical shear rate inside the capillary where the solution is projected is 9.1 s^{-1}. Thus, due to the fact that not all the solutions studied present a Newtonian behaviour, the viscosity results shown in the following tables (Tables 1 and 3) correspond to 10 s^{-1}.

Electrospinning processing parameters

There are several parameters that are closely related to the characteristics of the fibers obtained by electrospinning, so their control is indispensable. The parameters selected as reference for the processing of the different electrospun nanofiber systems were: 15 kV as the voltage applied; 0.4 mL/h as the flow rate and 10 cm as the distance between the tip of the needle and the collector. Humidity and temperature can modify the fibers obtained so they are remained in the range of 35 ± 5 % and 20 ± 5 ºC, respectively.

Characterization of nanofibers

Scanning Electron Microscopy (SEM): Microscopy examination of fibers has been assessed with a JEOL JSM 6460 LV (Tokyo, Japan) at an acceleration voltage of 25 kV. A digital processing software (Image J) is used to determine the fibers diameter.

Results and Discussion

Chitosan (CH)/ Polyethylene oxide (POE) systems

Solutions:

Table 1 shows the different properties measured of the CH/POE solutions prepared, varying the concentration of POE (3.0, 3.5 and 4.0%) and maintaining 0.85% CH.

Two opposite effects can be seen according to the previous results: The addition of POE produces solutions with a higher viscosity, which it could obstruct the syringe during the electrospinning process; however a decrease in the conductivity of the solutions is also produced. Considering the surface tension and the density of the solutions, no significant changes are produced by modifying the concentration of POE.

Table 1. Properties (Conductivity, suface tension, density and viscosity) of the CH/POE solutions. Values with different letters are significantly different (P≤0.05).

Systems	Conductivity (µS/cm)	Surface Tension (mN/m)	Density (g/mL)	Viscosity (mPa·s)
CH 0.85% POE 3.0%	807±1^{a}	50±1^{a}	1.02±0.01^{a}	1500±200^{a}
CH 0.85% POE 3.5%	780±2^{b}	50±2^{a}	1.02±0.01^{a}	3100±500^{b}
CH 0.85% POE 4.0%	764±1^{c}	53±2^{a}	1.02±0.01^{a}	5100±20^{c}

Fibers:

On the other hand, after the electrospinning process membranes of fibers are obtained and examined through SEM. It is interesting to point out that no fibers could be obtained for the system with a 4.0% of POE because of its high viscosity. The images of the membranes produced with the other CH/POE solutions can be seen in Figure 1:

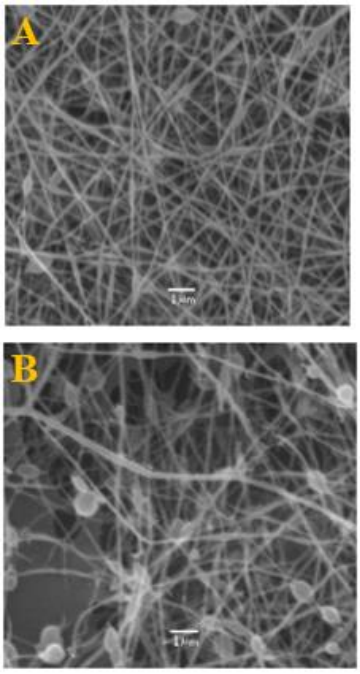

Figure 1. SEM images of the fibers produced from the CH/POE systems with a 0.85% of Chitosan and (A) 3.0% and (B) 3.5% of POE. All scale bars correspond to 1 µm.

Analysing the results obtained, it can be seen how the increase in the concentration of the PEO produces more disperse fibers, and even, it promotes the formation of aggregates with a spherical shape (named as spheroids).

In addition, these images are studied in order to obtain the mean diameter of the fibers obtained (Table 2). Interestingly, a decrease in the concentration of POE leads to a decrease in the fiber diameter. This effect could be explained by the variation of both conductivity and viscosity of the systems previous to the electrospinning process.

*Table 2. Fiber diameters of the CH/POE systems after performing electrospinning. * means that no fibers could be obtained.*

Systems	Fiber Diameter (nm)
CH 0.85% POE 3.0%	121±36
CH 0.85% POE 3.5%	151±32
CH 0.85% POE 4.0%	*

Collagen (CG)/Polyethylene oxide (POE) systems

Solutions:

Table 3 shows the different properties measured of the CG/POE solutions prepared, varying the concentration of POE (3.0, 3.5 and 4.0 %).

Table 3. Properties (conductivity, surface tension, density and viscosity) of the CG/POE solutions. Values with different letters are significantly different (P≤0.05).

Systems	Conductivity (µS/cm)	Surface Tension (mN/m)	Density (g/mL)	Viscosity (mPa·s)
CG 5.0% POE 3.0%	2038±1^{a}	49±1^{a}	1.03±0.01	71±1^{a}
CG 5.0% POE 3.5%	2028±5^{b}	52±1^{b}	1.03±0.01	390±30^{b}
CG 5.0% POE 4.0%	2018±5^{b}	54±1^{c}	1.03±0.01	850±10^{c}

The increase in the concentration of POE in the CG/POE solutions leads to a decrease of the conductivity of the solutions, as well as an increase in both the viscosity and the surface tension. However, the density is not affected (as it happened with the previous CH/POE solutions) by the addition of POE. Although the viscosity of the CH/POE solutions also increases with the concentration of POE present, the viscosity values reach are not high enough to obstruct the syringe and, consequently, the electrospinning process is completed. In fact, the viscosity values obtained are lower than the ones obtained for the CH-POE solutions evaluated in the previous section.

Fibers:

SEM images are also obtained from the CG/POE solutions (Figure 2). SEM images reveal that the fibers of the membranes obtained from the CG/POE are more uniform when the synthetic polymer content is higher (in this case, the concentration of POE). The fibers obtained for the systems with the lowest POE concentration (3.0%) (Figure 2A) shows spheroids in their structures. However, these spheroids tend to disappear by increasing the amount of POE used: 3.5% (Figure 2B) and 4.0% (Figure 2C).

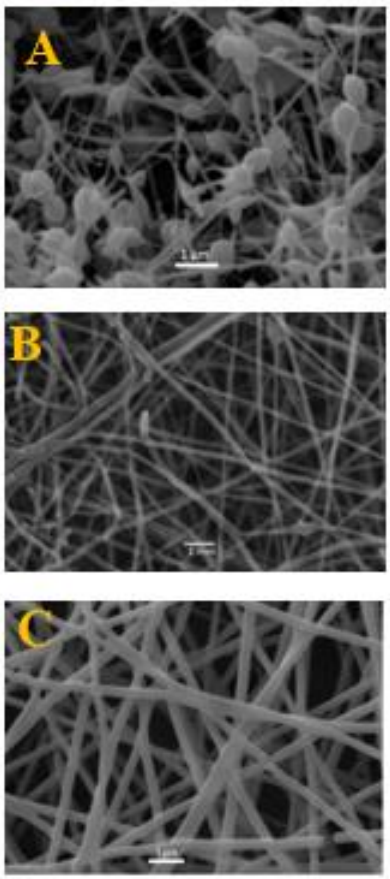

Figure 2. SEM images of the fibers produced from the CG/POE systems with a 5.0% of CG and (A) 3.0%, (B) 3.5% and (C) 4.0% of POE. All scale bars correspond to 1 µm.

Moreover, these images are also studied and the mean diameter obtained (Table 4). Considering the results obtained, a similar effect occurs because the diameter of the fibers is higher when the concentration of POE is increased and, thus, lowering the specific surface.

Table 4. Fiber diameter of the CG/POE systems after performing electrospinning

Systems	Fiber Diameter (nm)
CG 5.0% POE 3.0%	112 ± 26
CG 5.0% POE 3.5%	195 ± 39
CG 5.0% POE 4.0%	273 ± 28

Concluding remarks

The process of electrospinning is achieved and membranes of fibers are obtained using Polyethylene Oxide (POE) in combination with two different biopolymers: Chitosan (CH) and Collagen (CG).

Considering the CH/POE systems, the solutions exhibit a higher viscosity and a lower conductivity when the concentration of POE is increased. The fibers present a higher diameter by increasing the POE concentration. However, no fibers could be obtained from the system with the higher concentration of POE (4.0%) due to the high viscosity of this solution.

On the other hand, CG/POE systems show the same behaviour. A higher viscosity and a lower conductivity of the solutions as well as higher fiber diameter are found when the concentration of POE is higher.

Acknowledgements

This work is part of a research project sponsored "Ministerio de Economía y Competitividad" from the Spanish Government (Ref. CTQ2015-71164-P, MINECO/FEDER, UE). The authors gratefully acknowledge the University of Seville for the pre-doctoral scholarship of the VPPI-US of Victor M. Pérez Puyana, as well as "Ministerio de Educación y Cultura" for the Collaboration Grant of Leticia Cabrera Correa (csv:23561959618456302080873l). The authors gratefully acknowledge their financial support. The authors also thank the Microscopy Service (CITIUS-US) for providing full access and assistance to the JEOL 6460LV equipment.

References

1. Lee, K.Y., Jeong, L., Kang, Y.O., Lee, S.J., and Park, W.H. (2009). Adv. Drug Deliv. Rev. 61, 1020–1032.
2. Agarwal, S., Greiner, A., and Wendorff, J.H. (2009). Adv. Func. Tech. 19, 2863–2879.
3. Bhardwaj, N., and Kundu, S.C. (2010). Biotech. Adv. 28, 325–347.

Contact Address:

alromero@us.es
Department of Chemical Engineering
Faculty of Chemistry
University of Seville
C/ Profesor García González
Telf.: +34 954557179

Thermo-rheological properties of polypropylene modified bitumens for paving and roofing applications

A.A, Cuadri, F.J, Navarro, F.J, Martínez-Boza, P, Partal

Departamento de Ingeniería Química, Centro de Investigación en Tecnología de Productos y Procesos Químicos (Pro2TecS), Campus de 'El Carmen, Universidad de Huelva, 21071, Huelva (Spain)

Introduction

Bitumen, a by-product of fractional distillation of crude oil, can be described as a colloidal dispersion where the components of highest molecular weight, the asphaltenes, are dispersed into a medium constituted by the remaining components, the maltenes (resins, aromatics and saturates), composition commonly referred to as SARAs fractions [1]. Thus, this material presents a large set of interesting properties: impermeability, ductility, adhesivity, resistance to the effect of weathering and chemicals, etc. They all have favored the development of a wide field of applications that range from the construction of road pavements (~85 % of the total) to more specialized purposes, such as waterproof membranes for the roofing industry [2-4].

As for its major application, virgin polymers are very useful for road pavements, and waterproofing and roofing membranes in order to improve the main distresses associated with bitumen: a) at high in-service temperatures, rutting (permanent deformation under heavy vehicle loading) and fatigue cracking (cracks due to repetitive application of loads); b) at low in-service temperatures, thermal cracking (related to cracks due to the lack of asphalt flexibility) [5-7]. Thus, various virgin and recycled polymers included plastomers (e.g. polyethylene (PE), polypropylene (PP), ethylene–vinyl acetate (EVA), ethylene–butyl acrylate (EBA)) and thermoplastic elastomers (e.g. styrene–butadiene–styrene (SBS), styrene–isoprene–styrene (SIS), and styrene–ethylene/butylene–styrene (SEBS)) have been used [8-10]. On the other hand, the cost of polymer modified bitumens (PMBs) is quite relevant with the dosage of the added polymer, while this parameter has important influences on the final performance [3]. Thus, for road paving applications, economical reasons and workability requirements (easiness of producing, handling, pumping, placing and compacting) limit the amount of polymer in the mixture to low concentrations (usually lower than 5 wt.%). By contrast, roofing and waterproofing performance requires improved toughness, flexibility and adhesion in a very wide temperature window, which would need much higher concentrations (up to 30 wt.%) [11]. Consequently, from both environmental and economical point of views, bitumen modification with recycled polymers coming from agricultural or urban wastes have been recently reported [9], offering a sustainable life-cycle for some petroleum-derivative polymers. However, they are just limited to assess a thermo-mechanical characterization of their corresponding PMBs with polymer concentration lower than 10 wt.% in a wide range of in-service temperatures.

In response to the need of reusing polymer wastes, as well as reducing the cost of the polymer modified bitumens, the influence that polymer concentration exerts on the thermo-rheological properties and microstructure of recycled polypropylene modified bitumens were considered. With this aim, blends of a 160/220 penetration grade bitumen with different recycled polymer concentrations, ranging from 2 to 50 wt.%, were prepared. The evolution of the microstructure and rheological behavior of the different binders has been conducted by optical microscopy and oscillatory and dynamic mechanical thermal analysis (DMTA), respectively. From the experimental results obtained, it can be deduced that recycled polypropylene concentrations up to 5 wt. % lead to enhanced rheological properties of the modified bitumen useful for paving applications. Thus, the glassy region is shifted to lower temperatures and higher viscoelasticy moduli are obtained, improving the bitumen behavior at low and high in-service temperatures, respectively. On the other hand, the development of a continuous polymer-rich phase through the bituminous binders observed for larger recycled polymer concentrations yields modified binders suitable for roofing membranes.

Experimental

Materials

A 160/220 penetration grade bitumen, donated by Repsol YPF (Spain), and a recycled polypropylene (rPP), supplied by Eslava Plásticos, S.A. (Spain), were used as base components of the bituminous blends.

Sample preparation

Binary blends of bitumen and recycled polymer were prepared in the molten state, at 180 ºC, in an open batch reactor, using an IKA RW-20 mixer (Germany) with different propellers: a four blade propeller, for the lowest polymer concentrations (2%, 5% and 15 wt. %), and a helical ribbon impeller for 25 wt. % polymer content.

Blends containing 50 wt. % recycled polyethylene were processed in a modular batch mixing system (Polylab, Haake, Germany). The mixer tool used, Rheomix 3000p, enables batch testing of many highly viscous substances and consists of a batch mixer fitted with two counterrotating rollers, turning with different angular velocities (ratio 3:2).

Testing procedures

Dynamic temperature sweep tests between 30 and 130 ºC, in the linear viscoelastic range, were carried out in a controlled-stress rheometer RS-150 from Haake (Germany), using parallel plate geometries (20 and 35 mm diameter, 1 mm gap), at a constant frequency of 10 rad/s and a heating rate of 2 ºC/min (AASHTO-TP5).

DMTA experiments were done with a Seiko DMS 6100, Seiko Instruments (Japan), by using 50x10x3mm samples in double cantilever bending mode, and liquid nitrogen as fluid refrigerator. All the experiments were carried out at constant frequency (1 Hz) and a strain (within the linear viscoelastic region). The selected temperature ramp was 2 ºC/min. Temperature ranged from -40 to 130 ºC. In previous papers, authors checked that the selected heating ramp of 2 ºC/min is appropriate for conducting both measurements (e.g., dynamic temperature sweep tests and DMTA). On the other hand, the rheological data were collected until the linear viscoelastic functions values become negative.

Optical images were obtained by placing samples under an optical microscope (Olympus BX51, Japan), coupled with a LTS-350 Heating-Freezing Stage, manufactured by Linkam Scientific Instruments (UK). Samples were prepared by using standard microscope slides (76x26 mm), heating up to the molten state and, subsequently, cooling down to room temperature.

Results and Discussion

Rheological characterization: linear viscoelastic behavior

In order to analyze the mechanical response of the bitumen/rPP blends in a wide range of in-service temperatures, the linear viscoelastic functions obtained from DMTA in bending mode (E', E'') and oscillatory shear measurements (G', G'') were overlapped by using a shift-factor (b_T), which is called as Poisson's ratio.

As can be observed in Figure 1, the viscoelasticity functions of neat bitumen display a direct transition from the glassy to the Newtonian region by increasing temperature [12]. Moreover, no plateau at intermediate temperatures (like that which characterizes polymer melts and solutions) was detected, which demonstrates the non-existence of entanglements. On the contrary, the rPP mechanical spectrum presents a rubbery domain at low/intermediate temperature and a terminal region at high temperature. Thus, a maximum in E'', which characterises the onset of the glassy region, is also observed [12].

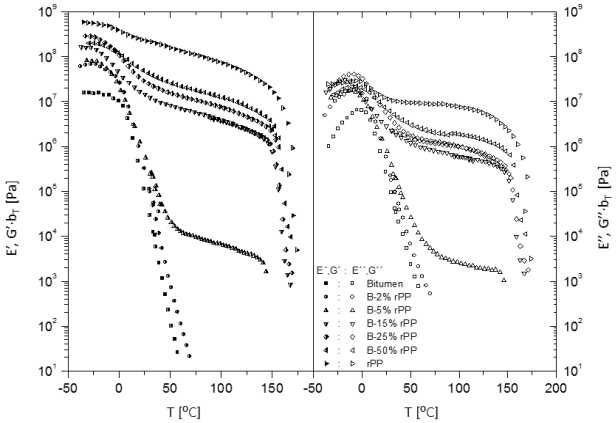

Figure 1. Evolution of linear viscoelastic functions with temperature for neat bitumen and its corresponding bitumen/rPP binders.

Regarding the bitumen/rPP blends, a strong dependence with the polymer concentration is clearly noticed on their mechanical spectrum. Compared to neat bitumen, while for the lowest concentration (2 wt.%) only slight differences are noticed, the effect of polymer modification on the bitumen/rPP viscoelastic behavior begins to become apparent when the rPP concentration increases up to 5 wt.%. For this blend, when the bitumen phase is soft enough, at temperature around 50 ºC, the presence of the polymer is revealed by an abrupt change of the slope for both moduli, developing a plateau-like region. In addition, the

behavior of the blends with concentrations higher than 5 wt.% rPP is clearly dominated by the polymer, showing an increase in the values of both moduli as polymer concentration rises. This fact has been related to an improvement of the in-service performance at high temperature and, consequently, better rutting resistance [13].

On the other hand, in order to establish a comparative analysis on the effect of modification on the low-temperature performance, a "mechanical" glass transition temperature ($T_{g,DMTA}$), taken as the values of temperature at the maximum in E'' curve [14] has been obtained. This parameter, which accounts for the onset of the glassy region (at which the binder is expected to be affected by thermal cracking under loading), has widely been used to evaluate the end-performance of polymer-modified bitumens at low temperatures [12]. In consequence, a decrease in the $T_{g,DMTA}$ is a highly desirable result of modification. It is worth noting that bitumen/rPP blends shows only a single peak in the low-temperature range which would indicate that both materials are compatible.

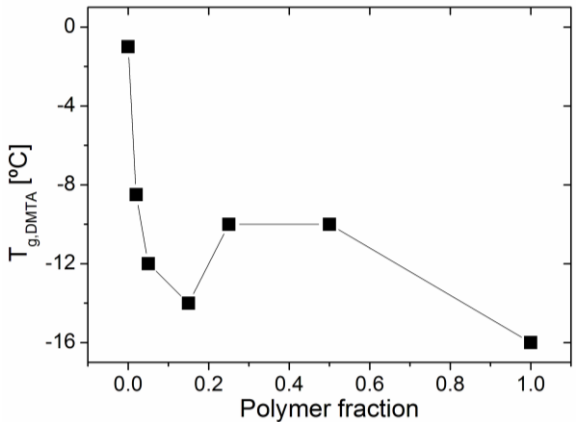

Figure 2. Evolution of "mechanical" glass transition temperature ($T_{g,DMTA}$) with polymer fraction for neat bitumen and its corresponding bitumen/rPP binders.

Microstructural characterization: optical microscopy

The morphology of the different bitumen/rPP blends was assessed using optical microscopy (Figure 3).

It is widely found in the literature that bitumen-polyolefins (e.g., polypropylene) blends display a multiphase morphology, where polymer-rich and bitumen-rich phases can be clearly visualized [15]. As can be seen in Figure 3, the photomicrographs of the blends with the lowest polymer content (2 wt.% rPP, Figure 3A) shows dispersed polymer domains (lightly toned regions), which are distributed homogeneously in a continuous bitumen phase (dark areas).

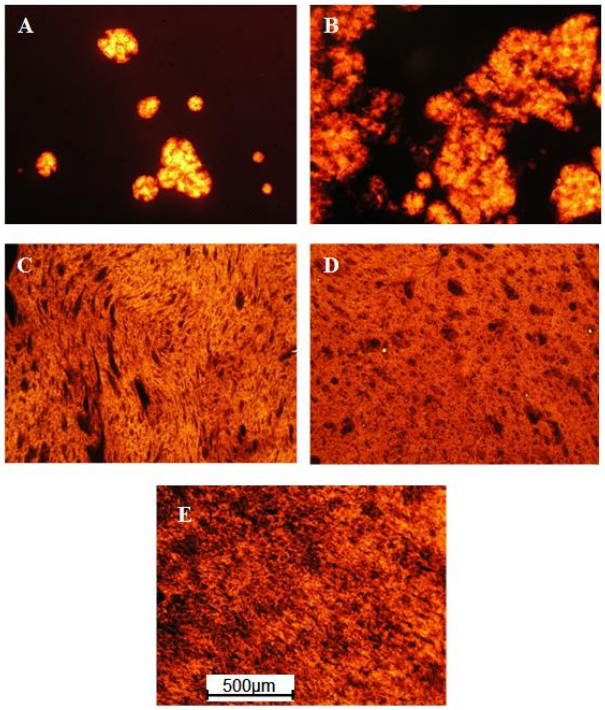

Figure 3. Photomicrographs for rPP/bitumen binders prepared with (A) 2, (B) 5, (C) 15, (D) 25 and (E) 50 wt.% polymer.

On the contrary, almost continuous polymer phase, and some large disperse regions of bituminous phase is noticed for 5 wt.% rPP (Figure 3B), whereas at higher concentrations phase inversion is clearly observed for 15 wt.% rPP (Figure 3C). Higher rPP concentration of 25 wt.% rPP (Figure 3D), and mainly of 50 wt.% rPP (Figure 3E), seems to yield different bitumen morphologies, showing a narrow dispersion of bitumen droplets in a polymer-rich continuous phase. Similar effect was also observed for bitumen/polyethylene blends [2]. This phase inversion observed by optical microscopy results from the addition of a partially compatible polymer to bitumen, and is of practical significance for roofing membranes, where a continuous polymer-rich phase is routinely sought [10].

Interestingly, the different rheological behavior for low and high polymer concentrations previously outlined, can be understood on the basis of this phase inversion [16]. Thus, the significant change observed in the linear viscoelastic properties, when polymer concentration increases from 5 to 15 wt.% rPP (Figure 1) is explained by the development of a continuous polymer-rich phase through the bitumen blend. This fact would highlight the role played by polymer swelling in the required rheological properties of waterproofing membranes, in particular at high in-service temperatures (Figure 1).

Therefore, due to its partial compatibility, polymer is swollen by some of the lighter maltenic compounds and,

therefore, the bituminous continuous phase is artificially enriched in asphaltenes by the so called ''physical distillation process'', leading to changes in the chemical composition of the matrix [1]. The absorption of some bitumen compounds by the rPP can be confirmed by means of image analysis, as shown in Table 1.

Thus, the polymer surface fraction increases beyond the proportion of wt.% rPP added for bitumen modification. Considering that polymer and bitumen densities are quite similar, polymer swelling by maltenic compounds may be clearly deduced [16]. In addition to that, the swelling ratio (defined as the ratio between the polymeric surface fraction and polymer concentration added) increases as polymer concentration decreases, getting values higher than 1, which is the system not swelled [16].

Table 1. Polymer-phase fraction and swelling ratio, from micrograph image analysis, for different rPP modified bitumen samples.

wt. % rPP	Polymer surface fraction (%)	Swellling ratio[a]
2	7.8	3.9
5	36.4	7.3
15	53.1	3.5
25	60.6	2.4
50	58.6	1.2
100	100	1.0

[a] Swelling ratio = Polymer surface fraction / wt.% rPP

Acknowledgements

This work is part of a research project sponsored by an MMA programme (Research Project 5,1–212/2005/3B, Ministerio de Medio Ambiente, Spain). The authors gratefully acknowledge its financial support.

References

1. Lesueur, D. (1985). Adv. Colloid Interface Sci. 145, 42-82.
2. Zhang, H., Yu, J., Wang, H., and Xue, L. (2011). Mater. Chem. Phys. 129, 769-776.
3. Izquierdo, M.A., García-Morales, M., Martínez-Boza, F.J. and Navarro, F.J. (2014). Mater. Chem. Phys. 146, 261-268.
4. Martín-Alfonso, M.J., Partal, P., Navarro, F.J., García-Morales, M. and Gallegos, C. (2008). Ind. Eng. Chem. Res. 47, 6933-6940.
5. Cuadri, A.A., Partal, P., Navarro, F.J., García-Morales, M. and Gallegos, C. (2011). Energy Fuels 25, 4055-4062.
6. Lu, X., Isacsson, J. and Ekblad, J. (2003). Mater. Struct. 36, 652-656.
7. Read, J. and Whiteoak, D. (2003). In The shell bitumen handbook; Shell Bitumen U.K.: Surrey, U.K., 2003.
8. Jiang, Z., Hu, C., Easa, S.M., Zheng, X. and Zhang, Y. J. (2017). Appl. Polym. Sci. 134, 44850.
9. García-Morales, M., Partal, P., Navarro, F.J., García-Morales, M. and Gallegos, C. (2007). Polym. Eng. Sci. 47, 181-191.
10. Pérez-Lepe, A., Martínez-Boza, F.J. and Gallegos, C. (2007). J. Appl. Polym. Sci. 103, 1166-1174.
11. Navarro, F.J., Partal, P., Martínez-Boza, F.J. and Gallegos, C. (2010). Polym. Test. 29, 588-595.
12. Partal, P., Martínez-Boza, F.J., Conde, B. and Gallegos, C. (1999). Fuel 78, 1-10.
13. Guisández, J., Tiemblo, P. and Gómez-Elvira, J.M. (2005). Polym. Degrad. Stab. 87, 543-553.
14. Martínez-Boza, F.J., Partal, P., Navarro, F.J. and Gallegos, C. (2001). Rheol. Acta 40, 135-141.
15. Cuadri, A.A., García-Morales, M., Navarro, F.J., Airey, G.D. and Partal, P. (2013). Rheol. Acta 52, 145-154.
16. González, O., Muñoz, M.E., Santamaría, A., Garcia-Morales, M., Navarro, F.J., Partal, P. (2004). Eur. Polym. J. 40, 2365-2372.

Contact Address:

frando@uhu.es
Departamento de Ingeniería Química,
Centro de Investigación en Tecnología de Productos y Procesos Químicos (Pro2TecS), Campus de 'El Carmen'
Universidad de Huelva
Avenida de las Fuerzas Armadas S/N, 21071, Huelva (Spain)
Telf.: +34 959 21 82 05; Fax: +34 959 21 99 83

Soy protein-based superabsorbent biopolymer materials functionalized with different acylation agents

C., Bengoechea[1], A.A., Cuadri[2], A., Romero[1], A., Guerrero[1]

[1] Universidad de Sevilla, Departamento de Ingeniería Química, c/ Prof. García González 1, 41012 Sevilla (Spain)
[2] Universidad de Huelva, Departamento de Ingeniería Química, Centro de Investigación en Tecnología de Productos y Procesos Químicos (Pro2TecS), Campus de 'El Carmen', 21071 Huelva (Spain)

Introduction

Superabsorbent polymer (SAP) materials are highly cross-linked macromolecules that can absorb and retain a significant amount of water or biological fluids (as high as ~10–1000 times their own weight) to form hydrogels [1,2]. Regarding their applications, SAP materials are momentous collection of resources with incredible applications in the field of engineering, biological and pharmaceutical sciences [3], highlighting the uses for water retention in agriculture and horticulture soils [4] and, mainly, for disposable diapers and feminine hygiene products [5]. SAPs are generally classified into synthetic and natural-based polymers. The former are frequently produced from acrylic acid and its derivatives [6]. However, some issues related to their poor biodegradability and high costs have been pointed out [1]. As a consequence, there is a growing need to develop natural SAPs that overcome these drawbacks, showing both great water uptake capacity and processability.

Soy protein isolate (SPI) would seem to be an adequate starting material for the manufacture of natural-based SAP materials when considering: (1) SPI is the main coproduct of the soybean oil industry, being available at an affordable price [7]; (2) SPI shows a high hydrophilic character, due to the high presence of aspartic and glutamic acids in its composition [8]; and (3) SPI, in combination with a suitable plasticizer (i.e., glycerol), displays excellent processability properties, allowing the production of different shaped products (e.g. by injection molding) [9]. A valuable way of improving the water absorption capacity of the soy protein could be through the functionalization of the protein matrix, giving rise to the presence of new water-solubilizing groups. One of the most common chemical modifications used for proteins is the acylation of the amino acid residues with acid anhydrides [10,11]. In this sense, soy protein modification with ethylenediaminetetraacetic dianhydride (EDTAD) or succinic anhydride (SA) are able to include a large number of carboxylate anions (COO-) into the soy protein molecule, creating numerous sites for water binding and, consequently, increasing its hydrophilic character [10,11].

Therefore, the main aim of the present work is to study the feasibility of obtaining natural-based SAP materials via soy protein (SPI) functionalization using different amounts of ethylenediaminetetraacetic dianhydride (EDTAD) or succinic anhydride (SA) as acylating agents.

Experimental

Materials

Soy protein isolate (SPI), with the trade name of SUPRO 500E IP, was supplied by PROANDA (Proveedora Andaluza, S.L., Sevilla, Spain). Its specifications, provided by the supplier, were: max. 6.0 % moisture, min. 90.0 % protein, max. 1.0 % fat, max. 5.0 % ash and pH (5 % slurry) in the range of 6.9-7.4. Glycerol (GL) was used as the plasticizer for soy protein isolate (SPI), and ethylenediaminetetraacetic dianhydride (EDTAD) and succinic anhydride (SA) were used as acylating agents. All these products were supplied by Panreac Química, S.A.

Functionalized protein

The SPI acylation by EDTAD and SA was performed according to the procedure reported by Hwang et al. [11] and Zhao et al. [10], respectively:

-Protein acylation by EDTAD:

The pH of a 4 wt. % solution of SPI was adjusted to 12 by adding the required amount of a 3.0 N NaOH solution and heating for 30 min at 65 ºC. The solution was then cooled down to room temperature and modified by the addition of the corresponding different amounts of EDTAD. The pH of the protein solution was kept constant at 12.0 throughout the chemical modification,

by adding the suitable amount of 1.0 N NaOH while stirring for 3 h. After that, the pH was decreased to 7.0 by the addition of 6 N HCl to prevent further modification.

Finally, the protein solution was dialyzed against dionized water for 48 h to remove salts (e.g. sodium salt of EDTAD) and excess reagents, recovering each acylated SPI sample through freeze-drying using a Telstar CRYODOS-80 (Telstar, Life Science Solutions, Madrid, Spain).

-Protein acylation by SA:

A 4 wt.% solution of SPI was dispersed in distilled water for 1 h using a magnetic stirrer. Subsequently, the pH of the solution was adjusted to 8 by adding the necessary amount of a 3.0 N NaOH solution. Then, different amounts of SA were added to three aliquots of this SPI solution. The pH of the solution was kept between 7.5 and 8.5 adding conveniently 3.0 N NaOH while stirring. After pH was stabilized around 8, the solution was kept stirred for 1 h. Afterwards, pH was decreased to 7.0 by the addition of 3 N HCl to prevent further modification. Finally, the protein solution was dialyzed against dionized water for 48 h and recovered through freeze-drying.

The acylation reaction occurs between the amino groups of the lysyl residue from the protein and the anhydride groups of the acylating agent [10,11]. In addition, SA possesses half anhydride groups compared to EDTAD. Therefore, to compare two acylated SPI samples, these should be prepared using the amount of acylating agent that provides the same anydride groups available to react with the amino groups of the protein. With this in mind, two acylated protein samples were prepared by the addition of adequate amount of EDTAD or SA to achieve 117 mol anhydride/10^5 g SPI. For this relationship, the EDTAD/SPI and SA/SPI mass ratio should be 0.15 and 0.116, respectively, taking into account that there is 0.56 g anhydride/g EDTAD and 0.72 g anhydride/g SA. These acylated samples will hereinafter be referred to as “a2SPI” and “a1SPI”, respectively, where “2” or “1” refers to the number of the anhydride group/molecule acylation agent (this is, prepared from EDTAD or SA, respectively).

Sample preparation

Blends containing 50 wt.% protein (unmodified SPI or acylated SPI systems) and 50 wt.% GL were properly manufactured by a thermomechanical procedure that consisted of two stages:

A) The ingredients were mixed in a two-blade counter-rotating batch mixer Haake Polylab QC (ThermoHaake, Karlsrube, Germany) at room temperature and 50 rpm for 10 min, at adiabatic conditions. During mixing, only a slight increase in temperature (always lower than 2 ºC) was detected whereas no significant increase in torque was observed, which excludes any significant contribution of shear induced crosslinking over the mixing stage. Samples were stored in sealed plastic bags at room temperature for 24 h, prior further processing.

B) The blends were processed by lab-scale injection molding using a MiniJet Piston Injection Molding System (ThermoHaake, Karlsrube, Germany) to obtain 60x10x1 mm rectangular shaped plastic specimens. Based on a previous study [12], when searching SPI/GL plastics with optimized water uptake capacity, it is advisable to select moderate processing conditions. Thus, the temperature, pressure and time in the pre-injection cylinder and in the mold were respectively: 50/120 ºC, 500/500 bar and 10/500 s. For the acylated SPIs, the pressure profile selected was 500/250 bar in order to obtain homogeneous bioplastic specimens. The plastic materials obtained from unmodified SPI will be referred to as SPI/GL.

Regarding the acylated systems, those obtained from acylated SPI with EDTAD will be abbreviated as a2SPI/GL and those from SA as a1SPI/GL.

Characterization

The water imbibing capacity (WIC) of all protein samples was measured in a Baummann apparatus according to a method modified by Wagner et al. [13]. A glass Buchner funnel equipped with a borosilicate filter (ROBU Glasfilter-Geraete GmbH, Germany) was connected to a horizontal graduated pipette filled with distilled water and located to the same level than the filter. A 30 mg sample was placed as thin layer on the filter while closing the funnel mouth with a hermetic lid. For each material, the amount of liquid water (ml or g) absorbed from the pipette at room temperature was recorded over time until equilibrium was reached, achieving the WIC value.

The tensile properties were evaluated at room temperature with a RSA3 (TA Instruments, New Castle, USA) in tensile mode using two medium clamps (length: 25 mm; width: 10 mm; thickness: 6 mm) for 60x10x1 mm rectangular probes. All tensile tests carried out at constant extensional rate of 1 mm/min. From them, the

maximum stress (σ_{max}), maximum strain (ε_{max}) and Young's Modulus (E) were obtained.

Water uptake of SAP plastic was determined according to UNE-EN ISO 62:2008 using 20x10x1 mm specimens immersed in distillate water for 24 h. The water uptake (WU) percentage was calculated as:

$$WU(\%) = \frac{m_2 - m_1}{m_1} x100 \qquad (1)$$

where: m_1 is the initial weight of the probe immediately weighed after being dried in an oven at 50 ºC for 24 h and cooled in a desiccator; and m_2 refers to the weight of the probe just after 24 h of water immersion.

Results and Discussion

Aiming to confirm the potential improvement on hydrophilic properties due to the increase in relative carboxylic content, the water imbibing capacity (WIC) for native SPI and its corresponding acylated SPI samples was determined. To that end, representative values for the kinetics of liquid water absorption, i.e. the amount of water absorbed by the sample over time, are displayed in Figure 1.

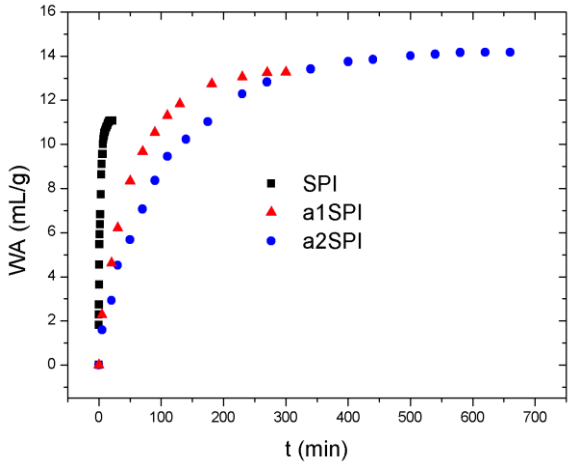

Figure 1. Kinetic of water absorption measured in a Baummann apparatus for native SPI and selected acylated SPI samples.

Compared to acylated SPI samples, the reference SPI took a shorter time to reach its swollen equilibrium (WIC), which is considered as the maximum spontaneous water absorption by the protein powder. However, the acylated samples display a sharp increase within the first ca. 170 min for a1SPI or ca. 330 min for a2SPI, and then increased gently until reaching its WIC value.

It is worth mentioning that the distribution of carboxylic groups, which is ultimately responsible for the increase in hydrophilicity of the protein, is different for acylated SPI when EDTAD (a2SPI) or SA (a1SPI) is used. Thus, a2SPI displays higher WIC value (14.2 mL/g) that a1SPI (13.4 mL/g).

On the other hand, Table 1 shows the results from the water uptake measurements obtained after immersion of bioplastic samples for 24 h. Regarding their water uptake capacity, those bioplastic samples prepared from acylated SP show strongly enhanced values as compared to the moderate value obtained for the reference sample. Moreover, all acylated SPI plastics here proposed comply the level required for being considered as superabsorbent (SAP) materials [14].

Table 1. Water uptake values obtained for SPI/GL samples.

Sample	WU (wt.%)	WU after re-swelling (wt.%)
SPI	161±10	130±9
a1SPI	3398±195	3278±175
a2SPI	3644±204	3596±198

On the other hand, the SAP-materials after their first water immersion were lyophilized and again subjected to water immersion for 24 h (named as re-swelling). Interestingly, no significant differences between water uptake and re-swelling capability are found in Table 1. In addition to that, no water-soluble loss matter (no data shown) was observed for the acylated samples after the second water immersion. This is particularly relevant from a practical point of view, since these findings imply that SPI superabsorbent materials can be re-used at least twice without losing their water uptake capacity.

Finally, representative results obtained from uniaxial strength measurements for the resulting plastic samples, after injection molding, are shown in Figure 2.

In Figure 2, the stress strain curves for the reference and acylated plastic systems are presented. All the curves exhibit an initial linear elastic behavior of high constant stress–strain slope yielding high values for the Young's Modulus (E), followed by a plastic deformation stage with a continuous decrease in the stress–strain slope after the elastic limit. A second constant slope is reached at the end of this plastic deformation stage. All the curves eventually reach a maximum value for the stress (σ_{max}) and the strain (ε_{max}), which is immediately followed by a sudden decrease in stress that corresponds to the rupture of the sample.

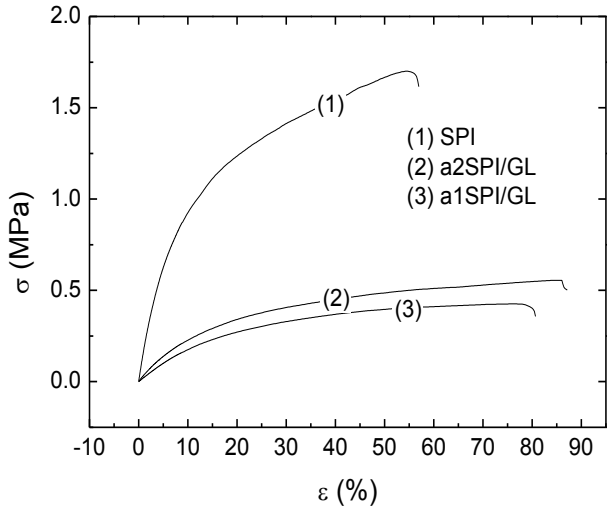

Figure 2. Stress versus strain curves for the reference plastic and its corresponding acylated plastic samples.

The values of the representative parameters σ_{max}, ε_{max} and E from these tensile tests performed on plastic specimens are shown in Table 2.

Table 2. Parameters from tensile strength measurements: Maximum stress (σ_{max}), maximum strain (ε_{max}) and Young's Modulus (E) for reference and acylated plastics.

Sample	σ_{max} (MPa)	ε_{max} (mm/mm)	E (MPa)
SPI/GL	1.7±0.15	0.567±0.03	17.01±1.2
a1SPI/GL	0.42±0.03	0.807±0.04	2.12±0.3
a2SPI/GL	0.56±0.03	0.862±0.03	3.41±0.4

As can be deduced, acylated plastics show lower values of σ_{max} and E compared to that obtained for the reference system. On the contrary, ε_{max} undergoes an increase when compared to the reference plastic up to 52 % and 43 % for the a2SPI/GL and a1SPI/GL, respectively. By comparing the results obtained from tensile tests and water uptake (WU) capacity, it can be assumed that the acylated SPI plastics with greater WU capacity display higher extensibility, as water imbibing capacity (WIC) increase, compared to the reference plastic. Therefore, it may be stated that the SPI chemical modification by acylation produces SAP plastics less fragile than the reference sample, which may be regarded as fairly positive for absorbent materials since it will favour the swelling behaviour of the biopolymer network.

Acknowledgments

This work is part of a research project sponsored by "Ministerio de Economía y Competitividad" from the Spanish Government, (MINECO/FEDER, UE), Ref. CTQ2015-71164-P. The authors gratefully acknowledge their financial support.

References

1. Shi, W., Dumont, M.J., and Ly, E.B. (2014). Eur. Polym. J., 54, 172–180.
2. Zohuriaan-Mehr, M.J., Pourjavadi, A., Salimi, H., and Kurdtabar, M. (2009). Polym. Adv. Technol., 20, 655–671.
3. Ullah, F., Othman, M.B.H., Javed, F., Ahmad, Z., and Akil, H.M. (2015). Mater. Sci. Eng. C, 57, 414–433.
4. Guilherme M.R., Aouada, F.A., Fajardo, A.R., Martins, A.F., Paulino, A.T., Davi, M.F.T., Rubira, A.F., and Muniz, E.C. (2015). Eur. Polym. J., 72, 365–385.
5. Kosemund, K., Schlatter, H., Ochsenhirt, J.L., Krause, E.L., Marsman, D.S., and Erasala, G.N. (2009). Regul. Toxicol. Pharmacol. 53, 81–89.
6. Zohuriaan-Mehr, M.J. and Kabiri, K. (2008). Iran. Polym. J., 17, 451-477.
7. Jamshidi, A., Ahmad Khan Beigi, F., Kabiri, K., and Zohuriann-Mehr, M.J. (2005). Polym. Test., 24, 825-828.
8. Tian, H.F., Wu, W.Q., Guo, G., Gaolun, B., Jia, Q.Q., and Xiang, A.M. (2012). J. Food Eng., 109, 496-500.
9. Fernández-Espada, L., Bengoechea, C., Cordobés, F., and Guerrero, A. (2016). J. Appl. Polym. Sci., 133, 42980.
10. Hwang, D.C. and Damodaran, D. (1996). J. Appl. Polym. Sci. 62, 1285-1293.
11. Yoshimura, T., Uchikoshi, I., Yoshimura, Y. and Fujioka, R. (2005). Carbohyd Polym 61, 322-326.
12. Félix, M., Martín-Alfonso, J.E., Romero A. and Guerrero, A. (2014). J. Food Eng.125, 7-16.
13. Wagner, J.R., Sorgentini, D.A. and Anon, M.C. (1996). J. Agr. Food Chem. 44, 1881-1889.
14. Zohuriaan-Mehr, M.J., Pourjavadi, A., Salimi, H. and Kurdtabar, M. (2009). Polym. Advan. Technol. 20, 655-671.

Contact Address:

bengoechea@us.es
Departamento de Ingeniería Química,
Facultad de Química
Universidad de Sevilla
C/Prof. García González 1, 41012 Sevilla (Spain)
Telf.: +34 954557179

Development of protein-based absorbent matrices containing zinc as micronutrient for horticulture

M. Jiménez-Rosado[1], S. Gamero-Roldán[1], F. Cordobés[2], M. Ruiz[1], A. Guerrero[2]

[1] Ingeniería Química, Escuela Politécnica Superior, Universidad de Sevilla (Spain)
[2] Ingeniería Química, Facultad de Química, Universidad de Sevilla (Spain)

Introduction

Superabsorbent biopolymers (SAB) are a good example of new type of materials, being based on renewable natural components with a reasonable low cost. Due to their superabsorbent properties, SAB materials possess an excellent potential in a great variety of applications including uses in personal hygiene products, as well as in horticulture and agriculture [1].

Superabsorbent polymer (SAP) materials are basically formed by a hydrophilic, polymeric matrix. This matrix is able to absorb and retain water from the environment, without dissolving, suffering a marked change of volume (swelling). A material is considered superabsorbent when its absorption capacity exceeds 10 times its own weight. Some of them can achieve up to 1000 times its weight. SAP market is dominated by synthetic polymers made from two basic monomers, acrylic acid and acrylamide. These SAPs show low biodegradability and some toxicity problems. Hence, there is a great interest in the development of sustainable SAP materials, based on raw material of natural and renewable origin, with greater cost efficiency and lower environmental impact.

The development of superabsorbent materials based on protein (SAB) show some apparent technological and economical benefits, in addition to the environmental advantages already mentioned. Proteins are among the most undervalued raw materials with respect to their industrial applications, and its use as SAB materials implies a high-added value [2].

The second most important application of SAPs is in horticulture. There are several commercial SAPs that are added to the land to store water and release micronutrients in a controlled manner, thus avoiding the typical excess of conventional fertilizers. The substitution of these materials by SAB matrices would provide great advantages in terms of their null toxicity and high biodegradability. Moreover, the matrix itself will entail an extra contribution of nutrients after their degradation. All these features makes these materials very attractive for their application in this field [3].

Protein from soybean is one of the most used biopolymer raw materials for bioplastic production, as it is a renewable source with an affordable price. Several soy products with different protein content are generally available, being soy protein isolate (SPI, 90%), soy protein concentrate (SPI, 72%) and soy flour (SF, 56%), the most used. Soy protein systems are typically hard to process unless a certain amount of plasticizer, denaturing agents, or a combination of both of them is present in the formulation of the bioplastic material. Plasticizers are low molecular weight agents that show the ability to increase the mobility of protein chains, reducing the number of intra and intermolecular interactions. Water and polyalcohols, especially glycerol, are widely used as plasticizers for soy protein. The ability of soy protein-based bioplastics to absorb huge amounts of water is the main reason to explore their use in the development of SAB materials [4].

The present work focuses on the development of soy protein-based matrices loaded with a micronutrient as SAB materials for their potential use in horticulture. Zinc cation has been selected as the micronutrient due to its important role on the growth and development of plants. Different procedures are assessed to introduce zinc in a soy protein-based matrix, evaluating the mechanical properties, water uptake capacity and loading level of zinc into the matrix.

Experimental

Materials

SPI (with min. 91 wt % protein, 6 wt % moisture) was supplied by Protein Technologies International (SUPRO 500E, Belgium).

Glycerol (Gly) from Panreac Química S.A. (Spain) was used as plasticizer.

Zinc was incorporated into the matrix as zinc sulphate. Two different zinc sulphate salts were used with different water content: zinc sulfate heptahydrate and zinc sulfate monohydrate, both of them purchased from Panreac Química S.A. (Spain).

Methods

The procedure for the preparation of SAB materials consisted of several stages, as can be seen in Figure 1.

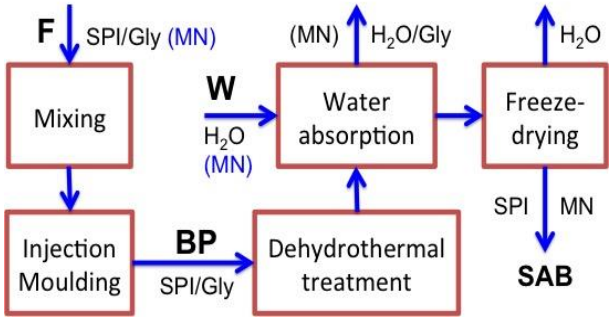

Figure 1. Processing stages for the preparation of SAB materials

The micronutrient (MN) was zinc sulfate incorporated either into the mixing (F) or absorption (W) stages.

First of all, SPI/Gly blends (1:1) were mixed in a two-blade counter-rotating mixer Polylab QC (ThermoHaake, Karlsruhe, Germany) at room temperature and 50 rpm for 10 min, under adiabatic conditions.

In the second stage, the dough-like blends obtained after mixing were subsequently processed by injection moulding (IM) using a MiniJet Piston Injection Moulding Sistem II (ThermoHaake, Karlsruhe, Germany) to obtain soy protein-based bioplastics (BP). In this stage, the processing parameters selected (that were selected from previous studies) are indicated in table 1 [4].

Table 1. Processing parameters for the injection moulding stage

Parameter	Standard IM Process	Modified IM Process
T_{cyl} (ºC)	40	40
P_{inj} (bar)	500	600
t_{inj} (s)	20	20
T_{mold} (ºC)	70	90
P_{hold} (bar)	200	200
t_{hold}(s)	30	30

where T_{cyl} and T_{mold} are the cylinder temperature, P_{inj} and t_{inj} is the injection time, T_{mol} is the temperature at the mould, and P_{hold} and t_{hold} are the holding pressure and time, respectively.

Subsequently, the probes were carried out to a dehydrothermal treatment that consisted of a heating stage in a conventional oven at 50ºC for 24 h. This stage was followed by an absorption process performed in a closed vessel with 300 mL of water for 24 h. Finally, the samples were introduced in a freeze-drying equipment (LyoQuest, Tesltar, Terrassa, Spain). Water uptake capacity and soluble matter loss were calculated at this point of the process.

Water absorption tests were carried according to a modification of the ASTM D570 norm (2005), using rectangular probes (55 × 10 × 1 mm). The water uptake capacity was calculated as follows:

$$Water\ uptake = \frac{m_2 - m_3}{m_3} \cdot 100 \qquad (1)$$

where m_3 is the weight of the matrix after freeze-drying stage and m_2 is the weight of the matrix after the absorption stage.

Moreover, soluble matter loss was estimated as:

$$Soluble\ matter\ loss = \frac{m_1 - m_3}{m_3} \cdot 100 \qquad (2)$$

where m_1 is the weight after the dehydrothermal stage.

The mechanical properties of BP matrices were also determined. Dynamic tensile and flexural tests were performed in a RSA3 DMA analyser (TA Instruments, USA).

In tensile tests, matrices were subjected to increasing axial stress until breaking. Thus, a crosshead speed of 1 mm/min was selected, and at least three replicates were tested for each sample.

In bending tests, BP matrices were subjected to a small amplitude oscillatory flexural stress or strain. First, a strain sweep test, at constant frequency of 1 Hz, was performed to determine the linear viscoelastic region. Frequency sweep tests (0.02-20 Hz) were carried out within the linear viscoelastic region.

Results and Discussion

Different procedures were assesed to introduce the micronutrient into the matrix. The simplest one consisted of incorporating different amounts of micronutrient (zinc sulfate heptahydrate) into the mixing stage of a 50/50 SPI/Gly blend. The blends obtained in this way were either poorly injected or leaded to excessively brittle samples after injection moulding. Similar results were obtained when zinc sulphate monohydrate was used as micronutrient.

At this point, IM conditions were modified in order to find more suitable conditions to process SPI/Gly/MN blends. Thus, injection pressure and mould temperature were increase up to 600 bar and 90 ºC, respectively. Under these processing conditions, loaded BP matrices were obtained that contained up to 10 wt % zinc sulfate monohydrate. Nevertheless, it was not possible to incorporate zinc sulphate heptahydrate as micronutrient into the BP matrices by injection moulding using either the standard or modified conditions. Water uptake capacity and mechanical properties of BP matrices with different content of zinc sulphate monohydrate (SPI/Gly 1:1) were studied.

Figure 2 shows water uptake capacity and soluble loss matter for SPI/Gly BP specimens as a function of MN content. As can be seen, the incorporation of micronutrient produces a remarkable decrease in water uptake capacity, regardless of the MN content loaded.

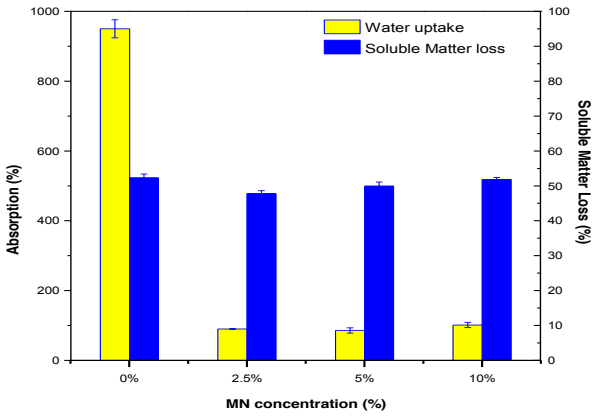

Figure 2. Water uptake capacity and soluble matter loss for SPI/Gly BP matrices at different zinc sulfate monohydrate content.

Tensile properties of SPI/Gly blends containing micronutrient were evaluated. In all cases, stress-strain curves exhibited an initial linear elastic behaviour of constant stress-strain slope yielding different values for the Young´s modulus. This linear behaviour was followed by a plastic deformation stage with a continuous decrease in the strain-stress slope after the elastic limit. All the curves eventually reached a maximum value for the stress (σ_{max}) and the strain (ε_{max}), which was immediately followed by the rupture of the sample (results not showed). Figure 3 shows the values of these parameters as a function of the MN content (zinc sulfate monohydrate). As can been observed, the incorporation of a micronutrient into the matrix produces obtaining an increase in the Young's modulus up to a maximum value (at about 5%) and progressively lower strain at break.

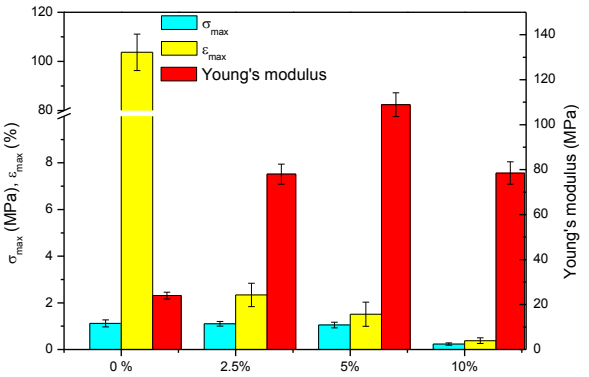

Figure 3.Tensile properties for SPI/Gly BP matrices at different zinc sulfate monohydrate content.

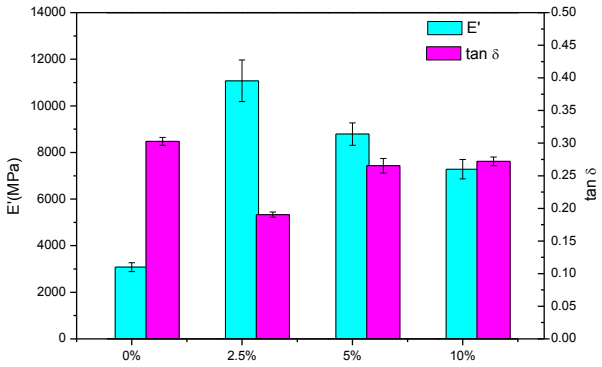

Figure 4. Dynamic flexural properties of matrices for SPI/Gly BP matrices at different zinc sulfate monohidrate content.

Dynamic flexural properties were obtained by means of small amplitude oscillatory bending frequency sweep tests. All the systems studied, showed a predominantly elastic response (E'>E'') over the whole frequency range studied. Both moduli showed a slight dependence on frequency (results not showed). Figure 4 shows values of the storage modulus (E') and loss tangent (tan δ) at 1 Hz. As can be observed, the incorporation of zinc sulfate monohydrate produces an enhancement of elastic properties and a decrease of the values of loss tangent. The SPI/Gly BP matrix with the lower content of salt shows the higher elastic response.

In order to improve loading level of zinc into the matrix, the incorporation of zinc sulfate heptahidrate was carried out at the absorption stage (W). Four different procedures of MN incorporation were assessed.

First of all, the BP matrix was immersed in a saturated solution of the salt. In the second option the immersion was initially carried out in distilled water and the micronutrient was added at different time intervals. However, none of these procedures leaded to significant loading levels. In both cases, absorption capacity was restricted due to the high ionic strength of the aqueous medium.

The third option consisted of three stages: Firstly, the absorption stage was carried out in distilled water (W) to produce swelling of the matrix and glycerol migration to the aqueous medium; Secondly, the above described dehydrothermal treatment was applied to the swelled matrix sample; Finally, a new absorption stage in a saturated solution of salt was perfomed. Matrices loaded with up to 6.18% MN (zinc sulphate heptahydrate) were obtained. It seems that the high swelling ratio taking place during the first stage compensate the effect of ionic strength, thus allowing a certain level of MN loading. Nevertheless, the amount of micronutrient incorporated into the matrix was lower than the previous ones obtained by the incorporation in the mixing stage.

Finally, this third procedure was modified by replacing the dehydrothermal stage by a freeze-drying operation. This fourth procedure leaded to a remarkable enhancement since a loading level up to 25.5% of the salt was obtained. These results indicate that the dehydrothermal heating stage induced a higher degree of crosslinking in the matrix that was detrimental for MN loading.

Figure 5 shows the results of water uptake and soluble matter loss of freeze-dried samples obtained after carrying out this fourth procedure. A comparison with one of the BP matrix loaded at the mixing stage may be also observed in this figure. As may be observed, the water uptake capacity is best for the procedure including the freeze-dried stage, which may be related with its high swelling capacity. The soluble matter loss is much lower in this case since part of this matter has been previously lost.

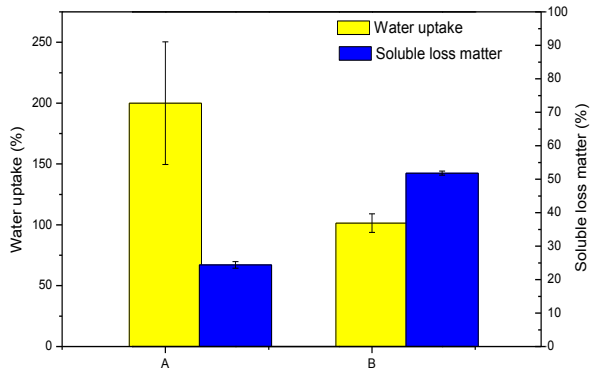

Figure 5. Water absorption capacity of the best matrices. A is matrices obtained by absorption (fourth option) with zinc sulfate heptahydrate and B is matrices obtained by mixing with zinc sulfate monohydrate.

Concluding Remarks

Fairly promising micronutrient loading and water uptake results of SPI-based SAB materials have been obtained that strongly depends on the process used. Thus, an important amount of an essential nutrient for a plant (Zn) has been incorporated to the matrix. However, the incorporation of salt to the matrix involves some reduction in water uptake capacity, due to the negative effect of ionic strength on water absorption. In addition, mechanical properties of the BP matrices are highly influenced by the presence of the salt.

When the salt was introduced in the absorption stage, higher hydrophilic properties were obtained. However, the process has to be reorganized in order to minimize the effect of ionic strength. This type of process is particularly successful when a freeze-drying stage was used instead of a dehydrothermal treatment.

In any case, the results obtained in this work opens up a great potential for the use of this SAB matrices as a source of supplying micronutrients for horticulture applications.

Acknowledgements

This research is part of a project supported by MINECO/FEDER, EU (CTQ2015-71164-P). The authors gratefully acknowledge their financial support.

References

1. Kamat, M., Malkani, R. and Indian, J. (2003). Pediatrics. 70 (11), 879–881.
2. Damodaran, S., Parkin, K.L. and Fennema, O.R. (2010). Fennema:quimica de los alimentos, 1st ed. Acribia, Madrid.
3. Mortain, L., Dez, I. and Madec, P.J. (2004). Comptes Rendus Chimie. 7 (6-7), 635-640.
4. Fernández-Espada, L., Bengoechea, C., Cordobés, F. and Guerrero, A. (2016) J. Appl. Polym. Sci., DOI: 10.1002/APP.43524.

Contact Address:

Mercedes Jiménez Rosado
mercedes9jimenez@hotmail.com
Ingeniería Química,
Escuela Politécnica Superior
Universidad de Sevilla
C/ Virgén de Africa 7, 41011, Sevilla (Spain)

Assessment of alginate/soy protein-based porous matrices

J.M. Aguilar, E. Álvarez, B. Sánchez, M.L. López, F. Cordobés

Department of Chemical Engineering, Escuela Politécnica Superior, University of Seville (Spain)

Introduction

Natural biopolymers, including protein and carbohydrate-based polymers, usually offer improved water solubility, biocompatibility, biodegradability and increased functional capability, which make them highly attractive materials in a wide range of applications.

Alginates (ALG) constitute a family of linear anionic polysaccharides isolated from coastal brown algae species such as Laminaria hyperborean. Alginates are composed of (1,4)-linked β-D-mannuronic acid (M) and α-L-guluronic acid (G) residues in homopolymer blocks of either similar or strictly alternating sections. In addition, alginate is a low cost material, being an interesting biopolymer for medical applications (e.g. drug delivery, wound healing or scaffolds for regenerative medicine). Polyvalent cations, save Mg^{2+}, have high affinities of binding to carboxylic groups of alginates and form gels via crosslinking. The gelation mechanism takes mainly place through the exchange of ions from the guluronic acids with the divalent cations, particularly Ca^{2+}. The cations bind G seguences in a highly cooperative manner to form egg-box dimmers, which can further grow into multimers by lateral association resulting in a gel with the characteristic egg-box structure [1, 2 and 3].

Thus, alginates have the ability to form gels with a large spectrum of textures, according to the number of junction zones between macromolecules. In fact, an increase in Ca^{2+} content will lead to a higher gel strength, achieving a maximum when the conversion degree is equal to 100% (it means that every Ca^{2+} is binding). On the contrary, an excess of Ca^{2+} content (e. g. 150%) will lead to syneresis and the gel will shrink and expel water [4].

However, since mechanical resistance of these hydrogels is reduced as Ca^{2+} are exchanged by monovalent cations from the medium, the addition of soy protein isolate (SPI) could overcome this limitation due to the structuring capability of their amino acids groups and side chains. Thus, positively charged amino groups of proteins can stabilize negatively charged alginate-based biomaterials and therefore mechanical properties can be optimized by adjusting processing parameters such as pressure and moulding temperature. Addition of a hydrophilic plasticizer such as glycerol (GL) is also advisable to properly process ALG/SPI bioplastic matrices.

The main objective of this work is focussed on the development of a porous matrix by thermo-mechanical conformation (i.e. injection moulding) and lyophilisation of bioplastics based on ALG/SPI blends.

Experimental

Materials

Two types of materials can be distinguished: those that conform the specimens (ALG, SPI and GL) and those being part of the medium where they are immersed ($CaCl_2$).

ALG is the alginic acid sodium salt produced from brown algae and commercialized by Sigma-Aldrich as medium viscosity specification. SPI were formulated by Protein Technologies International (Belgium) and provided by PROANDA (Spain), whose technical specifications are shown in Table 1. Glycerol (GL), pharma grade, was provided by PANREAC (Spain). Calcium Chloride anhydrous, technical grade (95%), were also provided by PANREAC (Spain).

Table 1. Technical specifications of Soy Protein Isolate (SPI)

Component	Value
Protein content	> 90%
Fat content	< 1 %
Ashes	< 5 %
Humidity	< 6 %
pH	7.07

Methods

Thermo-mechanical conformation of bioplastic specimens involved a two stages process, including the mixing of raw materials to obtain a dough-like mixture first, followed by injection moulding under pressure and heat. Mixing stage was performed at 25 ºC in a double-cylinder chamber containing two counter-rotating rollers by means of a Haake Polylab rheometer (Thermo Scientific, Germany). Rotational speed were initially set at 2-5 rpm until every component was added, being

increased since then until 50 rpm and maintaining this value during 30 min. Three alginate-based blends with Alginate/Soy protein (AL/SPI) weight ratios of 0/2, 1/2 and 2/2 were obtained by thermoplastic mixing, but maintaining the ratio between the sum of these two polymers (ALG+SPI) or also called active ingredient (AI) and the amount of plasticizer (GL) at a constant value of 1.33. The composition of this blends are illustrated in Table 2.

Table 2. Composition of blends under study

Blends	ALG/SPI ratio		
	0/2	1/2	2/2
Active Ingredient (AI)	57%	57%	57%
Alginate (ALG)	0,0%	19%	28,5%
Soy Protein (SPI)	57 %	38%	28,5%
Plasticizer (GL)	43 %	43%	43%

Samples where frozen after mixing at -18 ºC until the injection stage. Rectangular bioplastic specimens (60x10x1 mm) were performed using a piston injection moulding Mini Jet II (Haake, Germany). Injection parameters were previously studied [5], being fixed the following values for this study (T_{cyl}= 50ºC, T_{mol}= 70ºC, P_{iny}=500 bar, P_{hold}=500 bar, t_{iny}=20 s, t_{hold}=200 s).

Thermomechanical analysis of mixtures allowed us to optimize their composition and specimens were evaluated using a RSA III analyser (TA Instruments, USA) by frequency sweep (0.02-20 Hz) and breaking tensile test., being dynamic oscillatory test in the LVR.

Water absorption tests were also carried out in specimens following the D570-98 norm (ASTM, 2005). Suitable bioplastic specimens were immersed in aqueous medium with presence or absence of Ca^{2+} for stipulated times (2 or 24 h) and different Ca^{2+} concentrations (0, 0.3 and 0.5 M). Samples were introduced during 24 h in an oven at 50 ± 2ºC to eliminate moisture. Then, test pieces were immersed in the aqueous medium during the stipulated time and their wet weights were determined. Finally, specimens were introduced in the oven again (T=50 ± 2 ºC) to be dried and to determine their final dry weight. Water uptake capacity and loss of soluble matter were determined according to the technical specifications outlined in D570-98 norm (ASTM, 2005) [6].

After drying specimens in oven for 24 h at 50 ± 2ºC and immerse in water or a 0.3M $CaCl_2$ solution, matrices were obtained from selected specimens by freeze-drying process using a Telstar LyoQuest equipment.

Results and Discussion

Figure 1 shows the evolution of torque and temperature over time throughout the mixing stage. At the beginning of the test the torque undergoes a sudden increase up to a maximum torque value, followed by an asymptotic decrease that shortly reaches a flattened profile (after ca. 5 min) and a plateau value. The maximum value becomes more apparent as protein content is higher since its volume is bigger than alginate volume.

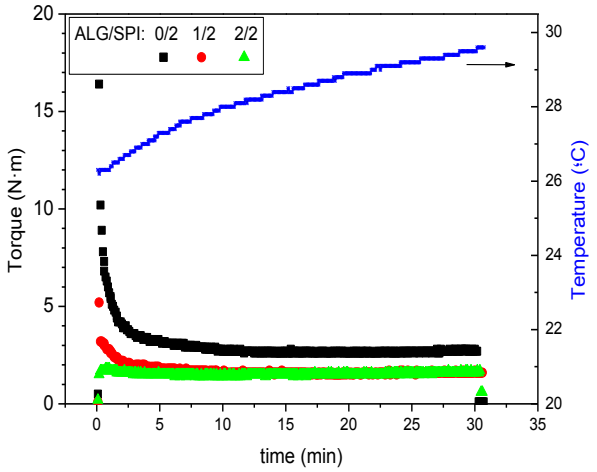

Figure 1. Evolution of torque and temperature profiles over mixing time

As it is shown in Fig. 2 regardless ALG/SPI ratio, all the specimens tested displayed higher elastic modules (E') than viscous modules (E''). It means that their behaviour are closer to a solid than a liquid (tan δ < 1). As the polysaccharide content increases both viscoelastic moduli decrease, which may be related to the observed less consistency of specimens.

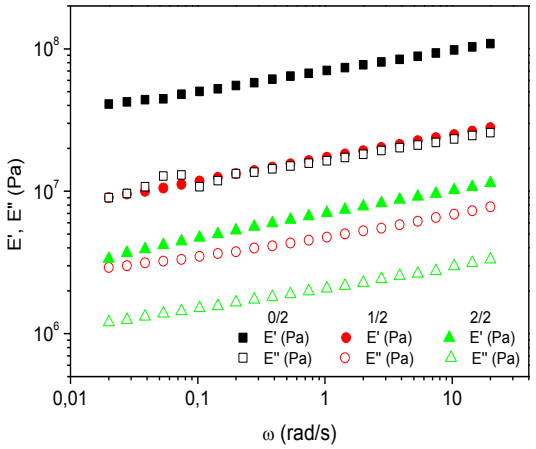

Figure 2. Frequency sweep tests obtained from dynamic mechanical analysis of specimens as a function of the Alginate/Soy Protein Isolate (ALG/SPI) ratio

In any case, all the blends prepared were properly injected with the selected processing conditions. However, it seems that specimens with a higher ALG

content become more brittle which makes more difficult their extraction from the mould. As it is shown in Fig. 2 regardless of the ALG/SPI ratio, all the bioplastic (BP) specimens tested displayed higher values for the elastic modulus (E') than for the viscous modulus (E"), as corresponds to a solid-like behaviour. When the polysaccharide content increases both viscoelastic moduli decrease, which may be related to the lower consistency observed for their blends.

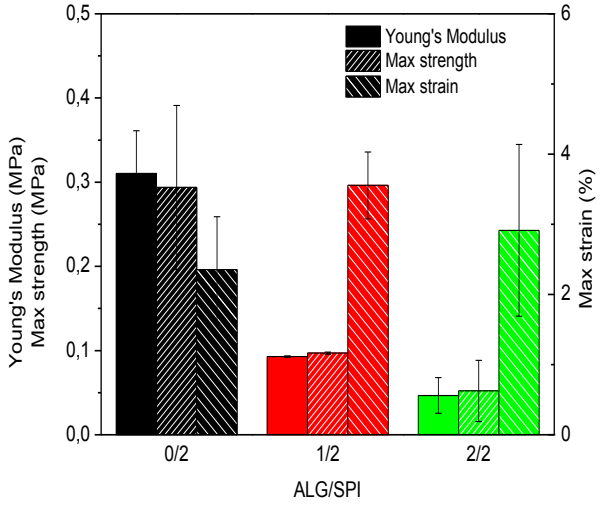

Figure 3. Parameters obtained from breaking tensile tests for specimens as a function of the Alginate/Soy Protein Isolate (ALG/SPI) ratio

Figure 3 shows some parameters obtained from the static tensile breaking tests, carried out on BP samples with different ALG/SPI ratio. The elastic modulus, also called Young's modulus corresponds to the slope of the line at the initial portion of the strain-stress curves [7]. Maximum tensile or ultimate strength (σ_{max}) and maximum tensile strain (ε_{max}) until rupture match with the higher values of strength and strain, respectively.

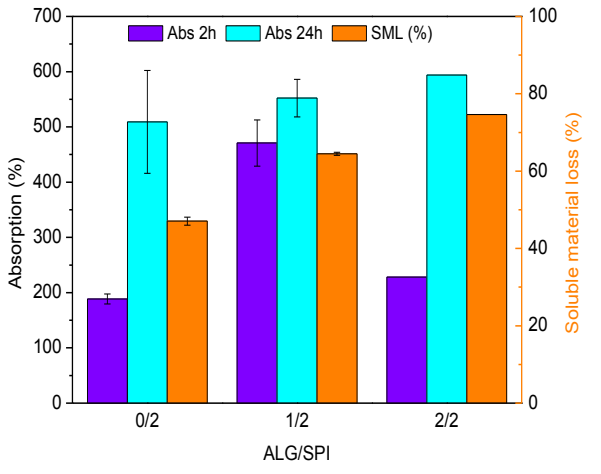

Figure 4. Water absorption capacity at 2 and 24 h, and soluble matter loss of specimens with different AlG/SPI ratio immerse in water

As can be observed, both Young's modulus and maximum strength increase as alginate composition is increased in the specimen. On the contrary, maximum strain increases moderately with the ratio ALG/SPI.

From data presented in Figure 4, it can be inferred that all of the compositions under study show a good water absorption capacity. Furthermore, soluble material loss (SML) becomes increasingly evident as the ALG/SPI ratio is higher when the specimens are immersed in water. In this way, these high values of the SML can be explained assuming that the total amount of the alginate and the glycerine and some of the soy protein are drawn from specimens. These results suggest that an increase in the BP porosity takes place, but at the expense of a decrease in the structural integrity of specimens.

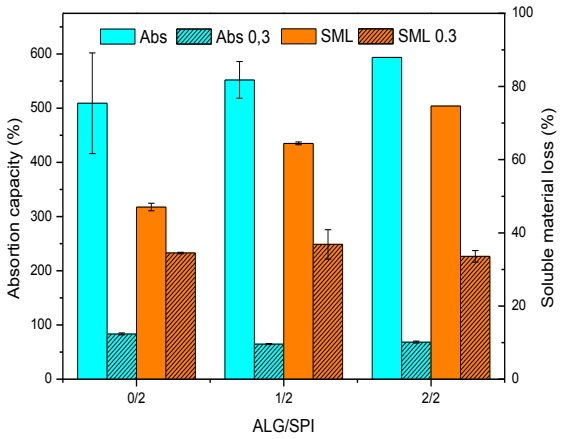

Figure 5. Water absorption capacity at 24 h and soluble matter loss of specimens with different ALG/SPI ratio immersed in water or $CaCl_2$ solution.

On the other hand, after immersing the specimens in a 0.3M solution of calcium chloride, the water absorption capacity of specimens decrease significantly, regardless of the ALG/SPI ratio (Figure 5). However, no significant changes are observed in the soluble material loss as ALG content increases. The fact that these values are approximately constant means that alginate is being retained in specimens as a consequence of its interaction with the calcium ions. Moreover, it is worth mentioning that the SML values are smaller than the glycerine content in specimens. Thus, these alginate-Ca^{2+} gels formed via crosslinking contribute to prevent some glycerine extraction.

Figure 6 shows frequency sweep of ALG/SPI porous matrices prepared after being immersed in the presence or absence of calcium. As may be seen, elastic modulus values remarkably decrease as ALG is added in the formulation of specimens when these are immersed in water. In contrast, presence of alginate seems to improve the elastic modulus of specimens when they are

immersed in a calcium chloride solution. Thus, this increase turns out to be more evident as the ratio ALG/SPI is higher.

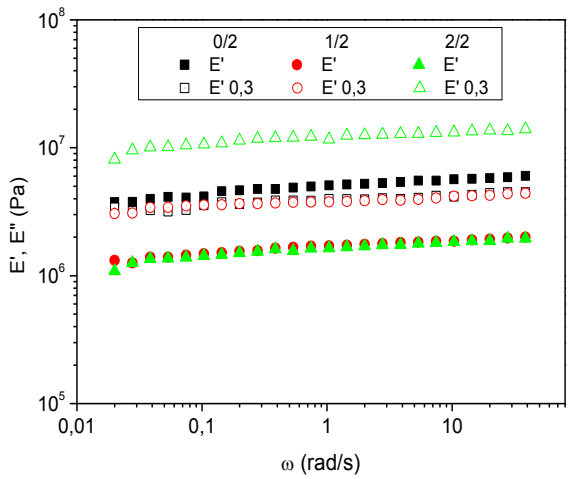

Figure 6. Frequency sweep tests carried out with different matrices subjected to immersion either in water or in 0.3M calcium chloride solution.

Conclusions

Specified mixing conditions in the present contribution led to specimens that are suitable for injection moulding.

All the specimens showed E' values higher than E'' and their mechanical properties were markedly modified by the ratio ALG/SPI. Thus, values of both moduli were lower as the composition of alginate was increased. Young's modulus and maximum tensile strength followed a similar evolution with the ALG/SPI ratio than that shown for both moduli.

The bioplastics studied showed large water absorption capacities but, unfortunately soluble matter losses were also high. The addition of calcium chloride in the immersion medium was able to retain all the alginate containing in specimens and some of the glycerine. Nevertheless, water absorption, porosity and swelling were significantly lower. On the other hand, stronger matrices with higher rheological consistency were obtained when the ratio ALG/SPI is raised and the inmersion liquid is calcium chloride.

References

1. Grant, G.T., Morris, E.R., Rees, D.A., Smith P.J.C., and Thom D. (1973) FEBS Lett. 32, 195–198.
2. Morris, E.R., Rees, D.A., and Boyd, J. (1978) Carbohydr. Res. 66, 145–154.
3. Khan, F. and Ahmad, S.R. (2013) Macromol. Biosci. 13, 395-421.
4. Molina, M.J. (1992) "Estudio de la estabilidad térmica del ácido algínico y derivados en diversas atmósferas". PhD. Thesis. Universidad Politécnica de Madrid.
5. Sánchez, B. (2015) "Desarrollo de matrices porosas basadas en alginato como soporte para ingeniería tisular. Degree Thesis. Universidad de Sevilla.
6. ASTM D570 – 98 (2010)e1 Standard Test Method for Water Absorption of Plastics. American Society for Testing Materials (ASTM).
7. ASM International (2004) Tensile testing, 2nd ed. American Technical Publishers, Hitchin Hertfordshire (U.K.)

Contact Address:

jmaguilar@us.es
Department of Chemical Engineering,
Escuela Politécnica Superior
University of Seville
c/ Virgen de África, 7. 41.011-Sevilla (Spain)
Telf.: (+34)95.455.71.80 / 79; Fax: (+34)95.455.64.47

Rheology and bonding performance of bioadhesives based on MDI-modified cellulose acetate and castor oil

A. Tenorio-Alfonso[1], M.C. Sánchez[1,2], J.M. Franco[1,2]

[1] Department of Chemical Engineering, University of Huelva, Campus El Carmen, Campus ceiA3, 21071, Huelva (Spain)
[2] Pro2TecS-Chemical Product and Process Technology Research Centre, University of Huelva, 21071, Huelva (Spain)

Introduction

Polyurethanes (PU) have been traditionally produced from petrochemical derivatives. Nevertheless, as a result of the petroleum exhaustion and the environmental consciousness, one of the main objectives in polyurethane synthesis is focused on completely or partially replacing those non-renewable raw materials by new eco-friendly alternatives, including, among others vegetable oils. [1]

The synthesis of such a versatile polymeric materials, what makes them so appealing choices to be used for industrial production [2, 3], is generally accomplished through the reaction of isocyanates (NCO) with compounds containing active hydroxyl groups (OH), along with a chain extender [4, 5]. Furthermore, polyurethanes are typically characterized by a multiblock structure, in the aftermath of the thermodynamic incompatibility between hard (*HS*) and soft segments (*SS*) domains [6, 7], which can interact with each other by means of hydrogen bonding [2]. The former comprises urethane/urea groups (diisocyanate and chain extender), while the latter are generally composed of polyester or polyether backbones (raw materials containing hydroxyl groups) [8]. The degree of phase separation, which is strongly dependent on chemical composition, chain length, synthesis processes, crystallization of both phases and hydrogen bond-formation, has a great influence on the final properties of the polyurethanes [2].

On the other hand, the hydroxyl groups source for polyurethane production may be replaced by cellulose derivatives and vegetable oils, as proposed in previous investigations [9, 10]. Regarding natural oils, taking into account economic factors, soybean, palm and rapseed oil could be considered as the most appealing alternatives [1]. However all of them require a previous modification aimed to create reaction sites willing to react with active isocyanate groups. Moreover, in order to avoid prior chemical modifications, lesquerella and castor oils have been previously employed to produce polyurethanes [11, 12], since they already contain active hydroxyl groups on their structures.

The objective of this study was to synthesize polyurethane adhesives from natural and sustainable raw materials analysing the influence of the initial NCO:OH molar ratio on their chemical structure and resulting rheological response and adhesion performance.

Experimental Methods

Materials

The raw materials employed to synthesized bio-based polyurethane adhesives were cellulose acetate (DS: 40 %, Mn ~ 30000), 4,4'-methylenebis(phenyl isocyanate) (MDI, ≥98.0% purity), toluene (purum grade ≥99.7%) used as solvent, and triethylamine (TEA, 99.5% for synthesis) as catalyst, all of them supplied by Sigma-Aldrich (St. Louis, MO, USA), together with castor oil which was provided by Guinama (Valencia, Spain).

Synthesis of bioadhesives

A two-stage protocol was followed to synthesize the polyurethane formulations [11]. In the first step, the solvent was introduced into a round-bottom flask and bubbled with a stream of argon through for 30 minutes. Then, cellulose acetate, previously dried, 4,4'-methylenebis(phenyl isocyanate) and triethylamine were added into the flask in different NCO:OH ratios, according to Table 1, and vigorously stirred for 24 hours at room temperature. Afterwards, solvent was removed by means of vacuum evaporation process, obtaining the biopolymers.

In the second stage, functionalized biopolymers were blended with castor oil with 1:1 biopolymer/castor oil weight ratio for 1 hour and at room temperature in an open vessel using a controlled-rotational speed mixing device (RW 20, Ika, Staufen, Germany) equipped with

an anchor impeller. The resulting products were left for curing.

Experimental techniques

Rheological characterization of the synthesized adhesives was carried out using a controlled-stress rheometer Physica MCR301 (Anton Paar Germany GmbH, Ostfildern, Germany). Torsional frequency sweeps (100-0.01 rad/s), within the linear viscoelastic region, were carried out from -5 to 200 ºC, as well as temperature ramps from room temperature to 200 ºC, at 1 Hz and heating rate of 2 ºC/min.

The chemical structure and curing process of these systems were analysed by means of Fourier transform infrared spectroscopy (FTIR) in a FT/IR-4200 Sprectrometer apparatus (JASCO Inc., Tokyo, Japan) with an attenuated total reflectance (ATR) accessory equipped with a monolithic diamond crystal. Infrared spectra were obtained as the result of an average of 97 scans with a resolution of 4 cm^{-1} and a 45º angle of incidence, in the spectral range 7800-350 cm^{-1}.

Thermal behaviour for the synthesized polyurethanes was studied by applying thermogravimetric analysis (TGA) and differential scanning calorimetry (DSC). TGA analysis were carried out using a Thermogravimetry/Differential Thermal Analyzer (TG/DTA) 6200 (Seiko Instruments, Tokyo, Japan) over 10-20 milligrams samples, at a heating rate of 10 ºC/min, from 30 up to 600 ºC and under nitrogen atmosphere (flow rate, 60 mL/min), while DSC tests were performed over 5-10 mg samples placed on hermetically sealed aluminium pans and submitted to a heating cycle from -85 to 200 ºC, also under inert environment of nitrogen (flow rate, 50 mL/min), using a Q100 Calorimeter (TA Instruments, New Castle, DE, USA).

Finally, the adhesion performance on metal (austenitic stainless steel, AISI 316L grade), wood (poplar wood) and polyester fabric substrates was analysed by means of standardized mechanical tests in terms of tension loading (ASTM D906, D1002) and peel strength (ASTM D903), using a Universal Testing Machine (Shimadzu, Kyoto, Japan) model AG-IS.

Results and Discussion

All polyurethanes exhibited a simple thermo-rheological behaviour, within the whole temperature range studied, after curing; being able to apply the t-T superposition principle (Figure 1), where the values for the shift factor strongly depend on the functionalization degree (Figure 2). Moreover, regardless molar NCO:OH ratio and the temperature, a predominant elastic behaviour was always observed, associated to the characteristic rubbery and glassy regions of the mechanical spectrum, with similar values for G' and G" at the glassy transition temperatures. This mechanical behaviour suggests the co-existence of segmented HS and SS domains [13, 14].

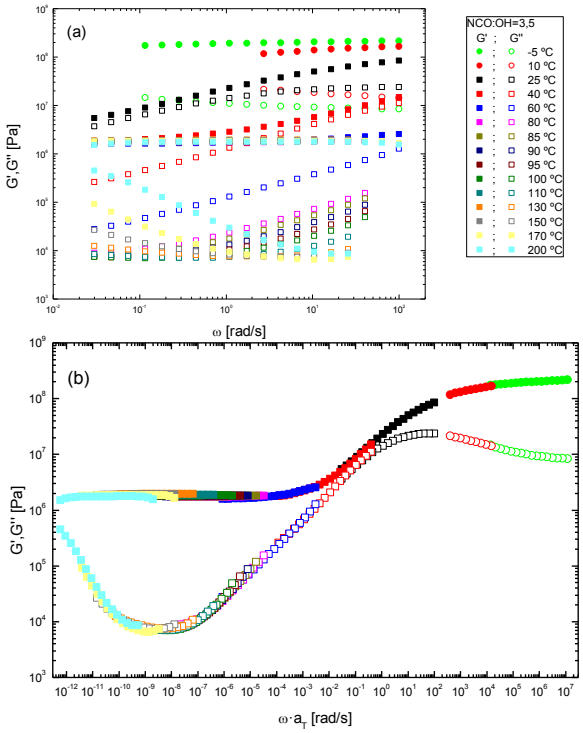

Figure 1: (a) Frequency sweep at different temperatures for a selected formulation (PU3.5); (b) t-T superposition applied taking 25 ºC as reference

Thermal and spectroscopic analysis corroborated the complete disappearance of free isocyanate during the first few days of curing. According to these results, the time required to reach a complete cure of the adhesives ranges from 3 hours to 3 days, continuously increasing with the functionalization degree. Moreover, according to FTIR-ATR spectra, the segmented chemical structure based on separated hard and soft domains was corroborated by the appearance of hydrogen bonded and non-hydrogen bonded urethane and urea linkages in the C=O stretching vibration (1760-1630 cm^{-1}).

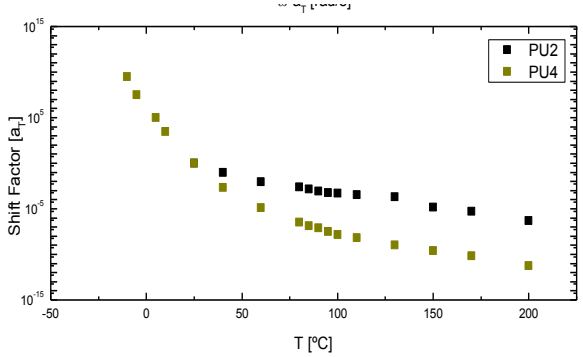

Figure 2: Shift factors comparison between polyurethanes PU2 and PU4

Table 1. Functionalization degrees and glassy transition temperatures

Sample	NCO:OH* molar ratio	Tg [ºC]
PU2	2:1	-10.2
PU2.5	2.5:1	6.1
PU3	3:1	17.0
PU3.5	3.5:1	21.6
PU4	4:1	26.5
PU4.53	4.53:1	27.6

*NCO:OH molar ratio in the first stage of the synthesis protocol

Furthermore, glassy transition temperatures corresponding to the soft segments ($T_{g,SS}$) obtained from DSC analysis are collected in Table 1. As can be noticed, T_g raises with NCO:OH ratio, because of a likely higher crosslinked structure, hampering the chain movements as a result of the greater production of stronger linkages, i.e. urea bonds, what was also confirmed by spectroscopic analysis.

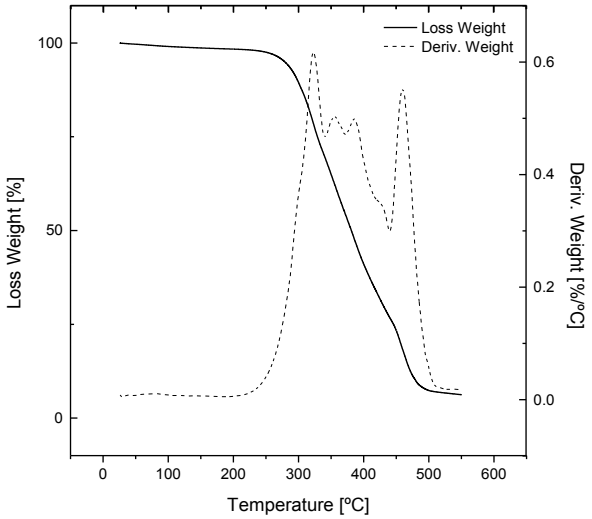

Figure 3: Thermogravimetric analysis (TGA) for a selected cellulose acetate-based polyurethane adhesive (PU4.53).

As for thermogravimetric analysis, completely cured MDI-based polyurethane underwent a four-stage decomposition process (Figure 3), remaining stable until 250-300 ºC. The first two steps are attributed to urethane bonds and cellulose acetate backbone (*hard segments*), the third thermal event is associated to castor oil thermal decomposition (*soft segments*), and the last step corresponds to excessively crosslinked polyurethane networks or due to C-C bonds cleavage [11, 15].

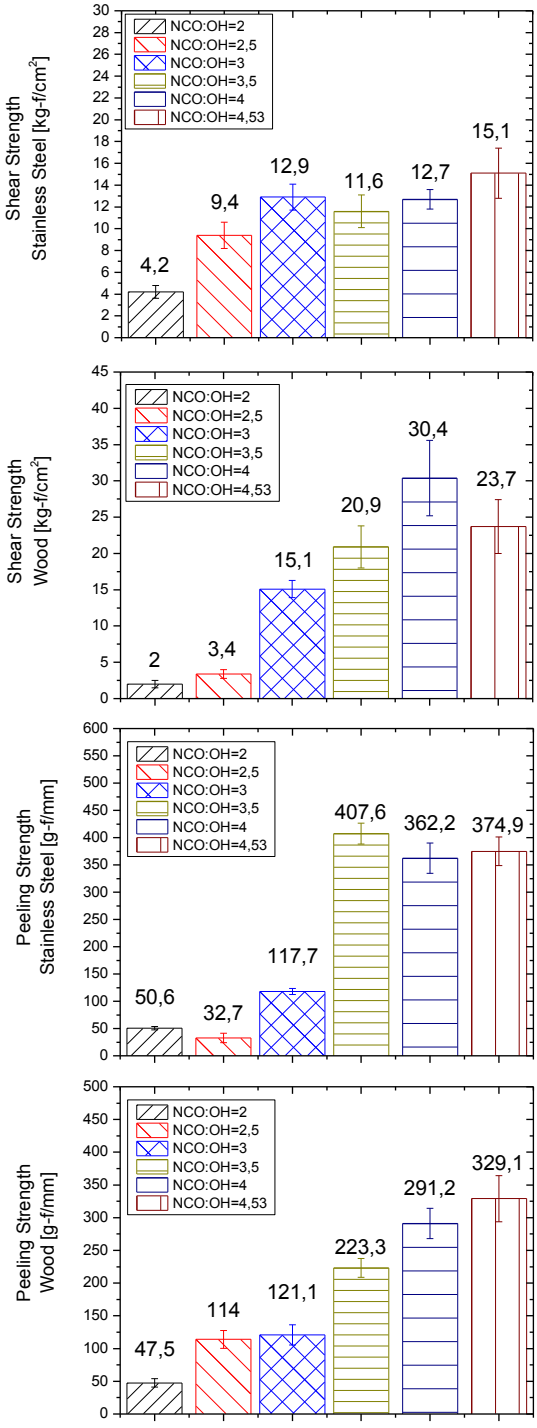

Figure 4: Mechanical standardized tests results for bio-based adhesive formulations studied.

On the other hand, those bio-based polyurethanes synthesized with an initial NCO:OH molar ratio ranging from 3 up to 4.53 exhibited similar peeling strengths, when stainless steel was used as substrate (Figure 4), much higher than those obtained with lower NCO:OH ratios. Moreover, when the substrate was replaced by wood, a more gradual increment in stripping strengths

with NCO:OH molar ratio was noticeable, achieving values almost seven times higher when NCO:OH molar ratio was increased from 2 to 4.53.

Regarding shear tests, the strength values also increased gradually with the functionalization degree when wood was considered as substrate, although the highest shear strength value was obtained with 4:1 NCO:OH molar ratio. However, when stainless steel was studied as substrate, most of the adhesives exhibited comparable strength values from a NCO:OH molar ratio of 3, which are generally lower than those obtained on wood surfaces, excepting for the lowest NCO:OH molar ratios (2 and 2.5).

Overall, the bio-based polyurethane formulation synthesized with 4:1 NCO:OH initial molar ratio seems to exhibit a more suitable adhesion performance to be applied as an adhesive on both wood and stainless steel substrates.

Concluding remarks

In this work, the effect of the functionalization degree of MDI/cellulose acetate/castor oil-based polyurethane over the chemical structure, thermomechanical and adhesion response was analysed by means of spectroscopic, thermal, rheological and mechanical tests. The results showed that all the polyurethane adhesives exhibited an apparent thermorheological simplicity throughout the whole temperature range studied. FTIR and thermal analysis verified that synthesized MDI-polyurethanes are comprised of a segmented chemical structure, whose thermomechanical and adhesion performance were optimised with an initial NCO:OH molar ratio of 4:1

Acknowledgments

This work is part of two research projects (CTQ2014–56038-C3-1R and TEP-1499) sponsored by MINECO-FEDER and Junta de Andalucía programmes, respectively. One of the authors (Adrián Tenorio) has also received a PhD. Research Grant from “Ministerio de Educación” (FPU13/01114). The authors gratefully acknowledge the financial support.

References

1. Datta, J. and Głowińska, E. (2014). Ind. Crop. Prod. 61, 84-91.

2. Fernández d'Arlas, B., Rueda, L., De la Caba, K., Mondragon, I. and Eceiza, A. (2008). Polym. Eng. Sci. 48, 519-529.

3. Ali, A., Yusoh, K. and Hasany, S. (2014). J. Nanomater. 2014, 1-9.

4. Güney, A. and Hasirci, N. (2014). J. Appl. Polym. Sci. 131, 1-13.

5. Norhisham, S.M., Maznee, T.T.N., Ain, H.N., Devi, P.K., Srihanum, A., Norhayati, M., Yeong, S., Hazimah, A., Schiffman, C.M. and Sendijarevic, A. (2017). Int. J. Adhes. Adhes. 73, 38-44.

6. Mattia, J. and Painter, P. (2007). Macromolecules. 40, 1546-1554.

7. Bistričić, L., Baranović, G., Leskovac, M. and Bajsić, E.G. (2010). Eur. Polym. J. 46, 1975-1987.

8. Queiroz, D.P., de Pinho, M.N. and Dias, C. (2003). Macromolecules. 36, 4195-4200.

9. Gallego, R., Arteaga, J., Valencia, C. and Franco, J. (2013). Cellulose. 20, 495-507.

10. Malik, M. and Kaur, R. (2016). Adv. Polym. Technol. 00, 1-7.

11. Tenorio-Alfonso, A., Sánchez, M.C. and Franco, J.M. (2017). Polymers. 9, 132-145.

12. Thames, S.F., Yu, H., Schuman, T.P. and Wang, M.D. (1996). Prog. Org. Coat. 28, 299-305.

13. Bagdi, K., Molnár, K., Sajó, I. and Pukánszky, B. (2011). Express Polymer Letters. 5, 417-427.

14. Van Ekeren, P. and Carton, E. (2011). Journal of Thermal Analysis and Calorimetry. 105, 591-598.

15. Corcuera, M., Rueda, L., d’Arlas, B.F., Arbelaiz, A., Marieta, C., Mondragon, I. and Eceiza, A. (2010). Polym. Degrad. Stab. 95, 2175-2184.

Contact Address

adrian.tenorio@diq.uhu.es
Department of Chemical Engineering, Physical Chemistry and Science of Materials
Campus El Carmen, Faculty of Experimental Sciences
University of Huelva
Address: Av. Fuerzas Armadas, S/N
PC: 21071
Telf.: 959219998

Influence of processing conditions on the rheological behaviour of NCO-functionalized lignin-based gel-like dispersions

A.M. Borrero-López [1], C. Valencia[1,2], J.M. Franco[1,2]

[1] Departamento de Ingeniería Química. Campus de "El Carmen". Universidad de Huelva. 21071 Huelva (Spain)
[2] Pro2TecS – Chemical Product and Process Technology Center. Universidad de Huelva. 21071 Huelva (Spain)

Introduction

Recently, the search of new materials which can mitigate climate change and resources extinction has changed industries focus on more environmentally aware attitudes. In the case of lubricant industries, this is increasingly yielding in the replacement of mineral oil into vegetable oil. However, still metallic soaps are used as gelling agents because of their high-grade functionality and microstructural performance [1]. Lignin, as the second most abundant biopolymer on earth, has been traditionally obtained as by-product in paper production although high-added valuable applications have not been explored in depth yet. However, its highly-branched aromatic structure and functional groups make it suitable for deeper research and use [2]. Diisocyanates are capable of reacting with OH groups of different raw materials including lignin and vegetable oils yielding a highly-entangled network, making feasible the oil confinement inside the structure for lubrication purpose [3].

In this work, the preparation protocol of renewable and eco-friendly oleogels based on lignin as thickener and castor oil as lubricant base oil was studied using different types of diisocyanates as crosslinkers, i.e., hexamethylene diisocyanate (HDI), isophorone diisocyanate (IDI), toluene diisocyanate (TDI), 4,4'-methylenebis(phenylisocyanate) (MDI), poly(hexamethylene diisocyanate) (pHDI) and 1,4-phenylene diisocyanate (PDI). Two processes for oleogel formation are analysed and compared: i) a two-step (TS) process previously reported [3] dealing with lignin functionalization first and further efficient dispersion in the vegetable oil, and ii) a new simpler and more environmentally careful direct process (D) in which all components are added and mixed simultaneously. Thermogravimetric analysis (TGA), Fourier-transform infrared spectroscopy (FTIR) and rheological tests were performed to characterize these formulations.

Experimental Methods

Materials

Lignin, triethylamine (Et_3N), toluene and diisocyanates used (98% purity except for TDI (80%)) were purchased from Sigma-Aldrich. Castor oil was acquired from Guinama (Spain).

Two-step process

Functionalization process

Lignin functionalization process was carried out based on previous studies [4]. Briefly described, lignin is added to a three-neck round bottom flask containing dry toluene under argon atmosphere together with Et_3N and the diisocyanate. The mixture was maintained for 24 hours under vigorous stirring at room temperature. The solvent and the catalyst from the mix were separated with a rotary evaporator and the product was directly used in the following step. 1:1 and 1:2 lignin/HDI weight ratios were selected, maintaining the same OH/NCO molar ratio for the rest of diisocyanates.

Gelling process

Gelling process consists on a mix of castor oil and the functionalized lignin (FL), using a controlled-rotational RW 20 (IKA) device equipped with an anchor stirrer and maintained during 24 hours at room temperature. For all samples, 30% was the FL concentration selected. No gel was obtained following this method when using pHDI as crosslinker or TDI at 1:2 lignin/diisocyanate ratio, because of an inefficient mixing between FL and CO, guiding to a heterogeneous sample, probably due to an extensively crosslinking formation.

One-step process

One-step process avoids the use of hazardous materials, like solvents, which could generate undesirable wastes. This process consists on a

simultaneous reaction of lignin, diisocyanate and castor oil using the device and parameters selected on the gelling process of the TS process. However, a 1:0.5 lignin/diisocyanate ratio was selected as higher ratios produce excessively crosslinked samples instead of desired soft gels for some of the diisocyanates.

Thermogravimetric analysis (TGA)

TGA were obtained using a Q-50 model (TA Instruments Water, USA) from room temperature to 600ºC at 10ºC/min under N_2 atmosphere. Characteristic parameters considered for each thermal event were temperature for the maximum weight loss rate (T_{max}) and weight loss (ΔW).

Fourier-transform infrared spectroscopy (FTIR)

The spectra were obtained using a JASCO FT/IR 4200 (Jasco inc. Japon) at 4 cm^{-1} resolution from 400 to 4000 cm^{-1}.

Rheological characterization

Small-amplitude oscillatory shear (SAOS) tests were accomplished inside the linear viscoelastic regime using ARES controlled strain rheometer (Rheometric Scientific) equipped with rough plate-plate geometries of 25 mm, 1 mm gap in a frequency range of 0.03-100 rad/s, at 25ºC. Rheological tests were performed one week after gel preparation, using fresh samples each time, and replicated at least twice.

Nomenclature used

TS systems have been named using TS followed by initial of diisocyanate selected and no number to 1:1 ratio and 2 for the 1:2 ratio. For direct systems, D followed by initial of diisocyanate selected was used for naming.

Results and Discussion

TGA and FTIR results

TGA profiles (data not shown) exhibit one main degradation event at around 380ºC, as a consequence of the CO degradation, which is generally surrounded by two shoulders, the first one from 311ºC to 340ºC, and the second one at around 424-454ºC. The first shoulder is related to urethane decomposition [5], while the second one is related to extended crosslinking, both of them dependant on the type of diisocyanate and concentration [6]. Thus, for instance, an increase in concentration generally implies higher losses in both shoulders. Characteristic parameters obtained from TGA profiles are collected in Table 1. As can be observed, HDI- and IDI-based oleogels prepared with the TS process yields higher weight losses for both shoulders, as a result of a higher crosslinking with CO. This is probably due to phenolic diisocyanates, with their more positive load on the NCO group carbon atom which favours a higher reactivity [7] with lignin, having less concentration available for CO. When one-step gels are regarded, again a generally higher centred peak is observed for phenolic diisocyanates, as a more probable reaction with lignin is feasible because of their reactivity. However, weight losses in the two shoulders are more similar for all diisocyanates studied, because of the similar concentration and the higher availability of CO in detriment of lignin.

According to FTIR results (data not shown), all spectra are similar as gel-like dispersions generate the same kind of bonds, i.e., urethane and urea [5], which are confirmed with new N-H stretching vibrations at around 3330 cm^{-1}, as well as in a wide range between 1800-1630 cm^{-1}, where the C=O stretching vibration of urethane and urea related to free and hydrogen-bonded moieties are present [8]. Moreover, N-H bending vibration is also noticeable at 1570 cm^{-1}. Lignin functionalization was confirmed in previous studies [4].

Table 1. TGA characteristic parameters for gel-like dispersions performed.

Sample	T_{max} (ºC)	ΔW (%)
TSH	379/439	83/11
TST	311/381/446	16/64/15
TSI	327/382/450	22/59/17
TSM	320/378/441	16/69/11
TSH2	343/381/445	28/53/12
TST2	311/381/439	21/61/11
TSI2	327/379/424	29/46/17
TSM2	320/386/454	19/67/13
TSP2	316/384/447	15/68/13
DH	334/378/432	22/48/13
DT	318/382/436	18/53/15
DI	332/378/469	23/54/11
DM	322/381/441	20/59/12
DpH	336/385/430	23/50/20
DP	319/380/434	17/60/12

Nevertheless, FTIR spectra of these dispersions show an internal process of curing, which may be monitored with the loss of intensity of -NCO moiety at 2270 cm^{-1}.

As can be seen in Figure 1, each diisocyanate possess a different curing trend. While phenolic diisocyanates experience a fast curing, free aliphatic diisocyanates disappear more gradually, which is even extended for IDI, easily explained again because of the higher aromatic reactivity and steric blockage of higher molecules which guides to difficulties in crosslinking [7].

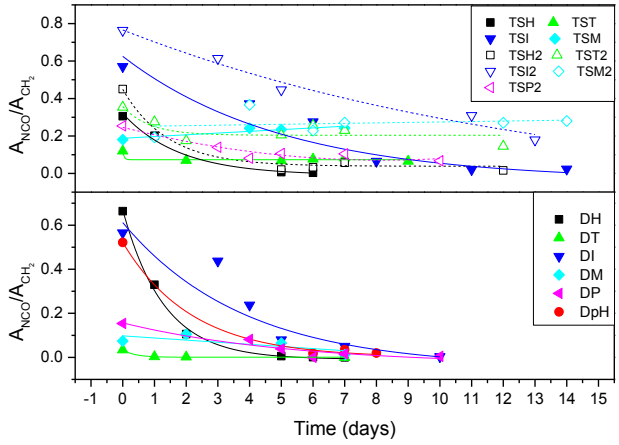

Figure 1. NCO loss evolution for TS (up) and one-step (down) oleogels.

Moreover, curing is strongly influenced by the type of processing, as can be seen in the case of TDI- and MDI-based oleogels. While applying a one-step process takes several days to lose all free diisocyanates, for the TS process, almost no curing is observed as the initial concentration is maintained, even for several months [4]. This fact is in agreement with the faster reaction with lignin in the first step, just making impossible to react consequently with CO due to steric impediment.

Rheological characterization

Apart from the differences discussed in TGA and FTIR results, rheological characterization demonstrates huge differences among all oleogels studied, as can be observed in Figure 2. Taking into account 1:1 TS oleogels (Figure 2a), only HDI is able to perform a suitable oleogel, as G' values are around 10^4 Pa and G'' values around one order of magnitude lower, similar to those found in commercial lubricating greases [3]. In contrast, TDI, MDI and IDI produce liquid-like viscoelastic dispersions. When increasing the weight ratio to 1:2 (Figure 2b), an increase in linear viscoelastic functions values is generally observed, as expected. On the other hand, IDI-based gel shows an unexpected behaviour at high frequency values, where a tendency to reach a crossover point between G' and G" was observed. For one-step oleogels (Figure 2c), a similar behaviour than that shown for 1:1 oleogels obtained with the TS process is observed, even when diisocyanate concentration is half. HDI-based oleogel depicts a slight decrease in linear viscoelastic functions values, as well as a shift in the crossover point at low frequencies. Regarding phenolic diisocyanates-based one-step gels, however, an increase in G' and G'' values is shown, except for PDI, which demonstrates a liquid-like behaviour. The improvement in DM overtakes even those values found with 1:2 lignin/ diisocyanate ratio with TS process. DT oleogel, in spite of it overcomes even DH values, exhibits a weak gel-like behaviour. Finally, DP oleogel, presents suitable G' and G'' values but, however, shows physical rubber-like appearance.

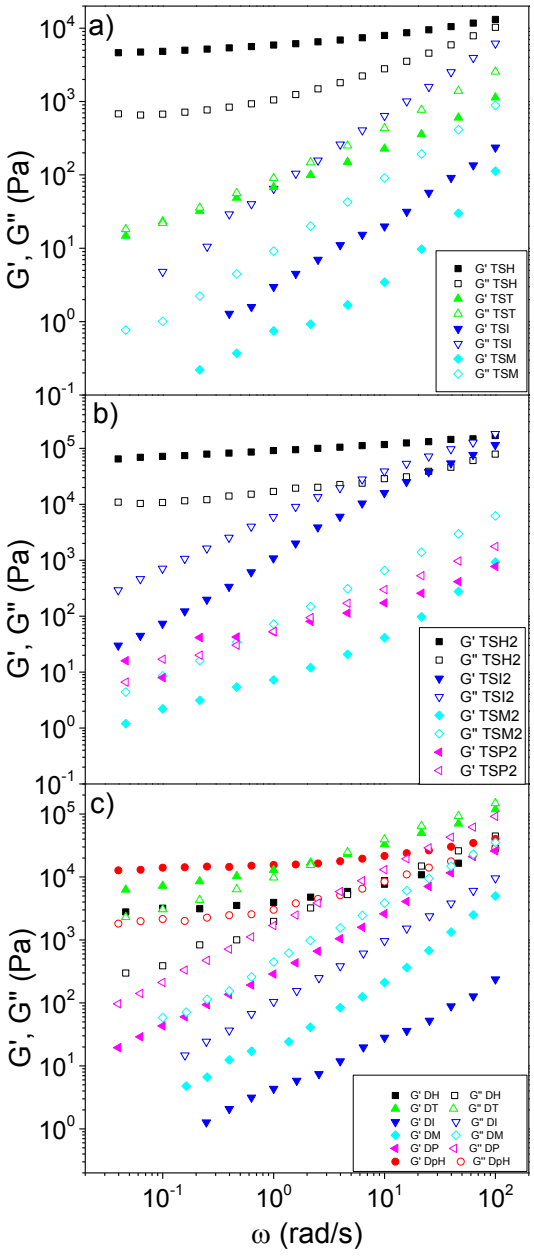

Figure 2. Frequency dependence of the storage, G', and loss, G", moduli of TS oleogels for a) 1:1 and b) 1:2 lignin/diisocyanate ratio and c) one-step oleogels.

Concluding Remarks

In this work, several diisocyanates were tested as crosslinkers for oleogel formation using lignin and castor oil. FTIR studies demonstrate urethane and urea bondings were generated in both FL and gel-like dispersions, thus crosslinking was successfully achieved between lignin and CO.

Rheological tests demonstrated a completely different behaviour depending on the nature of the diisocyanate, lignin/diisocyanate ratio and processing. Thus, in general, HDI was the most suitable crosslinker for gel formation no matter the type of processing and ratio, followed by TDI. Conversely, MDI- and IDI-based dispersions exhibited a general liquid-like behaviour. PDI produces a weak gel-like behaviour just for 1:2 TS gel. On the other hand, a rubber-like system is obtained for pHDI.

In conclusion, it can be considered that the nature of the diisocyanate, together with steric hindrance, are the key factors to obtain a gel with suitable properties to be used in the lubricant industry. For TS gels, the very high initial reactivity of some diisocyanates produces an excessive crosslinking degree, guiding to a worse combination with CO. Thus, for oleogels prepared in one-step process, a general increase in viscoelastic functions for aromatic compounds was observed in comparison with the TS process, while the others behave similar. Moreover, when high molecular weight diisocyanates were considered, different behaviour was also obtained.

Acknowledgements

This work is a part of two research projects (CTQ2014-56038-C3-1R and TEP-1499) sponsored by the MINECO-FEDER and Junta de Andalucía programmes, respectively.

References

1. Roman, C., Valencia, C., Franco, J.M. (2016). Tribol. Lett. 63(2)63:20.
2. Duval, A., and Lawoko, M. (2014). React. Funct. Polym. 85, 78–96.
3. Gallego, R., Arteaga, J.F., Valencia, C., Díaz, M.J., Franco, J.M. (2015). ACS Sustain. Chem. Eng. 3(9), 2130–2141.
4. Borrero-López, A.M., Valencia, C., Franco, J.M. (2017). Eur. Polym. J. 89(December 2016), 311–323.
5. Jena, K.K., Chattopadhyay, D.K., Raju, K.V.S.N. (2007). Eur. Polym. J. 43(5), 1825–1837.
6. Gallego, R., Arteaga, J.F., Valencia, C., Franco, J.M. (2013). Carbohydr. Polym. 98(1), 152–160.
7. Vilar, WD. (1998) Quimica e tecnologia dos poliuretanos. Vilar Consultoria.
8. Rueda-Larraz, L., d'Arlas, B.F., Tercjak, A., Ribes, A., Mondragon, I., Eceiza, A. (2009) . Eur. Polym. J. 45(7), 2096–2109.

Contact Address:

A.M. Borrero-López
Am.borrero@diq.uhu.es
Departamento de Ingeniería Química
Escuela Superior de Ingeniería
University of Huelva
Campus de "El Carmen", Av. De las Fuerzas Armadas s/n, 21071
Telf.: 0034959219998

Assessment of the adhesion performance of cellulose acetate and castor oil-based adhesives on different substrates by probe-tack tests

A. Tenorio-Alfonso[1], M.C. Sánchez[1,2], J.M. Franco[1,2]

[1] Department of Chemical Engineering, University of Huelva, Campus El Carmen, Campus ceiA3, 21071, Huelva (Spain)
[2] Pro2TecS-Chemical Product and Process Technology Research Centre, University of Huelva, 21071, Huelva (Spain)

Introduction

During the last century, the replacement of the traditionally petro-based raw materials by new eco-friendlier and sustainable substances in the industrial production and, in particular, in the polyurethane manufacture, has been the main focus of many researchers [1].

The production of polyurethane is, in most of the cases, conducted by means of a selective reaction between free active isocyanate (NCO) and hydroxyl (OH) groups, and using a chain extender (typically low molecular weight glycol or amine) [2], leading to a characteristically segmented chemical structure, which comprises separated soft (SS) and hard segments (HS) as a consequence of different interactions, such as hydrogen bonds between both microphases. This thermodynamically separated structure strongly influences the macromolecular properties of the final polyurethane [3].

As a result of their high-quality adhesion performance, excellent mechanical, thermal and chemical resistance, outstanding versatility, ease to handle, etc. [4] bio-based polyurethane adhesives have been recently developed, obtaining feasible alternatives to traditional formulations from vegetable oils or cellulose derivatives, as shown in previous studies [5, 6].

Furthermore, to carry out a more effective investigation of adhesives, the evaluation of the short and long term adhesion performance may be applied. The tack of an adhesive is the ability to form an instantaneous bond of measurable strength with a variety of substrates upon short contact time and pressure [7, 8]. A typical tack test, which traditionally includes two steps (bond formation and separation [9]), is quite dependent on factors like contact force, contact time, debonding speed and substrate nature, among others. One of the most relevant parameter obtained from tack tests is the energy of adherence (W_{adh}), which can be estimated as the area under the curve of stress versus strain plots [7].

The present contribution involves the study of the influence of the process conditions over the tack properties of a polyurethane synthesized through a solventless single-step protocol, by blending 1,6-hexamethylene diisocyanate, cellulose acetate and castor oil. Thus, tackiness was analysed as a function of contact pressure, contact time, debonding rate, curing times and substrate nature. Oscillatory torsional rheological measurements and standard mechanical tests were also performed and chemical structure was evaluated by means of differential scanning calorimetry (DSC) and Fourier transform infrared spectroscopy (FTIR).

Experimental

Materials and polyurethane synthesis

All the reagents used to synthesize bio-polyurethane adhesives were supplied from Sigma-Aldrich (St. Louis, MO, USA) including cellulose acetate (40 % DS acetyl groups, Mn ~ 30000) and 1,6-hexamethylene diisocyanate (≥98.0% of purity), whereas castor oil (211 cSt at 40 ºC) was purchased from Guinama (Valencia, Spain).

Bio-polyurethane synthesis

In this study, aiming to completely remove the use of environmentally hazardous products considered as solvents or catalysts, the several-stage synthesis protocol previously followed [10] has been modified and enhanced leading to a single-step production process. Thus, pre-dried cellulose acetate, 1,6-hexamethylene diisocyanate and castor oil were placed together in an open vessel and blended for 48 hours and at room conditions by using a controlled-rotational speed mixing device (RW 20, Ika, Staufen, Germany) equipped with an anchor impeller.

Methodology for polyurethane characterization

A probe tack test was employed to characterize the instantaneous adhesion of the synthesized polyurethane adhesive on different substrates (beech wood, stainless steel and aluminium). Immediate adhesion tests were carried out using an AG-IS Universal Testing Machine (Shimadzu, Kyoto, Japan), equipped with a 50 N load cell, a cylindrical and flat probe prepared with different adhesion substrates, and applying a custom-designed probe-tack method. 1.6 mm width of polyurethane adhesive film was compressed by two flat probes brought into contact at a speed of 5 mm/min and subsequently removed at a constant rate. Contact pressure was varied (0.52, 2.60, 5.6 and 7.8 kPa) and maintained for 1, 3 and 5 seconds. The probe was pulled out at a constant debonding speed ranging from 6 to 60 mm/min. All the tacking tests were performed at room conditions, during the first 5 hours after synthesis and replicated three times. The maximum stresses (σ_{max}), maximum deformations at failure (ε_{max}) and adhesion energies were recorded (W_{adh}).

Furthermore, totally cured polyurethane was rheologically characterized by performing temperature ramps under small-amplitude oscillatory torsional deformation (1 Hz frequency and 2 ºC·min^{-1} of heating rate) from room temperature up to 200 ºC, within the linear viscoelastic region, using a controlled-stress rheometer Physica MCR301 (Anton Paar Germany GmbH, Ostfildern, Germany).

The chemical structure and curing process of the synthesize bio-adhesive was studied by means of Fourier Transform Infrared Spectroscopy (FTIR) in a FT/IR-4200 Sprectrometer apparatus (JASCO Inc., Tokyo, Japan), equipped with an attenuated total reflectance (ATR) accessory provided with a monolithic diamond crystal. Infrared spectra were obtained as the result of an average of 101 scans with a resolution of 4 cm^{-1} and a 45º angle of incidence, in the spectral range 7800-350 cm^{-1}.

Differential scanning calorimetry tests were performed by using a Q100 Calorimeter (TA Instruments, New Castle, DE, USA), submitting 5-10 milligram-hermetically sealed aluminium pans to a heating cycle ranging from -85 to 200 ºC at a heating rate of 10 ºC/min, under nitrogen atmosphere (50 mL/min flow rate).

Final adhesion performance of the cellulose acetate-based adhesive was analysed on the same substrates considered for tacking tests, i.e. stainless steel, aluminium and wood, by means of standardized mechanical tests obtaining shear (ASTM D906, D1002) and peeling (ASTM D903) strength, using an AG-IS Universal Testing Machine (Shimadzu, Kyoto, Japan).

Results and Discussion

Tack tests provide the required force to separate a flat probe from an adhesive film. A typical stress vs strain curve in tack test is given in Figure 1.

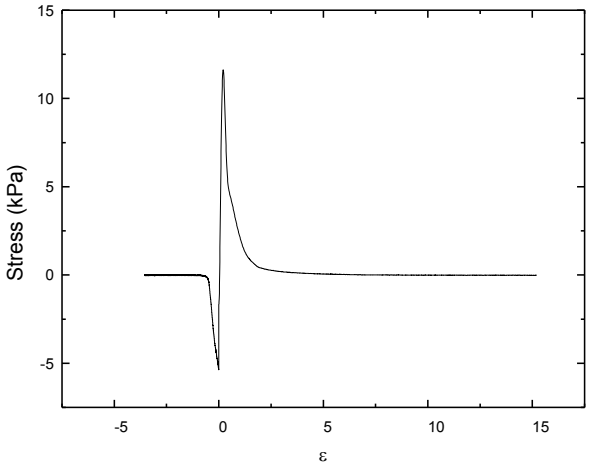

Figure 1. Typical tacking curve, plotting stress vs strain

According to previous studies [7], no matter the experimental conditions applied, cavitation was the main mechanisms observed during debonding, meaning that the energy of adherence presented a slight contribution of fibrillation. Thus, the different experimental conditions (Table 1) did not modify the failure mechanism, so that no greater fibrillation region was achieved.

Table 1. Tacking tests parameters

Test	Subs.	Deb. Rate (mm/min)	Contact time (s)	Pressure (kPa)
T1	SS	60	1	0.52
T2	SS	60	1	2.60
T3	SS	60	1	5.20
T4	SS	60	1	7.80
T5	SS	30	1	0.52
T6	SS	6	1	0.52
T7	SS	6	3	0.52
T8	SS	6	5	0.52
T9	Al	60	1	2.60
T10	W	60	1	2.60

Substrates: *SS* / Stainless steel; *Al* / Aluminium; *W* / Wood

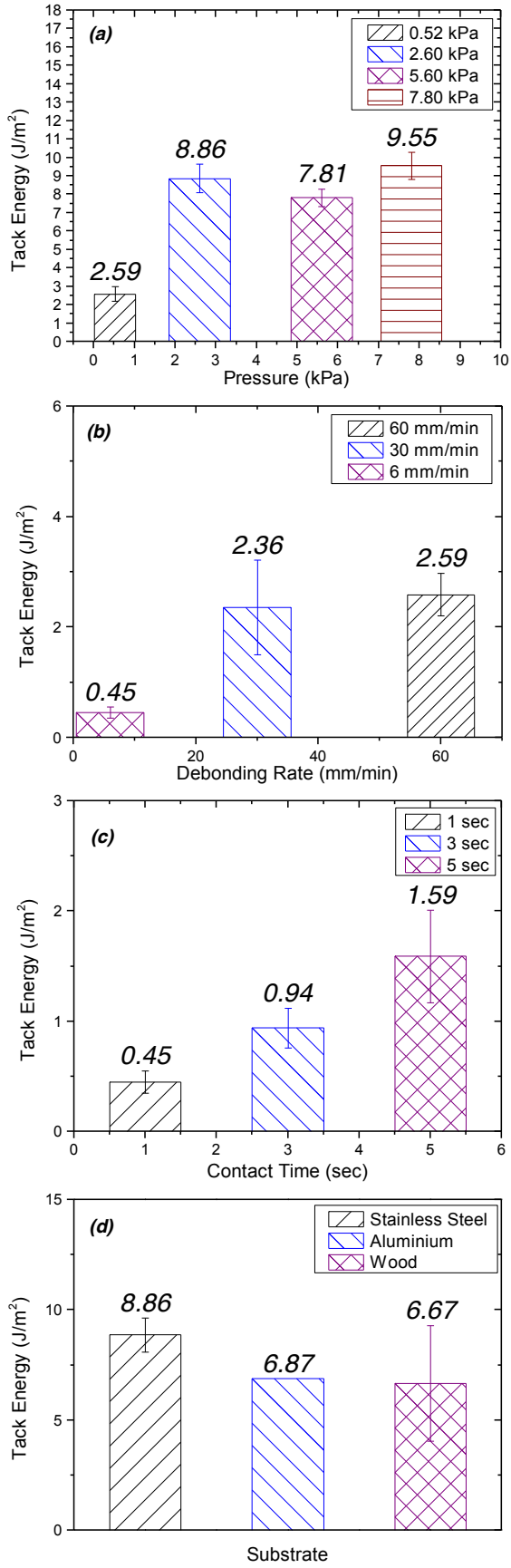

Figure 2. Tacking energy evolution with (a) pressure, (b) debonding speed, (c) contact time and (d) substrate.

Moreover, maximum stress and tack energy increased with contact pressure (tests T1-T4) and contact time (T6-T8), becoming more than twice when pressure was raised from 0.52 up to 7.8 kPa (Figure 2a). A similar evolution can be noticed when debonding rate was increased (tests T1, T5 and T6), obtaining higher maximum elongation with greater speeds. Moreover, despite the fact that bio-based adhesive exhibited the highest ultimate adhesion response with the most suitable failure (*substrate failure*) when wood was considered as substrate, at the first stages of curing time, the immediate adhesion turned to be the lowest on this surface (Figure 2d), being a third of the value reached in stainless steel, where tackiness was even higher than the corresponding to aluminium surface. Besides, under any probe-tack condition, a clear increase in the tack energy with curing time can be found during the first 5 hours of ageing, as a consequence of the higher crosslinking density.

Furthermore, as can be noticed from Figure 3, within the whole temperature range considered, the synthesized bio-based adhesive is characterised by a predominant elastic behaviour, what means storage modulus (G') unfailingly higher than the corresponding viscous modulus (G''), identified as the so called rubbery region of the mechanical spectrum.

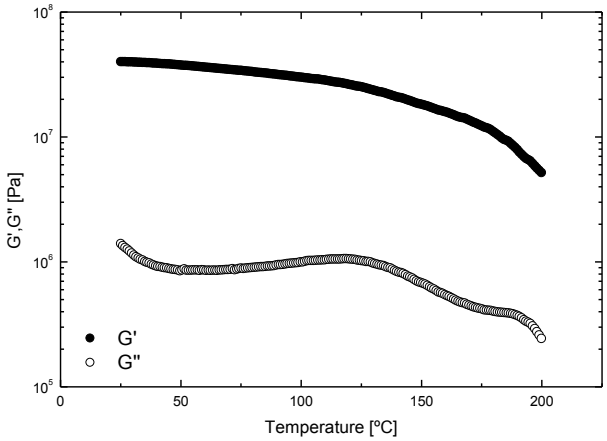

Figure 3. Evolution of linear viscoelastic moduli (G' and G'') with temperature

Moreover, the curing process was monitored by means of FTIR analysis, evaluating the disappearance of the characteristic free isocyanate peak (-N=C=O) located at 2263 cm^{-1}, and the characteristic absorption bands associated to urethane and urea linkages, particularly N-H, C-N and C=O stretching vibration with and without hydrogen bonding, leading to a segmented chemical structure, consisting of soft (SS) and hard segments (HS) domains, in accordance with previous studies [10].

This phase-separated structure was also confirmed by DSC results, since two glassy transition temperatures were obtained (Table 2) corresponding to both microdomains, soft ($T_{g,SS}$) and hard segments ($T_{g,HS}$). In terms of DSC and FTIR results, a period of 20 days can be assumed as the time required to achieve a completely cured adhesive.

Table 2. Glassy transition temperatures

Domain	Temperature (ºC)
Soft Segments (SS)	-15
Hard Segments (HS)	74

Regarding mechanical standard tests (Table 3), irrespectively of the substrate nature, peeling strengths were quite similar to each other, despite the fact that, as a consequence of the greater interaction between bio-based adhesive and wood, this material combination leads to a cohesion failure in contrast with adhesion failures achieved with the rest of substrates For this reason, shear strength provided by wood-wood joints became 30 % higher than the corresponding to both metal substrates. Indeed, the failure developed in shear tests when wood was considered as substrate turned to be the most appealing kind of failure, i.e. substrate failure. Finally, there was not significant difference between shear and peeling strengths in both metal substrates.

Table 3. Mechanical Results on different substrates

Tests	Value
Shear strength – W (kg-f/cm^2)	43,8 ± 11,0^c
Shear strength – Al (kg-f/cm^2)	33,1 ± 3,0^a
Shear strength – SS (kg-f/cm^2)	34,3 ± 4,3^a
Peeling Strength – W (g-f/mm)	269,5 ± 4,6^b
Peeling Strength – Al (g-f/mm)	285,8 ± 38,0^a
Peeling Strength – SS (g-f/mm)	288,9 ± 28,6^a

Failures: [a] Cohesion; [b] Adhesion; [c] Substrate

Acknowledgments

This work is part of two research projects (CTQ2014–56038-C3-1R and TEP-1499) sponsored by MINECO-FEDER and Junta de Andalucía programmes, respectively. One of the authors (Adrián Tenorio) has also received a PhD. Research Grant from “Ministerio de Educación” (FPU13/01114). The authors gratefully acknowledge the financial support.

References

1. Moubarik, A., Allal, A., Pizzi, A., Charrier, F. and Charrier, B. (2010). Eur. J. Wood Wood Prod. 68, 427-433.
2. Norhisham, S.M., Maznee, T.T.N., Ain, H.N., Devi, P.K., Srihanum, A., Norhayati, M., Yeong, S., Hazimah, A., Schiffman, C.M. and Sendijarevic, A. (2017). Int. J. Adhes. Adhes. 73, 38-44.
3. Bistričić, L., Baranović, G., Leskovac, M. and Bajsić, E.G. (2010). Eur. Polym. J. 46, 1975-1987.
4. Liu, H., Li, C. and Sun, X.S. (2017). Int J Adhes Adhes. 73, 66-74.
5. Gallego, R., Arteaga, J., Valencia, C. and Franco, J. (2013). Cellulose. 20, 495-507.
6. Malik, M. and Kaur, R. (2016). Adv. Polym. Technol. 00, 1-7.
7. Tramis, O., Brethous, R., Hassoune-Rhabbour, B., Fazzini, M. and Nassiet, V. (2016). Int J Adhes Adhes. 67, 22-30.
8. Maassen, W., Meier, M.A. and Willenbacher, N. (2016). Int J Adhes Adhes. 64, 65-71.
9. Z., C., W., A., A., H. and A., K. (2013). Int J Adhes Adhes. 40, 210-214.
10. Tenorio-Alfonso, A., Sánchez, M.C. and Franco, J.M. (2017). Polymers. 9, 132-145.
11. Corcuera, M., Rueda, L., d’Arlas, B.F., Arbelaiz, A., Marieta, C., Mondragon, I. and Eceiza, A. (2010). Polym. Degrad. Stab. 95, 2175-2184.

Contact Address

Author’s email: adrian.tenorio@diq.uhu.es
Department of Chemical Engineering, Physical Chemistry and Science of Materials
Campus El Carmen, Faculty of Experimental Sciences
University of Huelva
Address: Av. Fuerzas Armadas, S/N
PC: 21071
Telf.: 959219998

Formulation and rheological characterization of epoxidized lignin-based gel-like dispersions for lubricant applications

E. Cortés-Triviño[1], C. Valencia[1,2], M.A Delgado[1,2], J.M. Franco[1,2]

[1] Department of Chemical Engineering. University of Huelva, Campus El Carmen, Campus ceiA3, 21071 Huelva (Spain)
[2] Pro2TecS-Chemical Product and Process Technology Centre, University of Huelva, 21071 Huelva (Spain)

Introduction

Nowadays, as a result of the environmental awareness, the lubricant industry is intending to avoid or minimize hazardous effects caused by these products once disposed in the environment [1].

Although the use of vegetables oils as lubricant base oils to replace petroleum-derived products have been previously studied, a great interest to substitute the traditional thickening agents, including lithium, aluminium, sodium or calcium soaps, used in the lubricant formulations is currently arising. Some modified natural materials have been used in previous studies in order to minimize its impact over the environment and provide good rheological and thermal properties in lubricating performance [2].

Lignocellulosic materials represent the most abundant renewable organic resource on the earth [3]. One of their main constituents is lignin, which has been considered as non-commercialized waste of papermaking. Their biodegradable character and its great availability at moderately low prices seem to be good reasons to explore different valorisation pathways of this renewable resource. In addition, lignins present a complex structure with numerous functional groups susceptible to modification, which makes this by-product a potential source of innovative materials [4, 5].

Following this direction, a simple protocol was applied to chemically modify an alkali lignin (AL) with polyethylene glycol diglycidyl ether (PEGDGE) in alkaline medium in order to use it as thickener in lubricating greases formulations. The influence of the lignin/PEGDGE weight ratio used in the functionalization reaction was studied and the epoxidized compounds were dispersed in castor oil (CO) in order to analyze the rheological response of resulting gel-like dispersions.

Experimental

Materials

Castor oil, provided by Guinama (Spain), was used as base oil. A commercial alkali lignin, was modified with poly (ethylene glycol) diglycidyl ether (PEGDGE) (average Mn: 500 g/mol). Sodium hydroxide was used as catalyst. All reagents were supplied by Sigma-Aldrich

Modification of AL

Functionalization reaction was carried out following the protocol previously described [6]. Basically, 10 g of lignin were fully dissolved in a sodium hydroxide solution at 30 ºC placed in a round-bottle flask mounted with a thermometer, a magnetic stir bar and dropping funnel. Then, different amounts of PEGDGE (see Table 1) were dropwisely added and the reaction was kept at 30 ºC during 3 hours. Finally, the mixture was centrifuged at 4000 rpm and dried around 30 minutes in an oven at 80 ºC.

Preparation of gel-like dispersions

An open vessel and a controlled-rotational speed mixing device (70 rpm) RW 20 (Ika), equipped with an anchor impeller were used to prepare epoxide-functionalized compunds-based gel-like dispersions in castor oil. A 5% (wt.) concentration of the epoxidized compound was added in all cases. The reaction was kept for 24 hours at room temperature and then homogenized with an Ultra-Turrax T25 (Ika) rotor-stator turbine, at 10000 rpm for 1 minute. Reference systems containing only sodium hydroxide (Ref. 1 sample) and lignin/sodium hydroxide (Ref. 2 sample) dispersed in castor oil were also processed in order to quantify the effect of the epoxidized lignin on the rheological response of resulting gels.

Determination of the epoxy index

The presence of epoxy groups in the modified compounds was determined by titration with chloroform, glacial acetic acid, tetraethylammonium bromide and crystal violet with perchloric acid according to ISO 3001:1999(E).

Fourier transform infrared (FTIR) spectroscopy

FTIR spectra were obtained with a FT/IR-4200 spectrometer apparatus (JASCO) in a wavenumber range from 400 cm^{-1} to 4000 cm-1, at 4 cm^{-1}, in the transmission mode. PEGDGE-functionalized compounds were prepared as KBr pellets (32 mm x 3 mm).

Rheological characterization

Rheological characterization was carried out with a Physica MCR 501(Anton Paar) controlled-stress rheometer, equipped with a Peltier temperature controller, using a serrated plate-and-plate geometry (25 mm and 1 mm gap) Small amplitude oscillatory shear (SAOS) tests, inside the linear viscoelastic region, were performed in a frequency range of 0.03-100 rad/s, at 25ºC. Samples were measured 1 day, 1 week, 1 month and 2 months after its preparation.

Results and Discussion

Functionalization degree of samples

Table 1 provides information about the epoxidation degree of samples as a function of AL/PEGDGE weight ratio used in the functionalization reaction, as well as of the residual amount of sodium hydroxide present on the epoxidized compounds. As can be seen, a higher AL/PEGDGE ratio allows an increase in epoxidation index, also with a larger amount of sodium hydroxide retention. This fact may be explained attending to excessive epoxy ring opening in the alkaline aqueous medium and secondary reactions between epoxy groups when the amount of PEGDGE is raised.

Table 1. AL/PEGDGE ratio and the corresponding epoxy index and NaOH amount of EPL

Sample code	AL (g)	PEGDGE (g)	Epoxy Index (mol/kg)	NaOH (mol/kg)
EPL1	10	2.5	0.79	5.9
EPL2	10	5	0.52	5.4
EPL3	10	10	0.37	4.7
EPL4	10	20	0.28	2.8
EPL5	10	50	0.15	1.4

Fourier transform infrared (FTIR) spectroscopy

Main information inferred from the analysis of FTIR spectra of original alkali lignin and epoxidized samples is the appearance of new characteristic band at 865 cm^{-1}, related to the stretching vibrations of C-H contained in epoxide rings [7] and a significant simplification of the spectrum yielding a reduction in intensity the characteristic bands between 1033 and 1200 cm^{-1}.

Rheological characterization

Figure 1 shows the evolution of SAOS functions with frequency, at 25ºC, inside the linear viscoelastic range, two months after preparation for a selected epoxidized lignin-based gel-like dispersion (EPL1) compared with reference systems prepared with sodium hydroxide (Ref. 1) and lignin/sodium hydroxide (Ref. 2) dispersed in castor oil, in the same proportions, as well as for gel-like dispersions as a function of functionalization degree of thickener.

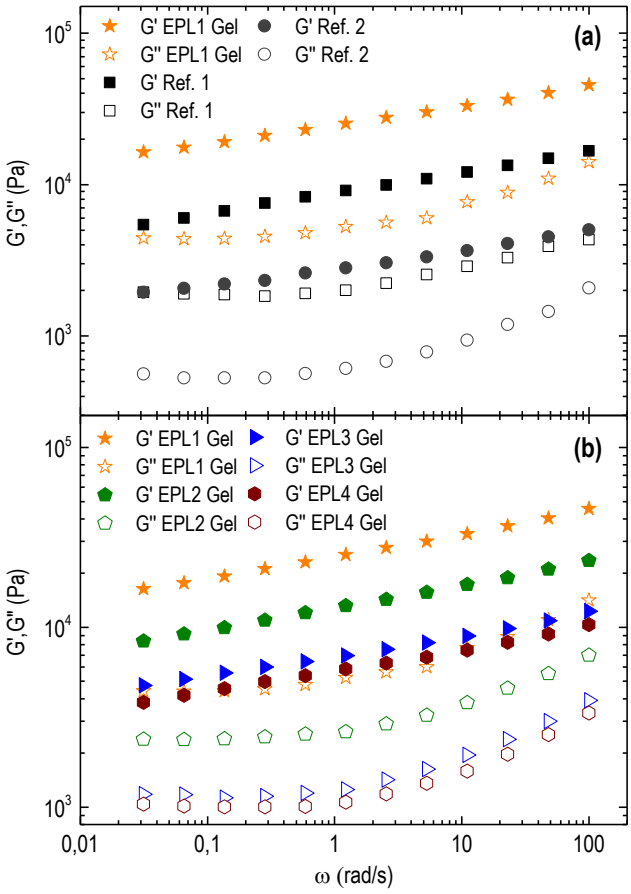

Figure 1 Frequency dependence of the storage, G', and loss, G", moduli for epoxide-functionalized lignin based oleogels as function of functionalization degree of samples (b) and for a selected sample (EPL1 Gel) compared with their corresponding reference systems (a) (G', closed symbols; G", open symbols).

In all cases, the typical response of particle gels was obtained, wherein the so-called "plateau region" of the mechanical spectrum was clearly noticed. Overall, from a qualitative point of view, this response is very similar to that previously found in commercial lubricating greases based on mineral oils and metallic soaps [8].

Moreover, as can be seen, a partial saponification process takes place between castor oil and residual NaOH, which provides even higher values of SAOS moduli than the epoxidized lignin-based dispersion one day after preparation. Nonetheless, after two months, the values of SAOS functions overtakes those found in the saponified oil only containing NaOH, due to the progress of the reaction between epoxy groups in the castor oil medium (Figure 1a). On the other hand, the rheological modification clearly increases with the epoxidation degree, as illustrated in Figure 1b.

The evolution of plateau modulus (G_N^0) as a function of epoxy index, one day and two months after preparation, was displayed in Figure 2. Reference systems didn't show changes on their rheological properties after on day. However, G_N^0 increased linearly with the epoxy index in epoxidized lignin gel-like dispersions, reaching a higher strength of microstructural network in those samples with a larger degree functionalization, as expected.

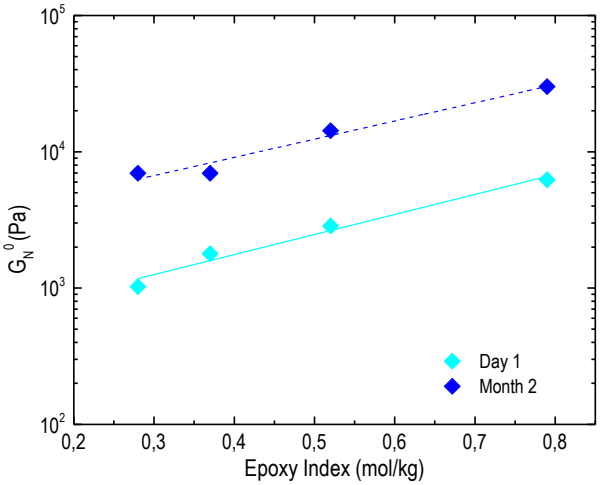

Figure 2. Evolution of G_N^0 with epoxy index as a function of the ageing time.

References

1. Bartz, WJ. (1998). Tribol. Int. 31, 35–47.
2. Zetzl, AK., Gravelle, AJ., Kurylowicz, M., Dutcher, J., Barbut, S., and Marangoni, AG. (2014). Food Struct. 2, 27–40.
3. Asada, C., Basnet, S., Otsuka, M., Sasaki, C., and Nakamura, Y. (2015). Int. J. Biol. Macromol. 74, 413–419.
4. Lora, JH., and Glasser, WG. (2002). J. Polym. Environ. 10.
5. Qin, Y., Mo, W., Yu, L., Yang, D., and Qiu, X. (2016). Holzforschung. 70, 4–11.
6. El Mansouri, N-E., Yuan, Q., and Huang, F. (2011). BioResources. 6, 2647–2662.
7. Lee, H., and Neville, K. (1967). Handbook of Epoxy Resin, McGraw-Hill, Inc., New York.
8. Sánchez, R., Valencia, C., and Franco, JM. (2014). Tribol. Trans. 57, 445–454.

Contact Address:

esperanza.cortes@diq.uhu.es
Department of Chemical Engineering,
Faculty of Experimental Science
University of Huelva
Campus de El Carmen, Av. 3 de Marzo S/N, 21071, Huelva, Spain.
Telf.: 34-959-219998

Improving thermal conductivity of alumina whisker composites by controlling the rheology and the whiskers selective location in PE/PA6 immiscible blends

A. Ares-Pernas[1], X. García-Fonte[1], C. Cerecedo[2], V. Valcárcel[2], M. J. Abad[1]

[1] Universidade da Coruña, Grupo de Polímeros, Centro de Investigacións Tecnolóxicas, Campus de Ferrol, 15471 Ferrol, Spain
[2] Neoker, S.L., Rúa da Xesta, 78A, 15895 O Milladoiro, Spain.

Introduction

For some electronic applications high thermal conductivity and high electrical resistivity composites are desired. In the literature there are several attempts to achieve this goal, introducing electrically insulating fillers with high thermal conductivity, using hybrid thermal conductive fillers, etc. Moreover, the most recent studies pointed out that this outcome can be achieved by controlling the selectively location of fillers in a phase of the polymer blend [1].

In these work, alumina whiskers composites were obtained by extrusion dispersing different amounts of electrically insulating filler, in different ratios of PE/PA6 blends. The mixing strategy, the ratio of PE/PA6 and the filler amount were well-designed with the aim to control the composite morphology and their rheology which can affect the macroscopic properties of materials as the electrical and the thermal conductivity [2].

The rheology characterization of designed composites was performed by small amplitude oscillatory shear experiments. With the aim to analyze the influence of PE/PA6 ratio in the rheological properties, coalescence experiments were realized too. Relationships between morphology and rheology were established appropriately by electronic microscopy. Using the laser flash technique, the thermal diffusivity and thermal conductivity of composites were measured.

The ultimate goal of this work is to optimize the thermal conductivity of composites using the minor amount of filler in an inmisicible polymer blend with a controlled morphology, which favours the formation of thermal conductive paths.

Experimental

Materials and composite processing

PE 25055E (Dow Chemical), PA6 Zytel 7335FA NC010 (DuPont) and the α-alumina fibres NKR$_v$® (α-Al2O3, corumdum, supplied and produced by NEOKER S. L. were used in this study. Composites of 60/40 PE/PA6 blend and different alumina contents were mixed by extrusion in two steps using a miniextruder Minilab Haake Rheomex CTW5 (Thermo Scien-tific) at 235ºC and 40 rpm. Firstly, the whiskers were introduced by extrusion in PE matrix and then, PE/whiskers blend was diluted with dry PA6 (drying for 6h at 90ºC) to obtain the desired PE/PA/whisker ratio. Samples were prepared by compression moulding and sprayed with a coating of graphite for thermal test. Figure 1 shows composites nomenclature.

Table 1. Samples nomenclature.

Sample nomenclature	PE (wt%)	PA6 (wt%)	Whiskers wt% (vol%)
PE	100	-	-
PA6	-	100	-
60/40	60	40	-
60/40/30	42	28	30 (10.1)
60/40/40	36	24	40 (14.9)
60/40/50	30	20	50 (20.8)

Characterization

Composites morphology was observed using a JEOL JSM-6400 SEM at accelerating voltage of 20 kV. Firstly, specimens were cryofractured using N_2 liquid and then sputter-coated with a thin layer of gold.

The rheological measurements were performed using a controlled strain rheometer (ARES, TA Instruments) with parallel-plate geometry (25 mm diameter,1 mm gap) at 225ºC in the linear viscoelastic region (LVE). Stability of samples with temperature during the test time was ensured. To promote the coalescence of dispersed phase, the rheological specimens were submitted to continuous flow at different shear rates of 0.02; 0.1 and 0.4 s^{-1} followed by frequency sweep tests.

Thermal diffusivities were measured at 25ºC with thermal analyser (LFA 447 Nanoflash, Germany). The

thermal conductivity of different composites was calculated from thermal diffusivity data, density and specific heat capacity of each sample.

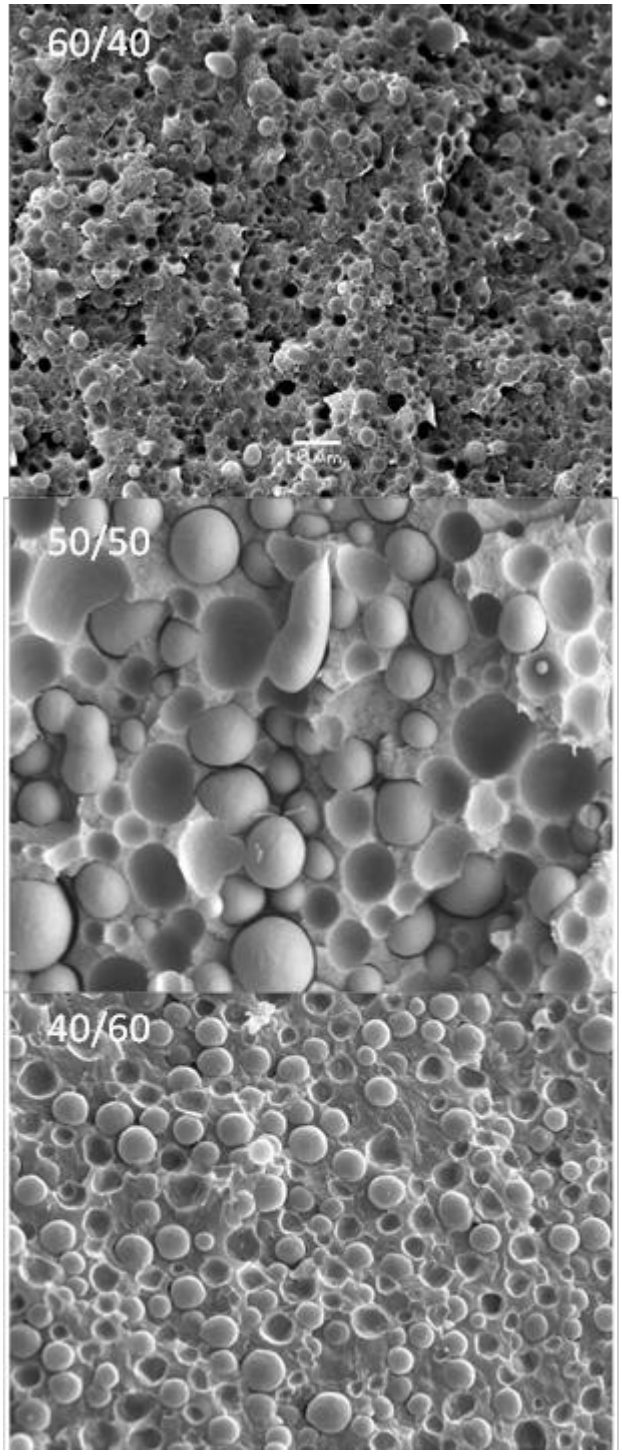

Figure 1. SEM micrographs of PE/PA6 blends (x1000)

Results and Discussion

According to the concept of double percolation, the phase's morphology plays a very important role in the thermal properties of the immiscible polymer blends reinforced with a filler. For this reason, at first, the most suitable morphology was selected by adjusting the weight ratio of PE/PA6 [4].

Three different immiscible blends were analysed 40/60; 50/50 and 60/40 wt%/wt% PE/PA6 blends (Figure 1). The typical sea-island morphology was observed in PE/PA6 blends, where PA spherical domains are dispersed in a continuous PE matrix (the phases identification was performed by etching using a selective dissolvent of PA6 (formic acid), micrograph not showed here).

Thermal conductivity data of binary blends were similar (0.28; 0.37 and 0.33 W/mK for 40/60; 50/50 and 60/40 respectively) and in all cases similar or higher than pure components (0.31 W/mK for raw PE and 0.30 W/mK for raw PA6). In view of this, the 60/40 blend was selected to continue the study since the size of PA domains is the lowest. Different amounts of alumina whiskers were introduced in 60/40 PE/PA blend and, to promote coalescence of PA domains, the samples were subject to different shear rates. Finally, the influence of these parameters in morphology, rheology and thermal properties of composites was analysed.

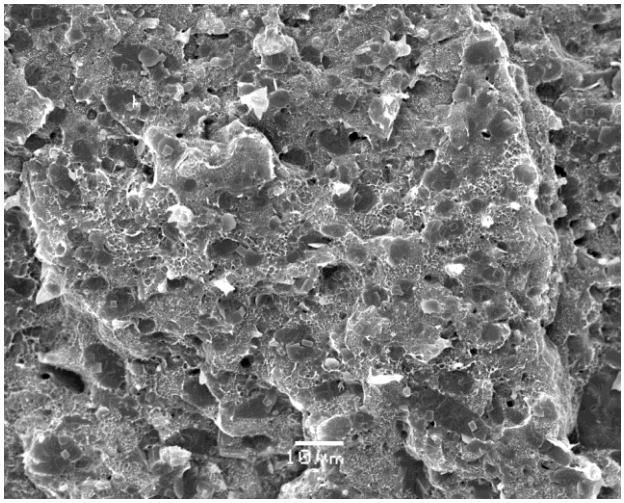

Figure 2. SEM micrographs of 60/40/30 PE/PA6/Alumina whiskers composite (x1000)

SEM micrographs show (Figure 2) that filler locates preferentially inside the PE phase. In Figure 3a, it can be seen that unfilled polymers and blend exhibit a predominantly viscous feature in the whole range of frequency investigated. Binary blend modulus is between the modulus of raw polymers as can be expected in immiscible blends. Storage modulus of the

composites increases with content of alumina whiskers. Incorporation of filler in the polymer transforms the liquid-like terminal behaviour to solid-like non-terminal behaviour that indicates the formation of an interconnected structure of nanotubes in the PE phase.

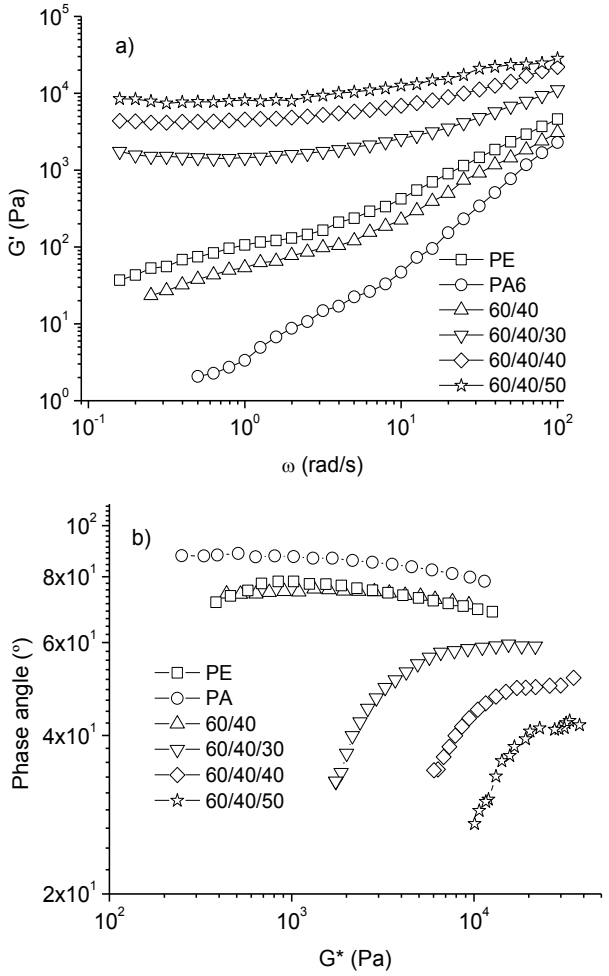

Figure 3. a) Storage modulus versus frequencies for neat polymers, 60/40 blend and alumina whiskers composites; b) Van Gurp-Palmen plot

This transition can be corroborated with Figure 3b in which the decrease in phase angle indicates that composites are rheologically percolated. The crossover points (Table 2) were clearly shifted to higher frequencies as filler increased until a solid-like behaviour in all frequency range is obtained (G'>G'') for more filled composite. The improvement of the elastic response in composites with high filler amounts indicates that the number of interfaces between whiskers has increased, that is, a denser percolated network was formed [5]. A denser network could improve the conductive paths into composite and consequently, enhance their thermal conductivity.

Table 2 shows that thermal conductivity is enhanced in all composites compared to the original blend and raw polymers.

Table 2. Crossover points of different composites. Thermal conductivity of pure components, blend and composites

Sample nomenclature	ω_c/G_c (rad.s^{-1}/Pa)	k (T=25ºC) (W/m.K)
PE	G''>G'	0.31
PA6	G''>G'	0.30
60/40	G''>G'	0.33
60/40/30	2,9 / 1903	0.46
60/40/40	13,3 / 7588	0.62
60/40/50	G'>G''	0.72
60/40/30 (0.4s^{-1})	-	0.63

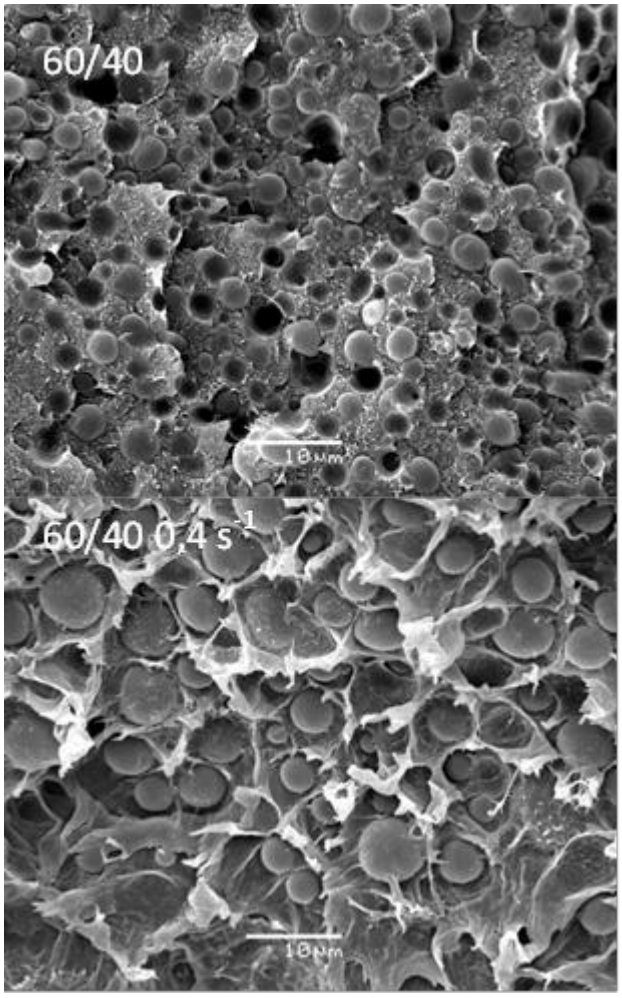

Figure 3. SEM micrographs of coalescence effects on 60/40 blend (x2000)

Besides, the use of an immiscible polymer blend as matrix, increases the thermal conductivity with respect to PA/alumina whiskers composite (k=0.48 W/mK for 60/40 wt%/wt% PA6/whiskers). It is due to the selective location of whiskers in PE matrix (continuous phase) which allows to increase the filler contacts (with the same filler content) and, in this way, increase the number of conductive paths. With the aim to improve

this effect, even more, PA domains coalescence will be studied.

The final properties of composites depend on the morphology of the system, which could be modified submitting them to different shear flows. One of the most important effects of flow on the blend morphology is coalescence [2, 4, 6].

Coalescence experiments were performed as can be described in experimental part. Slow continuous flows were applied to samples to favour mobility of droplets and to try to induce this phenomenon.

As can be observed in Figure 3, important morphological changes in 60/40 wt%/wt% PE/PA6 blend are observed with preshear. Same behaviour was obtained for 60/40/whiskers composites (not showed here). Size of the dispersed phase grows considerably with preshear and it could affect the rheological and thermal conductivity of the composites.

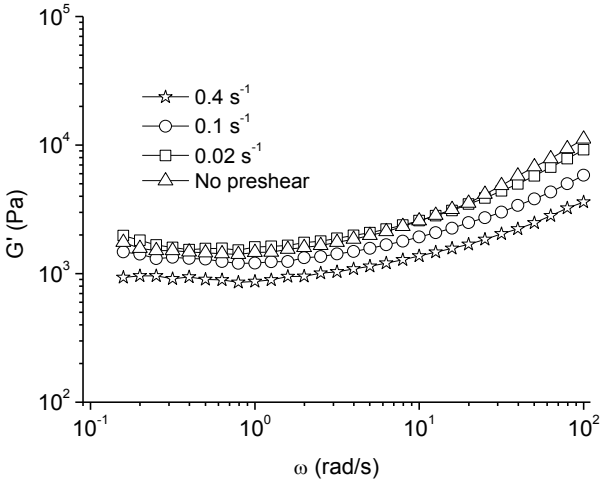

Figure 4. Coalescence experiments: effect of preshear in 60/40/30 PE/PA6/alumina whiskers composite

Effects of preshear in rheology behaviour are displayed in Figure 4. With a preshear of 0.02 s^{-1} no important changes in G' are observed with respect to the sample without preshear treatment. Moreover, when a preshear of 0.1 and 0.4 s^{-1} are applied to the sample an important diminution of storage modulus is observed. This diminution in storage modulus is due to the coalescence of PA domains. The growth of PA droplets could modify the distribution of the filler in the PE matrix and, in this way, change the thermal conductivity and other macroscopic properties of composites. To prove this fact, thermal conductivity of 60/40/30 composite was measured after a preshear of 0.4 s^{-1}. An increase about 40% in this parameter was obtained (Table 2), going from 0.46 (no preshear) to 0.63 W/m.K (preshear of 0.4 s^{-1}).

Conclusions

The use of an immiscible blend 60/40 wt%/wt% PE/PA6 to prepare alumina whiskers composites is a good option to improve thermal conductivity respect to composites with only PA.

Morphological changes can be followed easily with the analysis of rheological results that are strongly related with the macroscopic properties.

Coalescence of PA domains could enhance thermal conductivity (as it has already proved in preshear 60/40/30 composite) and other macroscopic properties, which is the aim of our future work.

Besides, rheology offers a feasible route to evaluate the coalescence of the dispersed phase in blends and composites.

Acknowledgements

Authors acknowledge the financial support to Xunta de Galicia – FEDER (Program of Consolidation and structuring competitive research units (GRC2014/036), Guangdong Innovative and Entrepreneurial Research Team Program and International Science&Technology Cooperation Program of China.

References

1. Cao, J.P., Zhao, J., You, F., Yu, H., Hu, G.H. and Dang, Z.M. (2013). Comp. Sci. and Tech. 89, 142–148.
2. Zhou, S., Luo, W., Zou, H., Liang, M. and Li, S. (2016). J. Comp. Mater. 50 (3), 327-337.
3. Kong, M., Huang, Y., Lv, Y., Wang, S., Yang, Q. and Li, G. (2014). Polym. 55, 4348-4357.
4. Filippone, G., Dintcheva, N. Tz., La Mantia, F.P. and Acierno, D. (2010). Polym. 51, 3956-3965.
5. Jyoti, J., Singh, B.P, Rajput, S., Singh, V.N. and Dhakate, S.R. (2016). J. Mater. Sci. 51, 2643-2652
6. Sangroniz, L.; Palacios, J.K., Fernández, M., Eguiazabal, J.I., Santamaría, A. and Müller, A. (2016). Eur. Poly. J. 83, 10-21.

Contact Address:

aares@udc.es
Grupo de Polímeros, Centro de Investigacións Tecnolóxicas
Universidade da Coruña
c/ Vazquez Cabrera s/n. Campus de Ferrol 15471, Spain
Telf.: 881013481

Design, mesomorphic properties and rheological characterization of a novel calamitic low molecular weight liquid crystal

M.T. Cidade[1], M. Cigl[2], V. Hamplova[2], A. Machado[1] and A. Bubnov[2]

[1]CENIMAT/I3N, Departamento de Ciência dos Materiais, Faculdade de Ciências e Tecnologia, Universidade Nova de Lisboa, 2829-516 Caparica, (Portugal)

[2]Institute of Physics, The Czech Academy of Sciences, 182 21 Prague (Czech Republic)

Introduction

Smart materials that are able to self-assemble into supramolecular structures with desirable functionality and physical properties at nano- and meso-scopic length scales represent currently an exciting area of intense research, which provides a highlighted approach for design and synthesis of new functional reactional mesogenic and macromolecular materials. One of the most exciting classes of organic materials, which are able to self-assembly, are those possessing the liquid crystalline behaviour. Liquid crystals (LC) constitute a fascinating class of soft matter which is characterized by the counterintuitive combination of fluidity and long-range order. LC materials exhibit a large number of different phases, most of which are spontaneously formed, i.e. they self-assemble into complex nano-structures. Moreover, the combination of fluidity and sensitivity to external stimulus like applied electric/magnetic fields (or illumination by UV-light in case of photosensitivity) makes polar fluids ideal for photonics, telecommunications, non-linear optics, energy conversion, etc. [1-4].

In order to stabilize the self-assembling materials and hence their functional structures the polymerization process can be used. Mesogenic units incorporated into the backbones or side-chains of weakly cross-linked polymers can become orientationally ordered. The resulting polymeric material combines the anisotropy and large susceptibility of low molar-mass liquid crystalline materials with mechanical elasticity and processability of polymers.

Search and design of new functional reactive mesogens exhibiting self-assembling behaviour [5-8] and contributing to better understanding molecular architecture – nano-organization properties of reactive mesogenic materials (to be used as functional side-chains for preparation of advanced siloxane based liquid crystalline polymers and elastomers) remains as an actual task in our days [9,10].

Nematic liquid crystals are well-known self-assembling materials responding to applied electric fields, which gave rise to LC display technology [11]. However, nematic LCs with positive dielectric anisotropy can be used also in electrorheological (ER systems), as they can be aligned by an applied electric field. The electrorheological (ER) effect, known as the enhancement of the viscosity when an electric field is applied perpendicular to the flow field, was first described by Winslow in 1949, when he observed an electrically induced fibration of small particles in fluid liquid suspension [12].

This work is devoted to design of several new calamitic reactive mesogenic materials together with characterisation of mesomorphic, structural and rheological properties.

Experimental

Synthesis and reagents

The synthesis of several new calamitic reactive mesogens was done according to the synthetic routes represented in Fig. 1. A brief description of the specific reactions and steps together with characterisation are presented in Results and Discussion Section. Chemical structure of reactive mesogens were confirmed by ^{1}H NMR, using a Varian VNMRS 300 instrument; deuteriochloroform ($CDCl_3$) and hexadeuteriodimethyl sulfoxide (DMSO-d6) were used as solvents and signals of the solvent served as internal standard. The chemical purity of all materials and intermediates was checked by high pressure liquid chromatography (HPLC), which was carried out using a silica gel column (Bioshere Si 100-5□m, 4x250, Watrex) with a mixture of 99.9 % of toluene and 0.1 % of methanol as an eluent, and detection of the eluting products by a UV-VIS detector (□ = 290 nm). The chemical purity was found between 99.5 % and 99.7 %.

Mesomorphic behaviour and structural properties

Sequence of mesophases was determined from the observation of textures and their changes in the polarising optical microscope (POM) - Nikon Eclipse E600POL (Nikon, Tokyo, Japan). Planar cells (bookshelf geometry) of 12 μm thickness (glasses with ITO transparent electrodes (5×5 mm^2) were supplied by Military University of Technology (Warsaw, Poland). The cells were filled with studied LC compounds in the isotropic phase by means of capillary action. The Linkam LTS E350 (Linkam, Tadworth, UK) heating/cooling stage with a TMS 93 temperature programmer was used for the temperature control, which enabled temperature stabilisation within ±0.1 K. The phase transition temperatures were determined by differential scanning calorimetry (DSC) using Pyris Diamond Perkin-Elmer 7 calorimeter (PerkinElmer, Shelton, CT, USA). The samples of about 4-8 mg, hermetically sealed in aluminium pans, were placed into the calorimeter chamber filled with nitrogen. Calorimetric measurements were performed on cooling/heating runs at a rate of 5 K min^{-1}. Temperature and enthalpy change values were calibrated on the extrapolated onset temperatures and the enthalpy changes of the melting points of water, indium and zinc.

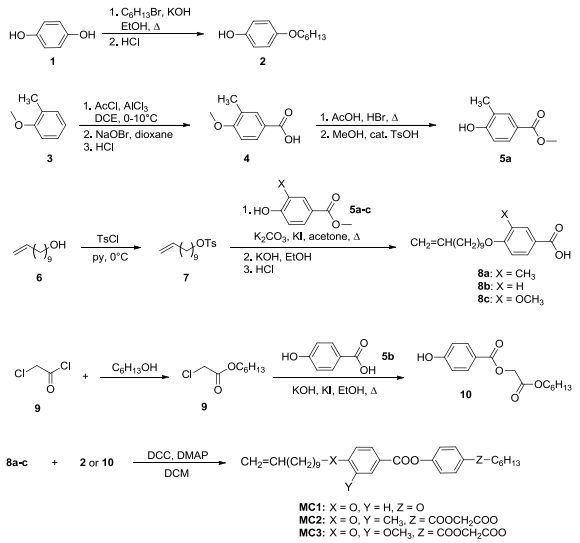

Figure 1. Routes to the synthesis of new calamitic reactive mesogens.

Rheological properties

Rheological characterization was performed using a Bohlin Gemini HR^{nano} rotational rheometer, to which a Bohlin electrorheological cell was coupled. Parallel plates (insulated upper plate of 50 mm diameter) geometry was used and the gap was set to 250 μm. Small angle oscillatory shear (SAOS) measurements and steady state measurements were performed at 60°C and 83°C, in the nematic and smectic A phases, respectively, without and with an electric field applied in the direction perpendicular to the flow direction, for electric fields strength up to 0–2 $kVmm^{-1}$. A pre-shear of 4 s^{-1} during 60 s, followed by an equilibration time of 120 s was imposed prior to the measurements. The electric field was generated by applying a high voltage to the gap between the plates. For the supply of high voltages, a DC power source (SPELLMAN SL150) was used.

Results and Discussion

Synthesis

All studied compounds have been synthesized according to the synthetic routes described in Figure 1 from commercially available starting materials. The methyl-substituted benzoate (5a) had to be synthesized since it was not commercially available. Its synthesis started from 2-methylanisole (3), which was acylated by acetyl chloride and obtained ketone was oxidized to benzoic acid via haloform reaction. After that, the hydroxylic group of the acid (4) was deprotected and finally the carboxylic group was esterified with methanol yielding desired benzoate (5a).The second part of the molecular core of MC2 and MC3 compounds was synthesized by the alkylative esterification of 4-hydroxybenzoic acid (5b) with *n*-hexyl chloroacetate (9), previously prepared by the reaction of choloroacetyl chloride (9) with *n*-hexanol. In the final step of the synthesis, benzoic acids (8) were esterified with phenols (2) or (10) using DCC coupling.

Properties of new materials

Mesomorphic behaviour

For newly designed liquid crystalline reactive mesogens, sequences of phases were determined by characteristic textures and their changes observed in POM. The phase transition temperatures and transition enthalpies were evaluated from DSC measurements. Sequence of phases and phase transition temperatures, measured on cooling, melting points, m.p. measured on heating and respective phase transition enthalpies, ΔH, obtained by DSC for all studied compounds are summarized in Table 1.

Let's compare the mesomorphic behaviour of three reactive mesogens with the same structure and differing

in the lateral substitution close to the polymerisable chain. In case of non-substitute MC1 reactive mesogen the nematic (N), the orthogonal smectic A (SmA) and orthogonal smectic B (SmB_{cr}) phases have been detected in a reasonably broad temperature range. A low temperature nematic phase has been detected for the MC2 reactive mesogen laterally substituted by the methyl group. Lateral substitution by the methoxy group fully suppresses the liquid crystalline behaviour of the MC3 reactive mesogen; melting point was found at about 65°C. The representative microphotographs of characteristic textures obtained by digital camera during observation of the planar samples in POM at crossed polarisers are presented in Fig. 2. For MC1 reactive mesogen the marble texture of the nematic phase (at 81°C) and the fan-shaped texture of the orthogonal SmA phase at (65°C) are presented on Fig. 2a and 2b, respectively. Typical Schlieren texture of the nematic phase (at 28°C) for MC2 reactive mesogen is presented in Fig. 2c. There was no considerable difference in the textures of the SmA and SmB_{cr} phases, hence the type of the lower temperature smectic phase for MC1 reactive mesogen was confirmed by the structural studies. Characteristic texture of the crystal phase (at 40°C) for MC3 reactive mesogen is shown on Fig. 2d.

Table 1. Sequence of phases and phase transition temperatures, T (°C), measured on cooling (5 K min^{-1}); melting points, m.p. (°C), measured on heating and phase transition enthalpies, ΔH [Jg^{-1}], obtained by DSC for the studied compounds ("●" the phase exists; "–"the phase does not exist).

	m.p./ΔH	Cr	T/ΔH	SmB_{cr}	T/ΔH	Sm A	T/ΔH	N	T/ΔH	Iso
MC1	59.0 [+96.3]	●	9.9 [-19.4]	●	44.4 [-9.7]	●	81.8 [-4.4]	●	83.6 [-4.6]	●
MC2	50.1 [+76.2]	●	-3.7 [-11.6]	-		-		●	31.7 [-2.6]	●
MC3	64.5 [+71.7]	●	51.8 [-71.7]	-		-		-		●

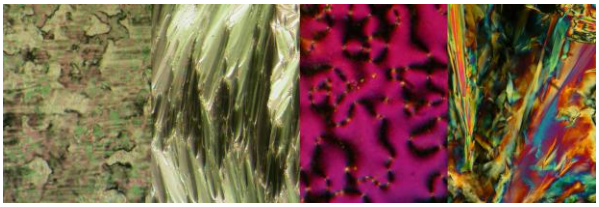

(a) (b) (c) (d)

Figure 2. Microphotographs of the textures obtained on cooling by POM on planar samples as indicated: (a) the marble texture of the nematic phase for MC1 at 81°C; (b) the fan-shaped texture of the orthogonal SmA phase for MC1 at 65°C; (c) the Schlieren texture of the nematic phase for MC2 at 28°C; (d) the structured lancets texture of the crystal phase for MC3 at 40°C.

Rheological characterization

Rheological studies without an applied electric field

Figure 3 presents the flow curves obtained for the SmA and nematic phases of MC1 reactive mesogen. It can be clearly observed that without applied electric field, this LC reactive mesogen presents a shear-thinning-type behaviour within the used shear rate range which may be attributed to the relatively high length of aliphatic chains and possible hydrogen bonding, both leading to intermolecular interactions. The values of the apparent viscosity are much higher for the SmA phase than that for the nematic phase, as expected, which is not only due to the decrease of the temperature but also to a higher order parameter characteristic of the smectic phases.

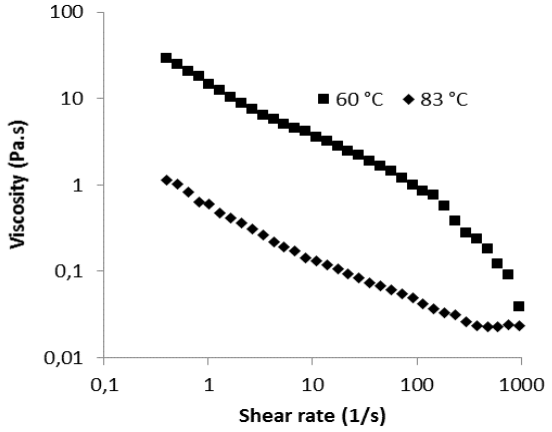

Figure 3. Shear rate dependence of the steady-state shear apparent viscosity in the SmA (at 60°C) and the nematic (at 83°C) phases of the MC1 reactive mesogen.

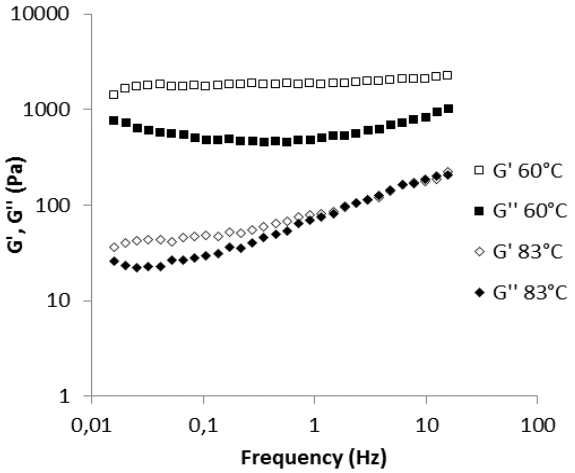

Figure 4. Angular frequency dependence of the complex viscosity and modulus obtained for the SmA (at 60°C) and the nematic (at 83°C) phases.

Figure 4 presents the elastic and viscous modulus (G' and G'') of MC1 reactive mesogen in the SmA and

nematic phases at selected temperatures. Its analysis shows higher values of both modulus for the SmA phase and that G' is much higher than G'' for this phase, which is expected in a phase showing a dominant elastic behaviour due to the layered organization. For the nematic phase G' and G'' present similar values, since the nematic is a much more fluid phase in character than the SmA phase.

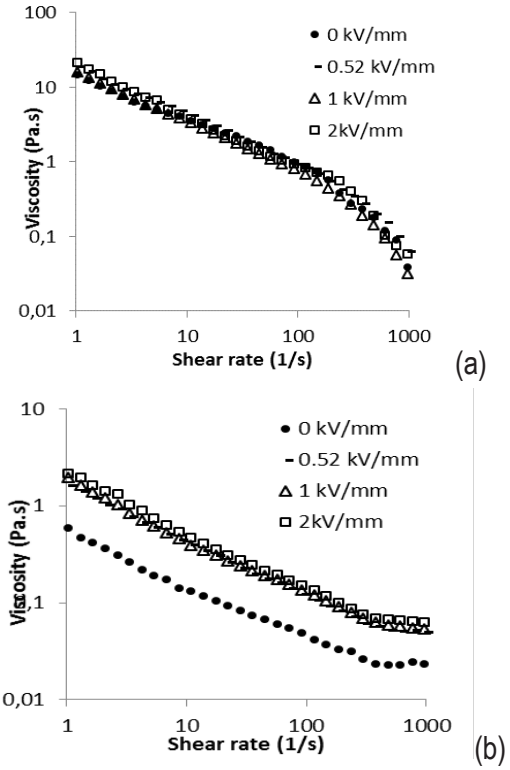

Figure 5. Shear rate dependence of steady state shear apparent viscosity for different electric field strengths (as indicated) for the SmA (a) and nematic (b) phases.

Rheological studies under applied electric field

The electroreological behaviour effect is observed in the nematic phase only. Figure 5 presents the viscosity curves obtained in the SmA (at 60ºC) and nematic (at 83ºC) phases of MC1 reactive mesogen under applied electric field ranging within 0-2 kV/mm.

In the nematic phase, the applied electric field increases the viscosity about four times, measured by the quotient between the viscosity at 2 kV/mm and the viscosity without electric field, for the smallest shear rate (1 s^{-1}), showing a positive ER effect. However, there are no significant differences under applied electric field from 0.52 kV/mm up to 1 kV/mm. This result indicates that the alignment of the molecules with the electric field occurs with a modest electric field and further increase of the electric field strength does not lead to better performance of the fluid in terms of the ER effect.

Acknowledgements

Authors greatly acknowledge the financial support from CSF 16-12150S research project and National Funds through FCT - Portuguese Foundation for Science and Technology, Reference UID/CTM/50025/2013 and FEDER funds through the COMPETE 2020 Programme under the project number POCI-01-0145-FEDER-007688.

References

1. Resetic A, Milavec J, Zupancic B, Domenici V, Zalar B. Polymer-dispersed liquid crystal elastomers. Nature Comm. 2016;7:13140.Kato T, Mizoshita N, Kishimoto K. (2006) Angew Chem Int Ed,;45, 38-68.
2. Lagerwall JPF, Scalia G. A. (2012) Curr Appl Phys, 12, 1387-1412.
3. Bubnov A, Iwan A, Cigl M, Boharewicz B, Tazbir I, Wójcik K, Sikora A, Hamplová V. (2016) RSC Advances, 6, 11577-11590.
4. Camacho-Lopez M, Finkelmann H, Palffy-Muhoray P, Shelley M. (2004) Nature Materials, 3, 307-310.
5. Jiang Y, Cong Y, Zhang B. (2016) RSC Advances, 6, 81902-81912.
6. A Bubnov, Kašpar M, Hamplová V, Glogarová M, Samaritani S, Galli G, Andersson G, Komitov L. (2006) Liquid Crystals, 33, 559-566.
7. Bubnov A, Novotná V, Hamplová V, Kašpar M, Glogarová M. (2008) Journal of Molecular Structure, 892, 151-157.
8. Kašpar M, Bubnov A, Sedláková Z, Stojanović M, Havlíček J, Obadović DŽ, Ilavsky M. (2008) European Polymer Journal, 44, 233-243
9. Resetic A, Milavec J, Zupancic B, Domenici V, Zalar B. (2016) Nature Comm, 7, 13140.
10. Zheng Y, Li S, Weng Z, Gao C. (2015) Chem Soc Rev., 44, 4091-4130.
11. Castellano JA. (2005). World Scientific Publishing. ISBN 978-981-238-956-5.
12. Winslow WM. (1949) J Appl Phys., 20, 1137-1140.

Contact Address:

Maria Teresa Cidade
mtc@fct.unl.pt
Department of Materials Science and Cenimat/I3N
Faculty of Sciences and Technologies
New University of Lisbon
2829-516 Caparica, Portugal
Telf.+351 212948584: ; Fax: +351 212957810

Effect of eco-friendly surfactant concentration on physical stability and rheological properties of green emulsions

L.A. Trujillo-Cayado, M.C. García, J. Santos, J.A. Carmona, M.C. Alfaro

[1] *Universidad de Sevilla, Grupo de Reología Aplicada. Tecnología de Coloides. Facultad de Química. C/ Profesor García González, 1, 41012, Sevilla (Spain)*

Introduction

Green solvents must meet a series of requirements such as being obtained from renewal raw materials, exhibiting fast biodegradability as well as low toxicity and playing the role of solvents to be substituted with the same or enhanced efficiency. This work deals with the development of emulsions containing green solvents, which may find applications as matrices for incorporation of agrochemical active ingredients. With a global population estimated to reach 9 billion people in 2050, the role of agrochemical turns out to be vital to increase the yield per hectare and to meet the requirements of food supply for all mankind. Emulsifiable concentrates (ECs) are among the most widely used agrochemical systems. However, in recent years there has been a strong trend to replace them with concentrated oil in water (O/W) emulsions (EWs). The partial removal of oil results in less phytotoxicity and skin irritation and the sizes of droplets can be adjusted to an optimum distribution, which is important for biological efficacy. In addition a formulation based on an aqueous continuous phase is by far more eco-friendly than the oil-based ECs. The use of green solvents, as alternatives to aromatic organic solvents, in agrochemical formulations follows the European Union guidelines towards the so-called sustainable development. In fact, many of classical solvents used in agrochemical applications have been banned or their use will be strongly restricted. Fatty acid dimethylamides (FAD) are among green solvents that can find applications in agrochemicals. α-Pinene is also a renewable solvent, which may be obtained from pine resins or distillation and can be formulated as O/W emulsions with the assistance of biopolymers. Polyoxyethylene glycerol esters derived from coconut oil are non-ionic surfactants, which fulfil the environmental and toxicological requirements to be used as emulsifiers in order to design eco-friendly products.

The most common emulsification methods are based on mechanical energy input. Rotor-stators, colloid mills, membranes, ultrasonic probes, high pressure-valve homogenizers and microfluidizers are currently used to prepare emulsions. Microfluidics is the methodology of choice if fluid-like emulsions with submicron mean diameters and narrow droplet size distributions (DSD) are the target, since they can reach extremely high shear rates [1].

Once emulsions are prepared, it is vital to detect at an early stage the onset of any destabilization process to shorten aging tests. In addition, determining the destabilization mechanisms provides outstanding feedback on formulation and processing variables. DSD is perhaps the most important factor in determining properties like biological efficacy, rheology or shelf-life stability of emulsions. On the whole, emulsions with smaller droplets and narrower DSDs result in longer stability. Rheology also provides useful information on the physical stability and handling properties of emulsions. A comprehensive assessment of emulsion stability involves monitoring the evolution of DSDs and key rheological variables over aging time. In any case, the most comfortable and informative technique to deal with the assessment of the physical stability of dispersions is Multiple Light Scattering (MLS). The cooperative information provided by the techniques listed above; along with microscopy usually offer a clear panoramic view of the stability of dispersions as a function of aging time.

The main objective of this work was to study the influence of surfactant concentration on the physical stability of slightly concentrated O/W emulsions formulated with these eco-friendly solvents. A further goal was to prepare stable fine emulsions developed by double channel microfluidization, which may be find applications as matrices for incorporation of active agrochemical ingredients. This formulation not only contains an eco-friendly surfactant but also a blend of two green solvents, which contributes to the increasing demand for the development of more sustainable chemical dispersions.

Experimental

30 wt% oil-in-water emulsions formulated with a non-ionic surfactant (glycereth-17 cocoate) at different concentrations were prepared using a mixture of green solvents, as dispersed phase. *N,N*-dimethyl decanamide (AMD-10™) and α-pinene were utilized with a 75/25 mass ratio.

Agnique AMD-10™ (density: 0.88 g/mL at 25ºC) was kindly provided by BASF. α-Pinene (density: 0.84 g/mL at 25ºC) was supplied by Sigma Chemical Company. The emulsifier used was a non-ionic surfactant derived from coconut oil. Namely, a polyoxyethylene glycerol fatty acid ester, glycereth-17 cocoate, received as a gift from KAO, was selected on account of its HLB number, 13. Its trade name is Levenol® C-201. The influence of Levenol® C-201 concentration on the stability and physicochemical properties of the emulsions was studied in the 1 to 5 wt% range.

Emulsions were prepared in two steps. First of all a Silverson L5M homogenizer equipped with a fine emulsor screen was used to prepare a coarse emulsion (primary homogenization). Subsequently, secondary homogenization was carried out with a Microfluidizer M110P so as to obtain lower droplet diameters and a narrower DSD.

DSD measurements were perfomed by laser diffraction with a Mastersizer X analyser (Malvern). These measurements were carried out after 1, 3, 13, 21 and 40 days aging time to check the possible occurrence of coalescence. The mean droplet diameter will be presented as volume mean diameter ($d_{4,3}$).

$$d_{4,3} = \frac{\sum_{i=1}^{N} n_i d_i^4}{\sum_{i=1}^{N} n_i d_i^3} \qquad \text{Eq. (1)}$$

Multiple light scattering (MLS) scans were carried out with a Turbiscan Lab-expert (Formulaction). Measurements were carried out for 40 days at 25 ºC to determine the predominant destabilization mechanism for each emulsion, as well as the kinetics of the destabilization process. The Turbiscan Stability Index (TSI) is a parameter that allows estimating emulsion stability. This parameter is a statistical factor and its value is obtained as the sum of all processes taking place in the studied probe. The TSI values were calculated according to the next equation:

$$TSI = \sum_{j} \left| scan_{ref}(h_j) \quad scan_i(h_j) \right| \qquad \text{Eq. (2)}$$

Where: H is the maximum height of the considered zone for the analysis, *h* is any given height from the bottom of the cell to the maximum height (H), and *i* is the number of scans. An increase of TSI values indicates that the system stability decreases.

The rheological characterization involved flow curves. Rheological experiments were conducted with a MARS controlled-stress rheometer (Haake, Germany) using a sandblasted Z20 coaxial cylinder geometry (R_i=1cm, R_e/R_i=1.085) for the curves and a sandblasted double-cone geometry (angle: 0.017 rad; diameter: 60 mm) for SAOS tests. The surface treatment of the sensor systems prevents wall-depletion (slip effects) from being significant under non-linear flow behaviour.

Flow curves tests were run by stepped shear rate ramps determined in controlled-stress mode (0.05-2 Pa). An approximation to steady state response of 0.01% for each step was used, fixing a maximum time per point of 180 s as cut off criterion.

All rheological measurements were carried out after 1, 3, 13, 21 and 40 days aging time to follow the effect of aging time and performed at 25ºC ± 0.1ºC, using a C5P Phoenix circulator (Thermo-Scientific, USA) for sample temperature control. Equilibration time prior to rheological tests was 180 s. All measurements were repeated 3 times for each emulsion. Results represent the mean of three measurements.

Resulting data from laser diffraction, multiple light scattering and rheological measurements have been analyzed using one-way analysis of variance (ANOVA) using StatPlus®:mac. All statistical calculations were conducted at a significance level of p = 0.05.

Results and Discussion

Figure 1 shows the volumetric mean diameters for emulsions formulated with a surfactant concentration from 1 to 5 wt%. These emulsions showed bimodal DSDs and an overwhelming number of submicron droplets. An increase of surfactant concentration up to 5 wt % resulted in a marked drop of volume mean diameters after 24 hours aging time as supported by standard deviation data and the ANOVA test ($p< 0.05$, p-value= 0.00). All $d_{4,3}$ values for the emulsion aged for one day were significantly different from each other except for 2 and 3 wt% (Tukey test, $p> 0.05$).

It is noteworthy that stable submicron emulsions were obtained at Levenol® C-201 surfactant concentrations within 2 and 3 wt%. The results obtained pointed to the occurrence of some coalescence for emulsions containing 1, 4 and 5 wt% surfactant. The increase in the $d_{4,3}$ values of the emulsion with less surfactant (1 wt%) can be ascribed to the occurrence of coalescence, enhanced by creaming of the bigger droplets. A depletion flocculation process may trigger coalescence in emulsions containing the higher surfactant

concentrations. This is provoked by exclusion of surfactant micelles between neighbouring oil droplets because of an osmotic pressure effect.

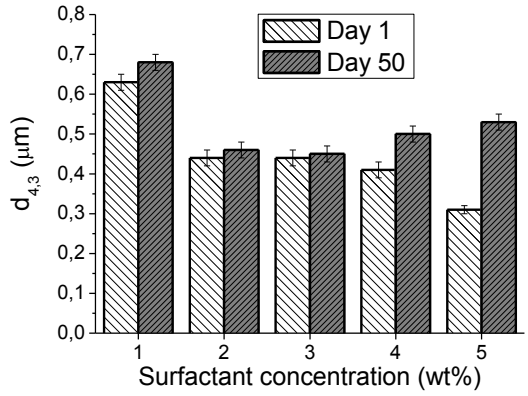

Figure 1. Volumetric mean diameter of oil droplets as a function surfactant concentration after one and fifty days aging time

Figure 2 shows the flow properties of emulsions aged for 24 hours as a function of surfactant concentration. The emulsion containing 1 wt% surfactant exhibited Newtonian behaviour (η= 5.02 mPa·s) at 20ºC. On the other hand, all emulsions in the (2-5) wt% concentration range exhibited shear-thinning behaviour. It must be noted that the rheological behaviour of emulsions aged for 24 h qualitatively shifted from Newtonian to non-Newtonian when increasing the Levenol® C-201 concentration by just 1 wt% (from 1 to 2 wt%). This is consistent with a marked drop in $d_{4,3}$, which must result in a substantial increase in the concentration of droplets (number of droplets per volume). In addition the non-Newtonian response is a clear indication of the formation of oil flocs, due probably to a depletion flocculation mechanism induced by the presence of surfactant micelles in the continuous phase.

The fluid-like behaviour of these emulsions at 20ºC was supported by their relatively low apparent viscosity values. By way of example, they increased at the maximum shear stress tested (2 Pa), from ca. 5 mPa·s for the Newtonian emulsions containing 1 wt% Levenol® C-201) to just ca. 30 mPa·s when the surfactant concentration was 5 wt%. Results for emulsions in the (2-5) wt% concentration range are consistent with the formation of slightly concentrated emulsions that are prone to form a weakly flocculated microstructure [2]. Their shear-thinning behaviour can be attributed to a shear-induced deflocculation process. Flow curves fitted modified power law equation (R^2>0.99) [2]:

$$= {}_1 \cdot \left(\frac{\dot{}}{1 s^{-1}} \right)^{n} \quad (3)$$

where τ_1 stands for the shear stress at 1 s^{-1}.

The values of fitting parameters corresponding to equation 3 are shown in table 1 for emulsions aged for 1 day. Table 1 illustrates the significant (according to the ANOVA test; $p < 0.05$) effects of both τ_1 (p-value= $2.28 \cdot 10^{-10}$) and n (p-value= $7.86 \cdot 10^{-13}$) on emulsions aged for 24 hours containing different surfactant concentrations.

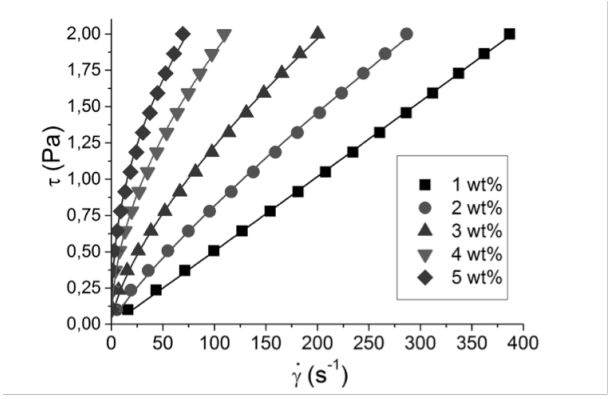

Figure 2. Flow curves of emulsions aged for 24 hours as a function of surfactant concentration. Continuous lines correspond to the power-law fitting equation. Standard deviation of the mean (three replicates) for τ_1 < 8%. Temperature = 20ºC.

Means with the same letter are not significantly different from each other (Tukey test, p> 0.05). The increase in τ_1, and consequently in apparent viscosity, as well as the drop in power law index values with surfactant concentration for emulsions aged for 1 day may be due to the formation of droplets with progressively lower mean diameters as well as to the increasingly greater number of micelles in the continuous phase,which yields a steady increase in viscosity of the continuous phase and also to the formation of increasingly flocculated emulsions due to depletion flocculation induced by surfactant micelles in the continuous phase [3].

Table 1. Flow curves fitting parameters for all emulsions studied aged for 24h.

Surfactant (wt%)	τ_1 (mPa)	n
1	4.75 ± 0.40	0.99 ± 0.01
2	17.40 ± 1.32	0.84 ± 0.01
3	53.19 ± 4.31	0.68 ± 0.01
4	162.68 ± 12.98	0.53 ± 0.01
5	299.5 ± 24.11	0.44 ± 0.02

Figure 3 shows the shear viscosity of emulsions at 1 Pa ($\eta_{T=1Pa}$) as a function of aging time and surfactant concentration. The increase in $\eta_{T=1Pa}$ after 1 day aging timee with surfactant concentration may be due to progressively lower mean droplet diameters and higher viscosities off continuous phases. The clear drop in viscosity of emulsions containing high surfactant

concentration was a further indication of coalescence induced by a previous depletion flocculation process, as also pointed by laser diffraction results.

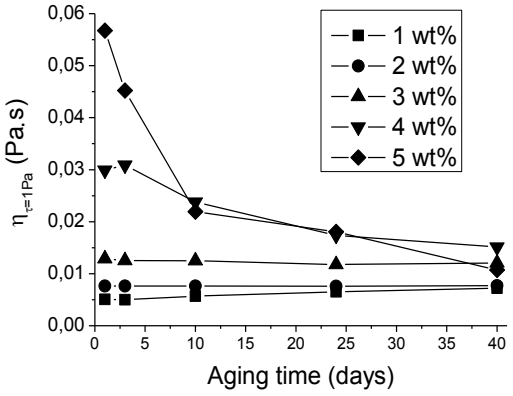

Figure 3. Shear viscosity at 1 Pa for all emulsions as a function of aging time and surfactant concentration.

Emulsions with 1, 4 and 5 wt% surfactant showed high values of TSI at the bottom of an emulsion sample placed in a Turbiscan measuring cell, which is indicative of a higher creaming rate (see Figure 4). This may be ascribed in the case of the emulsion containing 1 wt % surfactant to the facts it possessed the highest droplet size and the lowest zero-shear viscosity. It is noteworthy that the mean droplet sizes of emulsions with 4 and 5 wt % surfactant turned out to be quite low. Therefore, the reason behind the relatively high TSI values of these emulsions was different and must be likely due to the depletion flocculation process described above. Yet the formation of droplet aggregates can accelerate the creaming process without a change in the droplet size.

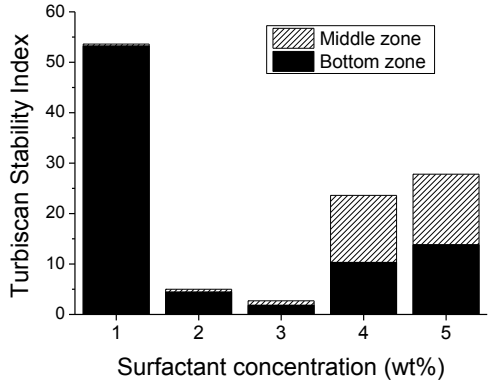

Figure 4. *TSI for emulsions aged for 40 days as a function of surfactant concentration in the middle and bottom zone of the measurement cell.*

The fact that TSI remained nearly constant in the intermediate zone suggests that de stabilization mechanisms like flocculation and coalescence were not significant in the 1-3 wt% range. Conversely, the higher TSI values in the intermediate zone for emulsions formulated with 4 or 5 wt % surfactant confirmed they underwent a flocculation process resulting eventually in some coalescence, as experimentally checked by laser diffraction (Fig 1) as well as by the rheological results obtained (Fig 3).

Concluding Remarks

Surfactant concentration exerted a marked influence on the droplet size distribution, rheological properties and physical stability of emulsions. The cooperative information provided by laser diffraction, multiple light scattering and rheology allows the physical destabilization of emulsions to be monitored and the dominant destabilization mechanism to be identified.

The emulsion containing 1 wt% of the nonionic Levenol® C-201 surfactant undergoes fast creaming after a rather short aging time, although coalescence later becomes the dominant destabilization mechanism as demonstrated by the cooperative information provided by multiple light scattering, shear flow curves and laser diffraction.

Depletion flocculation triggers coalescence, which becomes the main destabilization mechanism for emulsions formulated with the higher surfactant concentrations (4 wt% and 5 wt%).

Emulsions containing 2 wt% and 3 wt% nonionic Levenol® C-201 surfactant present the best results. The emulsion with 3 wt% surfactant exhibits the longest physical stability since it shows the longest delayed times for the onset of the creaming and coalescence mechanisms.

Acknowledgements

The financial support received (Project CTQ2015-70700) from the Spanish Ministerio de Economía y Competitividad and from the European Commission (FEDER Programme) is kindly acknowledged.

References

1. Santos, J., Trujillo-Cayado, L. A., Calero, N., Alfaro, M.C., & Munoz, J. (2016). *Journal of Industrial and Engineering Chemistry*, *36*, 90-95.

2. Trujillo-Cayado, L. A., Alfaro, M. C., Raymundo, A., Sousa, I., & Muñoz, J. (2016). Colloids and Surfaces B: Biointerfaces, *145*, 430-437

3. Pal, R. (2011). Current Opinion in Colloid & Interface Science, *16*(1), 41-60.

Contact Address:

Luis Alfonso Trujillo Cayado (ltrujillo@us.es)
Department of Chemical Engineering
Faculty of Chemistry, University of Seville
C/ Profesor García González, 1, 41012, Sevilla (Spain)
Telf.: +34 954 557180 ; Fax: 34 954 556447

Pharmaceuticals, Cosmetics and Medical Applications

A Preformulation Study of Hydrogels through a Double Crosslinking Strategy

*M. Pleguezuelos-Villa[2], A. Nácher[1-2], S. Mir-Palomo[2], M. J. Hernández[3], O. Vila Buso[4], V. Alonso Usero[5], A. Torrens[6], O. Díez-Sales[1,2 *]*

1 Instituto Interuniversitario de Investigación de Reconocimiento Molecular y Desarrollo Tecnológico (IDM), Universitat Politècnica de València, Universitat de València.
2 Departament of Pharmacy and Pharmaceutical Technology and Parasitology. Univ. Valencia (Spain)
3 Department of Earth Physics and Thermodynamics. Univ. Valencia (Spain)
4 Departament of Physical Chemistry.Univ. Valencia (Spain)
5 Department of Dermatology, Hospital 9 Octubre. Valencia (Spain)
6 Sesderma S.L.Valencia (Spain).

Introduction

Hydrogels (HG) are polymeric three-dimensional macromolecular networks formed by basic elements physically or chemically interconnected and swollen by a solvent. Polymeric HG has multiple applications. Due to their excellent biocompatibility they are used in materials for parenteral administration [1]. They are also frequently used as drug delivery systems because of their ability to hold liquids and bioactive compounds [2]. In this work, a polymeric HG has been prepared with highly biocompatible components such as gelatin (GL) and hyaluronic acid (HA), including different concentrations of genipin (GN), a compound derived from gardenia fruit. Gelation is attributed to the Schiff-base reaction between amino and aldehyde groups of biopolymers, and the subsequent crosslinking with GN.

In this HG a model drug as Propranolol HCl has been used. Rheological properties were determined by means of flow and dynamical tests. Moreover, HG has also been tested as drug carrier systems.

Experimental

A RheoStress 1 rheometer (Thermo Haake, Germany) equipped with control and data logging software (RheoWin 4.0.1) and a Haake D30 thermostat for sample temperature control were used for the measurements. After loading the samples they were kept at rest for at least 600 seconds prior to measurement, in order to remove any assembling strain. All measurements were performed in triplicate, at 25ºC, using a cone-plate sensor (2º, 35 mm diameter cone).

Three types of rheological measurements were performed: flow curves, oscillatory and creep-recovery tests.

Step flow curves were performed in controlled stress mode, so shear stress range was chosen in order to obtain viscosities corresponding to very low shear rates until approx. 100 s^{-1} (30 s each step).

In order to establish the linear viscoelastic range (LVR), stress sweeps at a frequency of 1 Hz were performed for all the samples.

Oscillatory measurements at a constant stress in LVR were performed, varying the frequency from 0.01 to 10 Hz (9 points per decade).

Creep and recovery tests in 300 s period each were also carried out (100 points recorded in logarithmic distribution).

Franz cells (Figure 1) were used to assess the drug release from hydrogels through artificial membranes to a receptor compartment, in a thermostatic bath (37.0 ± 0.5 °C). These conditions were chosen in order to represent the physiological conditions of human skin. The concentration of the drug in the obtained samples, after determined delivery times (from 0.5 to 24 h), were measured by HPLC.

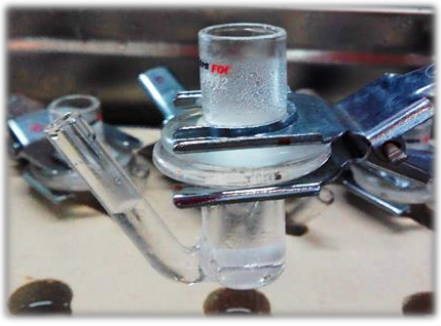

Figure 1. Franz'cells pictures.

Results and Discussion

The flow curves obtained for the different studied polymers are plotted in Figure 2. They were fitted ($r > 0.99$) to the Carreau simplified model

$$\eta = \frac{\eta_0}{\left[1+\left(\frac{\dot{\gamma}}{\dot{\gamma}_c}\right)^2\right]^s} \quad (1)$$

where η_0 is the zero shear viscosity, $\dot{\gamma}_c$ the critical shear rate and "s" the shear thinning index. The values obtained for these parameters and their standard deviations are indicated in Table 1.

Table 1. Mean and standard deviation for the parameters of the different polymers fitted to Carreau model (Eq. 1).

	η_0 (Pa s)	$\dot{\gamma}_c$ (s^{-1})	s (0.01)
GL/HA	245 (6)	0.046 (0.006)	0.29
GL/HA GN (0.04%)	2700 (70)	0.007 (0.001)	0.42
GL/HA GN (0.08%)	3645 (50)	0.003 (0.001)	0.42

The experimental values obtained in both rheological and delivery tests were analized using *SigmaPlot 10.0®* and *KaleidaGraph® (Synergy Software 4.03).*

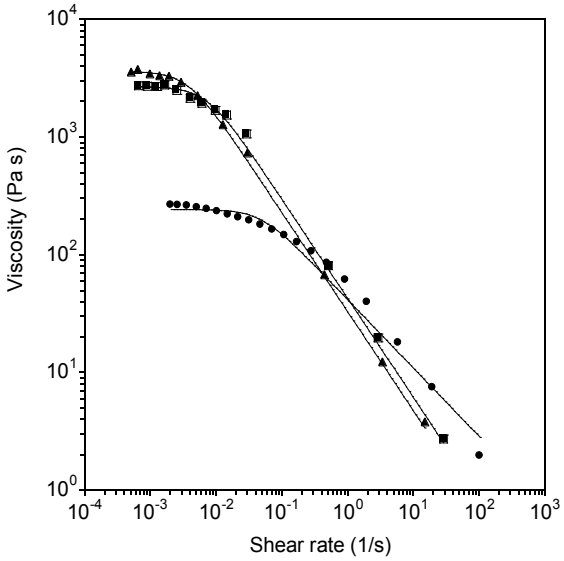

Figure 2. Flow curves fitted to Carreau model. GL/HA (●), GL/HA 0.04% GN (■) and GL/HA 0.08% GN (▲).

As it can be observed in Figure 2 and Table 1 the presence of GN increased both η_0 and shear thinning index (s) values. Including GN in GL/HA gels developed systems with zero shear viscosity one order de magnitude greater. This increment also depended on the concentration of GN. On the other hand, as a result of the differences in shear thinning behaviour and critical shear rates, the values of viscosity for high shear rates are greater for the hydrogels without GN.

In order to obtain information about the internal structure of the molecules, oscillatory tests were carried out. Obtained values for the elastic modulus or storage modulus (G') and loss modulus or viscous modulus (G") are shown in Figure 3.

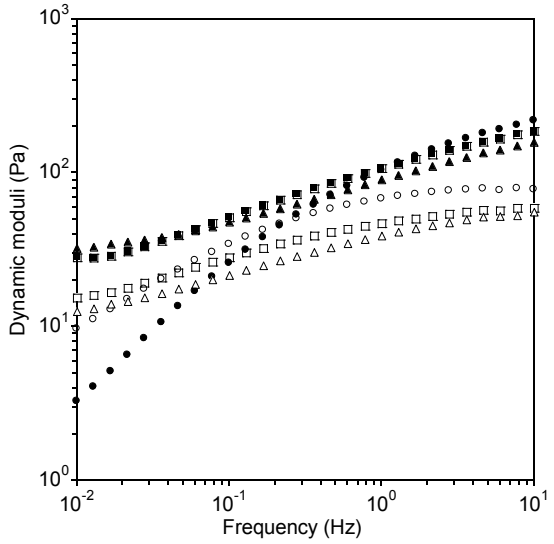

Figure 3. Dynamic moduli, G' (closed symbols) and G" (open symbols) versus frequency.GL/HA (●), GL/HA 0.04% GN (■) GL/HA 0.08% GN (▲).

It is interesting to point out that all HG had the same behaviour at high frequencies. However, the HG without GN presents a cross point for G' and G" at 0.2 Hz. Below this frequency, the viscous modulus is greater than the storage modulus, what could indicate the system presents macromolecular entanglements, but not a three-dimensional network. It seems that the presence of GN developed an internal network, as the systems GL/HA/GN present G'>G" for all the frequency range tested, with a typical weak gel dynamic spectrum.

In Figure 4, the corresponding loss tangent values are shown. The viscous behaviour the system without GN is clear, as tan δ are greater than 1 and strongly dependent on frequency. On the other hand, the HG including GN presented lower tan δ, almost no frequency dependent. Moreover, the values for the highest concentration of GN are lower, so we could

conclude the structuring increased with GN concentration.

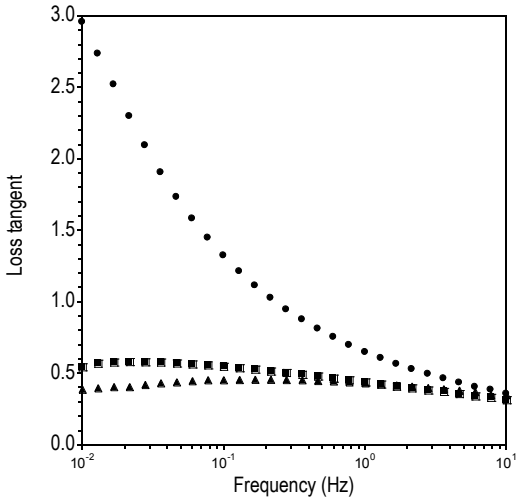

Figure 4. Loss tangent versus frequency.GL/HA (●), GL/HA 0.04% GN (■) GL/HA 0.08% GN (▲).

Figure 5 shows the creep-recovery tests for the HG assayed. The compliance values, J, for the creep part were fitted to Burger model

$$J(t) = \frac{1}{G_0} + \frac{1}{G_1}\left[1 - \exp\left(\frac{-G_1 t}{\eta_1}\right)\right] + \frac{t}{\eta_0} \qquad (2)$$

where G_0 is the elastic modulus of the Maxwell spring and G_1 is the elastic modulus of the Kelvin-Voigt unit. The residual viscosity, η_0, corresponds to the dashpot of the Maxwell element. The viscosity associated with the dashpot of the Kelvin-Voigt unit is known as the internal viscosity, η_1. This mechanical model is widely used due to its relative simplicity and the acceptable results obtained in many cases [3].

The values obtained for these parameters are indicated in Table 2. As it can be observed, the presence of GN provoked an increase in η_0 and G_0, when comparing to the control sample without GN. Therefore, including GN in the HG developed systems that are less deformable and more structured.

On the other hand, the total recovery percentage (R, %) have been calculated

$$R\,(\%) = \left(\frac{J_{Max} - J_{Min}}{J_{Max}}\right) \times 100 \qquad (3)$$

where J_{Max} the maximum compliance, prior to recovery, and J_{Min} the compliance at the end of the recovery time considered. For all systems assayed, the total recovery was similar, about 45%.

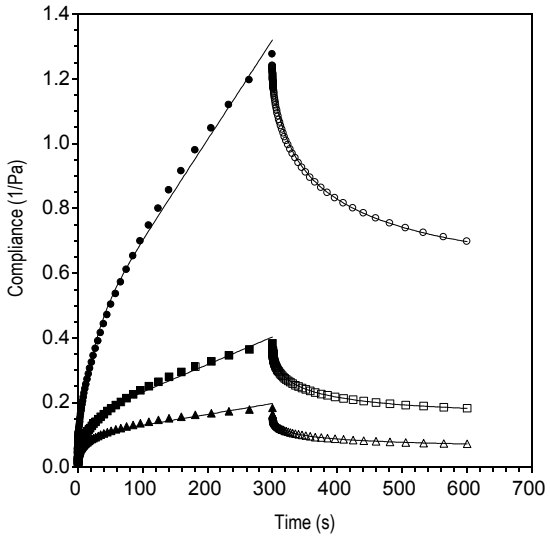

Figure 5. Creeps and recovery test for HG. GL/HA (●), GL/HA 0,04% GN (■) and GL/HA 0.08% GN (▲).

Table 2. Elastic moduli (G_o, G_1) and dashpot viscosities (η_0 and η_1) for mechanical Burguer model HG formulations.

	η_0 (Pa s)	G_o (Pa)	η_1 (Pa s)	G_1 (Pa)
GL/HA	32 (7)	18 (1)	65 (3)	2.9 (0.1)
GL/HA GN (0.04%)	1180 (40)	40 (2)	123 (8)	8.2 (0.2)
GL/HA GN (0.08%)	2950 (140)	41 (2)	142 (13)	13.9 (0.4)

Finally, Figure 6 shows the percentages of propranolol released at 25 h for the different formulations. The mean release profiles (% cumulative drug release) were fitted according to Korsmeyer-Peppas equation to describe the drug release mechanism.

$$\frac{M_t}{M_\infty} = K\,t^n \qquad (4)$$

where M_t and M_∞ are the absolute amount of drug released at t and infinite time, respectively, K is a constant reflecting structural and geometric characteristics of the device and n is the release exponent characterizing the diffusion mechanism.

Taking into account the results obtained the HG with 0.08% GN [K= 4.1 (± 0.1) h^{-1}] provided a drug release slower than 0.04% GN [K= 0.66 (±0.01) h^{-1}] and the n value was close to 1.0 indicating zero – order release kinetics (n > 0.7).

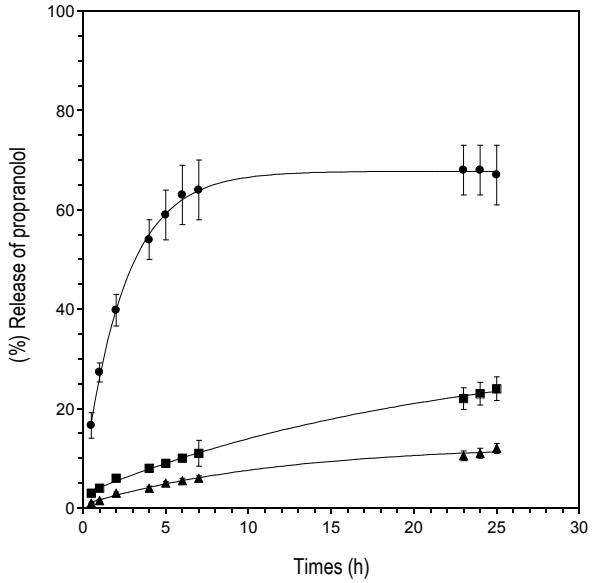

Figure 6. Propanolol percentages released from hydrogels formulated. GL/HA (●), GL/HA 0.04% GN (■) and GL/HA 0.08% GN (▲).

In conclusion, this study demonstrates that double crosslinked GL/HA with GN hydrogels have ideal rheological properties and could be potentially used for drug sustained release.

References

1. Jalani, G. Rosenzweig, DH. Makhoul, G. Abdalla, S. Cecere, R. Vetrone, F. (2015). Tough, in-situ thermogelling, injectable hydrogels for biomedical applications, Macromol Biosci, 15 (4), 473-80.
2. Reyes-Ortega, F. Cifuentes, A. Rodríguez, G. Aguilar, MR. González-Gómez, Á. Solis (2015). Bioactive bilayered dressing for compromised epidermal tissue regeneration with sequential activity of complementary agents, Acta Biomater, 23,103-115.
3. Dolz M, Corrias F, Díez-Sales O, Casanovas A., Hernandez-Lucas M.J. (2009). Influence of Test Times on Creep and Recovery Behavior of Xanthan Gum Hydrogels. Appl Rheol.; 19 (3), 34201–34208.

Contact Address:

**Octavio.diez.uv.es*
Department of Pharmacy and Pharmaceutical Technology,
Faculty of Pharmacy
Univ. Valencia
Spain

A comparative rheological study of several dentifrices trademarks

J.A. Picó[1], J. Peris[1], A.Sánchez[1], M.J. Hernández[2] A. Nacher[3], O. Diez-Sales[3]

[1]Research and Development Department, KOROTT, SL. Polígono Santiago Payá, 03801 Alcoy (Spain)
[2]Department of Earth Physics and Thermodynamics, Faculty of Physics, University of Valencia, 46100 Burjassot, Valencia (Spain)
[3]Dep. Pharmacy and Pharmaceutical Technology and Parasitology, Fac. Pharmacy, Univ. Valencia, 46100 Burjassot (Spain)

Introduction

Dentifrices are considered to be semi-solid products which are designed to clean the teeth and provide a fresh and pleasant breath. The attributes that initially attract consumers in the purchase of the toothpaste are: advertising and promotion, the design of its container and aroma given off when being used. On the other hand, the acceptance of daily use is a combination of the stability of the product, the viscosity of the dentifrice in its tube and immediately after extrusion, viscosity in the oral cavity during brushing, etc. The rheological characterization of toothpastes plays an important role in the definition and control of these attributes [1]. In order to be an acceptable product it should be easily extrudable from the package ("squeezing out"), it should keep enough tightness ("stand up") over the toothbrush (Figure 1), and also generate a pleasant foam and have a good flavor for the consumer [2, 3] .

"Stand up"

"Squeezing out"

Figure 1.Important rheological properties

The main objective is this work is the rheological characterization of the products manufactured by different toothpaste brands, comparing the values obtained for some of those characteristic parameters.

Experimental

Toothpastes studied

A total of 13 dentifrices manufactured by the 5 trademarks with the greatest sales volume that are distributed in mass markets in Spain were studied. Commercial names and composition are shown in Table 1. Main ingredients (humectants, thickening and abrasive agents) are listed in decreasing order depending of the concentration (exacts amounts are unknown). The hydrocolloid used is also listed in Table 1, as we consider it could be important for the final texture of the product.

Table1. Composition of the dentifrices studied.

	Main ingredientes	***Hydrocolloid***
"Accion total"		
Colgate®Total	Aqua/Glycerin/ Hydrated Silica /PVM/MA copolymer	Cellulose /Carrageenan
Colgate® Protección caries	H_5CaO_6P/Aqua/Glycerin	Cellulose
Binaca® Antiplaca	Aqua/Sorbitol/Hydrated Silica/(Bradosol®)	Xanthan
Sensodyne® Protección total	Aqua/Sorbitol/Hydrated silica/Glycerin/KNO_3	Xanthan
Kemphor® Original	Aqua/Glycerin/Hydrated Silica/Sorbitol	Cellulose
Colgate® triple acción	Aqua/Glycerin/Hydrated Silica/PEG-12	Cellulose
Korott® Acción total	Aqua/Sorbitol/Hydrated Silica/Glycerin/PEG-12	Cellulose
"Blanqueante"		
Signal ® Blanqueador	Aqua/Sorbitol/Hydrated Silica/$NaHCO_3$/PEG-32	Cellulose
Colgate® Sensation Blanqueador	Aqua/Hydrated Silica/Glycerin/Sorbitol/ $NaHCO_3$	Carrageenan
Sensodyne® Blanqueante	Aqua/Hydrated Silica/ Sorbitol/ Glycerin/$Na_5O_{10}P_3$ x H/ KNO_3	Xanthan
Korott® Blanqueante	Aqua/Sorbitol/Hydrated Silica /Glycerin/ $Na_4P_2O_7$	Cellulose
"Gel"		
Colgate® Max fresh	Sorbitol/Aqua/ Hydrated Silica	Hydroxypropyl Metyl cellulose
Korott® Gel	Sorbitol/Agua/Hydrated Silica/Glycerin/PEG-12	Cellulose

They are grouped in three categories, according to their commercial denomination. "Acción total" are those with a

general action, ready to be used in the daily oral care. "Blanqueante" dentifrices include whitening agents and they have a more abrasive composition for a dental stains removal function and a deeper cleaning. "Gels" dentifrices have a characteristic transparency which is achieved with a higher concentration of sorbitol (in order to equal silica refraction index). They are also perceived with a fresher flavor by the consumers.

Rheological measurements

Experiments were carried out at 20ºC in a controlled stress rheometer DHR-1 (TA Instruments) with a Peltier plate for temperature control. Serrated and smooth 40 mm diameter parallel plates (1 mm gap) were used. All measurements were repeated at least twice.

Steady-state flow curves (3% tolerance) were performed, in CS mode, varying stresses from 10 to 15000 μNm.

After determining linear viscoelastic region from oscillatory stress sweeps, dynamic moduli were obtained through frequency sweeps in the range of 0.05 to 100Hz, at different stress amplitudes between 0.4 and 1 Pa.

Results and Discussion

Flow curves

All analyzed toothpastes had a strong dependence of viscosity with shear rate and they were fitted satisfactorily (r >0.995) to the Carreau simplified model

$$\eta = \frac{\eta_0}{\left[1+\left(\frac{\dot{\gamma}}{\dot{\gamma}_c}\right)^2\right]^s} \qquad (1)$$

where η_0 is the zero shear viscosity, $\dot{\gamma}_c$ the critical shear rate and s the shear thinning index.

The flow curves and the corresponding fits are shown in Figure 2. All the dentifrices are highly shear thinning products. This is in accordance with the functionality of this kind of products, as they must be firm and tight on the brush but easily spreadable when brushing on the teeth.

The zero viscosity, η_0, corresponding to the constant plateau for very low shear rates in Figure 2, can be related to the "stand up" parameter (Figure 1). High values ranging from 10^3 to 10^4 Pa s are observed in Figure 2, while viscosities corresponding to brushing shear rates are about 1 Pa s.

In order to simplify the comparison between products, the viscosity "at rest", η_0, and viscosity for movement, at 10 s^{-1}, η_{10}, are shown in bar graphs in Figure 3 (in a linear scale). It is interesting to point out that the different dentifrices manufactured by Colgate® showed slightly lower values compared to the rest of brands products.

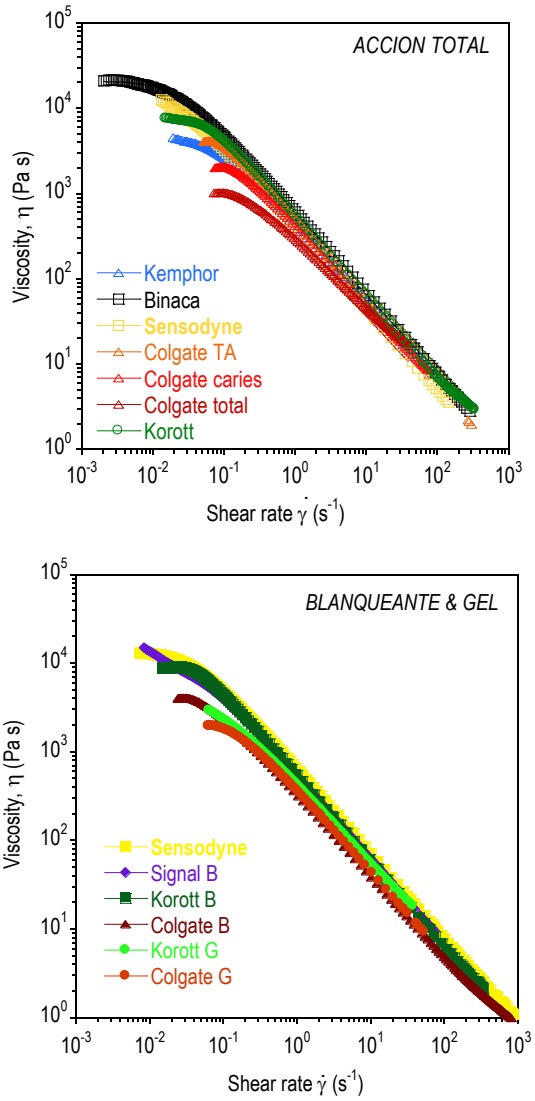

Figure 2. Flow curves for all the toothpastes studied, grouped as indicated in Table1.

The variability observed in zero viscosity values, η_0, or "stand up", is large between the different toothpastes, even an order of magnitude (Figure 2). However, differences are minimized when comparing η_{10}, since all of them are around 50 Pa s. From a practical point of view, this indicates that the differences appreciated between the pastes just out of the tube won't be noticed in the mouth during brushing.

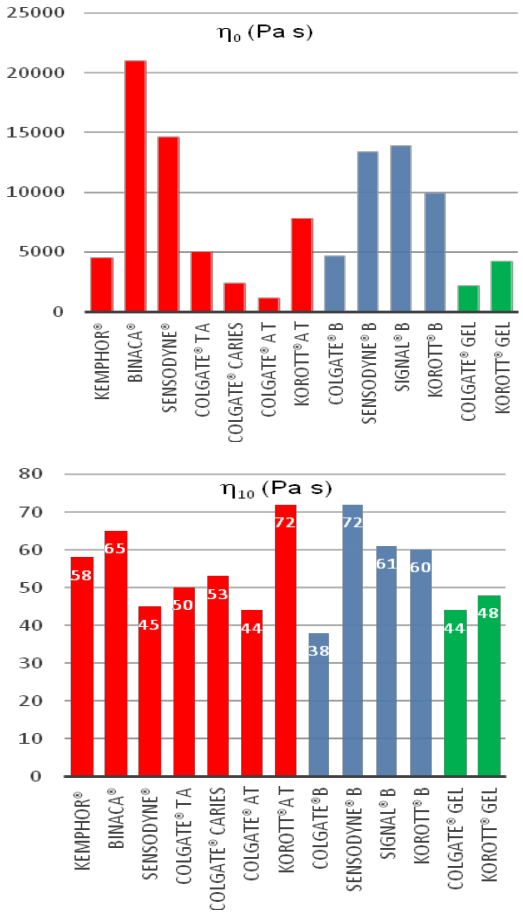

Figure 3. Zero viscosity and viscosity at 10 s^{-1} measured in the different toothpastes tested (■ "acción total", ■ "blanqueante" and ■ "gel").

The practical "squeezing out" parameter, characterizing toothpaste, could be related with the yield stress, σ_0. These values had been obtained from the viscosity versus stress plots, calculating the value of stress corresponding to the beginning of the viscosity drop. They are shown in Figure 4 in a bar chart.

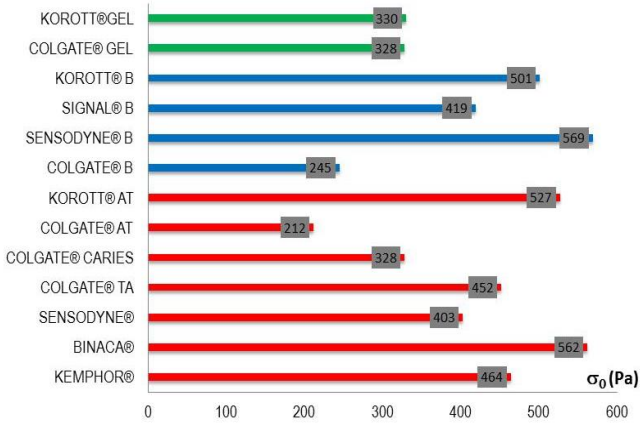

Figure 4. Toothpastes yield stress values (■ "acción total", ■ "blanqueante" and ■ "gel".)

The yield stresses obtained ranged from 300 to 550 Pa approx. A high value for the minimum stress necessary to flow is characteristic of dentifrices. Again Colgate® products stand over the rest, showing the lower σ_0, only comparable to Korott® gel (even lower than 300 Pa)

Viscoelastic properties

All the toothpastes studied from the different trademarks had a predominance of elastic moduli over viscous moduli (G'>G") in common, which indicates a gel-like behavior, typical of systems with a complex internal structure.

Since all the storage moduli obtained were straight lines in log-log plots of G' versus frequency, there were fitted to empirical power equations in order to compare the results

$$G' = G'_1 \nu^m \qquad (2)$$

where G'_1 corresponded to the storage modulus for 1 Hz and exponent m gave information about frequency dependence. The obtained values for these fits are shown in Table 2.

Table2. Values of the parameters G'_1, m obtained from fitting G', to eq. (2).

	G'_1 (Pa)	m
"Accion total"		
Kemphor®	6410 (63)	0.173 (0.002)
Binaca®	12110 (57)	0.083 (0.002)
Sensodyne®	18452 (85)	0.040 (0.002)
Colgate® TA	2921 (12)	0.170 (0.001)
Colgate® caries	1970 (15)	0.223 (0.002)
Colgate® AT	728 (12)	0.371 (0.004)
Korott ®	5938 (18)	0.141 (0.001)
"Blanqueante"		
Colgate® B	1936 (18)	0.150 (0.003)
Sensodyne® B	9191 (38)	0.115 (0.001)
Signal® B	10186 (40)	0.080 (0.002)
Korott® B	5024 (33)	0.128 (0.002)
"Gel"		
Colgate® G	3327 (47)	0.151 (0.005)
Korott® G	4075 (41)	0.143 (0.003)

In order to evaluate and compare the viscoelastic nature of the toothpastes, loss angles, δ, were also calculated. They are plotted in Figure 5 as a function of frequency.

The two dentifrices with the highest values of yield stress presented also the highest values of storage modulus, and the lowest values of loss angle, δ (Binaca® and Sensodyne® in "accion total"). This

indicated they are the systems with a strongest internal structure, maybe responsible of the greatest σ_0.

On the other hand, the dentifrice with a lowest zero viscosity and the lowest yield stress (Colgate® AT), also presented the lowest value for storage modulus and the highest values of loss angle, which implied it had the weakest structure, maybe responsible of its easy flow.

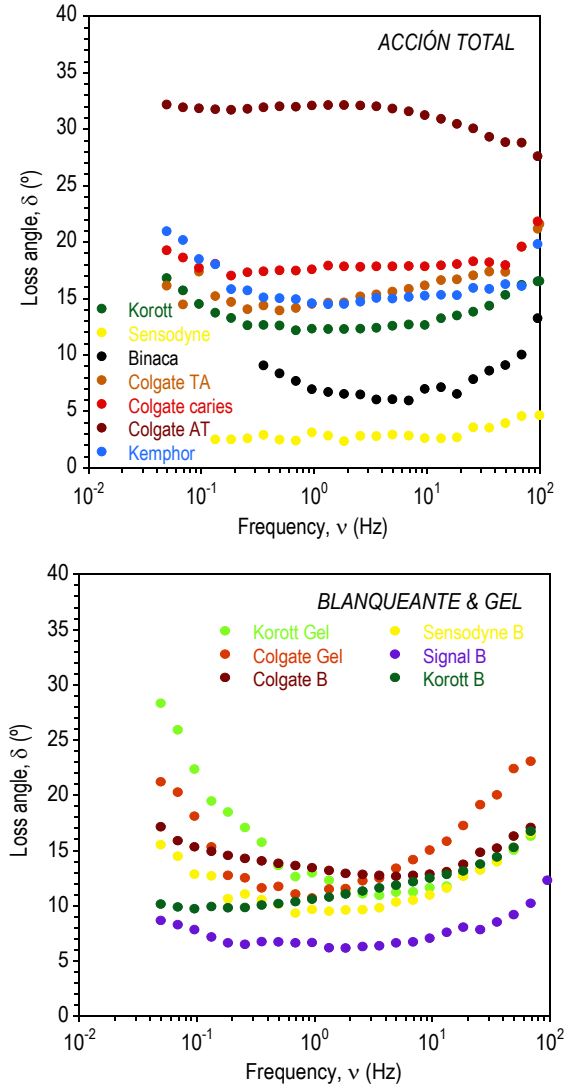

Figure 5. Loss angle δ as a function of frequency for the toothpastes studied.

These differences observed in viscosity and viscoelasticity of Colgate® toothpastes would be attributable to the absence of sorbitol, or just a small amount in the majority of its formulations.

Moreover, the results obtained for Sensodyne® and Binaca® could be due to the use of xanthan gum and potassium salts in their formulations, what contributes to a formation of an internal gel network.

Conclusions

All the dentifrices studied (pastes and gels) showed a highly shear thinning and viscoelastic behaviour, with a typical weak gel-like structure. As a result of the different shear thinning behavior, the differences observed in visual consistency ("stand up") on the brush are reduced for higher shear rates, when the brush is moving on the teeth.

The variability in the concentration of moisturizers, silica and hydrocolloid provides a different structure in the analyzed toothpastes.

References

1. Pader, M. (1988) *Oral hygiene products and practice*. Cosmetic science and technology series, vol. 6. Marcel Dekker, Inc., New York.
2. Laba, D.(1993) *Rheological properties of cosmetics and toiletries*. Cosmetic science and technology series, vol. 13. Marcel Dekker, Inc., New York.
3. Prencipe, M., Masters, J.G., Thomas, K.P. & Norfleet, J. (2016), 01-02-2016-last update, *Squeezing out a better toothpaste* [Homepage of British American Tobacco], https://industrydocuments.library.ucsf.edu/tobacco/docs/#id=sgfb0205 [1995, Febrero 2013]

Contact Address:

japico@korott.com
Research and Development Department, KOROTT, SL.
Address: Polígono Santiago Payá, 03801 Alcoy (Spain)
Telf.+34 966526550 ; Fax:+34 966522718

The impact of thickeners and surfactants on the rheology of hair cleansing products

A Nunes[1], J Marto[2], J Sotomayor[3], HM Ribeiro[2]

[1] Departamento de Química, Faculdade de Ciências e Tecnologia, Universidade Nova de Lisboa, Caparica, Portugal
[2] Research Institute for Medicine and Pharmaceutical Science (iMed.ULisboa), Faculty of Pharmacy, Universidade de Lisboa, Lisboa, Portugal
[3] LAQV, REQUIMTE, Departamento de Química, Faculdade de Ciências e Tecnologia, Universidade Nova de Lisboa, Caparica, Portugal

Introduction

Shampoos are products designed to cleanse, condition and provide a pleasant fresh, clean residual scent to hair.

The shampoo formulation comprises, among others, water, surfactants, thickening agents and other components. The main constituent of hair cleansing product is the surfactant due to its detergent properties. With the growth in demand for environmentally-friendly products steadily on the rise, it's natural that only naturally-derived surfactants are a category sparking interest among formulators.

The detergents molecules or surfactants are considered amphiphiles, being composed of long carbon chains with a polar end. The carbon chains present in surfactants are hydrophobic (lipophilic) sites that attract the soluble components (oils). On the other hand, the polar end consists of hydrophilic groups, consequently, attract the water soluble components (water) [1-6]

Rheological (thickening) agents are multi-functional, ubiquitous ingredients found in most formulations that can significantly impact stability and performance. Learning how to choose the correct technology for formulation can dramatically improve in use product performance and stability.

To meet this objective, 16 formulations composed of naturally-derived surfactants, (sugar based), in this case, by decyl glucoside and acylamino acids (amino acids based). Different thickeners such as cocamide DEA, PEG-18 glyceryl oleate, PEG-free formed by sorbitan sesquicaprylate and, finally, HPMC were used to assess the rheological characterization, foaminess and pH and compared with a formulation with sodium laureth sulfate (SLES).

Experimental

The surfactants used in this study were: EcoSense® 1000 from Dow (decyl glucoside), AMILITE® ACS-12 (Sodium Cocoyl Alaninate), AMILITE® GCS-12K (Sodium Cocoyl Glycinate) from Ajinomoto.

Different thickeners, cocamide DEA (Rewomid® DC212 S from Evonik), sugar based composed of PEG-18 glyceryl oleate (Antil® 171 from Evonik), PEG-free formed by sorbitan sesquicaprylate (Antil® Soft GC from Evonik) and, finally, HPMC (Sigma) were used to assess the rheological characterization, the foaminess and pH.
16 formulations were prepared using the same amount of active substance (detergent) (9%).

A formulation with sodium laureth sulfate (SLES, Texapon® N40 from BASF) was used as control.

The pH was measured with a potentiometer while the foaminess and foam stability were determined using a vortex for 15 seconds and measuring the foam height for 90 minutes. The rheological characteristics of the shampoos were examined at high shear rates using continuous shear techniques and in the viscoelastic region using oscillation techniques. These experiments were performed with a controlled stress Kinesus Rheometer (Malvern) using cone and plate geometry (truncated cone angle 4° and radius 40mm). The frequency sweep method was performed between 0.1Hz and 10Hz, with a shear strain of 0.8%, at 25ºC, while the table of shear rate method was performed by increasing the shear rate from $0.1s^{-1}$ to $100s^{-1}$, at 25ºC. The shear stress was measured by this method and the apparent viscosity was calculated by dividing the shear stress by the shear rate. This last method was used to verify the behavior of formulation with the increase of shear rate.

Results and Discussion

Most of the created formulations showed low viscosity, being liquid. All SLES formulations and amino-acid based, when HPMC was used as thickener, presented acceptable viscosity for shampoos. Thus, these were the only analysed in this work and its composition is found in table 1.

Table 1 – Formulations with acceptable viscosity for shampoos.

	Formulations (%)					
Ingredients	**1**	**2**	**3**	**4**	**12**	**16**
Water	80.00	80.00	80.00	83.00	83.00	83.00
SLES	37.04	37.04	37.04	37.04	-	-
Sodium cocoyl alaninate	-	-	-	-	33.33	-
Sodium cocoyl glycinate	-	-	-	-	-	33.33
PEG- free	5.00	-	-	-	-	-
PEG-18 glyceryl oleate	-	5.00	-	-	-	-
Cocamide DEA	-	-	5.00	-	-	-
HPMC	-	-	-	5.00	5.00	5.00

Concerning the pH values, it can be stated that the values vary between 8.91 and 5.73 appropriate for shampoos. The formulation with higher pH it's the one that has the SLES as surfactant and the traditional thickener while, the formulation with SLES as surfactant and a sugar based thickener has the lowest pH as can be seen in table 2.

The pH values obtained were expected since these results are in accordance with each ingredient's pH. For example, formulation 3 is the one that presents a higher pH as cocamide DEA has a pH between 8 and 10.5, causing an increase in pH's formulation.

Table 2 - pH values of each one of the formulations analysis.

	1	**2**	**3**	**4**	**12**	**16**
pH	6.16	5.73	8.91	6.55	7.92	8.11

Concerning the stability of the formed foam, it has been found that when SLES is used as a surfactant, it promotes stable foam, unlike the amino acid based surfactant (table 3). The formulation with higher foam stability it's the one that has the SLES as a surfactant and cocamide DEA as a thickener (formulation 3) while, the formulation with the sodium cocoyl alaninate as a surfactant and the HPMC as a thickener (formulation 12) did not produce higher foam.

Table 3. Length of the formed foam (in centimetres) in function of the time (in minutes).

	Time (min)			
Formulations	**0**	**30**	**60**	**90**
1	0.4	0.2	0.2	0.2
2	1.2	1.1	1.0	0.9
3	0.4	0.3	0.2	0.2
4	0.7	0.4	0.4	0.3
12	1.5	0.4	0.4	0.3
16	1.0	0.7	0.5	0.4

All formulations are comprised of anionic surfactants, where the hydrophilic polar group is negatively charged. As described before, the stronger the link between the water and the surfactant, the greater the stability of surfactant foam formed. Thus, the anionic surfactants, due to the strong bond with the water, presents high and stable foam when compared with non-ionic surfactants. Through the analysis of table 3, SLES formulations present higher foam stability. The anionic surfactants sodium cocoyl glycinate and sodium cocoyl alaninate present two oxygen atoms in the polar end of the molecule being thus able to make bonds with water. On the other hand, SLES have at least four oxygen atoms available to interact with water producing a foam with great stability, regardless of the thickener used.

Water-soluble polymers, such HPMC, can interact with the surfactants creating both an increased surface viscosity and a stearic repulsion between the two surfaces (surface and bulk) in the foam lamellae, thus enhancing the stability of the foam.

The shampoos were analysed by observing the behaviour of viscosity as a function of shear rate applied and the behaviour of elastic and viscous component of the shampoos as a function of frequency.

Analysing the figures 1 and 2, representing the apparent viscosity as a function of shear rate, it is possible to identify the thickener (HPMC) that is responsible for the shampoo's higher viscosity values regardless the surfactant used. Swellable polymers (HPMC) are the most common rheological agents used in water formulations because they thicken water continuous formulations.

Sodium cocoyl alaninate is the surfactant which was answerable for the higher shampoos' viscosity regardless of the thickener used.

The increase of the viscosity of a formulation is entirely related to the number of carbons in the carbon chain of the main surfactant. With increase in the number of

carbons, in the carbon chain of the molecule, there is an increase in molecular weight and, consequently, a higher viscosity in the formulations. Sodium cocoyl alaninate presents a carbon chain C15, while SLES presents a C12-C14 carbon chain and the sodium cocoyl glycinate, a C11. Thus, sodium cocoyl alaninate is the one that offers greater viscosity due to the biggest length of its carbon chain.

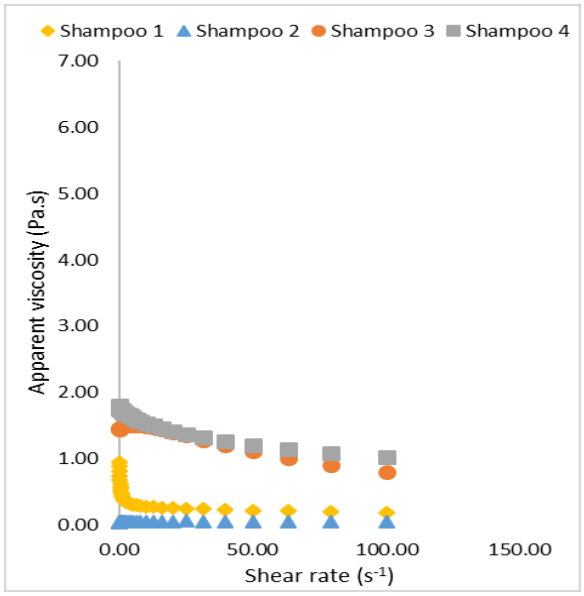

Figure 1. Apparent viscosity Vs shear rate for shampoos with SLES as a surfactant

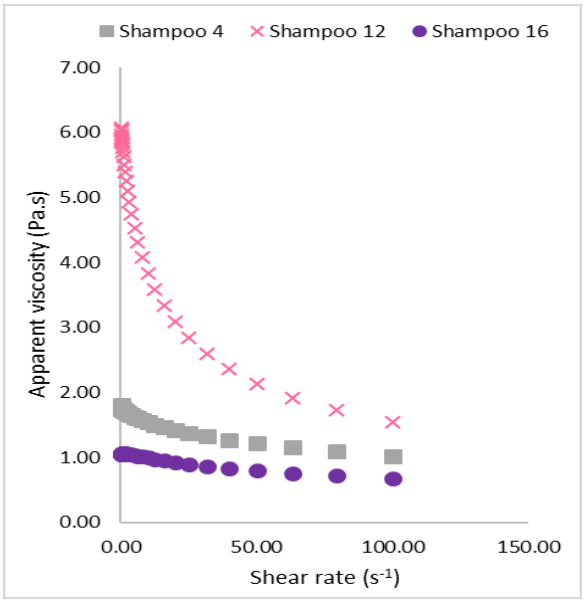

Figure 2 . Apparent viscosity Vs Shear rate for shampoos with Cellulose HPHC as a thickener.

In all formulations, the G" > G', meaning, these formulations have the viscous modules superior to the elastic modules presenting a weak network that allows the good flow allowing a good spreadability of the products on the hair (figure 3). Thus, in the formulations depicted in these figures the only change is the type of thickener used, making it possible to compare these two components with the type of thickener. Shampoo 3 presents the maximum value of elasticity, while shampoo 2 has a lower value.

It can be verified that when the cocamide DEA and HPMC are used as thickeners with SLES, the viscosity increases, in comparison with the other thickeners used. The smallest value of viscosity is when the PEG-18 glyceryl oleate is used as thickener, independent of the surfactant used.

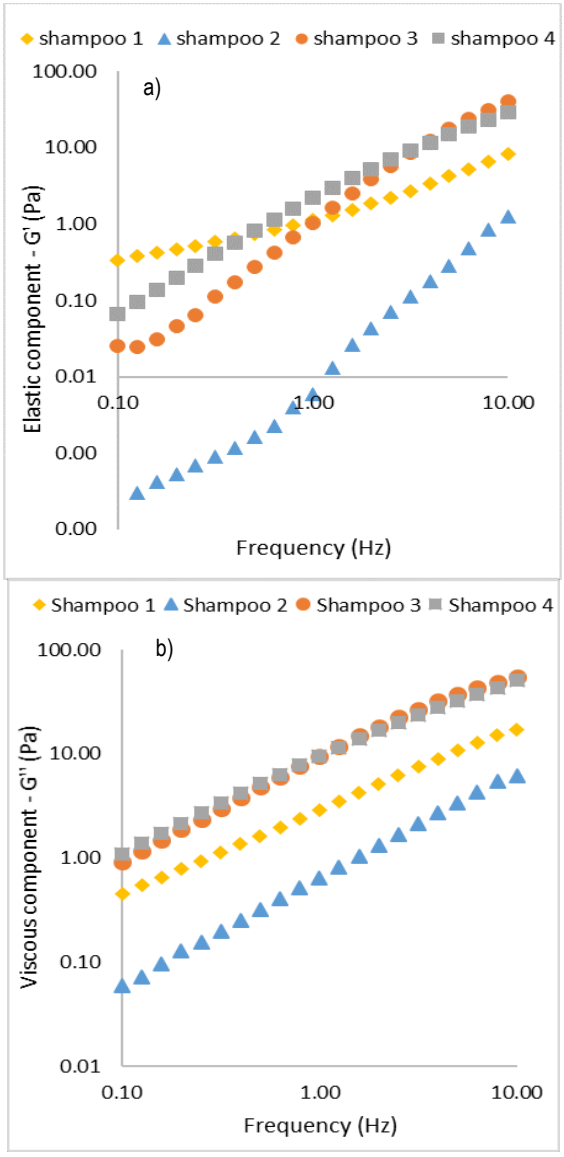

Figure 3 . a) Elastic component (G') for 4 different shampoos; b) and Viscous component (G") for 4 different shampoos.

In conclusion, both thickeners and surfactants have great impact in hair cleansing products properties depending on their chemical origin of the raw material.

References

1. Barata, E. (1991). *A cosmetologia*. 2nd Edition, Fim de século.
2. Dias, M. (2015). Hair cosmetics: An overview. *International Journal of Trichology,* 7, 2-15.
3. Draelos, Z. (2010). Essentials of Hair Care often Neglected: Hair Cleansing. *International Journal of Trichology,* 2, 24-29
4. D'Souza P, Rathi SK. (2015). Shampoo and conditioners: What a dermatologist should know? *Indian J Dermatol.* 60, 248-254.
5. Gray, J. MBBS, MRCGP and MIT. (2001). Hair Care and Hair Care Products. *Clinics in Dermatology*. 19, 227-236.
6. WOLF, R. Wolf, D. Tüzün, B. Tüzün,Y. (2001). Soaps, Shampoos, and Detergents. *Clinics in Dermatology*. 19, 393-397.
7. Daltin, D. (2011). *Tensoativos: química, propriedades e aplicações.* 1st Edition, Blucher. São Paulo (Brasil).

Contact Address:

hribeiro@campus.ul.pt
LAQV, REQUIMTE, Departamento de Química
Faculdade de Ciências e Tecnologia
Universidade Nova de Lisboa
Caparica, Portugal

Rotational and translational motion observed in *Escherichia coli* aggregates during shear

R. Portela[1], J.M. Franco[2], P. Patrício[3,4], P. L. Almeida[3,5], R. G. Sobral[1] and C. R. Leal[3,6]

[1] UCIBIO@REQUIMTE, Departamento de Ciências da Vida, Faculdade de Ciências e Tecnologia, Universidade Nova de Lisboa, 2829-516 Caparica (Portugal)
[2] Departamento de Ingeniería Química, Facultad de Ciencias Experimentales da Universidad de Huelva (Spain)
[3] ISEL, Rua Conselheiro Emídio Navarro 1, P-1959-007 Lisboa (Portugal)
[4] CEDOC, Faculdade de Ciências Médicas, Universidade Nova de Lisboa, 1169-056 Lisboa (Portugal)
[5] CENIMAT/I3N, Faculdade Ciências e Tecnologia, Universidade Nova de Lisboa, 2829-516 Caparica (Portugal)
[6] Centro de Investigação em Agronomia, Alimentos, Ambiente e Paisagem, LEAF, Instituto Superior de Agronomia, Universidade de Lisboa, Tapada da Ajuda 1349 - 017 Lisboa (Portugal)

Introduction

Recently, the growth of an *Escherichia coli* culture was studied using real-time and in situ rheology and rheo-imaging measurements, allowing to characterize their rheological behavior during time [1]. In the *lag phase*, bacteria are adapting to the new environmental growth conditions, with a characteristic slow division rate. Accordingly, the viscosity shows a slow and constant increase with time. In the *exponential phase* the viscosity presents a dramatic increase, but exhibits several drops and recoveries. In the *late phase* of growth, the viscosity increase slows down, reaching an intermittent plateau of maximum viscosity, with several drops and recoveries. In this phase, the highest bacteria density is attained: bacteria still grow and divide, but at a lower rate; big and irregular bacteria aggregates are observed, which keep moving in suspension and no significant sedimentation is observed; the aggregates present translational motion in the shear flow direction and rotational motion in the vorticity direction; the aggregates become larger along time, due to the incorporation of smaller aggregates; due to the rotational motion, the aggregates become elongated along the rotational axis; apparently, the size of the aggregates does not influence the rotational motion, since almost all aggregates rotate with the same angular velocity, which is related to the applied shear rate. As a first approximation, and because an explicit individual motion of the cells within each aggregate is not observed, this behavior is interpreted in light of a simple rigid-body motion, in which shear rate and angular velocity are dependent, which will be presented as a microscopic model.

Experimental

Bacteria strain and growth conditions

Escherichia coli DH5α (Invitrogen, USA) was used. Cultures were grown at 37ºC with aeration in Miller Lysogeny broth (LB) (NZYtech, Portugal). Cultures grown overnight were used to inoculate fresh medium at an initial optical density (OD_{620nm}) of 0.005, for rheological characterization. To monitor bacterial growth, we measured the optical density at discrete time intervals, resorting to a spectrophotometer Ultrospec 2100 pro. In parallel, we also determined the population colony-forming units (cfu/ml), which provides an estimation of the viable cells, by plating serial dilutions of the bacterial cultures in Miller Lysogeny agar (LA) (NZYtech,Portugal). The plates were incubated for 48 h at 37ºC and the colonies were counted.

Rheology

Rheological measurements were performed in a controlled stress rotational rheometer Bohlin Gemini HRnano. A steel plate-plate geometry, with a diameter of 40 mm and a 2000 μm gap (to ensure a good signal), was used for the measurements of the viscosity growth curve, at a constant shear rate of 10 s^{-1}, at 37ºC (to allow optimal bacterial growth), see Fig.1. A solvent trap was used in all measurements to avoid evaporation.

Rheo-imaging

Real-time image acquisition was performed during steady- state shear flow measurements in ThermoHaake RheoScope equipment, which combines the principles of a conventional controlled stress rheometer with an optical microscope. A constant shear rate of 10 s^{-1} was imposed using a cone-plate geometry with a 70 mm

diameter and an angle of 1º, at 37ºC. The cone had a mirror surface and the plate a cover glass, to allow optical microscopic observations (20×) during shear (schematic details are in Fig. 2), at an intermediate radius plate fixed position. A sequence of one photo image per minute was extracted from the video. In these tests, the growth of an *E. coli* culture was followed by starting measurements already at the exponential phase (approximately at an OD_{620nm} = 2.5). Video image acquisition was performed over 150 min. At the end of these measurements two videos with a higher frame rate acquisition (1 frame/s) were recorded, each with a duration of 3 min, under the same rheological conditions.

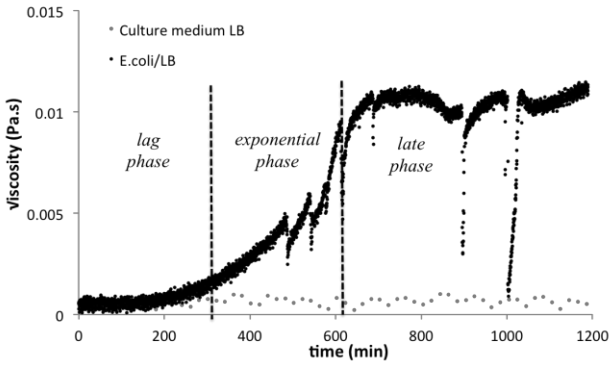

Figure 1. E. coli culture steady-state shear growth curve, η(t) measured at a constant shear rate of 10s⁻¹ – in LB culture medium (dark grey) and culture medium LB (light gray) (representative curve), at 37ºC. Dashed lines separate distinct growth phases: lag, exponential and late phases.

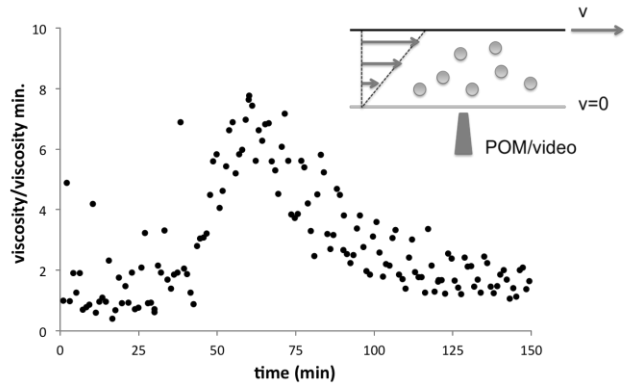

Figure 2. Relative steady-state shear viscosity growth curve of a E. coli culture, measured at a constant shear rate of 10 s⁻¹; measurements were started with a culture already at the exponential phase of growth; inset: schematic details on the image acquisition setup at an intermediate radius / plate position. Measurements were performed at 37ºC.

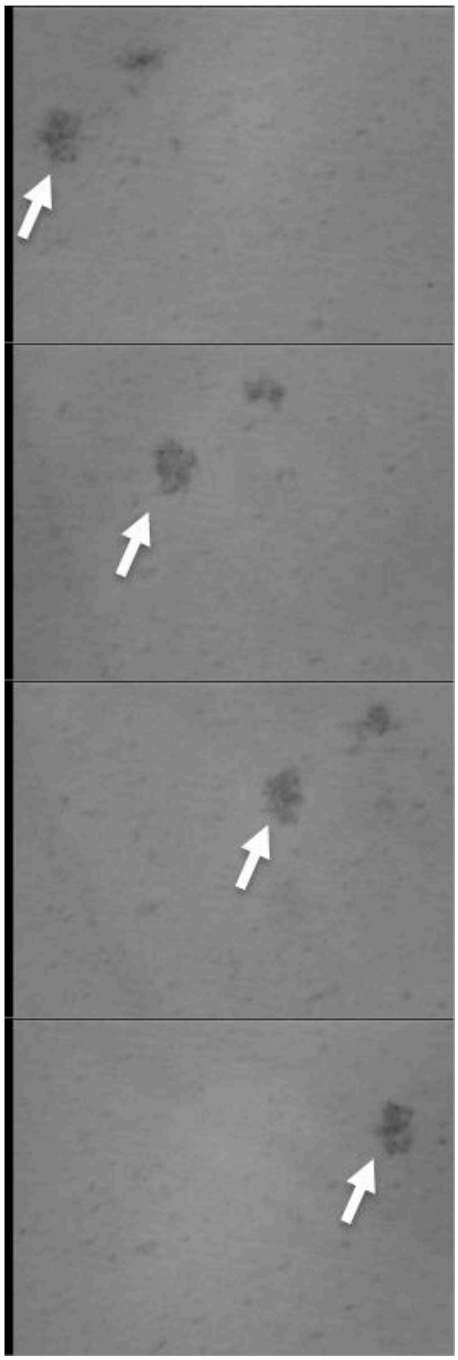

Figure 3. Four-image sequence (1 image/s) extracted from rheoimaging measurements of an E. coli culture, in order to illustrate the aggregates' rotational motion (the rotating aggregates are indicated by the white arrows and a full rotation may be seen in this sequence). The images were collected during steady-state shear, at a constant shear rate of 10 s⁻¹, in the late phase of growth. Each image is 225 μm wide (640 × 480 pixels). Measurements were performed at 37ºC.

Microscopic model

Consider the cells as small individual particles (not perturbing the flow and inertia effect neglected), connected by rigid links or filaments, thus forming a global rigid body.

In particular, if the vorticity direction coincides with one of the principal directions of the aggregate's moment of inertia, the aggregate may rotate only in the plane of the flow, according to the classic equation, proposed by Jeffery [2]:

$$\frac{d\theta}{dt} = -\frac{\dot{\gamma}}{2}(1 - d\cos 2\theta) \qquad (1)$$

From which the average mean value of the angular velocity can be obtained:

$$\dot{\theta}_m = \frac{\dot{\gamma}}{2}\sqrt{1-d^2} \qquad (2)$$

where d is related to the principal second order moments in the rotational plane, I_1 and I_2, respectively, and is given by:

$$d = (I_2 \quad I_1)/(I_1 + I_2) \quad |d| \quad 1 \qquad (3)$$

Discussion and Conclusions

In this study, real-time and *in situ* rheoimaging rheology was applied to the animal commensal bacteria *E. coli* during cell growth. As the density of bacteria in the medium increases, cells may rearrange themselves in different aggregates, capable of strongly influencing their environment and leading to three different physical rheological responses, corresponding to the three distinct phases of growth, the *lag*, *exponentia*l, and *late* phases.

In the *lag* phase, bacteria are adapting to the new environmental growth conditions, with a characteristic slow division rate. Accordingly, the viscosity shows a slow and constant increase with time. In the *exponential* phase the viscosity presents a dramatic increase, but exhibits several drops and recoveries. In the *late* phase of growth, the viscosity increase slows down, reaching an intermittent plateau of maximum viscosity, with several drops and recoveries. In this phase, the highest bacteria density is attained: bacteria still grow and divide, but at a lower rate. Big and irregular bacteria aggregates are observed, which keep moving in suspension. No significant sedimentation is observed. The aggregates present translational motion in the shear flow direction and rotational motion in the vorticity direction. The aggregates become larger in time, due to the incorporation of smaller aggregates. Due to the rotational motion, the aggregates become elongated along the rotational axis. Apparently, the size of the aggregates does not influence the rotational motion, since almost all aggregates rotate with the same angular velocity, which is related to the applied shear rate.

As a first approximation, and because we do not observe an explicit individual motion of the cells within each aggregate, we interpret this behavior in light of a simple rigid-body motion. *Considering eq.(2), the average value of the angular velocity of the aggregates was estimated to be 2,2 ± 0,7 rad/s (the error associated to this estimation is mainly due to the acquisition frame rate, which is 1 frame/s), and is roughly 1/4 of the shear rate (10 ± 0.01 1/s).*

This would correspond to a fairly asymmetric aggregate (in the rotational plane, which is perpendicular to the plane of the images, and leading to a large value of d), not suggested by the pictures.

However, the role of the *E. coli* intrinsic motility is surely an important ingredient to understand the rheological behavior of the aggregates and to address in future studies.

Acknowledgements

This article is based upon work from COST Action MP1305, supported by COST (European Cooperation in Science and Technology). This work was also supported by FEDER through COM PETE 2020; FCT Projects No. UID/CTM/50025/2013 and PTDC/FIS-NAN/0117/2014 (P.L.A.); ESCMID Grant No. 2015 (R.G.S.); and the Unidade de Ciências Biomoleculares Aplicadas, which is financed by national funds from FCT/MEC (Grant No. UID/Multi/04378/2013) and cofinanced by the ERDF under the PT2020 Partnership Agreement No. POCI-01-0145- FEDER-007728.

References

1. R. Portela, R., Patrício, P., Almeida, P. L., Sobral, R. G., Franco, J. M., and Leal, C. R. (2016). Phys. Rev. E 94, 062402.
2. Jeffery, G. B. (1922). Proc. R. Soc. London Ser. A 102, 161.

Contact Address:

C.R. Leal
cleal@adf.isel.pt
ISEL
Rua Conselheiro Emídio Navarro 1,
P-1959-007 Lisboa, Portugal
Telf.:+351218317000, ext: 1195; Fax:+351218317138

Polymers and Biopolymers

Shear rheology of welan gum solutions

J.A. Carmona, L.A. Trujillo-Cayado, M.C. García, N. Calero, P.Ramírez

Universidad de Sevilla, Grupo de Reología Aplicada. Tecnología de Coloides. Facultad de Química. c/ P. García González, 1, 41012, Sevilla (Spain)

Introduction.

Welan gum is a microbial polysaccharide produced by Alcaligenes sp. Its structure consists of a backbone chain with l-mannose, l-rhamnose, d-glucose, and d-glucuronic acid [1]. This gum has also been used for upstream operations of the petroleum industry and can find potential applications in fracking. However, it is mainly used for improving the mechanical properties of cement formulation due to its thickening, suspending and binding properties [2]. Therefore, studying the rheological properties of this gum is of key importance.

The overall objective of this research was to gain a deeper insight into the rheology of concentrated aqueous dispersions of polysaccharides, using standard step-wise flow curves, linear and non-linear creep tests and parallel superposition experiments. Shear stress values corresponding to either the zero-shear viscosity plateau region or the non-Newtonian region out of the linear zone were used to carry out the parallel superposition tests. The specific aim of this study was to determine the steady-state shear rate dependence of viscosity for concentrated welan gum aqueous solutions. In order to achieve this goal, we challenge the information provided by step-wise flow curves, by using linear and non-linear creep tests. Last but not least, the most important target of this research is to assess the information provided by the parallel superposition technique for this type of concentrated gum solutions.

Experimental

Materials and solution preparation.

A commercial welan gum sample (K1A96 “Industrial grade”) kindly donated by CP Kelco was used. The solutions studied were prepared with ultrapure Milli-Q water, by means of a standard procedure. All samples contained 0.1 (m/m) % sodium azide, as preservative.

Rheological measurements

Rheological tests were carried out with a CS DHR3 rheometer (TA Instruments). A serrated surface steel plate & plate geometry of 40 mm diameter was used for all experiments made. The measuring temperature was always 20 ± 0.1 ºC, using a Peltier system and a solvent trap to inhibit evaporation.

Step-wise flow curves from 0.01 Pa to 20 Pa were run selecting a steady state approximation of 0.01% and a maximum measuring time of 2 minutes per point. Linear and nonlinear creep tests were realized at different shear stress values for an experimental time which ranged from 15 min to 30 min, depending on the applied shear stress.

Parallel superposition tests were done in two steps. 1) Samples were pre-sheared by means of a creep test. 2) The shear stress applied in step 1 was maintained for a given experimental time while an oscillatory shear experiment was conducted in parallel. These dynamic viscoelastic tests consisted of a stress sweep at 6.28 rad/s to determine the linear viscoelastic range (LVR). Subsequently, a frequency sweep from 30 to 0.1 rad/s was carried out.

Results and Discussion

Shear rate dependence of viscosity

Figure 1 illustrates the shear rate dependence of viscosity for some welan gum solutions. Data derived from step-wise flow curves as well as from linear and non-linear creep tests are shown. Viscosity values closer or within the zero-shear plateau region calculated from creep tests turned out to be higher and higher than those of step-wise flow curves as the gum concentration was increased. This highlights the limitations of flow curves to provide steady-state viscosity values at very low shear rates (typically, below 0.01 s^{-1}) for some viscoelastic fluids since the experimental time of flow curves is usually shorter than the required time to reach the steady-state response [4]. This is clearly the case for the flow curves obtained at 0.4 m/m % and 0.6 m/m % welan gum concentration, despite the fact that flow curves were run for roughly 1 hour.

The shear rate dependence of viscosity at steady-state between 0.2 % (m/m) and 0.6 % (m/m) welan gum

showed a limiting low shear Newtonian viscosity or at least a clear tendency to reach the zero-shear viscosity, followed by a shear thinning region. The zero-shear viscosity and the slope of the power-law region increased with welan gum concentration as a consequence of the formation at quiescent state of a more complex structure based on macromolecular entanglements.

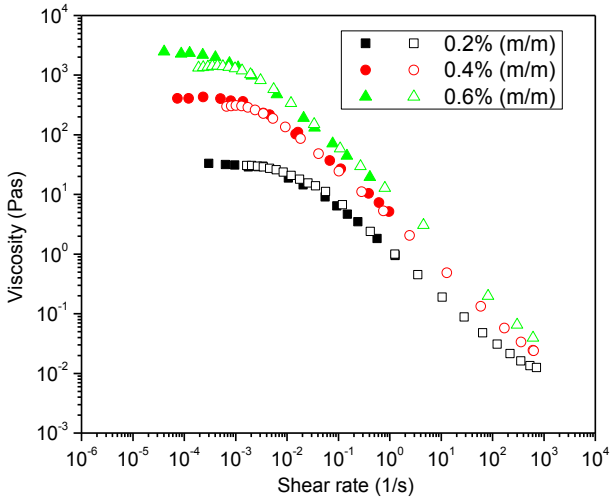

Figure 1. Viscosity versus shear rate for welan gum aqueous solutions with 0.2, 0.4 and 0.6% (m/m) gum. Closed symbos: data from creep. Open symbols: data from step-wise flow curves. T=20ºC.

Paralell superposition

Prior conducting dynamic viscoelastic tests with a steady shear stress in parallel, samples were presheared until a constant shear rate was achieved. The experimental time for the preshear step was different for each sample since it depended on welan gum concentration and the applied stress. Similarly to the standard protocol to carry out small amplitude oscillatory shear (SAOS) tests, the LVR was checked by means of oscillatory shear stress sweeps at 1Hz. Figure 2 shows the results obtained for the solution containing 0.4 % (m/m) welan by way of example. The values of the critical shear stress and strain amplitudes limiting the LVR fell down as the steady shear stress increased. This may be a consequence of the fact that macromolecular chains are likely to show a tendency to orient themselves in the shear flow direction, disrupting to some extent the original entanglements and weak gel structure.

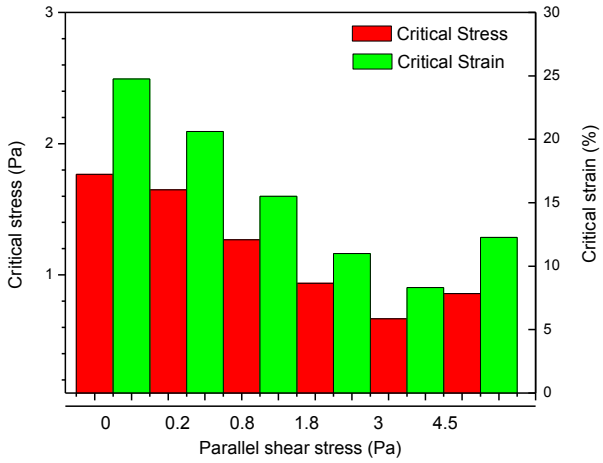

Figure 2. Critical oscillatory stress (left-axis) and strain (right-axis) for a welan aqueous solution 0.4% (m/m) at different parallel shear stresses. T=20ºC.

Figure 3 shows the influence of angular frequency on the loss tangent tan(δ). Regardless of the welan gum concentration in the 0.2 – 0.6 % (m/m) range, tan(δ) was not significantly affected by shear stress values as long as they corresponded to the limiting low shear rate viscosity plateau. By way of example, the frequency dependence of the loss tangent at 0.6% (m/m) welan gum was not influenced by a parallel shear stress until 0.5 Pa (Figure 3C). Whenever this shear stress was not exceeded, the 0.6% (m/m) welan gum solution exhibited weak gels properties since tan(δ) < 1 and the frequency dependence was rather weak. In addition, the sample at 0.5 Pa and lower shear stress values did not flow in practice since the corresponding shear rates were below 0.001 s^{-1}.

When parallel shear stress values exceeded those limiting the zero-shear viscosity plateau region for each gum concentration, a marked increase in the loss tangent took place such that a crossover of G' and G'' could be observed at the angular frequency where tan(δ) = 1. This crossover highlighted a change in the viscoelastic properties, which was consistent with a shear induced shift from weak gel [tan(δ)<1] to entanglement solution behaviour [tan(δ)>1]. It must be noted that this structural transition shifts to higher angular frequencies when the parallel shear stress applied increased, as previously reported for other polymers [5]. This is consistent with the occurrence of more marked fluid-like viscoelastic properties as the macromolecular network is weakened by parallel shear stress.

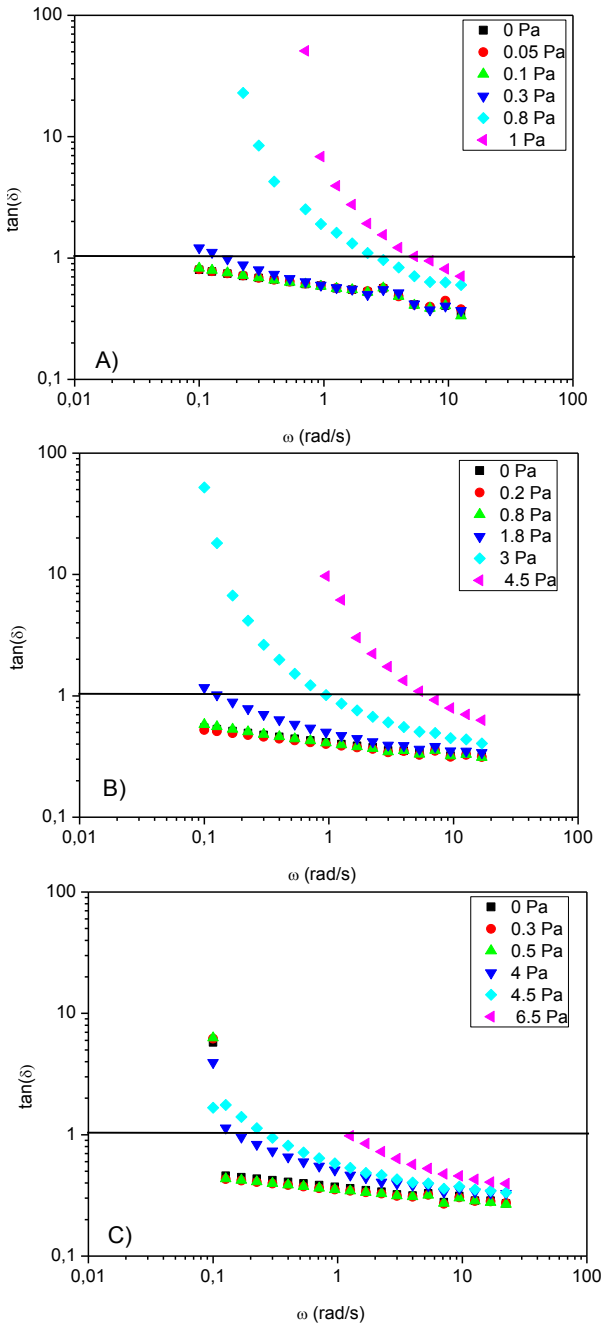

Figure 3. Dependency of tan(δ) with the angular frequency for welan gum solutions at different gum concentrations and shear stress values. A) 0.2 % (m/m), B) 0.4% (m/m), C) 0.6% (m/m). T=20ºC.

Conclusions

Flow curves need the assistance of creep compliance tests to determine the shear rate dependence of steady-state viscosity value of structured dispersions as demonstrated for welan gum/water systems in the (0.2-0.6) % m/m range. They exhibited a zero-shear Newtonian plateau region followed by a shear thinning region.

Parallel superposition tests are an alternative to LAOS tests to provide information on viscoelastic properties of samples when the applied shear stress values are above the limiting value for linear viscoelastic behaviour. In other words, parallel superposition tests allowed a sort of mechanical snaphot of structural disruption to be captured throughout the whole flow curve. Parallel superposition tests are quite useful to monitor the shear-induced change from mechanical spectra typical of weak gels to those of entanglement solutions as shear stress is applied above the critical shear stress limiting the linear viscoelastic range.

Acknowledgements

The financial support received (Project CTQ2015-70700-P) from the Spanish Ministerio de Economía y Competitividad and from the European Commission (FEDER Programme) is kindly acknowledged. The authors are also grateful to CP Kelco for providing materials for this research, and to Servicios Centrales de Investigación (CITIUS), Universidad de Sevilla.

References

1. Kaur, V., Bera, M. B., Panesar, P. S., Kumar, H., & Kennedy, J. F. (2014). Welan gum: microbial production, characterization, and applications. International Journal of Biological Macromolecules, 65, 454-461.
2. Khayat K.H. ,Yahia A. (1997). Effect of welan gum-high-range water reducer combinations on rheology of cement grout, ACI Materials Journal, 94, 365-372.
3. Walters K. (1975), Rheometry, Chapman and Hall, London, p.p. 201.
4. Santos J, Trujillo LA, Calero N, Alfaro MC, Muñoz J. (2013) Physical characterization of a commercial suspoemulsion as a reference for the development of suspoemulsiones. Chemical Engineering & Technology. 36, 1883-1890.
5. Booij, H. C. (1968). Influence of superimposed steady shear flow on the dynamic properties of non-Newtonian fluids. Rheologica Acta, 7(3), 202-209.

Contact Address:

joseacarmona@us.es
Departamento de Ingeniería Química
Facultad de Química
Universidad de Sevilla
c/ P. García González, 1, 41012, Sevilla (Spain).
Telf.: 954 556447

Rheological properties of aqueous solutions of diutan gum

M.C. Garcia, J.A. Carmona, M.J. Martin, J. Santos, M.C. Alfaro

Universidad de Sevilla, Grupo de Reología Aplicada. Tecnología de Coloides. Facultad de Química. c/ P. García González, 1, 41012, Sevilla (Spain)

Introduction

Diutan gum (DG) is an anionic polysaccharide obtained by aerobic fermentation from Sphingomonas sp. ATCC 53159. Its structure is composed of a repeated configuration of rhamnose, glucose, glucuronic acid and glucose units [1]. The main applications of DG are in personal care formulations, industrial, oilfield and civil engineering due to its capability to modify the rheology of different aqueous solutions.

Nowadays, Diutan gum is mainly employed in cement formulation [2] due to its capability to modify the rheological properties and performance of cement paste [3]. In addition, Diutan gum may play an important role in oil recovery as a consequence of its ability to endure the severe conditions of salinity and temperature existing in the petroleum reservoirs [4].

This study assesses the influence of DG concentration, on the rheological properties of 0.5% wt NaCl aqueous solutions. Several rheological measurements have been carried out in order to determine a) linear viscoelastic properties by small amplitude oscillatory shear and b) shear flow properties by running step-wise flow curves.

Experimental

Several Diutan gum (CP Kelco, San Diego, USA) solutions at different gum concentrations within the (0.1 - 0.5) wt %, containing 0.5 wt % NaCl (Panreac) were prepared.

A serrated plate & plate geometry (35 mm diameter) with a sample gap of 1mm was used for oscillatory shear tests carried out using a CS AR2000 rheometer (TA instruments). The LVR (linear viscoelastic range) was estimated by oscillatory shear stress sweeps at three fixed frequencies, 0.1,1 and 3 Hz. Rheokinetics tests were done at 1Hz and frequency sweeps were run from 3 Hz to $8 \cdot 10^{-3}$ Hz, in both cases within the LVR. A solvent- trap was used to avoid sample drying.

Additionally, a Haake-MARS CS rheometer (Thermo) was used to study flow properties by carrying out step-wise flow curves. A coaxial Z20 DIN cylinder geometry with sandblasted surfaces was used. The ratio of radii is 1.0847, the gap between the external surface of the rotor and the inner wall of the cup is 0.85mm, the rotor length being 30 mm.

Stepwise flow curves were run between 1 Pa and 15 Pa, fixing a steady state approximation of 0.01% and a maximum measuring time of 3 minutes per point.
All rheological tests were done at 20ºC.

Results and Discussion

Estimation of the equilibration time

First of all the rest, or better equilibration, time required to achieve the structural recovery of samples after being loaded into the measuring system was estimated by rheokinetics. Namely, an oscillatory shear test was done at 1Hz as a function of time within the LVR. The equilibration time was calculated using a first-order kinetic equation (1), as reported by Muñoz et al. (2001) [5].

$$G' = G_0' + (G_\infty' - G_0')[1 - \exp(-k \cdot t)]^m \qquad (1)$$

Where, G´ is the storage modulus, G_0' is the instantaneous value of G' for null recovery time, G_∞' is the values of G´ for full structural recovery, k is a kinetic coefficient and m, which is a fitting parameter, was given a value of 1, in agreement with first-order kinetics. Upon analysing the results obtained, an equilibration time of 120 s was used for all samples studied.

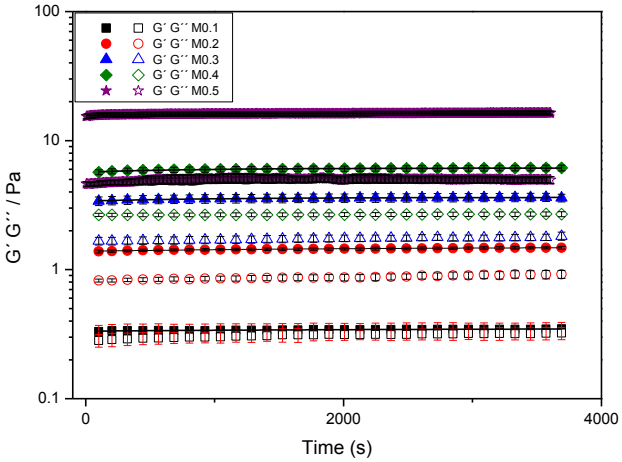

Figure 1. Influence of Diutan gum concentration on the time-dependent evolution of G' and G" immediately after samples were loaded into the parallel plate measuring system. NaCl concentration: 0.5wt %. T=20ºC

Determination of the Linear Viscoelastic Range (LVR)

Stress sweeps at three different frequencies (0.1, 1 and 3 Hz) were carried out to determine the linear viscoelastic range.

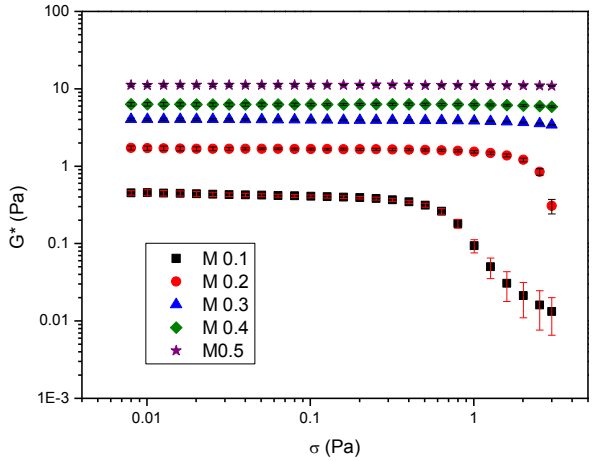

Figure 2. Influence of the Diutan gum concentration on stress sweeps at 0.1 Hz. T=20ºC

The results obtained (data not shown) supported that the critical stress and critical strain amplitudes increased with Diutan gum concentration. Figure 1, 2 and 3 also revealed that the complex modulus increased with Diutan gum concentration, although data obtained at 3 Hz could be biased by inertial effects.

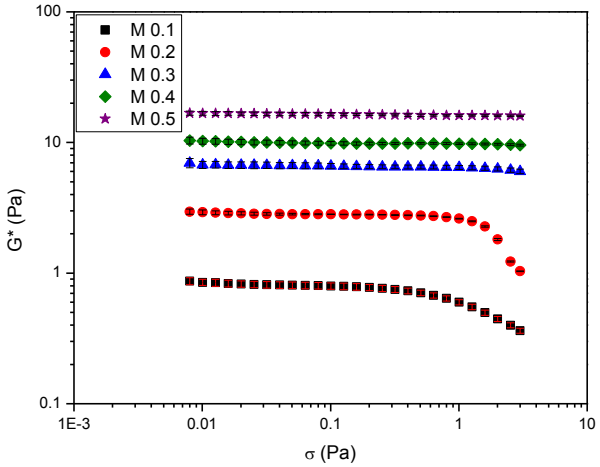

Figure 2. Influence of the Diutan gum concentration on stress sweeps at 1 Hz.T=20ºC

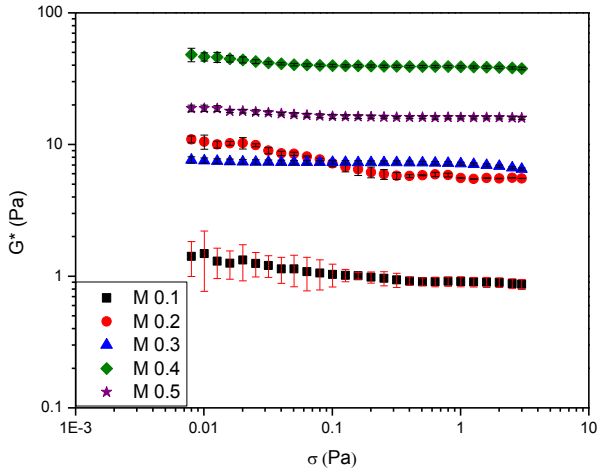

Figure 3. Influence of the Diutan gum concentration on stress sweeps at 3 Hz.T=20ºC

Mechanical spectra

The mechanical spectra illustrated the viscoelastic response of the Diutan gum solutions studied. Figure 4 shows the increase in complex viscosity with Diutan gum. In all cases a tendency towards a limiting $|\eta^*_0|$ value was observed.

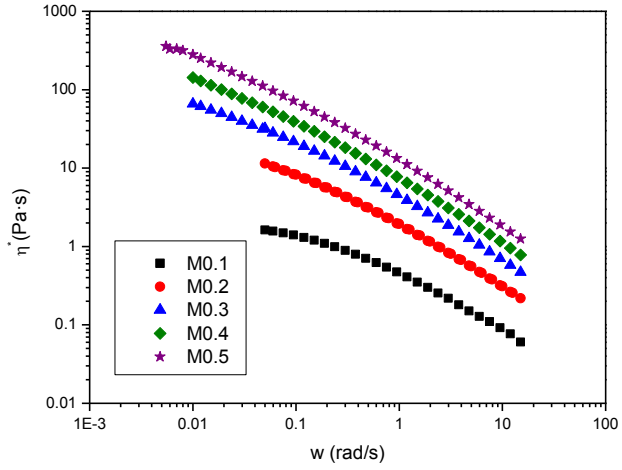

Figure 4. Influence of Diutan gum concentration on $|\eta^*|$ values calculated from frequency sweeps. T=20ºC

Flow curves

Figure 5 exhibit the influence of Diutan gum concentration on the flow curves. All samples showed shear thinning behaviour and fitted the Herschel-Bulkley equation.

$$\sigma = \sigma_0 + K \cdot (\dot{\gamma})^n \qquad (2)$$

where K is the so-called consistency index $(Pa \cdot s)^n$, whose units depend on the flow index value; σ is the shear stress, σ_0 and n are the apparent yield stress and the flow index values predicted by the Herschel-Bulkley equation.

The values of the apparent yield stress calculated from the Herschel-Bulkley equation (1) are shown in table 1. As can be observed, the apparent yield stress increased with Diutan gum concentration. The same effect was detected regarding the consistency index values. Additionally, an increase in Diutan concentration brought about a tendency of the flow index to decrease.

Table 1. Fitting parameters to the Herschel-Bulkley equation for Diutan gum solutions.

	σ_0 (Pa)	$E_{\sigma 0}$	K	E_K	n	En	R^2
M0.1	0.37	0.05	0.18	0.03	0.41	0.03	0.99
M0.2	1.78	0.12	0.13	0.04	0.53	0.05	0.99
M0.3	3.70	0.21	0.34	0.11	0.42	0.08	0.99
M0.4	3.9	0.46	1.58	0.40	0.24	0.03	0.99
M0.5	5	-	3.04	0.04	0.19	0.003	0.99

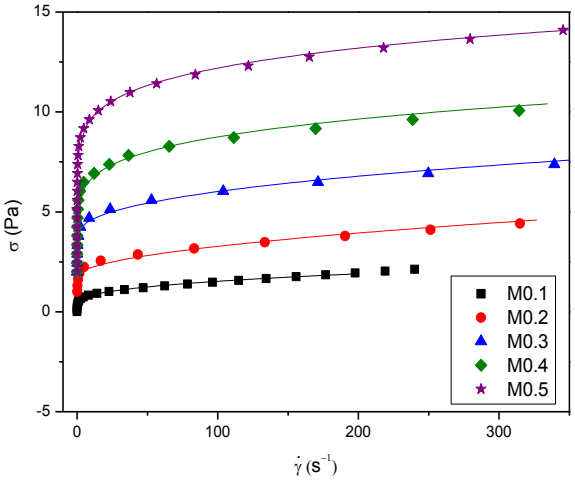

Figure 5. Influence of Diutan gum concentration on the flow curves. T=20ºC

Concluding remarks

Frequency sweeps assisted by oscillatory shear time tests were used to determine the mechanical spectra of Diutan gum solutions, which exhibited clear viscoelastic properties an increasing complex viscosity values as gum concentration increased. Step-wise flow curves were consistent with shear thinning behaviour. The Herschel-Bulkley equation was used the fit the flow curves, which were consistent with a rise of the apparent yield stress and a drop of flow index as Diutan gum concentration was increased.

Acknowledgements

The financial support received from the Spanish Ministerio de Economía y Competitividad (MINECO) and FEDER, UE is kindly acknowledged (project CTQ2015-70700-P).

References

1. Chowdhury, T. A., Lindberg, B., Lindquist, U., Baird, J. (1987).Carbohydr Res 164,117–122.
2. Roussel, N., Lemaître, A., Flatt, J. R., Coussot, P. (2010). Cement and Concrete Research, 40, 77–84.
3. Zhang, J., Weissinger, E. A., Peethamparan, S., Scherer, G. W. (2010). Cement and Concrete Research, 40, 1023–1033
4. Xu, L., Gong, H., Dong, M., Li, Y.(2015). Carbohydrate polymers 132, 620-629.
5. Muñoz, J., Hudson, N.E. Vélez, G. Alfaro, M.C., Ferguson, J. (2001). Rheol. Acta 40, 162-175.

Contact Address:

joseacarmona@us.es
Departamento de ingeniería Química
Facultad de Química
Universidad de Sevilla
c/ P. García González, 1, 41012, Sevilla (Spain).
Telf.: 954 556447

Morphology-rheology relationship on novel PA6-HNBR blends

A. Burgoa[1], R. Hernandez[1], A. M. Zaldua[1], A. Arrillaga[1], J. L. Vilas[2]

[1] Leartiker S. Coop, Xemein Etorbidea, 12-A E-48270, Markina-Xemein, Bizkaia (Spain)
[2] Department of Physical-Chemistry, University of the Basque Country, Faculty of Science and Technology, Barrio Sarriena, s/n E-48940, Leioa, Bizkaia (Spain)

Introduction

Rubber-plastic blends are attracting a growing interest for use as thermoplastic elastomers. Blending of rubber materials with plastics gives rise to a new class of materials that combine the properties of conventional rubbers with the advantage of being repeatedly processable, like thermoplastics. They do not need to be vulcanized during fabrication into end-use parts. Blending is a smart and economical strategy to obtain new high performance TPEs from the existing rubber and plastic materials.

Although a wide range of possible rubber-plastic combinations exist, the full potentialities of TPE blends have not yet been completely explored. This is due to the fact that the majority of polymers are immiscible with one another, as has been repeatedly shown in many research works, due to the thermodynamics [1]. These blends can be commercially successful only if they are efficiently compatibilized [2].

The final properties of immiscible blends are not only determined by the intrinsic properties of the components and the use of compatibilizers, but they are also significantly dependent on the morphology of the blend. Rheology-morphology relationship in immiscible polymer blends are complex and depend on several factors [3]. The present investigation reports our observations on the rheology-morphology relationships on the blends of a high temperature resistant thermoplastic, polyamide 6 (PA6), and a rubber material with high resistance to oils and temperature, hydrogenated acrylonitrile butadiene rubber (HNBR). Partially carboxylated hydrogenated acrylonitrile butadiene rubber (HXNBR) has been added to enhance the adhesion between the rubber and thermoplastic phases.

Experimental

Materials

The polyamide 6 (PA6) used in this study was supplied by Lanxess. Hydrogenated acrylonitrile butadiene rubber (HNBR) and partially carboxylated hydrogenated acrylonitrile butadiene rubber (HXNBR) were supplied by Arlanxeo. The basic characteristics of the above materials are given in Table 1.

Table 1. Basic characteristics of the raw materials

Material (trade name)	Characteristics
PA6 (Durethan B 30 S)	Density: 1.14 g/cm^3 Melting point: 222°C Moisture content: 0.03-0.12 %
HNBR (Therban AT 3904 VP)	Specific gravity: 0.96 Acrylonitrile content: 39 wt % Mooney viscosity ML (1+4) 100°C: 40 Residual double bonds : 0.5 %
HXBR (Therban XT KA 8889 VP)	Specific gravity: 0.97 Acrylonitrile content: 33 wt % Mooney viscosity ML (1+4) 100°C: 74 Residual double bonds : 3.5 %

Blend preparation

For the rubber phase the selected grades were blended at four different blend ratios (100:0, 70:30, 50:50, and 30:70) in a two-roll mill. The rubber sheets obtained were cut into small pieces and extruded (using a Gumix extruder) into strands for subsequent palletization using talc powder as the partition agent. Extrusion was carried out at 90°C at a rotor speed of 15 rpm. Designation of HXNBR/HNBR rubber blends is given in Table 2.

Many research works have shown that among all the possible plastic/rubber blends, those with 40 plastic/60 rubber composition (w/w) showed the best TPE characteristics [4], for that reason, this particular composition was selected for the present investigation. Uncrosslinked rubber/plastic blends based on HNBR/HXNBR and PA6 at 60/40 blend ratio were prepared in a Brabender DSE 20/40 corrotating twin screw extruder. Rubber pellets and the predried nylon 6 granules were manually premixed and fed into the twin screw extruder using a gravimetric feeder at a constant

1 kg/h rate. All blends were prepared at a rotor speed of 100 rpm. The temperature profile of the extruder from feeding to the die is listed in Table 3. After extrusion the blended samples were quenched in a water bath and subsequently pelletized. All blends were dried in a vacuum oven and re-extruded using the previous extrusion conditions in order to homogenize the mixtures.

Table 2. Designation of the rubber blends

Sample name	HNBR	HXNBR
$H_{100}X_0$	100	0
$H_{70}X_{30}$	70	30
$H_{50}X_{50}$	50	50
$H_{30}X_{70}$	30	70

Table 3. Temperature profile of the extruder

Stage	Barrel temperature (°C)
Hopper	235
1	235
2	240
3	240
4	240
Die	240

Characterization

The morphology of the blends was analysed using a scanning electron microscope (SEM, Hitachi S-3400 N) and an optical microscope (Nikon ECLIPSE 80i) equipped with a LINKAM LTS420 hot stage. SEM analysis was carried out by inspecting the cryofractured surface of the samples. The surface was sputter coated with gold prior to the SEM observation. Optical microscopy measurements were performed using the following procedure: thin films were obtained by placing a pellet between two cover glasses and heated up to 240 °C; the temperature was then lowered rapidly to 30 °C allowing the material to crystalize.

Rheological analysis of the blends were performed on a capillary rheometer Rosand Rh 7/2 (Malvern) and on a Thermo Haake Mars III oscillatory rheometer with parallel plate geometry. Capillary rheometer measurements were performed at 240 °C using a capillary die of 0.5 mm diameter and L/D ratio of 32, which was sufficient large to ensure that the measured stress does not need to be corrected. In the case of dynamic shear measurements frequency sweeps from 10 Hz to 0.01 Hz were performed at 240 °C.

Results and Discussion

Morphology

Figure 1 shows the SEM results of the cryofractured surfaces of all the blends. Optical microscopy results of $60H_{100}X_0$/40PA6 and $60H_{50}X_{50}$/40PA6 are shown in Figure 2. The use of polarized optical microscopy enables the distinction between crystalline (light) and amorphous (dark) regions. The SEM and optical microscopy results demonstrate that the rubber particles are dispersed on microscale in the PA6 matrix. The component with higher volume fraction and lower viscosity has a tendency to encapsulate the other, becoming the matrix.

In addition, microscopy images clearly show the effect of using HXNBR. SEM micrographs show that after addition of HXNBR the blend shows a finer dispersion of rubber particles. On the other hand, with increasing the HXNBR content the blend phases are less defined, showing a better compatibility. The optical micrograph obtained for the $60H_{100}X_0$/40PA6 blend shows a thin layer between the rubber and the thermoplastic phases but in the case of the blends with HXNBR it was not possible to distinguish clearly the two phases.

So the obtained micrographs confirmed not only the immiscibility between PA6 and HNBR, but also the adhesion and fine dispersion of rubber phase within the PA6 matrix achieved using HXNBR. This result can be interpreted in terms of the formation of an interface during melt-mixing due to the reaction of the carboxylic functionalities of HXNBR with the amine groups on PA6.

Rheological properties

Figure 3 shows the viscosities of PA6 and the TPE blends. The curves show the stress response to the sinusoidal oscillation and the pressure response to the capillary flow. As it was discovered by Cox and Merz [5] the dynamic and steady flow viscosities overlap. PA6 exhibits a shear-thinning behaviour at high shear rates and a Newtonian plateau at low shear rates. On the other hand, blends show a decrease of the viscosity followed by a pseudo-Newtonian plateau and by a second non-Newtonian flow (pseudoplastic) in the region of high shear rates. This is a typical behaviour for systems in which one polymer is the matrix and the other acts as a filler dispersed in it [6]. So, the rheological information is in agreement with the rubber particulate morphology obtained by SEM and optical microscopy.

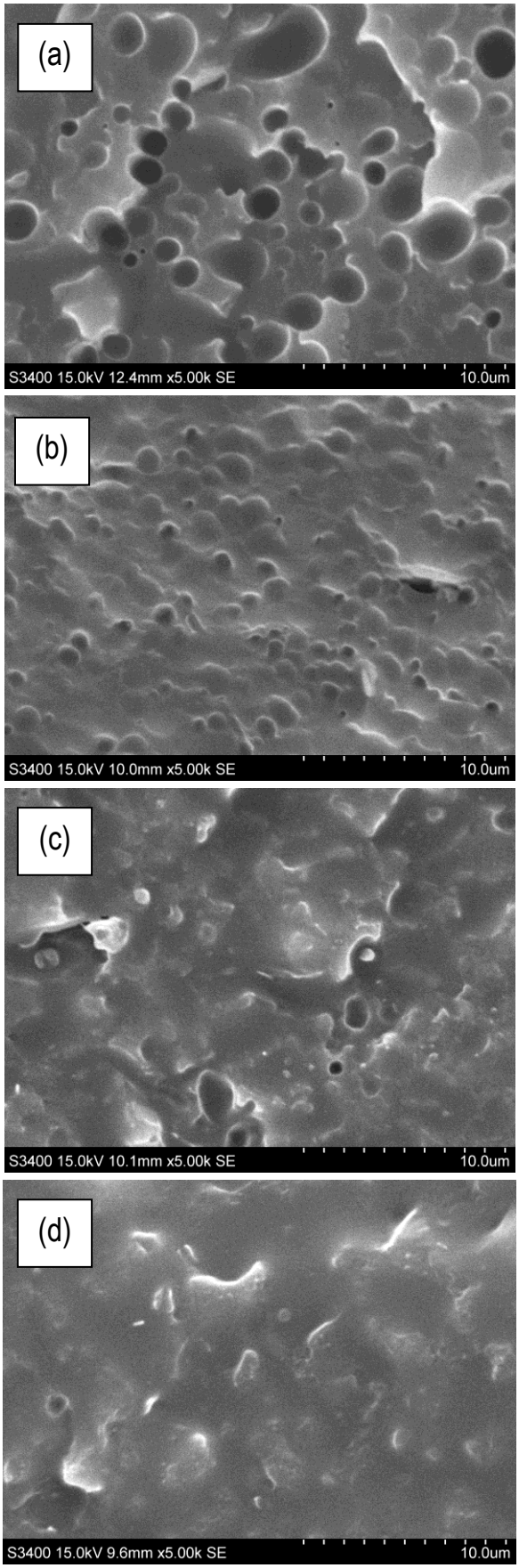

Figure 1. SEM micrographs of cryofractured surfaces: (a) $60H_{100}X_0$/40PA6; (b) $60H_{70}X_{30}$/40PA6; (c) $60H_{50}X_{50}$/40PA6; (d) $60H_{30}X_{70}$/40PA6.

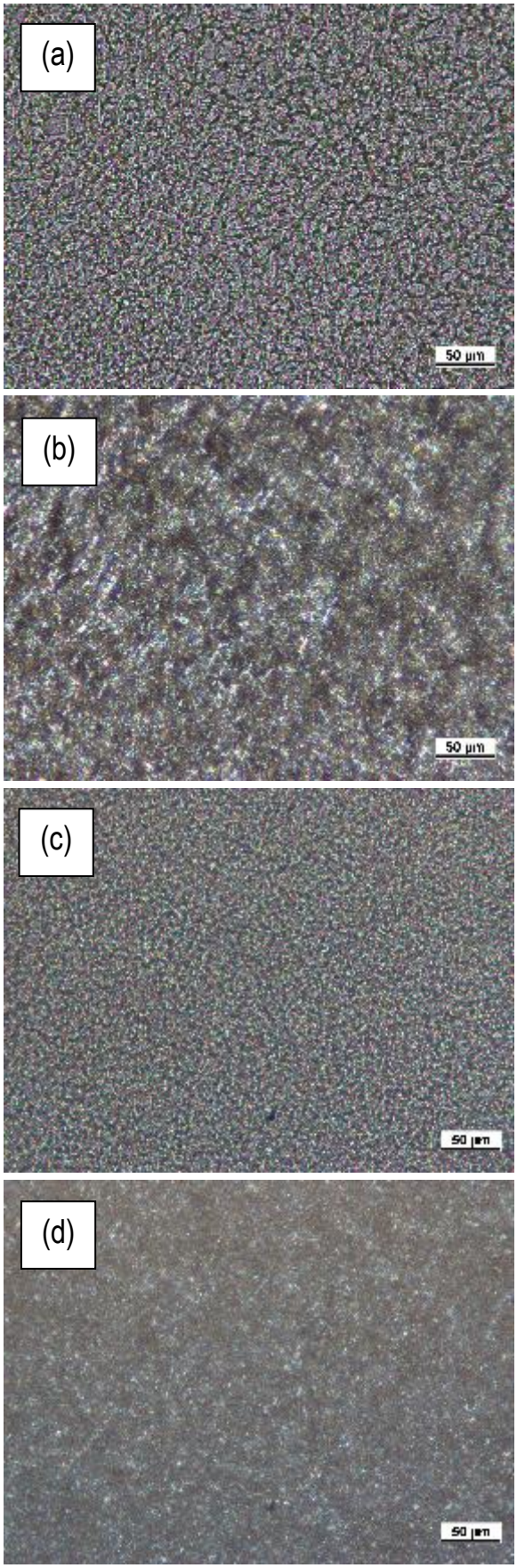

Figure 2. Optical micrographs: (a) $60H_{100}X_0$/40PA6; (c) $60H_{50}X_{50}$/40PA6. Polarized optical micrographs: (b) $60H_{100}X_0$/40PA6; (d) $60H_{50}X_{50}$/40PA6.

The mechanism responsible for the pseudo-Newtonian plateau that appears in the blends is the yield phenomena. The fundamental mechanism causing variation of the viscosity with the shear rate are the changes of structure of the flowing liquid under the influence of the shear rate [3]. In our particular case the appearance of the yield phenomena could be a consequence of the formation of rubber aggregates leading to the increase of the effective volume fraction of rubber particles.

The unlimited increase of viscosity at low shear rates is associated with the formation of filler structure having a certain strength and distinct relaxation properties from the polymer matrix. In the case of high shear rates the filler structure is broken down and the blends behave like conventional melts and, as it can be seen in Figure 3, the flow curves of the blends overlap with the flow curve of PA6 [6].

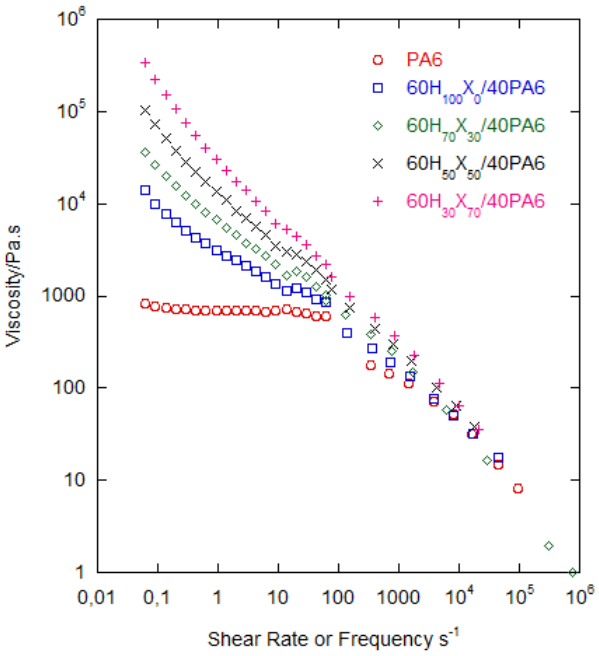

Figure 3. Viscosities of the blends measured by using oscillatory rheometer and capillary rheometer.

Acknowledgments

This research was supported by the Basque Government in terms of the predoctoral grant from the Department of Education.

References

1. Olabisi, O., Robeson, L.M., and Shaw, M.T. (1979). Polymer-Polymer Miscibility, Academic Press, New York, London, Toronto, Sydney, San Francisco.
2. Banerjee, S. S, and Bhowmick, A. K. (2016). Rubber Chemistry and Technology. 90, 1–36.
3. Utracki, L.A. (1989). Polymer Alloys and Blends: Thermodynamics and Rheology, Hanser Publishers, Munich, Vienna, New York.
4. Banerjee, S. S, and Bhowmick, A. K. (2016). Journal of Material Science. 51, 6722-6734.
5. Cox, V. P., and Merz, E. H. (1958). Polymer Chemistry. 28, 619-622.
6. Vinogradov, G.V., and Malkin, A. Ya. (1980). Rheology of Polymers. Mir publishers, Moscow, Springer-Verlag, Berlin, Heidelberg, New York.

Contact Address:

aburgoa@leartiker.com
Leartiker S. Coop.
Xemein Etorbidea, 12-A E-48270, Markina-Xemein, Bizkaia (Spain)
Telf.:+34 946169167

Morphology-rheology relationship in PET-PE-TiO_2 multiphasic systems: Analogies with recycled milk bottles

L. Sangroniz[1], J.L. Ruiz[1], M. M. Fernández[1], A. Santamaria[1], A.J. Müller[1-2]

[1] POLYMAT and Polymer Science and Technology Department, Faculty of Chemistry, University of the Basque Country UPV/EHU (Spain)
[2] IKERBASQUE, Basque Foundation for Science (Spain)

Introduction

In the last few years, it has been shown that it is possible to compatibilize immiscible polymer blends adding fillers [1]. For blends with droplet matrix morphology, the addition of fillers can reduce the dispersed phase size. The presence of fillers also modifies the rheological properties of the blends. In this contribution, the addition of titanium dioxide (TiO_2) to polyethylene terephthalate / low density polyethylene immiscible blends is studied, focusing on the rheological properties of the blends in continuous flow. This blend is interesting from a technological point of view, since in the last years PET bottles filled with TiO_2 have been introduced in the market for milk packaging. Taking into account that PET filled with TiO_2 is not compatible with actual PET recycling processes, an alternative solution is to obtain innovative materials recycling milk bottles with the bottle caps, usually made from polyolefins, which leads to PET/polyolefins immiscible blends with TiO_2 particles. Therefore, it is necessary to study the morphology of the blends and the rheological properties for the processing of the material.

The morphological analysis revealed that for PET/LDPE blends the titanium dioxide is located preferentially at the interface. The size of the dispersed phase is reduced, which can be attributed to the barrier effect of the particles located at the interface, preventing the coalescence of the droplets, to the changes in the viscosity of the phases or to the reduction of the interfacial tension [2]. Regarding to the rheological properties, the results showed that some of the blends exhibit a viscoplastic behaviour. The study of blends with different compositions allowed us to determine the factors that provoke the appearance of a viscoplastic behaviour, not reported before in literature for these blends. According to our analysis the requirements to obtain a viscoplastic behaviour are the following: a) emulsion like structure, b) the presence of TiO_2 particles and c) optimum size of the LDPE dispersed phase. Interestingly, the yield stress seems to be inversely proportional to the size of the LDPE droplets. Continuous flow experiments were complemented with small amplitude oscillatory shear experiments, demonstrating the effect of the morphology on the dynamic viscoelastic results in the terminal or flow region, in particular when a viscoplastic behaviour occurred.

A feasible and straightforward rheological method is proposed to characterize recycled materials, contributing to the development of a “Circular Economy” of polymers.

Experimental

The blends were prepared using a Collin co-rotating twin screw extruder, at 270ºC and 40 rpm. PET/LDPE blends were prepared in 90/10, 80/20 and 70/30 w/w ratio and for the nanocomposites TiO_2 was added as 5% with respect to the total amount of the blend. The samples were compression molded using a hydraulic press at 265ºC during 5 min.

The morphology was analysed by Scanning Electron Microscopy SEM (Hitachi S-2700 electron microscopy); for that the samples were cryogenic fractured and coated with gold. Transmission Electron Microscopy TEM (TECNAI G2 20 TWIN) was also employed to determine the location of the TiO2 particles.

The rheological properties of the blends in extrusion flow were analysed using a Gottfert Rheograph 25. The measurements were carried out at 270ºC in a shear rate range between 10 and 1000 s^{-1}.

The dynamic viscoelastic measurements in the linear regime were performed using an ARG2 rheometer under nitrogen atmosphere using parallel plates geometry (d=25 mm) at 270ºC. Frequency sweeps were carried out in the range of 628-0.2 rad/s.

Results and Discussion

Morphology

The morphological analysis of the blends shows that the blends exhibit a sea-island morphology, where LDPE forms the dispersed phase and PET the matrix. As an

example, the size of the dispersed phase for PET/LDPE 80/20 blend and the nanocomposite are indicated in Table 1. In the binary blend the LDPE droplets have an average size in number of 10.5 μm. The addition of TiO_2 provokes a significant reduction of the dispersed phase, since a value of 3.58 μm is obtained. In addition to the refinement of the morphology, the presence of TiO2 particles leads to a narrower distribution of the droplets size, as can be seen in Figure 1; thus more homogeneous blends are obtained.

The TEM image shown in Figure 2 demonstrates that TiO_2 particles are mostly located at the interface, surrounding LDPE droplets, although some particles are also present in the matrix and in the dispersed phase. As mentioned in the Introduction, different factors are involved on the refinement of the morphology: Reduction of the interfacial tension, changes in the viscosity of the phases and the barrier effect of the particles which are surrounding LDPE droplets, which inhibit the coalescence of the droplets. [1-3]

Table 1. Average diameter in number of the PET/LDPE binary blend (80/20) and the nanocomposite containing 5% TiO_2(76/19/5).

Sample	d_n (μm)
PET/LDPE 80/20	10.5
PET/LDPE/TiO_2 76/19/5	3.58

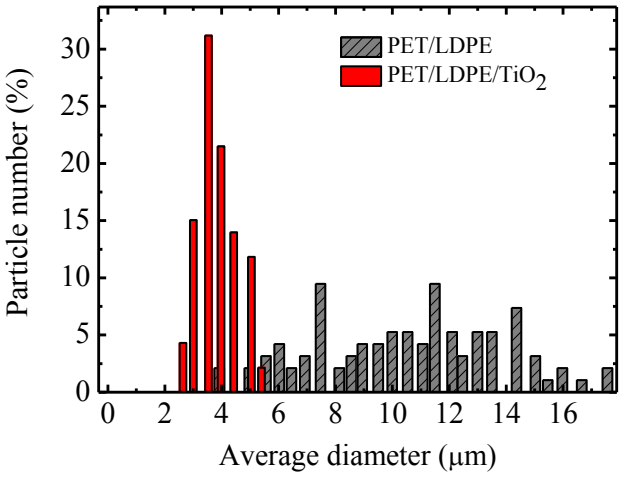

Figure 1. Particle size histogram for binary blend (PET/LDPE 80/20) and nanocomposite (PET/LDPE/TiO_2 76/19/5).

Regarding to the location of nanoparticles, thermodynamic and kinetic aspects have to be considered. The final location of the particles that results from thermodynamic interactions can be predicted considering surface and interfacial tension of the blend components using different equations. For PET/PP systems it has been reported that the interfacial tension between PP and TiO_2 is higher than for PET/TiO_2, so TiO_2 locates at the PET phase. Thus, taking into account only thermodynamic aspects it should be expected that in PET/LDPE blend nanoparticles would locate at PET phase. But, since polymers have a high viscosity is not possible to achieve thermodynamic equilibrium. For the system studied in this work, we can assume that TiO_2 locate at the beginning at PP phase because this phase is melted earlier in the extruder. During extrusion particles tend to migrate to PET phase, since it is thermodynamically more favoured; but the viscosity of the polymers is high, avoiding equilibrium to be attained. Different physico-chemical factors affect the final location of the particles. In this case, TiO_2 particles locate mainly at the interface, but also in the PET as well as in the LDPE phase, as can be seen in Figure 2.

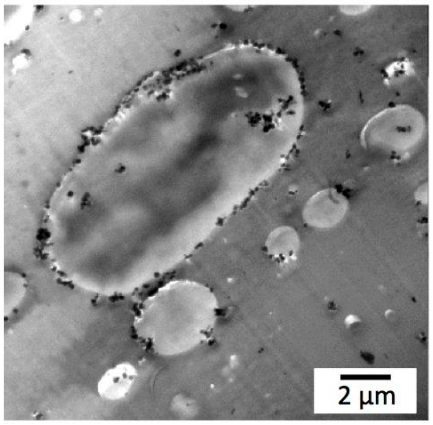

Figure 2. TEM image of PET/LDPE/TiO2 blend, TiO2 particles (black spots) are located mainly at the interface.

Therefore, the interface is not fully saturated by TiO_2 nanoparticles In literature [1-4] PET/PP 25/75 blends have been studied and it has been found that the addition of 4% of TiO_2 reduces the size of PET droplets (d_v) almost a 60%. In our case the reduction is near to 30%. It should be noted that the major phase is different: in the case of our blends the continuous phase is PET, whereas for the blends studied in literature, the continuous phase is PP. In addition, for the blends analysed in literature small TiO_2 particles have been employed, with a diameter of 15 nm, whereas our particles have a size of 150 nm. This can affect the ability of the nanoparticles to reduce the size of the dispersed droplets [5].

Rheology

Figure 3 shows the flow curves obtained for the binary blend PET/LDPE 80/20 and the nanocomposite

containing TiO_2. As can be seen, the binary blend exhibits a pseudoplastic behaviour. However, the presence of TiO_2 particles changes drastically the behaviour of the blend: The nanocomposite shows a viscoplastic behaviour, as the viscosity tends to increase at low shear rates, instead of reaching a constant value. This behaviour results from the increase of the interactions between PET and LDPE phases, promoted by the TiO_2 particles located at the interface. Above a critical shear rate, the applied stress is high enough to break the interactions reducing the viscosity. The viscosity of the binary blend has been fitted to the Cross equation, Eq. (1)

$$(\dot{}) = \frac{0}{1 + (\dot{} \; 0)} \qquad (1)$$

In where λ is the inverse of the critical shear rate, η_0 is the Newtonian viscosity, $\dot{\gamma}$ is the shear rate and α is the slope of the pseudoplastic regime.

For the nanocomposite, PET/LDPE/TiO_2, the data has been fitted to a modified Cross model, Eq. (2), in order to obtain the yield stress value, σ_y,

$$(\dot{}) = \frac{y}{\dot{}} + \frac{0}{1 + (\dot{} \; 0)} \qquad (2)$$

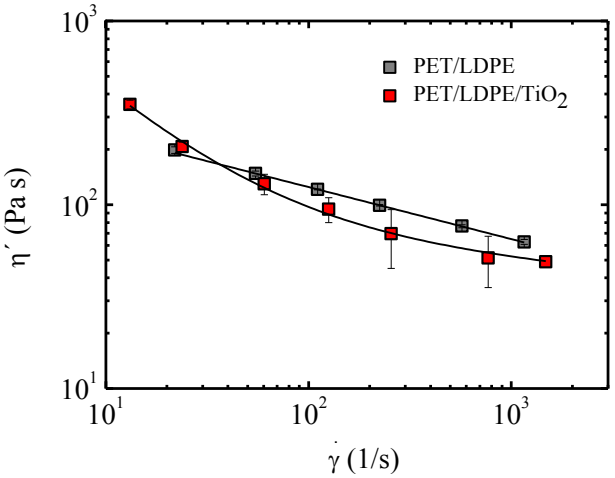

Figure 3. Flow curves for binary blend (PET/LDPE 80/20) and nanocomposite (PET/LDPE/TiO2 76/19/5) at 270ºC. For the nanocomposite a yield stress value of 3558 Pa is obtained.

PET and LDPE containing TiO_2 and blends with different composition have been also studied concluding that the following requirements are necessary to obtain a viscoplastic behaviour:

a) Emulsion like structure is needed, since only immiscible polymer blends show yield stress.

b) There is an optimum LDPE droplets size because not all the blends show viscoplastic behaviour. Large LDPE droplets do not favour viscoplastic behaviour because the interfacial surface is decreased, reducing the elastic component.

c) The presence of TiO_2 is necessary as the binary blends do not show viscoplastic behaviour.

From a technological point of view, the addition of TiO_2 facilitates the processing of the material since lower viscosity values are obtained for the nanocomposite at intermediate and high shear rates.

The rheological properties of the blends have been also analysed in the linear viscoelastic regime by small amplitude oscillatory shear measurements, SAOS. As shown in Figure 4, the blend containing TiO_2 exhibits higher viscosity than the binary blend. This result differs from that obtained under continuous flow. However, it should be considered that the results obtained with SAOS can not be compared with the results from continuous flow where the measurements are performed in the non linear regime and thus interactions are broken. Therefore, it can be stated that for the measurements performed in the linear regime, the interactions between LDPE and PET phases, promoted by the presence of TiO2, are not broken, and the blend containing TiO_2 shows higher viscosity values.

The binary blend shows a pseudoplastic behaviour, since the viscosity values at low frequencies tend to a plateau. However, the nanocomposite exhibits a viscoplastic behaviour, characterized by a viscosity increase as frequency is reduced. The same behaviour is observed under extrusion flow at different shear rates.

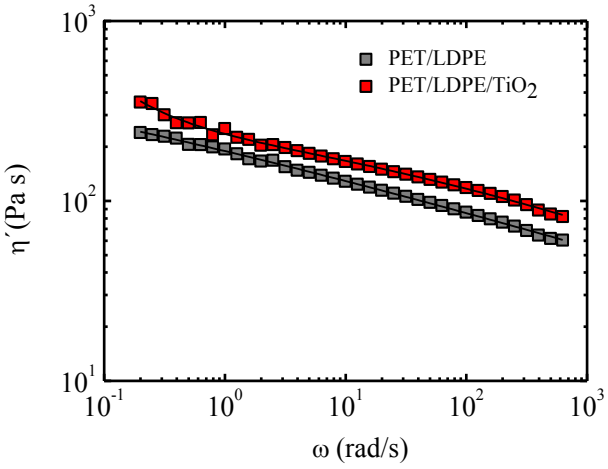

Figure 4. Viscosity against frequency obtained by SAOS for binary blend (PET/LDPE 80/20) and nanocomposite (PET/LDPE/TiO2 76/19/5) at 270ºC.

In figure 5 the storage modulus against frequency is plotted. The figure shows that at low and intermediate frequencies the blend containing nanoparticles exhibits higher modulus values than the binary blend. Indeed, the nanocomposite shows a plateau at low frequencies which arises from the formation of a percolated network due to the interactions between polymer chains and the nanoparticles. This network hinders the motion of the chains supressing the flow [6]. SAOS reveals as a valuable technique to characterize precisely the viscoelastic properties of the blend.

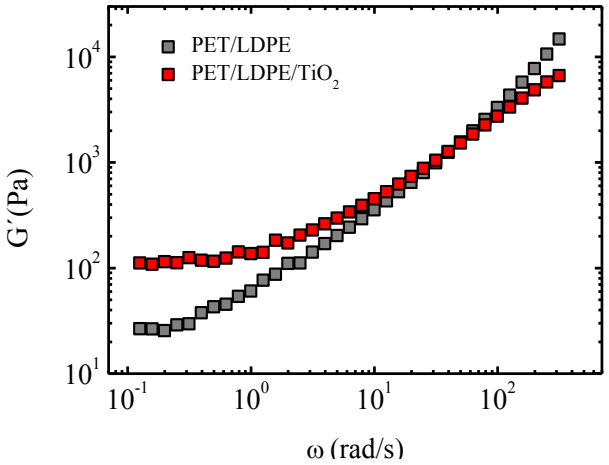

Figure 5. Storage modulus for binary blend (PET/LDPE 80/20) and nanocomposite (PET/LDPE/TiO2 76/19/5) at 270ºC.

Concluding Remarks

PET/LDPE blends with and without TiO_2 particles have been investigated. The morphological analysis reveals that the particles tend to localize at the interface which leads to the reduction of the LDPE droplets size.

Regarding to the viscoelastic properties, binary blend exhibits a pseudoplastic behaviour under continuous and SAOS flow, whereas the nanocomposite shows a viscoplastic behaviour. This behaviour arises from the presence of TiO_2 which promotes the interactions between LDPE and PET phase.

The rheological properties in continuous flow show that the presence of TiO2 reduces the viscosity, facilitating the processability of this blend. On the other hand, SAOS measurements allow us to gain insight into the relationship between the morphology and the viscoelastic properties.

Acknowledgements

We gratefully acknowledge funding by EU/FEDER funds through the Interregional Project REVALPET, POCTEFA EFA064/15 and the financial support from Basque Government, GIC IT-586-13. L.S. acknowledges a FPU thesis grant from Spanish Government.

References

1. Laoutid, F., Estrada, M., Michell, R.M., Bonnaud, L., Müller, A.J., Dubois, P. (2013). Polymer 54, 3982-3993.
2. Taguet, A., Cassagnau, P., Lopez-Cuesta, J.M. (2014). Prog. Polym. Sci. 39, 1526-1563.
3. Scaffaro, R., Botta, L. (2014). In Nanostructured Polymer Blends (Thomas, S:, Shanks, R., Chandrasekharakurup, S., Eds.), pp. 133-160 Elsevier, Amsterdam.
4. Li, W., Karger-Kocsis, J., Schlarb, A.K. (2009). Macromol. Mater. Eng. 294, 582-589.
5. Li, W., Karger-kocsis, J., Thomann, R. (2009). J Polym. Sci. B Polym. Phys. 47, 1616-1624.
6. Fernandez, I., Santamaria, A., Muñoz, M.E. Castell, P. (2007). Eur. Polym. J. 43, 3171-3176.

Contact Address:

leire.sangroniz@ehu.eus
POLYMAT and Polymer Science and Technology Department
Faculty of Chemistry
University of the Basque Country UPV/EHU
Address: Manuel de Lardizabal 3, 20018 Donostia-San Sebastián, Spain
Telf.: +34 943 018 494

Improving the properties of biodegradable Poly(butylene adipate-co-terephthalate) for packaging: From processing to application

L. Sangroniz, A. Sangroniz, M. Iriarte, A. Etxeberria, A. Santamaria

POLYMAT and Polymer Science and Technology Department, Faculty of Chemistry, University of the Basque Country UPV/EHU, Paseo Manuel de Lardizabal 3, 20018 Donostia-San Sebastián , Spain

Introduction

Nowadays commodity polymers are widely used in packaging applications; however, the major drawback of these polymers is that once they are used they are disposed in landfills or in incinerators. In order to overcome this problem, biodegradable polymers have been widely studied in the last years. In general biodegradable polymers exhibit poor mechanical and barrier properties, thus different techniques have been used to improve their features, so they can be suitable for the required application [1].

Poly(butylene adipate-co-terephthalate) (PBAT) is a biodegradable and compostable polymer that presents interesting properties such as high elongation at break, tear resistance and degradability. However this polymer shows poor barrier properties making it unsuitable for many packaging applications [2].

Several approaches have been carried out to improve the barrier character of polymers; one route is blending with another polymer that presents a better barrier performance.

In this work Poly(butylene adipate-co-terephthalate) is blended with a non-biodegradable polymer commercially known as Blox, which is a poly(amino-ether) resin. This is an amorphous thermoplastic polymer with high optical clarity. It presents excellent barrier properties, especially to oxygen and carbon dioxide. Furthermore, it shows adequate toughness and good adhesion to different substrates [3].

The obtained PBAT/ Blox blends are immiscible and the characterization of the barrier properties to different penetrants shows that the addition of Blox leads to a huge improvement. Since this blend has potential applications in the packaging sector, the study of its properties related to processing conditions becomes a necessary task.

In industry, films are obtained usually by blown film extrusion, so the rheological properties of the blends in shear and in elongation flow have to be studied. For that, small amplitude oscillatory shear (SAOS) measurements in the molten state have been performed, studying the effect of adding Blox on the viscoelasticity, which is relevant for processing. On the other hand, from an academic point of view, it is interesting to study the effect of the composition of the blend on the linear viscoelastic properties and the estimation of the interfacial tension of the blends. Regarding to the elongational flow, the blend has to exhibit adequate melt strength to be suitable for processing by blown film extrusion. In addition, the mechanical properties of the blends have been studied by DMTA measurements in order to assess its suitability for the final application [1, 4].

Experimental

In this work Poly(butylene adipate-co-terephthalate) (PBAT) which is also known as Ecoflex (Basf) and poly(amino ether) resin, that will appear as Blox (Dow Chemical) have been used. The following blends were prepared using a Model CS-183 MMX mixer at 190ºC and 40 rpm: 75 PBAT/ 25 Blox, 50 PBAT/ 50 Blox and 25 PBAT/ 75 Blox.

Thermal properties were measured in a differential scanning calorimeter model Q2000 V24 TA Instruments with heating and cooling rates of 10ºC/min.

The morphological analysis was carried out using a Scanning Electron Microscopy (Hitachi S-2700 electron microscopy). Previous to analyse the surface of the samples, the blends were cryogenically fractured and coated with gold.

Rheological measurements in the linear viscoelastic regime were performed in ARG2 rheometer. Small amplitude oscillatory shear experiments were carried out, under nitrogen atmosphere at 150ºC and using parallel plates geometry with a diameter of 25 mm.

Results and Discussion

Thermal analysis

Glass transition temperature is analysed to determine the miscibility of the system: Miscible blends show a single T_g, whereas immiscible ones have two T_g´s [5]. As can be seen in the data reported in Table 1, all the blends show two glass transition temperatures, indicating that the systems are immiscible.

Table 1. Glass transition temperature of PBAT/ Blox blends.

Sample	T_g (°C)
PBAT	-27
75 PBAT/ 25 Blox	-27, 72
50 PBAT/ 50 Blox	-27, 72
25 PBAT/ 75 Blox	-30, 73
Blox	77

Morphological analysis

The morphological analysis of PBAT/ Blox blends shows that for the studied compositions droplet matrix morphology is obtained. In Figure 1 SEM micrograph of 25 PBAT/ 75 Blox is shown; as can be seen the dispersed PBAT phase is spherical in shape and the droplets are homogeneously distributed in the Blox matrix. The adhesion between both components is good and not debonding is observed. The 75 PBAT/ 25 Blox blend shows also a droplet matrix morphology, however the 50 PBAT/ 50 Blox blend exhibits a co continuous morphology.

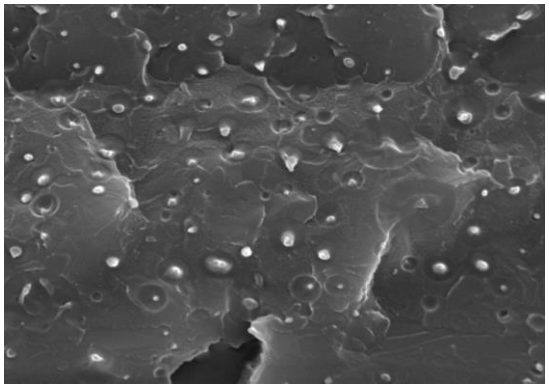

Figure 1. SEM micrograph of 25 PBAT/ 75 Blox blend.

Rheology

Cole Cole plots were used to investigate the viscoelastic properties of the blends. In this plot both components of the complex viscosity are represented: η´´ vs η´. Cole Cole plots are a valuable technique to distinguish between homogeneous and heterogeneous systems. If the system is homogeneous the plots will exhibit only one arc, as it is observed for PBAT and Blox polymers in Figure 2. However, in the case of a heterogeneous system two arcs can appear, if the relaxation time of each phase is different. For 50 PBAT/ 50 Blox an arc and a tail is observed, the other blends studied in this work (not shown in the plot) exhibit a similar behaviour regardless of the morphology. However, it has been reported in literature that depending on the morphology of the system the shape of Cole Cole plots can change. For droplet matrix morphology two semicircles are obtained; the first one corresponds to the matrix relaxation whereas the second one arises from the relaxation of the droplets. For co continuous morphologies an arc and a tail is observed, the tail corresponds to the network relaxation of interpenetrating phases. This behaviour has been reported for polymethyl methacrylate/poly(styrene-co-maleic anhydride) [6] and polystyrene/styrene-ran-acrylonitrile copolymer [7].

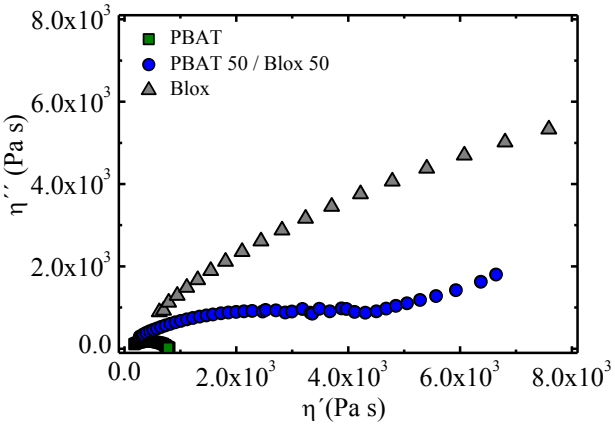

Figure 2. Cole Cole plots for PBAT, Blox and 50 PBAT/ 50 Blox blends. Only PBAT and Blox show a single arc that corresponds to homogeneous system.

Analogous to Cole Cole plots, the plot proposed by Han can also be employed, i.e., storage modulus vs loss modulus. For systems that obey time temperature superposition, Han's plot provides a temperature independent master curve without the need of further calculations. The independence of this plot from temperature is explained from the Doi and Edward tube model,

$$\ln G' = 2\ln G'' + \ln\left(\frac{6M_c}{5\rho RT}\right) \qquad (1)$$

where M_c is the entanglement molecular weight, ρ is the density, R the universal constant of gases and T temperature [8].

As can be seen in Figure 3, the data of the 50 PBAT/ 50 Blox blend deviates with respect to that of neat PBAT and Blox. The deviation is more pronounced for 25 PBAT/ 75 Blox blend, not shown in the figure. It should be taken into account that 50 PBAT/ 50 Blox blend has a co continuous morphology, whereas 25 PBAT/ 75 Blox blend shows a droplet matrix morphology. For the latter, droplets are smaller than for 75 PBAT/ 25 Blox blend and, consequently, the interfacial surface is higher. This leads to a more severe deviation in Han's plots, because the interfacial elastic contribution is higher.

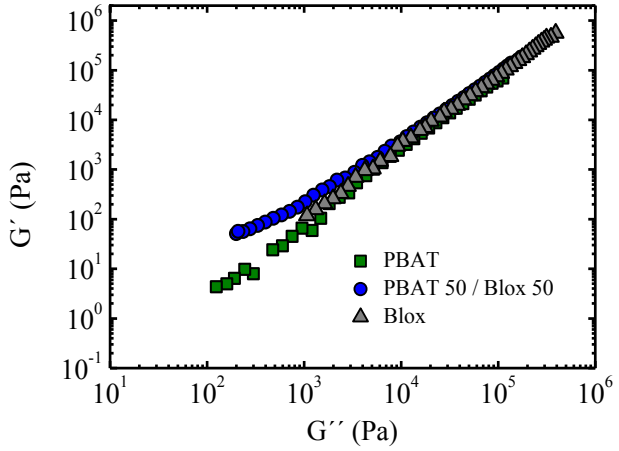

Figure 3. Han plots for PBAT, Blox and 50 PBAT/ 50 Blox. As can be seen the behaviour of the blend deviates respect from the pure polymers.

From a technological point of view it is important to study the effect of adding Blox to PBAT, since the viscoelastic properties of the blend change. In Figure 4 the viscosity is shown as a function of frequency, for PBAT, Blox and 50 PBAT/ 50 Blox. Neat PBAT, Blox and 75 PBAT/ 25 Blox blend exhibit a Newtonian behaviour followed by a pseudoplastic behaviour, since a viscosity constant value is only observed at low frequencies. However, for 50 PBAT/ 50 Blox and 25 PBAT/ 75 Blox blend a viscoplastic behaviour is observed, this response being more pronounced in the latter. Instead of reaching a constant value, the viscosity increases as frequency is decreased. Considering the morphology of the blends we can state that viscoplasticity is exhibited only when the size of the droplets is small enough to increase significantly the interface surface. In the case of 50 PBAT/ 50 Blox blend, viscoplasticity is not really observed. Instead, a second Newtonian plateau can be perceived at low frequencies. More research will be necessary to clarify this feature.

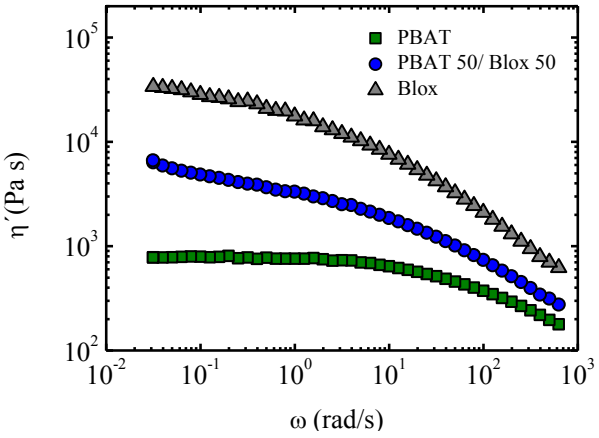

Figure 4. Viscosity against frequency for the systems studied in this work.

Although there are huge differences in the viscosity for the different blends at low and intermediate frequencies, at high frequencies the differences are diminished. In Figure 5 the viscosity corresponding to a frequency of 100 rad/s is analysed as a function of composition. In general, high frequency data match well with results obtained under processing conditions. As can be seen in the figure, the viscosity of the blends increases as Blox concentration is increased. The data can be fitted to the reciprocal mixing rule:

$$\frac{1}{\eta} = \frac{\phi}{\eta_A} + \frac{(1-\phi)}{\eta_B} \qquad (2)$$

The equation represents the viscosity of an infinitely layered mixture of two Newtonian liquids [9, 10], where Φ is the volume fraction, η_A and η_b are the viscosity of each phase and η is the viscosity of the blend. As can be seen the experimental data deviate slightly from the equation.

The blend containing 75 PBAT/ 25 Blox shows an interesting behaviour, since the addition of Blox does not increase the viscosity, showing a similar value to that obtained with PBAT. This arises from the high pseudoplasticity showed by the blend. Therefore 75 PBAT/ 25 Blox blend is a very adequate material, since with a small Blox content the permeability is reduced drastically, while the viscosity remains practically unchanged respect pure PBAT. Good permeability and adequate processability are, therefore, combined.

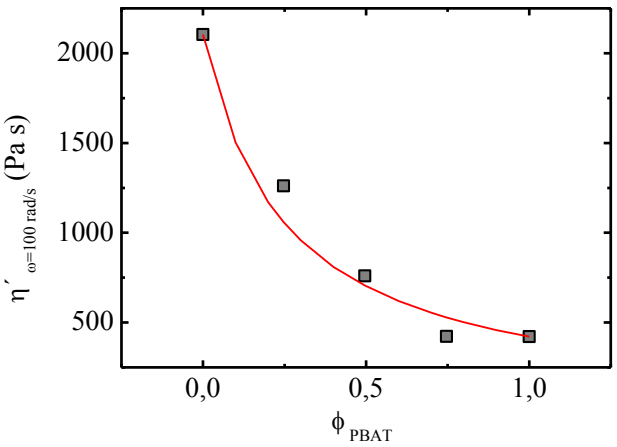

Figure 5. Viscosity taken at w = 100 rad/s has been plotted against the composition of PBAT.

Conclusions

Thermal analysis shows that the blends are immiscible, since two T_g's are obtained for all the blends. The morphological analysis shows that 25 PBAT/ 75 Blox and 75 PBAT/ 25 Blox blends exhibit droplet in matrix morphology whereas 50 PBAT/ 50 Blox exhibits a co continuous morphology.

The analysis of the viscoelastic properties carried out by Cole Cole and Han´s plots shows that the blends exhibit the typical behaviour of heterogeneous systems. Han´s plot shows that 50 PBAT/ 50 Blox and 75 PBAT/ 25 Blox blends bring about a more pronounced elastic contribution.

Although the addition of Blox provokes a huge increase of the viscosity at low and intermediate frequencies, at high frequencies the differences are very diminished, due to the pseudoplastic behaviour of the blends. This is an interesting result from the industrial processing point of view.

Acknowledgements

Authors thank the Basque Government for financial support (IT586-13 and IT618-13) and the Spanish Ministry of Innovation and Competitiveness MINECO (MAT2016-78527-P). L.S. acknowledges a FPU thesis grant from the Spanish Government and A.S. thanks the thesis grant from the Basque Government.

References

1. Eslami, H., Kamal, M.R., (2013). J. Appl. Polym. Sci. 129, 2418-2428.
2. Jiang, L., Wolcott, M.P., Zhang, J., (2006). Biomacromolecules 7, 199-207.
3. Granado, A., Eguiazabal, J.I., Nazabal, J., (2008). J. Appl. Polym. Sci. 109, 3892-3899.
4. Al-Itry, R., Lamnawar, K., and Maazouz, A., (2015) Polymers 7, 939-962.
5. Olabisi, O., Robeson, L.M., Shaw, M.T. (1979), In Polymer-Polymer Miscibility, pp. 117-193 Academic Press, New York.
6. Li, R., Yu, W., Zhou, C., (2006). J. Macromol. Sci. B, 45, 889-898.
7. Lopez-Barron, C.R., Macosko, C.W., (2014). J. Rheol., 58, 1935-1953.
8. Han, C.D., Kim, J.K. (1993). Polymer 34, 2533-2539.
9. Grizzuti, N., Buonocore, G., Iorio, G., (2000). J. Rheol. 44, 149-164.
10. Van Oene, H. (1978). In Polymer Blends (Paul, D.R., and Newman, S., eds.), Academic, New York.

Contact Address:

leire.sangroniz@ehu.eus
POLYMAT and Polymer Science and Technology Department
Faculty of Chemistry
University of the Basque Country UPV/EHU
Address Manuel de Lardizabal 3, 20018 Donostia-San Sebastián, Spain
Telf.: +34 943 018 494

A rheological study of epoxy resins mixed with ionic liquids and its implications in sustainable chemistry

M.M. Fernández, E. Garro, A. Santamaría

Polymer Science and Technology Department and Institute for Polymer Materials (POLYMAT), Faculty of Chemistry, University of the Basque Country (UPV/EHU) (Spain).

Introduction

Epoxy resins are the most important thermosetting polymers, because they possess a set of properties which make them apt for many applications in different industrial sectors. However, epoxy resins have a weak point from an environmental point of view, which concerns the use of volatile and toxic chemical agents, such amines, to carry out the curing (crosslinking) process. On the other hand, ionic liquids (IL) have gained ground in recent years as "green solvents", because of their high thermal stability, low volatility and recyclability, among other advantages.

In recent years the use of ionic liquids as catalysts and curing aiders of epoxy resins has been reported in the literature [1], but, notwithstanding the practical relevance of the subject, the origin of the interactions between both substances remains unclear. The use of rheological measurements to gain insight into epoxy-IL interactions has not been considered, so far.

In this work a rheological study of epoxy-IL systems is carried out, using hydrophobe an hydrophilic ionic liquids and considering the following aspects: a) Analysis of the terminal viscoelastic zone of epoxy-IL mixtures in the liquid state, using SAOS flow b) Time scans under isothermal conditions by SAOS experiments, to investigate the reduction of curing time, temperature and amine content, when ILs are added c) Dynamic mechanical thermal analysis (DMTA) and dielectric tests to evaluate the mechanical and electrical properties of the cured samples and correlate the results with the confinement or phase separation of the ionic liquid in the epoxy network.

Experimental

Materials

The polymer matrix of the prepared composites is a commercial resin produced by Gairesa (Spain), under the name of Bepox 1622, which is supplied as two components, epoxy/hardener in proportion 2.38 to 1 in weight, and formulated to fulfil a wide range of technical parameters.

The ILs used in the study were all commercial grade ILs supplied by Aldrich:

1-butyl-3methyl imidazolium bis (trifluoromethyl sulfonyl) imide $[C_{10}H_{15}F_6N_3O_4S_2]$, Trihexyl (tetradecyl) phosphonium chloride $[[CH_3(CH_2)_5]_3P(Cl)(CH_2)_{13}CH_3]$ and Trihexyl (tetradecyl) phosphonium dicyanamide $[[CH_3(CH_2)_5]_3P[N(CN)_2](CH_2)_{13}CH_3$.

Preparation of Epoxy/IL blends and curing process

Different amounts of the ILs were dissolved in the epoxy resin under mechanical stirring at room temperature for 10 min. The solutions were degassed in an ultrasound bath for 20 min. Then, the hardener component was added and stirred for 10 min. The curing protocol used was 2 h at 80ºC and 2h at T=120ºC.
The effect of the addition of Ionic Liquid on the epoxy network is investigated

Characterization

The rheological analysis was carried out in oscillatory mode using a Haake Rheostress 6000 rheometer equipped with parallel plates with a diameter of 20 mm.

Electrical characterization was performed using an Agilent impedance analyzer adapted to an ARES Rheometer (TA Instrument) by alternating current (AC) Measurement were carried out in the frequency range from 100 to 10^5 Hz.

The analysis of the epoxy/IL mixtures before curing was performed at room temperature and a frequency range from 0.1 to 100 Hz. An amplitude of 10% was applied to ensure a linear viscoelasticity response. The curing process was evaluated by rheological and electrical characterization at T = 80ºC.

Dynamic mechanical thermal analysis was performed in a Triton Tritec 2000 DMTA using bending cantilever mode. Heating Temperature sweep tests with a constant

heating rate of 4ºC/min were performed at a frequency of 1 Hz.

Results and Discussion

In Figure 1 the storage (elastic) modulus G' of pure epoxy and epoxy/ IL dispersions are plotted as a function of frequency. The data correspond to experiments at room temperature. Whereas the characteristic linear viscoelastic response of a liquid is observed for the pure epoxy resin, approaching scaling laws $G' \propto \omega^2$ and $G'' \propto \omega$, the G' slope is reduced and a plateau is observed at the lower frequencies for mixtures containing higher than 20% IL (expressed in weight percent of IL dispersed in the epoxy resin).

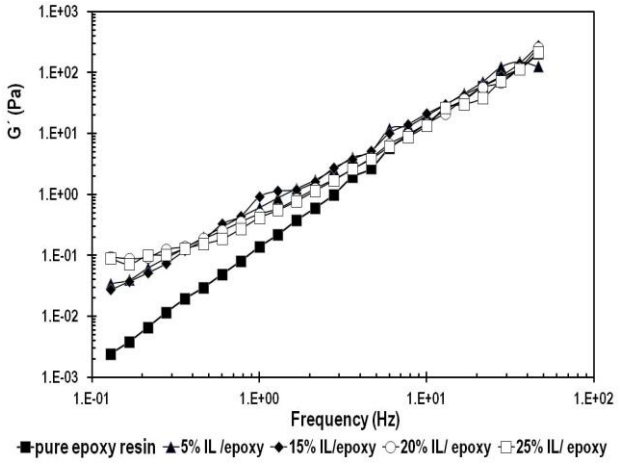

Figure 1. The storage modulus, G' taken at T=25ºC for pure epoxy and selected IL concentrations: 5%, 15%, 20% and 25%. Selected IL is 1-butyl-3methyl imidazolium bis (trifluoromethyl sulfonyl) imide [$C_{10}H_{15}F_6N_3O_4S_2$]

The evolution of storage modulus and loss modulus during isothermal curing process at T=80ºC for the pure epoxy resin and resin/ILs dispersions with different IL content is shown in Figure 2. The selected IL corresponds to 1-butyl-3methyl imidazolium bis (trifluoromethyl sulfonyl) imide [$C_{10}H_{15}F_6N_3O_4S_2$]. The time required for the G'=G'' cross over is taken as the gel point. The gel point is based on the transition from a liquid sate characterized by G''>G', to a solid state for which both moduli are frequency independent and G'>G''. The presence of IL resulted in a reduction of the gel time in 15-30 min with respect to pure thermosetting epoxy resin, depending on the IL concentration. Hence, IL accelerates the curing process of the epoxy resin. The result deals with the ability of Imidazolium-based IL to act as active promoter of curing for epoxy system [2].

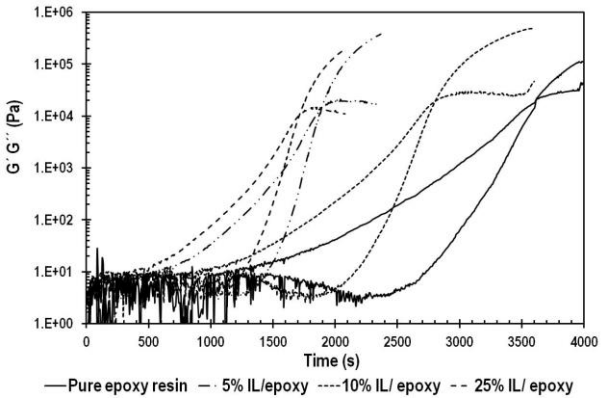

Figure 2. Variation of storage modulus, G' and loss modulus G'', (taken at a frequency of 1 Hz) with time during the curing process at T=80ºC for pure epoxy resin, and selected IL concentrations: 5%, 10% and 25%. Selected IL is 1-butyl-3methyl imidazolium bis (trifluoromethyl sulfonyl) imide [$C_{10}H_{15}F_6N_3O_4S_2$]:

The reduction of hardener content in the thermosetting system epoxy/hardener was also investigated. The curing process of the epoxy resin is considerably accelerated even when the hardener amount is reduced. This is seen in Figure 3 for the formulation containing 20% wt of IL and epoxy/hardener in proportion 2.38 to 0.75 in weight. However, we have to differentiate the observed acceleration from the effective curing effect. According to literature, the reaction activity of ionic liquids toward epoxy resin is expected to be connected with its thermal decomposition characteristics [3]. Considering the low range of temperatures used in this work, it was expected that the IL acted only accelerating the first stage of the curing process. In fact, the thermo-mechanical properties of the formulated resin with reduced hardener content, showed below, was consistent with the mentioned behaviour.

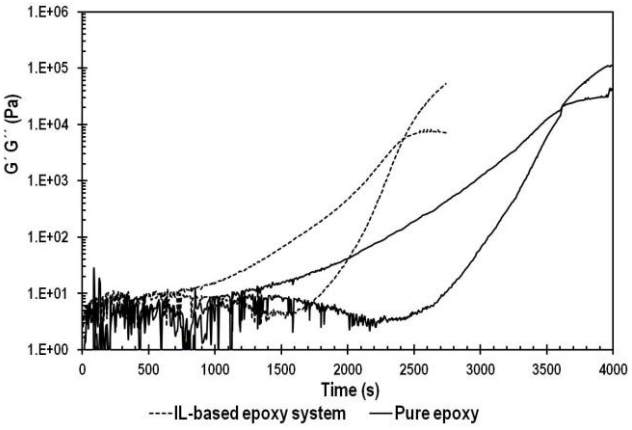

Figure 3. Variation of storage modulus, G' and loss modulus G'', (taken at a frequency of 1 Hz) with time during the curing process at T=80ºC for pure epoxy resin, epoxy/hardener in proportion 2.38 to 1 in weight, and 20% IL concentration 1-butyl-3methyl imidazolium bis (trifluoromethyl sulfonyl) imide [$C_{10}H_{15}F_6N_3O_4S_2$]: epoxy/hardener in proportion 2.38 to 0.75 in weight

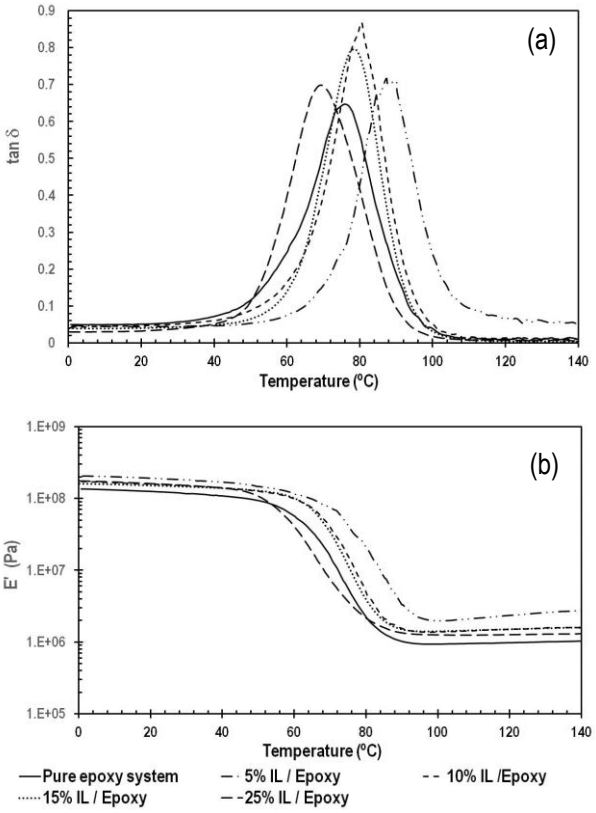

Figure 4. Dynamic mechanical thermal properties, DMTA, taken at a frequency of 1 Hz . a) Tan delta b) Storage modulus E', for pure epoxy resin, and IL concentrations: 5%, 10%, 15% and 25%. The selected IL is 1-butyl-3methyl imidazolium bis (trifluoromethyl sulfonyl) imide [$C_{10}H_{15}F_6N_3O_4S_2$]

The mechanical performance of the ILs-modified epoxy networks can be affected by the accelerated process. The DMTA curves presenting E' storage modulus and tan δ dependences for pure and ILs based epoxy thermosetting materials are given in Figure 4. Higher values of *E'* were obtained for all selected compositions; the highest values were noticed for the composition containing the lower amount of IL, which is 5%. In addition, the temperature for the *tan* δ peak, which stands for the glass transition temperature, *Tg*, was not affected for samples containing medium concentrations of IL i.e. 10% and 15%. The highest Tg value corresponded to the 5% IL composition, whereas the lower Tg value was observed for the 25% IL composition.

The results can be summarized as follows: 1) The crosslink density was not greatly affected, since tan δ peak values were only slightly higher than that of the pure epoxy system, 2) IL-based systems displayed higher storage moduli than that of the pure epoxy network in the temperature range below glass transition to rubbery state, suggesting an improvement of stiffness due to interactions between ILs and the epoxy matrix, and 3) A plasticizing effect, associated to a Tg reduction, was observed for the sample of the higher concentration of IL, 25% wt.

On the other hand, the mechanical performance of the 1-butyl-3methyl imidazolium bis (tri fluoro methyl sulfonyl) imide/IL sample that contains epoxy/hardener in proportion 2.38 to 0.75 in weight, so reducing the amount of the hardener with respect to the original formulation, indicated that the system was not effectively crosslinked.

As can be seen in Figure 5a, the IL modified system presented higher tan δ values, due to its reduced crosslinking density. Certainly, the ionic liquid accelerated the curing process, but at the selected temperature for curing, T=80ºC, it should be taken as non-reactive for stoichiometric consideration.

Interestingly, according to the results of Figure 5b the IL formulated system showed higher storage moduli at temperatures below glass transition (glassy state), due to the effect of interactions between ILs and epoxy matrix. But, in the rubber state, the modulus was clearly lower than that of the neat epoxy resin, owing to the mentioned reduced crosslinking density.

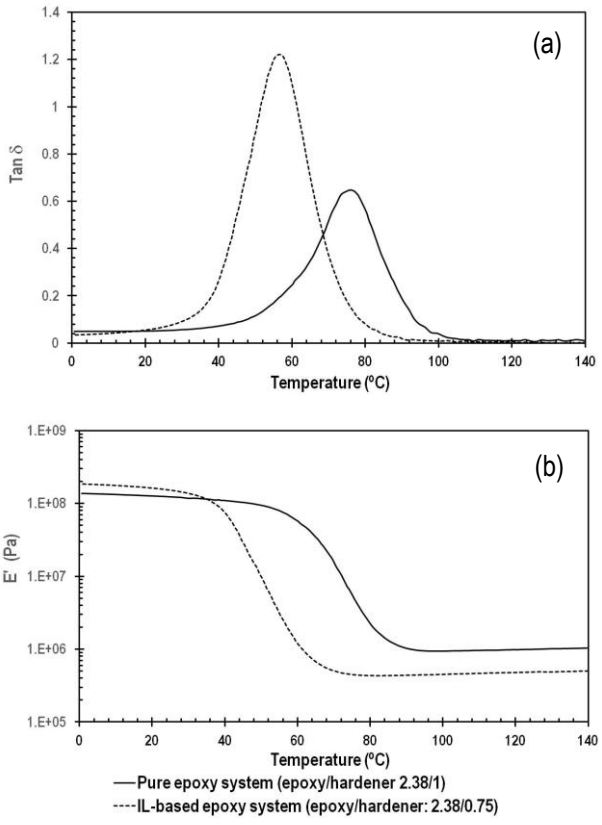

Figure 5. Dynamic mechanical thermal properties, DMTA, taken at a frequency of 1 Hz for pure epoxy resin, (epoxy/hardener in proportion 2.38 to 1 in weight), and 20% wt IL concentration (epoxy/hardener in proportion 2.38 to 0.75 in weight). Selected IL is 1-butyl-3methyl imidazolium bis (trifluoromethyl sulfonyl) imide [$C_{10}H_{15}F_6N_3O_4S_2$].
a) Tan delta, b) Storage modulus, E'..

Rheological characterization of the modified epoxy/IL system allowed us to study the effectiveness of the use of IL as additive on the formulation of commercial epoxy thermosetting resin. All the compositions of IL studied in this work were efficient accelerating the curing process. On the other hand, the interactions between epoxy resin/IL affected not only the viscoelastic behaviour of the system before curing, but also the mechanical performance of the cured material. The increase of the storage moduli of the cured IL-based system revealed the interactions effect on the network stiffness. The results also revealed the plasticizing effect of ionic liquid above a certain composition.

Acknowledgments

The authors gratefully acknowledge financial support from the the Grupo de investigación del Sistema Universitario Vasco IT 586-13

References

1. Nguyen T.K.L. et al. (2016) Sustainable Chemistry and Engineering Vol. 4, pp. 481-490
2. Soares, B.G., Livi, S., Duchet-Rumeau, J. Gerard, J.F., (2012) Polymer , Vol. 53, pp. 60-66.
3. Maka, H., Spychaj, T. and Zencker, M. (2015) Journal of industrial engineering Chemistry, Vol. 31, pp 192-198

Contact Address:

Dr. Mercedes Fernández San Martín
mercedes.fernandez@ehu.es
Polymer Science and Technology Department and Institute for Polymer Materials POLYMAT
Faculty of Chemistry
University of the Basque Country (UPV/EHU)
Paseo Manuel de Lardizabal, 3
20018 San Sebastian
Telf.: 943 018494; Fax: 943 017065

Effect of the addition of cellulosic fibers on the physico-chemical properties of soy protein bioplastics

S. Gamero-Roldán, M. Jiménez-Rosado, J. Fuente, C. Bengoechea

Departamento de Ingeniería Química, Facultad de Química, Universidad de Sevilla, (Spain)

Introduction

Plastics derived from petrochemicals have been extensively used in many applications for a very long time, which eventually have resulted in a serious environmental issue mainly due to the non-biodegradability of those materials. Thus, the progressive replacement of those traditional plastics by new plastics based on ingredients with a higher degradability is of special interest in the industry. Some of these environmentally friendly materials are based on biopolymers (e.g. proteins, polysaccharides).

Throughout the years, different protein sources as crawfish, potato, bloodmeal, gluten or soybean have been used as basis of the formulation of bioplastics. Soybean is the source of a vegetable protein that possesses a high amount of hydrophilic aminoacids (e.g. aspartic acid, glutamic acid), which eventually may lead to bioplastics with an enhanced water uptake capacity, even if the mechanical properties are diminished. Previous research has pointed out how certain ingredients (e.g. sodium carbonate) or chemical modifications (e.g. acylation) may increase the water uptake of soy protein based bioplastics [1,2]. The latter approach has even managed to obtain water absorption values high enough to be named superabsorbents. Superabsorbent materials (SAMs) are three-dimensionally cross-linked hydrophilic polymer networks that can absorb extremely large volumes of aqueous fluids in a short time, being able to retain the absorbed water even under heating or some pressure. SAMs can absorb water between 10 and 1000 times their own mass. The SAM market is mainly ruled by acrylic polymers. These are often toxic, non-biodegradable, and/or made from non-renewable materials. Thus, it is important to develop SAMs derived from natural and renewable sources, which would result in a much lower environmental impact (i.e. highly biodegradable), and are also characterized by lower production costs [3,4,5].

These biodegradable SAMs are a good example of a new type of materials with an excellent potential in a great variety of applications among which may include personal hygiene products, agriculture and horticulture.

The development of SAMs based on proteins presents both technological and economic benefits. In addition, they would be less polluting to the environment than most commercially used SAMs.

Natural fibers present typical properties as low density, biodegradability and proper specific mechanical properties. Those properties would make natural fibres an attractive ingredient to include in the soy-based bioplastics, in order to improve their mechanical properties without altering critically their biodegradability. Moreover, they are also characterized by good moisture absorption, which may favour their potential application as SAM.

The objective of the present study has been to study the effect of cellulose fibers on the development and properties of hydrophilic matrixes based on a soy protein isolate. Two different cellulose fibers have been used: a bleached fiber (0.4% lignin) and an unbleached fiber (5.15% lignin), with a fiber concentration within the range of 0.1 to 10.0% w/w. Thus, the optimization of both the composition and the processing have been considered.

Experimental

Materials

Soy protein isolate (SPI, min. 90% protein content, SUPRO 500E, Protein Technologies International, Inc. (USA)) was kindly supplied by PROANDA (Spain). Glycerol, from Panreac Quimica S.L.U. (Spain), was used as plasticiser, and cellulosic and lignocellulosic fibers (lignin content: 0.4 and 5.15%, respectively) were included within the formulation.

Sample preparation

A SPI/GL mass ratio equal to 1:1 was kept constant in all formulations. Blends mixing were achieved using a Polylab DC mixer (Thermo scientific, Haake, Germany), which can be used in batch processing operations and which provides the required agitation. The angular velocity of the slower blade was 50 rpm, and the blending process took 10 minutes. The blend was produced at room temperature, under adiabatic conditions, following the same protocol as in previous papers [6]. Injection moulding procedure was carried out in a Minijet Piston Injection Molding System (Thermo Haake, Germany) always at the same processing conditions (injection chamber temperature: 40ºC; mould temperature: 70 ºC; injection pressure: 500 bars). The shape of the specimens obtained was rectangular (60 × 10 × 1 mm) for dynamic tests or dumbshell for tensile tests.

Characterization

Dynamic tests were Strain sweep tests were performed with a RSA3 rheometer (TA Instruments, New Castle, DE, USA) using dual cantilever geometry in bending mode. First, the linear viscoelastic region (LVR) was determined through strain sweep tests at 1 Hz. Then, at a constant strain within the LVR, frequency sweep tests were performed at room temperature. At least two replicates of each measurement were performed.

Tensile tests were performed with a 10 kN ElectromechanicalTesting System (MTS), according to ISO527-2:1993 (Tensile Properties of Plastics) with an extension rate of 1 mm/min, at room temperature. At least five tests were carried out.

Water absorption tests were carried out according to ASTM D570 (2005). The water absorption percentage was calculated as:

$$\text{water uptake}\,(\text{wt}\%) = \frac{\text{wet wt.} - \text{conditioned wt.}}{\text{conditioned wt.}} \times 100 \quad (1)$$

where: wet wt, refers to the weight of the probe just after 24 h of water immersion; reconditioned wt, is the final weight of the wet sample after 24 h of drying in an oven at 50ºC. At least three replicates of each measurement were performed.

All results were obtained on samples 24 hours after of the manufacture and are reported as means and standard deviations.

Results and Discussion

Dynamic properties

Figure 1 displays the results obtained from the frequency sweep tests performed within the LVR for bioplastics containing either a lignocellulosic or a cellulosic fiber. The fiber concentration ranged from 1 to 5% (w/w).

It may be observed that in every case, as expected for a solid sample, the elastic modulus, E', is always higher than the viscous modulus, E'', independently of the fiber content.

When both fibers are compared, they seem to display a different evolution for E' and E'' when their content is increased: no apparent modification of the mechanical spectra takes place when varying the cellulosic fiber content (Figure 1, bottom); on the other hand, when using lignocellulosic fibers, the addition of fiber within the range of 0.1 to 1% results in a decrease in the mechanical properties. It may be related to weak fiber/matrix interfacial bonding [7]. Anyway, it seems that it improves when a fiber content equal to 5% is used.

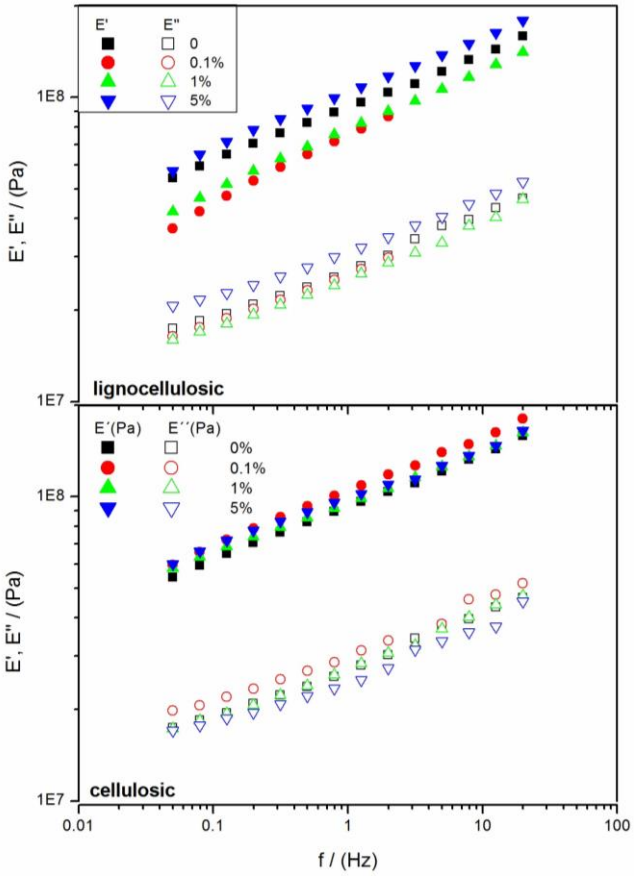

Figure 1. Mechanical spectra for SPI/GL bioplastics containing lignocellulosic (top) or cellulosic (bottom) fibers (0, 0.1, 1, 5% (w/w)

Mechanical properties

Previously, some researchers have justified the presence of fibers within a bioplastic material on terms of the expected strengthening of the mechanical properties of the material.

Figure 2 shows the evolution of characteristical mechanical parameters obtained from tensile tests with the fiber content: Young modulus (top), tensile strength (σ_{max}) (middle) and strain at break (ϵ_{max}) (bottom).

Even if no clear evolution is found for Young modulus, due to the high standard deviation of the results obtained, it is possible to observe how at least for the lignocellulosic fiber, an enhancement is observed when a fiber content of 5% is used. Thus, for a lignocellulosic fiber content from 0 to 1%, E is between 19-23 MPa, and when it is increased up to 5%, E reaches a value close to 29MPa. The cellulosic fiber does not seem to promote a significant enhancement of the Young modulus. These results match the previous results obtained from dynamic tests, even if no significant decrease in E is found for the lower lignocellulosic content

Tensile strength for bioplastics containing lignocellulosic fibers show an upward evolution as the fiber content increases. Anyway it should be noticed that differences are not significant for consecutive fiber contents. This evolution of tensile strength onto higher values as the fiber content increases is also observed for bioplastics containing cellulosic fibers. In this case, there is a significant and important enhancement of the tensile strength for the sample with 5% of cellulosic fiber content. Anyway, no significant differences are to be found for this parameter between samples containing lignocellulosic or cellulosic fibers.

When observing the maximum strain obtained with these samples, in both cases, the maximum value is observed at 5% fiber content, being significantly higher for the sample with lignocellulosic fiber.

Water uptake

Fibers are characterized by good moisture absorption, which considering the hydrophilic character of soy protein, could lead to bioplastics with a high water uptake capacity. Soy protein is rich in polar aminoacids (e.g. aspartic and glutamic acid) and, moreover, may be modified through functionalization to include a higher amount of polar groups like carboxyl groups (acylation) [2]. The mild conditions used in the processing of these bioplastics (temperatures lower than 70ºC) also would favour a higher water uptake capacity than that expected at more drastic conditions.

Figure 3 shows the results obtained for bioplastics containing either lignocellulosic or cellulosic fibers at different contents (0 to 5%). From these results, it seems that the inclusion of lignocellulosic fiber do not alter the water uptake capacity of the bioplastics significantly, when fiber content is lower than 1%.

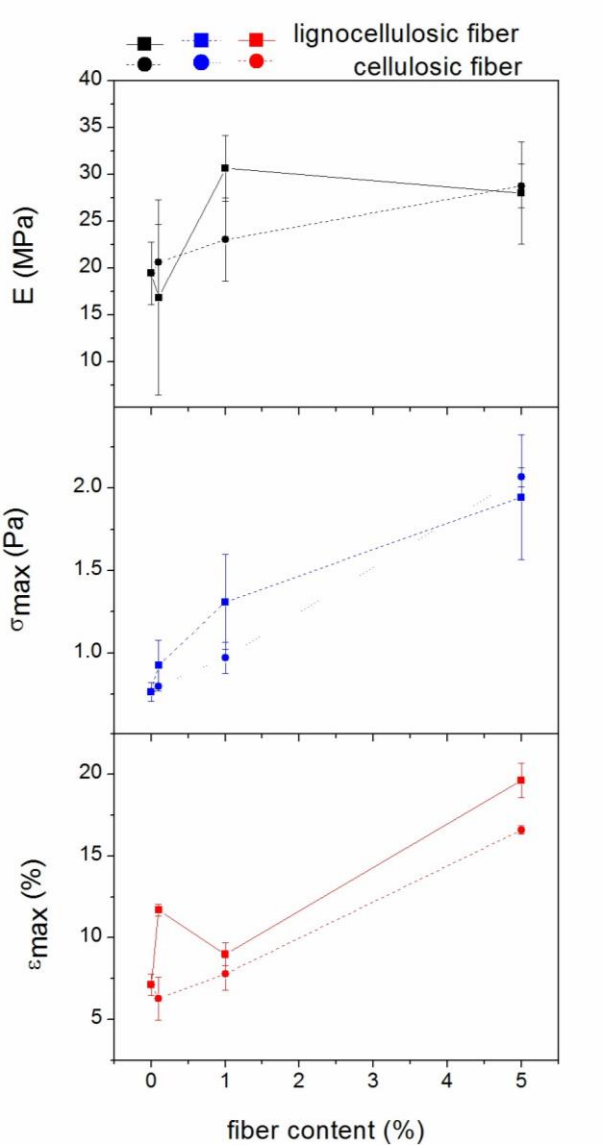

Figure 2. Mechanical parameters for SPI/GL bioplastics containing lignocellulosic (square) or cellulosic (circle) fibers (0, 0.1, 1, 5% (w/w)

On the other hand, cellulosic fibers do make a significant contribution to the water uptake properties of the materials, as it increases from 320% (0% fiber) up to 375% (0.1% fiber). From this data, it seems than in order to improve the absorption of water the cellulosic fiber content should be in the lower content range

(<1%). Thus, the addition of a 5% of fiber, either lignocellulosic or cellulosic, results in a decrease of the water uptake capacity. The decrease is more important when lignocellulosic fibers are used in the formulation.

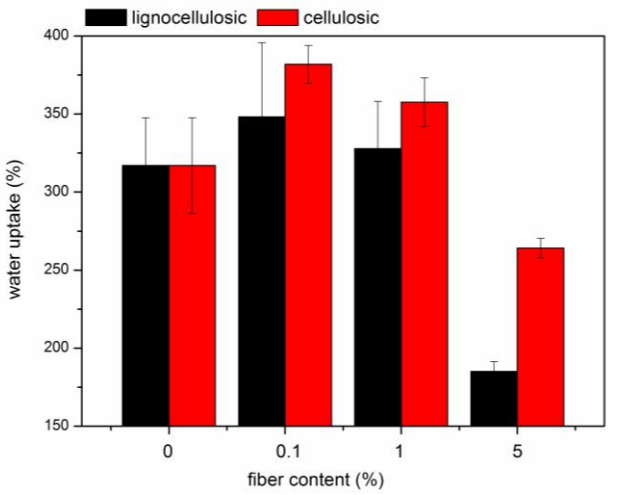

Figure 3. water uptake values for SPI/GL bioplastics containing lignocellulosic (black) or cellulosic (red) fibers (0, 0.1, 1, 5% (w/w)

Concluding remarks

The processing of bleaching the cellulosic fiber in order to extract the lignin clearly affects its properties when used as ingredient in the formulation of soy protein based bioplastics. Thus, the addition of lignocellulosic fiber in the bioplastics produces a modification of the mechanical spectra, displaying a maximum in E' and E'' at a fiber content equal to 5%. When bleached cellulosic fiber is used, mechanical spectra of the bioplastics basically remains unaltered, independently of the fiber content.

When observing the tensile properties, both tensile strength and maximum strain generally increases independently of the nature of the fiber.

Water uptake of the bioplastics is most affected when bleached cellulosic fibers are used, reaching higher values than the reference bioplastic for fiber contents lower than 1%. At 5% fiber content, a reduction in the water uptake was observed.

Acknowledgements

This work is part of a research project sponsored by "Ministerio de Economía y Competitividad" from Spanish Government (CTQ2015-71164-P (MINECO/FEDER, UE)). The authors gratefully acknowledge their financial support.

References

1. Fernández-Espada, L. (2016), PhD Thesis, Universidad de Sevilla
2. Cuadri, A.A., Romero, A., Bengoechea, C., Guerrero, A. (2017). Polymer Testing, 58, 126-134.
3. Zohuriaan-Mehr, M.J., Pourjavadi, A., Salimi, H., Kurdtabar, M. (2009). Polymers for Advanced Technologies, 20(8), 655-671.
4. M. Kamat, R. Malkani and J Indian, *Pediatrics,* 2003, 70 (11), 879-881.
5. M. Teodorescu, A. Lungu, P.O. Stanescu and C. Neamtu, *Ind Eng Chem Res,* 2009, 48 (14), 6527-6534.
6. Fernández-Espada, L., Bengoechea, C., Cordobés, F., Guerrero, A. (2016). Journal of Applied Polymer Science, 133 (24), 43524.
7. Abdul Khalil, H.P.S., Issam, A.M., Ahmad Shakri, M.T., Suriani, R. and Awang, A.Y. (2007) Industrial Crops and Products, 26, 3, 315–323.

Contact Address:

cbengoechea@us.es
Departmento de ingeniería química
Facultad de química
Universidad de Sevilla
C/Profesor García González, 1, 41012
Sevilla
Telf.: +34 954 557 179

Viscosity index improvers for multi-grade oil of copolymers polyethylene-propylene and hydrogenated poly(isoprene-co-styrene)

I. Stanciu

Department of Physical Chemistry, Faculty of Chemistry, University of Bucharest (Romania)

Introduction

The temperature range at which the oil is exposed in a vehicle engine is quite wide: from cold in winter with high temperatures during the summer when it is heated. Oil viscosity decreases with increasing temperature, and such a difference can be covered only by a single grade oil.

High temperature lubrication can be improved with the advent of oil viscosity index improvers or modifiers [1-5]. These polymers with low viscosity oils add their viscosity-temperature characteristic improves engineering and thicken them effectively at high temperatures [6-9]. Extends lubricating effect of a wider range of temperatures and thus called multi-grade oils.
Viscosity index is an empirical number indicating the degree of viscosity of an oil change on a given temperature range [10, 12]: high value means low variation and low value - high variation. The range of VI normal chain paraffinic oils without additives is between 95 and 105.

Viscosity decrease with increasing temperature can be reduced by using lubricating additives, also called viscosity index improver or viscosity modification. They are special polymers that - add low viscosity oils - viscosity-temperature characteristics improve them. [11, 13, 15] The additives effectively thickens the oil at all temperatures, but the increase in viscosity is more pronounced at high temperatures. The oil viscosity continues to decrease logarithmically with increasing temperature, but the slope is reduced considerably.
Extends lubricating effect so a higher temperature range and the oil turns from monograde in multigrade. The slope of the straight line log (viscosity)-log (temperature) is determined for a given polymer, the nature and concentration of the polymer, and the nature of the oil [10-12].

Importance VI can be demonstrated by considering the auto lubricants: an excessively thick VI oil when the engine is cold, start promoting rapid and prompt circulation and excessive thinning when the engine is hot, provides full lubrication and prevents consumption excessive oil.

The object of the present paper is the determination of viscosity indices or multigrade correspondence of some Infineum SV 260 and Paratone 8900 copolymers solutions – recommended as viscosity improvers for multi-grade mineral oils. We determined their effectiveness prevailed paraffinic oil SAE 10W.

Experimental

Dissolution of the two polymers in the oil SAE 10W was conducted at room temperature with gentle stirring for several weeks. Solutions of concentration 6 g / dL brew was then diluted with mineral oil SAE 10W to achieve concentrations of 3, 3.5, 4, 4.5 and 5g/dL.

The kinematic viscosities of the mineral oil SAE 10W and concentrated copolymer solutions 3, 3.5, 4, 4.5 and 5g/ dL were determined using a set of Schott Ubbelohde-type viscometers selected according to the values of their constants and viscosities of solutions, so that the margins of the uncertainty, inherent in the Hagebach-Couette correction, does not exceed the error allowed for the measurements. The measurements were carried out at 40 ± 0.1 and 100 ± 0.1°C, according to the recommandation of ASTM D2270. They were possible only for 3, 3.5, 4, 4.5 and 5 g/dL solutions with the available set of viscometers.

Results and Discussion

Viscosity is a measure of an oil thickness and ability to flow at certain temperatures, while viscosity index is a lubricating oil quality indicator, an arbitrary measure for the change of its kinematic viscosity with temperature and provides an insight into the oil's ability to perform at high and low temperatures.

The criteria for classification of mineral oils for engines take into account either the viscosity - that cause lubricating ability or performance - indicating the temperature which can be used.

The most used classification that takes into consideration the viscosity is done by Society of Automotive Engineers, SAE shortened. Based on measurements of viscosity SAE viscosity classification standard developed oils for cars J 300. For engine oils there are two types of SAE viscosity grades: one denoted by number and "W" and the only other number. The differences between the two types of classes are the following oils: oils "W" are upper limits for the dynamic viscosity and pumping cracking at low temperatures and minimum limits kinematic viscosity at 100°C, while no W oils have upper and lower for kinematic viscosity at 100°C and lower limit for viscosity at operating temperature (150°C) and shear rate (10^5 s^{-1}) large, but not for the viscosity at low temperatures. So classes W shows the performance at low temperatures and for those without W are provided only performance at high temperature.

If oils meet the requirements of only one class are called monograde, and if you meet the requirements of both classes are multi-grade. The multi-grade oils do not become too viscous at low temperatures and meet, also, the corresponding requirements class they belong to high temperatures. This means that their viscosity decreases with increasing temperature less than the grade oils.

Viscosity is a measure of an oil thickness and ability to flow at certain temperatures, while viscosity index is a lubricating oil quality indicator, an arbitrary measure for the change of its kinematic viscosity with temperature and provides an insight into the oil's ability to perform at high and low temperatures.

The criteria for classification of mineral oils for engines take into account either the viscosity - that cause lubricating ability or performance - indicating the temperature which can be used.

The most used classification that takes into consideration the viscosity is done by Society of Automotive Engineers, SAE shortened. Based on measurements of viscosity SAE viscosity classification standard developed oils for cars J 300. According to this, classes of oils - are defined according to dynamic and kinematic viscosity in different conditions.

For engine oils there are two types of SAE viscosity grades: one denoted by number and "W" and the only other number. The differences between the two types of classes are the following oils: oils "W" are upper limits for the dynamic viscosity and pumping cracking at low temperatures and minimum limits kinematic viscosity at 100°C, while no W oils have upper and lower for kinematic viscosity at 100°C and lower limit for viscosity at operating temperature (150°C) and shear rate (10^5 s^{-1}) large, but not for the viscosity at low temperatures. So classes W shows the performance at low temperatures and for those without W are provided only performance at high temperature.

If oils meet the requirements of only one class are called monograde, and if you meet the requirements of both classes are multi-grade. The multi-grade oils do not become too viscous at low temperatures and meet, also, the corresponding requirements class they belong to high temperatures. This means that their viscosity decreases with increasing temperature less than the grade oils.

The viscosity-temperature relationship shows how the viscosity of a fluid varies with the inverse temperature. From the mathematical relationship that exists between the two quantities is possible to predict fluid viscosity oil chart at any temperature within a limited range if known viscosity at two temperatures. Thus, according to ASTM Standard Viscosity-Temperature Charts for Liquid Petroleum Products, available in 6 ranges, are used: the two known viscosity-temperature points are located on the chart and a straight line is drawn through them. The other viscosity-temperature values of the given fluid will fall on this line.

Multi-grade oils typically begin as base oils. Then special oil-soluble organic polymers, called viscosity index improvers, are added in an effort to bring the difference in viscosities closer together. The viscosity still varies logarithmically with temperature, but the slope representing the change is lessened [2, 10, 12]. This slope, which represents the change in viscosity with temperature, depends on the nature and amount of the additives to the base oil.

The kinematic viscosities of 3, 3.5, 4, 4.5 and 5 g/dL copolymer solutions Infineum SV 260 and Paratone 8900 in SAE 10W as solvent were measured at 40 and 100°C, according to ASTM D2270, and the viscosity indices were determined using the ASTM D-341 diagram, shown in Figure 1 and Figure 2.

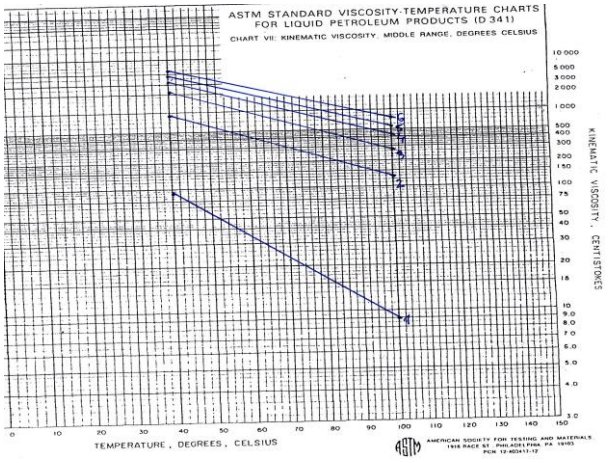

Figure 1. ASTM D-341diagram for determination of viscosity indices of SAE 10W oil and concentrated copolymer Paratone 8900 solution: 1- oil SAE 10W, 2- solution 3 %, 3- solution 3.5 %, 4 – solution 4 %, 5 – solution 4.5 % and 6 – solution 5 %

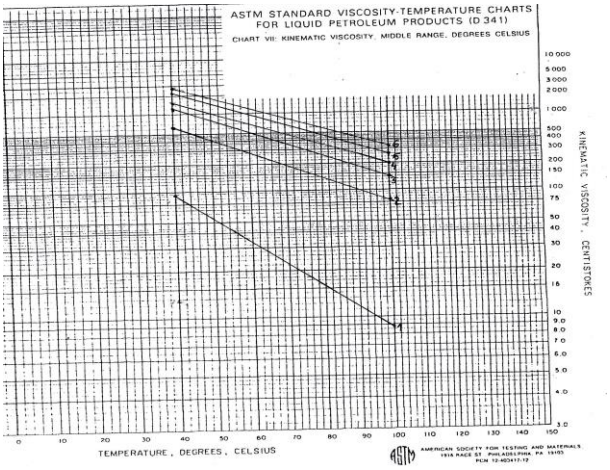

Figure 2. ASTM D-341diagram for determination of viscosity indices of SAE 10W oil and concentrated copolymer Infineum SV 260 solution: 1- oil SAE 10W, 2- solution 3 %, 3- solution 3.5 %, 4 – solution 4 %, 5 – solution 4.5 % and 6 – solution 5 %

The values obtained for the viscosity indices of 3, 3.5, 4, 4.5 and 5 % Infineum SV 260 and Paratone 8900 solutions are given in Table 1, together with their kinematic viscosities at 40 and 100°C and viscosity-temperature coefficients.

The value of its viscosity index corresponds also with literature data, typical viscosity indices for most paraffinic, solvent-refined mineral-based industrial oils falling in the range of 90 to 105.

As may be noticed greatly increases the viscosity index for the two copolymers, their values surpassing those of any synthetic fluid, which varies between 80 and 400 [7] produced by Paratone 8900 growth is higher than that produced by Infineum SV 260 at all concentrations. Thus, the VI of 3% Infineum SV 260 solution is 3.13 times higher than that of SAE 10W oil, the VI of 3.5% Infineum SV 260 solution is 4.21 times higher than that of SAE 10W, the VI of 4% Infineum SV 260 solution is 4.42 times higher than that of SAE 10W, the VI of 4.5% Infineum SV 260 solution is 4.57 times higher than that

of SAE 10W and that of 5% solution 4.71 times, while that of 3 % Paratone 8900 solution is 4.38 times higher, that of 3.5% Paratone 8900 solution is 4.7 times higher, that of 4 % Paratone 8900 solution is 4.86 times higher, that of 4.5% Paratone solution is 5.18 times higher and that of 5% is 5.33 times.

A copolymer solution Paratone 8900 shows a greater increase of viscosity at all concentrations. The dependences of viscosity indices on concentration of copolymers Infineum SV 260 and Paratone 8900 are shown in Figure 3.

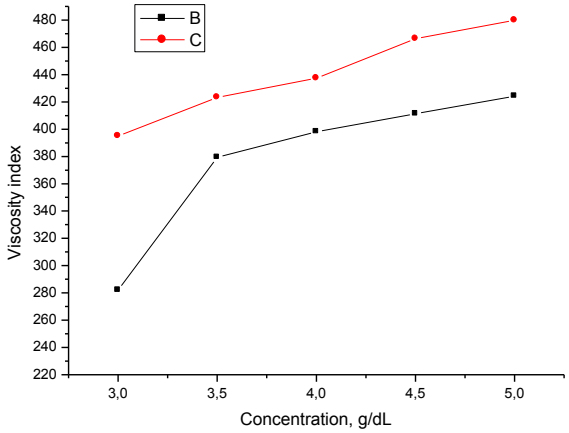

Figure 3. Dependence of viscosity indices on copolymer concentration: B – Infineum SV 260; C – Paratone 8900

As can be seen from the Figure, the values of VI of Paratone 8900 solutions increase almost linearly with concentration, whilst those of Infineum SV 260 tend towards a limiting value. The higher the concentration, the higher the differences between the viscosity indices of the two copolymer solutions are. This demonstrates that Paratone 8900 is a better viscosity index improver for the mineral oil SAE 10W irrespective of concentration, in accordance with the previous results, which shown that the viscosities of solutions of this polymer are less dependent on temperature for all the concentration, that is it is a better viscosity improver compared with Infineum SV 260.

Another indication of the change in kinematic viscosity with temperature, which is less arbitrary than the

viscosity index, is the viscosity-temperature coefficient, VTC, defined by the relationship:

$$VTC = (a - b)/a \quad (1)$$

where a is the viscosity (cSt) at 40°C and b – viscosity at 100°C. The lower the viscosity-temperature coefficient, the higher the viscosity index is. They are in accordance with the values of VI and the previously published results on the efficiency of the two copolymers as viscosity improvers obtained using the dynamic viscosities [5]. The lowest values were obtained for Paratone 8900 solutions, which prove once more that this copolymer is a better viscosity index improver.

Conclusions

The viscosity indices of 3, 3.5, 4, 4.5 and 5% solutions of copolymers Infineum SV 260 and Paratone 8900, recommended as viscosity index improvers, in SAE 10W mineral oil as solvent were determined using the ASTM 2270-93 diagram.

Infineum SV 260 produces a lower increase of viscosity indices comparative with Paratone 8900: 3.13 times for a concentration of 3%, 4.21 times for 3.5%, 4.42 times for 4%, 4.57 times for 4.5% and 4.71 times for 5% compared with 4.38, 4.7, 4.86, 5.18 and 5.33 times, respectively.

The values of viscosity-temperature coefficients, calculated from the kinematic viscosities of solutions at 40 and 100°C, show also that Paratone 8900 is a better viscosity index improver than Infineum SV 260 irrespective of concentration.

References

1. Fernandes, C. M., Amaro, P. M., Martins, R. C., & Seabra, J. H. (2013). Torque loss in thrust ball bearings lubricated with wind turbine gear oils at constant temperature. Tribology International, 66, 194-202.
2. Smeeth, M., Spikes, H., & Gunsel, S. (1996). Boundary film formation by viscosity index improvers. Tribology transactions, 39(3), 726-734.
3. Gunsel, S., Smeeth, M., & Spikes, H. (1996). Friction and wear reduction by boundary film-forming viscosity index improvers (No. 962037). SAE Technical Paper.
4. Wang, J., Ye, Z., & Zhu, S. (2007). Topology-engineered hyperbranched high-molecular-weight polyethylenes as lubricant viscosity-index improvers of high shear stability. Industrial & engineering chemistry research, 46(4), 1174-1178.
5. Horne, W. V. (1949). Polymethacrylates as viscosity index improvers and pour point depressants. Industrial & Engineering Chemistry, 41(5), 952-959.
6. Eckert, R. J. A., & Covey, D. F. (1988). Developments in the field of hydrogenated diene copolymers as viscosity index improvers. Lubrication Science, 1(1), 65-80.
7. Mueller, H. G. (1978). Mechanism of action of viscosity index improvers.TRIBOLOGY international, 11(3), 189-192.
8. Fan, J., Müller, M., Stöhr, T., & Spikes, H. A. (2007). Reduction of friction by functionalised viscosity index improvers. Tribology Letters, 28(3), 287-298.
9. Jukic, A., Vidovic, E., & Janovic, Z. (2007). Alkyl methacrylate and styrene terpolymers as lubricating oil viscosity index improvers. *Chemistry and Technology of Fuels and Oils*, *43*(5), 386-394.
10. Port, W. S., O'Brien, J. W., Hansen, J. E., & Swern, D. (1951). Viscosity Index Improvers for Lubricating Oils. Polyvinyl Esters ofLong-Chain Fatty Acids.Industrial & Engineering Chemistry, 43(9), 2105-2107.
11. Smeeth, M., Spikes, H., & Gunsel, S. (1996). Performance of viscosity index improvers in lubricated contacts. Langmuir, 12(19), 4594-4598.
12. Kapur, G. S., Sarpal, A. S., Mazumdar, S. K., Jain, S. K., Srivastava, S. P., & Bhatnagar, A. K. (1995). Structure—performance relationships of viscosity index improvers: I microstructural determination of olefin copolymers by NMR spectroscopy. Lubrication science, 8(1), 49-60.

Contact Address:

istanciu75@yahoo.com
Department of Physical Chemistry
Faculty of Chemistry
Universityof Bucharest
Address 4-12 Elisabeta Blvd

Magnetorheology of alginate ferrogels

C. Gila-Vílchez, M. T. López-López, A. B. Bonhome-Espinosa, J. D. G. Durán

Department of Applied Physics, Faculty of Science, University of Granada (Spain)

Introduction

Hydrogels consist on cross-linked networks of hydrophilic polymer chains dispersed in a continuous aqueous medium. Due to their interesting properties for applications, such as high water content, softness, flexibility and biocompatibility, hydrogels have been widely studied [1]. In particular, they have found extensive applications as biomaterials: they have been used for the delivery of drugs and cells [2-4] or as scaffolds in tissue engineering [5-9].

Although hydrogels are very soft materials, microparticles can be incorporated into them to change their mechanical properties [10]. Indeed, the mechanical properties of these materials can be controlled by an external magnetic field when magnetizable microparticles are embedded in the polymer network, obtaining magnetic-field sensitive gels called magnetic gels or ferrogels [11]. This smart property might be used, for example, in technological applications as magneto-controlled dampers, vibration and shock absorbers [12]. They have also found several applications as scaffolds in the field of tissue engineering, where their mechanical properties can be matched by magnetic field application to those of potential target tissues [13]. Furthermore, the presence of magnetic particles within the hydrogels plays an important role for nearby cells. In particular, it stimulates cell adhesion and proliferation [14-16]. Finally, the presence of magnetic particles also allows visualization by magnetic resonance imaging [17].

On account of the wide range of applications of the hydrogels, the fundamental investigation of their rheological properties is nowadays an active field of research. Measurements may involved from simple frequency sweep tests to more complex tests such as steady-state storage modulus, gelation kinetics or sol-gel transition of hydrogels [18-23].

This work focuses on the rheology of alginate hydrogels with silica-covered iron microparticles embedded in them. The mechanical versatility of these ferrogels makes them attractive candidates for further development in biomedical and technological applications.

Experimental Methods

Alginate ferrogel preparation

A standard sample preparation procedure was performed in order to ensure a high reproducibility of the rheological measurements.

Sodium alginate (empirical formula $(C_6H_8O_6)_n$) obtained from the extracellular matrix of brown algae, with a molecular weight of 176.10 g/mol (Sigma Aldrich, USA), was used as material for the preparation of the polymer network. As source of calcium ions to initiate gelation calcium carbonate ($CaCO_3$) was used in combination with D-glucono-δ-lactone (GDL) (Sigma Aldrich, USA). We used silica-covered iron particles (Fe-CC), whose density was 7.5 g cm^{-3}, (BASF, Germanny) as magnetic phase in the preparation of ferrogels. Figure 1 shows that the iron particle surface was completely covered by the silica coating even thought its thickness was not totally uniform. Moreover, these particles presented a typical ferromagnetic behaviour with a saturation magnetization (M_S) value of 1587 ± 2 kA m^{-1} (Fig. 2)

For the preparation of the ferrogels, we proceeded as follows. First, sodium alginate was dissolved in distilled water at a concentration of 1% w/v. For a final volume of 5 mL, we added 7.5 mg of $CaCO_3$ and 26.7 mg of GDL to the sodium alginate solution and stirred the mixture by a vortex mixer for a few seconds to initiate gelation. Approximately 90 min after the gelation was initiated, we stirred the hydrogel again by a vortex mixer and added the required Fe-CC powder to attain the desired concentration of particles. Then, this mixture was sonicated for 10 min and placed in a culture dish for 120 min. Finally, we added 5 additional mL of calcium chloride at a concentration of 45 mM to the samples and they were placed overnight in a wet ambient at room temperature. For comparison, we also prepared non-

magnetic hydrogels by following the same protocol without particle addition.

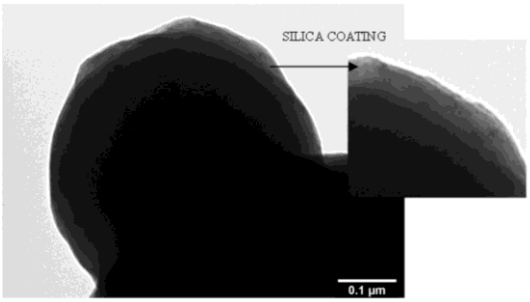

Figure 1. HREM (High-Resolution Episcopic Microscopy) micrograph of the silica coated iron particles (Fe-CC). Taken with permission from [24].

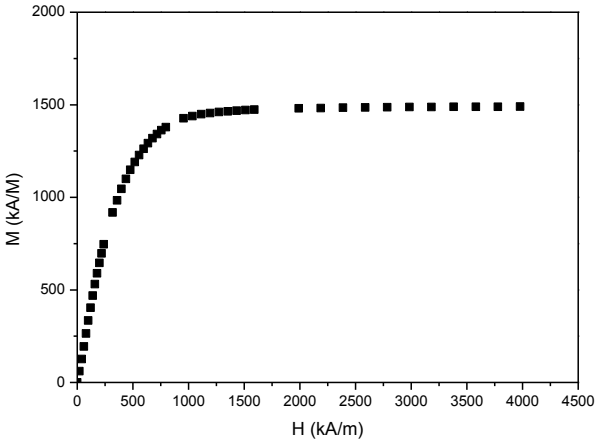

Figure 2. Magnetization curve of Fe-CC particles.

Oscillatory rheometry of alginate ferrogels

A rotational (magneto)rheometer (Physica MCR 300) with a plate-plate geometry (20 mm of diameter) was used to carry out the rheological measurements, at a constant temperature of 25 ± 0.1 ºC.

In order to determine the viscoelastic linear region (VLR) of the different ferrogels, we carried out a deformation amplitude sweep test at a constant frequency of 1 Hz and stepwise increasing strain. Afterwards, we did a frequency test at strain amplitude within the VLR, and angular frequency in the range 0.3 to 100 rad/s, for the different ferrogels, and under different magnetic field intensities.

During all the measurements we imposed a constant normal force of 0.1 N to ensure that there was always contact between the plate and the ferrogel –note that ferrogels experience magnetostriction. Differences in the gap thickness within an amplitude or frequency sweep were always smaller than 10%.

Results and Discussion

We investigated the rheological response of our ferrogels at different concentrations of Fe-CC particles and under the application of an external magnetic field. In all cases, the storage modulus (G') was considerably higher than the loss modulus (G''), indicating that our ferrogels were more elastic than viscous, as expected for cross-linked networks.

Results for the storage (G') and loss modulus (G'') show that these quantities were considerably enhanced for ferrogels with respect to nonmagnetic hydrogels – i. e., there was a substantial enhancement of the mechanical properties of ferrogels with respect to non-magnetic ones (Fig. 3) that is connected with the addition of particles, but not with their magnetic character. Furthermore, we have observed that this enhancement is more pronounced at larger concentrations (results not shown here). Thus, it must be explained by changes induced by the particles in the internal structure of the hydrogels when they were added in the formulation. To be precise, this enhancement can be explained by the additional cross-linking between alginate fibres imparted by the particles – a similar enhancement was previously observed for fibrin-based magnetic biomaterials [11].

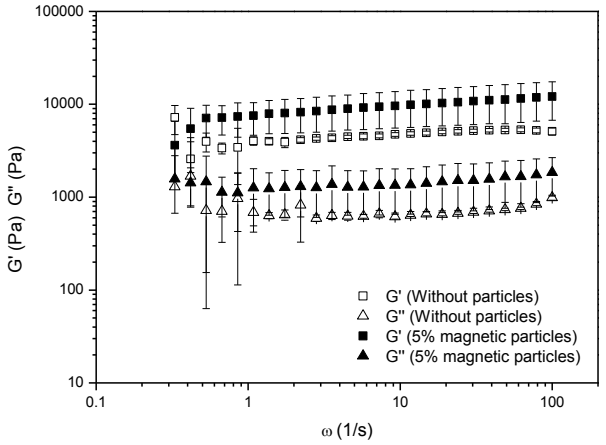

Figure 3. Storage (G') and loss (G'') moduli as a function of oscillation frequency for a non-magnetic hydrogel and a ferrogel containing a volume concentration of particles of 5%.

On the other hand, it was also observed an enhancement of the mechanical properties of the ferrogels which was related to the application of an external magnetic field (Fig. 4). The reason is that, in the presence of an external magnetic field, the particles embedded in the hydrogel get magnetized and attract each other, forming field aligned structures. Due to these structures, induced by the dipole moments of the magnetic particles, the ferrogel experience a shape

change of its internal structure and therefore a higher hardness. Note that this increase of G' and G'' with the intensity of the applied magnetic field was more pronounced as the particle concentration is higher (results not shown here for brevity). Given that the particle concentration is higher, there are more particles in contact forming field aligned structures.

Furthermore, the increase on G' and G'' is more pronounced due to the application of an external magnetic field than that only due to the increase in particle concentration.

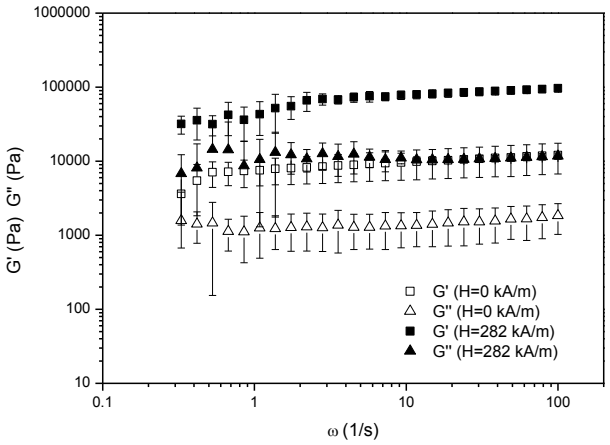

Figure 4. Storage (G') and loss (G'') moduli as a function of oscillation frequency and for two magnetic field intensities (H). Ferrogel containing 5% volume concentration of magnetic particles.

What is more, the limit of the VLR has been also determined, concluding that the VLR of the ferrogel is narrowed both by the increase in the particle concentration and in the magnetic field intensity (Fig. 5). As we have previously discussed, when the concentration of magnetic particles and the intensity of the applied magnetic field were increased, the ferrogels became harder due to the changes induced in the polymer network. However, the harder the ferrogels become, the more rigid are with respect to deformation. This result is reflected in the decrement of their critical strain, which was considered as the point where the storage modulus deviates 10% from the plateau level.

As it is shown in Figure 5, above the critical strain the storage modulus decreases strongly in all cases. However, we observe different behaviours of the loss modulus as a function of the Fe-CC concentration and the intensity of the applied magnetic field, which passes through a distinct maximum (related to the maximum dissipation of energy) before decreasing. When the shear strain amplitude exceeds the critical strain the field-aligned chains formed by Fe-CC particles start to split and thus to break the ferrogel in smaller pieces. Each one of these parts is more solid-like than liquid-like, so we still observed G' values higher than G'' values despite the fact that the ferrogel was actually broken.

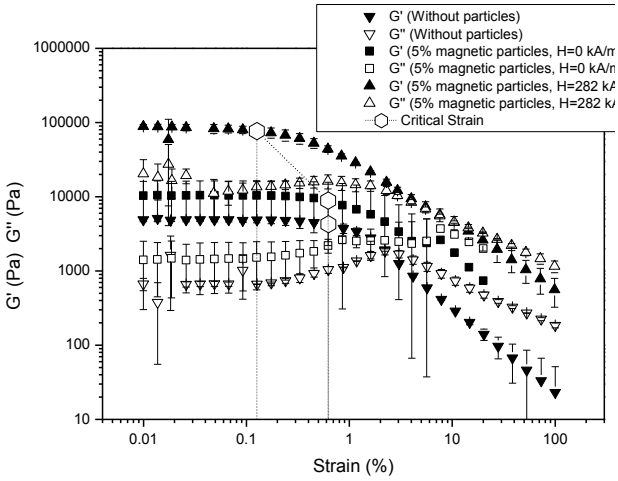

Figure 5. Storage (G') and loss (G'') moduli as a function of amplitude strain for a non-magnetic hydrogel and a ferrogel (under two magnetic field intensities, H) containing a 5% volume concentration of particles and at a frequency of 1 Hz.

Conclusions

We have obtained macroscopically homogeneous magnetic hydrogels with silica-covered iron particles embedded in an alginate network at different particle concentrations. We have found that these magnetic hydrogels show superior mechanical properties as compared with non-magnetic hydrogels. Furthermore, this enhancement increases as a function of the volume concentration of particles embedded in the hydrogels due to the role of the Fe-CC particles as cross-linkers of the alginate network.

We have also observed a more pronounced enhancement of the mechanical properties of the ferrogels when a magnetic field is applied. The reason for this enhancement is that the magnetic field induces the formation of Fe-CC structures which provide a higher hardness and rigidity. In fact, we have observed that the linear viscoelastic region is narrowed because of the internal structure changes previously mentioned.

To conclude, we have developed a new protocol for the preparation of such kinds of ferrogels with improved mechanical properties. Indeed, we intend this to be the first step in the further development of other similar materials, which can provide a wide range of new applications.

Acknowledgements

This study was supported by project FIS2013-41821-R (Plan Nacional de Investigación Científica, Desarrollo e Innovación Tecnológica, Ministerio de Economía y Competitividad, Spain, co-funded by ERDF, European Union). C. Gila Vílchez also acknowledges financial support from MECD, Spain.

References

1. Caló, E., and Khutoryanskiy, V.V. (2015). European Polymer Journal, 65, 252–267.
2. Langer, R. (1990). New methods of drug delivery, Science, 249, 1527-1533.
3. Mitragotri, S. and Lahann, J. (2009). Nature Materials, 8, 15-21.
4. Choi, N.W., Cabodi, M., Held, B., Gleghorn, L., Bonassar, J. and Stroock, A.D. (2007). Nature Materials, 6, 908-915.
5. Atala, A., Bauer, S.B., Soker, S., Yoo, J.J. and Retik, A.B. (2006). Lancet, 367, 1241-1246.
6. Boucard, N., Viton, C., Agay, D., Mari, E., Roger, T., Chancerelle, Y. and Domard, A. (2007). Biomaterials, 28, 3478-3488.
7. Rodriguez, I.A., López-López, M.T., Oliveira, A.C., Sánchez-Quevedo, M.C., Campos, A., Alaminos, M. and Durán, J.D.G. (2012). Journal of Tissue Engineering and Regenerative Medicine, 6 (8), 636.
8. Carriel, V., Garrido-Gomez, J., Hernandez-Cortes, P., Garzon, I., Garcia-Garcia, S., Sáez-Moreno, J.A., Sánchez-Quevedo, M.C., Campos, A. and Alaminos, M. (2013). Journal of Neural Engineering, 10, 026022.
9. García-Martínez, L., Campos, F., Godoy-Guzmán, C., Sánchez-Quevedo, M.C., Garzon, I., Alaminos, M., Campos, A. and Carriel, V. (2016). Histochemistry and Cell Biology, doi: 10.1007/s00418-016-1485-9.
10. Ilg, P. (2013). Soft Matter, 9, 3465-3468.
11. López-López, M.T., Scionti, G., Oliveira, A.C., Durán, J.D.G., Campos, A., Alaminos, M., and Rodríguez, I.A. (2015). PLoS ONE, 10(7): e0133878.
12. López-López, M.T., Durán, J.D.G., Iskakova, L.Y., and Zubarev, A.Y. (2016). Journal of Nanofluids, 5, 479–495.
13. López-López, M.T., Rodríguez, I.A., Rodríguez-Arco, L., Carriel, V., Bonhome-Espinosa, A.B., Campos, F., Zubarev, A., and Durán, J.D.G. (2016). Journal of Magnetism and Magnetic Materials, 431, 110-114.
14. Bañobre-López, M., Piñeiro-Redondo, Y., De Santis, R., Gloria, A., Ambrosio, L., Tampieri, A., Dediu, V. and Rivas, J. (2011). Journal of Applied Physics, 109, 07B313.
15. Bock, N., Riminucci, A., Dionigi, C., Russo, A., Tampieri, A., Landi, E., Goranov, V.A., Marcacci, M. and Dediu, V. (2010). Biomaterialia, 6, 786-796.
16. Zeng, X.B., Hu, H., Xie, L.Q., Lan, F., Jiang, W., Wu, Y. and Gu, Z.W. (2012). International Journal of Nanomedicine, 7, 3365-3378.
17. Ziv-Polat, O., Skaat, H., Shahar, A. and Margel, S. (2012). International Journal of Nanomedicine, 7, 1259-1274.
18. Adibnia, V. and Hill, R.J. (2016). Journal of Rheology, 60, 541-548.
19. Calvet, D., Wong, J.Y. and Giasson, S. (2004). Macromolecules, 37, 7762-7771.
20. Cho, J., Heuzey, M.C. and Hamdine, M.L. (2007). Macromolecular Materials and Engineering, 292, 571.
21. Curtis, D.J., Holder, A., Badiei, N., Claypole, J., Walters, M., Thomas, B., Barrow, M., Deganello, D., Brown, M.R., Williams, P.R. and Hawkins, K. (2015) Journal of Non-Newtonian Fluid Mechanics, 222, 253-259.
22. Rubistein, M. and Colby, R.H. (2003).Polymer Physics, Oxford University, New York, NY.
23. Bonhome-Espinosa, A.B., Campos, F., Rodriguez, I.A., Carriel, V., Marins, J.A., Zubarev, A., Duran, J.D.G. and Lopez-Lopez, M.T. (2017). Soft Matter, 13, 2928-2941.
24. Gómez-Ramírez, A., López-López, M.T., González-Caballero, F., Durán, J.D.G. (2011). Smart Materials and Structures, 20, 045001.

Contact Address:

gila@ugr.es
Department of Applied Physics,
Faculty of Science
University of Granada
Avda. Fuentenueva s/n, 18017, Granada (Spain)
Telf.: +34 958249099; Fax: +34 958243214

Crucial viscoelastic features for polymer 3D printing

M. I. Calafel[1], R. H. Aguirresarobe[1], A. Santamaria[1], N. Sadaba[2], M. Boix[3], B. Pascual[3], I. Conde[3]

[1]Institute of Polymer Materials (POLYMAT) and Polymer Science and Technology Department, Faculty of Chemistry, University of the Basque Country (UPV/EHU), Paseo Manuel de Lardizabal 3, 20018 Donostia-San Sebastián (Spain)
[2] Institute of Polymer Materials (POLYMAT), Mining-Metallurgy Engineering and Materials Science Department, Faculty of Engineering, University of the Basque Country (UPV/EHU), Alameda de Urquijo s/n, 4013 Bilbao (Spain)
[3] ERCROS S.A., Innovation and Technolgy Department, Chlorine Derivatives Division, Diagonal 595. 08014-Barcelona (Spain)

Introduction

The so called "Additive manufacturing" is a new manufacturing process which consists in translating virtual solid model data into physical models in a quick and easy process [1]. The most known example is 3D printing. This technology is considered a revolutionary route for processing and is currently being used in automotive and aerospace industries, as well as in medicine.

Many practical applications of 3D are carried out using polymers, for instance, biopolymers for tissue engineering [2] and composites with thermoplastic matrices and a broad range of filler materials such as metals, metal oxides, and plant fibres [3]. But the number of scientific papers dealing with the physical basis of printing polymers is scarce [4].

In the most common process, the melted polymer is extruded from the nozzle while the extrusion head is rastered around the build surface building a layer-by-layer 3 dimensional part. Unfortunately, in parts prepared by this process the weld is typically the point of failure [5]. Welding polymer layers implies a diffusion process of the polymer chains from one sheet to the other, which is governed by the viscoelastic behaviour in the terminal or flow zone. The time span of the terminal zone depends on temperature, in a way which is conditioned by the micro-structure and molecular mass distribution of the polymer. The time interval for the diffusion of the chains, which is equivalent to the time span of the terminal zone, is reduced as temperature is decreased. Therefore, in 3D printing of amorphous polymers welding becomes practically impossible at temperatures close to the glass transition Tg.

Therefore, knowing the welding process involved in the additive manufacturing during 3D printing is a crucial issue, to implant the pillars of a sound knowledge in this field. As well as, knowing the melt processability of polymers is highly dependent on the rheological properties of these systems, viscosity measurements, in particular, should be considered as a more central part of the material characterization tool for selecting suitable candidates for 3D printing.

In this contribution we analyse the dynamic viscoelasticity of novel random copolymers of polyvinyl chloride and different polyacrylates, to determine the frequency and temperature limits of the terminal zone. This permits to ascertain the priority of the materials to be used in 3D printing, considering the established printing velocity and temperature. An advanced printing machine is used to manufacture objects and, so, account for the relationship between the viscoelastic data and the quality of the elaborated articles.

Experimental

Materials

The PVC homopolymer and PVC-acrylate copolymers were obtained by Single Electron Transfer–Degenerative Chain Transfer Living Radical Polymerization (SET-DTLRP). The reagents used and the method of synthesis were described in a previous publication [6,7].

Samples Preparation

To evaluate the properties of random copolymers it was necessary to prepare pressed sheets obtained by formulating copolymers with 2 phr of a Ca/Zn stabilizer and 3 phr of epoxydated soy bean oil wherein "phr" is an abbreviation for "parts per hundred parts of resin". Formulations were fused and homogenized in a two-roll mill at a temperature of 160 ºC and pressed at the same temperature to mould the specific samples for each test.

Dynamic Mechanical Thermal Analysis (DMTA)

A Dynamic Mechanical Analyzer, Triton 2000 DMA from Triton Technology, was used in bending mode to carry out Mechanical Dynamic Thermal Analysis (DMTA). The samples were heated from -50 ºC to 120 ºC at a

constant heating rate of 4 ºC/min and a frequency of 1.0 Hz; this allowed detecting the glass transition temperature given by a maximum peak in loss tangent, tanδ.

Rheometry

The dynamic viscoelastic behaviour of the samples in the molten state was investigated using an AR-G2 stress controlled rheometer (TA Instruments) with a parallel-plate fixture (12 mm diameter), conducting oscillatory frequency sweep experiments in the linear regime at the temperatures indicated. The combined effect of temperature and frequency on the shear elastic modulus, G´, shear loss modulus, G´´, and complex viscosity, η^*, was investigated in the terminal zone (low frequencies).

Thermogravimetry

The thermal degradation of the materials was evaluated by high resolution (Hi-Res™) TGA in a Thermogravimetric Analyzer, TA, model Q500, in the temperature range from 50ºC to 550ºC at a heating rate of 40ºC/min and a resolution setting of 6, under a nitrogen flow rate of 75mL/min.

3D Bioplotter

A 3D-bioplotter (Developer Series, EnvisionTEC GmbH) was used for 3D printing process. Printed samples were originally designed in Solidworks 2016 x64 Editor. The preliminary proofs were performed between 140ºC and 160ºC, with 0.001 mm of resolution, and a maximum pressure of 10 bar. The needles used have an inner diameter of between 0.1 to 0.4 mm.

Results and Discussion

In Figure 1 the elastic and viscous moduli, G' and G'', respectively, of pure PVC and commercial PVC with 35 phr DOP are plotted as a function of frequency at T= 160ºC. As it is observed, the value of the elastic modulus is much higher than that of the viscous modulus for all the frequencies, both in the pure PVC and plasticized PVC. The same behaviour is noticed whatever the temperature we investigate. This result leads us to deduce that neat and plasticized PVC are not good candidates at all to be used in 3D, because the observed elastic prevailing behaviour impedes chain diffusion and, therefore, welding between layers.

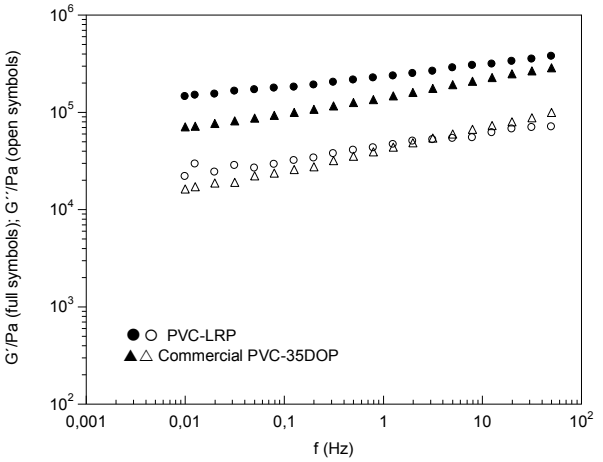

Figure 1. Elastic modulus (G´) (full symbols) and viscous modulus (G´´) (open symbols) as a function of frequency at T=160ºC, for pure PVC-LRP and commercial PVC-DOP formulation.

To surmount this deficiency, we auto-plasticized neat PVC *via* its copolymerization with poly(butyl acrylate), reducing the glass transition of the system. Dynamic mechanical thermal analysis (DMTA) results of Figure 2 show that the glass transition of PVC is shifted from 90ºC to 30ºC, when butyl acrylate monomers are introduced in a random way between VC monomers. This provokes a dramatic change in the molten state of PVC/BA copolymer, with respect to pure PVC. To the difference of the results of Figure 1, the viscous modulus overcomes the elastic modulus in wide range of frequency, allowing the diffusion of chains in an extent period of time. Then, welding, which implies chains inter-diffusion between layers, is possible in this copolymer, making it a suitable choice for 3D printing.

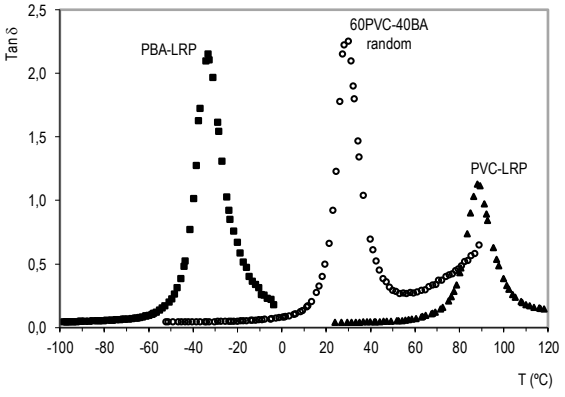

Figure 2. Loss tangent as a function of temperature obtained in DMTA for PVC-LRP (▲), PBA-LRP (■) and 60PVC-40BA random copolymer (○).

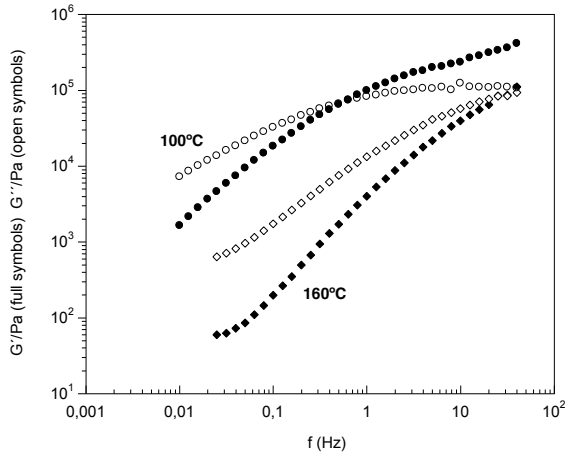

Figure 3. Elastic modulus (G´) (full symbols) and viscous modulus (G´´) (open symbols) as a function of frequency at T=160ºC (■,□) and 100ºC (●,○) for 60PVC-40BA random copolymer.

But, extrusion flow, which is involved in 3D manufacturing, should not be disregarded, because the polymer should be transfer from the reservoir to the printing plate. Although the welding conditions raised in the initial hypothesis are accomplished even at low temperatures, because G''>G' (Figure 3), the viscosity may be too high, avoiding proper flow in the capillary.

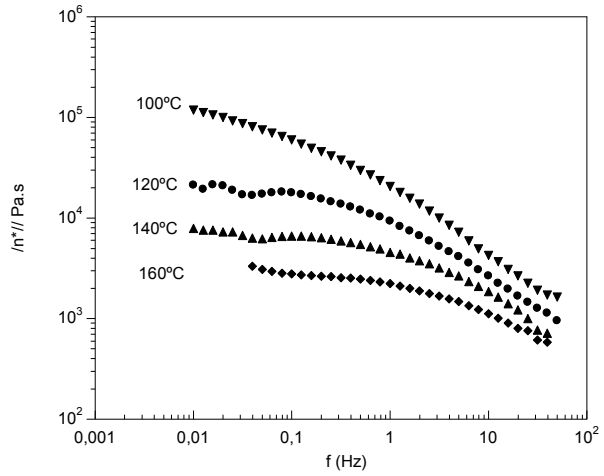

Figure 4. Complex viscosity (/η/) as a function of frequency at T=100ºC (▼), 120ºC (●), 140ºC (▲) and 160ºC (✦) for 60PVC-40BA random copolymer.*

The perceptive analysis of the viscosity results is presented in Figure 4, where the complex viscosity at different temperatures is displayed as a function of temperature. These viscosity data mark the apparently final step of the selection of the material conditions for 3D printing: Only at temperatures above 140ºC the viscosity is sufficiently low to yield flow from the reservoir to the plate. The criterion used is based on preliminary calculations and observations that take into account the viscoelasticity of the material, the internal dimensions of the reservoir, the needle and the maximum pressure that the equipment is capable of exerting (10 bar).

Before inserting the material into the printer the thermal stability of the copolymer has been evaluated by high resolution thermogravimetry. In Figure 5 the weight loss curves of PVC-LRP and 60PVC-40BA random copolymers is shown. As can be seen, the initial temperature of decomposition, which indicates the maximum processing and manufacturing temperature, of both, the PVC homopolymer and 60PVC-40BA, is above 190ºC. Thus, no thermal degradation should take place in the reservoir.

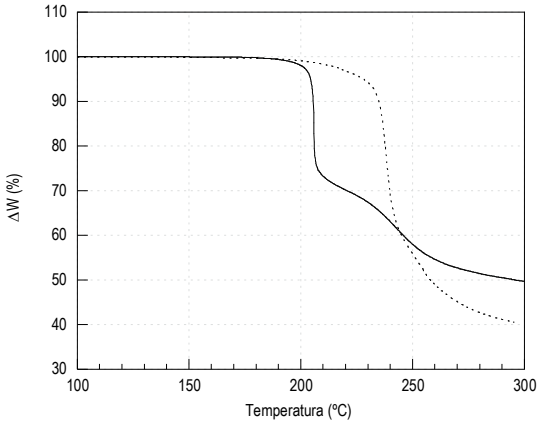

Figure 5. Thermogravimetric curves for PVC-LRP (····) and for 60PVC-40BA random copolymer (–).

The first 3D printing scaffold-test is showed in Figure 6. Still, a non expected result was obtained for 3D printing of the PVC/PBA sample which fulfilled the viscoelastic conditions: Degradation of the material took place during manufacturing, as can be observed in Figure 7.

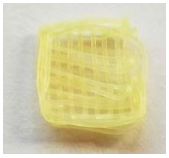

Figure 6. Image of scaffold-test obtained by 3D printing of 60PVC-40BA random copolymer at 160ºC.

Figure 7. Image of the material remaining into the nozzle after 2 hours at 160ºC of 60PVC-40BA random copolymer.

Conclusion

It is demonstrated that PVC/PBA copolymers can be chemically tuned to give adequate viscoelasticity and viscosity, so delivering good welding and capillary flow in 3D printing. But, in this type of materials, controlling degradation is an added task that should be necessarily considered.

References

1. Gibson, I., Rosen D., Stucker B. (2015). Additive Manufacturing Technologies, Springer Science, New York.
2. Wu G., Hsu, S. (2015). J. Med. biol. Eng. 35, 285-292.
3. Torrado, A. R., Shemelya, C. M., English, J. D., Lin, Y., Wicker, R. B., Roberson, D. A. (2015). Additive Manufacturing 6, 16-29.
4. K. Migler et al. (2016). XVIIth International Congress on Rheology, 2016, Kyoto, Japan.
5. Ge, T., Grest, G. S., Robbins, M. O. (2014). Macromolecules 47, 6982-6989.
6. Calafel, I., Muñoz, M. E., Santamaria A., Boix, M., Conde, J. I., Pascual, B. (2015). J. Vinyl. Addit. Technol. 21, 24-32. 21:24–32, 2015
7. Calafel, I., Muñoz, M. E., Santamaria A., Boix, M., Conde, J. I., Pascual, B. (2015). Eur. Polym. J. 73, 202-211.

Contact Address: Antxon Santamaria

antxon.santamaria@ehu.eus
Institute of Polymer Materials (POLYMAT) and Polymer Science and Technology Department
Faculty of Chemistry, University of the Basque Country (UPV/EHU)
Paseo Manuel de Lardizabal 3, 20018 Donostia-San Sebastián (Spain)

Extremely slow reptation dynamics of Rod-Coil-Rod Triblock Copolymers

P. Troya[1], J. Ramírez[1,2], B.D. Olsen[2]

[1] Department of Chemical Engineering, Universidad Politécnica de Madrid (Spain)
[2] Department of Chemical Engineering, Massachusetts Institute of Technology (USA)

Introduction

Rod-coil block copolymers are a family of polymeric materials with non-homogeneous stiffness along the backbone. Frequently, one of the block types is very flexible, whereas the other type is completely rigid. These materials have attracted a lot of interest in the last decade for their potential use as nanostructured soft materials with functional domains in organic electronics [1] and biomaterial applications [2, 3]. The equilibrium self-assembly of these materials has been thoroughly investigated and is very different from the analogue flexible block copolymers due to the mismatch between the block topologies and the liquid crystalline interactions between the rigid blocks [4, 5], but a fundamental understanding of their dynamics, which is necessary for the design of materials with the right diffusion, mechanical and processing properties, is still not complete.

Previous theoretical and experimental results of tracer entangled rod-coil diblock and coil-rod-coil triblock copolymers in a mesh of very high molecular weight flexible chains suggest the appearance of new mechanisms of diffusion that slow down the dynamics of rod-coil diblock and triblock copolymers, with diffusivities that are smaller than both rod and coil homopolymers by over an order of magnitude in some cases [6,7]. As a result, a modified reptation theory has been introduced that attributes the slow dynamics of rod-coils to the mismatch between the curvatures of the entanglement tubes of the rod and coil blocks [8].

The present work extends the theoretical and simulation study to the case where both molecular ends are occupied by rigid blocks. In this new configuration, arm retraction is not possible because the rods cannot retract along their rigid tubes, and activated reptation is extremely difficult because any motion of the chain along its tube needs to drag both end rods along the flexible tube corresponding to the coil block. In addition, any new tube segment created by reptation of the chain must be stiff, and therefore, in the absence of constraint release, the whole tube must have a very small curvature. The reptation of the coil block inside the straight tubes created by the end rods is entropically unfavourable (see Figure 1). Therefore, new relaxation mechanisms must emerge that result in even slower relaxation dynamics than in the case of similar rod-coil and coil-rod-coil block copolymers.

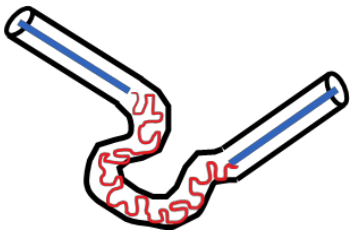

Figure 1. Schematic view of the reptation of a rod-coil-rod triblock copolymer.

Model and Methods

Molecular Dynamics (MD) simulations of tracers of entangled rod-coil-rod block copolymers in a mesh of very long, flexible coils, have been run using LAMMPS ((Large-scale Atomic/Molecular Massively Parallel Simulator") [9]. Chains are represented by a small modification of the standard Kremer-Grest model for entangled polymers [10]. Polymers are represented by bead-spring chains of N monomers, and the excluded volume and bonded interactions are chosen carefully so that the probability of two chains crossing each other is virtually zero. The non-bonded interaction consists on a purely repulsive shifted Lennard-Jones potential:

$$U_{LJ} = 4\varepsilon\left(\left(\frac{\sigma}{r_{ij}}\right)^{12} - \left(\frac{\sigma}{r_{ij}}\right)^{6} + \frac{1}{4}\right), \quad r_{ij} \le 2^{\frac{1}{6}}\sigma \quad (1)$$

and the bonded interaction of the springs is modelled by means of a FENE potential:

$$U_S = -\frac{1}{2}kR_0^{\,2}\ln\left(1-\left(\frac{r_{ij}}{R_0}\right)^2\right), \quad r_{ij} < R_0 \quad (2)$$

In both equations, r_{ij} is the separation between monomers *i* and *j*. Position, energy, and time are measured using standard non-dimensional LJ units. We use the standard parameter values from the original paper [10], and introduce a small modification to the

Kremer-Grest model so that rod-like blocks can be incorporated into the system. The rods are modelled using a stiff bending potential between any three neighbor beads along the rod:

$$U_\theta = 1000\varepsilon(1+\cos\theta) \quad (3)$$

Simulations are run with periodic boundary conditions at a monomer density ρ=0.85, and the size of the simulation box is chosen such that the density of rods is less than $L^{-3/2}$ (where L is rod length, and the factor of 2 comes from the two rods per molecule), which minimizes rod-rod interactions. In addition, we add a soft repulsive potential,

$$U_R = 25\exp(-4r_{ij}), \quad r_{ij} < 3\sigma \quad (4)$$

between rod monomers to counteract possible depletion interactions [11]. The magnitude of this potential does not affect overall diffusion in the simulations. Matrix chains are large in order to supress constraint release during the characteristic time of tracer disengagement.

In order to generate initial configurations, we use a fast equilibration proposed recently [12] which is a modification of the standard fast 'push-off' method [13].

Results and Discussion

Systems of symmetric rod-coil-rod diluted tracers of molecular weight 200 and rod lengths ranging from L=0 to L=24 in a mesh of matrix chains of molecular weight M=1000 have been generated, equilibrated and run for long enough to reach the terminal time. Enough independent copies of each simulation have been run so that there are 400 tracers in total of each case. On Table 1, a summary of the systems studied in this work is shown. Matrix chains are long enough so that their disengagement time scale is much longer than that of tracers, and constraint release events can be discarded.

Table 1. Rod-coil-rod systems studied in this work.

L	Tracer chains	Matrix chains	Total Particles	Copies
0	40	62	70000	10
4	40	62	70000	10
8	40	62	70000	10
12	40	110	118000	10
16	25	170	175000	16
20	16	215	218200	25
24	10	234	236000	40

Static properties

On Figure 2, the mean-squared end-to-end distance of the rod-coil-rod tracers is represented as a function of the length of the rod L. The overall size of tracer molecules grows as the square of the rod size, which can be understood by using a simple scaling argument. The flexible block has N-2L monomers and its size can be calculated by using the characteristic ratio of the Kremer-Grest model. The two rods behave as two freely jointed chain segments with length Lσ. Therefore, the total molecule size can be expected to be:

$$\langle R^2 \rangle = (N-2L)C_\infty + 2L^2 \quad (5)$$

On Figure 2, the scaling is fitted to the data from simulations, obtaining a characteristic ratio of 1.7, which is close to the reported value of 1.88 [12].

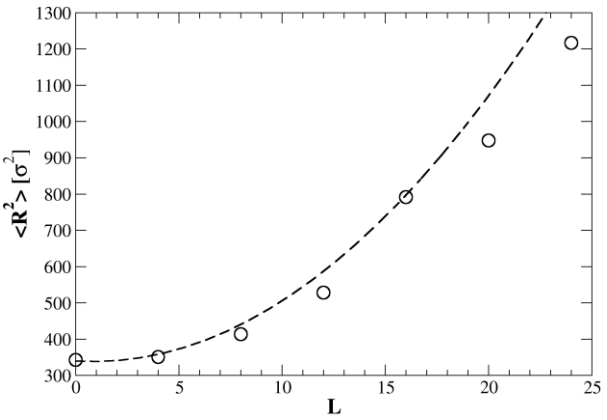

Figure 2. Mean-squared end-to-end distance of the tracers. The dashed line represents a scaling expression discussed in the text (see Eq. 5).

On Figure 3, the mean-square distance between monomers i and j along the chain, divided by $|j-i|$, starting from the middle monomer, is represented in order to check the Gaussian statistics of the chains.

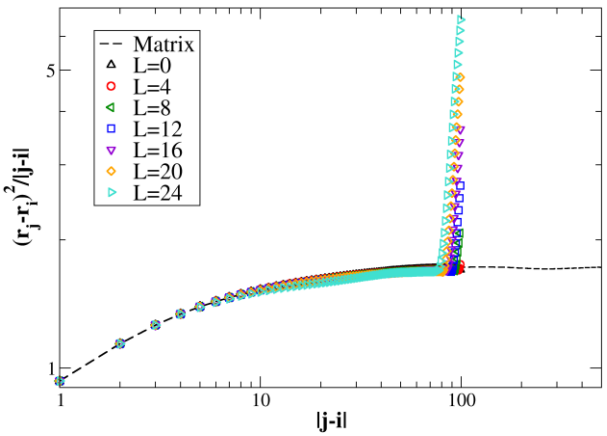

Figure 3. Normalized mean-squared monomer distance, starting from the middle monomer, showing expected Gaussianity of tracers and matrix chains.

As expected, the chains are ideal up to the end rods, with a characteristic ratio of 1.72, whereas the rods deviate strongly from Gaussian behaviour.

Dynamical properties

The dynamical properties of the tracer chains have been studied by measuring the diffusion and orientational relaxation of the chains.

On Figure 4, the mean-squared displacement of the center of mass of tracer chains is shown as a function of time. The motion of the tracers is subdiffusive up to their respective terminal times, when it becomes Fickian, which is the expected behaviour for entangled linear polymer chains. As the length of the rod increases, the diffusion of the chains slows down significantly, to the point that chains with L=24 have a self-diffusion coefficient that is almost one order of magnitude smaller than tracers with L=0. Matrix chains diffuse at least one order of magnitude slower than the slowest tracers.

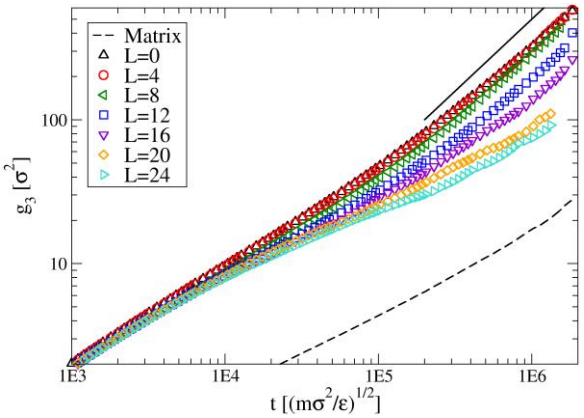

Figure 4. Mean-squared displacement of the centre of mass of the tracer rod-coil-rod triblock copolymers. The dashed line shows the matrix chains and the continuous line shows the Fickian (slope 1) scaling.

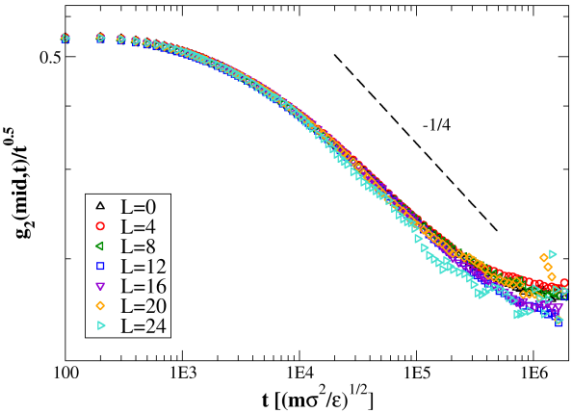

Figure 5. Mean-square displacement of the middle monomer of the tracer block copolymers, showing reputation scaling in intermediate timescales.

Reptation of the chains can also be evidenced by measuring the mean-square displacement of the middle monomer of the chains, which is shown on Figure 5 divided by $t^{1/2}$, in order to manifest the different scaling regimes. As predicted by Doi and Edwards [4] the mean-square displacement of the middle monomer scales roughly with time to the power of 1/4 from τ_e, the Rouse time of one entanglement, up to τ_R, the Rouse time of the chains.

On Figure 6, the end-to-end relaxation of the tracer chains, which is the slowest relaxation mode for linear chains, is shown. Again, as the rod length increases, the tracers relax more slowly. On the same plot, the end-to-end relaxation of the matrix chains is also depicted. It is clear that the terminal time of matrix chains is at least one order of magnitude larger than that of the tracers, which is necessary if we want to minimize the effect of constrain release on the relaxation of tracer chains.

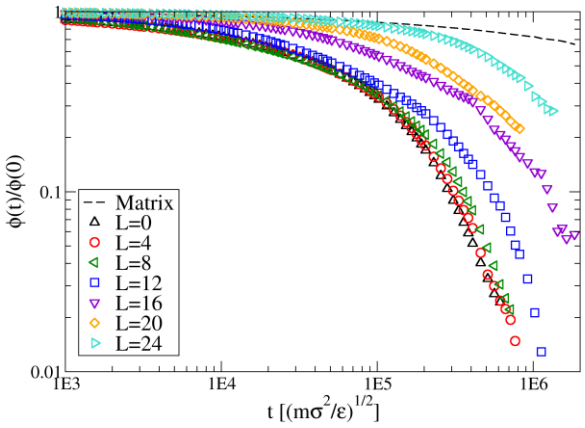

Figure 6. End-to-end vector relaxation of the tracers. The behaviour of matrix chains is shown as a dashed line.

In order to quantify the effect of the length of the rods on the dynamics of rod-coil-rod (RCR) triblock copolymers, we have calculated the self-diffusion coefficient from the slope of the Fickian regime region on Figure 4, as well as the terminal time from fitting an exponential decay to the terminal region of the end-to-end vector relaxation of the tracers on Figure 6. Both quantities are represented as a function of the length of the rods on Figure 7. In order to better understand the effect of the rods, both the diffusion coefficient and the terminal time are normalized by their corresponding values for a tracer with no rods, i.e. with L=0.

The self-diffusion coefficient shows a monotonic decay with increasing rod length, up to a maximum slowdown of a factor of 5 for L=24. The decay can be compared to that observed for coil-rod-coil (CRC) block copolymers, where the rod occupies the middle block. The slowdown effect in CRC copolymers (black symbols) is clearly not as acute as for RCR chains (red symbols). A similar trend as that observed for the self-diffusion coefficient can be seen for the terminal time of RCR polymers, with terminal times that are more than a factor of 6 larger than those of tracers with no rods.

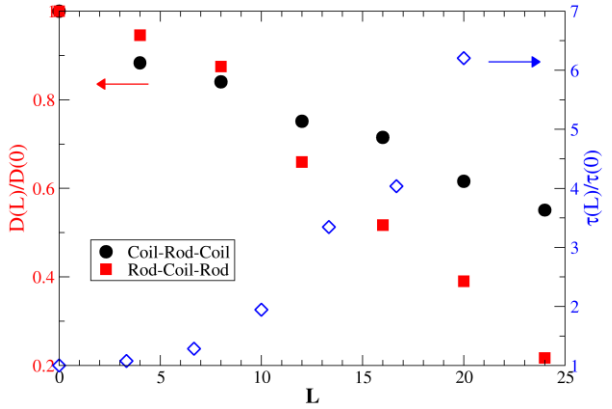

Figure 7. Normalized diffusion constant of coil-rod-coil (black) and rod-coil-rod (red), and normalized terminal time of rod-coil-rod block copolymers (blue) as a function of rod length L.

The slow-down effect can be understood in terms of reptation dynamics. In CRC polymers, as the rods get longer than the tube diameter, the reptation is hindered by the fact that the rods cannot easily reptate along the curved tubes of the flexible blocks. Reptation becomes then an activated process, and chains must wait until a sufficiently large fluctuation occurs that allows the rod to diffuse a long distance along the primitive path of the flexible tube. As the rods grow, a new arm retraction mechanism becomes favourable and the slow down process gets less severe. In that sense, CRC polymers with long rod blocks can relax by arm retraction, in a similar way as stars or branched polymers do.

Instead, in RCR polymers, the reptation gets much more difficult because there are two rods that need to diffuse along the curved contour of the primitive path corresponding to the flexible block. At the same time, arm retraction is not possible, because the rigid rods at the ends of the chain prevent it from happening. In addition, the reptation of the flexible block along the straight tube segments created by the end rods violates Gaussian statistics and is entropically unfavourable.

Since the size of the molecule does not change appreciably with rod size, the dramatic drop in the value of D must be a consequence of an increase of several orders of magnitude in the disengagement time. A linear polymer that takes such a long time to disentangle is expected to also entangle at a very slow pace. From a technological point of view, a material with such slow reentanglement dynamics would be of interest in itself, because it would show a very low steady state viscosity. Thus, the detailed knowledge of the molecular mechanisms of motion and relaxation of rod-coil block copolymers is of utmost importance for the prediction of their flow properties and their kinetics of self-assembly, and will encourage innovations in the applications, processing methods and self-assembly kinetics of these technologically relevant materials.

Acknowledgements

We acknowledge the computer resources and technical assistance provided by the Centro de Supercomputación y Visualización de Madrid (CeSViMa), as well as computer resources Comet through a generous XSEDE allocation No. TG-DMR160175. JR acknowledges funding from Real Colegio Complutense at Harvard.

References

1. Segalman, R.A., McCulloch, B., Kirmayer, S., and Urban, J.J. (2009). Macromolecules 42, 9205-9216.
2. van Hest, J.C.M. (2007). Polym. Rev. 47, 63-92.
3. Kohn, W.D., Mant, C.T., and Hodges, R.S. (1997). J. Biol. Chem. 272, 2583.
4. Damasceno, P.F., Engel, M., and Glotzer, S.C. (2012). Science 337, 453-457.
5. Olsen, B.D., Shah, M., Ganesan, V., and Segalman, R.A. (2008). Macromolecules 41, 6809-6817.
6. Wang, M., Alexander-Katz, A., and Olsen, B.D. (2012). ACS Macro Lett., 1 (6), pp 676–680.
7. Wang, M., Timachova, K., and Olsen, B.D. (2015). Macromolecules, 48 (9), pp 3121–3129.
8. Wang, M., Likhtman, A.E. and Olsen, B.D. (2015). J. Chem. Phys. 143, 184904.
9. Plimpton, S. (1995). J Comp Phys, 117, 1-19.
10. Kremer, K., and Grest, G.S. (1990). J Chem Phys 92, 5057-5086.
11. Asakura, S., and Oosawa, F. (1958). J. Polym. Sci. 33, 183-192.
12. Sliozberg, Y.R., and Andzelm, J.W. (2012). Chem. Phys. Lett. 523 139–143.
13. Auhl, R., Everaers, R., Grest, G.S., Kremer, K., and Plimpton, S.J. (2003). J Chem Phys 119, 12718.
14. Doi, M., and Edwards, S.F. (1986). *The theory of polymer dynamics*, Oxford University Press, New York.

Contact Address:

jorge.ramirez@upm.es
Department of Chemical Engineering,
ETSI Industriales, Universidad Politécnica de Madrid
José Gutiérrez Abascal, 2
+34 913363182

IBEREO valencia 2017
The multidisciplinary science of rheology
Towards a healthy and sustainable development

Colloids and Suspensions

Interfacial and emulsifying properties of bio-based surfactants obtained from coconut oil

P. Ramírez[*], *L. A. Trujillo, J.A. Carmona, M.J. Martín, M.C. García*

Universidad de Sevilla, Grupo de Reología Aplicada. Tecnología de Coloides. Facultad de Química. C/ Profesor García González, 1, 41012, Sevilla (Spain)

Introduction

In recent years, interest to explore eco-friendly surfactants, obtained directly from renewable natural material, has increased for various industrial and environmental applications. Polyoxyethylene-based non-ionic surfactants are widely used in industrial applications such as detergents, cosmetics and personal care products, food dispersions, agricultural formulations, petroleum industry applications, and in general to stabilize foams and emulsions.

As a class of relatively new non-ionic surfactants, polyoxyethylene glycerol esters derived from coconut oil are produced from renewable resources. Due to the fact that these surfactants are fully innocuous for human skin and hair and their properties are adequate in order to design eco-friendly products, they have received considerable research interests and have been used in many fields in recent years. At present, there is a marked trend towards the use of eco-friendly surfactants derived from inexpensive renewable resources in detergent formulations.

The influence of the hydrocarbon chain length as well as of the number of ethylene oxide (EO) groups on the adsorption of polyoxyethylene-based non-ionic surfactants at the air/water and oil/water interfaces has been previously reported. In addition, the surface properties of two polyoxyethylene glycerol esters derived from cocoa oil with two and seventeen EO groups, namely equilibrium adsorption, dynamic surface tension and surface rheology, have been recently reported [1-2]. However, Glyceret-6 cocoate (Levenol® F-200) adsorption and the air/water interface have not been yet studied. In addition, taking into account that most of the technical applications of these surfactants involve events occurring at the interfaces, gaining a deeper knowledge of the interfacial properties and of these surfactants is of key importance in order to rationally design new formulations. The interest in interface rheology, which has been proven to be related to the stabilities of foams and emulsions, has increased in recent years.

For an oil/water system, the interfacial system is determined by the natures of the surfactant and oil, concentration and other environmental factors, such as temperature. α-Pinene is a renewable biosolvent, which may be obtained from pine resins or distillation. This solvent exhibits a good biodegradability; hence it may be proposed as an interesting alternative to typical organic solvents that are more environmentally damaging. α-Pinene is completely miscible with oils and insoluble in water.

The main goals of the present work was to characterize the surface and interfacial properties (equilibrium, dynamics and dilatational rheology) at the α-pinene/water interface of an eco-friendly surfactant, Levenol F-200, in order to complete the previous studies carried out with Levenol C-201 and Levenol H&B [2]. The other target of this investigation was to compare the yield of these three surfactants derived from coconut oil for the development of oil-in-water emulsions formulated with a green solvent (α-pinene). Rheology, laser diffraction and multiple light scattering were the main techniques used to assess the emulsification properties of the surfactants.

Experimental

Three commercial polyoxyethylene glycerol ester surfactants derived from coconut oil have been studied. These surfactants differ in the number of EO groups. Namely Levenol® C-201 (Glycereth-17 cocoate), Levenol F-200 (Glycereth-6 cocoate) and Levenol® H&B (Glycereth-2 cocoate), which are technical grade surfactants with 17, 6 and 2 average EO groups respectively. They were kindly provided by KAO and used as received. The solutions were prepared with Milli-Q water. All glassware was cleaned with sulfuric acid (98%) containing 8 gL^{-1} of ammonium disulfure. α-Pinene (0.84 g/mL at 25ºC) was purchased from Sigma–Aldrich® and purified with Florisil® resins (Fluka, 60–10 mesh) prior to use.

Interfacial tension measurements were performed with a drop profile analysis tensiometer (CAM200, KSV,

Finland). The drop was formed inside a thermostatted cuvette at 20ºC and controlled using a custom-built control unit consisting of a syringe with a piston that is driven by a stepper motor. The control procedure was as follows: once the drop was formed the contour of the drop was acquired and then the drop initial area calculated. Every 10 seconds the area was calculated and the actual and initial value were compared. Whenever the values differed, the stepper motor drove the piston in the respective direction to correct the difference.

The continuous phases were prepared by dissolving the emulsifier in ultrapure water cleaned using a Milli-Q water purification system. The samples (total amount of 250 g) were prepared in two steps. Firstly, the mixture of solvents was added slowly at 4000 rpm for 30 s to the aqueous phase. Subsequently, secondary homogenization was carried out with a rotor-stator device equipped with a mesh screen (Silverson L5M) using a rotational speed of 7500 rpm over 90 s. Temperature was fixed at 20ºC. The emulsifying capacity was determined from the measurement of the droplet size. The droplet size distributions and droplet mean diameters of emulsions aged for 24 hours were measured by laser diffraction using a Malvern Mastersizer X. Occurrence of coalescence and/or Ostwald ripening was assessed from the change in droplet-size distribution and mean diameters with aging time. The mean droplet diameter was expressed as Sauter mean diameter ($D_{3,2}$) and volume mean diameter ($D_{4,3}$):

$$d_{3,2} = \frac{\sum_{i=1}^{N} n_i d_i^3}{\sum_{i=1}^{N} n_i d_i^2} \quad (1)$$

$$d_{4,3} = \frac{\sum_{i=1}^{N} n_i d_i^4}{\sum_{i=1}^{N} n_i d_i^3} \quad (2)$$

To determine the distribution width of droplet sizes, "span" was used calculating from the following formula:

$$span = \frac{D(v,0.9) \quad D(v,0.1)}{D(v,0.5)} \quad (3)$$

D(v,0.9), D(v,0.5), D(v,0.1) are diameters at 90%, 50% and 10% of cumulative volume, respectively.

Emulsion physical stability against creaming, coalescence and flocculation was evaluated by multiple light scattering measurements. A Turbiscan Lab Expert (Formulaction, France) was used during 30 days at 20 ºC. This technique makes it possible to determine the predominant mechanism of destabilization in each sample as well as the kinetics of the destabilization process. To characterize the creaming process, the creaming index was used (CI):

$$CI = \frac{H_S}{H_E} \times 100 \quad (4)$$

Where, H_E is the total height of the emulsion and H_S is the height of the serum layer. The initial slope of the plot of CI versus aging time is related to the creaming rate (ω) [3]:

$$= \frac{d(CI)}{dt} \times \frac{H_E}{100} \quad (5)$$

The rheological characterization of emulsions were carried out by means of flow curves performed with a Haake MARS rheometer (Germany) with a sandblasted Z20 coaxial cylinder geometry at 20ºC. Rheological measurements were carried out for five different aging time: 1, 6, 15, 21 and 30 days.

Results and Discussion

Table 1 show the equilibrium surface tension ($\gamma_{A\text{-}W}$) and interfacial tension ($\gamma_{O\text{-}W}$) values of Levenol F-200. First of all, a decrease in the surface and interfacial tensions with the bulk concentration were observed and secondly, a constant value region was achieved once the interfacial layer became saturated. The crossing point of both regions made it possible to estimate the critical micelle concentration (cmc). At the air-water interface, the cmc of Levenol F-200 (0.12 molm^{-3}) turned out to be higher than that of Levenol® C-201 (0.07 molm^{-3}) but lower than that of Levenol® H&B (0.3 molm^{-3}). This supported the higher surface activity of Levenol® C-201.

Table 1. Equilibrium surface tension ($\gamma_{A\text{-}W}$) and interfacial tension ($\gamma_{O\text{-}W}$) values of Levenol F-200

C (g/L)	$\gamma_{A\text{-}W}$ (mN/m)	$\gamma_{O\text{-}W}$ (mN/m)
0	71.0	35.0
0.001	71.0	31.0
0.002	71.0	29.7
0.005	69.0	28.0
0.01	62.5	26.0
0.02	52.1	21.0
0.05	39.0	17.0
0.1	31.0	14.0
0.2	30.5	12.1
0.5	30.0	9.5
1	29.0	8.5
2	29.0	7.8
5	28.5	6.4

The cmc value for these surfactants is similar than those obtained for other widely used non-ionic surfactants (e.g. Tween 20) and for other eco-friendly surfactants like vanillin derived surfactants. The CMC value at the -pinene/water interface is shifted toward higher bulk surfactant concentration values. From the dynamic surface tension response of Levenol F-200 (data not shown) a minimum in surface tension is obtained above 0.5 gL^{-1}. This anomalous behavior can be ascribed to the occurrence of a fast diffusion and adsorption of surfactants molecules at the interface followed for a slower solubilization of the previously adsorbed surfactants into the adjacent oil phase [2].

Figure 1 and Table 2 show the droplet size distributions, Sauter and volumetric mean diameters and span values for emulsions with different surfactants aged for 24 hours. First, it should be stated that Levenol H&B emulsion have lower mean Sauter mean diameter than Levenol C-201 and Levenol F-200 emulsions. However, that emulsion has the highest span value and a bimodal distribution. Results showed that the use of this pure biosolvent and these surfactants produced macroemulsions with droplet size greater than 1 µm. None of the emulsions showed an increase of droplet sizes with aging time.

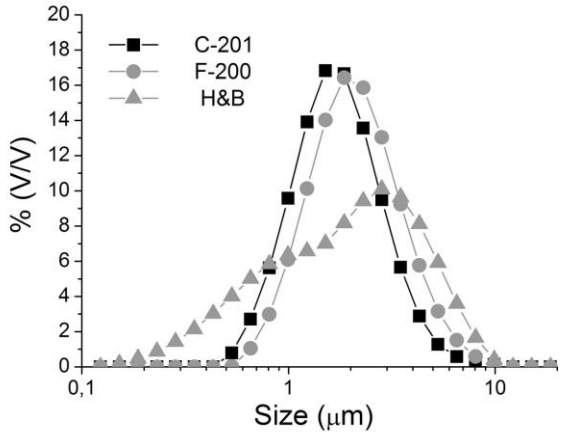

Figure 1. Droplet size distributions for all studied emulsions aged for 24 hours.

Table 2. Span, $d_{3,2}$ and $d_{4,3}$ values for emulsions aged for 24 hours. Standard deviation of the mean (3 replicates) for span < 10%, d3,2 < 6% and d4,3 < 8%.

Surfactant	Sp	$d_{3,2}$ (nm)	$d_{3,2}$ (nm)
Levenol C-201	1.386	1370	1750
Levenol F-200	2.229	1080	2200
Levenol H&B	1.420	1660	2130

In Figure 2, the creaming index was plotted as a function of aging time for the emulsion prepared with different surfactants. The creaming index was lower for the samples developed using Levenol C-201, which exhibited the lower volumetric mean diameter and span values.

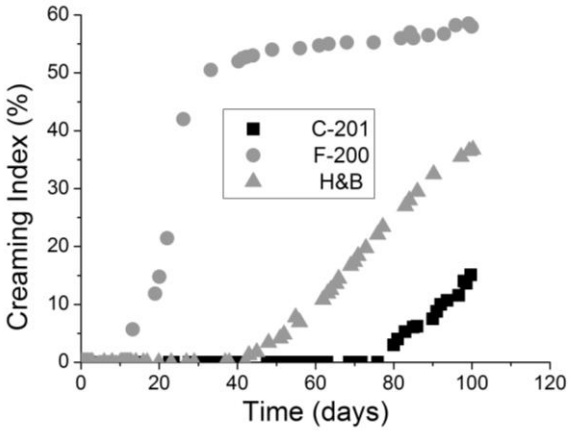

Figure 2. Creaming index (CI) as a function of aging time for all emulsions studied. Samples kept under storage at 20 ºC.

Emulsions processed Levenol C-201 and Levenol H&B showed a nearly linear dependence of the creaming index with aging time and a delay time for creaming lower than 42 days (see table 3). To study the destabilization kinetics due to creaming, the slope of the linear region was used to determine the creaming rate. The emulsion prepared with Levenol F-200 showed the highest creaming index at 100 days and the greatest creaming rate (see Figure 2 and table 3). The similar values of creaming rate for emulsions prepared with Levenol C-201 and Levenol H&B should be noted. However, important changes in these parameters were found for the emulsions developed Levenol F-200. The best emulsion was that obtained with Levenol C-201. This supports the laser diffraction and rheological characterization results.

Table 3. Creaming rate and delay time for creaming values for all studied emulsions.

Surfactant	Creaming rate (%/day)	Delay time (day)
Levenol C-201	0.23	76.1
Levenol F-200	0.28	42.0
Levenol H&B	1.23	12.5

Flow curves representing the shear stress dependence on the shear rate for emulsions studied as a function of surfactant after one day of aging time are shown in Figure 3. Firstly, the Newtonian behavior of these emulsions should be noted (n= 1), so that their viscosity (slope of the plot of stress vs. shear rate) remain a constant no matter how fast they are forced to flow.

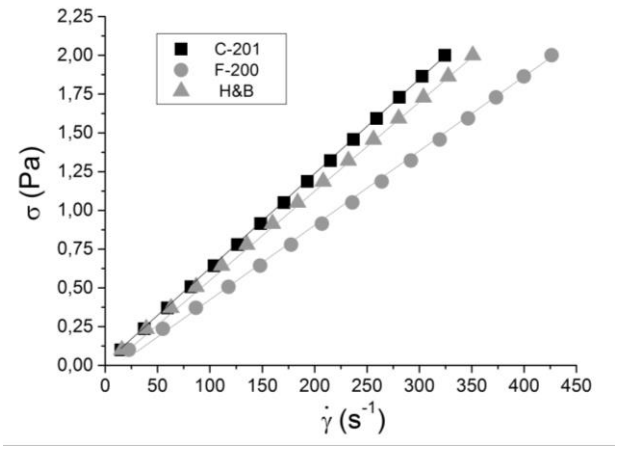

Figure 3. Flow curves for all emulsions studied aged for 24 hours. Samples kept under storage at 20 ºC.

Table 4 shows the viscosity values emulsions aged for 24 h as a function of the surfactant. The emulsion prepared with Levenol F-200 showed a lower viscosity value than those emulsions prepared with Levenol C-201 and Levenol H&B. This is consistent with the different mean diameters between the studied emulsions. The droplet-size effect in the rheology is particularly important for fine dispersions with droplets around than 1 μm [4].

Table 4. Viscosity values for all studied emulsions aged for 24 hours.

Surfactant	η (mPa· s)
Levenol C-201	6.17
Levenol F-200	4.69
Levenol H&B	5.70

Concluding Remarks

We have carried out a study of the interfacial properties at the air/water and α-pinene/water interfaces of an eco-friendly surfactant (Levenol F-200) and of the emulsion stabilizing properties of three polyoxyethylene glycerol ester surfactants derived from coconut oil (Levenol C-201, Levenol F-200 and Levenol H&B), which has recently become commercially available. Dynamic surface tension measurements showed the occurrence of two processes with different kinetics: a first diffusion stage was followed by a slower rearrangement or compression of the previously adsorbed molecules. Moreover, for Levenol F-200 an intermediate cmc value between Levenol® C-201 and Levenol H&B values was obtained. The cmc value at the α-pinene/water interface is shifted toward higher bulk surfactant concentration value in comparison with air/water interface results. Moreover, a minimum in the dynamic surface tension curve for Levenol F-200 at high surfactant bulk concentration was observed. This result is consistent with the fact that this surfactant is partly solubilized in α-pinene.

Regardless of the emulsifier used, the use of these surfactants led to obtain concentrated emulsions with α-pinene as dispersed phase. The physical stability of the emulsions was studied by means of laser diffraction and multiple light scattering techniques. In addition, the results provided by multiple light scattering demonstrated that the emulsions with smaller droplet sizes exhibited enhanced stability against creaming. The most stable emulsion was the one prepared with Levenol C-201.

Nevertheless, it has been demonstrated that the use of the non-ionic surfactant with higher number of ethoxylated groups (Levenol C-201) is adequate for two reasons: (a) it provides the sufficient viscosity to prevent creaming and (b) it is the best to avoid destabilization by coalescence.

Acknowledgements

The financial support received (Project CTQ2015-70700) from the Spanish Ministerio de Economía y Competitividad and from the European Commission (FEDER Programme) is kindly acknowledged.

References

1. Trujillo-Cayado, L.A., Ramírez, P., Pérez-Mosqueda, L.M., Alfaro, M.C., Muñoz, J. (2014) Colloids Surf. A, 458, 195.
2. Tujillo-Cayado, L.A., Ramírez, P., Alfaro, M.C., Ruíz, M., Muñoz, J. (2014) Colloids Surf., B: Biointerfaces 122, 623.
3. Santos, J., Trujillo-Cayado, L.A., Calero, N., Muñoz, J. (2014) AIChE. J 60, 2644.
4. Pal, R. (1996) AIChE J. 42, 3181.

Contact Address:

Pablo Ramírez del Amo (pramirez@us.es)
Department of Chemical Engineering
Faculty of Chemistry
University of Seville
C/ Profesor García González, 1, 41012, Sevilla (Spain)
Telf.: +34 954 557180 ; Fax: 34 954 556447

Effect of surfactants on shear and microstructural properties of aqueous sepiolite gels

J.A. Carmona, A. Caro, J. Santos, R. LLinares, P. Ramírez

Universidad de Sevilla, Grupo de Reología Aplicada. Tecnología de Coloides. Facultad de Química. c/ P. García González, 1, 41012, Sevilla (Spain).

Introduction

Sepiolite is a phyllosilicate whose structure consists of two tetrahedral layers with an octahedral layer in between, containing Mg^{2+} cations. Sepiolites exhibit either a fiber-like or a needle-type structure at the microscale. They also contain channels which extend themselves along the whole length of fibers. This microstructure is responsible for their specific rheological, catalytic and adsorbing properties [1].

Sepiolites are mainly used as thickener, gelling agent and modifier of rheological properties. They are used in several agrochemical, cosmetic and pharmaceutical products. This is not only due to their thickening properties but also to the fact that they can hold drugs and pesticides, which may be delivered at controlled rate [2]. In addition, sepiolites are also used as fillers in some paints, coatings, detergents, plastics, adhesives and cement [1].

The aim of this research was to study the influence of ionic surfactants of different nature on the rheological and microstructural properties of sepiolite gels prepared at 3 % (m/m). Cetyl trimethylammonium bromide (CTAB) and sodium dodecyl sulfate (SDS) were used as cationic and anionic surfactant, respectively.

Experimental

Materials and preparation of gels.

A commercial clay (Pangel S9), provided by Tolsa Group (Madrid, Spain), was used. Pangel S9 contains 85 % (m/m) sepiolite and 15% (m/m) of others clays.

Gels, containing 3 % (m/m) the commercial clay and CTAB or SDS, were prepared with a high-shear homogenizer at room temperature. CTAB and SDS surfactants were purchased from Sigma Aldrich.

Rheological measurements

Rheological measurements were carried out using a CS Haake-MARS rheometer (Thermo, Karlsruhe, Germany). A serrated surface steel plate & plate sensor system (35 mm diameter) was used for oscillatory shear tests. The FL16 vane (16 mm diameter) was utilized to carry out flow curve measurements, with a sandblasted cylindrical cup of 20 mm diameter. All rheological tests were conducted at 20ºC, using a solvent- trap to avoid sample drying.

Stepwise flow curves with different stress intervals were run, fixing a steady state approximation of 0.01% and a maximum measuring time of 2 minutes per point. The linear viscoelastic range (LVR) in oscillatory shear was estimated by oscillatory stress sweeps at 1Hz. Frequency sweeps were carried out from 3 to 0.01 Hz, using a shear stress amplitude of 0.2 Pa.

Microscopy

The samples were freeze-dried using a laboratory freeze dryer, model LyoQuest 85 (Telstar, United States). A Scanning electron microscope (SEM) JEOL 6460LV (JEOL Ltd, Japan) was used. Freeze-dried samples were mounted on the specimen holder and sputter-coated with gold. Finally, each sample was collocated into the microscope where it was observed at 5 kV and a vacuum of 10^{-5} Pa.

Results and Discussion

Flow curves

Figure 1 shows flow curves of sepiolite gels without surfactants and with either SDS (Figure 1A) or CTAB (Figure 1B). All flow curves were typical of the so-called "very shear thinning" materials. Therefore, an apparent or better, a practical yield stress (σ_0) could be estimated. At a shear stress slightly above (σ_0), a dramatic increase in shear rate was observed; i.e. an abrupt drop of viscosity took place.

The flow curve pattern hardly changed at low either SDS or CTAB concentrations. The apparent yield stress for sepiolite gels containing 5mM surfactant were 9.9 Pa and 8.8 Pa, for gels formulated with SDS and CTAB, respectively. These values were not markedly different to that of the sepiolite gel without surfactant (11.6 Pa).

On the other hand, a marked decrease in viscosity and apparent yield stress, which dropped to 1.2 Pa, was

observed above 5mM SDS (Figure 1a). Conversely, both viscosity and the yield stress (45.2 Pa) increased at 10mM CTAB.

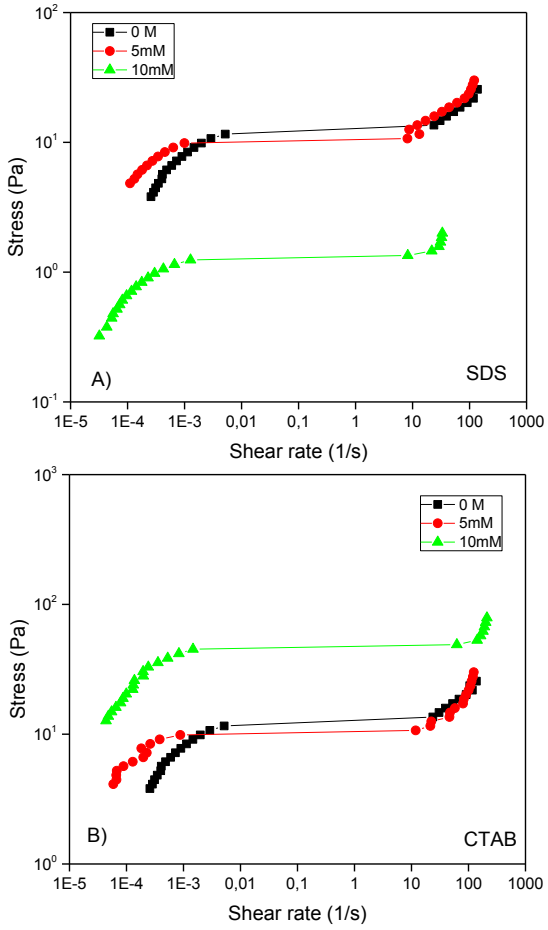

Figure 1. Shear stress versus shear rate for sepiolite aqueous gels with 3% (m/m) and different concentrations of SDS and CTAB. A) SDS concentration 0, 5 and 10 mM. B) CTAB concentration 0, 5 and 10 mM. T=20ºC.

Viscoelasticity

Figure 2 shows the frequency dependence of the argument of complex modulus, $|G^*|$, which can be defined as in terms of G' and G'' (equation 1).

$$|G^*| = [(G')^2 + (G'')^2]^{(1/2)} \quad (1)$$

The frequency dependence of G' as well as that of G" suggest that the rheological response was consistent with a weak gel behaviour; i.e G' > G'' throughout the whole frequency range covered (data not shown) and the frequency dependence of both viscoelastic is rather weak on the log-log plot. Likewise the flow properties of sepiolite gels containing SDS, $|G^*|$ values at low concentration (5mM) of this surfactant were not significantly different to those of the sepiolite gel without surfactant. Above 5mM SDS, $|G^*|$ dropped by about two orders of magnitude, congruently with the formation of a weaker gel-like structure.

Addition of the cationic surfactant CTAB in the (5-10) mM range (Figure 2b) yielded a slight increase in the gel strenght as demonstrated by the greater $|G^*|$ values. However, no significant differences were observed upon increasing the CTAB concentration from 5mM to 10 mM.

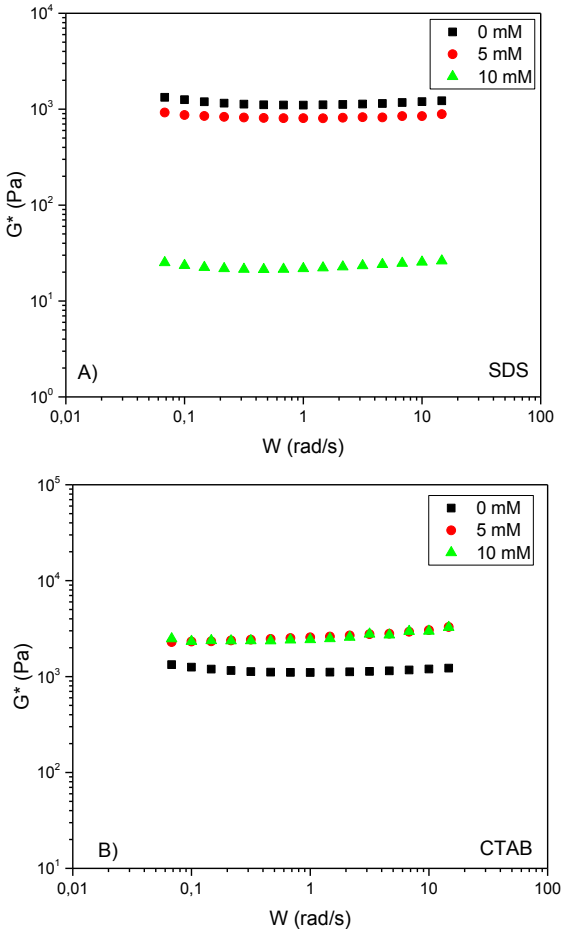

Figure 2. Complex viscoelastic modulus *vs* angular frequency for sepiolite aqueous gels with 3% (m/m) and different content in SDS and CTAB. A) SDS concentration 0, 5 and 10 mM. B) CTAB concentration 0, 5 and 10 mM. T=20ºC.

Microscopy

Scanning electron microscopy (SEM) micrographs of different sepiolite gel-like systems are shown in Figure 3 (A, B, C). Figure 3A shows the microstructure of the 3 % (m/m) sepiolite gel without surfactant. The main feature of this microstructure consisted of small layers randomly distributed such that cell-like structures, similar to those formed by cork, are formed. This implies a certain organization degree, which explains the gel-like rheological properties observed for these samples.
Figure 3b illustrates that the incorporation of 10mM SDS resulted in a more open microstructure. This may be attributed to the electrostatic repulsions between

negative SDS molecules and sepiolite, which is also negatively charged. This resembles the microstructure of expanded cork.

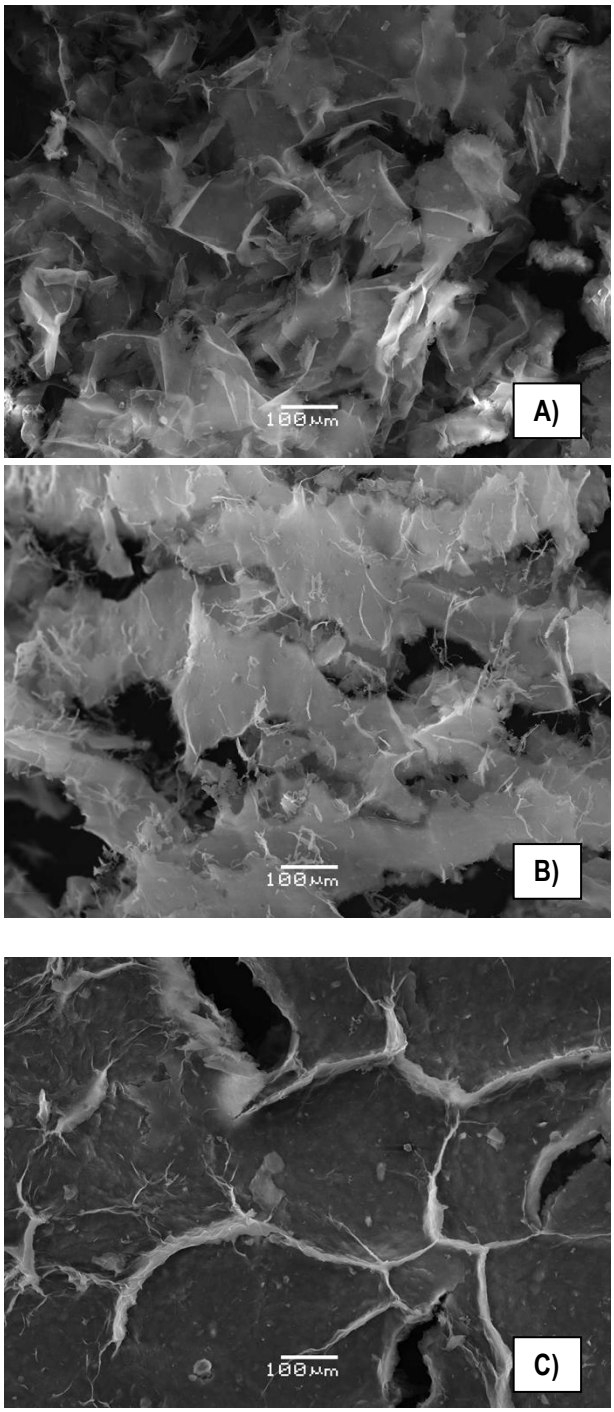

Figure 3. SEM micrographs of freeze-dried sepiolite gel with 3% (m/m) and different concentrations of SDS and CTAB. A) Without surfactant B) 10mM SDS C) 10mM CTAB.

Figure 3C shows the microstructure of a sepiolite gel formulated with 10mM CTAB consisting of a cellular structure; i.e based on the formation of more compact cells than those exhibited by the sepiolite gel formulated without surfactant. Water and surfactant micelles are likely to be found within the holes formed by sepiolite gels. This complex microstructure hinders the relative movement of cells and may be responsible for the increase in a) viscosity, b) apparent yield stress and c) the dynamic viscoelastic functions G' and G''.

The microstructure of sepiolite gels containing CTAB is based on attractive interactions between negative charges of sepiolite and positive charges of CTAB, such that cohesive forces among particles are promoted.

Conclusions

The rheological properties of sepiolite gels are markedly influenced by the charge and concentrations of ions in the continuous phase. Thus, addition of SDS in concentrations above 5mM results in a drop of yield stress, viscosity and gel-like strength. Conversely, the addition of a cationic surfactant, such as CTAB at concentrations above 5mM yields the opposite effects. These results are consequence of electrostatic interactions between surfactant molecules and the gel-like structure of sepiolite.

SEM micrographs of sepiolite gels exhibit a network based on alumino-silicate fibers. Addition of SDS of sepiolite gels results in a more open structure than that of the sepiolite gel without surfactant. Conversely, gels containing CTAB show a more compact structure, which supports the increase of viscosity, yield stress and gel-strength.

Acknowledgements

The financial support received (Project CTQ2015-70700-P) from the Spanish Ministerio de Economía y Competitividad and from the European Commission (FEDER Programme) is kindly acknowledged. The authors are also grateful to the following companies for providing materials for this research, Tolsa Group and the Microscopy Service of CITIUS (Univ. Sevilla).

References

1. Galan, E. (1996). Properties and applications of palygorskite-sepiolite clays. Clay Minerals, 31(4), 443-453.
2. Maqueda, C., Partal, P., Villaverde, J., & Perez-Rodriguez, J. L. (2009). Characterization of sepiolite-gel-based formulations for controlled release of pesticides. Applied Clay Science, 46(3), 289-295.

Contact Address:

pramirez@us.es
Departamento de Ingeniería Química
Facultad de Química
Universidad de Sevilla
c/ P. García González, 1, 41012, Sevilla (Spain).
Telf.: +34 954 556447

Emulsions stabilised with legume proteins. From interfacial to bulk rheology

M. Felix[1], N.C. Isaurralde[2], J. A. López Osorio[3], C. Carrera[1], A. Guerrero[1]

[1] Universidad de Sevilla, Departamento de Ingeniería Química, c/ Prof. García González 1, Sevilla (Spain).
[2] Universidad Nacional del Litoral (UNL) - Facultad de Ingeniería Química (FIQ) - Instituto de Investigaciones en Catálisis y Petroquímica (INCAPE-CONICET) (Argentina)
[3] Facultad de Ingeniería, Programa de Alimentos, Universidad de Caldas, calle 65 # 26-10, 275, Manizales, Caldas (Colombia)

Introduction

Nowadays, food industry is showing great interest in the development of low-fat oil-in-water (O/W) emulsions in order to obtain healthier food emulsions. Most of food emulsions are currently stabilised by milk or eggs proteins [1]. Unfortunately, the costs of these proteins are high and their use may involve some health problems (e.g. food allergies and intolerance). For this reason, food industry is currently focused on the use of plant proteins to substitute animal proteins. Among them, legume proteins seem to be excellent candidates [2]. However, further efforts to extend research on functional properties of legume proteins would be necessary to enable their use in novel applications [3]. In addition, plant proteins may be also regarded as being highly efficient in producing and stabilizing food products like emulsions, by reducing interfacial tension. However, they not only favour breakup of droplets but also may contribute to stabilize oil droplets by forming fairly stable viscoelastic interfacial films. In this sense, interfacial properties play and essential role in the emulsification process and stability of O/W interfaces, dominating the dynamics of complex fluid-fluid interfaces. The behaviour of proteins molecules at the O/W interface has been extensively studied for model proteins (i.e. β-Lactoblobulina, albumen or BSA). However, the behaviour of commercial proteins has not been examined in sufficient depth, mainly because of its high complexity [4]. This complex behaviour found at the O/W interface may come from a variety of molecular interactions between protein chains, aggregates, polymers and/or colloidal particles at the fluid-fluid interface. To elucidate the nature of these interactions, the evaluation of interfacial-shear rheological properties have been postulated as the most useful tool for the assessment of the microstructure of complex fluid-fluid interfaces [5]. Moreover, rheological properties from interfacial shear measurements have been related to the long-term stability of emulsions. In relation to this, the characterisation of emulsion microstructure over ageing time is one of the best ways to follow the stability of emulsions [6].

The objective of this work has been to establish a relationship between interfacial properties and bulk rheology of chickpea-stabilised emulsions. The later properties have been previously used in combination with droplet size distribution (DSD) measurements to make predictions on the stability of protein-based emulsions [7]. Therefore, a further objective would be to find links between interfacial shear rheology and emulsion stability. To achieve this objective, chickpea protein has been used to stabilise O/W protein-based emulsions at three different pH values (2.5, 5.0 and 7.5).

Experimental

Materials

A protein flour from milled chickpea was supplied by DOSBIO (San José de la Rinconada, Seville, Spain). This chickpea flour was dispersed into water (10 wt.%) and the pH value was adjusted at 8.0 using 4 M NaOH (to achieve alkaline solubilization). The flour dispersion was stirred over 30 min and subsequently centrifuged for 15 min at 15000 × g and 10 ºC. The supernatant was separated from the pellet and the pH value was set at 3.5 using 4 M HCl (to carry out isoelectric precipitation). Dispersion was again centrifuged for 15 min at 15000 × g and 10 ºC. The pellet was freeze-dried in a Telstar LyoQuest (Terrassa, Barcelona, Spain).

Interfacial characterisation

Interfacial dilatational measurements were carried out using a pendant drop tensiometer (Tracker, IT Concept, France). The droplet profile was digitized and analysed through a CCD camera. Droplet profiles were processed according to the Laplace equation as was described by Castellani et al. [8]. The complex dilatational viscosity of protein-based O/W layers (η_i^*) was determined at 10% strain amplitude after reaching the pseudo equilibrium state (10,800 s) from 0.0075 to 0.1 Hz. All the tests were carried in an optical glass cuvette containing the oil phase, which was thermoset at 20.0 ± 0.1 °C.

Interfacial shear rheology was carried out using a double-wall-ring geometry (DWR) connected to a sensitive magnetic air bearing stress-controlled rheometer (DHR-3, TA Instruments, USA). The procedure was carried out as indicated Vandebril et al. [9]. Complex shear viscosity (η_i^*) from O/W interface was obtained from frequency sweep tests (from 0.0075 to 7.5 Hz) after reaching the pseudo equilibrium state (10,800 s). Additionally, flow curves were carried out at O/W interface from $4 \cdot 10^{-4}$ to 100 s^{-1}.

Emulsion preparation

After the rheological characterisation of the interfacial layers, emulsions were prepared using a high-pressure homogenizer EmulsiFlex-C5 (Avestin). Firstly, a pre-emulsion was obtained by homogenising for 2 min in a Ultraturrax® mixer at the selected pH value, using an aqueous dispersion of 2.0 wt.% freeze-dryed chickpea protein and sunflower oil at a 50/50 O/W ratio.

Emulsion characterisation

Droplet size distributions (DSD) of emulsions were determined with a particle size analyser by means of laser diffraction (Mastersizer X, Malvern). To avoid the presence of floccules during DSD tests, emulsions were diluted 1:10 into 1 wt.% SDS solution (pH 8.0), and then gently stirred. The volumetric mean droplet diameter (D[4,3]) was calculated as follows:

$$D[4,3] = \frac{\sum n_i d_i^4}{\sum n_i d_i^3} \quad (1)$$

where n_i is the number of droplets with a diameter d_i.

Small Amplitude Oscillatory Shear (SAOS) tests were carried out for all the emulsions by means of a stress-controlled rheometer (AR-2000, TA Instruments), using serrated plate-plate geometry to avoid slipping effects. Frequency sweep test (from 0.05 to 50 s^{-1}) and flow curves (from $1 \cdot 10^{-3}$ to 1000 s^{-1}) were carried out 1 and 30 days after emulsification.

Statistical analysis

At least 3 replicates of each measurement were carried out. Uncertainty was expressed as standard deviation.

Results and Discussion

Interfacial characterisation

Figure 1 shows the complex viscosity (η_i^*) obtained from dilatational measurements as a function of frequency (from 0.0075 to 0.1 Hz) and pH (2.5, 5.0 and 7.5). This figure puts forward the development of a fairly viscoelastic O/W interface after protein adsorption, which depends on the pH value (2.5, 5.0 or 7.5).

As may be observed, the pH value has a strong influence on η_i^*. The higher values were obtained for the system at pH 2.5, whereas the lower were obtained for the system at pH 7.5. The complex viscosity, η_i^*, is also frequency-dependent, showing a power-law decay with frequency for all the systems studied.

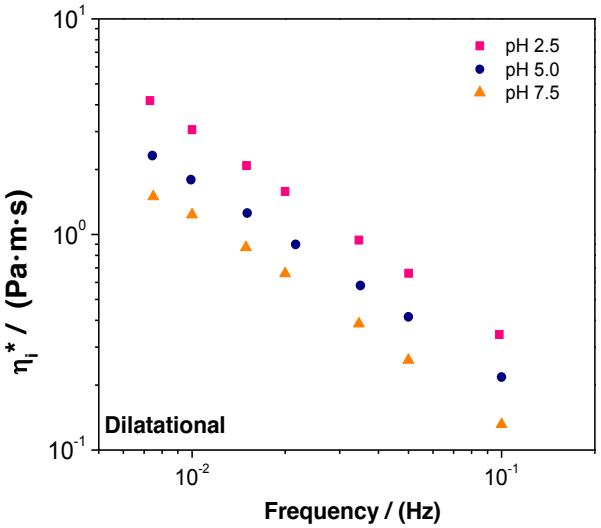

Figure 1. Values of the interfacial dilatational complex viscosity, η_i^*, obtained at the O/W interface as a function of frequency and pH.

Despite the fact that rheological dilatational properties are typically determined by subjecting interfaces to oscillatory deformations, different contributions may affect the dynamic properties of the interface. Hence, dilatational measurements may not be able to show only the response of protein-protein interactions at O/W interfaces, which determine the stability of a complex fluid-fluid interface [5]. In that case, a combination with interfacial shear tests is needed to understand the true dynamic of the complex fluid-fluid interface. According to Sagis [10], the response of the interface to an applied deformation by dilation may be the result of the contribution of three terms. Apart from changes in surface tension, deformations may induce deviatoric stresses in complex interfaces, and the bending rigidity of the interface may also contribute to the response of an interface. Thus, the effective interfacial tension may be expressed as follows:

$$\sigma_{eff} = \sigma - kC_o \frac{1}{R} + tr(\boldsymbol{\tau}^i) \quad (2)$$

The three terms in the right hand of Eq. (2) represent the interfacial tension (σ), the bending rigidity (where R is the drop radius) and the deviatoric stresses, respectivey. The effective interfacial tension (σ_{eff}), measured at various droplet sizes, fits a linear equation with the reciprocal of the drop radius (1/R) giving rise to negative slopes that depend on pH (- 45, - 54 and -19 μN at pH 2.5, 5.0 and 7.5, respectively). This linear dependence indicates that the response to a dilatational deformation is dominated by the second term and provides information on bending rigidity rather than on a true dilatational modulus. The lower slope found at pH 7.5

reflects that the predominant role of bending rigidity is less pronounced at this pH.

With the above limitations in mind, Small Amplitude Oscillatory Shear measurements were carried out at the O/W interface (SAOS). Figure 2 exhibits the interfacial complex viscosity (η_i^*) obtained from SAOS tests as well as the interfacial apparent viscosity (η_i) obtained from flow tests at the O/W interface after the protein adsorption as a function of pH (2.5, 5.0 and 7.5). This figure corroborates the relevance of protein interactions at the O/W after protein adsorption, which are particularly strong at the lowest pH, as reflected by the values of both η_i^* and η_i. However, these interactions are not as strong as they would be expected from the results shown by dilatational measurements. This difference also supports the contribution of other factors (i.e. the bending rigidity of the interface) to the response obtained by dilatational measurements.

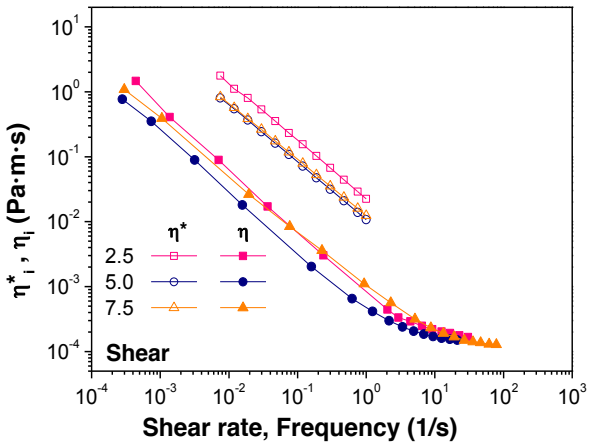

Figure 2. Values of the interfacial shear complex and apparent viscosity, η_i^* and η_i, obtained at the O/W interface as a function of pH (2.5, 5.0 and 7.5).

Moreover, Figure 2 also displays the interfacial shear flow properties as a function of pH. As may be observed, the interfacial layers always show a very shear-thinning behaviour, with similar slopes in the power-law decay region, and a clear tendency to reach a high-shear-rate limiting viscosity. This figure also attempts to test the applicability of the Cox-Merz [12] rule for the interfacial O/W layers. This rule, which is applicable for the bulk rheological properties of many polymer melts and concentrated and semi-dilute polymer solutions, generally fails for either cross-linked or entangled gelled systems [11]. As may be observed in Figure 2, a quite remarkable deviation from the Cox-Merz rule takes place at the O/W interface that confirms formation of the two-dimensional gel-like behaviour.

Emulsion characterisation

Table 1 shows D[4,3] parameter from DSD profiles obtained according to Eq. (1), as a function of pH. First of all, it is worth pointing out the strong dependence of droplet sizes on pH. Thus, the lowest sizes were obtained at pH 2.5 and 7.5, far from the isoelectric point (IEP) which is ca. 3.7. At these pH values, the electrostatic interactions among droplet surfaces are relevant since their zeta potential values are -26.5 and 28.4 mV, respectively. However, at pH 5.0 the zeta potential is -11.0 mV, hence the electrostatic repulsions may be regarded as moderate. In any case, according to the values shown in Table 1, all the emulsions studied can be considered stable in terms of the slight evolution of droplet size shown after one month. As may be observed, the shortest change in droplet size was found at pH 2.5, which was the system with the highest η_i^*. In addition, it is noticeable that the mean volume diameters were in the same size range than those obtained for other protein-based emulsions [13,14].

Table 1. Evolution over storage time of D[4,3] parameter from DSD of chickpea-stabilized emulsions as function of pH (2.5, 5.0 and 7.5)

	D [4,3]	
	Day 1	**Day 30**
pH 2.5	1.3 ± 0.1	1.4 ± 0.1
pH 5.0	6.4 ± 0.2	6.9 ± 0.1
pH 7.5	1.7 ± 0.1	2.0 ± 0.1

Dynamic frequency sweep and flow tests were carried out for all the emulsions studied to determine both, the frequency dependence of complex viscosity (η^*), and the shear-rate dependence of the steady sate apparent viscosity (η). Figure 3 shows the values of η^* obtained 1 day after emulsion preparation as well as 30 days later at three different pH values (2.5, 5.0 and 7.0). The values of the apparent viscosity (η), 1 day after emulsification, are also shown in Figure 3.

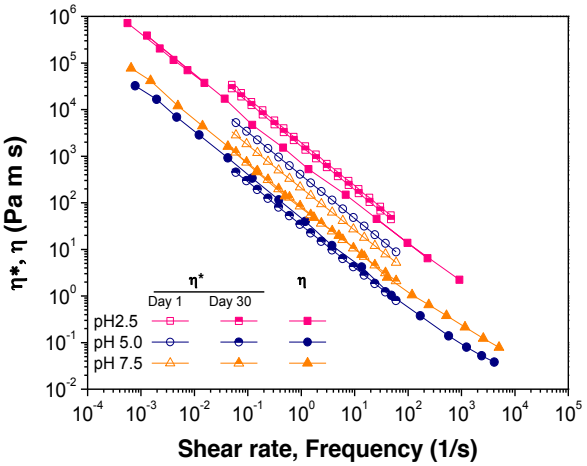

Figure 3. Complex viscosity (η^*) from SAOS measurements (1 and 30 days after emulsification) and steady state apparent viscosity (η) from shear flow tests (1 day after emulsification) at three different pH values (2.5, 5.0 and 7.5)

As may be observed, values of η^* and η show a strong dependence on pH. The highest values of both variables correspond to pH 2.5, at which positively charged protein surfaces located at the O/W interface provide strong electrostatic repulsions that help to prevent emulsion destabilization (e.g. by flocculation and coalescence). On the other side, the lowest values of η^* and long-term η correspond to pH 5.0, at which electrostatic interactions are only slight since protein surfaces show moderate negative charges. As a result, the more stable emulsions (lower changes of η^* over storage time) were found far from the IEP (particularly at pH 2.5). These results are in accordance with D[4,3], where the lowest value was obtained for the emulsion at pH 2.5, whereas the highest value was obtained for the emulsion at pH 5.0. Interestingly, all emulsions exhibit a very shear-thinning behaviour with slopes between -0.94 and -0.90 that are very close to the values shown by the O/W interface.

Finally, this figure also shows that chickpea-stabilized emulsions do not match the empirical Cox-Merz rule. This fact as has been typically found in emulsion rheology, where high concentrated emulsions have been described as a system forming a well developed gel-like elastic network [11,15].

Concluding remarks

Achieving high values of complex viscosity (η_i^*), chickpea proteins provide suitable interfacial properties for stabilizing O/W interface. However, the interfacial response is highly pH-dependent, finding the best response at pH 2.5. The comparison between dilatational and interfacial shear rheology indicates that η_i^* values obtained from dilatational measurements are affected by bending rigidity. Thus, despite the fact that this contribution takes place at all the pH values studied, the lower contribution was found at pH 7.5.

Results seem to support the assumption that a direct relationship exists between the bulk linear viscoelastic properties of chickpea-based emulsions and interfacial SAOS data for chickpea-absorbed O/W interfaces. Emulsion destabilization occurs over storage time for those emulsions showing lower values of both interfacial and bulk LVE properties.

Previous results obtained for highly concentrated protein-stabilized emulsions reported that the complex modulus could be used to predict long-term emulsion stability [14]. As a consequence, interfacial SAOS can be regarded as a powerful tool that might be used to make predictions on the stability of protein-based emulsions, even before carrying out emulsification.

Acknowledgements

This work is part of a research project sponsored by the "Ministerio de Economía y Competitividad", Ref. CTQ2015-71164-P (MINECO/FEDER, EU).

References

1. Guerrero, A., and Ball, H.R. (1994). J. Texture Stud. (1994), 25, 363–381.
2. Zhang, T., Jiang, B., Mu, W., and Wang, Z. (2009). Food Hydrocolloid 23, 146–152.
3. Makri, E., Papalamprou, E., and Doxastakis, G. (2005). Food Hydrocolloid 19, 583–594.
4. Fuller, G. G., and Vermant, J. (2012). Annu. Rev. Chem. Biomol. Eng. 3, 519–543.
5. Sagis, L.M.C., and Fischer, P. (2014). Curr. Opin. Colloid Interface Sci. 19, 520–529.
6. McClements, D. J. (2004). Food Emulsions: Principles, Practice and Techniques, 2nd ed., Press, C. R. C., Ed., Boca Raton: Florida.
7. Romero, A. Cordobés, F., Puppo, M.C., Guerrero, A., and Bengoechea, C. (2008). Food Hydrocolloid 22, 1033–1043.
8. Castellani, O., Al-Assaf, S., Axelos, M., Phillips, G. O., and Anton, M. (2010). Food Hydrocolloid 24, 121–130.
9. Vandebril, S., Franck, A., Fuller, G. G., Moldenaers, P., Vermant, J. (2010). Rheol. Acta 49, 131–144.
10. Sagis L.M.C. (2013). Eur. Phys. J. Special Topics 222, 39–46.
11. Al-Hadithi, T.S.R., Barnes, H.A. and Walters, K. (1992) Colloid Polym. Sci. 270, pp. 40-46.
12. Felix, M., Romero, A., Guerrero, A. (2017). Food Hydrocoll. 64, 9–17.
13. Bair, S.; Yamaguchi, T.; Brouwer, L.; Schwarze, H.; Vergne, P. (2014) Tribol. Int., 79, 126–131.
14. Romero, A., Cordobés, F., Puppo, M.C., Guerrero, A., Bengoechea, C. (2008). Food Hydrocoll. 22, 1033–1043.
15. Bengoechea, C., Puppo, M.C., Romero, A., Cordobés, F., Guerrero, A. (2008). J. Food Eng. 87, 124–135.

Contact Address:

M. Felix (mfelix@us.es)
Dpto. Ingeniería Química, Universidad de Sevilla,
C/ Profesor García Gonzalez, 1-41012 Sevilla, Spain
Telf.:+34 954 557179

Rheological study of the aggregation state of alumina nanofluids

J.L. Arjona-Escudero[1], I.M. Santos-Ráez[1], A.I. Gómez-Merino[2], F.J. Rubio-Hernández[2]

[1] Department Ingeniería Mecánica, Térmica y de Fluidos, Escuela de Ingenierías Industriales, University of Málaga (Spain)
[2] Department Física Aplicada II, Escuela de Ingenierías Industriales, University of Málaga (Spain)

Introduction

Nanofluids are dilute suspensions of functionalized nanoparticles or composite materials developed about a decade ago with the specific aim of increasing the thermal conductivity of heat transfer fluids, which have now evolved into a promising nanotechnological area. Nanofluids contain particles with size generally less than 100 nm. The presence of solid particles is adequate for the use as heat exchanger fluids [1,2]. The effect of nanoparticle size on thermal properties of nanofluids is still today a question which is far from being answered. In this respect, the results reported in the literature are contradictory [3], probably due to the formation of aggregates when particles are dispersed in the liquid phase. Regarding to the nanoparticle shape influence in thermal conductivity, cylinders and spheres have been considered as the more effective in heat transfer. In relation to the nanoparticle concentration effect, it has been proved that thermal conductivity increases with volume fraction [4]. Volume concentration (or volume fraction) can be accounted for as one of the most important parameters of nanofluids. The solid particles have higher thermal conductivity than liquids, therefore as the percentage of dispersed nanoparticles increases, the thermal conductivity of the whole mixture increases as well. Several studies confirmed that nanofluid heat transfer coefficients could be improved by more than 20% in the case of low nanoparticle concentrations (< 5%) [5]. However, the effect of nanoparticle size is still a question to be answered.

Recently [6], the relationship between shear rheology and aggregation state of suspensions has been reviewed. Mechanical and physical properties of the resultant materials depend on shape, size and size distribution, which are considered determining parameters in the formation of particle aggregates. Hence the importance of a good characterization of nanofluids to study the effect of shape, size, volumetric fraction, and so on, over thermophysical properties. For example, sometimes can be considered to have a small particle size when in fact these particles come together to form larger aggregates, which could lead to even contradictory conclusions about the effect of particle size.

Spherical nanoparticles of alumina, which is one of the most dispersed nanoparticle in water, were used in this study. The aim of this work is the characterization of alumina nanofluids related to particle shape, size and size distribution using TEM (Transmission Electron Microscopy), DLS (Dynamic Light Scattering) and rheological assessment.

Theory

The flow field of a suspension is mainly governed by the volume fraction occupied by solid particles (ϕ). When the suspension is concentrated, the interactions of particles should be considered. In this case, several expressions for the relation between viscosity and volume fraction of particles have been proposed. Krieger and Dougherty [7] and Mooney [8] derived two expressions in which the maximum packing fraction of particles (ϕ_m) appears as a second parameter,

$$\eta_r = \left(1 - \frac{\phi}{\phi_m}\right)^{-[\eta]\phi_m} \quad (1)$$

$$\eta_r = exp\left(\frac{[\eta]\phi}{1-\left({}^{\phi}/_{\phi_m}\right)}\right) \quad (2)$$

In these expressions, $\eta_r = {}^{\eta}/_{\eta_0}$, η_0 is the viscosity of the liquid phase, $[\eta]$ is the intrinsic viscosity, which depends on the aspect ratio, defined as the proportion between two characteristics lengths of the particle. When $[\eta] = 2{,}5$, particles are spheres. Finally, ϕ_m, is the maximum packing fraction, that expresses the ability of the particles to achieve the most compact distribution.

Frequently, the viscosity curves are governed by the mathematical model of power law, whose expression is:

$$\eta = K \cdot (\dot{\gamma})^{n-1} \quad (3)$$

Where *n* explains the Newtonian behavior ($n \cong 1$), shear thickening ($n>1$) or shear thinning ($n<1$) of the material.

Experimental Methods

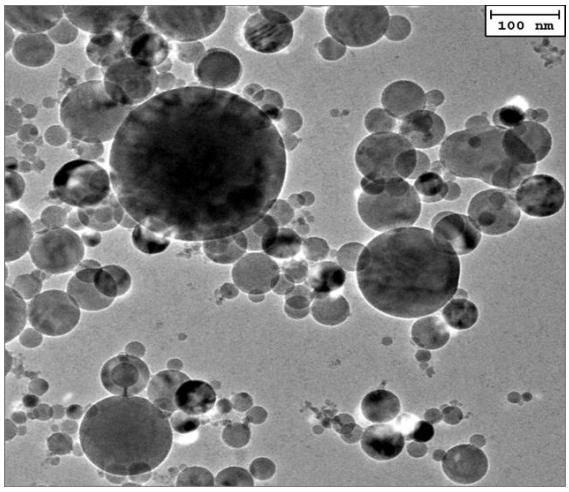

Figure 1. Representative TEM micrograph and particle morphology of Al_2O_3 nanoparticles used in the study

Al_2O_3 powder has been supplied by Sigma-Aldrich with a particle size of 50 nm.

TEM images were recorded on a JEOL JEM-100CX and on a FEI TECHNAI G20 transmission electron microscope. The particle powder was dispersed in pure water with 1.10^{-4} M KCl as a background electrolyte and was left in an ultrasound bath for 20 min. Samples were attached to Formvar copper grids by placing one drop on the grid and evaporating the solvent.

Samples were prepared by a two-step procedure was. The nanoparticules were dispersed into water as base fluid by ultrasonication process with different durations.

Dynamic Light Scattering (DLS) technique were used to characterize the size of agglomerates in solution. Measurements were performed using a Zetasizer Nano-S system (Malvern Instruments, UK). This instrument uses the backscattering detection system (scattering angle θ=173°), is equipped with a Helium–Neon laser source (632.8 nm and 4.0 mW) and has a built-in Peltier temperature control with an accuracy of ±0.1 °C. Agglomerate size was obtained from the correlation function using the CONTIN algorithm [9].

Rheological measurements were performed in a Haake Rheostress-600 rheometer (Thermoelectron, Germany). Cone-plate geometry with a cone angle of 1º and diameter of 60 mm was utilized. Steady flow curves were performed by applying discrete shear rates at increasing ramps in the range of 10^{-3} to 10^{3} s^{-1}. Each measure was recorded after shearing the sample until the steady response was obtained.

Results and Discussion

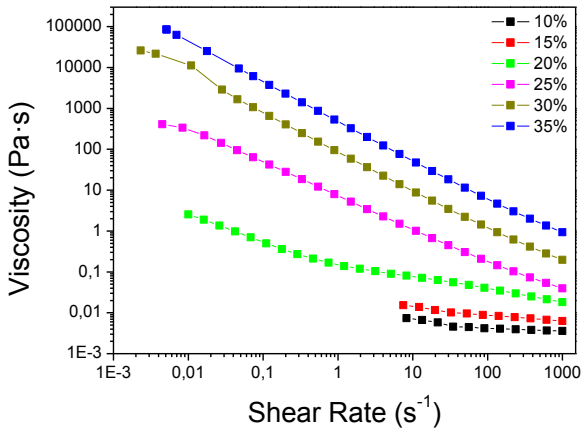

Figure 2. Effect of shear rate and particle volume fraction on the viscosity of Al_2O_3 water nanofluids at native pH and 5ºC.

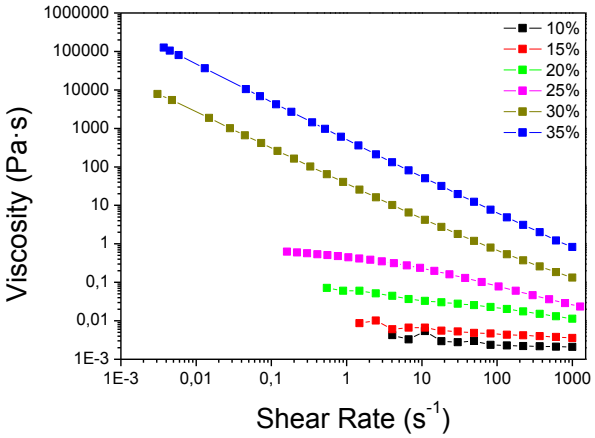

Figure 3. Effect of shear rate and particle volume fraction on the viscosity of Al_2O_3 water nanofluids at native pH and 25ºC.

TEM images showed spherical nanoparticles with a mean average diameter of 50±10 nm, although polydispersity was observed, with few particles of 200±20 nm in diameter (Fig. 1).

DLS analysis indicates that the size of the agglomerates decreases insignificantly with temperature and this size increases considerably when the pH is raised to the value of the isoelectric point, which for alumina suspensions is close to 9. However, at the working pH (native) the particle size remains approximately constant. The diameter average, at native pH, is about 200±30 nm with a poorly dispersed size distribution, so the solid particles are agglomerated and remain stable over time.

In the steady shear flows (Figs. 2 and 3) a Power Law is observed for high values of the volumetric fraction and an almost Newtonian behaviour for volumetric fractions

that do not exceed 15%. The power law adjustments are summarized in Table 1. In all cases, the flow index is negative (the coefficient n<1), as it can be expected in shear thinning behavior, and K, the consistency, increases with volume fraction and decreases with temperature.

Table 1. Predicted values of K and n according Power Law model. All the uncertainties of n are under 0.05.

Temperature 5ºC			
ϕ	*K* [Pa·s]	*n*	R^2
10%	0.01±0.01	0.83	0,8702
15%	0.02±0.01	0.81	0,9660
20%	0.123±0.003	0.34	0,9974
25%	15±1	0.37	0,9858
30%	330±10	0.27	0,9815
35%	480±10	0.017	1,0000
Temperature 25ºC			
ϕ	*K* [Pa·s]	*n*	R^2
10%	0.005±0.012	0.84	0,5936
15%	0.01±0.01	0.85	0,8351
20%	0.06±0.01	0.76	0,9911
25%	0.4±0.1	0.72	0,9731
30%	40±10	0.09	0,9997
35%	320±10	0.02	1,0000

Table 2. Predicted values of ϕ_m and $[\eta]$ at low and high shear rate obtained by fitting the measured data with the Krieger Dougherty and Mooney models.

Temperature 5ºC			
Model	**Parameter**	**Low shear rate**	**High shear rate**
KD equ (1)	$[\eta]$	15.44±0.04	10.28±0.01
	ϕ_m	0.37±0.05	0.48±0.01
	R^2	0.8583	0.9993
M equ (2)	$[\eta]$	16.02±0.02	9.29±0.01
	ϕ_m	0.51±0.05	0.71±0.02
	R^2	0.8599	0.9995
Temperature 25ºC			
Model	**Parameter**	**Low shear rate**	**High shear rate**
KD equ (1)	$[\eta]$	17,70±0.01	9,93±0.02
	ϕ_m	0,37±0.02	0,44±0.01
	R^2	0,9941	0,9992
M equ (2)	$[\eta]$	20,43±0.03	8,64±0.01
	ϕ_m	0,57±0.04	0,63±0.02
	R^2	0,9946	0,9994

Table 3. Volume fraction of particles in a cluster (ϕ_{pc}) in the KD and M models. All the uncertainties of ϕ_{pc} are under 0.001.

Temperature 5ºC			
Model	**Parameter**	**Low shear rate**	**High shear rate**
KDequ	ϕ_{pc}	0.162	0.243
Mequ	ϕ_{pc}	0.156	0.269
Temperature 25ºC			
KDequ	ϕ_{pc}	0.141	0.252
Mequ	ϕ_{pc}	0.122	0.289

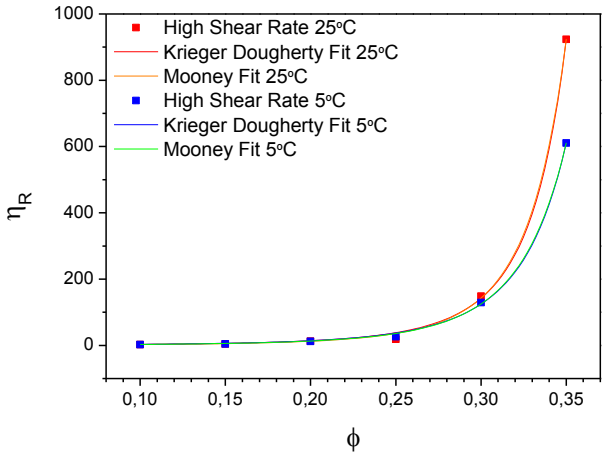

Figure 4. Dependence of the relative viscosity on the particle volume fraction: Krieger Dougherty and Mooney Fits at different temperatures.

As mentioned above, the steady shear flow has shown a shear thinning behaviour, consequently the clusters measured by means of DLS technique, when they are at rest, are formed by highly branched aggregates that erode when shear rate increases, until a suspension of individual particles is achieved. These results are in good agreement with the intrinsic viscosity obtained by Mooney and Krieger-Dougherty models (Table 2). In both cases, these values are far from 2.5 typical of spherical particles.

Fig. 4 shows the adjustments of Krieger Dougherty and Mooney models carried out at various temperatures and high shear rate. Both models fit reasonably well the experimental curves and, as it is shown in Fig. 4, they agree in the adjustment, overlapping both models the experimental data.

A quantity that can give an idea regarding the compaction degree of clusters is the volume fraction of particles in a Cluster (ϕ_{pc}). This can be obtained by means of using the relation derived by Smith and Bruce [10]:

$$\phi_{pc} = 2.5/[\eta] \qquad (4)$$

Using Eq. (4) the results obtained are shown in Table 3. These relatively low results suggest that clusters are ramified or have opened structures at the low shear rate region [11]. However, the values of the maximum packing fraction, that are obtained when both models fit the relative viscosity vs. particle volume fraction data (Fig. 4), are relatively small for both models. It could be interpreted that M model provides better values than K-D model at low shear rates. While at high shear rates the M values are too high for a system of clusters with different shapes and sizes.

The temperature effect was also taken into account. The adjustments summarized in Table 2 indicate that the shape of the agglomerates varies little with temperature since the coefficients of intrinsic viscosity and maximum packing fraction are not very different at temperatures of 5ºC and 25ºC. This little influence of temperature on the aggregate size was also observed by DLS. Measurements of particle size at 5 ºC and 25 ºC did not experiment much change, giving in both cases an average value of 220 ±40 nm at 5ºC and 200±20 nm at 25 ºC.

Concluding Remarks

The flow and viscosity curves of alumina nanoparticle suspensions were performed varying particle volume fraction and temperature. The nanofluid suspension shows a nearly Newtonian behavior when the volume fraction do not exceed 0.15 and a shear thinning when the volume fraction is higher than 0.15. It was also observed that viscosity increases with volume particle fraction and decreases with temperature.

The analysis of the experimental data using the Mooney and Krieger Dougherty models indicated that nanoparticles formed agglomerates because the intrinsic viscosity is far from 2,5, which is the value corresponding to spherical particles. This result was also supported by DLS measurements, which provided diameter average of particles higher than 50 nm. This last was the nanosphere elemental size observed by electron microscopy (TEM).

The steady shear flow and the high values of the maximum packing fraction at high shear rates have suggested that these clusters, when they are at rest, are formed by highly branched aggregates that erode, when the shear rate increases, until a suspension of individual particles is achieved. The two tested models (Krieger-Dougherty and Mooney) fit the experimental data.

References

1. El Bécaye Maïga, S., Tam Nguyen, C., Galanis, N., Roy, G., Maré, T., and Coqueux, M. (2006). International Journal of Numerical Methods for Heat & Fluid Flow 16 (3), 275-292.
2. Jang, S.P., and Choi, S.U. (2006). Applied Thermal Engineering 26 (17), 2457-2463.
3. Lomascolo, M., Colangelo, G., Milanese, M. and de Risi, A. (2015). Renewable and Sustainable Energy Reviews 43, 1182-1198.
4. Vanaki, Sh M., P. Ganesan, Mohammed, H.A. (2016) Renewable and Sustainable Energy Reviews 54 1212-1239.
5. Godson L, Raja B, Mohan Lal D, Wongwises S.(2010) Renewable Sustainable Energy Reviews 14 629–41.
6. Genovese, D.B. (2012). Adv. Colloid Interface Sci. 171, 1-16.
7. Krieger, I.M., and Dougherty, T.J. (1959). Trans. Soc. Rheol. 3, 137-152.
8. Mooney, M. (1951). J. Colloid Interface Sci 6, 162-170.
9. Provencher, S.W. (1982). Computer Physics Communications 27 (3), 229-242.
10. Smith, T. L., & Bruce, C. A. (1979). J. Colloid Interface Sci, 72(1), 13.
11. Prasher, R., Phelan, P. E., & Bhattacharya, P. (2006). Nano letters, 6(7), 1529-1534.

Contact Address:

aimerino@uma.es
Department of Fisica Aplicada II,
Escuela de Ingenierías Industriales
University of Málaga (Spain)
C/ Dr. Ortiz Ramos, s/n, Málaga (Spain)
Telf.: 951 952 294 ; Fax:

Gibbs free energy of activation for viscous flow in alumina suspensions

I.M. Santos-Ráez[1], J.L. Arjona-Escudero[1], A.I. Gómez-Merino[2], F.J. Rubio-Hernández[2]

[1] Department of Ingeniería Mecánica, Térmica y de Fluidos, Escuela de Ingenierías Industriales, University of Málaga (Spain)
[2] Department of Física Aplicada II, Escuela de Ingenierías Industriales, University of Málaga (Spain)

Introduction

The presence of alumina solid nanoparticles in aqueous phase induces the appearance of two main effects: the distortion of the flow field, which in turn increases the viscosity of the suspension when compared to the viscosity of the carrier liquid, and the change from Newtonian to non- Newtonian flow depending on the size, shape and concentration of particles. In addition, the presence of solid particles produces an increase in the thermal conductivity of the nanofluids. For this specific application is mandatory to avoid the solid phase sedimentation [1-3]. Particle sedimentation is preceded by particle flocculation, which is controlled by the zeta-potential.

Very often, the viscosity curves of moderately concentrated ceramic suspensions exhibit a sigmoidal shape: a low shear Newtonian plateau precedes a sharp fall in viscosity with increasing rate (shear-thinning), which very often ends in a high shear Newtonian plateau [4]. This shape flatten with temperature. The shear-thinning behavior usually has been explained by considering a less structurated system as a consequence of applying a shear, which lines up the particles and reduces the viscosity of the suspension. This alignment of particles diminishes the distortion of the shear flow. When the shear rate increases the rest structure progressively erodes. At the high shear rate region a Newtonian plateau is expected to be achieved. It is widely accepted [5] that this second Newtonian plateau results from the formation of ordered sheets formed by basic units (virtually the individual particles). As the liquid phase can easily flow between them, a reduction in the viscosity value is expected.

Few physical magnitudes, apart from the rheological parameters already mentioned, are used to justify the shear thinning mechanism. The purpose of this work is to assess the influence of some thermodynamic parameters, which could affect the shear thinning process, in order to contribute to the knowledge of the physical mechanism that result in this rheological behavior. With this aim, the Gibbs energy together with the volume activation in aqueous alumina nanoparticle suspensions was determined.

Experimental Methods

Al_2O_3 powder was supplied by Sigma-Aldrich; specific surface area of 43 m^2/g; density of 3880 kg/m^3.

Nanoparticles of 250±10 nm average diameter (measured by dynamic light scattering (DLS) at a native pH), were dispersed into the base fluid (aqueous solution 10^{-4} M of KCl) and sonicated for 30 min. Two volume fractions (ϕ) were prepared for this study, 0.224 and 0.150.

Rheological measurements were performed in a Haake Rheostress-600 rheometer (Thermoelectron, Germany) using a cone-plate geometry (20 mm/1°). Flow curves were recorded until the steady response was obtained in the range of 10^{-4} to 10^{3} s^{-1}.

Results and Discussion

Fig. 1 shows the viscosity curve of alumina suspensions at several temperatures and ϕ=0.224. It exhibits shear-thinning behavior with light Newtonian regions at low and high shear rate (this last less pronounced). A similar results were obtained for ϕ=0.150.

It is clear than more than one type of flow is involved in the behaviour of alumina suspensions, although the predominant is shear thinning. In all cases the viscosity of the suspension is related with the solid volume fraction, the shear rate and the temperature.

As first approach, the viscosity could be analyzed in terms of the well-known Arrhenius equation, in which is assumed that the pre-exponential factor could be a function of shear rate and volume fraction. Therefore, in order to express the relative viscosity dependence with temperature a modified version of the Andrade-Eyring equation was proposed [6]:

$$\eta_r = f(\phi, \dot{\gamma}) e^{\frac{\Delta G}{RT}} \quad (1)$$

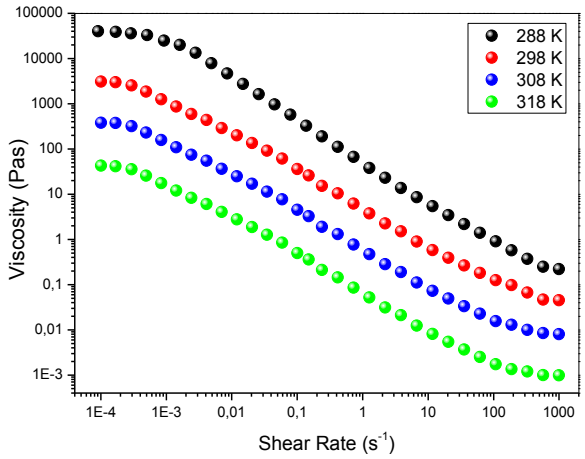

Figure 1. Effect of shear rate and temperature on the viscosity of Al_2O_3 water nanofluids at native pH, ϕ=0.224. Error bars have been omitted for clarity. All the uncertainties are under 5%.

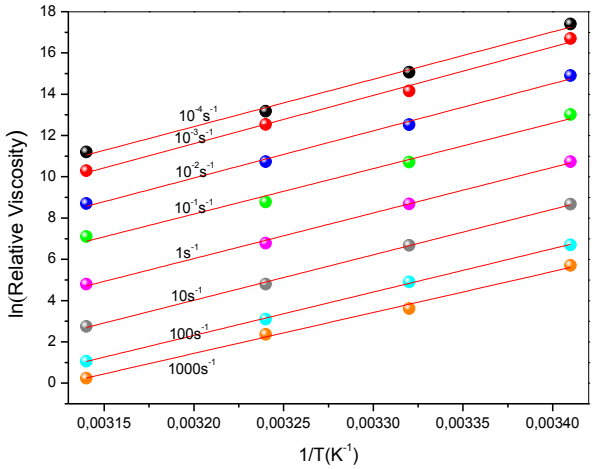

Figure 2. Relative viscosity versus the reciprocal of temperature. Effect of shear rate and (ϕ = 0.224), on the relative viscosity of Al_2O_3 water nanofluids at native pH.

where ΔG is the molar Gibbs free energy of activation representing the strength of flow obstacles, R the universal gas constant and T the thermodynamic temperature. The function $f(\phi,\dot{\gamma})$ is the pre-exponential factor, associated with the diffusion coefficient for the particles. In principle, it could be a function of shear rate and volume fraction.

Fig. 2 shows the effect of shear rate and temperature on the relative viscosity of alumina suspensions at ϕ = 0.224, by plotting ln of the relative viscosity versus reciprocal temperature (1/T). In all cases a linear dependency with reciprocal temperature was found, which indicates that the slope is independent on temperature. As expected, similar results were observed at ϕ = 0.150.

The values of the Gibbs activation energy and the pre-exponential factor can be obtained from the slopes and intercepts of the linear adjustment shown in Fig. 2. The activation energy values for alumina suspensions are shown in Fig. 3. A light decrease of the Gibbs energy with the increment of the shear rate was observed. This result could be related with the Newtonian behavior at high and low shear rates and the decrease of the slope in the viscosity curves.

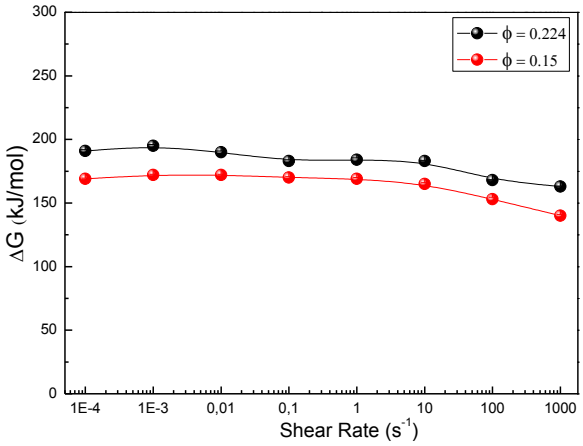

Figure 3. Gibbs activation energy at various shear rates, at the two volume fraction studied. Error bars have been omitted for clarity. All the uncertainties are under 5%.

Concerning the effect of the volume, it can be seen that, although the magnitude represented is the molar energy, the higher the concentration of particles the more activation energy was observed. Values for ΔG appear to be relatively high as compared to most fluids but lie within the normal range of between about 80–300 kJ/mol. It is probable due to the fact that the high activation energies are associated with the formation of clusters that erode under the shear [7]. By contrast, values of the pre-exponential factor are very small. Similar results of slopes and intercepts were obtained by other authors, although with different systems [8, 9].

On the other hand, the modified Arrhenius relationship may be written in the form [10]:

$$\eta = \eta_\infty e^{\frac{\Delta G - V\tau}{RT}} \qquad (2)$$

where η is the viscosity of the suspension, V is the activation volume (m^3/mol), defined as the difference between the molar volume during the shear thinning process and the molar volume at rest (by comparing with the transition state theory, TST) at the same temperature and pressure, τ is the shear stress; η_∞ is a constant which represents the viscosity at very high shear rate.

This equation has the advantage as compared to the conventional empirical approach in having material parameters that are, at least in principle, related to physical quantities.

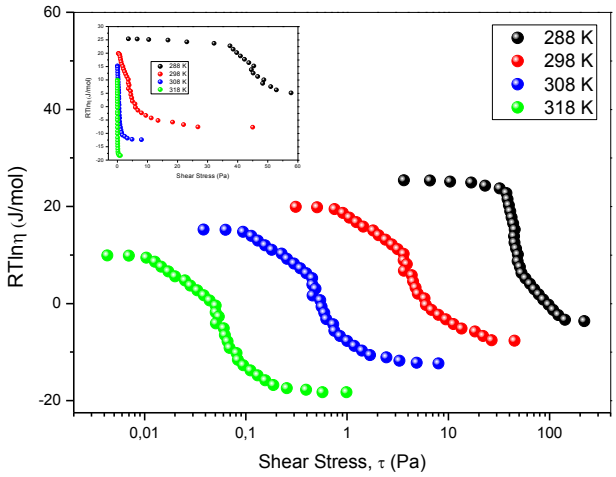

Figure 4. According to Eq. (3), curves of RT lnη plotted against shear stress for alumina suspensions at ϕ=0.224, at native pH and various temperatures as indicated. Horizontal trends correspond to the Newtonian behavior parts.

Eq. (2) can be rewritten as:

$$RTln\eta = RTln\eta_{\infty} + \Delta G - V\tau \qquad (3)$$

Fig. 4 shows the curves obtained by plotting RTlnη versus shear stress, according to Eq. (3). The Newtonian behavior corresponds to the horizontal trends and the sloping lines correspond to the non-Newtonian behavior. For clarity, the shear stress axis was represented in the logarithmic scale. The linear scale was also included in the Fig. 4 to show more clearly that the slope of the curves increases with temperature. In other words, the molar volume (slope in Eq. (3)) augments with temperature. This result endorses Eq. (3) as an appropriate expression to modelate the relationship between viscosity and temperature. Notice that the curve at the higher temperature presents the Newtonian region at low shear rate while the lower temperature curve exhibits the Newtonian plateau at a higher shear rate. This tendency was also observed in Fig. 1, where the low temperature (288 K) curve insinuates a sigmoidal-like shape more pronouncedly than the other temperature curves.

The experimental curves of Fig. 4 may be written in a general form as:

$$RTln\eta = A\tau + B \qquad (4)$$

The intercept of Eq. (4) corresponds to $\boldsymbol{RTln\eta_{\infty} + \Delta G}$. When this quantity is plotted against temperature a trend towards linearity is found. Fig. 5 exhibits the results for the Newtonian and non-Newtonian parts of the two different volume fractions. The intercept of Fig. 5 provides de value of ΔG. The results obtained from Fig. 5 are shown in Table 1. These values are consistent with those determined by means of Eq. (1), and plotted in Fig. 3.

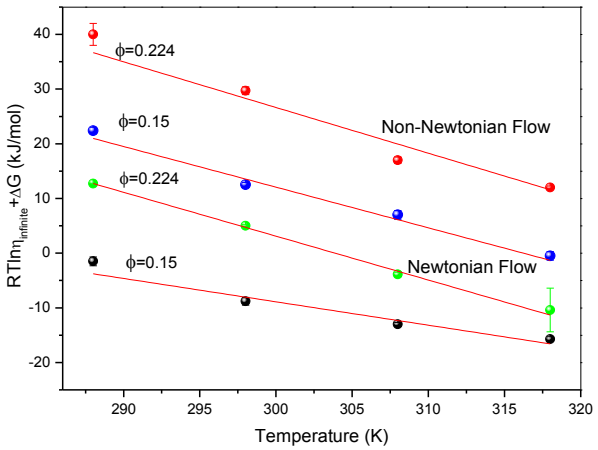

Figure 5. Values of RT lnη∞+ΔG, obtained from the intercepts of both the Newtonian and non-Newtonian parts of RTlnη vs shear stress curves such as those of Fig. 4, plotted against temperature for alumina suspensions, ϕ=0.224 and ϕ=0.150.

According to Table 1, the activation energy increases with the volume fraction and is higher for the non-Newtonian flow.

Besides, in the shear thinning region the activation Gibbs energy is higher than the corresponding to the Newtonian region, as expected from Fig.3. In addition, the slopes of Fig.5 are proportional to the lnη∞. The values calculated for alumina suspensions are also presented in Table 1.

Table 1. Values obtained from intercept (ΔG) and slope (η∞) from Fig.5.

Newtonian Flow		
$\boldsymbol{\phi}$	**ΔG [kJ/mol]**	$\boldsymbol{\eta_{\infty}}$**[Pa s]**
0.224	244±7	0.98±0.02
0.150	120±20	0,95±0.08
Non Newtonian Flow		
$\boldsymbol{\phi}$	**ΔG [kJ/mol]**	$\boldsymbol{\eta_{\infty}}$**[Pa s]**
0.224	270±40	0.90±0.13
0.150	230±20	0.91±0.08

On the other hand, slopes from shear thinning and Newtonian curves of Fig. 4, which represent values of the activation volume, are plotted against temperature in Fig. 6, for alumina nanofluids at the two volume fractions. Results can be tentatively assumed as linear for an initial interpretation. The activation volume increases dramatically with temperature in the non-Newtonian flow, while the Newtonian flow is

characterized by a small increase of the activation volume. This result can be easily quantified considering a linear relationship of the activation volume with temperature, that is:

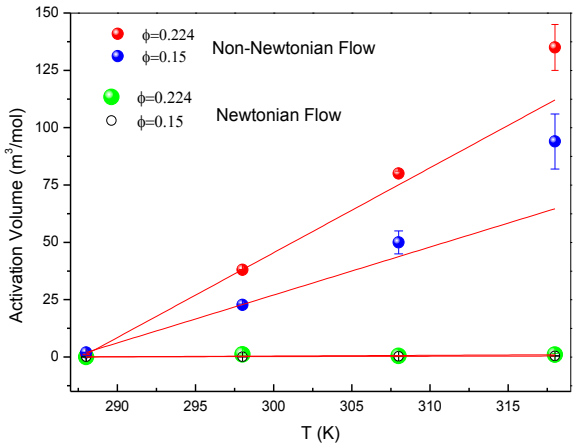

Figure 6. Activation volume determined from the slopes of RT lnη vs shear stress curves (Fig. 4) plotted against temperature, Eq. (5).

$$V = V_0 + \upsilon T \qquad (5)$$

The values of V_0, the temperature independent parameter, and υ, the temperature dependent parameter, are summarized in Table 2. The values of V_0 are always negative, which indicate a reduction of volume during the shear process. However, the temperature dependent parameter, υ, is always positive, as it is shown in Table 2, resulting an activation volume positive, as it is observed in Fig. 6. This means an increment of the activation volume in all cases, but significantly higher under the conditions of non-Newtonian flow and greater temperature.

Table 2. Values determined from intercept and slope of Fig.6.

Newtonian Flow		
ϕ	V_0 [m³/mol]	υ [m³/molK]
0.224	-9±4	0.03±0.01
0.150	-3.7±0.8	0.013±0.001
Non Newtonian Flow		
ϕ	V_0 [m³/mol]	υ [m³/molK]
0.224	-830±3	2.89±0.01
0.150	-595±3	2.073±0.001

Concluding Remarks

The effect of temperature and shear on the relative viscosity was modelated with a modified version of the Andrade-Eyring equation. The activation Gibbs energy was calculated for various shear rates. The non-Newtonian flow requires more activation energy than the Newtonian flow.

The modified Arrhenius model was also checked. The activation Gibbs energies in the Newtonian and non-Newtonian flow were evaluated. The results were consistent but higher than those obtained by using the Andrade-Eyring model.

The activation volume during the flow was also evaluated. The non-Newtonian flow requires higher activation volumes when the temperature of the system increases.

References

1. Silambarasan, M. Manikandan, S., Rajan, K.S. (2012). International Journal of Heat and Mass Transfer 55, 7991-8002.
2. Lomascolo, M., Colangelo, G., Milanese, M., de Risi, A. (2015). Renewable and Sustainable Energy Reviews 43, 1182-1198.
3. Jarahnejad, M., Haghighi, E. B., Saleemi, M., Nikkam, N., Khodabandeh, R., Palm, B., Muhammed, M. (2015). Rheologica Acta, 54, 411-422.
4. Larson, R.G. (1999). The Structure and Rheology of Complex Fluids. New York: Oxford University Press.
5. Chandler, H.D. (2014). Powder Technology, 268, 368-372.
6. Chen, H., Ding, Y., Tan, C. (2007). New Journal of Physics, 9, 367.
7. Gómez-Merino, A. I., Rubio-Hernández, F. J., Velázquez-Navarro, J. F., Aguiar, J., Jiménez-Agredano, C. (2014). Ceramics International, 40, 14045-14050.
8. Chandler, H. D. (2013). Journal of Colloid and Interface Science, 409, 98-103.
9. Rubio-Hernández, F. J., Gómez-Merino, A. I., Delgado-García, R., Páez-Flor, N. M. (2017). Powder Technology, 308, 318-323.
10. Chandler, H. D. (2010). Rheologica Acta 49, 345.

Contact Address:

fjrubio@uma.es
Departamento de Física Aplicada II
Escuela de Ingenierías Industriales
Universidad de Málaga (Spain)
C/ Dr. Ortiz Ramos, s/n, Málaga (Spain)
Tel.: +34 951 952 296

Rheometry and Experimental Methods

Following Phase Transitions with Rheometry and Simultaneous Raman-Spectroscopy

F. Meyer, J.P. Plog

Thermo Fisher Scientific, Karlsruhe (Germany)

Introduction

The use of a coupled rheometer and Raman spectrometer to obtain comprehensive insight into material's behaviour is presented.

Rheology is the study of flow and deformation of matter. During a rheological measurement the response of a material to a mechanical excitation (stress or strain) is measured using a rotational rheometer. The obtained data represents the overall response of the material which is exposed to the shear field in the measuring geometry. The mechanical properties of the material are directly related to its materials microscopic and molecular structure. However, rheological measurements alone do not provide any information about the structure and the changes that occur on the microscopic and/or molecular level.

Raman spectroscopy has shown its ability as a powerful, effective and non-invasive method for chemical analysis. Coupling a rheometer with a Raman spectrometer provides direct information about molecular reaction kinetics and mechanical properties. This is extremely useful for studying phase transition behaviour such as the crystallization of polymer melts during processing. It can also provide insight for in-situ characterization and monitoring, which can be challenging when working with on-line techniques as only relative flow fields are characterized.

Finally, the coupling gives the researcher the advantage of maximizing and synchronizing the information gathered from a single measurement as well as enabling transient information on their materials during fast processing conditions.

In this contribution we present results obtained with the new combination of a commercially available rotational rheometer with a Raman spectrometer. Details of this unique set-up as well as selected results will be presented.

Experimental

The experimental set-up shown in Fig. 1 represents a novel integration of commercial instrumentation. A Raman spectrometer (Thermo Scientific iXR Raman) and rotational rheometer (Thermo Scientific HAAKE MARS) are coupled through an optically transparent base modified from the Thermo Scientific RheoScope Module.

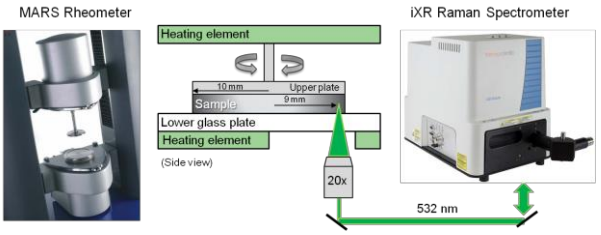

Figure 1. Schematic drawing of the experimental setup enabling simultaneous collection of rheological and Raman spectroscopy data.

To demonstrate the capabilities of the RheoRaman setup, simultaneous Raman and rheological measurements were performed on high density polyethylene (SRM 1475, National Institute of Standards and Technology, Gaithersburg, MD) during crystallization [1].

An HDPE sample of thickness 750 µm was heated for 5 minutes at 155 °C, cooled at 10 °C/min to 134 °C, and then cooled at a slower rate of 2 °C/min to 124 °C and held at temperature to crystallize. The crystallization was investigated by means of rheological measurements in oscillation mode using a 20 mm stainless steel parallel plate rotor.

The excitation source for Raman spectroscopy was a 532 nm laser with 10 mW laser power at the sample. The typical laser spot size at the focal point was approximately 5 µm. A 20x objective of the HAAKE RheoScope was used to direct the beam into the sample and to collect the 180° Raman back scattering.

Results and Discussion

The Raman spectra of HDPE in both semi-crystalline and amorphous state are shown in Fig. 2.

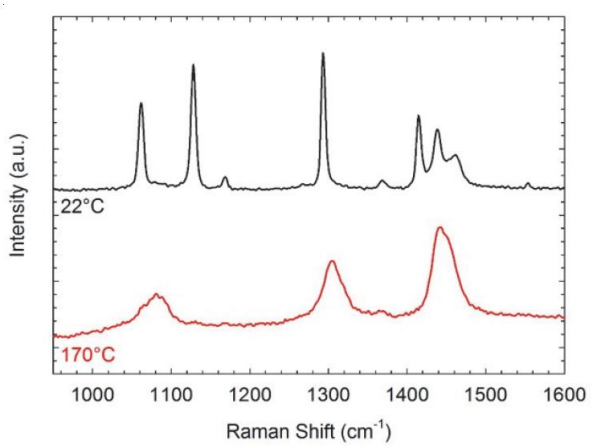

Figure 2. Raman spectra of polyethylene at temperatures corresponding to the semi-crystalline state (22 °C) and the amorphous state (170 °C).

The spectrum at room temperature shows sharp peaks corresponding to the C-C stretch, CH_2 twist, and CH_2 bend. At 170 °C HDPE is in the melt state and the sharp peaks are replaced with broader spectral features. The Raman spectra of HDPE can be analyzed to quantify the crystallinity of the sample. Specifically, the area under the peak at 1416 cm^{-1} in the HDPE spectra is directly proportional to the mass fraction of crystallinity in the sample. In order to calculate the crystallinity, the integrated peak area I_{1416} is normalized by the total area under the peaks in the CH_2 twist region and a scale factor N_c (Eq.1).

$$\alpha_{cr} = \frac{I_{1416}}{(I_{1296} + I_{1303})N_c} \qquad (1)$$

For HDPE on the RheoRaman setup, the measured scale factor is N_c = 0.80 ± 0.03. Although this is larger than calculated values of N_c from previous measurements [2], the Raman peak intensities of HDPE (and therefore the scale factor values) are strongly dependent upon the polarization state of the incoming and collected light as well as the scattering angle [3]. The crystallinity for the room temperature sample in Fig. 2 is (73 ± 4) % which agrees with the crystallinity value of (74 ± 5)% measured via DSC.

Fig. 3 shows the results of simultaneous rheological and Raman measurements during HDPE crystallization. The complex modulus is measured during small-amplitude oscillatory shear using a fixed strain amplitude of 0.01 and oscillation frequency of 1 Hz. Fig. 3 shows that early times in the crystallization process are characterized by G' < G'', but over time a crossover occurs in the modulus as the values of G' and G'' increase over 2 orders of magnitude. The plateau in G' and G'' at later times indicates the end of crystallization.

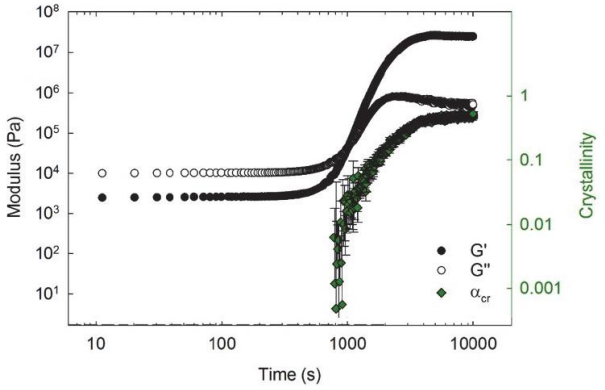

Figure 3. Complex modulus and crystallinity of PE versus time duringisothermal crystallization at 124 °C.

Fig. 3 also shows the instantaneous mass fraction of crystalline material, which first exceeds the measurement noise at approximately 800 s and increases over time. The appearance and increase in crystallinity as measured by Raman spectroscopy correlates well with the increase in the complex modulus near the crossover point. It can be concluded, that the phase transition in the investigated sample is clearly driven by crystallization.

Summary

Due to the sensitivity of the crystallization process on temperature, relating Raman and rheological measurements would be difficult using multiple instruments. By using the presented coupled RheoRaman set-up, it is possible to correlate changes in the complex modulus with structural and conformational changes during the crystallization of a HDPE melt.

References

1. Kotula, A.P et. Al., (1975). Review of Scientific Instruments 87, 105105.
2. Migler, K.B., Kotula, A.P and Hight Walker A.R., (2015). Macromolecules 48.
3. Hendra, P.J., Jobic H.P., Marsden E.P. and Bloor, D. (1977). Spectrochim. Acta, Part A 33.

Micro-capillary Flow Behavior of Magnetorheological Fluids

J. R. Morillas, K. Shahrivar, J. de Vicente

Biocolloid and Fluid Physics Group, Department of Applied Physics, Faculty of Sciences, University of Granada

Introduction

Magnetorheological (MR) fluids are non-Brownian field-responsive suspensions that experience a dramatic rheological change upon the application of a magnetic field. In the absence of a magnetic field they typically behave as quasi-Newtonian fluids. However, in the presence of a magnetic field, particles become magnetized and aggregate forming elongated structures in the field direction. As a result, the fluids exhibit a strongly non-linear behavior and in some cases the onset of an apparent yield stress [1].

Traditionally, the flow behavior of these materials has been studied under steady shear flow through the use of torsional rheometers, despite the fact that in most of the applications where these fluids are used, a different kinematics is applied. Moreover, recently, a Universal Master Curve has been proposed for steady shearing flow using the Mason number (that measures the importance of shear over magnetostatic interactions) [2, 3]. In the present manuscript we aim to elucidate whether a similar Master Curve applies in the case of microcapillary flows.

Experimental Methods

MR fluids used in this work were based on carbonyl iron microparticles (EW grade from BASF-SE, Germany) dispersed in pure glycerol (viscosity 0.125 Pa·s, Scharlau) at a low concentration (5 vol%). Although these MR fluids sediment under gravity in the course of some minutes, the experiments duration was short enough to safely suppose that the concentration is constant in the bulk.

Microcapillary flow tests were carried out in straight glass microchannels under pressure driven flow to precisely elucidate the yielding behavior of the fluids. Overall, the whole circuit consists of i) an inlet pressure pump, ii) the microchannel in whose extremes two pressure sensors are placed (max. 5 bar), iii) a valve, iv) two flow rate sensors (operational range between 1-50 and 0.4-7 μL/min) and v) an outlet pressure pump.

The microchannel employed was a straight one (length 22 mm) with a semi cylindrical cross section (radius of approx. 100 μm). It was placed inside a home-made external electromagnetic circuit that was capable of generating strong uniaxial DC fields (up to 64 kA m^{-1}) perpendicular to the flow direction.

Flow curves were obtained by reducing the pressure difference between inlet and outlet pumps (max. 3.5 bar), in steps of 250 mbar. Simultaneously, the pressure difference along the microchannel, and flow rate in the whole circuit were monitored. For safety reasons, and in order to avoid the entrance of iron particles in the flow rate sensors, we used a valve to make MR fluid to push filtered mineral oil, so that the flow rate is directly measured on this latest fluid. Final data, pressure difference and related flow rate come from time averaging when their signal become stationary: each step is kept during 3 minutes while time averaging is done in the latest 30 seconds at every step.

Results and Discussion

In Figure 1 we show the pressure difference along the channel versus the flow rate when the MR fluid flows through the microchannel under different magnetic fields. As it can be seen, the MR fluid behaves as a Newtonian one when there is no magnetic field (c.f. the straight line), however when the field is applied the sample develops a field-dependent apparent yield stress, that is, there is no flow for pressure differences below this threshold value. For each magnetic field strength, the flow curve was repeated at least three times.

In order to determine the shear viscosity and the yield stress it is necessary to relate the pressure difference (ΔP) and the flow rate (Q) with the shear stress (τ_w) and the shear strain ($\dot{\gamma}_w$) at the wall, respectively. The former relationship can be obtained from a global force

balance supposing a fully developed flow inside the channel according to:

$$\tau_w = \frac{\Delta P}{L}\frac{\pi R}{2(\pi+2)} \qquad (1)$$

Here, L is the length and R the radius of the channel.

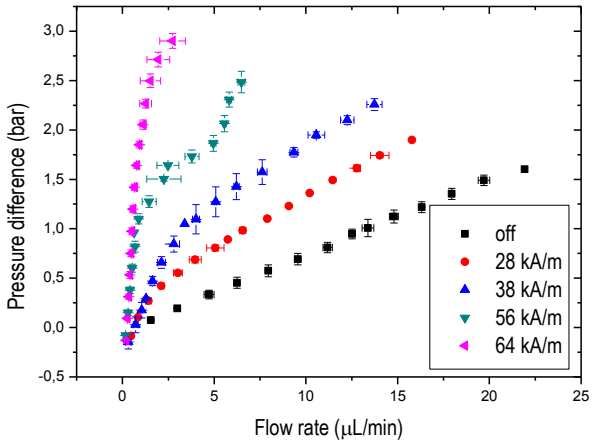

Figure 1. Pressure difference versus flow rate in 5 vol% carbonyl iron based MR fluids at different magnetic field strengths.

On the other hand, the relationship between the flow rate and the shear rate imply knowing an analytical expression for the velocity field inside the channel. However, this is a very complicated task for our geometry. For this reason we performed Finite Element Method (FEM) simulations (using COMSOL Multiphysics) to relate both magnitudes in the semi cylindrical geometry obtaining this expression: $\dot{\gamma}_{wa} = 3.783\,Q/R^3$. Here $\dot{\gamma}_{wa}$ is the "apparent" shear rate, that is, the shear rate developed by a Newtonian fluid. For non-Newtonian fluids, of interest in this work, it is necessary to introduce a correction of the form:

$$\dot{\gamma}_w = \dot{\gamma}_{wa}\left[m + n\frac{d\ln(\dot{\gamma}_{wa})}{d\ln\tau_w}\right] \qquad (2)$$

where m and n are constants which depend on the geometry of the channel. For a semi cylindrical shape, we get (again using FEM simulations) $m = 4/5$ and $n = 1/5$.

With this in mind, the calculated shear viscosity of the MR fluid in the off state (i.e. the high shear viscosity) was found to be $\mu_\infty = 0.1644 \pm 0.0017$ Pa·s. For this, a linear fit was carried out to the shear stress versus shear rate curve in the absence of magnetic fields. Next, we fit experimental data to a master curve (figure 2) in the form of non-dimensional viscosity $\mu/\mu_\infty = \tau_w/\dot{\gamma}_w\mu_\infty$ versus Mason number Mn as it is usually done in torsional shear mode. Here, the Mason number is defined as the ratio between hydrodynamic forces and magnetostatic ones:

$$Mn = \frac{72\mu_\infty\dot{\gamma}_w}{\mu_0 M^2} \qquad (3)$$

where M is the particle magnetization (dependent on the applied magnetic field) and μ_0 is the vacuum permeability.

As it can be seen in figure 2, a reasonably good fit is obtained in the flow regime (at large Mason numbers) where hydrodynamic forces dominate. However, for the lower Mason numbers investigated, the curves do not collapse as otherwise expected. This is due to experimental limitations since to get trusty data in this region, longer acquisition time (in our case restricted by sedimentation time) and accurate measuring sensors are needed.

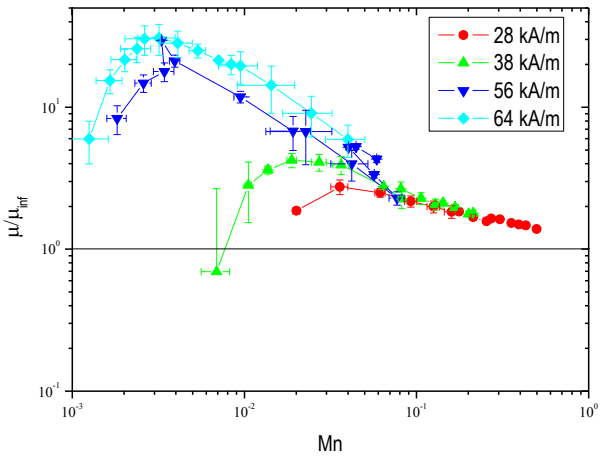

Figure 2. Rheological Master Curve in MR fluids under microchannel flow conditions at different magnetic field strengths. Error bars correspond to the standard deviation for at least three repetitions.

Concluding Remarks

We demonstrate that a rheological Master Curve can be obtained in the case of MR fluids subjected to microcapillary flows using a Mason number. This curve exhibits similarities to other master curves obtained in conventional steady shear flows using torsional rheometry in the bulk [2, 3]

Acknowledgements

This work was supported by MAT 2016-78778-R, MAT 2013-44429-R and PCIN-2015-051 projects (MINECO and FEDER, Spain) and by Junta de Andalucía P11-FQM-7074 project (Spain). J. R. M. acknowledges FPU14/01576 fellowship.

References

1. de Vicente, J. (2013). e-rheo-iba. 1,1-18.
2. Ruiz-López, J.A., Fernández-Toledano, J.C., Hidalgo-Álvarez, R. and de Vicente, J. (2016). Soft Matter. 12, 1468-1476.
3. Ruiz-López, J.A., Fernández-Toledano, J.C., Klingenberg, D.J., Hidalgo-Álvarez, R. and de Vicente, J. (2016). Journal of Rheology. 60(1), 61-74.

Contact Address:

José Rafael Morillas Medina jmorillas@ugr.es
Keshvad Shahrivar kshahrivar@ugr.es
Juan de Vicente Álvarez-Manzaneda jvicente@ugr.es

Department of Applied Physics
Faculty of Sciences
University of Granada
C/ Fuentenueva s/n, 18071-Granada, Spain
Telf.: 0034 958245148; Fax: 0034 958 243214

Remedying slip effects in the shear flow of gellan sheared gels

M.C. García, S. Sánchez, J. Santos, M.C. Alfaro, J. Muñoz

Universidad de Sevilla, Grupo de Reología Aplicada. Tecnología de Coloides. Facultad de Química. c/ P. García González, 1, 41012, Sevilla (Spain).

Introduction

Gellan gum is an anionic polysaccharide commercially obtained by microbial fermentation from Sphingomonas elodea (ATCC 41462) [1] and is in the group of the biopolymers efficient to produce fluid gels at very low concentrations. It is available in two forms, high acyl (HA) and low acyl (LA) content. The present project has been exclusively developed with low acyl gellan gum (LA).

The principal applications of fluid gels are as a suspensions agent [1], emulsions stabilized, and a possible satiety agent.

Gellan gum fluid gels are aqueous dispersions with a structure based on the existence of a network based on gelled particles. As a consequence of their structure, they exhibit an apparent yield stress [2, 3].

The main goal of this work has been to determine the apparent yield stress of low-acyl gellan gum fluid gels with Ca^{+2} ions as promoters of gel formation. However, the results obtained in the rheological measurements carried out to determine of the value of this yield stress could be influenced by the occurrence of wall-slip on the smooth surface of the sensor system. For this reason, it has previously been studied the influence of wall slip phenomena studying the effects of a change in the measurement geometry as well of the type of surface and the effect of the thickness of the sample on the flow behaviour of gellan gum fluid gels.

Experimental

0.2 wt% low-acyl gellan gum (Kelcogel FTM, supplied by CP Kelco) containing 0.15 wt% calcium chloride (Panreac) were produced by the method reported in a previous work [2].

The time necessary to avoid the effects of sample loading, 17 min, was determined by SAOS/time test.
Steady state flow in 0.5 – 25 Pa shear stress range was performed to study the existence of wall-slip by changing the sensor system geometry, surface properties and measuring gap (500-1000μm). The sensor systems used were a) parallel plates with smooth surfaces and 60 mm of diameter (PP60L), b) an upper plate with serrated surface (TA Instruments plate SST ST X-HATCH) and 60 mm of diameter with a lower homemade serrated plate (PP60R) and c) cone & plate with 60mm of diameter and angle of 1.059º (CP60).
In addition, the value of yield stress was obtained by two different ways. Firstly, it was determined by flow curves in 0.5-25 Pa range and using parallel plate with serrated surface.

Subsequently, the yield stress was determined by creep compliance test in the (1 - 8 Pa) range for 2 min at 20ºC. These tests were also performed with the same sensor system than the flow curves. All rheological measurements were conducted by a control stress rheometer, AR2000 (TA Instrument) and at 20ºC.

Results and Discussion

Steady state flow obtained with different geometries

Various results were provided by flow curve as result of the use of different geometries with different surfaces to perform the flow curve. The tests performed with rough surface sensor system showed the occurrence of a Newtonian zone at low shear stresses or rates. However, the results obtained with smooth surfaces' geometries undervalued the viscosity values at low shear stress. These facts point out the existence of wall slip phenomenon. For this reason, the use of a sensor system with rough surface is required to avoid this effect on the flow curve.

Additionally, the results obtained from steady state flow revealed gellan gum fluid gels presented a marked shear thinning behaviour; i.e. the viscosity decreases as shear stress increases. Nevertheless, it is necessary to overcome a minimal shear stress (yield stress, τ_0) in order to the fluid gels can flow.

Finally, the flow curves have been well fitted to the Herschel-Bulkley equation (1) which allowed a value of the τ_0 to be obtained. It is worth noting that the apparent yield stress values with smooth surfaces (PP60L and CP60) were lower than that obtained with

rough surfaces (PP60R) as result of the wall slip phenomenon (Table 1).

$$\tau = \tau_0 + K \cdot \dot{\gamma}^{n} \qquad (1)$$

Table 1. τ_0 as a function of sensor system used

Sensor system	τ_0 (Pa)	SD (Pa)
PP60R	3.10	0.27
PP60L	1.68	0.26
CP60	0.47	0.12

From these results the optimal sensor system for carrying out these measurements was found to be the parallel plate with serrated surface.

Steady state flow obtained with different measuring gap

The measurements conducted to determine the influence of measuring gap in 500-1000 μm range on the flow behaviour were carried out with parallel plate with serrated surface. The gap used to perform these tests did not affect the results obtained (Table 2).

According to that, the measuring gap to perform the following test was 1000μm since it is frequently used with parallel plate sensor.

Table 2. τ_0 as a function of sensor system used

Measuring gap (μm)	τ_0 (Pa)	SD (Pa)
500	3.66	0.29
750	3.30	0.32
1000	3.10	0.27

Creep compliance tests

Figure 1 shows the evolution of the strain as function of the shear time for two minutes at the nominal stress of 1 Pa on the fluid gels containing 0.2 wt% gellan gum and 0.15 wt% calcium chloride.

The results obtained are characterized by very low slope values. The apparent linear zone at the end of this measurement could suggest that the steady state has been reached. However, previous work demonstrated that gellan gum fluid gels require 3600 seconds to achieve the steady state [4].

The results obtained at 4.3 Pa are exhibited in figures 2 and 3. Four replicates at this value of nominal stress were performed. Two of them showed a shape of the curve similar to figure 2, which was analogous at figure 1, while the other two replicates were like figure 3.

As can be observed, the replicates shown in figure 2 correspond with those characteristic of linear creep flow. Conversely, figure 3 exhibits results typical of the onset of shear flow. The abrupt change in the observed behaviour indicates that this value of shear stress can be considered as the apparent yield stress.

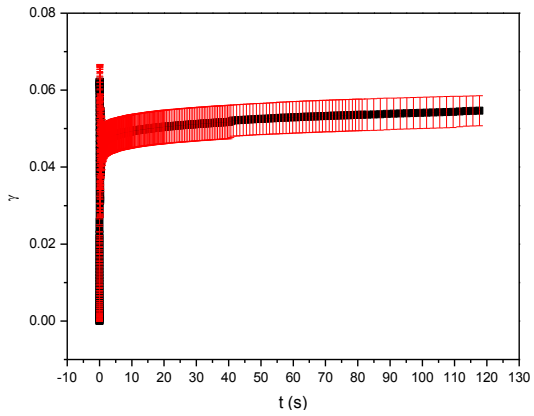

Figure 1. Creep test at 1 Pa on the fluid gels containing 0.2 wt% gellan gum and 0.15 wt% $CaCl_2$. Vertical bars indicate standard deviation data. PP60R. T=20ºC.

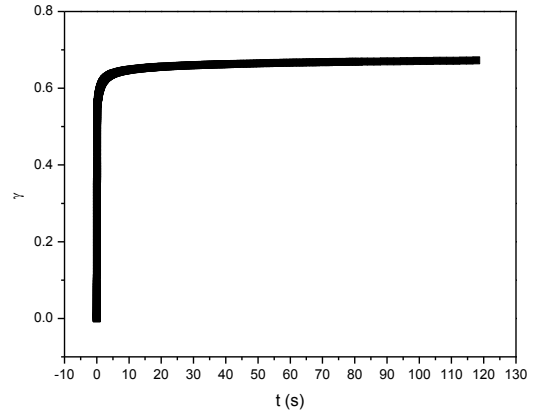

Figure 2. Creep test at 4.3 Pa on the fluid gels containing 0.2 wt% gellan gum and 0.15 wt% $CaCl_2$. Runs 1 and 3. PP60R. T=20ºC.

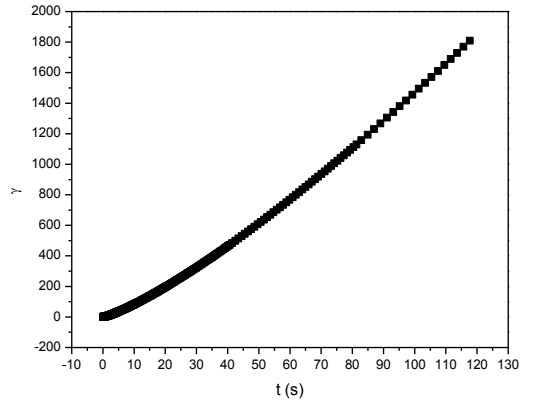

Figure 3. Creep test at 4.3 Pa on the fluid gels containing 0.2 wt% gellan gum and 0.15 wt% $CaCl_2$. Runs 2 and 4. PP60R. T=20ºC.

Figure 4 shows a practically linear evolution of strain with the time. This result can be associated to that the steady state was promptly achieved.

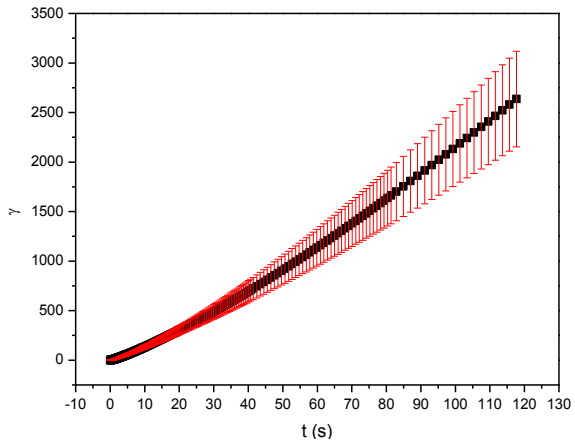

Figure 4. Creep test at 5 Pa on the fluid gels containing 0.2 wt% gellan gum and 0.15 wt% $CaCl_2$. Vertical bars indicate standard deviation data. PP60R. T=20ºC.

Concluding remarks

The results reveal the existence of wall slip effect in the obtaining the flow curves of gellan gum fluid gels. Therefore, this evidences the need of using a sensor system with rough surface. In the same way, using a rough geometry in 500-1000μ measuring gap range, there was no influence on the flow curves. Based on these results, parallel plate geometry with serrated surface and a measuring gap of 1000μm is established to determinate the apparent yield stress value by creep flow test. The value correspond to the yield stress has been 4.3 Pa. The comparison of methods used (fitting the flow curve to Herschel-Bulkley's model and creep tests) allow us to conclude that creep is the rheological test of choice to accurately determine the yield stress.

Acknowledgements

The financial support received from the Spanish Ministerio de Economía y Competitividad (MINECO) and FEDER, UE is kindly acknowledged (project CTQ2015-70700-P).

References

1. Sworn,G. (2008). In Handbook of Hydrocolloids, 2nd ed. (Philips, G.O. and Williams, P.A., eds), pp. 204-227.
2. García, M.C. Alfaro, M.C, Muñoz,J. (2015). J. Food Eng., 159, 42-47.
3. García, M.C. Alfaro, M.C, Muñoz,J. (2016). Biochemical Engineering Journal, 114, 257-261
4. Muñoz, J., Alfaro, M.C., García, M.C., Claro, J.G., Pérez, L.M., Calero, N., (2008).In Rheology in Product Design and Engineering. (Guerrero, A., Muñoz, J., Franco, J.M., eds)

Contact Address:

José Muñoz
jmunoz@us.es
Departamento de Ingeniería Química,
Facultad de Química
Unviversidad de Sevilla
C/ Profesor García González, 1, 41012,Sevilla, Spain
Telf:+34 954 556447.

Author Index